frontiers | Research Topics

Monitoring the immune/tumor microenvironment to improve cancer immunotherapy

Edited by
Jinhwan Kim and Kelsey P. Kubelick

Published in
Frontiers in Immunology

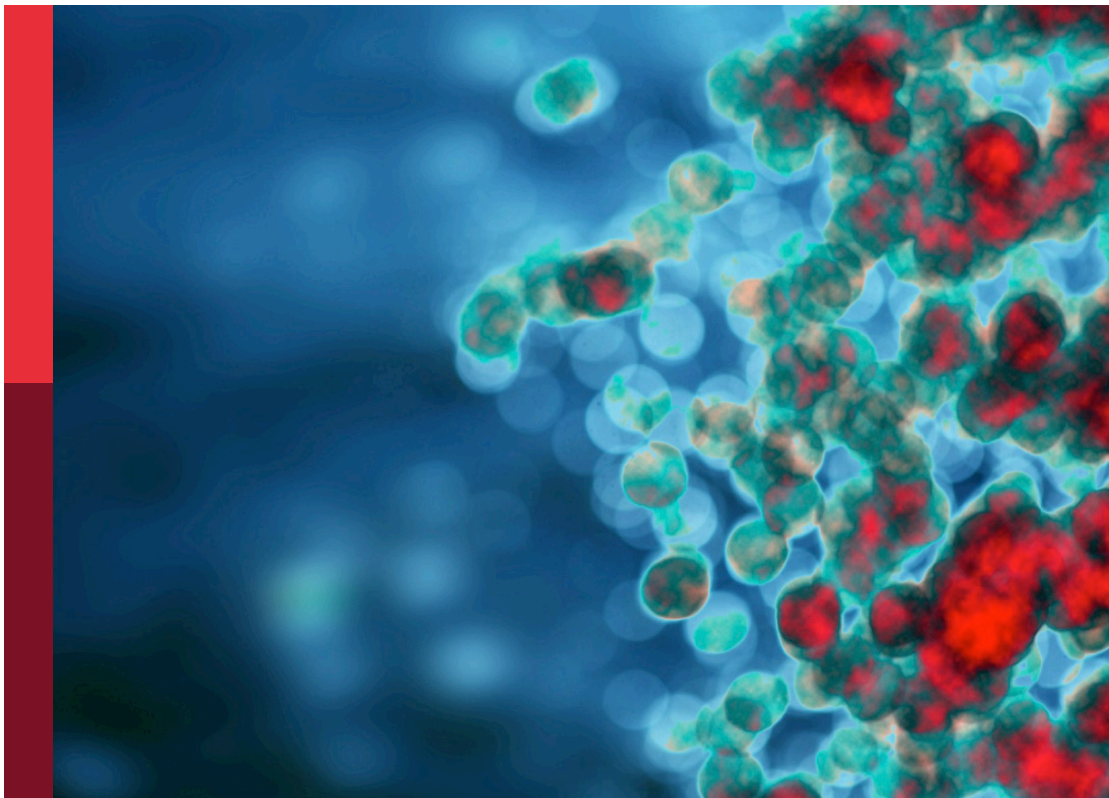

ISSN 1664-8714
ISBN 978-2-8325-7013-5
DOI 10.3389/978-2-8325-7013-5

Generative AI statement
Any alternative text (Alt text) provided alongside figures in the articles in this ebook has been generated by Frontiers with the support of artificial intelligence and reasonable efforts have been made to ensure accuracy, including review by the authors wherever possible. If you identify any issues, please contact us.

About Frontiers

Frontiers is more than just an open access publisher of scholarly articles: it is a pioneering approach to the world of academia, radically improving the way scholarly research is managed. The grand vision of Frontiers is a world where all people have an equal opportunity to seek, share and generate knowledge. Frontiers provides immediate and permanent online open access to all its publications, but this alone is not enough to realize our grand goals.

Frontiers journal series

The Frontiers journal series is a multi-tier and interdisciplinary set of open-access, online journals, promising a paradigm shift from the current review, selection and dissemination processes in academic publishing. All Frontiers journals are driven by researchers for researchers; therefore, they constitute a service to the scholarly community. At the same time, the *Frontiers journal series* operates on a revolutionary invention, the tiered publishing system, initially addressing specific communities of scholars, and gradually climbing up to broader public understanding, thus serving the interests of the lay society, too.

Dedication to quality

Each Frontiers article is a landmark of the highest quality, thanks to genuinely collaborative interactions between authors and review editors, who include some of the world's best academicians. Research must be certified by peers before entering a stream of knowledge that may eventually reach the public - and shape society; therefore, Frontiers only applies the most rigorous and unbiased reviews. Frontiers revolutionizes research publishing by freely delivering the most outstanding research, evaluated with no bias from both the academic and social point of view. By applying the most advanced information technologies, Frontiers is catapulting scholarly publishing into a new generation.

What are Frontiers Research Topics?

Frontiers Research Topics are very popular trademarks of the *Frontiers journals series*: they are collections of at least ten articles, all centered on a particular subject. With their unique mix of varied contributions from Original Research to Review Articles, Frontiers Research Topics unify the most influential researchers, the latest key findings and historical advances in a hot research area.

Find out more on how to host your own Frontiers Research Topic or contribute to one as an author by contacting the Frontiers editorial office: frontiersin.org/about/contact

Monitoring the immune/tumor microenvironment to improve cancer immunotherapy

Topic editors

Jinhwan Kim — University of California, Davis, United States

Kelsey P. Kubelick — University of Virginia, United States

Citation

Kim, J., Kubelick, K. P., eds. (2025). *Monitoring the immune/tumor microenvironment to improve cancer immunotherapy*.

Lausanne: Frontiers Media SA. doi: 10.3389/978-2-8325-7013-5

Table of contents

frontiers | Frontiers in Immunology

TYPE Editorial
PUBLISHED 06 October 2025
DOI 10.3389/fimmu.2025.1706172

OPEN ACCESS

EDITED AND REVIEWED BY
Peter Brossart,
University of Bonn, Germany

*CORRESPONDENCE
Jinhwan Kim
jjnkim@ucdavis.edu
Kelsey P. Kubelick
kpkubelick@virginia.edu

RECEIVED 15 September 2025
ACCEPTED 25 September 2025
PUBLISHED 06 October 2025

CITATION
Kim J and Kubelick KP (2025) Editorial: Monitoring the immune/tumor microenvironment to improve cancer immunotherapy.
Front. Immunol. 16:1706172.
doi: 10.3389/fimmu.2025.1706172

Editorial: Monitoring the immune/tumor microenvironment to improve cancer immunotherapy

Jinhwan Kim[1,2]* and Kelsey P. Kubelick[3]*

[1]Department of Biomedical Engineering, University of California, Davis, Davis, CA, United States, [2]Department of Surgery, School of Medicine, University of California, Davis, Sacramento, CA, United States, [3]Department of Biomedical Engineering, University of Virginia, Charlottesville, VA, United States

KEYWORDS

cancer immunotherapy, tumor microenvironment, biosensor, monitoring tumor, immune cell tracking, monitoring immune responses, theranostics

Editorial on the Research Topic
Monitoring the immune/tumor microenvironment to improve cancer immunotherapy

Although cancer immunotherapies have demonstrated remarkable clinical success across various cancer types, their potential is constrained by heterogeneous patient responses and immune-related toxicities (1). An effective immune response against cancer necessitates the coordinated activity of multiple cellular and molecular mediators within the cancer-immunity cycle, which encompasses antigen release and presentation, immune cell priming, their trafficking and infiltration, and ultimately tumor cell killing (2). Unfortunately, each step can be impacted by the immunosuppressive tumor microenvironment (TME), and failure at any single step can lead to resistance or relapse.

It is important to recognize that the TME is not a static compartment but a dynamic ecosystem where malignant cells, immune effectors, vasculature, and soluble mediators interact in both synergistic and antagonistic ways (3). Traditional methods of studying the immune response within the TME, such as invasive biopsy-based histological analyses or snapshot-like endpoint assays, fail to capture the spatiotemporal dynamics and heterogeneity that shape clinical outcomes (4). Recent advancements in bioimaging, biosensing, and computational modeling now enable us to observe the immune response in real-time, non-invasively, and longitudinally (5, 6). This allows us to map cell-cell interactions *in situ*, monitor therapeutic interventions based on the imaging feedback, and link these observations to patient outcomes. This Research Topic includes 12 contributions (6 original research articles, 3 reviews, 2 mini-reviews, and 1 opinion piece) that collectively illustrate the cutting-edge technologies for visualizing and quantifying the complex spatiotemporal dynamics of the immune-tumor microenvironment. These advanced imaging and diagnostic strategies offer profound insights into mechanisms of resistance, guide the optimization of current cancer immunotherapies, and inspire novel treatment strategies.

A comprehensive review article by Racacho et al. framed the tumor/immune microenvironment (TIME) as a central determinant of cancer progression and therapeutic response, describing how cellular and molecular interactions drive immune activation or suppression and how modern immunotherapies aim to reprogram these processes. Moreover, their study highlighted emerging trends in imaging and artificial intelligence (AI) that enable precise visualization of immune dynamics, setting the stage for research advances in this field. A complementary mini-review article by Purl et al. focused on adoptive cellular therapies for liver metastases, emphasizing how the hepatic niche restricts immune cell trafficking and persistence and how advanced imaging platforms, including PET and MRI, can be leveraged to track and optimize therapeutic cell delivery.

Articles in this Research Topic also emphasized the significance of direct visualization of immune responses. Opinion, review, and research articles by Zhang et al., Zhang et al., and Frecot et al. underscored the need to move beyond static endpoints and adopt spatiotemporal imaging techniques. These techniques, including multiplex tissue imaging, intravital microscopy, and PET tracers targeting CD8 or OX40 to image T cell status, enabled longitudinal and functional monitoring for the identification of earlier and more accurate indicators of therapeutic response.

Advanced imaging strategies have led to the identification of new structural features within the immune-tumor microenvironment. For example, tertiary lymphoid structures (TLS) can serve as organizational centers that underpin therapeutic responses, highlighting their potential role as predictive biomarkers of cancer immunotherapy. In the context of ovarian cancer, a review article by Varghese et al. presented evidence linking TLS, improved survival, and responsiveness to checkpoint blockade therapies. In contrast, a research article by Munoz-Erazo et al. demonstrated how digital pathology methods can be utilized in colorectal cancer to standardize TLS analysis and correlate with clinical outcomes.

Advancements in computational modeling and molecular profiling have further expanded monitoring capabilities. A research article by Liu et al. showcased how a multimodal deep learning framework that integrates pathology, radiology, and clinical data enhanced the prediction of PD-L1 status, immunotherapy response, and survival in esophageal cancer, demonstrating the power of AI-driven data fusion. Complementary bioinformatics and single-cell studies revealed microenvironment-linked biomarkers across tumor types. For instance, research articles by Zheng et al. found RFC4 overexpression in lung adenocarcinoma, Huang et al. identified disulfidptosis/ferroptosis-related gene signatures in endometrial carcinoma, and Miao et al. identified high FGF12 expression in stromal sarcoma. These findings emphasize the importance of interpreting tumor-intrinsic biology through the lens of the immune context. The microenvironment ultimately determines whether molecular changes translate into therapeutic vulnerability.

Finally, Wang et al. provided a mini-review that exemplifies the context-specific nature of immune regulation. Their review focused on IL-37 in gastrointestinal disease, highlighting how this cytokine's effects vary depending on the tissue and disease stage. This complexity underscores the importance of tailoring immunotherapy strategies to the unique characteristics of local immune environments.

Together, the contributions in this Research Topic highlight how the field of cancer immunotherapy monitoring is evolving through a deeper understanding and real-time assessment of the tumor/immune microenvironment. Articles in this Research Topic demonstrate how non-invasive imaging can capture the dynamics of immune engagement, how to standardize and utilize TLS as actionable biomarkers, how to integrate multimodal approaches and leverage AI to enhance predictive power, how bioinformatics and single-cell approaches can reveal novel immune-linked targets, and how context-specific regulation continues to complicate and enrich our understanding of the tumor/immune microenvironment. Effective cancer immunotherapy demands a united effort to design potent interventions along with tools to monitor, visualize, and guide immune responses as they unfold within the tumor microenvironment.

Finally, we would like to express our gratitude to all of the authors and reviewers for their invaluable contributions to this Research Topic. Their work exemplifies the growing power of interdisciplinary collaboration that integrates immunology, oncology, radiology, engineering, and data science to advance cancer immunotherapy through real-time monitoring of the tumor/immune microenvironment.

Author contributions

JK: Writing – original draft, Writing – review & editing. KK: Writing – original draft, Writing – review & editing.

Conflict of interest

The authors declare that the research was conducted in the absence of any commercial or financial relationships that could be construed as a potential conflict of interest.

Generative AI statement

The author(s) declare that no Generative AI was used in the creation of this manuscript.

Any alternative text (alt text) provided alongside figures in this article has been generated by Frontiers with the support of artificial intelligence and reasonable efforts have been made to ensure accuracy, including review by the authors wherever possible. If you identify any issues, please contact us.

Publisher's note

References

1. Sambi M, Bagheri L, Szewczuk MR. Current challenges in cancer immunotherapy: multimodal approaches to improve efficacy and patient response rates. *J Oncol.* (2019) 2019:4508794. doi: 10.1155/2019/4508794

2. Zhang Y, Zhang Z. The history and advances in cancer immunotherapy: understanding the characteristics of tumor-infiltrating immune cells and their therapeutic implications. *Cell Mol Immunol.* (2020) 17:807–21. doi: 10.1038/s41423-020-0488-6

3. Murciano-Goroff YR, Warner AB, Wolchok JD. The future of cancer immunotherapy: microenvironment-targeting combinations. *Cell Res.* (2020) 30:507–19. doi: 10.1038/s41422-020-0337-2

4. Kulkarni AD, Mukarrama T, Barlow BR, Kim J. Recent advances in non-invasive *in vivo* tracking of cell-based cancer immunotherapies. *Biomater Sci.* (2025) 13:1939–59. doi: 10.1039/d4bm01677g

5. Kubelick KP, Kim J, Kim M, Huang X, Wang C, Song S, et al. *In vivo* ultrasound and photoacoustic imaging of nanoparticle-engineered T cells and post-treatment assessment to guide adoptive cell immunotherapy. *ACS Nano.* (2025) 19:6079–94. doi: 10.1021/acsnano.4c12929

6. Lee Y, Castellanos AMS, Kim M, Kulkarni AD, Lee J, Jhunjhunwala A, et al. Nanoengineered cytotoxic T cells for photoacoustic image-guided combinatorial cancer therapy. *BioMed Eng Lett.* (2025). doi: 10.1007/s13534-025-00499-z

frontiers | Frontiers in Immunology

TYPE Review
PUBLISHED 12 July 2024
DOI 10.3389/fimmu.2024.1428541

OPEN ACCESS

EDITED BY
Kelsey P. Kubelick,
University of Virginia, United States

REVIEWED BY
Xinpei Deng,
Sun Yat-sen University Cancer Center (SYSUCC), China
Ajay Kumar Sharma,
Johns Hopkins University, United States

*CORRESPONDENCE
Yaming Li
ymli2001@163.com
Xuena Li
lixuenacmunm@163.com

†These authors have contributed equally to this work

RECEIVED 06 May 2024
ACCEPTED 27 June 2024
PUBLISHED 12 July 2024

CITATION
Zhang J, Du B, Wang Y, Cui Y, Wang S, Zhao Y, Li Y and Li X (2024) The role of CD8 PET imaging in guiding cancer immunotherapy.
Front. Immunol. 15:1428541.
doi: 10.3389/fimmu.2024.1428541

The role of CD8 PET imaging in guiding cancer immunotherapy

Jiani Zhang†, Bulin Du†, Yuxiang Wang†, Yan Cui, Shu Wang, Yuxuan Zhao, Yaming Li* and Xuena Li*

Department of Nuclear Medicine, The First Hospital of China Medical University, Shenyang, Liaoning, China

Currently, immunotherapy is being widely used for treating cancers. However, the significant heterogeneity in patient responses is a major challenge for its successful application. CD8-positive T cells ($CD8^+$ T cells) play a critical role in immunotherapy. Both their infiltration and functional status in tumors contribute to treatment outcomes. Therefore, accurate monitoring of $CD8^+$ T cells, a potential biomarker, may improve therapeutic strategy. Positron emission tomography (PET) is an optimal option which can provide molecular imaging with enhanced specificity. This review summarizes the mechanism of action of $CD8^+$ T cells in immunotherapy, and highlights the recent advancements in PET-based tracers that can visualize $CD8^+$ T cells and discusses their clinical applications to elucidate their potential role in cancer immunotherapy.

KEYWORDS

immunotherapy, CD8 + T cells, PET, clinical application, cancer

1 Introduction

Immunotherapy has advanced rapidly in the recent past (1–3). Key methods involving immune checkpoint inhibitors (ICIs) and adoptive cell therapy (ACT) have achieved notable success in the clinical management of various cancers (4, 5). However, durable and effective responses are only observed in a section of patients (6). Efforts have been made to further optimize immunotherapeutic strategies and several studies have attempted to identify potential biomarkers for improving the therapeutic efficacy (7–9).

$CD8^+$ T lymphocytes, critical immune effector cells, play a vital role in cancer immunotherapy (10, 11). Studies have shown that improved outcomes correlate positively with $CD8^+$ T cell infiltration in several types of tumors (12–14), including melanoma (15), non-small cell lung cancer (NSCLC) (16), breast cancer (17), and cervical cancer (18). In addition to the quantity of infiltration, the functional status of $CD8^+$ T cells within the tumor microenvironment (TME), which is influenced by interactions with cells and may change with time, also significantly affect response to therapy (19, 20). Both infiltration and functional status greatly contribute to the heterogeneity in response to immunotherapy (6, 8, 9). Therefore, monitoring of $CD8^+$ T cells *in vivo* is crucial for improving patient understanding and implementation of precision medicine.

Tumor biopsy, a conventional invasive method, is used in clinical practice to analyze $CD8^+$ T cells. However, due to its inherent limitations, this invasive approach poses several challenges, including difficulty in re-assessment and the inability to provide spatial and dynamic information (21). In contrast, non-invasive methods using various imaging modalities and direct/indirect labeling of target cells or construction of radiolabeled agents play significant roles in monitoring the immune response *in vivo* (22, 23). Positron emission tomography (PET) is a promising molecular technique that can provide whole-body images with considerable specificity and sensitivity (24). The binding of targeted vectors to specific radionuclides forms the foundation of PET radiotracers, and PET enables non-invasive real-time monitoring of the target cells by detecting radionuclide decay emissions (25, 26). PET radiotracers have been extensively used to characterize $CD8^+$ T cells, and thus effectively quantify early therapy-induced alterations in immune status (27).

Currently, existing PET radiotracers for visualizing $CD8^+$ T cells can be generally divided into two categories: 1) those directly targeting CD8, a dimeric co-receptor, indicating the presence of $CD8^+$ cells, and 2) those indirectly reflecting the functionality or status of $CD8^+$ T cells by targeting potential biomarkers. This review offers an overview of the development of PET imaging of $CD8^+$ T cells, briefly summarizes current information on relevant $CD8^+$ T cell biology and innovative PET tracers and discusses the future potential applications of PET in the field of cancer immunotherapy.

2 Mechanisms of action of $CD8^+$ T cells

2.1 $CD8^+$ T cells in immunology

Common T cells originate from lymphoid progenitor cells in the red bone marrow. These immature precursor T cells then migrate to the thymus (28). $CD8^+$ T cells gradually mature via several specific processes, including the development of the T cell receptor's (TCR's) affinity for major histocompatibility complex class-1 (MHC-1), positive selection, and negative selection (28, 29).

The direct interaction between $CD8^+$ T cells and corresponding antigens is pivotal for $CD8^+$ T cell activation. MHC-1, presented by malignant cells or antigen-presenting cells (APCs), is recognized by the TCR of $CD8^+$ T cells (30). Following activation of the TCR signal, additional signals from co-receptors such as CD28 complexed with B7 molecules (CD80/86), along with the influence of cytokines or chemokines, further facilitate the activation of $CD8^+$ T cells (31, 32). Consequently, $CD8^+$ T cells can identify and target tumor sites. Upon reaching the site, $CD8^+$ T cells begin to infiltrate and combat tumor cells.

2.2 $CD8^+$ T cells in anti-tumor immunity

Several studies have established the critical function of $CD8^+$ T cells in anti-tumor immunity (33, 34). The mechanisms via which $CD8^+$ T cells contribute to tumor-killing activity are complex and involve multiple factors. A primary pathway involves the release of granules containing perforin and granzymes by $CD8^+$ T cells, directly leading to the apoptosis of malignant cells (34). Perforin creates pores in tumor cell membranes, allowing granzymes to enter the TME and exert cytotoxic effect (35). The FAS ligand (FASL) pathway is another crucial pathway, which is cytotoxic for tumor cells (36). The interaction between FAS on malignant cells and FASL on $CD8^+$ T cells triggers a signal that activates the FAS-associated death domain protein, resulting in caspase activation and subsequent apoptosis of tumor cells. Additionally, $CD8^+$ T lymphocytes contribute to the destruction of tumor cells by secreting cytokines, including interferon-γ (IFN-γ) and tumor necrosis factor-alpha (37, 38). Various mechanisms collaborate to achieve tumor cell elimination, with several factors playing integral roles, including effector cytokines that impact the $CD8^+$ T cells and the dynamic metabolic state of these cells (39, 40) (Figure 1).

2.3 $CD8^+$ T cells in cancer immunotherapy

$CD8^+$ T lymphocytes possess the potent ability to kill malignant cells. However, owing to prolonged exposure in the TME, many $CD8^+$ T cells gradually exhibit characteristics of "exhaustion" (41, 42). In this state, the proliferation, effector cytokine production, and cytolytic activity of the $CD8^+$ T cells tend to decrease, while cell surface expression of inhibitory receptors, including programmed death-1 receptor (PD-1) and cytotoxic T lymphocyte antigen-4 (CTLA-4), increase concurrently (43, 44). Tumor cells exploit this by overexpressing inhibitory immune checkpoints, thereby achieving immune escape and diminishing the effectiveness of the immune response against tumors (45).

Immunotherapy, which leverages natural immune function to eliminate tumor cells, can be generally categorized into ICIs, ACT, cancer vaccines, oncolytic virus therapies, and cytokine therapies (46). ICIs block immune checkpoint pathways, aiding in the reversal of the exhausted state of $CD8^+$ T cells (47, 48). In recent years, ICIs have been shown to improve anti-tumor effects and exhibit excellent results (49, 50). A global study (KEYNOTE-042, NCT02220894) compared first-line monotherapy with pembrolizumab (a representative of ICIs) with platinum-based chemotherapy in patients with locally advanced/metastatic NSCLC without epidermal growth factor receptor/anaplastic lymphoma kinase alterations and programmed death-ligand 1 (PD-L1) tumor proportion score of ≥ 1%. Durable benefit was observed in pembrolizumab groups, in which higher 5-year overall survival (OS) rates were evident (51). Moreover, immunotherapy-based combinations demonstrated promise in further improving outcomes (52). The use of a combination of nivolumab, ipilimumab, and chemotherapy confirmed a significant improvement in OS compared with chemotherapy alone in a phase 3 trial (CheckMate 9LA, NCT03215706) involving patients with NSCLC (53). In addition to ICIs, ACT is a promising option for cancer therapy. Chimeric antigen receptor T cell therapy (CAR-T), based on gene editing in $CD8^+$ T cells and reinfusion into the human body, enhances the effectiveness of immune cells (54). These engineered cells can target malignant cells better than other cells

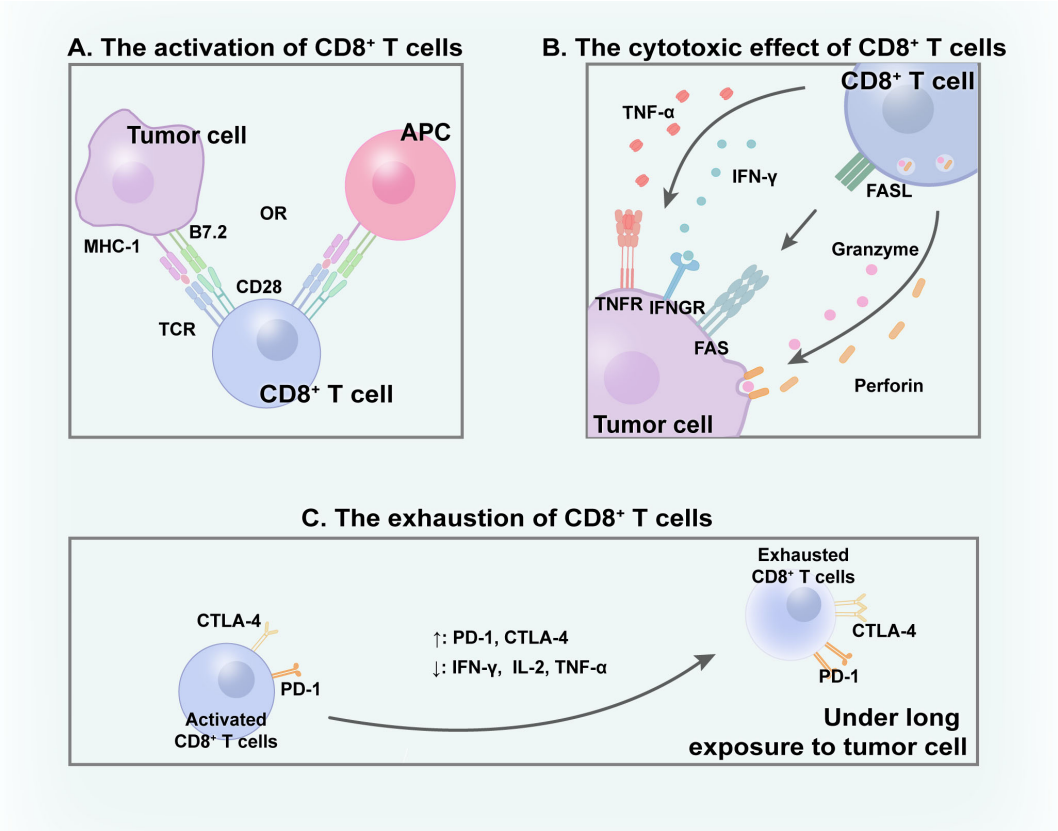

FIGURE 1
CD8$^+$ T cells within TME. **(A)** With the interaction with APC/tumor cells, CD8$^+$ T cells get activated and **(B)** subsequently excrete cytotoxic effect to eliminate tumor cells through various mechanisms. **(C)** Under long time exposure to tumor, activated CD8$^+$ T cells gradually become exhausted.

and exert cytotoxic effects (55). Moreover, oncolytic virus therapies selectively replicate in tumor cells while promoting the anti-tumor immunity of CD8$^+$ T cells (56). Cancer vaccines activate APCs loaded with tumor antigens, inducing efficient CD8$^+$ T cell responses (57). To some extent, various immunotherapy methods directly or indirectly boost the anti-tumor effect of CD8$^+$ T lymphocytes, aiding in the eradication of tumor cells (58). Furthermore, novel combination therapies with radiotherapy aim to overcome immune resistance and increase CD8$^+$ T cell infiltration, thereby enhancing efficacy (59). Consequently, CD8$^+$ T lymphocytes play an indispensable part in immunotherapy (Figure 2).

3 CD8$^+$ T cell imaging tracers

PET is a powerful clinical technique (60) utilized for non-invasively and dynamically visualizing CD8$^+$ T cells in cancer immunotherapy. Currently, the design and development of tracers for CD8$^+$ T cells have improved considerably. Ideal radiotracers should possess high specificity, sensitivity, and a relatively low radiation burden. Both the choice of radionuclides and vectors are critical considerations in this process (27).

Previously, zirconium-89 (^{89}Zr) was a popular choice. Owing to its relatively long half-life, this radionuclide pairs well with intact antibodies that also have long serum half-lives, potentially providing reliable information several hours or days after injection (61, 62). Copper-64 (^{64}Cu) is another promising candidate for a long-lasting imaging agent that can be used in the human body (63). However, its high signal intensity in the liver and intestines may limit the clinical application of ^{64}Cu-labeled probes (27). In contrast, gallium-68 (^{68}Ga) and fluorine-18 (^{18}F) are better options for obtaining sequential images in clinical settings due to their shorter half-lives (64).

Studies utilizing full-sized antibodies, which are relatively easy to produce as imaging agents, have been successfully used in immuno-PET (27). However, their use is challenging, because their size exceeds the renal filtration cutoff, which may impede diffusion and penetration (65). With the advancement of radiotracers, current choices for targeting vectors extend beyond full-length antibodies, with options such as minibodies, cys-diabodies, and nanobodies emerging. Smaller antibody fragments, particularly nanobodies, which consist solely of a heavy chain structure, are preferred in many studies for their rapid pharmacokinetics, better tissue penetration, and low immunogenicity (66, 67). When combined with radionuclides with short half-lives such as ^{68}Ga and ^{18}F, nanobodies can facilitate the creation of high-quality images with lower radiation doses, aiding their translation into clinical practice. The currently developed radiotracers used for visualizing CD8$^+$ T cells are summarized in the Table 1.

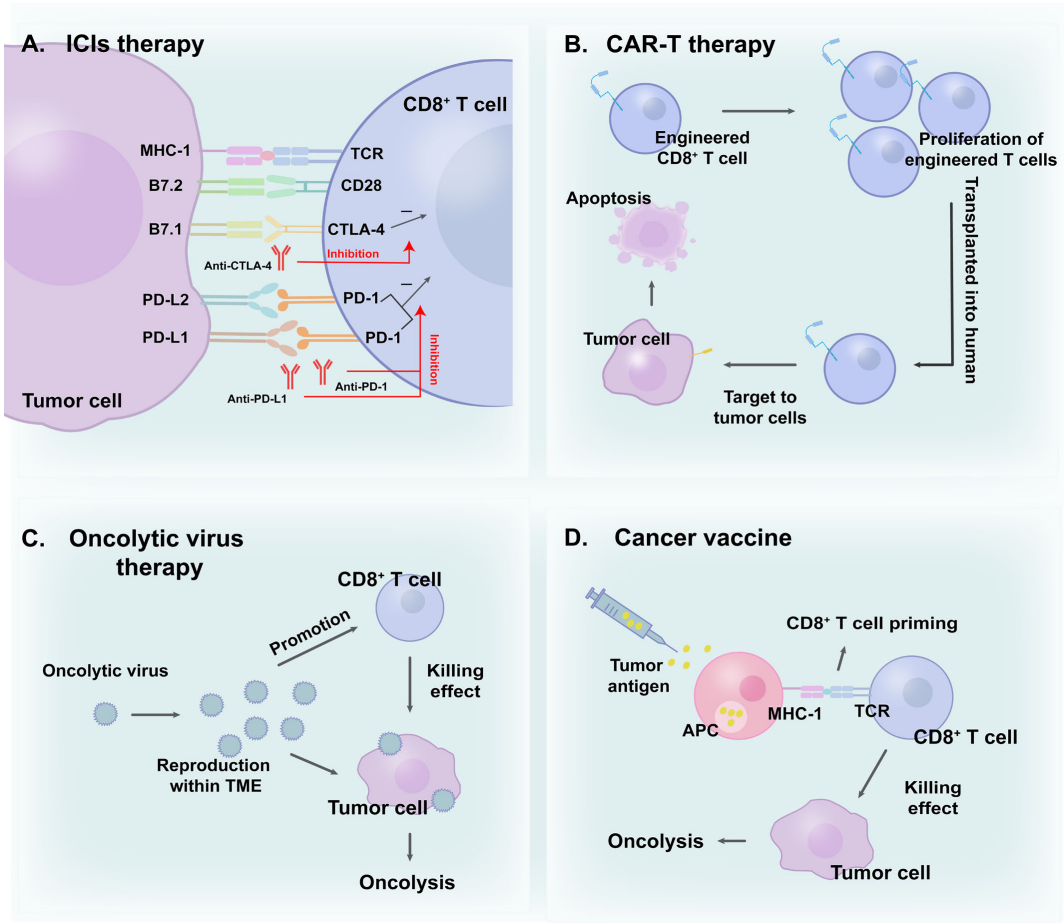

FIGURE 2
CD8$^+$ T cells in **(A)** ICIs therapy; **(B)** CAR-T therapy; **(C)** Oncolytic virus therapy and **(D)** Cancer vaccine. CD8$^+$ T cells play a vital role in cancer immunotherapies.

4 Quantitative visualization of CD8$^+$ T cells

The immune status within TME is dynamic, with CD8$^+$ T cells, other immune cells, and effector molecules being constantly in flux (93, 94). Therefore, real-time monitoring of CD8$^+$ T cell infiltration can provide accurate and significant information for personalized therapy. Due to its unique advantages, the PET tracer has emerged as an attractive tool, and many studies have investigated its potential clinical applications.

4.1 Feasibility of using CD8 PET tracers

4.1.1 Minibody

CD8-targeted tracers, primarily derived from antibodies, minibodies, cys-diabodies, and nanobodies, have shown promising results. The feasibility of using two ^{64}Cu-labeled engineered minibodies, ^{64}Cu-NOTA-2.43 and ^{64}Cu-NOTA-YTS169, for monitoring CD8$^+$ T cells has been confirmed in non-tumor murine models (68). The interaction between murine CD8α (one of the isoforms of CD8) and these tracers was verified without diminishing CD8$^+$ T cell populations. Both tracers accumulated in the lymph nodes and spleen in antigen-positive mouse models, with notably decreased uptake in immunodeficient or antigen-depleted models (68). To delineate the TME more accurately in clinical patients, ^{64}Cu-DOTA-IAB22M2C, a CD8-targeted minibody, has been effectively used in a xenograft model of orthotopic glioblastoma, demonstrating its ability to monitor both peripheral and intratumoral CD8$^+$ T cells (79). Notably, tracer accumulation in the brain indicated that ^{64}Cu-DOTA-IAB22M2C could potentially complement ^{18}F-FDG, particularly in addressing its limitations in brain tumor imaging.

Building upon these animal studies, clinical trials using tracers with high affinity to human CD8 have been designed. Research on ^{89}Zr-Df-IAB22M2C, a ^{89}Zr-labeled anti-CD8 minibody, has progressed considerably (77, 95–97). Preclinical studies have demonstrated its uptake in targeted lesions with an ideal target-to-background ratio in mouse models. Subsequently, a phase I first-in-human study (NCT03107663) assessed the optimal mass doses

TABLE 1 PET tracers visualizing $CD8^+$ T cells.

Classification	Target	Radiotracer	Radioisotope	Imaging agent	Study design	Main findings	Author (year)
Quantitative Visualization of $CD8^+$ T Cells	CD8	^{64}Cu-NOTA-2.43	^{64}Cu	Minibody	Preclinical	These two tracers both can detect mouse CD8 expression in preclinical models.	Tavaré et al. (2014) (68)
		^{64}Cu-NOTA-YTS169	^{64}Cu	Minibody			
		^{89}Zr-malDFO-2.43	^{89}Zr	Cys-diabody	Preclinical	This tracer can be used to monitor the proliferation, localization of $CD8^+$ T cells *in vivo*.	Tavaré et al. (2015) (69)
		^{89}Zr-malDFO-169	^{89}Zr	Cys-diabody	Preclinical	This tracer is potential to tract endogenous $CD8^+$ T cells and evaluate the alterations induced by three distinct immunotherapies (ACT, anti-CD137/4-1BB, anti-PD-L1).	Tavaré et al. (2016) (70)
		^{64}Cu-169cDb	^{64}Cu	Cys-diabody	Preclinical	This tracer is able to visualize $CD8^+$ T cells alterations induced by CpG and αPD-1 therapy.	Seo et al. (2018) (71)
		^{89}Zr-DFO-CD8a	^{89}Zr	F(ab)'2 fragments	Preclinical	This tracer is of capacity to depict $CD8^+$ T cells *in vivo* and predict outcome to a novel PD-1 checkpoint inhibitor (Sym021).	Kristensen et al. (2019) (72)
		^{89}Zr-PEGylated anti-CD8 VHH	^{89}Zr	Nanobody	Preclinical	This tracer could visualize the increase of $CD8^+$ T cells induced by anti-PD-1 treatment and show the potential to evaluate therapy efficacy.	Rashidian et al. (2019) (73)
		^{64}Cu-NOTA-CD8a	^{64}Cu	F(ab)'2 fragments	Preclinical	This tracer is able to provide images of $CD8^+$ T cells changes induced by radiotherapy and CTLA-4 therapy.	Kristensen et al. (2020) (74)
		ZED88082A	^{89}Zr	Monovalent antibody	Preclinical	This tracer was developed for assessing $CD8^+$ T cells levels *in vivo* without affecting its activity.	Gill et al. (2020) (75)
					Phase 1&2 (NCT04029181)	This uptake of ZED88082A can greatly reflect the dynamic alterations of $CD8^+$ T cells in cancer patients undergoing ICIs and shows the prognostic value in the field of immunotherapy.	Kist de Ruijter et al. (2022) (76)
		^{89}Zr-Df-IAB22M2C	^{89}Zr	Minibody	Phase 1 (NCT03107663)	This tracer passed the safety assessment in human subjects and has the potential to draw a whole-body picture of $CD8^+$ T cells in human bodies.	Pandit-Taskar et al. (2020) (77)
					Phase 2 (EudraCT-number 2021-004328-13)	This tracer can assess $CD8^+$ T cells infiltration through PET/MRI and show uptake in lymphatic organs.	Schwenck et al. (2023) (78)
		^{64}Cu-NOTA-IAB22M2C	^{64}Cu	Minibody	Preclinical	This tracer could be used to evaluate $CD8^+$ T cells both in peripheral blood and inside GBM.	Nagle et al. (2021) (79)
		^{68}Ga-NOTA-SNA006a	^{68}Ga	Nanobody	Preclinical		

(Continued)

10.3389/fimmu.2024.1428541

TABLE 1 Continued

Classification	Target	Radiotracer	Radioisotope	Imaging agent	Study design	Main findings	Author (year)
						This nanobody-based tracer could rapidly visualize $CD8^+$ T cells with great affinity.	Zhao et al. (2021) (80)
		^{68}Ga-NODAGA-SNA006	^{68}Ga	Nanobody	Phase 1 (NCT05126927)	This novel tracer is able to quantitatively monitor $CD8^+$ T cells in human body and dynamically interpret the complex therapy-induced changes.	Wang et al. (2022) (81)
		^{18}F-VHH5v2	^{18}F	Nanobody	Preclinical	This tracer could detect different $CD8^+$ T cells *in vivo* at early time points.	Sriraman et al. (2022) (82)
		^{89}Zr-DFO-REGN5054	^{89}Zr	Antibody	Preclinical	This tracer could detect $CD8^+$ T cells during therapy and is demonstrated safe and well-tolerated in non-human mammals.	Tavaré et al. (2022) (83)
		^{89}Zr-IAB42M1-14	^{89}Zr	Minibody	Preclinical	This tracer can assess the infiltration of $CD8^+$ T cells in tumor, lymphoid tissues and alterations induced by ICOS monotherapy or ICOS/PD-1 combination therapy.	Alsaid et al. (2023) (84)
Functional Visualization of $CD8^+$ T Cells	Granzyme B	^{68}Ga-NOTA-GZP	^{68}Ga	Peptide	Preclinical	The tracer could assess granzyme B expressions reflecting the cytotoxic function and stratify patients.	Larimer et al. (2017) (85)
		^{18}F-AlF-mNOTA-GZP	^{18}F	Peptide	Preclinical	The uptake of this tracer is greatly associated with the levels of GZB-expressing $CD8^+$ T cells and may inform the evaluation of immunotherapy.	Hartimath et al. (2022) (86)
		^{68}Ga-grazytracer	^{68}Ga	Non-aldehyde peptidomimetics	Phase 1 (NCT05000372)	This tracer is able to distinguish pseudoprogression with tumor progression and is demonstrated the potential to reflect immune response in patients.	Zhou et al. (2022) (87)
	IFN-γ	^{89}Zr-anti-IFNγ	^{89}Zr	Antibody	Preclinical	This IFN-γ-targeted tracer could detect the alterations of such cytokine and thus indirectly depict the function of immune cells.	Gibson et al. (2018) (88)
		^{89}Zr-DFO-NCS-anti-IFN-γ HL-11	^{89}Zr	Diabody	Preclinical	This tracer is developed to target IFN-γ *in vivo* and confirmed the one with best properties among distinct choices of linker lengths	Rezazadeh et al. (2022) (89)
	IL-2R	^{18}F-FB-IL2	^{18}F	Protein	Preclinical	This tracer could specifically attach to IL-2R and possesses the capacity to reveal activated T cells in pathologic conditions.	Di Gialleonardo et al. (2012) (90)
					Phase 1 (NCT02922283)	The feasibility of applying this tracer to human beings was demonstrated safe. Current data	P.p et al. (2021) (91)

(Continued)

10.3389/fimmu.2024.1428541

TABLE 1 Continued

Classification	Target	Radiotracer	Radioisotope	Imaging agent	Study design	Main findings	Author (year)
						shows this tracer can't evaluate therapy-induced changes.	
	AraG	^{18}F-AraG	^{18}F	Small molecule	Preclinical	This tracer could detect the immune response to immunotherapy and has the potential to distinguish patients from responders to non-responders.	Levi et al. (2021) (92)

(1.5 mg) and imaging timings (24 hours post-injection) among 15 patients in varying treatment states using ^{89}Zr-Df-IAB22M2C (97). The optimal conditions for its clinical application are being investigated in an ongoing phase II clinical trial (NCT03802123).

4.1.2 Nanobody

Existing CD8-targeted minibody-based PET tracers are mainly labeled with ^{89}Zr or ^{64}Cu which has long half-live. Consequently, these tracers require a long time (usually several hours or days after injection) before the image acquisition and which may cause difficulties for clinical practice. In contrast, nanobodies have emerged as highly potent alternatives, offering rapid targeting, high signal-to-background ratios, and other superior characteristics (98).

Considering the advantages of ^{68}Ga over ^{89}Zr, a novel CD8-targeted nanobody, ^{68}Ga-NOTA-SNA006a, was developed to monitor human CD8 antigen using PET (80). *In vitro* binding assays was conducted to assess the binding capacity of vectors to human CD8 protein and results demonstrated strong binding affinity with positive binding rate constant. *In vivo* studies assessing specificity and stability in humanized mouse models demonstrated its significant uptake in CD8-positive tumors and organs (lung, spleen and liver). An optimized variant with reduced kidney uptake, ^{68}Ga-NODAGA-SNA006, was obtained by removing the His6 tag from ^{68}Ga-NOTA-SNA006a (81). This nanobody's ability to quantify CD8$^+$ T lymphocytes has been shown not only in preclinical models but also in three lung cancer volunteers (NCT05126927). Notably, a patient who underwent immunotherapy displayed comparably high uptake in tumor lesions, suggesting the potential of this tracer to evaluate therapy-induced changes (81).

4.2 Patient stratification for immunotherapy

Immunotherapy has been successfully applied in various clinical settings, particularly in cancer treatment. However, its wider clinical application is hindered by the generally low patient response rate, with immune heterogeneity being a key deterrent. Therefore, visualization of CD8$^+$ T cells may be a potent strategy for detecting immune heterogeneity and guiding patient stratification.

Kristensen developed ^{89}Zr-DFO-CD8a, which was created from the F(ab')2 fragments of a rat-anti-mouse CD8a antibody conjugated to the p-SCN-Bn-desferrioxamine chelator (72). This preclinical study investigated the correlation between baseline PET imaging of CD8 levels (tumor-to-heart ratios) and tumor suppression induced by a PD-1 checkpoint inhibitor. Groups with higher numbers of baseline CD8$^+$ T lymphocytes exhibited significant tumor suppression, while the efficacy in groups with fewer CD8$^+$ T lymphocytes was less pronounced. This finding suggests the potential for stratifying patients from responders to non-responders before starting immunotherapy (72). Notably, significant difference in the maximum ^{89}Zr-DFO-CD8a tumor-to-heart ratio between responding and non-responding groups was not observed, highlighting the necessity of understanding the

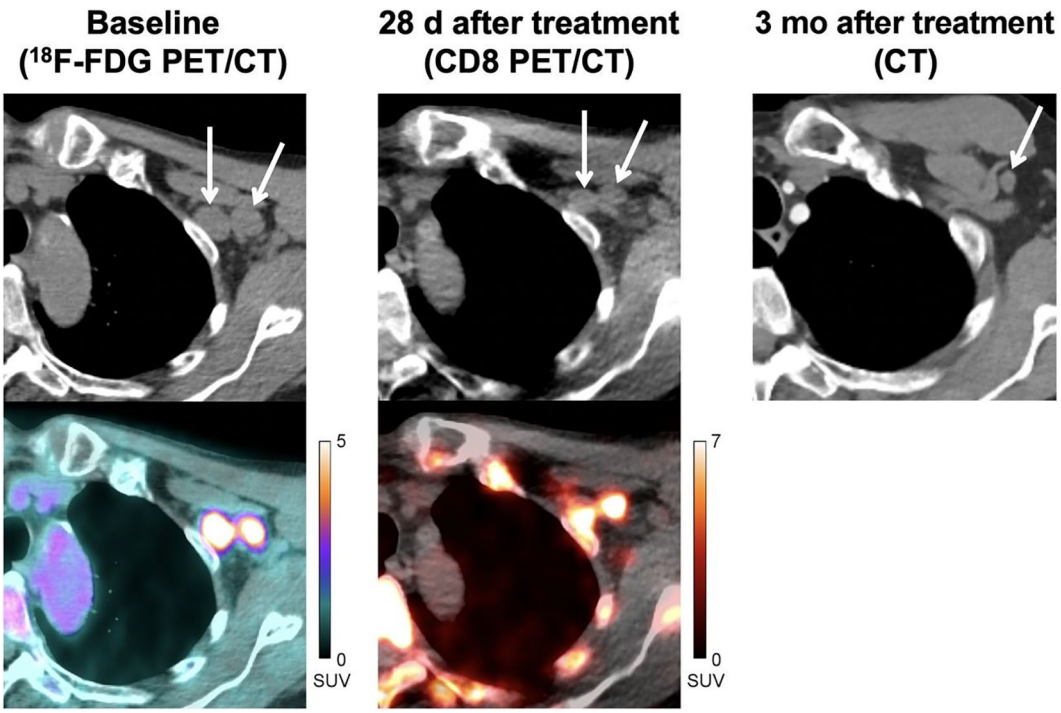

FIGURE 3
A 71 years old patient (locally advanced stage III melanoma) with immunotherapy (pembrolizumab). CD8 PET/CT images, which performed 28 days after pembrolizumab, show evident uptake in metastases indicating significant infiltration of $CD8^+$ T cells. CT images performed 3 months after treatment confirmed the efficacy of immunotherapy. Reproduced from Farwell MD et al. (97).

relationship between specific quantitative parameters and the patient population suitable for immunotherapy.

4.3 Evaluating the efficacy of immunotherapy

Owing to its unique mechanism, atypical patterns of response may emerge during immunotherapy (99, 100). Pseudoprogression, for example, is an atypical phenomenon that differs from actual progression, characterized by increasing tumor size due to therapy-induced immune cell infiltration (101). The existence of atypical patterns brings great challenges to the evaluation of efficacy in clinical practice (102). CD8 PET tracers can directly monitor the immune alterations caused by immunotherapy unaffected by atypical phenomenon, which may provide accurate evaluation at an early stage and thus favor follow-up decision making.

The use of ^{89}Zr-malDFO-169cDb, an ^{89}Zr-desferrioxamine-labeled anti-CD8 cys-diabody, enabled tracking of endogenous $CD8^+$ T cells and assessment of changes induced by three different immunotherapies in murine models (70). The study compared tumor-to-blood ratios between responders and non-responders in each of the three models, noting that the difference in the anti-PD-L1 therapy group was less significant (70). In addition to monotherapy, Kristensen has evaluated the efficacy of combination therapy. The use of ^{64}Cu-NOTA-CD8a for evaluating the response to combination therapy, external radiation therapy with anti-CTLA-4 therapy, has been validated demonstrating the tracer's utility (74). This finding suggests a potential for using CD8-targeted probes for evaluating therapeutic efficacy and providing valuable information for clinical decision-making.

In clinical settings, a study involving patients with metastatic melanoma undergoing immunotherapy showed that CD8 PET tracer (^{89}Zr-Df-IAB22M2C, performed 28 days after immunotherapy) was noticeably incorporated during metastases, indicating infiltration of $CD8^+$ T cells. This positive indication was consistent with conventional computed tomography (CT) imaging (performed 3 months after immunotherapy) which suggested a complete response to therapy (Figure 3) (97). This study demonstrated the promising potential of CD8 PET in evaluating immunotherapeutic efficacy at rather early stage. Additionally, another clinical study suggested the feasibility of using ^{89}Zr-Df-IAB22M2C PET/MRI in assessing $CD8^+$ T cells infiltration for efficacy evaluation in a retrospective cohort of eight patients (78). However, future studies involving larger prospective cohorts are required to strengthen these findings.

4.4 Dynamic surveillance of ICI therapy

For more effective and precise immunotherapy, dynamic and non-invasive surveillance of the therapeutic process is urgently

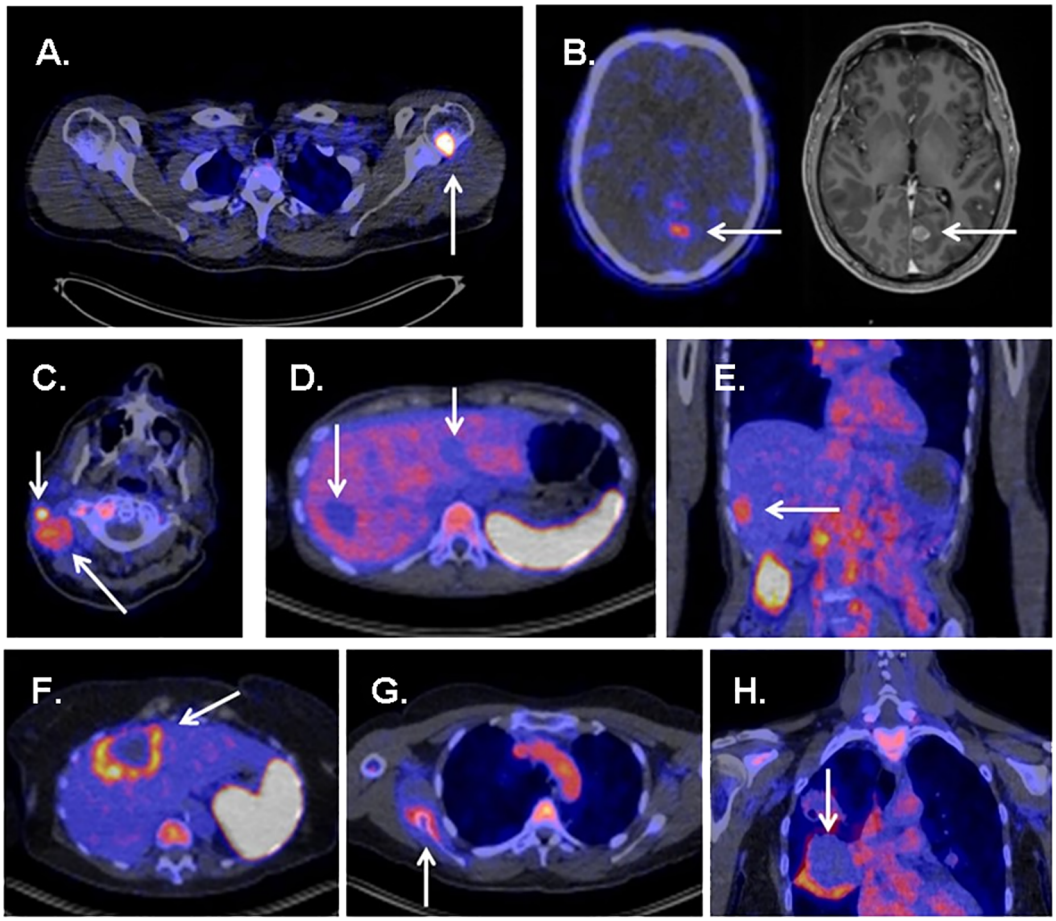

FIGURE 4
Several examples showing uptake of ^{89}ZED88082A in tumor sites and metastases. **(A)** High uptake in bone metastasis of a patient with melanoma. **(B)** Uptake in a brain metastasis of a patient with melanoma. **(C)** Evident uptake in multiple cervical lymph node metastases in a patient with cutaneous squamous cell carcinoma. **(D)** Several liver metastases showing no uptake in a patient with ovarian clear cell carcinoma. **(E)** Uptake in a liver metastasis in a patient with squamous cell oesophageal cancer. **(F)** Liver metastases with rim uptake in a patient with colorectal cancer. (G) Uptake in bone lesion of a patient with squamous cell vulvar cancer. **(H)** Rim uptake in lung metastasis of a patient with cervical cancer. Reproduced from Kist de Ruijter L et al (76).

required. Rashidian used ^{89}Zr-PEGylated camelid single-domain antibody fragments to successfully visualize the dynamic increase in CD8$^+$ T lymphocytes within tumors during ICI therapy. They observed a significant trend of CD8$^+$ T lymphocytes migrating from the periphery to the central position in tumor sites in murine models (73). This finding underscores the unique advantages of dynamic surveillance in this context.

Additionally, the occurrence of adverse events during immunotherapy, which are crucial factors in dynamic surveillance, should not be overlooked. Based on the results of a phase 1/2 trial (NCT04029181), the potential of ZED88082A in detecting inflammation in non-malignant areas has been investigated. The results suggest its ability to characterize CD8-related immune-related adverse events (irAEs) (76). This study investigated the potential applications of CD8-targeted PET tracers and provided practical directions for further clinical translation. However, irAEs may also be induced by other factors, such as B cells, indicating a potential limitation of CD8 PET tracers in obtaining comprehensive information on irAEs. More datasets in the future are required to confirm these findings.

4.5 Predicting the prognosis of ICI therapy

ZED88082A, based on a monoclonal antibody, was used to visualize CD8 infiltration in patients with solid tumors during ICI therapy (75, 76, 103). Thirty-nine patients (excluding one because of tracer extravasation) were used to assess tracer uptake both at baseline and during therapy (Figure 4) (76).

In an average follow-up of 5.6 months, baseline tracer uptake correlated positively with the best overall response per the Response Evaluation Criteria in Solid Tumors. The tracer accumulation in patients with no progressive disease, which included one showing complete response, eight showing partial responses, and four cases of stable disease, was 40% higher than that in patients with progressive disease. The study also found that patients with

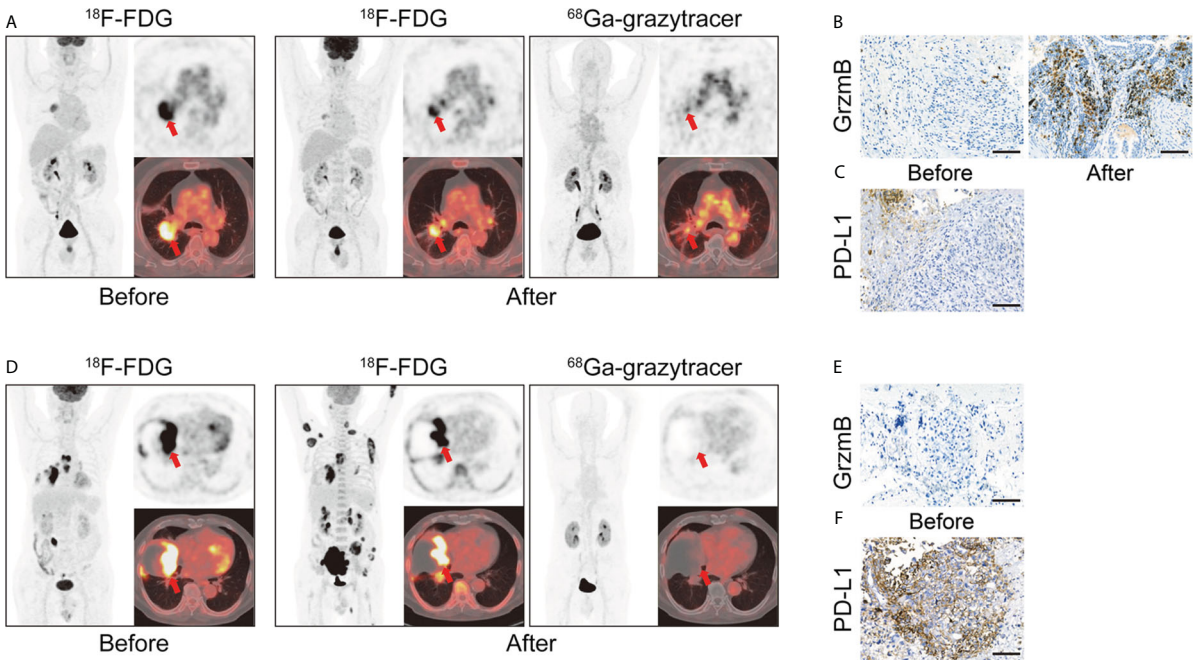

FIGURE 5
(A) A 66 years old patient (lung adenocarcinoma, cT2bN2M0 IIIa) with combination therapy (pemetrexed disodium + cisplatin + toripalimab). ^{68}Ga-grazytracer PET/CT images, which performed 3 circles after treatment, demonstrate uptake in tumor lesions indicating the cytotoxic effect against tumor cells (SUVmax 4.1). Follow-up evaluation confirmed a positive prognosis for this patient. **(B, C)** Immunohistochemistry (IHC) staining of granzyme B and PD-L1 of corresponding patient. **(D)** A 70 years old patient (pulmonary sarcomatoid carcinoma, cT4N3M1c IVb) with immunotherapy (pembrolizumab). ^{68}Ga-grazytracer PET/CT images, which performed 1 circle after treatment, reveal relatively fewer uptake (SUVmax 2.0) with follow-up evaluation suggesting a negative prognosis for this patient. **(E, F)** IHC staining of granzyme B and PD-L1 of corresponding patient. Reproduced from Zhou H et al. (87).

above-median baseline geometric mean maximum standardized uptake values (SUVmax) (> 5.2) tended to have better progression-free survival (PFS) and superior OS than others (76). This demonstrates the potential of ZED88082A in predicting prognosis for ICI therapy.

Studies focusing on CD8-targeted PET imaging have made significant advancements, and current developments demonstrate the feasibility of using CD8-targeted radiotracers in the field of immunotherapy. To a certain extent, these tracers have improved the efficacy of immunotherapies and may be used to assess the efficacy of newly developed treatments.

5 Functional visualization of CD8$^+$ T cells

CD8-targeted PET tracers not only reveal the number of effector CD8$^+$ T cells but also that of naïve and exhausted CD8$^+$ T cells. However, the effector CD8$^+$ T cells are the primary subtype contributing to anti-tumor immunity (104). Therefore, targeting of effector CD8$^+$ T cells results in a functional representation of all CD8$^+$ T cells, offering a comprehensive and accurate assessment of their status after combining both quantitative and functional visualization.

CD8 has been identified to be a reliable target for monitoring immunotherapy in numerous studies. Considering the variable functional states of CD8$^+$ T lymphocytes (such as exhausted T cells), and the diverse impacts of various factors on these cells, several researchers have focused on the cytokines produced during the tumor-killing process and throughout T cell activation, which can indicate the activation of cytotoxic T lymphocytes (105).

5.1 Granzyme B

Granzyme B, released by activated effector CD8$^+$ T lymphocytes, participates in the direct tumor-killing mechanism. As a potent representative of the anti-tumor immune response, granzyme B is considered a potential predictive biomarker for cancer therapy (106, 107). Larimer designed a novel peptide-based imaging probe, ^{68}Ga-NOTA-GZP, which specifically represents granzyme B expression. They demonstrated a correlation between tracer uptake and therapeutic efficacy, verifying the granzyme B tracer's potential as an immunotherapy predictive biomarker (85, 108). Another granzyme B-targeted tracer, ^{68}Ga-grazytracer, showed comparably higher uptake at tumor sites than ^{68}Ga-NOTA-GZP (87). This novel radiotracer, designed by Zhou, has demonstrated the ability to monitor granzyme B levels and the potential to evaluate the efficacy of ICIs and ACT therapy. Furthermore, it can assess intrinsically-induced immune responses, as shown by its ability to distinguish true progression from pseudoprogression in mouse models, potentially complementing the results obtained using ^{18}F-FDG. This study also investigated the feasibility of clinical translation in five patients, obtaining positive results consistent with preclinical findings (Figure 5) (87).

Evidence suggests that the granzyme B tracer is a valuable tool for characterizing the tumor-killing function in the context of immunotherapy. However, control of the imaging time point remains a hurdle to be overcome due to the variable time window between granzyme B secretion from cytotoxic $CD8^+$ T cells and its arrival at malignant cells, which can be influenced by several factors (109).

5.2 IFN-γ

IFN-γ, which partially reflects the function of $CD8^+$ T cells, may act as a promising biomarker for immuno-PET considering its significant role in the anti-tumor response. Studies have also investigated the feasibility of using IFN-γ as a therapeutic agent in immunotherapy (110, 111). ^{89}Zr-anti-IFNγ, developed by Gibson, can be used to assess IFN-γ levels and may be potentially used as a probe for assessing active anti-tumor T cell activity and predicting treatment outcomes in animal models (88). Unlike CD8-targeted tracers, ^{89}Zr-anti-IFNγ can directly represent effector function, addressing the limitation that $CD8^+$ T cells might become dysfunctional despite the presence of tumor-infiltrating lymphocytes. However, $CD8^+$ T cells are not the only subset capable of secreting this cytokine. Depending on the cell subset, IFN-γ might not only exert an anti-tumor effect but also potentially promote tumor progression (112). Therefore, the feasibility and practical value of targeting IFN-γ for immuno-PET has to be verified. Further investigation on IFN-γ-targeted tracers is required not only to evaluate the efficacy of immunotherapy but also to promote the development of IFN-γ-based therapeutic methods.

5.3 Arabinofuranosyl guanine

An ^{18}F-labeled analog of AraG, which acts as a substrate for deoxyguanosine kinase (dGK), significantly influences T cell activation and functionality, particularly from a metabolic perspective, and can be used to elucidate the status of immune cells (113, 114). ^{18}F-AraG can be used to detect the immune response to immunotherapy, as it shows pronounced accumulation in human immune cells (92, 115–116). In contrast, macrophages and dendritic cells negligibly affected the tracer uptake, while a significant increase in ^{18}F-AraG uptake correlated with the activation of $CD8^+$ T lymphocytes. Unlike ^{18}F-FDG, which reflects tumor metabolism, ^{18}F-AraG can directly illustrate the course of the immune response, overcoming a major limitation of ^{18}F-FDG in immuno-PET applications (92). Levi and colleagues have demonstrated the significant value of ^{18}F-AraG in evaluating anti-PD-1 therapy and chemotherapy. However, the variability in individual response kinetics may challenge its clinical translation. Further investigation is required to determine whether this tracer is sufficiently sensitive to detect authentic clinical changes and to optimize its use in the future.

5.4 Interleukin-2 receptor

IL-2 plays an active role in both differentiation and activation of T lymphocytes and induces cytotoxic effects by binding to their receptors on target cells (117, 118). IL-2 receptors can be categorized into monomeric, dimeric, and trimeric IL-2Rs. The high-affinity IL-2R consists of CD25, CD122, and CD132 subunits, all of which exist on activated T cells (119). A PET-based tracer, N-(4-18F-fluorobenzoyl) interleukin-2 (^{18}F-FB-IL2), can be used to visualize activated T cells in animal models (90, 120). A clinical study (NCT02922283) involving 19 melanoma patients was conducted to investigate the biodistribution and kinetics in human subjects and assess its translational feasibility (91). Furthermore, 11 patients underwent ^{18}F-FB-IL2 scans both at baseline and after receiving immunotherapy. Results indicated that the tracer could identify tumor lesions; however, uptake was generally low, and significant correlation was not observed between tracer uptake and therapy-induced changes (91). Therefore, related tracers have to be optimized further to determine whether IL-2R is a suitable target that can accurately and authentically reflect changes induced by ICIs. It is noteworthy that IL-2 has been approved by the Food and Drug Administration of USA for cancer immunotherapy; however, the subsequent results did not meet the initial expectations (121). IL-2R-based PET tracers may be used to develop innovative IL-2 therapeutic strategies.

6 Conclusion and future prospects

While immunotherapy is recognized as a groundbreaking advancement in oncology, questions regarding the varying immunogenic statuses of tumors, especially in terms of $CD8^+$ T lymphocyte infiltration and their diverse responses to immunotherapy, remain. $CD8^+$ T cells play a pivotal role in immune-mediated tumor killing, and hence, CD8-targeted PET radiotracers have become research hotspots. They can be used to track alterations in $CD8^+$ T lymphocytes, contributing to the generation of a comprehensive immune profile. A series of preclinical and clinical studies have investigated the potential applications of such radiotracers, demonstrating their capacity to stratify patients, predict outcomes, and evaluate the efficacy of immunotherapies. Notably, baseline CD8 imaging has shown a correlation with better overall responses, indicating its potential as an early predictive biomarker. Furthermore, the emergence of PET tracers that depict the functional status of $CD8^+$ T cells, distinguishing activated effector cells, offers the possibility of guiding individualized immunotherapy in a precise manner.

It is noteworthy that the patient numbers and tumor types in most clinical trials are relatively limited. For a more comprehensive investigation on the feasibility of clinical translation and standardized applications, future studies using larger cohorts, multidisciplinary integration, and long-term longitudinal design are required. The current tracers that visualize activated $CD8^+$ T cells are limited, and additional biomarkers reflecting the function of $CD8^+$ T cells remain underexplored. Some emerging PET imaging parameters require further validation in preclinical studies and multi-center collaborations. A large number of the existing PET tracers based on antibodies have yielded positive results in preclinical studies; however, their radiation burden and long serum half-lives will hinder their subsequent clinical application. Low molecular weight/

peptide-based PET tracers coupled with short half-life radioisotopes such as ^{68}Ga and ^{18}F, which possess the advantages of low radiation burden and shorter image acquisition time, are required for clinical translation. In clinical strategies for tackling malignancies, the trend is shifting toward the use of combination therapy. The dynamic evaluation of such therapies using PET tracers still warrants further investigations.

In conclusion, *in vivo*, systematic, quantifiable, and visual molecular imaging technology may significantly aid clinicians in devising optimal regimens for immunotherapy in precision oncology.

Author contributions

JZ: Visualization, Writing – original draft, Writing – review & editing. BD: Funding acquisition, Writing – original draft, Writing – review & editing. YW: Writing – original draft, Writing – review & editing. YC: Investigation, Writing – review & editing. SW: Investigation, Writing – review & editing. YZ: Investigation, Writing – review & editing. YL: Funding acquisition, Supervision, Writing – review & editing. XL: Conceptualization, Investigation, Supervision, Writing – review & editing.

Funding

The author(s) declare financial support was received for the research, authorship, and/or publication of this article. This work was supported by National Natural Science Foundation of China (grant no. 81971652, 82171987, 82272043).

Conflict of interest

The authors declare that the research was conducted in the absence of any commercial or financial relationships that could be construed as a potential conflict of interest.

Publisher's note

References

1. Demaria O, Cornen S, Daëron M, Morel Y, Medzhitov R, Vivier E. Harnessing innate immunity in cancer therapy. *Nature*. (2019) 574:45–56. doi: 10.1038/s41586-019-1593-5

2. Peterson C, Denlinger N, Yang Y. Recent advances and challenges in cancer immunotherapy. *Cancers*. (2022) 14:3972. doi: 10.3390/cancers14163972

3. Yang Y. Cancer immunotherapy: harnessing the immune system to battle cancer. *J Clin Invest*. (2015) 125:3335–7. doi: 10.1172/JCI83871

4. Ribas A, Wolchok JD. Cancer immunotherapy using checkpoint blockade. *Science*. (2018) 359:1350–5. doi: 10.1126/science.aar4060

5. Singh AK, McGuirk JP. CAR T cells: continuation in a revolution of immunotherapy. *Lancet Oncol*. (2020) 21:e168–78. doi: 10.1016/S1470-2045(19)30823-X

6. Sharma P, Hu-Lieskovan S, Wargo JA, Ribas A. Primary, adaptive, and acquired resistance to cancer immunotherapy. *Cell*. (2017) 168:707–23. doi: 10.1016/j.cell.2017.01.017

7. Gibney GT, Weiner LM, Atkins MB. Predictive biomarkers for checkpoint inhibitor-based immunotherapy. *Lancet Oncol*. (2016) 17:e542–51. doi: 10.1016/S1470-2045(16)30406-5

8. Pan Y, Fu Y, Zeng Y, Liu X, Peng Y, Hu C, et al. The key to immunotherapy: how to choose better therapeutic biomarkers for patients with non-small cell lung cancer. *biomark Res*. (2022) 10:9. doi: 10.1186/s40364-022-00355-7

9. Zeng DQ, Yu YF, Ou QY, Li XY, Zhong RZ, Xie CM, et al. Prognostic and predictive value of tumor-infiltrating lymphocytes for clinical therapeutic research in patients with non-small cell lung cancer. *Oncotarget*. (2016) 7:13765–81. doi: 10.18632/oncotarget.v7i12

10. Hiam-Galvez KJ, Allen BM, Spitzer MH. Systemic immunity in cancer. *Nat Rev Cancer*. (2021) 21:345–59. doi: 10.1038/s41568-021-00347-z

11. Giles JR, Globig AM, Kaech SM, Wherry EJ. CD8+ T cells in the cancer-immunity cycle. *Immunity*. (2023) 56:2231–53. doi: 10.1016/j.immuni.2023.09.005

12. Duffy MJ, Crown J. Biomarkers for predicting response to immunotherapy with immune checkpoint inhibitors in cancer patients. *Clin Chem*. (2019) 65:1228–38. doi: 10.1373/clinchem.2019.303644

13. Dejardin D, Kraxner A, Blank A, Rieder N, Teichgräber V, Städler N, et al. A composite decision rule of CD8+ T-cell density in tumor biopsies predicts efficacy in early-stage, immunotherapy trials. *Clin Cancer Res*. (2024) 30:877–82. doi: 10.1158/1078-0432

14. Fridman WH, Zitvogel L, Sautès-Fridman C, Kroemer G. The immune contexture in cancer prognosis and treatment. *Nat Rev Clin Oncol*. (2017) 14:717–34. doi: 10.1038/nrclinonc.2017.101

15. Haywood S, Garioch J, Ramaiya A, Moncrieff M. Quantitative and spatial analysis of CD8+/PD-1 tumor-infiltrating lymphocytes as a predictive biomarker for clinical response of melanoma in-transit metastases to topical immunotherapy. *Ann Surg Oncol*. (2021) 28:1029–38. doi: 10.1245/s10434-020-08713-1

16. Yu Y, Zeng D, Ou Q, Liu S, Li A, Chen Y, et al. Association of survival and immune-related biomarkers with immunotherapy in patients with non-small cell lung cancer: A meta-analysis and individual patient-level analysis. *JAMA Netw Open*. (2019) 2:e196879. doi: 10.1001/jamanetworkopen.2019.6879

17. Semiglazov V, Tseluiko A, Kudaybergenova A, Artemyeva A, Krivorotko P, Donskih R. Immunology and immunotherapy in breast cancer. *Cancer Biol Med*. (2022) 19:609–18. doi: 10.20892/j.issn.2095-3941.2021.0597

18. Otter SJ, Chatterjee J, Stewart AJ, Michael A. The role of biomarkers for the prediction of response to checkpoint immunotherapy and the rationale for the use of checkpoint immunotherapy in cervical cancer. *Clin Oncol (R Coll Radiol)*. (2019) 31:834–43. doi: 10.1016/j.clon.2019.07.003

19. Kurtulus S, Madi A, Escobar G, Klapholz M, Nyman J, Christian E, et al. Checkpoint blockade immunotherapy induces dynamic changes in PD-1-CD8+ Tumor-infiltrating T cells. *Immunity*. (2019) 50:181–194.e6. doi: 10.1016/j.immuni.2018.11.014

20. Wang C, Zeng Q, Gül ZM, Wang S, Pick R, Cheng P, et al. Circadian tumor infiltration and function of CD8+ T cells dictate immunotherapy efficacy. *Cell*. (2024) 187:2690–2702.e17. doi: 10.1016/j.cell.2024.04.015

21. Yamashita K, Iwatsuki M, Harada K, Koga Y, Kiyozumi Y, Eto K, et al. Can PD-L1 expression evaluated by biopsy sample accurately reflect its expression in the whole tumour in gastric cancer? *Br J Cancer*. (2019) 121:278–80. doi: 10.1038/s41416-019-0515-5

22. Liu Z, Li Z. Molecular imaging in tracking tumor-specific cytotoxic T lymphocytes (CTLs). *Theranostics*. (2014) 4:990–1001. doi: 10.7150/thno.9268

23. Wei W, Jiang D, Ehlerding EB, Luo Q, Cai W. Noninvasive PET imaging of T cells. *Trends Cancer*. (2018) 4:359–73. doi: 10.1016/j.trecan.2018.03.009

24. Phelps ME. PET: the merging of biology and imaging into molecular imaging. *J Nucl Med*. (2000) 41:661–81.

25. Juweid ME, Cheson BD. Positron-emission tomography and assessment of cancer therapy. *N Engl J Med*. (2006) 354:496–507. doi: 10.1056/NEJMra050276

26. Pantel AR, Mankoff DA. Molecular imaging to guide systemic cancer therapy: Illustrative examples of PET imaging cancer biomarkers. *Cancer Lett*. (2017) 387:25–31. doi: 10.1016/j.canlet.2016.05.008

27. Wei W, Rosenkrans ZT, Liu J, Huang G, Luo QY, Cai W. ImmunoPET: concept, design, and applications. *Chem Rev*. (2020) 120:3787–851. doi: 10.1021/acs.chemrev.9b00738

28. Kumar BV, Connors TJ, Farber DL. Human T cell development, localization, and function throughout life. *Immunity*. (2018) 48:202–13. doi: 10.1016/j.immuni.2018.01.007

29. Gascoigne NR, Rybakin V, Acuto O, Brzostek J. TCR signal strength and T cell development. *Annu Rev Cell Dev Biol*. (2016) 32:327–48. doi: 10.1146/annurev-cellbio-111315-125324

30. Guerder S, Flavell RA. T-cell activation. Two for T. *Curr Biol*. (1995) 5:866–8. doi: 10.1016/S0960-9822(95)00175-8

31. Zumerle S, Molon B, Viola A. Membrane rafts in T cell activation: A spotlight on CD28 costimulation. *Front Immunol*. (2017) 8:1467. doi: 10.3389/fimmu.2017.01467

32. Pennock ND, White JT, Cross EW, Cheney EE, Tamburini BA, Kedl RM. T cell responses: naive to memory and everything in between. *Adv Physiol Educ*. (2013) 37:273–83. doi: 10.1152/advan.00066.2013

33. Raskov H, Orhan A, Christensen JP, Gögenur I. Cytotoxic CD8+ T cells in cancer and cancer immunotherapy. *Br J Cancer*. (2021) 124:359–67. doi: 10.1038/s41416-020-01048-4

34. Farhood B, Najafi M, Mortezaee K. CD8+ cytotoxic T lymphocytes in cancer immunotherapy: A review. *J Cell Physiol*. (2019) 234:8509–21. doi: 10.1002/jcp.27782

35. Voskoboinik I, Whisstock JC, Trapani JA. Perforin and granzymes: function, dysfunction and human pathology. *Nat Rev Immunol*. (2015) 15:388–400. doi: 10.1038/nri3839

36. Fu Q, Fu TM, Cruz AC, Sengupta P, Thomas SK, Wang S, et al. Structural basis and functional role of intramembrane trimerization of the fas/CD95 death receptor. *Mol Cell*. (2016) 61:602–13. doi: 10.1016/j.molcel.2016.01.009

37. Bhat P, Leggatt G, Waterhouse N, Frazer IH. Interferon-γ derived from cytotoxic lymphocytes directly enhances their motility and cytotoxicity. *Cell Death Dis*. (2017) 8:e2836. doi: 10.1038/cddis.2017.67

38. van Horssen R, Ten Hagen TL, Eggermont AM. TNF-alpha in cancer treatment: molecular insights, antitumor effects, and clinical utility. *Oncologist*. (2006) 11:397–408. doi: 10.1634/theoncologist.11-4-397

39. Martínez-Lostao L, Anel A, Pardo J. How do cytotoxic lymphocytes kill cancer cells? *Clin Cancer Res*. (2015) 21:5047–56. doi: 10.1158/1078-0432.CCR-15-0685

40. Leone RD, Powell JD. Metabolism of immune cells in cancer. *Nat Rev Cancer*. (2020) 20:516–31. doi: 10.1038/s41568-020-0273-y

41. Philip M, Schietinger A. CD8+ T cell differentiation and dysfunction in cancer. *Nat Rev Immunol*. (2022) 22:209–23. doi: 10.1038/s41577-021-00574-3

42. Wang Q, Qin Y, Li B. CD8+ T cell exhaustion and cancer immunotherapy. *Cancer Lett*. (2023) 559:216043. doi: 10.1016/j.canlet.2022.216043

43. van der Leun AM, Thommen DS, Schumacher TN. CD8+ T cell states in human cancer: insights from single-cell analysis. *Nat Rev Cancer*. (2020) 20:218–32. doi: 10.1038/s41568-019-0235-4

44. Hashimoto M, Kamphorst AO, Im SJ, Kissick HT, Pillai RN, Ramalingam SS, et al. CD8 T cell exhaustion in chronic infection and cancer: opportunities for interventions. *Annu Rev Med*. (2018) 69:301–18. doi: 10.1146/annurev-med-012017-043208

45. Schreiber RD, Old LJ, Smyth MJ. Cancer immunoediting: integrating immunity's roles in cancer suppression and promotion. *Science*. (2011) 331:1565–70. doi: 10.1126/science.1203486

46. Zhang Y, Zhang Z. The history and advances in cancer immunotherapy: understanding the characteristics of tumor-infiltrating immune cells and their therapeutic implications. *Cell Mol Immunol*. (2020) 17:807–21. doi: 10.1038/s41423-020-0488-6

47. Pardoll DM. The blockade of immune checkpoints in cancer immunotherapy. *Nat Rev Cancer*. (2012) 12:252–64. doi: 10.1038/nrc3239

48. Sadreddini S, Baradaran B, Aghebati-Maleki A, Sadreddini S, Shanehbandi D, Fotouhi A, et al. Immune checkpoint blockade opens a new way to cancer immunotherapy. *J Cell Physiol*. (2019) 234:8541–9. doi: 10.1002/jcp.27816

49. Dermani FK, Samadi P, Rahmani G, Kohlan AK, Najafi R. PD-1/PD-L1 immune checkpoint: Potential target for cancer therapy. *J Cell Physiol*. (2019) 234:1313–25. doi: 10.1002/jcp.27172

50. Rowshanravan B, Halliday N, Sansom DM. CTLA-4: a moving target in immunotherapy. *Blood*. (2018) 131:58–67. doi: 10.1182/blood-2017-06-741033

51. de Castro GJr, Kudaba I, Wu YL, Lopes G, Kowalski DM, Turna HZ, et al. Five-year outcomes with pembrolizumab versus chemotherapy as first-line therapy in patients with non-small-cell lung cancer and programmed death ligand-1 tumor proportion score ≥ 1% in the KEYNOTE-042 study. *J Clin Oncol*. (2023) 41:1986–91. doi: 10.1200/JCO.21.02885

52. Desai A, Peters S. Immunotherapy-based combinations in metastatic NSCLC. *Cancer Treat Rev*. (2023) 116:102545. doi: 10.1016/j.ctrv.2023.102545

53. Paz-Ares L, Ciuleanu TE, Cobo M, Schenker M, Zurawski B, Menezes J, et al. First-line nivolumab plus ipilimumab combined with two cycles of chemotherapy in patients with non-small-cell lung cancer (CheckMate 9LA): an international, randomised, open-label, phase 3 trial. *Lancet Oncol*. (2021) 22:198–211. doi: 10.1016/S1470-2045(20)30641-0

54. Hong M, Clubb JD, Chen YY. Engineering CAR-T cells for next-generation cancer therapy. *Cancer Cell*. (2020) 38:473–88. doi: 10.1016/j.ccell.2020.07.005

55. Ma S, Li X, Wang X, Cheng L, Li Z, Zhang C, et al. Current progress in CAR-T cell therapy for solid tumors. *Int J Biol Sci*. (2019) 15:2548–60. doi: 10.7150/ijbs.34213

56. Shalhout SZ, Miller DM, Emerick KS, Kaufman HL. Therapy with oncolytic viruses: progress and challenges. *Nat Rev Clin Oncol*. (2023) 20:160–77. doi: 10.1038/s41571-022-00719-w

57. Lin MJ, Svensson-Arvelund J, Lubitz GS, Marabelle A, Melero I, Brown BD, et al. Cancer vaccines: the next immunotherapy frontier. *Nat Cancer*. (2022) 3:911–26. doi: 10.1038/s43018-022-00418-6

58. Chen Y, Yu D, Qian H, Shi Y, Tao Z. CD8+ T cell-based cancer immunotherapy. *J Transl Med*. (2024) 22:394. doi: 10.1186/s12967-024-05134-6

59. Zboralski D, Osterkamp F, Christensen E, Bredenbeck A, Schumann A, Hoehne A, et al. Fibroblast activation protein targeted radiotherapy induces an immunogenic tumor microenvironment and enhances the efficacy of PD-1 immune checkpoint inhibition. *Eur J Nucl Med Mol Imaging*. (2023) 50:2621–35. doi: 10.1007/s00259-023-06211-6

60. Dercle L, Sun S, Seban RD, Mekki A, Sun R, Tselikas L, et al. Emerging and evolving concepts in cancer immunotherapy imaging. *Radiology*. (2023) 306:32–46. doi: 10.1148/radiol.210518

61. van Dongen GAMS, Beaino W, Windhorst AD, Zwezerijnen GJC, Oprea-Lager DE, Hendrikse NH, et al. The role of 89Zr-immuno-PET in navigating and derisking the development of biopharmaceuticals. *J Nucl Med*. (2021) 62:438–45. doi: 10.2967/jnumed.119.239558

62. De Feo MS, Pontico M, Frantellizzi V, Corica F, De Cristofaro F, De Vincentis G. 89Zr-PET imaging in humans: a systematic review. *Clin Transl Imaging*. (2022) 10:23–36. doi: 10.1007/s40336-021-00462-9

63. da Silva DA, De Luca A, Squitti R, Rongioletti M, Rossi L, MaChado CML, et al. Copper in tumors and the use of copper-based compounds in cancer treatment. *J Inorg Biochem*. (2022) 226:111634. doi: 10.1016/j.jinorgbio.2021.111634

64. Sanchez-Crespo A. Comparison of Gallium-68 and Fluorine-18 imaging characteristics in positron emission tomography. *Appl Radiat Isot*. (2013) 76:55–62. doi: 10.1016/j.apradiso.2012.06.034

65. Chomet M, van Dongen GAMS, Vugts DJ. State of the art in radiolabeling of antibodies with common and uncommon radiometals for preclinical and clinical immuno-PET. *Bioconjug Chem*. (2021) 32:1315–30. doi: 10.1021/acs.bioconjchem.1c00136

66. Rashidian M, Ploegh H. Nanobodies as non-invasive imaging tools. *Immunooncol Technol*. (2020) 7:2–14. doi: 10.1016/j.iotech.2020.07.001

67. Abousaway O, Rakhshandehroo T, Van den Abbeele AD, Kircher MF, Rashidian M. Noninvasive imaging of cancer immunotherapy. *Nanotheranostics*. (2021) 5:90–112. doi: 10.7150/ntno.50860

68. Tavaré R, McCracken MN, Zettlitz KA, Knowles SM, Salazar FB, Olafsen T, et al. Engineered antibody fragments for immuno-PET imaging of endogenous CD8+ T cells. *vivo*. *Proc Natl Acad Sci U.S.A*. (2014) 111:1108–13. doi: 10.1073/pnas.1316922111

69. Tavaré R, McCracken MN, Zettlitz KA, Salazar FB, Olafsen T, Witte ON, et al. Immuno-PET of murine T cell reconstitution postadoptive stem cell transplantation using anti-CD4 and anti-CD8 cys-diabodies. *J Nucl Med*. (2015) 56:1258–64. doi: 10.2967/jnumed.114.153338

70. Tavaré R, Escuin-Ordinas H, Mok S, McCracken MN, Zettlitz KA, Salazar FB, et al. An effective immuno-PET imaging method to monitor CD8-dependent responses to immunotherapy. *Cancer Res*. (2016) 76:73–82. doi: 10.1158/0008-5472.CAN-15-1707

71. Seo JW, Tavaré R, Mahakian LM, Silvestrini MT, Tam S, Ingham ES, et al. CD8+ T-cell density imaging with 64Cu-labeled cys-diabody informs immunotherapy protocols. *Clin Cancer Res*. (2018) 24:4976–87. doi: 10.1158/1078-0432.CCR-18-0261

72. Kristensen LK, Fröhlich C, Christensen C, Melander MC, Poulsen TT, Galler GR, et al. CD4+ and CD8a+ PET imaging predicts response to novel PD-1 checkpoint inhibitor: studies of Sym021 in syngeneic mouse cancer models. *Theranostics*. (2019) 9:8221–38. doi: 10.7150/thno.37513

73. Rashidian M, LaFleur MW, Verschoor VL, Dongre A, Zhang Y, Nguyen TH, et al. Immuno-PET identifies the myeloid compartment as a key contributor to the outcome of the antitumor response under PD-1 blockade. *Proc Natl Acad Sci U.S.A*. (2019) 116:16971–80. doi: 10.1073/pnas.1905005116

74. Kristensen LK, Christensen C, Alfsen MZ, Cold S, Nielsen CH, Kjaer A. Monitoring CD8a+ T cell responses to radiotherapy and CTLA-4 blockade using [64Cu]NOTA-CD8a PET imaging. *Mol Imaging Biol*. (2020) 22:1021–30. doi: 10.1007/s11307-020-01481-0

75. Gill H, Seipert R, Carroll VM, Gouasmat A, Yin J, Ogasawara A, et al. The production, quality control, and characterization of ZED8, a CD8-specific 89Zr-labeled immuno-PET clinical imaging agent. *AAPS J*. (2020) 22:22. doi: 10.1208/s12248-019-0392-0

76. Kist de Ruijter L, van de Donk PP, Hooiveld-Noeken JS, Giesen D, Elias SG, Lub-de Hooge MN, et al. Whole-body CD8+ T cell visualization before and during cancer immunotherapy: a phase 1/2 trial. *Nat Med*. (2022) 28:2601–10. doi: 10.1038/s41591-022-02084-8

77. Pandit-Taskar N, Postow MA, Hellmann MD, Harding JJ, Barker CA, O'Donoghue JA, et al. First-in-humans imaging with 89Zr-df-IAB22M2C anti-CD8 minibody in patients with solid Malignancies: preliminary pharmacokinetics,

biodistribution, and lesion targeting. *J Nucl Med*. (2020) 61:512–9. doi: 10.2967/jnumed.119.229781

78. Schwenck J, Sonanini D, Seyfried D, Ehrlichmann W, Kienzle G, Reischl G, et al. *In vivo* imaging of CD8+ T cells in metastatic cancer patients: first clinical experience with simultaneous [89Zr]Zr-Df-IAB22M2C PET/MRI. *Theranostics*. (2023) 13:2408–23. doi: 10.7150/thno.79976

79. Nagle VL, Henry KE, Hertz CAJ, Graham MS, Campos C, Parada LF, et al. Imaging tumor-infiltrating lymphocytes in brain tumors with [64Cu]Cu-NOTA-anti-CD8 PET. *Clin Cancer Res*. (2021) 27:1958–66. doi: 10.1158/1078-0432.CCR-20-3243

80. Zhao H, Wang C, Yang Y, Sun Y, Wei W, Wang C, et al. ImmunoPET imaging of human CD8+ T cells with novel 68Ga-labeled nanobody companion diagnostic agents. *J Nanobiotechnology*. (2021) 19:42. doi: 10.1186/s12951-021-00785-9

81. Wang Y, Wang C, Huang M, Qin S, Zhao J, Sang S, et al. Pilot study of a novel nanobody 68 Ga-NODAGA-SNA006 for instant PET imaging of CD8+ T cells. *Eur J Nucl Med Mol Imaging*. (2022) 49:4394–405. doi: 10.1007/s00259-022-05903-9

82. Sriraman SK, Davies CW, Gill H, Kiefer JR, Yin J, Ogasawara A, et al. Development of an 18F-labeled anti-human CD8 VHH for same-day immunoPET imaging. *Eur J Nucl Med Mol Imaging*. (2023) 50:679–91. doi: 10.1007/s00259-022-05998-0

83. Tavaré R, Danton M, Giurleo JT, Makonnen S, Hickey C, Arnold TC, et al. Immuno-PET monitoring of lymphocytes using the CD8-specific antibody REGN5054. *Cancer Immunol Res*. (2022) 10:1190–209. doi: 10.1158/2326-6066.CIR-21-0405

84. Alsaid H, Cheng SH, Bi M, Xie F, Rambo M, Skedzielewski T, et al. Immuno-PET monitoring of CD8+ T cell infiltration post ICOS agonist antibody treatment alone and in combination with PD-1 blocking antibody using a 89Zr anti-CD8+ Mouse minibody in EMT6 syngeneic tumor mouse. *Mol Imaging Biol*. (2023) 25:528–40. doi: 10.1007/s11307-022-01781-7

85. Larimer BM, Wehrenberg-Klee E, Dubois F, Mehta A, Kalomeris T, Flaherty K, et al. Granzyme B PET imaging as a predictive biomarker of immunotherapy response. *Cancer Res*. (2017) 77:2318–27. doi: 10.1158/0008-5472.CAN-16-3346

86. Hartimath SV, Ramasamy B, Xuan TY, Rong TJ, Khanapur S, Cheng P, et al. Granzyme B PET imaging in response to *in situ* vaccine therapy combined with αPD1 in a murine colon cancer model. *Pharmaceutics*. (2022) 14:150. doi: 10.3390/pharmaceutics14010150

87. Zhou H, Wang Y, Xu H, Shen X, Zhang T, Zhou X, et al. Noninvasive interrogation of CD8+ T cell effector function for monitoring early tumor responses to immunotherapy. *J Clin Invest*. (2022) 132:e161065. doi: 10.1172/JCI161065

88. Gibson HM, McKnight BN, Malysa A, Dyson G, Wiesend WN, McCarthy CE, et al. IFNγ PET imaging as a predictive tool for monitoring response to tumor immunotherapy. *Cancer Res*. (2018) 78:5706–17. doi: 10.1158/0008-5472.CAN-18-0253

89. Rezazadeh F, Ramos N, Saliganan AD, Barr S, Peraino N, Schomburg F, et al. Evaluation and selection of a lead diabody for interferon-γ PET imaging. *Nucl Med Biol*. (2022) 114-115:162–7. doi: 10.1016/j.nucmedbio.2022.06.001

90. Di Gialleonardo V, Signore A, Glaudemans AW, Dierckx RA, De Vries EF. N-(4-18F-fluorobenzoyl)interleukin-2 for PET of human-activated T lymphocytes. *J Nucl Med*. (2012) 53:679–86. doi: 10.2967/jnumed.111.091306

91. van de Donk PP, Wind TT, Hooiveld-Noeken JS, van der Veen EL, Glaudemans AWJM, Diepstra A, et al. Interleukin-2 PET imaging in patients with metastatic melanoma before and during immune checkpoint inhibitor therapy. *Eur J Nucl Med Mol Imaging*. (2021) 48:4369–76. doi: 10.1007/s00259-021-05407-y

92. Levi J, Goth S, Huynh L, Lam T, Huynh TL, Schulte B, et al. 18F-araG PET for CD8 profiling of tumors and assessment of immunomodulation by chemotherapy. *J Nucl Med*. (2021) 62:802–7. doi: 10.2967/jnumed.120.249078

93. Gajewski TF, Schreiber H, Fu YX. Innate and adaptive immune cells in the tumor microenvironment. *Nat Immunol*. (2013) 14:1014–22. doi: 10.1038/ni.2703

94. Lei X, Lei Y, Li JK, Du WX, Li RG, Yang J, et al. Immune cells within the tumor microenvironment: Biological functions and roles in cancer immunotherapy. *Cancer Lett*. (2020) 470:126–33. doi: 10.1016/j.canlet.2019.11.009

95. Griessinger CM, Olafsen T, Mascioni A, Jiang ZK, Zamilpa C, Jia F, et al. The PET-tracer 89Zr-df-IAB22M2C enables monitoring of intratumoral CD8 T-cell infiltrates in tumor-bearing humanized mice after T-cell bispecific antibody treatment. *Cancer Res*. (2020) 80:2903–13. doi: 10.1158/0008-5472.CAN-19-3269

96. Maresca KP, Chen J, Mathur D, Giddabasappa A, Root A, Narula J, et al. Preclinical evaluation of 89Zr-df-IAB22M2C PET as an imaging biomarker for the development of the GUCY2C-CD3 bispecific PF-07062119 as a T cell engaging therapy. *Mol Imaging Biol*. (2021) 23:941–51. doi: 10.1007/s11307-021-01621-0

97. Farwell MD, Gamache RF, Babazada H, Hellmann MD, Harding JJ, Korn R, et al. CD8-targeted PET imaging of tumor-infiltrating T cells in patients with cancer: A phase I first-in-humans study of 89Zr-df-IAB22M2C, a radiolabeled anti-CD8 minibody. *J Nucl Med*. (2022) 63:720–6. doi: 10.2967/jnumed.121.262485

98. Yang E, Liu Q, Huang G, Liu J, Wei W. Engineering nanobodies for next-generation molecular imaging. *Drug Discovery Today*. (2022) 27:1622–38. doi: 10.1016/j.drudis.2022.03.013

99. Ramon-Patino JL, Schmid S, Lau S, Seymour L, Gaudreau PO, Li JJN, et al. iRECIST and atypical patterns of response to immuno-oncology drugs. *J Immunother Cancer*. (2022) 10:e004849. doi: 10.1136/jitc-2022-004849

100. Persigehl T, Lennartz S, Schwartz LH. iRECIST: how to do it. *Cancer Imaging*. (2020) 20:2. doi: 10.1186/s40644-019-0281-x

101. Chen MY, Zeng YC. Pseudoprogression in lung cancer patients treated with immunotherapy. *Crit Rev Oncol Hematol*. (2022) 169:103531. doi: 10.1016/j.critrevonc.2021.103531

102. Chai LF, Prince E, Pillarisetty VG, Katz SC. Challenges in assessing solid tumor responses to immunotherapy. *Cancer Gene Ther*. (2020) 27:528–38. doi: 10.1038/s41417-019-0155-1

103. Ogasawara A, Kiefer JR, Gill H, Chiang E, Sriraman S, Ferl GZ, et al. Preclinical development of ZED8, an 89Zr immuno-PET reagent for monitoring tumor CD8 status in patients undergoing cancer immunotherapy. *Eur J Nucl Med Mol Imaging*. (2023) 50:287–301. doi: 10.1007/s00259-022-05968-6

104. St Paul M, Ohashi PS. The roles of CD8+ T cell subsets in antitumor immunity. *Trends Cell Biol*. (2020) 30:695–704. doi: 10.1016/j.tcb.2020.06.003

105. Obst R. The timing of T cell priming and cycling. *Front Immunol*. (2015) 6:563. doi: 10.3389/fimmu.2015.00563

106. Trapani JA, Smyth MJ. Functional significance of the perforin/granzyme cell death pathway. *Nat Rev Immunol*. (2002) 2:735–47. doi: 10.1038/nri911

107. Rousalova I, Krepela E. Granzyme B-induced apoptosis in cancer cells and its regulation (review). *Int J Oncol*. (2010) 37:1361–78. doi: 10.3892/ijo_00000788

108. Larimer BM, Bloch E, Nesti S, Austin EE, Wehrenberg-Klee E, Boland G, et al. The effectiveness of checkpoint inhibitor combinations and administration timing can be measured by granzyme B PET imaging. *Clin Cancer Res*. (2019) 25:1196–205. doi: 10.1158/1078-0432.CCR-18-2407

109. Thiery J, Keefe D, Boulant S, Boucrot E, Walch M, Martinvalet D, et al. Perforin pores in the endosomal membrane trigger the release of endocytosed granzyme B into the cytosol of target cells. *Nat Immunol*. (2011) 12:770–7. doi: 10.1038/ni.2050

110. Dunn GP, Koebel CM, Schreiber RD. Interferons, immunity and cancer immunoediting. *Nat Rev Immunol*. (2006) 6:836–48. doi: 10.1038/nri1961

111. Ni L, Lu J. Interferon gamma in cancer immunotherapy. *Cancer Med*. (2018) 7:4509–16. doi: 10.1002/cam4.1700

112. Gocher AM, Workman CJ, Vignali DAA. Interferon-γ: teammate or opponent in the tumour microenvironment? *Nat Rev Immunol*. (2022) 22:158–72. doi: 10.1038/s41577-021-00566-3

113. Buck MD, O'Sullivan D, Klein Geltink RI, Curtis JD, Chang CH, Sanin DE, et al. Mitochondrial dynamics controls T cell fate through metabolic programming. *Cell*. (2016) 166:63–76. doi: 10.1016/j.cell.2016.05.035

114. Almeida L, Lochner M, Berod L, Sparwasser T. Metabolic pathways in T cell activation and lineage differentiation. *Semin Immunol*. (2016) 28:514–24. doi: 10.1016/j.smim.2016.10.009

115. Levi J, Lam T, Goth SR, Yaghoubi S, Bates J, Ren G, et al. Imaging of activated T cells as an early predictor of immune response to anti-PD-1 therapy. *Cancer Res*. (2019) 79:3455–65. doi: 10.1158/0008-5472.CAN-19-0267

116. Namavari M, Chang YF, Kusler B, Yaghoubi S, Mitchell BS, Gambhir SS. Synthesis of 2'-deoxy-2'-[18F]fluoro-9-β-D-arabinofuranosylguanine: a novel agent for imaging T-cell activation with PET. *Mol Imaging Biol*. (2011) 13:812–8. doi: 10.1007/s11307-010-0414-x

117. Sun Z, Ren Z, Yang K, Liu Z, Cao S, Deng S, et al. A next-generation tumor-targeting IL-2 preferentially promotes tumor-infiltrating CD8+ T-cell response and effective tumor control. *Nat Commun*. (2019) 10:3874. doi: 10.1038/s41467-019-11782-w

118. Damoiseaux J. The IL-2 - IL-2 receptor pathway in health and disease: The role of the soluble IL-2 receptor. *Clin Immunol*. (2020) 218:108515. doi: 10.1016/j.clim.2020.108515

119. Boyman O, Sprent J. The role of interleukin-2 during homeostasis and activation of the immune system. *Nat Rev Immunol*. (2012) 12:180–90. doi: 10.1038/nri3156

120. Di Gialleonardo V, Signore A, Willemsen AT, Sijbesma JW, Dierckx RA, de Vries EF. Pharmacokinetic modelling of N-(4-[(18)F]fluorobenzoyl)interleukin-2 binding to activated lymphocytes in an xenograft model of inflammation. *Eur J Nucl Med Mol Imaging*. (2012) 39:1551–60. doi: 10.1007/s00259-012-2176-y

121. Jiang T, Zhou C, Ren S. Role of IL-2 in cancer immunotherapy. *Oncoimmunology*. (2016) 5:e1163462. doi: 10.1080/2162402X.2016.1163462

frontiers | Frontiers in Immunology

TYPE Mini Review
PUBLISHED 14 August 2024
DOI 10.3389/fimmu.2024.1431495

OPEN ACCESS

EDITED BY
Gaia Codolo,
University of Padua, Italy

REVIEWED BY
Maria Rosaria Galdiero,
University of Naples Federico II, Italy

*CORRESPONDENCE
Caiping An
1156507154@qq.com
Shisan Bao
profbao@hotmail.com

†These authors have contributed equally to this work

RECEIVED 12 May 2024
ACCEPTED 31 July 2024
PUBLISHED 14 August 2024

CITATION
Wang Q, Zhang G, An C, Hambly BD and Bao S (2024) The role of IL-37 in gastrointestinal diseases.
Front. Immunol. 15:1431495.
doi: 10.3389/fimmu.2024.1431495

The role of IL-37 in gastrointestinal diseases

Qiang Wang[1†], Guangrun Zhang[2†], Caiping An[3*], Brett D. Hambly[4] and Shisan Bao[5,6*]

[1]Department of Anatomy, School of Basic Medicine, Gansu University of Chinese Medicine, Lanzhou, China, [2]School of Traditional Chinese and Western Medicine, Gansu University of Chinese Medicine, Lanzhou, China, [3]Department of Nephrology, Gansu Provincial Hospital, Lanzhou, China, [4]Centre for Healthy Futures, Torrens University Australia, Sydney, NSW, Australia, [5]Foreign Affairs Office, The Third Affiliated Hospital of Gansu University of Chinese Medicine, Baiyin, China, [6]Foreign Affairs Office, The First People's Hospital of Baiyin, Baiyin, China

Gastrointestinal mucosal surface is frequently under challenge due to it's the large surface area and most common entry of microbes. IL-37, an anti-inflammatory cytokine, regulates local and systemic host immunity. *H. pylori* infection leads to the inhibition of IL-37 in the gastric mucosa, contributing to heightened mucosal inflammation and destruction, thereby facilitating increased proliferation of *H. pylori*. Food allergy, due to immune dysregulation, also contribute to GI injury. On the other hand, elevated levels of IL-37 observed in gastric cancer patients align with reduced host immunity at the cellular and humoral levels, indicating that IL-37 may contribute to the development of gastric cancer *via* suppressing pro-inflammatory responses. While IL-37 provides protection in an IBD animal model, the detection of highly produced IL-37 in IBD patients suggests a stage-dependent role, being protective in acute inflammation but potentially exacerbates the development of IBD in chronic conditions. Moreover, elevated colonic IL-37 in CRC correlates with overall survival time and disease time, indicating a protective role for IL-37 in CRC. The differential regulation and expression of IL-37 between upper- and lower-GI organs may be attributed to variations in the microbial flora. This information suggests that IL-37 could be a potential therapeutic agent, depending on the stage and location.

KEYWORDS

IL-37, gastrointestinal, inflammation, cancer, colorectal cancer

Introduction

Intestinal mucosal immunity and GI defense

The gastrointestinal (GI) system, encompassing the largest mucosal surface area in the body (1), is highly susceptible to both specific and non-specific microbial invasion (2). Gut-associated lymphoid tissues (GALT) within the GI system protects against such threats, and consists of lamina propria lymphocytes, intraepithelial lymphocytes (3), in addition to

mesenteric lymph nodes. Any compromise or hyperactivity in GALT immunity can lead to severe consequences. For instance, a deficiency in IFNγ compromises host intestinal immunity at the cellular and humoral levels by impairing macrophage function in response to *Salmonella* challenge, resulting in salmonellosis and septicemia (4). On the other hand, exogenous IFNγ has been shown to protect the host against lethal salmonellosis *in vivo* in mice (5). Conversely, TNF, a pro-inflammatory cytokine, plays a crucial protective role in acute inflammatory bowel disease within the GI tract. Studies indicate that a deficiency in TNF could exacerbate colitis in a DSS-induced colitis murine model (6), maybe *via* upregulating IL-1β production, which is supported by their testing, using bone marrow derived dendritic cells from TNF KO mice (7), highlighting the protective function of TNF during acute inflammation. On the other hand, TNF is significantly upregulated, both circulating and within local affected intestinal tissues, indicating its pro-inflammatory role during chronic intestinal inflammation, which is supported by clinical findings, showing that anti-TNF antibody therapy significantly improves the condition of IBD patients at both the macroscopic and microscopic levels (8). Furthermore, if chronic inflammation persists without proper management in the intestine, it may lead to the induction of malignancy (9). This underscores the delicate balance required to maintain optimal GI health, with both excessive and insufficient immune responses posing significant risks. This review focuses on the role of IL-37 in both upper and lower GI infection/inflammation, as well as malignancies, which could provide a useful perspective for both basic scientists and clinicians.

IL-37

IL-37, also known as interleukin-1 family member 7 (IL-1F7), exists in five different splice variants (a-e) (10). The IL-37 protein ranges in size from 17 to 26 kDa, corresponding to a gene size of 3.617 kb (11). It has been identified in various tissues, including lymph nodes, thymus, lung, intestine, uterus, as well as in leucocytes such as NK cells, activated B cells, and monocytes. Additionally, IL-37 has been detected in epithelial cells, suggesting a potential role in regulating intestinal mucosal immunity (12). The involvement of IL-37 in host immunity has demonstrated that IL-37 acts as an anti-inflammatory cytokine by inhibiting pro-inflammatory responses (12), and is able to attenuate both innate (13) and adaptive immunity (14). Additionally, dysregulated expression of IL-37 has been observed in autoimmune diseases such as psoriasis, Graves' disease, and systemic lupus erythematosus (15), highlighting its crucial role in maintaining host homeostasis. Additionally, inflammatory bowel disease (IBD) involves, in part, an effector T cell response against commensal microbiota, which contributes towards disease severity, since ongoing inflammation in IBD leads to the loss of tolerance toward commensals and subsequent worsened disease outcomes. Specifically, the intestinal mucosal immune response is dependent on the differentiation of pro-inflammatory commensal antigen-specific T cells (e.g. against CBir1-bacterium) prior to intestinal damage (16). Thus, the role of IL-37 in regulating gastrointestinal mucosal immunity may also depend on the local immune response to various stimuli, leading to diverse outcomes.

IL-37 in *H. pylori* gastric infection/inflammation

The ground-breaking discovery of the critical role played by *H. pylori* infection in contributing to gastric ulceration, and subsequent gastric cancer was elegantly demonstrated by Nobel laureates Drs Marshall and Warren (17). This revelation revolutionized the management of *H. pylori* infected gastritis patients, leading to fundamental improvements in their outcomes. The Nobel Committee commented on the significance of this discovery, stating, "Thanks to the pioneering discovery by Marshall and Warren, peptic ulcer disease is no longer a chronic, frequently disabling condition but a disease that can be cured by a short regimen of antibiotics and acid secretion inhibitors" (18).

Thus, the first research focus has been on the relationship between *H. pylori* gastric infection and IL-37 expression. A notable decrease in IL-37 expression was identified in the ulcerated gastric mucosa of biopsy samples from patients with *H. pylori* infection, in comparison to those without *H. pylori* infection (19). Furthermore, diminished IL-37 levels were also noted in the mucosa affected by gastritis with *H. pylori* infection, even in the absence of stomach ulceration (19). Surprisingly, no significant disparity in suppressed mucosal IL-37 levels was observed between *H. pylori*-infected patients with and without stomach ulceration.

These data imply that *H. pylori* promotes local inflammation *via* inhibiting the production of IL-37 in gastric mucosa, which in turn enhances the production of pro-inflammatory cytokines and chemokines (13), such as IFN-γ and TNF (20). Although pro-inflammatory responses provide defense, if the inflammation persists too long, particularly among susceptible individuals without proper management, local inflammation may not be sufficiently efficient to eradicate *H. pylori* infection, but rather will contribute to more severe disturbance in the stomach mucosa, resulting in persistent chronic infection. The severely inflamed tissues in the stomach mucosa may not then respond well to either pro and/or anti-inflammatory cytokine/chemokine signaling, which may promote further *H. pylori* infection. Thus, as stated above, these data highlight the role of pro-inflammatory mediators (e.g., IFN-γ (4) and TNF (6)) in providing protection against the severity of pathogenic challenges in the gastrointestinal mucosa, highlighting the pivotal role of pro-inflammatory mediators in preventing overwhelming inflammation.

The source of gastric mucosal IL-37 production remains unclear, but IL-37 is likely produced by immune and non-immune cells, including epithelial cells (21) in response to *H. pylori* challenge in an autocrine and paracrine fashion.

The discovery of a reduction in IL-37 in stomach tissue infected with *H. pylori in vivo* is consistent with findings *in vitro* (20), showing that reduction in mucosal IL-37 in the microenvironment may contribute to elevated levels of pro-inflammatory mediators, including chemokines, *in vivo*, and also in challenged GI epithelial cells *in vitro* (22). This is supported by findings indicating

substantial IL-37-modulated chemokine production *in vitro* by GI epithelial cells, potentially leading to the persistence of chronic inflammation in the stomach. There are consistent findings of the function of IL-37 between *in vivo* and *in vitro* systems, supporting the view that gastric mucosal IL-37 might contribute to chronicity *via* suppressing local inflammation/immunity.

Overall, the suppressed IL-37 levels observed in patients with *H. pylori* infection may lead to a decrease in local anti-inflammatory responses and an increase in maladaptive damaging pro-inflammatory responses. While an enhanced pro-inflammatory response is typically crucial for defense against *H. pylori* infection, susceptible individuals may experience a disturbance in their host immunity. This disturbance could result in severe ulceration and inflammation of the gastric mucosa, potentially further promoting *H. pylori* infection and progressing to precancerous and/or gastric cancer stages. This aligns with the notion that chronic inflammation plays a critical role in the development of gastric cancer in infected individuals (23), and in some cases, a smaller number of patients may even develop extra-gastric mucosa-associated lymphoid tissue (MALT) lymphoma (24).

Food allergy and coeliac disease

Food allergy and coeliac disease still lead to substantial morbidity in humans, despite extensive clinical and basic research over the last few decades (25). Following an extensive literature search, no published data on the role of IL-37 in food allergy or coeliac disease has been found. However, it has been reported that IL-37 is substantially reduced in asthmatic children (26), suggesting the important role of IL-37 in asthma. Additionally, exogenous IL-37 ameliorates allergic inflammation in asthmatic animal models, by suppressing pro-inflammatory cytokines, e.g. IL-1 and IL-33 (27), which is supported by findings in IL-37 transgenic mice. Considering that both intestinal and respiratory mucosal surfaces belong to mucosal-associated lymphoid tissues (MALT) (28), it is reasonable to speculate that IL-37, acting as an anti-inflammatory cytokine, could inhibit food allergy by upregulating $CD35^+$ Treg cells (29), thereby dampening hyperactive MALT responses (30). Consequently, IL-37 could serve as a therapeutic target for managing food allergy, similar to the role described for IL-33 (31), which requires verification in future studies. The precise underlying mechanism of IL-37 in regulating allergic response remains to be clarified. A recent report finds that IL-37 ameliorates local inflammation in atopic dermatitis by regulating gut microbiota through the AMPK-mTOR signaling pathway (32), further supporting the concept that IL-37 may act on both local and systemic responses *via* manipulating intestinal mucosal microbiota, an idea that requires further investigation.

Coeliac disease, an autoimmune disorder primarily affecting the small intestine, results from the ingestion of gluten-containing foods by genetically susceptible individuals with specific HLA alleles (33). Histopathological examination of coeliac disease reveals varying degrees of mucosal inflammation, characterized by cellular and humoral immune responses, including leukocyte infiltration, swelling, and neovascularization (34). Elevated levels of pro-inflammatory cytokines and reports of anti-inflammatory cytokines in coeliac disease patients correlate with clinical severity (35), suggesting a close association between coeliac disease and heightened pro-inflammatory cytokine production. However, attempts to mitigate inflammation in this setting, through anti-inflammatory cytokines, may be insufficiently effective. Recent studies have clarified the gluten-specific host response, demonstrating a strong correlation between gluten intake and clinical symptoms and signs in coeliac patients compared to controls (36). This observation aligns with significantly increased levels of pro-inflammatory cytokines, such as IL-2, IL-6, CCL20, CXCL8, CXCL9, IFN-γ, alongside elevated anti-inflammatory cytokines including IL-10 and IL-22. Because there is no direct evidence of the relationship between IL-37 and coeliac disease, based on the above data, it is also reasonable to speculate that IL-37, acting as an anti-inflammatory cytokine, would be enhanced among coeliac disease patients, particularly acutely following the ingestion of gluten contained food. This speculation is purely based on indirect evidence and consequently requires further verification.

IL-37 in gastric cancer

Persistent chronic stomach ulceration, particularly in the presence of *H. pylori* infection, substantially boosts the incidence of gastric cancer (37). Notably, circulating IL-37 is significantly higher in gastric cancer patients, compared to sex and age matched healthy controls (38), suggesting a possible pro-tumor effect of IL-37, since elevated IL-37 promotes an anti-inflammatory response *via* suppressing both innate (13) and adaptive immunity (14), resulting in compromised host immune surveillance against malignancy (39). These data are supported by the finding that IL-37 inhibits the immune response at both the cellular and humoral levels (40), which likely promotes gastric cancer development *via* inhibiting host gastric mucosal immunity against the development of gastric cancer. These data are further consistent with the finding that there is an inverse correlation between circulating IL-37 expression and 5-year survival (38). The pro-cancer role of IL-37 in gastric cancer is further sustained from multivariate analysis, which provides a more reliable prediction than univariate, showing that while the depth of invasion (T1-2 *vs* T3-4) and stage (I-II *vs* III-IV) were significant under univariate analysis, IL-37 expression (low *vs* high) remained significant under multivariate analysis and was the most reliable predictor for overall survival and progression free survival using multi-variate analysis. Interestingly, only high circulating IL-37 expression is a reliable predictive factor for low progression-free survival. Additionally, an elevated level of circulating IL-37 was correlating with poor differentiation. Surprisingly, there is no evidence in the literature about the specific underlying mechanism concerning the pro-cancer activity of IL-37 in gastric cancer, which warrants further investigation. There is at least a partial explanation that IL-37 inhibits immunosurveillance, although these data are not specific for gastric cancer, they are a more general immunological observation (13, 39–41). The underlying mechanism in gastric cancer has not been specifically examined.

Interestingly, in most other cancers examined to date, elevated levels of IL-37 have correlated with anti-tumor activity and with improved survival (12). IL-37 has been shown to be protective during the development of a number of cancers, including hepatocellular carcinoma (42, 43), colorectal cancer (44), non-small cell lung cancer (45), renal cell carcinoma and oral and cervical squamous cell carcinoma (46). Possible anti-tumor mechanisms of IL-37 include inhibition of both angiogenesis and tumor-promoting inflammation, and promotion of anti-tumor immunity (47). Paradoxically, high circulating levels of IL-37 have been shown to associated with decreased survival in patients with metastatic epithelial ovarian cancer (48).

However, the detailed data within the literature are very variable, as some studies investigated circulating IL-37, while others have measured cancer vs normal tissue levels of IL-37. Data derived from other cancers suggest that the best indicator of IL-37 activity is likely to be the level of the IL-37 in cancer tissue as a function of severity/survival.

Such speculation is aligned with our previous findings, showing that there is an inverse correlation between IL-31, -32, -33 (49) and IL-34 (50) in gastric cancer survival, suggesting a pro-cancer role of these cytokines. Taken together, these data align with the concept that host immunity plays a critical role in immune surveillance against the development of gastric cancer, i.e. both mucosal and systemic immunity may be compromised among gastric cancer patients due to significantly upregulated IL-37, which inhibits potentially protective pro-inflammatory responses (51).

Interestingly, a recent report shows that IL-37 can play a dual role in malignancy, i.e. IL-37 possesses both anti-inflammatory and pro-inflammatory functions (52), depending on which subset units of IL-37 are activated. A protective role of IL-37 during the development of gastric cancer has been demonstrated, where the processed form of IL-37 binds to SMAD-3, relocates to the nucleus, and hinders the transcription of various pro-inflammatory genes. Both the precursor and cleaved versions of IL-37 are actively secreted. They associate with the IL-18Rα chain, shared by IL-18 as a receptor subunit, and recruit Toll/IL-1R (TIR)-8 to facilitate intracellular signaling. IL-37 suppresses the activation of NF-κB and MAPK while activating the Mer-PTEN-DOK pathway. It exerts negative regulation on signaling induced by TLR agonists, proinflammatory cytokines, and IL-1RF ligands. Additionally, IL-37 influences cell metabolism by inhibiting mTOR and GSK-3α/β, and activating AMPK (53).

By contrast to gastric cancer, it has been reported that IL-37 suppresses hepatocellular carcinoma (HCC) growth through inhibiting tumor-associated macrophages (TAM) (54), by promoting TAM polarization from the pro-tumorigenic M2 subtype to the anti-tumorigenic M1 subtype (55). A possible explanation for this discrepancy is that the exposure of the epithelial cells of the liver and stomach to microbiological flora are completely different, although both belong to the GI system. Thus, GI mucosal immunity may play different regulatory roles in maintaining homeostasis in these two different organs. This is in line with a report showing that the anti-inflammatory role of IL-37 contributes to the suppression of chronic inflammation, particularly among patients with non-alcoholic fatty liver disease (NAFLD), and subsequently reduces the risk of malignancy (56).

Surprisingly, no studies have examined local gastric mucosal expression of IL-37 amongst either GC patients or HCC up to date. It is understandable that there are ethical challenges to obtaining gastric mucosa or hepatic tissue from HCC cohorts, but certainly the detection of IL-37 in GC tumor and adjacent normal gastric mucosa warrants further clarification. Importantly, recent research indicates that IL-37 could serve as a novel therapeutic tool for cancer patients (53), and there is growing evidence suggesting its potential role as a prognostic marker across various human cancers (56).

IL-37 in IBD

Inflammatory bowel disease (IBD) serves as an umbrella term encompassing chronic gastrointestinal inflammation, which includes conditions such as ulcerative colitis and Crohn's Disease (57). The etiology of IBD is intricate, involving factors such as environmental influences, genetics, and infections (57). The global incidence of IBD is 6.8 million (58). Notably, IBD is a lifelong condition currently lacking a cure, making it a significant focus of attention (58).

The protective role IL-37 during the development of experimental colitis has been demonstrated in IL-37 transgenic mice following DSS challenge, showing substantially reduced clinical signs and symptoms and histopathology severity from IL-37 overexpression transgenic mice, compared to that of wildtype counterparts (59). Importantly the induced IL-37 mRNA inversely correlates with intestinal barrier breakdown (59). The reduced intestinal mucosal inflammation in the IL-37 transgenic mice was found to be consistent with suppressed pro-inflammatory mediators (TNF and IL-1β, IL-17, IL-6 and CXCL1), but enhanced anti-inflammatory mediator (IL-10) production, and reduced recruitment of leucocytes (neutrophils, dendritic cells, macrophages, eosinophils) in the lamina propria (59). It has been elegantly demonstrated that hemopoietic-derived IL-37 provides an essential protective role from DSS colitis, by adoptive transfer of bone marrow from IL-37 transgenic mice, compared to that of the control bone marrow. Additionally, correlating with improved histopathology, increased Ki67 demonstrated proliferation and regeneration of intestinal mucosa. Furthermore, there was no significant difference in the group receiving anti-IL-10 receptor blocking antibody, possibly because IL-10 did not exhibit a syngeneic role with IL-37. Alternatively, the antibody may not have maintained a therapeutic effect for sufficient time.

Interestingly, conflicting results have emerged from IL-37 transgenic mice following DSS stimulation, revealing that IL-37 transgenic mice exhibited more severe colitis under conventional conditions compared to wildtype mice (60). Conversely, under SPF conditions, IL-37 transgenic mice displayed less severe colitis. This implies that the protective role of IL-37 is contingent upon the gut microbiota, specifically whether dysbiosis is present. This observation suggests a potential link between environmental factors and the pathogenesis of colitis, in conjunction with the

integrity of the intestinal mucosal epithelial barrier. This barrier plays a pivotal role in recruiting neutrophils and NK cells, as well as preventing the invasion of pathogenic bacteria into the colon lamina propria and its draining lymph nodes (16), because intestinal damage is required for the pro-inflammatory differentiation of commensal antigen-specific T cells, for example against the CBir1-bacterium.

Therefore, the roles of intestinal mucosal IL-37, influenced by the state of the intestinal microbiota, may contribute to either the exacerbation or alleviation of IBD occurrences. The regulation of host cellular and/or humoral immunities based on gut pathogenic bacteria, or the maintenance of intestinal microbial and immune homeostasis, emerges as a promising therapeutic strategy for IBD (60).

The findings in the animal model of IBD are aligned with observations in patients with IBD, showing that significantly higher expression of IL-37β is observed in biopsies from inflamed mucosa from active ulcerative colitis patient (61), but there is no obvious expression of IL-37β in the normal intestinal mucosa. The upregulation of IL-37β is consistent with and likely a consequence of a high level of proinflammatory mediators, particularly TNF (61). These findings indicate that heightened levels of intestinal mucosal IL-37β in individuals with ulcerative colitis may play a protective or immunosuppressive role in response to local inflammation. However, persistent chronic inflammation in susceptible cohorts, potentially due to either inadequate activation of downstream pathways and/or ineffective receptors for IL-37 (61), compromise IL-37 action and subsequently disrupt the local immunological balance.

Eventually irreversible permanent damage occurs within the intestinal mucosa, despite the application of different approaches, e.g. NSAIDs, steroids, the anti-TNF monoclonal antibody biologics (infliximab, golimumab, certolizumab and adalimumab, and the fusion protein etanercept). There is no literature concerning the involvement of other subsets of IL-37 in IBD, which warrants further exploration. In particular, the role of specific subsets of IL-37, i.e. IL-37α and γ in patients with IBD remains to be explored in future.

The crucial role of IL-37 in the development of IBD is highlighted by findings in a pediatric patient (62), who developed infantile ulcerative colitis, as a consequence of the over-expression of an inactivated homozygous IL-37 variant that was functionally unable to suppress pro-inflammatory cytokine production. The patient's mother was identified as heterozygous for the inactivating IL-37 variant mutation. This genetic variant may contribute to the destabilization of the protein structure of IL-37, leading to increased solvent accessibility of the substituted polar residue (62). These clinical findings offer insights into the role of IL-37 during IBD development and suggest it could be a potential therapeutic target for managing patients with IBD in the future.

Further mechanistic investigation from this study illustrates that the mutant Ile177Thr IL-37 exhibits lower stability than wild-type IL-37, rendering the mutant IL-37 more susceptible to eradication, determined using cycloheximide chase assays, despite the elevated protein expression of I177T IL-37 (62). This insight is supported by *in vitro* studies, demonstrating that primary monocyte-derived dendritic cells from this IL-37 variant patient produce higher levels of TNF and IFN-γ compared to wild-type cells. Furthermore, these cells are unable to effectively inhibit pro-inflammatory responses *in vitro*, confirming the underlying mechanism of the IL-37 variant in response to pro-inflammatory stimulation.

It is important to highlight the substantial differences between IBD in humans and animal models. For instance, the duration of IBD often exceeds 10 years in humans, whereas in animal models, it typically spans only a few weeks. Consequently, there are significant variations in host immunity between chronic and acute conditions.

IL-37 in colorectal cancer

Colorectal cancer (CRC) remains a formidable global health challenge, despite extensive research efforts spanning both basic and clinical domains over several decades (63). CRC is still ranked as one of the leading prevalent malignancies worldwide, with an annual incidence of 1.93 million new cases (64). Effectively managing CRC continues to prove to be a significant struggle for clinicians and patients alike. Consequently, patients often experience unfavorable outcomes and a low five-year survival rate (65), primarily due to a substantial proportion being diagnosed at advanced stages characterized by deep bowel wall invasion and/or distant metastasis, with palliative care being the only option for these patients. It is well known that host immunity plays a critical role in tumorigenesis, especially in CRC, consistent with reports showing that there is a positive correlation between pro-inflammatory mediators and the severity of CRC (66), especially in the majority of CRC that are associated with MMR/MSI incompetent tumors (67).

The precise role of IL-37, an anti-inflammatory cytokine, during the development of CRC remains to be explored in detail. However, it has been hypothesized that IL-37 may provide protection *via* regulating host MALT immunity during the development of CRC, based partly on the observation that colonic IL-37 is significantly diminished in CRC tissues, evident at both the mRNA and protein levels, when compared to non-cancerous tissues (66).

The proposed protective role of IL-37 in CRC is supported by the observation that an inverse correlation occurs between colonic IL-37 and CRC invasion and differentiation (66). Additionally, a positive correlation occurs between IL-37 expression levels and both disease-free survival and overall survival (66), further supporting our hypothesis. Another study has revealed that IL-37 is localized in the cytoplasm of colonic epithelial cells, and the expression of colonic IL-37 in CRC tissue is consistently reduced compared to that in non-CRC colonic epithelial cells (68). Notably, in this study, colonic tumor IL-37 expression exhibits an inverse correlation with the depth of CRC invasion, consistent with CRC progression (68). Surprisingly, no significant correlation was observed between colonic tumor IL-37 expression and differentiation of CRC by the second research team (68). This discrepancy, i.e. the correlation between IL-37 and differentiation of CRC, reported by these two groups, may be due to different patient demographics, such as different regional, genetic and/or environmental backgrounds, which should be further verified. No differences have been

observed in the role and expression of IL-37 in CRC as a function of the location of the CRC (right *vs* left colon) (69), or patient sex (70) or age (71).

In contrast to the aforementioned findings, increased IL-37 levels appear to promote CRC tumorigenesis in the context of chronic inflammatory bowel disease, revealing a more intricate mechanism (72). To investigate how IL-37 contributes to CRC promotion, researchers utilized IL-37 transgenic mice to induce CRC in the presence of chemically-induced colitis (72). Compared to wild-type (WT) mice with colitis, the IL-37 over-expression transgenic mice showed more severe colitis and a greater number of tumors. Notably, IL-37 transgenic mice exhibited compromised $CD8^+$ T cell function, leading to enhanced evasion of immune surveillance. Moreover, dysfunctional $CD8^+$ T cells mediated IL-37's inhibition of IL-18-induced proliferation and effector function, a process dependent on SIGIRR (single immunoglobulin interleukin-1 receptor-related protein) (72). These findings underscore that the overall impact of IL-37 expression heavily relies on the pre-existing inflammatory status of the mucosa.

At the molecular and signaling levels, IL-37, recognized as an anti-inflammatory cytokine (13), plays a critical role in maintaining the integrity of intestinal mucosal homeostasis. When the mucosa faces various pathological stimuli or challenges, including exacerbations of IBD, colonic IL-37 is released to alleviate inflammation (73). This process can help prevent the transformation of colonic epithelial cells into a malignancy by suppressing the pro-proliferative stimulus of pro-inflammatory cytokines. However, if the underlying pathological stimuli are not effectively addressed or halted, chronic inflammation persists, for example, chronic inflammation associated with IBD, disrupting tissue homeostasis (67), despite ongoing efforts by colonic IL-37 to suppress local inflammation. As mentioned earlier, immune surveillance against malignancies relies on host immunity and inflammation; therefore, prolonged and excessive suppression of pro-inflammatory responses may potentially promote tumorigenesis by hindering the local inflammation necessary for tumor cell destruction (74). This aligns with previous research demonstrating a positive correlation between pro-inflammatory mediators and CRC histopathology (67) (Figure 1).

Comparison between up and low GI cancers

Moreover, the regulatory role of IL-37 varies between gastric cancer and colorectal cancer, promoting carcinogenesis through the up-regulation of IL-37 in gastric cancer or the down-regulation of IL-37 expression in colorectal cancer within the local mucosa. This

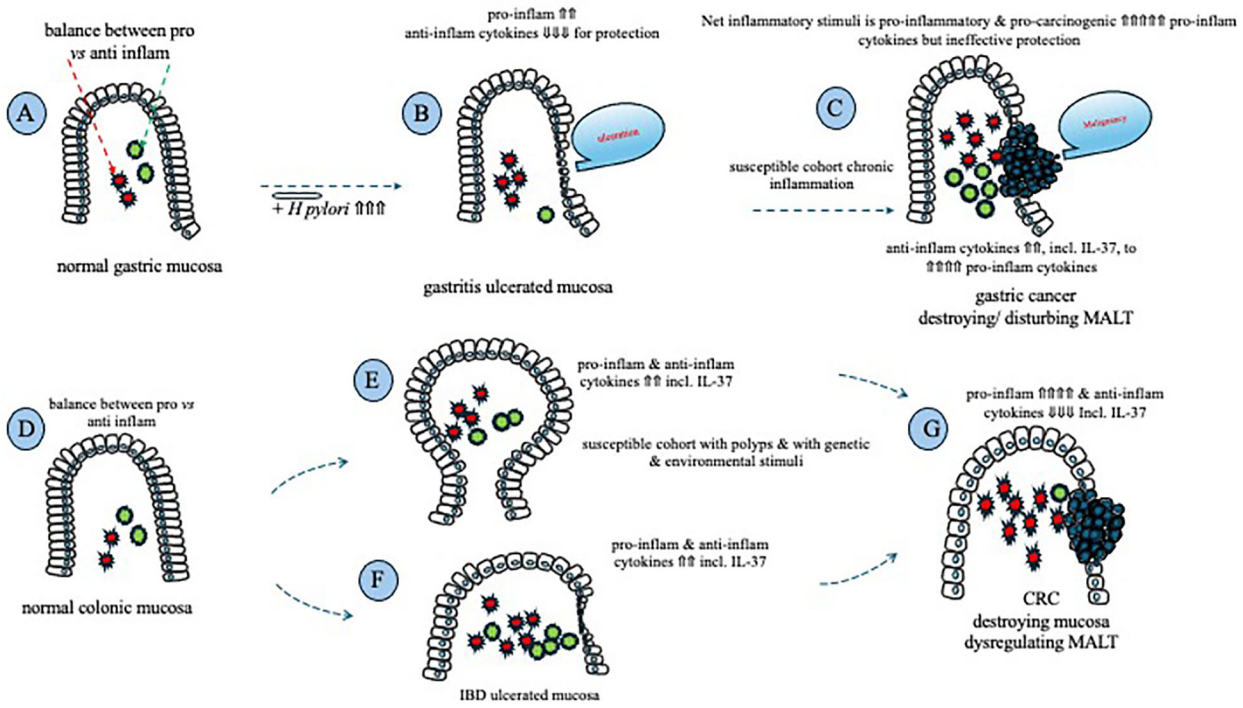

FIGURE 1
Schematic that summarizes the involvement of inflammatory cytokines in mucosal ulceration and cancer formation in the stomach and the colon. Homeostasis between pro- and anti-inflammatory cytokines exists within the normal gastric mucosa **(A)**; chronic *H. pylori* infection results in an increase in pro-inflammatory cytokines, with a reduction in anti-inflammatory cytokines, including IL-37, leading to gastric ulceration **(B)**; following prolonged ulceration, anti-inflammatory cytokine expression rises, but is unable to suppress a continued rise in pro-inflammatory/pro-carcinogenic cytokines, ultimately leading to gastric cancer **(C)**. Homeostasis between pro- and anti-inflammatory cytokines exists within the normal colonic mucosa **(D)**; both pro- and anti-inflammatory mucosal cytokines are increased within a cancer-susceptible cohort **(E)**, +/- the presence of IBD **(F)**, in an attempt to maintain homeostasis; prolonged pro-inflammatory/pro-carcinogenic cytokine stimulation leads to neoplastic transformation of colonic mucosal epithelial cells that reduce their production of anti-inflammatory cytokines, including IL-37, resulting in the formation of CRC **(G)**.

difference can be attributed to the substantial variations between these two gastrointestinal organs. A significant factor is the distinction in the microenvironments of the colon and stomach, despite both being part of the MALT system (28). In addition, genetic contributions to tumorigenesis in both gastric cancer and colorectal cancer, local microenvironments also play a role in carcinogenesis, such as *H. pylori* in gastric cancer (37) and ultra-processed rich food in colorectal cancer (75). These differences necessitate distinct host mucosal regulatory responses to maintain homeostasis. Consequently, the signaling pathways for gastric cancer and colon cancer differ, suggesting the induction of different immune-regulatory mechanisms, particularly on IL-37 during tumorigenesis.

The above observations invite speculation that development of gastric cancer and CRC is partially due to substantially impaired/disturbed local and possible systemic host immunity among susceptible individuals, for example intestinal mucosal IL-37 production. Dramatic impaired host immunity compromised immune surveillance against the development of malignancy, resulting in initiation of cancers (51).

Interestingly, IL-37 has been shown to exert protective effects in various cancer types. For instance, in hepatocellular carcinoma (76), it may operate through the inhibition of M2 macrophages (54). In lung cancer (77), IL-37 demonstrates protective effects by inhibiting angiogenesis, as illustrated in an animal model study (78). From a mechanistic standpoint, elevated levels of IL-37 have been associated with increased infiltration of $CD1a^{+}$ dendritic cells, which notably correlates with the overall survival rate in hepatocellular carcinoma (79). The implications of enhanced dendritic cells in anti-tumor immunity may involve heightened professional antigen presentation, leading to a subsequent increase in the differential polarization of macrophages (79). This phenomenon could elucidate the varying roles of macrophages in the development of malignancies, potentially exhibiting diverse mechanisms of carcinogenesis or microenvironments. The differential role of IL-37 in the GI tract and among different cancers may be due to the host differential immunological response(s) to various challenges, with different outcomes.

Conclusion

H. pylori infection leads to the inhibition of IL-37 in the gastric mucosa, contributing to heightened mucosal inflammation and destruction, thereby facilitating increased proliferation of *H. pylori*. Elevated levels of IL-37 observed in gastric cancer patients align with reduced host immunity at the cellular and humoral levels, indicating that IL-37 may not play a protective role in gastric cancer. It is speculated that IL-37 may protect individuals from food allergy and/or coeliac disease. While IL-37 provides protection in an IBD animal model, the detection of highly produced IL-37 in IBD patients suggests a stage-dependent role, being protective in acute inflammation but potentially promoting IBD in chronic conditions. Moreover, elevated colonic IL-37 in CRC correlates with overall survival time and disease time, indicating a protective role for IL-37 in CRC, except possibly in IBD-associated CRC. The differential regulation and expression of IL-37 between upper- and lower-GI organs may be attributed to variations in the microbial flora. This information suggests that IL-37 could be a potential therapeutic agent, acting as a key suppressor of innate immunity and allergic immune responses mediated by leucocytes.

Author contributions

QW: Conceptualization, Writing – original draft. GZ: Conceptualization, Writing – original draft. CA: Conceptualization, Writing – review & editing. BH: Writing – review & editing. SB: Writing – review & editing, Conceptualization, Supervision.

Funding

The author(s) declare financial support was received for the research, authorship, and/or publication of this article. The current study is partially supported by a grant from Gansu Provincial Science and Technology Project (Project No: 23JDKD0001).

Conflict of interest

The authors declare that the research was conducted in the absence of any commercial or financial relationships that could be construed as a potential conflict of interest.

The author(s) declared that they were an editorial board member of Frontiers, at the time of submission. This had no impact on the peer review process and the final decision.

Publisher's note

References

1. Klatt EC. The gastrointestinal tract. In: Kumar V, Abbas A, Aster JC, editors. *Robbins & Cotran Pathologic Basis of Disease*. Amsterdam, Netherlands: Eleservier (2015). p. 177–223.

2. Dekaboruah E, Suryavanshi MV, Chettri D, Verma AK. Human microbiome: an academic update on human body site specific surveillance and its possible role. *Arch Microbiol.* (2020) 202:2147–67. doi: 10.1007/s00203-020-01931-x

3. Morbe UM, Jorgensen PB, Fenton TM, von Burg N, Riis LB, Spencer J, et al. Human gut-associated lymphoid tissues (GALT); diversity, structure, and function. *Mucosal Immunol*. (2021) 14:793–802. doi: 10.1038/s41385-021-00389-4

4. Bao S, Beagley KW, France MP, Shen J, Husband AJ. Interferon-gamma plays a critical role in intestinal immunity against Salmonella typhimurium infection. *Immunology*. (2000) 99:464–72. doi: 10.1046/j.1365-2567.2000.00955.x

5. Kiderlen AF, Kaufmann SH, Lohmann-Matthes ML. Protection of mice against the intracellular bacterium Listeria monocytogenes by recombinant immune interferon. *Eur J Immunol*. (1984) 14:964–7. doi: 10.1002/eji.1830141019

6. Xu Y, Hunt NH, Bao S. The correlation between proinflammatory cytokines, MAdCAM-1 and cellular infiltration in the inflamed colon from TNF-alpha gene knockout mice. *Immunol Cell Biol*. (2007) 85:633–9. doi: 10.1038/sj.icb.7100112

7. De Santis S, Kunde D, Galleggiante V, Liso M, Scandiffio L, Serino G, et al. TNFalpha deficiency results in increased IL-1beta in an early onset of spontaneous murine colitis. *Cell Death Dis*. (2017) 8:e2993.

8. Genaro LM, Gomes LEM, Franceschini A, Ceccato HD, de Jesus RN, Lima AP, et al. Anti-TNF therapy and immunogenicity in inflammatory bowel diseases: a translational approach. *Am J Transl Res*. (2021) 13:13916–30.

9. Schottenfeld D, Beebe-Dimmer J. Chronic inflammation: a common and important factor in the pathogenesis of neoplasia. *CA Cancer J Clin*. (2006) 56:69–83. doi: 10.3322/canjclin.56.2.69

10. Nicklin MJ, Weith A, Duff GW. A physical map of the region encompassing the human interleukin-1 alpha, interleukin-1 beta, and interleukin-1 receptor antagonist genes. *Genomics*. (1994) 19:382–4. doi: 10.1006/geno.1994.1076

11. Boraschi D, Lucchesi D, Hainzl S, Leitner M, Maier E, Mangelberger D, et al. IL-37: a new anti-inflammatory cytokine of the IL-1 family. *Eur Cytokine Netw*. (2011) 22:127–47. doi: 10.1684/ecn.2011.0288

12. Su Z, Tao X. Current understanding of IL-37 in human health and disease. *Front Immunol*. (2021) 12:696605. doi: 10.3389/fimmu.2021.696605

13. Nold MF, Nold-Petry CA, Zepp JA, Palmer BE, Bufler P, Dinarello CA. IL-37 is a fundamental inhibitor of innate immunity. *Nat Immunol*. (2010) 11:1014–22. doi: 10.1038/ni.1944

14. Luo Y, Cai X, Liu S, Wang S, Nold-Petry CA, Nold MF, et al. Suppression of antigen-specific adaptive immunity by IL-37 via induction of tolerogenic dendritic cells. *Proc Natl Acad Sci*. (2014) 111:15178–83. doi: 10.1073/pnas.1416714111

15. Ye L, Ji L, Wen Z, Zhou Y, Hu D, Li Y, et al. IL-37 inhibits the production of inflammatory cytokines in peripheral blood mononuclear cells of patients with systemic lupus erythematosus: its correlation with disease activity. *J Transl Med*. (2014) 12:69. doi: 10.1186/1479-5876-12-69

16. Sorini C, Cardoso RF, Tripathi KP, Mold JE, Diaz OE, Holender Y, et al. Intestinal damage is required for the pro-inflammatory differentiation of commensal CBir1-specific T cells. *Mucosal Immunol*. (2023) 17:81–93. doi: 10.1016/j.mucimm.2023.11.001

17. Marshall BJ, Warren JR. Unidentified curved bacilli in the stomach of patients with gastritis and peptic ulceration. *Lancet*. (1984) 1:1311–5. doi: 10.1016/S0140-6736(84)91816-6

18. Marshall B. Helicobacter pylori–a Nobel pursuit? *Can J Gastroenterol*. (2008) 22:895–6. doi: 10.1155/2008/459810

19. Ahmadnia Z, Ranaee M, Mohammadi Abandansari R, Bagheri N, Shirzad H. Evaluating the microRNA expression of IL-35 and IL-37 in helicobacter pylori-infected patients with gastritis and gastric ulcer. *Iran J Allergy Asthma Immunol*. (2022) 21:20–6. doi: 10.18502/ijaai.v21i1.8609

20. Feng XX, Chi G, Wang H, Gao Y, Chen Q, Ru YX, et al. IL-37 suppresses the sustained hepatic IFN-gamma/TNF-alpha production and T cell-dependent liver injury. *Int Immunopharmacol*. (2019) 69:184–93. doi: 10.1016/j.intimp.2019.01.037

21. Cavalli G, Dinarello CA. Suppression of inflammation and acquired immunity by IL-37. *Immunol Rev*. (2018) 281:179–90. doi: 10.1111/imr.12605

22. Gunaltay S, Ghiboub M, Hultgren O, Hornquist EH. Reduced IL-37 production increases spontaneous chemokine expressions in colon epithelial cells. *Dig Dis Sci*. (2017) 62:1204–15. doi: 10.1007/s10620-016-4422-9

23. Chai EZ, Siveen KS, Shanmugam MK, Arfuso F, Sethi G. Analysis of the intricate relationship between chronic inflammation and cancer. *Biochem J*. (2015) 468:1–15. doi: 10.1042/BJ20141337

24. Varon C, Azzi-Martin L, Khalid S, Seeneevassen L, Menard A, Spuul P. Helicobacters and cancer, not only gastric cancer? *Semin Cancer Biol*. (2022) 86:1138–54. doi: 10.1016/j.semcancer.2021.08.007

25. Figueroa-Gomez X, Oliveras-Lopez MJ, Rodriguez Silva JM, Poyanco M, Lopez H, Araya M. Experiences and perceptions of people with celiac disease, food allergies and food intolerance when dining out. *Front Nutr*. (2024) 11:1321360. doi: 10.3389/fnut.2024.1321360

26. Raedler D, Ballenberger N, Klucker E, Bock A, Otto R, Prazeres da Costa O, et al. Identification of novel immune phenotypes for allergic and nonallergic childhood asthma. *J Allergy Clin Immunol*. (2015) 135:81–91. doi: 10.1016/j.jaci.2014.07.046

27. Schroder A, Lunding LP, Zissler UM, Vock C, Webering S, Ehlers JC, et al. IL-37 regulates allergic inflammation by counterbalancing pro-inflammatory IL-1 and IL-33. *Allergy*. (2022) 77:856–69. doi: 10.1111/all.15072

28. Cesta MF. Normal structure, function, and histology of mucosa-associated lymphoid tissue. *Toxicol Pathol*. (2006) 34:599–608. doi: 10.1080/01926230600865531

29. Osborne DG, Domenico J, Fujita M. Expression of IL-37 induces a regulatory T-cell-like phenotype and function in jurkat cells. *Cells*. (2022) 11. doi: 10.3390/cells11162565

30. Traxinger BR, Richert-Spuhler LE, Lund JM. Mucosal tissue regulatory T cells are integral in balancing immunity and tolerance at portals of antigen entry. *Mucosal Immunol*. (2022) 15:398–407. doi: 10.1038/s41385-021-00471-x

31. Galand C, Leyva-Castillo JM, Yoon J, Han A, Lee MS, McKenzie ANJ, et al. IL-33 promotes food anaphylaxis in epicutaneously sensitized mice by targeting mast cells. *J Allergy Clin Immunol*. (2016) 138:1356–66. doi: 10.1016/j.jaci.2016.03.056

32. Hou T, Sun X, Zhu J, Hon KL, Jiang P, Chu IM, et al. IL-37 ameliorating allergic inflammation in atopic dermatitis through regulating microbiota and AMPK-mTOR signaling pathway-modulated autophagy mechanism. *Front Immunol*. (2020) 11:752. doi: 10.3389/fimmu.2020.00752

33. Catassi C, Verdu EF, Bai JC, Lionetti E. Coeliac disease. *Lancet*. (2022) 399:2413–26. doi: 10.1016/S0140-6736(22)00794-2

34. Verkarre V, Brousse N. [Histopathology of coeliac disease]. *Pathol Biol (Paris)*. (2013) 61:e13–9. doi: 10.1016/j.patbio.2011.03.003

35. Goel G, Tye-Din JA, Qiao SW, Russell AK, Mayassi T, Ciszewski C, et al. Cytokine release and gastrointestinal symptoms after gluten challenge in celiac disease. *Sci Adv*. (2019) 5:eaaw7756. doi: 10.1126/sciadv.aaw7756

36. Goel G, Daveson AJM, Hooi CE, Tye-Din JA, Wang S, Szymczak E, et al. Serum cytokines elevated during gluten-mediated cytokine release in coeliac disease. *Clin Exp Immunol*. (2020) 199:68–78. doi: 10.1111/cei.13369

37. Wroblewski LE, Peek RM Jr., Wilson KT. Helicobacter pylori and gastric cancer: factors that modulate disease risk. *Clin Microbiol Rev*. (2010) 23:713–39. doi: 10.1128/CMR.00011-10

38. Zhang Y, Tang M, Wang XG, Gu JH, Zhou LN, Jin J, et al. Elevated serum levels of interleukin-37 correlate with poor prognosis in gastric cancer. *Rev Esp Enferm Dig*. (2019) 111:941–5. doi: 10.17235/reed.2019.6460/2019

39. Zitvogel L, Tesniere A, Kroemer G. Cancer despite immunosurveillance: immunoselection and immunosubversion. *Nat Rev Immunol*. (2006) 6:715–27. doi: 10.1038/nri1936

40. Conti P, Carinci F, Lessiani G, Spinas E, Kritas SK, Ronconi G, et al. Potential therapeutic use of IL-37: a key suppressor of innate immunity and allergic immune responses mediated by mast cells. *Immunol Res*. (2017) 65:982–6. doi: 10.1007/s12026-017-8938-7

41. Lou S, Cao Z, Chi W, Wang X, Feng M, Lin L, et al. The safety concerns regarding immune checkpoint inhibitors in liver cancer patients rising mainly from CHB. *Front Pharmacol*. (2023) 14:1164309. doi: 10.3389/fphar.2023.1164309

42. Li P, Guo H, Wu K, Su L, Huang K, Lai R, et al. Decreased IL-37 expression in hepatocellular carcinoma tissues and liver cancer cell lines. *Oncol Lett*. (2020) 19:2639–48. doi: 10.3892/ol

43. Muscari F, Maulat C. Preoperative alpha-fetoprotein (AFP) in hepatocellular carcinoma (HCC): is this 50-year biomarker still up-to-date? *Transl Gastroenterol Hepatol*. (2020) 5:46. doi: 10.21037/tgh.2019.12.09

44. Wang D, Zhang B, Liu X, Kan LL, Leung PC, Wong CK. Agree to disagree: The contradiction between IL-18 and IL-37 reveals shared targets in cancer. *Pharmacol Res*. (2024) 200:107072. doi: 10.1016/j.phrs.2024.107072

45. Takada K, Okamoto T, Tominaga M, Teraishi K, Akamine T, Takamori S, et al. Clinical implications of the novel cytokine IL-38 expressed in lung adenocarcinoma: Possible association with PD-L1 expression. *PloS One*. (2017) 12:e0181598. doi: 10.1371/journal.pone.0181598

46. Ouyang P, Wu K, Su L, An W, Bie Y, Zhang H, et al. Inhibition of human cervical cancer cell invasion by IL-37 involving runt related transcription factor 2 suppression. *Ann Transl Med*. (2019) 7:568. doi: 10.21037/atm

47. Mei Y, Liu H. IL-37: An anti-inflammatory cytokine with antitumor functions. *Cancer Rep (Hoboken)*. (2019) 2:e1151. doi: 10.1002/cnr2.1151

48. Huo J, Hu J, Liu G, Cui Y, Ju Y. Elevated serum interleukin-37 level is a predictive biomarker of poor prognosis in epithelial ovarian cancer patients. *Arch Gynecol Obstet*. (2017) 295:459–65. doi: 10.1007/s00404-016-4258-8

49. Liu Q, Zhang J, Xia L, Wise SD, Hambly BD, Tao K, et al. Clinical implications of interleukins-31, 32, and 33 in gastric cancer. *World J Gastrointest Oncol*. (2022) 14:1808–22. doi: 10.4251/wjgo.v14.i9.1808

50. Liu Q, Zhang Y, Zhang J, Tao K, Hambly BD, Bao S. Inverse correlation between Interleukin-34 and gastric cancer, a potential biomarker for prognosis. *Cell Biosci*. (2020) 10:94. doi: 10.1186/s13578-020-00454-8

51. Swann JB, Smyth MJ. Immune surveillance of tumors. *J Clin Invest*. (2007) 117:1137–46. doi: 10.1172/JCI31405

52. Zhu Y, Qin H, Ye K, Sun C, Qin Y, Li G, et al. Dual role of IL-37 in the progression of tumors. *Cytokine*. (2022) 150:155760. doi: 10.1016/j.cyto.2021.155760

53. Abulkhir A, Samarani S, Amre D, Duval M, Haddad E, Sinnett D, et al. A protective role of IL-37 in cancer: a new hope for cancer patients. *J Leukoc Biol*. (2017) 101:395–406. doi: 10.1189/jlb.5RU0816-341R

54. Zhang Z, Zhang J, He P, Han J, Sun C. Interleukin-37 suppresses hepatocellular carcinoma growth through inhibiting M2 polarization of tumor-associated macrophages. *Mol Immunol*. (2020) 122:13–20. doi: 10.1016/j.molimm.2020.03.012

55. Andon FT, Digifico E, Maeda A, Erreni M, Mantovani A, Alonso MJ, et al. Targeting tumor associated macrophages: The new challenge for nanomedicine. *Semin Immunol*. (2017) 34:103–13. doi: 10.1016/j.smim.2017.09.004

56. Gu M, Jin Y, Gao X, Xia W, Xu T, Pan S. Novel insights into IL-37: an anti-inflammatory cytokine with emerging roles in anti-cancer process. *Front Immunol*. (2023) 14:1278521. doi: 10.3389/fimmu.2023.1278521

57. Guan Q. A comprehensive review and update on the pathogenesis of inflammatory bowel disease. *J Immunol Res*. (2019) 2019:7247238. doi: 10.1155/2019/7247238

58. Collaborators G.B.D.I.B.D. The global, regional, and national burden of inflammatory bowel disease in 195 countries and territories, 1990-2017: a systematic analysis for the Global Burden of Disease Study 2017. *Lancet Gastroenterol Hepatol*. (2020) 5:17–30. doi: 10.1016/S2468-1253(19)30333-4

59. McNamee EN, Masterson JC, Jedlicka P, McManus M, Grenz A, Collins CB, et al. Interleukin 37 expression protects mice from colitis. *Proc Natl Acad Sci U.S.A*. (2011) 108:16711–6. doi: 10.1073/pnas.1111982108

60. Cong J, Wu D, Dai H, Ma Y, Liao C, Li L, et al. Interleukin-37 exacerbates experimental colitis in an intestinal microbiome-dependent fashion. *Theranostics*. (2022) 12:5204–19. doi: 10.7150/thno.69616

61. Imaeda H, Takahashi K, Fujimoto T, Kasumi E, Ban H, Bamba S, et al. Epithelial expression of interleukin-37b in inflammatory bowel disease. *Clin Exp Immunol*. (2013) 172:410–6. doi: 10.1111/cei.12061

62. Zhang ZZ, Zhang Y, He T, Sweeney CL, Baris S, Karakoc-Aydiner E, et al. Homozygous IL37 mutation associated with infantile inflammatory bowel disease. *Proc Natl Acad Sci U.S.A*. (2021) 118. doi: 10.1073/pnas.2009217118

63. Keum N, Giovannucci E. Global burden of colorectal cancer: emerging trends, risk factors and prevention strategies. *Nat Rev Gastroenterol Hepatol*. (2019) 16:713–32. doi: 10.1038/s41575-019-0189-8

64. WHO. *Cancer*. (2021). Available at: https://www.who.int/news-room/fact-sheets/detail/cancer.

65. Society AC. Survival rates for colorectal cancer(2021). Available online at: https://www.cancer.org/cancer/colon-rectal-cancer/detection-diagnosis-staging/survival-rates.html. January 29, 2024.

66. Yan X, Zhao J, Zhang R. Interleukin-37 mediates the antitumor activity in colon cancer through beta-catenin suppression. *Oncotarget*. (2017) 8:49064–75. doi: 10.18632/oncotarget.v8i30

67. Medzhitov R. Origin and physiological roles of inflammation. *Nature*. (2008) 454:428–35. doi: 10.1038/nature07201

68. Zhu B, Luo J, Jiang Y, Yu L, Liu M, Fu J. Prognostic significance of nomograms integrating IL-37 expression, neutrophil level, and MMR status in patients with colorectal cancer. *Cancer Med*. (2018) 7:3682–94. doi: 10.1002/cam4.1663

69. Dang J, He Z, Cui X, Fan J, Hambly DJ, Hambly BD, et al. The role of IL-37 and IL-38 in colorectal cancer. *Front Med (Lausanne)*. (2022) 9:811025. doi: 10.3389/fmed.2022.811025

70. Lin JH, Giovannucci E. Sex hormones and colorectal cancer: what have we learned so far? *J Natl Cancer Inst*. (2010) 102:1746–7. doi: 10.1093/jnci/djq444

71. Sahin IH, Akce M, Alese O, Shaib W, Lesinski GB, El-Rayes B, et al. Immune checkpoint inhibitors for the treatment of MSI-H/MMR-D colorectal cancer and a perspective on resistance mechanisms. *Br J Cancer*. (2019) 121:809–18. doi: 10.1038/s41416-019-0599-y

72. Wang Z, Zeng FL, Hu YW, Wang XY, Zhao FL, Zhou P, et al. Interleukin-37 promotes colitis-associated carcinogenesis via SIGIRR-mediated cytotoxic T cells dysfunction. *Signal Transduct Target Ther*. (2022) 7:19. doi: 10.1038/s41392-021-00820-z

73. Jemal A, Siegel R, Xu J, Ward E. Cancer statistics, 2010. *CA Cancer J Clin*. (2010) 60:277–300. doi: 10.3322/caac.20073

74. Ullman TA, Itzkowitz SH. Intestinal inflammation and cancer. *Gastroenterology*. (2011) 140:1807–16. doi: 10.1053/j.gastro.2011.01.057

75. Wang L, Du M, Wang K, Khandpur N, Rossato SL, Drouin-Chartier JP, et al. Association of ultra-processed food consumption with colorectal cancer risk among men and women: results from three prospective US cohort studies. *BMJ*. (2022) 378:e068921. doi: 10.1136/bmj-2021-068921

76. Zhao JJ, Pan QZ, Pan K, Weng DS, Wang QJ, Li JJ, et al. Interleukin-37 mediates the antitumor activity in hepatocellular carcinoma: role for CD57+ NK cells. *Sci Rep*. (2014) 4:5177. doi: 10.1038/srep05177

77. Ge G, Wang A, Yang J, Chen Y, Yang J, Li Y, et al. Interleukin-37 suppresses tumor growth through inhibition of angiogenesis in non-small cell lung cancer. *J Exp Clin Cancer Res*. (2016) 35:13. doi: 10.1186/s13046-016-0293-3

78. Gao W, Kumar S, Lotze MT, Hanning C, Robbins PD, Gambotto A. Innate immunity mediated by the cytokine IL-1 homologue 4 (IL-1H4/IL-1F7) induces IL-12-dependent adaptive and profound antitumor immunity. *J Immunol*. (2003) 170:107–13. doi: 10.4049/jimmunol.170.1.107

79. Liu Y, Zhao JJ, Zhou ZQ, Pan QZ, Zhu Q, Tang Y, et al. IL-37 induces anti-tumor immunity by indirectly promoting dendritic cell recruitment and activation in hepatocellular carcinoma. *Cancer Manag Res*. (2019) 11:6691–702. doi: 10.2147/CMAR

frontiers | Frontiers in Immunology

TYPE Original Research
PUBLISHED 15 October 2024
DOI 10.3389/fimmu.2024.1480091

OPEN ACCESS

EDITED BY
Kelsey P. Kubelick,
University of Virginia, United States

REVIEWED BY
Timo De Groof,
Vrije University Brussels, Belgium
Anja Lux,
Friedrich-Alexander-University
Erlangen-Nürnberg, Germany

*CORRESPONDENCE
Ulrich Rothbauer
ulrich.rothbauer@uni-tuebingen.de

RECEIVED 13 August 2024
ACCEPTED 30 September 2024
PUBLISHED 15 October 2024

CITATION
Frecot DI, Blaess S, Wagner TR, Kaiser PD, Traenkle B, Fandrich M, Jakobi M, Scholz AM, Nueske S, Schneiderhan-Marra N, Gouttefangeas C, Kneilling M, Pichler BJ, Sonanini D and Rothbauer U (2024) Making the effect visible – OX40 targeting nanobodies for *in vivo* imaging of activated T cells.
Front. Immunol. 15:1480091.
doi: 10.3389/fimmu.2024.1480091

Making the effect visible – OX40 targeting nanobodies for *in vivo* imaging of activated T cells

Desiree I. Frecot[1,2], Simone Blaess[3,4], Teresa R. Wagner[3], Philipp D. Kaiser[3], Bjoern Traenkle[3], Madeleine Fandrich[3], Meike Jakobi[3], Armin M. Scholz[5], Stefan Nueske[5], Nicole Schneiderhan-Marra[3], Cécile Gouttefangeas[2,6,7], Manfred Kneilling[2,4,8], Bernd J. Pichler[2,4,7], Dominik Sonanini[2,3,4,9] and Ulrich Rothbauer[1,2]*

[1]Pharmaceutical Biotechnology, University Tübingen, Tübingen, Germany, [2]Cluster of Excellence iFIT (EXC2180) "Image-Guided and Functionally Instructed Tumor Therapies", University of Tübingen, Tübingen, Germany, [3]NMI Natural and Medical Sciences Institute at the University of Tübingen, Reutlingen, Germany, [4]Werner Siemens Imaging Center, Department of Preclinical Imaging and Radiopharmacy, University of Tübingen, Tübingen, Germany, [5]Livestock Center of the Faculty of Veterinary Medicine, Ludwig Maximilians University Munich, Oberschleissheim, Germany, [6]Institute for Immunology, University of Tübingen, Tübingen, Germany, [7]German Cancer Consortium (DKTK) and German Cancer Research Center (DKFZ) partner site Tübingen, Tübingen, Germany, [8]Department of Dermatology, University of Tübingen, Tübingen, Germany, [9]Department of Medical Oncology and Pneumology, University of Tübingen, Tübingen, Germany

Purpose: Human OX40 (hOX40/CD134), a member of the TNF receptor superfamily, is mainly expressed on activated T lymphocytes. Triggered by its ligand OX40L (CD252), it provides costimulatory signals that support the differentiation, proliferation and long-term survival of T cells. Besides being a relevant therapeutic target, hOX40 is also an important biomarker for monitoring the presence or infiltration of activated T cells within the tumor microenvironment (TME), the inflammatory microenvironment (IME) in immune-mediated diseases (IMIDs) and the lymphatic organs. Here, we developed novel single domain antibodies (nanobodies, Nbs) targeting hOX40 to monitor the activation status of T cells by *in vivo* molecular imaging.

Methods: Nbs against hOX40 (hOX40-Nbs) were selected from an immunized Nb-library by phage display. The identified hOX40-Nbs were characterized *in vitro*, including determination of their specificity, affinity, stability, epitope recognition and their impact on OX40 signaling and T cell function. A lead candidate was site-specifically conjugated with a fluorophore via sortagging and applied for noninvasive *in vivo* optical imaging (OI) of hOX40-expressing cells in a xenograft mouse model.

Results: Our selection campaign revealed four unique Nbs that exhibit strong binding affinities and high stabilities under physiological conditions. Epitope binning and domain mapping indicated the targeting of at least two different epitopes on hOX40. When analyzing their impact on OX40 signaling, an agonistic effect was excluded for all validated Nbs. Incubation of activated T cells with hOX40-Nbs did not affect cell viability or proliferation patterns, whereas differences in cytokine release were observed. *In vivo* OI with a fluorophore-conjugated lead candidate in experimental mice with hOX40-expressing xenografts demonstrated its specificity and functionality as an imaging probe.

Conclusion: Considering the need for advanced probes for noninvasive *in vivo* monitoring of T cell activation dynamics, we propose, that our hOX40-Nbs have a great potential as imaging probes for noninvasive and longitudinal *in vivo* diagnostics. Quantification of OX40$^+$ T cells in TME or IME will provide crucial insights into the activation state of infiltrating T cells, offering a valuable biomarker for assessing immune responses, predicting treatment efficacy, and guiding personalized immunotherapy strategies in patients with cancer or IMIDs.

KEYWORDS

OX40, nanobody, T cell activation, tumor microenvironment (TME), monitoring immunotherapies, *in vivo* imaging

Introduction

Immunotherapies that specifically modulate the patient's immune system, e.g. to fight malignant tumor cells or attenuate autoimmune reactions, have opened a new chapter in personalized medicine (1–4). Although such therapies have shown remarkable success in some cases, the reasons why patients respond differently need to be understood. It is generally accepted that treatment outcomes are highly dependent on the individual immune system and the composition of the tumor (TME) or inflammatory microenvironment (IME), which is why sophisticated diagnostic approaches are required. To overcome the limitations of invasive procedures including histopathology or liquid biopsies (5, 6), noninvasive techniques such as *in vivo* imaging have been implemented in diagnostics and therapy monitoring. This has led to an increasing interest in the development of novel probes, that recognize specific immune cell populations and are capable of visualizing their infiltration into the TME, IME as well as primary and secondary lymphatic organs (7). Considering cytotoxic CD8$^+$ T cells as one of the most relevant immune cells in the context of immunotherapies, a growing number of different antibody-derived imaging probes for preclinical and also clinical *in vivo imaging* of CD8$^+$ T cells have recently been reported (7–13). In addition, comparable probes have been developed to visualize other populations such as CD4$^+$ T cells, which increasingly gained importance in the context of tumor immunotherapy (14–17). Furthermore, also probes targeting myeloid cells including tumor-associated macrophages (18, 19) or detecting immune checkpoints expressed on antigen-presenting cells (APCs) and/or tumor cells have been reported (reviewed in (20, 21). Since the presence or absence of specific cell populations alone does not give information about their functional states, visualizing of particularly activation, could enable more precise patient stratification and monitoring of therapeutic responses. This was demonstrated by visualization of the inducible T cell costimulatory receptor (ICOS) (22), the early T cell activation marker CD69 (23), or soluble factors such as granzyme B (24, 25) or interferon-γ (IFN-γ) (67) which both are released by activated cytotoxic T cells.

OX40 (CD134/TNFRSF4), has been described as a surface marker for T cell activation (26–30). It is mainly expressed on activated CD8$^+$ and CD4$^+$ T cells, but also on activated regulatory T cells (Tregs), natural killer T cells (NKTs) and neutrophils (27, 31–33). OX40 binds to the OX40 ligand (OX40L, CD252) presented by activated APCs including B cells, dendritic cells and macrophages (34–36). OX40-OX40L engagement is key to potentiate T cell responses, including differentiation, proliferation, long-term survival, and enhancement of T cell effector functions, such as cytokine production (37). Recently, mouse-specific OX40 monoclonal antibodies (mAbs) were developed and applied for immune positron emission tomography (immunoPET) imaging in proof-of-principle studies to predict responses to cancer vaccines (38) or T cell response to glioblastoma (39) in preclinical mouse models. Beside cancer, OX40-specific immunoPET has also been applied to follow the development of acute graft-versus-host disease (40) or rheumatoid arthritis (41). However, the long systemic half-life of mAbs (up to seven days after injection), which is due to a reduced renal clearance, binding to Fc gamma receptor (FcγRs)-presenting cells and slow tissue penetration, delays prompt immunoPET imaging and leads to high radiation exposure. Moreover, this leads to a high tissue and blood background, which limits its sensitivity in detecting small populations of activated T cells (42). Consequently, there is a high demand for advanced molecules targeting human OX40 (hOX40) for diagnostic immunoPET imaging (43).

Antibody fragments derived from heavy-chain-only antibodies of camelids, referred to as VHHs or nanobodies (Nbs) (44), have emerged as versatile medical *in vivo* imaging probes [reviewed in (45–47)]. Nbs are characterized by a high stability in hydrophilic environments, small size (~15 kDa) and lack of the Fc moiety and thus show a fast renal clearance. In combination with highly sensitive and/or quantitative whole-body molecular imaging techniques based on optical or radionuclide-based modalities, *in vivo* binding of Nbs to their targets could be detected within minutes after systemic application (46, 48). Here, we describe the first set of hOX40-specific Nbs to monitor the activation status of human T cells and demonstrate the capability of a lead candidate

10.3389/fimmu.2024.1480091

for whole-body *in vivo* optical imaging (OI) of hOX40-expressing tumor cells in a mouse xenograft model.

Results

Identification and characterization of hOX40 specific Nbs

For the generation of hOX40-specific Nbs, two alpacas (*Vicugna pacos*) were immunized with the extracellular domain of hOX40, which contains the amino acid residues from Leu29 to Ala216. A positive immune response in both animals was confirmed on day 63 by serum ELISA (Supplementary Figure S1). Starting from peripheral blood lymphocytes (PBLs), we established a Nb-phagemid library representing the VHH repertoire of both animals (size: ~3 x 10^7 clones), from which hOX40-Nbs were enriched against recombinant hOX40 in two consecutive rounds of phage display. The selective binding of individual clones was tested in a whole-cell phage ELISA with U2OS cells stably expressing hOX40 (U2OS-hOX40). Subsequent sequencing revealed four unique hOX40-Nbs, namely O7, O12, O18 and O19, which exhibited highly diverse complementarity determining regions (CDRs) 3 (Figure 1A, Supplementary Table S1). All selected Nbs were expressed in *Escherichia coli* (*E. coli*) and purified by immobilized metal ion affinity chromatography (IMAC) followed by size exclusion chromatography (SEC), yielding high purity binding molecules (Figure 1B). To initially assess their binding affinities, we performed biolayer interferometry (BLI) and determined K_D values in the pico- to low nanomolar range (0.2 - 3.4 nM), while O7 showed a substantially weaker affinity as reflected by a K_D of ~ 150 nM (Figure 1C, Supplementary Figure S2A). In addition, we determined the folding stability of the selected candidates using differential scanning fluorimetry (nanoDSF). All Nbs showed high thermal stabilities with melting temperatures (T_M) between 50°C and 74°C without aggregation. Notably, this was not affected by an accelerated aging period of 10 days at 37°C (Figure 1D, Supplementary Figure S2B).

For the fluorescent functionalization of hOX40-Nbs, we took advantage of a sortase-based approach to selectively attach an

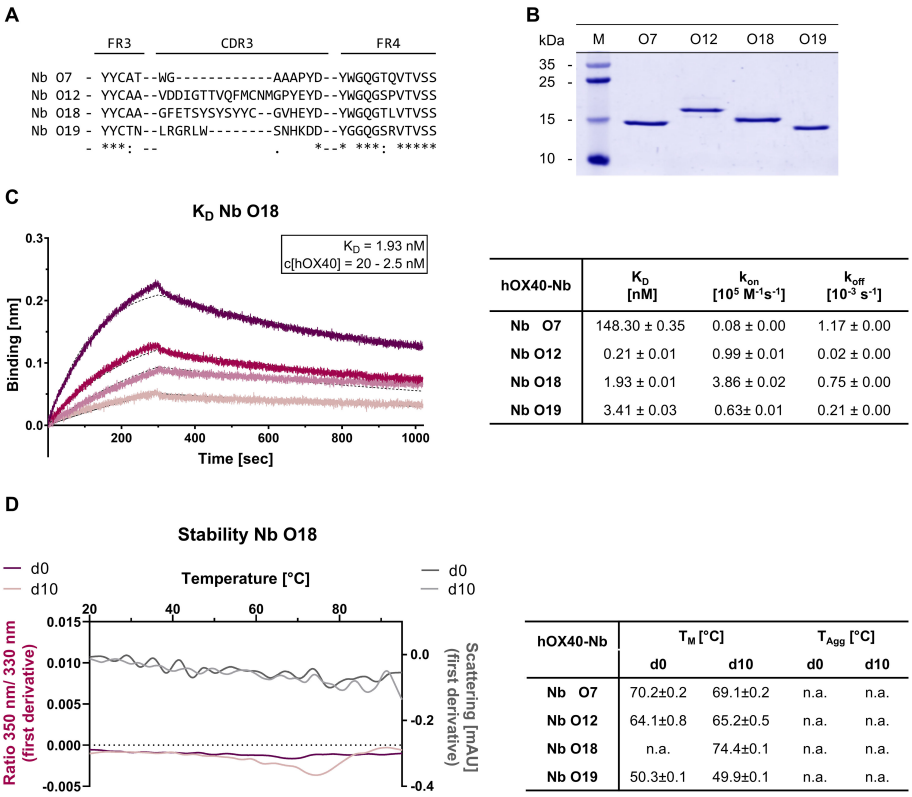

hOX40-Nb	K_D [nM]	k_{on} [10^5 $M^{-1}s^{-1}$]	k_{off} [10^{-3} s^{-1}]
Nb O7	148.30 ± 0.35	0.08 ± 0.00	1.17 ± 0.00
Nb O12	0.21 ± 0.01	0.99 ± 0.01	0.02 ± 0.00
Nb O18	1.93 ± 0.01	3.86 ± 0.02	0.75 ± 0.00
Nb O19	3.41 ± 0.03	0.63± 0.01	0.21 ± 0.00

hOX40-Nb	T_M [°C]		T_{Agg} [°C]	
	d0	d10	d0	d10
Nb O7	70.2±0.2	69.1±0.2	n.a.	n.a.
Nb O12	64.1±0.8	65.2±0.5	n.a.	n.a.
Nb O18	n.a.	74.4±0.1	n.a.	n.a.
Nb O19	50.3±0.1	49.9±0.1	n.a.	n.a.

FIGURE 1
Biochemical characterization of hOX40-Nbs. **(A)** Amino acid (aa) sequences of the complementarity determining region (CDR) 3 from 4 unique hOX40-Nbs identified by two consecutive rounds of bio panning (full sequences are displayed in Supplementary Table S1). **(B)** Coomassie-stained SDS-PAGE of 2 µg purified hOX40-Nbs after purification using immobilized metal affinity chromatography (IMAC) and size exclusion chromatography (SEC). **(C)** Biolayer interferometry (BLI)-based affinity measurements exemplarily shown for Nb O18. Biotinylated Nb was immobilized on streptavidin biosensors. Kinetic measurements were performed using four concentrations of recombinant hOX40 ranging from 2.5 nM - 20 nM (displayed with gradually lighter shades of color; left). Summary table (right) shows affinities (K_D), association constants (k_{on}), and dissociation constants (k_{off}) determined by BLI using four concentrations of purified Nbs as mean ± SD. **(D)** Stability analysis using nano scale differential scanning fluorimetry (nanoDSF) displaying fluorescence ratio (350 nm/330 nm) (red) and light scattering (gray) shown as first derivative for day 0 (dark shade) and after an accelerated aging period of 10 days at 37°C (light shade), exemplary shown for Nb O18 (left) and summarized for all hOX40-Nbs in the table (right). Data are shown as mean value of three technical replicates.

azide-group to the C-termini of the Nbs, which served as chemical handle for the addition of a AlexaFluor647(AF647)-conjugated dibenzocyclooctyne (DBCO-AF647) group utilizing click chemistry (16). As a result, we obtained Nbs comprising a C-terminal fluorophore with a defined labeling ratio of 1:1. The fluorescent Nbs were used to determine corresponding K_D (half-maximum binding at equilibrium) values on U2OS-hOX40 cells by flow cytometry. In accordance with the BLI-determined affinities, a strong functional binding for O12 and O18 with K_D values in the subnanomolar range (~ 0.1 nM for O12; ~ 0.3 nM for O18) was determined, whereas O7 and O19 displayed slightly weaker affinities (Figure 2A, Supplementary Figure S3A). To further confirm specific binding of the selected Nbs to hOX40 localized at the plasma membrane of mammalian cells, we used the fluorescent Nbs for live cell staining of U2OS-hOX40 cells in comparison to wild-type U2OS (U2OS-WT) cells. The images displayed intense signals localized at the cellular surface for all tested binders, which was comparable to the staining with a commercially available anti-hOX40 mAb, while none of the tested Nbs showed non-specific binding to U2OS-WT cells (Figure 2B). In addition, we used this approach to test a potential cross-reactivity of the Nbs to murine OX40 (mOX40) which has a ~63% sequence homology and performed live cell imaging on U2OS cells transiently expressing mOX40. Only O7 bound to mOX40, while all other candidates showed no staining of mOX40 expressing U2OS cells (Supplementary Figure S3B). In summary, we identified four hOX40-Nbs that bind recombinant as well as cell-resident hOX40. With respect to O12, O18 and O19 we selected high-affinity binders with K_D values in the pico- to low nanomolar range that exhibited strong specific binding to membrane-exposed hOX40. Notably, only O7 was less affine to recombinant hOX40 but showed additional cross-reactivity towards mOX40.

Characterization of binding epitopes on hOX40

To localize the binding sites of the selected hOX40-Nbs within the natively folded hOX40, we generated cellular expression constructs comprising domain-deletion mutants of hOX40 domains 1-3, which we transiently expressed in U2OS cells. Nb binding to truncated versions of hOX40 was visualized by immunofluorescence imaging of live cells. An anti-hOX40 mAb directed against domain 4 was used as a positive control (Figure 3A). Based on these results, we allocated binding of O7 and O19 to domain 3 and of O12 and O18 to domain 1 of hOX40 (Figure 3B). To examine a potential combinatorial binding of the different hOX40-Nbs, we further performed epitope binning analysis by BLI (Figure 3C). As expected from the domain mapping, O12 and O18, both targeting domain 1, simultaneously bound hOX40 in complex with O7 or O19, each targeting domain 3.

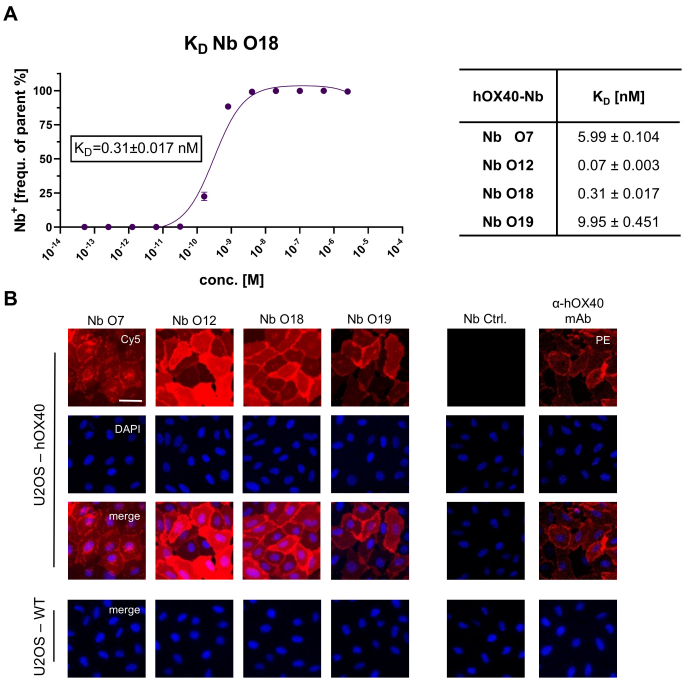

hOX40-Nb	K_D [nM]
Nb O7	5.99 ± 0.104
Nb O12	0.07 ± 0.003
Nb O18	0.31 ± 0.017
Nb O19	9.95 ± 0.451

FIGURE 2
Characterization of cellular binding of hOX40-Nbs. **(A)** Determination of hOX40-Nb binding to cellular expressed hOX40 by flow cytometry (n=3), exemplary shown for Nb O18 labeled with AlexaFluor647 (AF647; left). The percentage of positively stained U2OS-hOX40 (frequency of parent) was plotted against indicated concentrations of AF647-labeled hOX40-Nbs and K_D values shown in table (right) were calculated from a four-parametric sigmoidal model based on the mean ± SD of three replicates. **(B)** Representative images of U2OS-hOX40 cells (upper panel) and U2OS-WT cells (lower panel) stained with 1000 nM AF647-labeled hOX40-Nbs (left) as well as non-binding AF647-labeled PEP-Nb (Nb Ctrl.) as negative and phycoerythrin (PE)-labeled anti-hOX40 mAb as positive control (right). Shown are individual Nb staining (red), nuclei staining (Hoechst, blue) and merged signals; scale bar: 50 µm.

10.3389/fimmu.2024.1480091

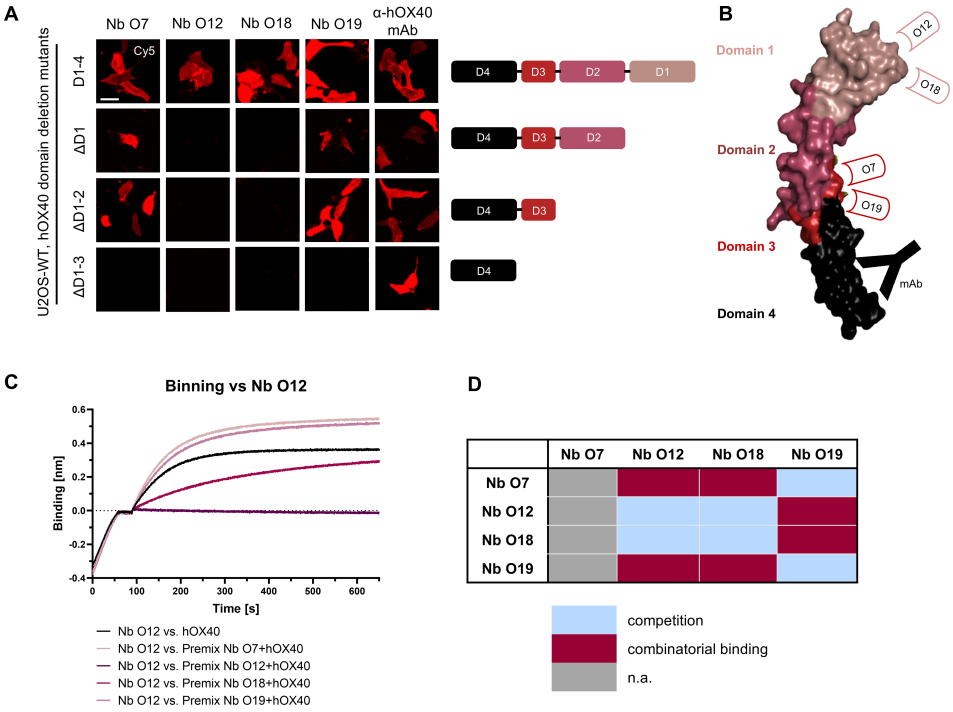

FIGURE 3
Characterization of binding epitopes of hOX40-Nbs. **(A)** Domain mapping by immunofluorescence staining with hOX40-Nbs on U2OS cells displaying either surface exposed hOX40 full length (D1-4), or domain deletion mutants as indicated. Shown are representative images of living cells stained with individual AF647-labeled Nbs or anti-hOX40 mAb; scale bar: 50 µm. **(B)** Schematic overview summarizing the results of domain mapping analysis (crystal structure OX40 PDB: 2HEV). **(C)** Epitope binning analysis of hOX40-Nbs by BLI. Representative sensograms of combinatorial Nb binding to recombinant hOX40 on sharing/overlapping epitopes or on different epitopes are shown. **(D)** Graphical summary of epitope binning analysis.

However, only weak combinatorial binding was observed for Nbs addressing the same domain, suggesting that O12 and O18, as well as O7 and O19 address identical or at least overlapping epitopes (Figure 3D, Supplementary Figure S4).

hOX40-Nbs bind to activated human T lymphocytes

Having demonstrated that all selected Nbs recognize recombinant and exogenously overexpressed cellular hOX40, we next investigated their specificity for binding to endogenous hOX40 on activated T cells. Therefore, human peripheral blood mononuclear cells (hPBMCs) from three healthy donors (K025, K029 and K034) were either left untreated or incubated for 24 h with phytohaemagglutinin L (PHA-L) as a pan T cell stimulus and interleukin 2 (IL-2) to induce expression of OX40 (49) (Figure 4A). Subsequently, hPBMCs were double-stained with fluorescently labeled hOX40-Nbs, the non-binding PEP-Nb (50) (Nb Ctrl.) or a phycoerythrin (PE)-labeled anti-hOX40 mAb in combination with a T cell-specific anti-CD3 mAb, and the percentage of $OX40^+$ positive T cells ($CD3^+$) was analyzed by flow cytometry (Figure 4C, gating: Supplementary Figure S5A). The obtained data show that all hOX40-Nbs except O7 bound specifically to T cells upon PHA-L-/IL-2 mediated activation, comparable to the anti-hOX40 mAb. Notably, no binding prior to stimulation was observed (Figures 4B, C, Supplementary Figure S5B). Determination of mean fluorescence intensities (MFI) normalized to the negative control (PEP-Nb) revealed differences that reflect the affinities of the Nbs previously determined with BLI (Supplementary Figure S5C). To further investigate the binding of hOX40-Nbs to different T cell subpopulations, we performed flow cytometry analysis of activated hPBMCs with Nbs O12, O18, O19, non-binding PEP-Nb or the anti-hOX40-mAb in combination with antibodies indicative for main T cell populations including anti-CD4, anti-CD8 as well as anti-CD25 and anti-FoxP3 antibodies for the assessment of Tregs (Supplementary Figure S6A). As shown in Figure 4D, the results indicated that the selected hOX40-Nbs bind to OX40 on all three analyzed T cell subpopulations upon activation, comparable to the anti-hOX40 mAb. Furthermore, differences in OX40 expression were found for the various T cell populations and the donors analyzed. While we observed a higher percentage of OX40-expressing cells in non Treg $CD4^+$ T cells and Tregs, lower expression of OX40 on $CD8^+$ T cells was observed for all three tested donors (Figure 4D). In summary, the flow cytometric analysis confirmed the specificity of three of the selected hOX40 Nbs for their antigen and their functionality to bind endogenous hOX40 exclusively on activated T cells.

10.3389/fimmu.2024.1480091

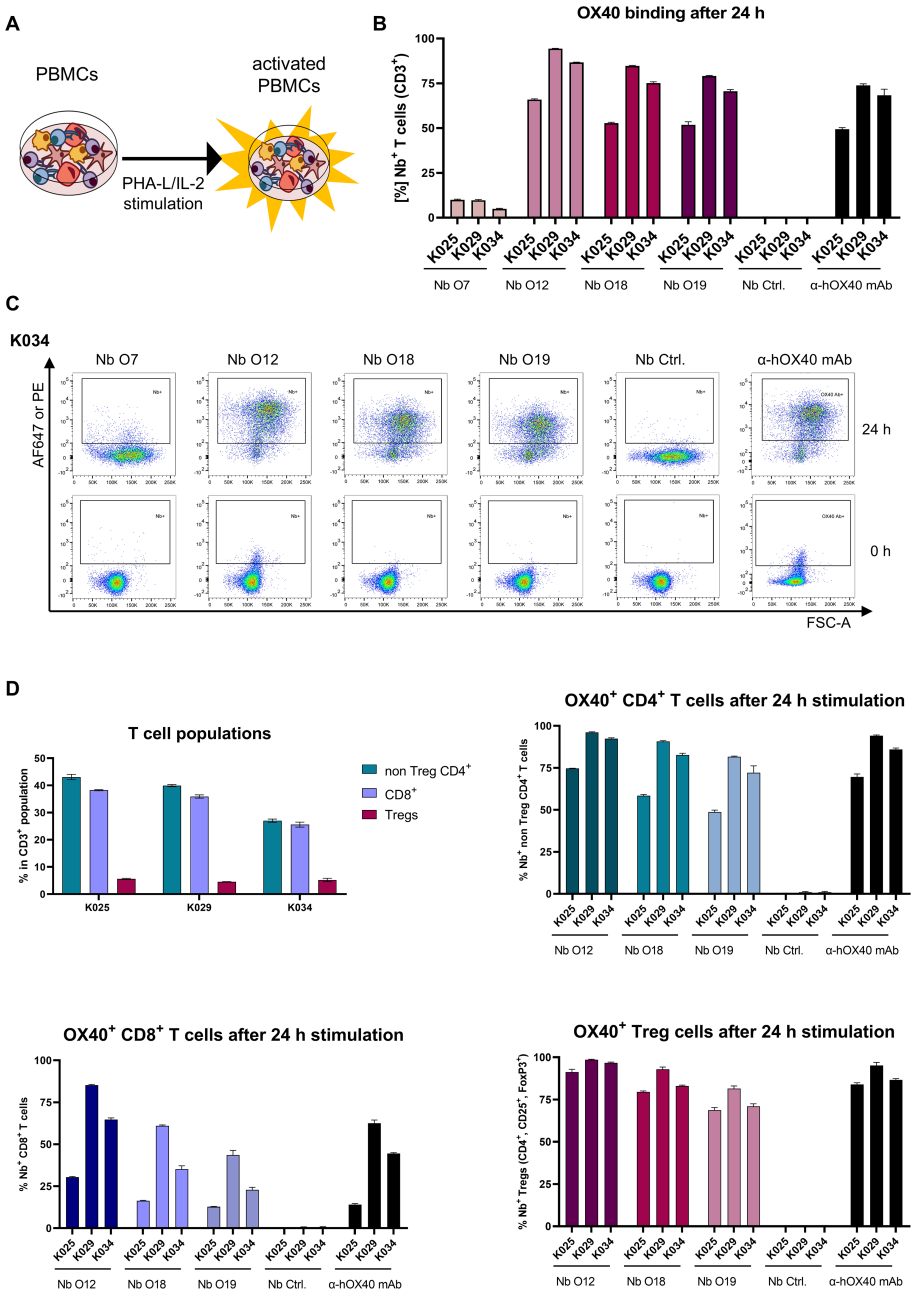

FIGURE 4
Validation of hOX40-Nb binding to activated T cells. **(A)** Schematic outline of activation of human peripheral blood mononuclear cells (hPBMCs) by phytohaemagglutinin L (PHA-L) and IL-2. **(B)** Flow cytometry analysis of hOX40-Nbs staining on $CD3^+$ hPBMCs from three different donors (K025, K029 and K034) after 24 h of PHA-L and IL-2 stimulation shown as bar graph. Data are presented as mean ± SD of three replicate stains. **(C)** Exemplary results of flow cytometry analysis of $CD3^+$ hPBMCs derived from donor K034 stained with AF647-labeled hOX40-Nbs, a non-binding PEP-Nb (Nb. Ctrl.) or a PE-labeled anti-hOX40 mAb before (0 h, lower panel) and after (24 h, upper panel) stimulation. **(D)** Flow cytometry analysis of hOX40-Nb staining on non Treg $CD4^+$, $CD8^+$ and regulatory (Treg) T cells from the three same donors after 24 h of PHA-L and IL-2 stimulation. Bar graphs summarizing the percentages of the different T cell subpopulations for each donor (upper left), Nb binding to non Treg $CD4^+$ T cells (upper right), Nb binding to $CD8^+$ T cells (lower left) and Nb binding to Tregs (lower right) in comparison to non-binding PEP-Nb (Nb. Ctrl.) or a PE-labeled anti-hOX40 mAb. Data are presented as mean ± SD of three replicate stains.

Agonistic and antagonistic effects of Nbs on OX40 signaling

Targeting OX40, can trigger strong immune responses (51). Therefore, we next investigated whether binding of the Nbs exerts agonistic or antagonistic effects on OX40-mediated signaling by using a genetically engineered Jurkat T cell-based bioassay. These effector cells express hOX40 and contain a luciferase reporter driven by a response element downstream of the OX40 signaling axis. Non-stimulated OX40 effector cells exhibited a weak luminescent signal, which was not further enhanced by addition of increasing concentrations of Nbs O12, O18, and O19. However, when using OX40L as positive control, we observed a strong concentration-dependent induction of NF-kB promotor activity, reflected by an

10.3389/fimmu.2024.1480091

increasing luminescence signal, as expected (Figure 5A). Next, we used this assay to analyze a possible competition between OX40L and Nbs for hOX40 binding. Therefore, we preincubated the OX40 effector cells with serial dilutions of Nbs ranging from 0.13 µM to 0.002 nM before adding OX40L at the saturation concentration of 0.12 µM. In this setting, we observed a reduction in luminescence in the presence of Nb O12 and, to a minor extent, of O18, whereas pre-incubation with O19 did not have any effect on OX40L-mediated induction of OX40 signaling (Figure 5B). These results were consistent with a BLI-based competition assay in which we monitored the binding of OX40L to recombinant hOX40 in the presence or absence of Nbs (Supplementary Figure S7). From these findings, we concluded that none of the Nbs augment OX40-mediated signaling. However, O12 and, to a minor degree, O18, which both target domain 1 of hOX40, competed with the binding of the natural ligand OX40L and could therefore potentially exert an antagonistic effect.

Impact of hOX40-Nbs on proliferation and cytokine release of immune cells

To further explore possible effects of hOX40-Nb binding on T cells, we next investigated its influence on proliferation and cytokine release in hPBMCs. Therefore, hPBMCs from three donors (K025, K029 and K034) were labeled with carboxyfluorescein succinimidyl ester (CFSE) followed by induction of hOX40 expression by PHA-L

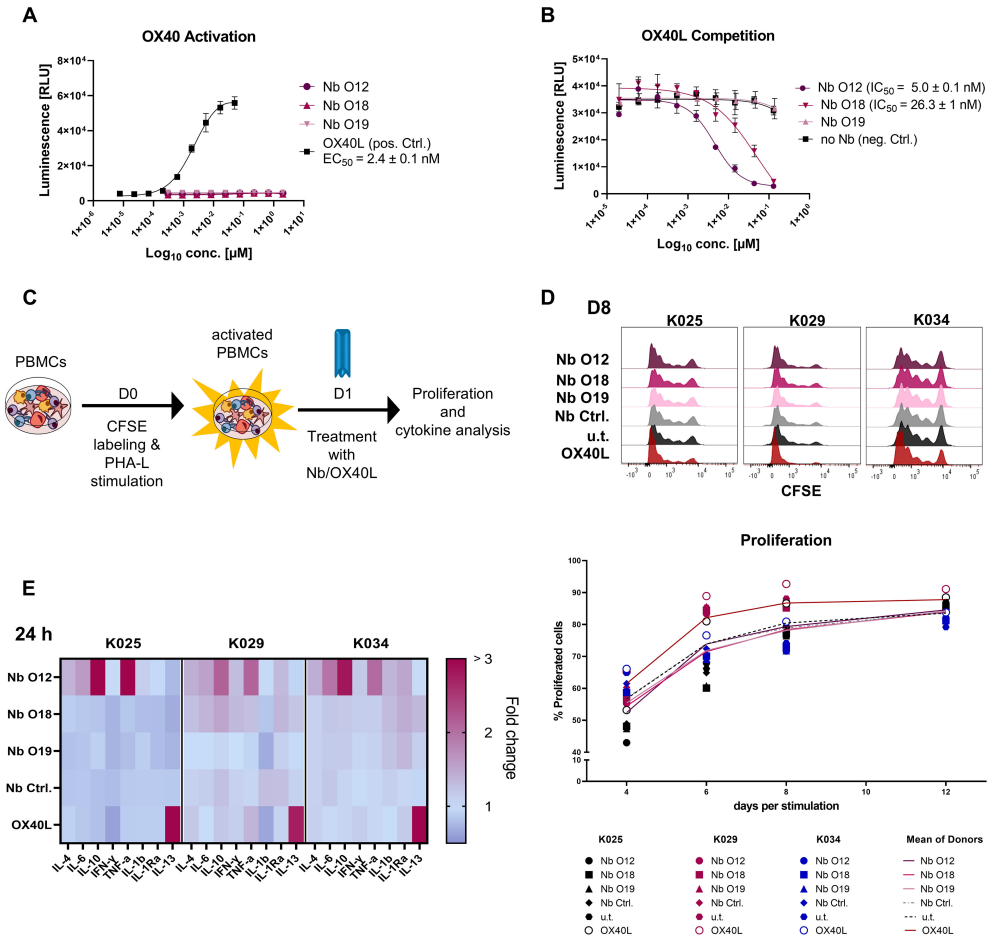

FIGURE 5
Analysis of hOX40-Nbs on OX40 signaling. **(A, B)** Assessment of agonistic or antagonistic activities of hOX40-Nbs on OX40 signaling in a cell-based OX40 bioassay. **(A)** For determining agonistic effects OX40 effector cells were treated for 5 h with serial dilutions of Nbs O12, O18, O19 or OX40L as positive control (pos. Ctrl.) followed by luminescence detection. Data are shown as a three-parameter logistic regression dose-response curve based on the mean ± SD of three replicates (n = 3), with EC_{50} value of ~ 2.4 nM for OX40L. **(B)** For analysis of a potential OX40L competition, OX40 effector cells were preincubated with serial dilutions of Nbs ranging from 0.13 µM to 0.002 nM before adding OX40L at the saturation concentration of 0.12 µM followed by luminescence detection. Three-parameter logistic regression dose-response curves based on the mean ± SD of three replicates showed an antagonistic effect of Nb O12 and O18 with IC_{50} values of ~ 5.0 nM or 26.3 nM, respectively. **(C)** Schematic workflow for testing the impact of Nbs on T cell proliferation and cytokine release. hPBMCs of three donors (K025, K029, K034) were CFSE-labeled and stimulated with PHA-L/IL-2. After 24 h, hPBMCs were treated with 0.5 µM hOX40-Nbs, non-binding PEP-Nb (Nb Ctrl.), OX40L or left untreated (u.t.). Proliferation at days 4, 6, 8 and 12 after stimulation and cytokine release after 24, 72 and 168 hours of Nb treatment were monitored. **(D)** Proliferation was analyzed by flow cytometry (CFSE-low/negative fraction), exemplary shown for day 8 (D8, upper panel). Mean percentages of all three donors are shown as plain or dotted lines (lower panel). **(E)** Determination of cytokines secreted after treatment with hOX40-Nbs displayed as a heat map, exemplary shown for 24 hours (24 h) after Nb treatment. Values are shown as fold change compared to the untreated control based on the mean of three technical replicates.

and IL-2 stimulation for 24 h. After confirming successful activation and hOX40 expression by flow cytometry (Supplementary Figures S8A, B), hPBMCs were either left untreated or incubated with Nbs O12, O18, O19 or the non-binding PEP-Nb as a negative control (each 0.5 µM). For targeted hOX40 stimulation 0.5 µM OX40L was used (Figure 5C). Cell proliferation was monitored on days 4, 6, 8 and 12 by flow cytometry (Figure 5D). The results revealed similar proliferation profiles in the hPBMC samples from the same donor upon Nb treatment compared to the untreated samples, while treatment with OX40L induced a ~10% increase at day 6 and 8 in proliferation (Figure 5D, Supplementary Figures S8C, D). In addition, we investigated effects of hOX40-Nbs on the release of cytokines. Therefore, we determined the concentration of a panel of pro- and anti-inflammatory cytokines (Supplementary Table S2) in the supernatant of samples collected after 24, 72 and 168 hours post Nb treatment using a previously reported microsphere-based sandwich immunoassay (16). While Nb O18 and O19 showed only minor effects on cytokine release compared to the untreated control or samples incubated with a non-binding PEP-Nb, a significant increase of the NFκ-driven cytokines TNF and IL-6 and of the Th2 cytokines IL-4, and IL-10 upon treatment with O12 was observed. Interestingly, the cytokine release of O12-treated samples differed from samples treated with OX40L, in which only elevated levels of IL-13 were observed (Figure 5E, Supplementary Figure S9).

hOX40-Nb for *in vivo* imaging

For *in vivo* OI, we chose the fluorescently-labeled Nb O18 ($O18_{AF647}$) as it showed the strongest binding to cellular exposed hOX40 with only minor blocking effect on OX40L and did not modulate T cell function or cytokine expression. CD1 nude mice with subcutaneous HT1080-hOX40 or HT1080-WT tumors were intravenously (*i.v.*) injected with 5 µg of $O18_{AF647}$ and non-invasively *in vivo* investigated by OI over 6 h. The signal intensity (SI) of $O18_{AF647}$ in both the HT1080-hOX40 and the HT1080-WT tumors peaked within 5 min after injection. While the SI continuously decreased over time in the HT1080-WT tumors, it remained stable in the HT1080-hOX40 tumors between 3 h and 6 h post injection, indicating target-specific accumulation after the initial clearing phase of $O18_{AF647}$. Importantly, we determined an increased $O18_{AF647}$-related SI in the HT1080-hOX40 tumors compared to HT1080-WT tumors at all imaging time points with the greatest difference 6 h post injections of ~7-fold (Figures 6A, B). Finally, mice were sacrificed, and the presence of $O18_{AF647}$ within the explanted tumors was analyzed by *ex vivo* OI. Consistent with the *in vivo* data, HT1080-hOX40 tumors exhibited a significantly higher uptake (SI) when compared to HT1080-WT control tumors, indicating a specific binding of the Nb O18 to its target antigen and a favorable signal-to-background ratio for this Nb-derived immunoprobe (Figure 6C). These findings demonstrated a specific binding for $O18_{AF647}$ *in vivo*, highlighting its potential as a promising tool for noninvasive monitoring of OX40 expression in immune diagnostics.

Discussion

hOX40 is a recognized theranostic marker that is relevant for both diagnostic and therapeutic applications in the emerging field of immunotherapies (52). On tumor infiltrating T cells, expression of hOX40 correlates with a beneficial outcome and overall survival

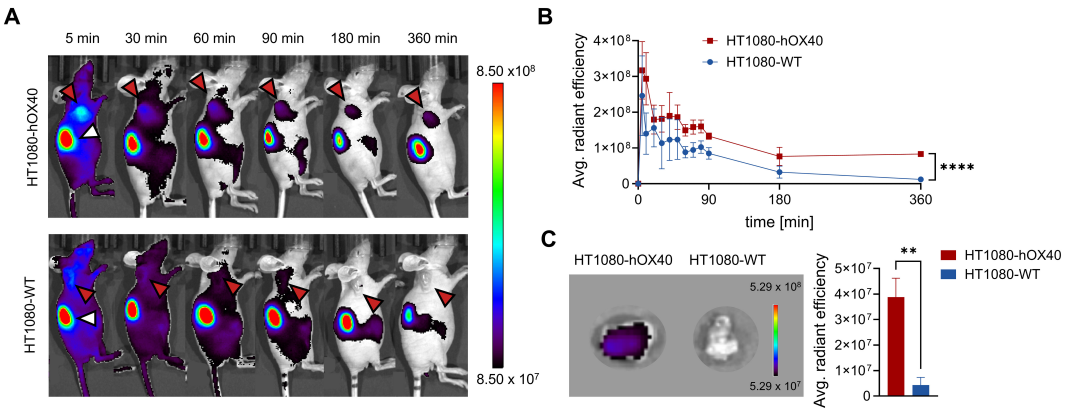

FIGURE 6
In vivo optical imaging (OI) with $O18_{AF647}$ in HT1080-hOX40 and HT1080-WT tumor bearing mice. 5 µg of $O18_{AF647}$ were administered intravenously (i.v.) to CD1 nude mice which previously were subcutaneously injected with human HT1080-hOX40 or HT1080-WT cells at the right upper flank for tumor formation. Tumor biodistribution of $O18_{AF647}$ was monitored by repetitive OI measurements over the course of 6 h. **(A)** Acquired images of different measurement time points of one representative $O18_{AF647}$-injected mouse with HT1080-hOX40 tumor (top) or HT1080-WT tumor (bottom, control). Red arrows indicate the tumor localization at the right upper flank. The kidney is marked with a white arrow at the 5 min time point. **(B)** Quantification of the fluorescence signal from the tumors (n = 3 per group, arithmetic mean of the average radiant efficiency ± SD, unpaired t test, corrected for multiple comparisons using the Holm-Sidak method revealing a significance of p = 0,00004 indicated by ****) determined at indicated time points. **(C)** Representative *ex vivo* OI of harvested tumor (left) and organ quantification of $O18_{AF647}$ in HT1080-hOX40 and HT1080-WT tumors. After the last imaging time point, tumors were harvested for *ex vivo* OI, confirming significantly increased accumulation of $O18_{AF647}$ in HT1080-hOX40 tumors (n = 3 per group, arithmetic mean ± SD; unpaired t test revealing a significance of p = 0,0017 indicated by **). Data are shown as individual and mean value of three technical replicates. $p < 0.05$ was considered statistically significant (*) and marked as ** for $p < 0.01$ and **** for $p < 0.0001$.

of patients with solid tumors such as colorectal cancer, cutaneous melanoma, non-small cell lung cancer and ovarian cancer (53–57). In the context of IMIDs such as rheumatoid arthritis, systemic lupus erythematosus or ulcerative colitis, increased expression of hOX40 often correlates with disease activity and severity (51, 58). Building on this potential, anti-OX40-specific mAbs were developed to monitor OX40 expression on activated T cells in preclinical mouse models and used in noninvasive medical imaging of OX40 in cancer vaccination (38), T cell response to glioblastoma (39), acute graft-versus-host disease (40), and rheumatoid arthritis (41).

Due to their unique properties, including specific binding, rapid and deep tissue penetration, short systemic half-life and low immunogenicity, Nbs have emerged as promising building blocks for the development of next-generation imaging probes (46) evidenced by an increasing number of preclinical and first in-human clinical trials (59–62). Here, we developed the first hOX40-specific Nbs as novel probes to specifically address activated T cells. As we focused on developing these binders as potential *in vivo* imaging probes, we aimed for Nbs that have minimal to no effects on OX40 signaling. In total, we identified four hOX40-Nbs with high binding affinity and long-term stability. Epitope mapping categorized the Nbs into two groups addressing either domain 1 or domain 3 of hOX40. However, a precise molecular insight into the recognized structural epitopes remains to be investigated. A more detailed analysis, e.g. by hydrogen-deuterium exchange mass spectrometry (HDX-MS), as already described for other Nbs (16, 19, 63), could facilitate the identification of Nbs that can be used for combinatorial binding, e.g., with OX40 antibodies currently in therapeutic development (64, 65). Three of the selected hOX40-Nbs (O12, O18 and O19) specifically bound to physiologically expressed hOX40 on the surface of activated T cells. A detailed analysis of the main T cell subpopulations further revealed comparable Nb binding to OX40 when expressed on activated $CD8^+$, non Treg $CD4^+$ and also Treg $CD4^+$ T cells. Regarding the surveillance of activated T cells that infiltrate the tumor after immunotherapy, for example, binding to OX40 on activated Tregs could be considered a potential limitation, since not only anti-tumor effector T cells are visualized by hOX40-Nb. However, the specific binding of the hOX40-Nbs demonstrates the potential to provide a comprehensive picture of the activation status of T cells in the TME.

In vitro assessment of potential biological effects revealed that none of the selected hOX40 Nbs triggered OX40 signaling, while binding of O12 and to a lesser extent O18, both targeting domain 1 of hOX40, seems to compete with the natural ligand OX40L. Interestingly, although no agonistic effect was observed, treatment with O12 resulted in an increased release of NFκB induced cytokines and Th2 cytokines, which may be caused by a cross-reactivity of this Nb with other members of the tumor necrosis factor receptor superfamily (TNFRSF) or induction of an immune response by an unknown mechanism. For *in vivo* imaging applications, we chose Nb O18 as a lead candidate due to its strong affinity for recombinant and cellularly-exposed hOX40. Bearing in mind that only very small amounts of tracer are needed for imaging, we considered the observed weak competition with OX40L to be acceptable especially since binding of O18 showed no obvious effects on proliferation and cytokine release of T cells. Apparently, site-directed functionalization employing C-terminal sortagging and DBCO-mediated click chemical conjugation to AF647 (16, 66) did not affect its binding properties. OI of HT1080-hOX40 tumors in a mouse xenograft model designed as the first *in vivo* "proof-of-concept" analysis, showed rapid target-specific accumulation of fluorescently labeled O18 on antigen-expressing cells and sustained binding over a prolonged period indicating a high *in vivo* binding functionality with a low off-rate. Even though demonstrated in a rather artificial model, which at this stage does not yet provide information on the visualization of activated T cells or their dynamic distribution within the TME, we envisage that O18 has the potential to be further developed into a radiolabeled immunoprobe for non-invasive monitoring of OX40 expression in immunodiagnostics.

In summary, several probes for visualizing T cell activation markers have been developed to date, including imaging probes based on peptides that bind granzyme B (24), mAbs against ICOS (22), IFN-γ (67), murine OX40 (38), or a CD69 antibody as an early phenotypic activation marker (23, 68). Perspectively, diagnostic imaging using these probes can support therapy monitoring and patient selection for personalized immunotherapies such as immune checkpoint inhibitor therapies, where a high number of activated T cells within the TME is advantageous. Our first hOX40-specific Nbs described here now expand this list. Because of their high binding functionality, their unique properties in terms of tissue penetration and their improved signal-to-noise ratio without unwanted modulation of OX40 signaling, we expect that our hOX40-Nbs, once further engineered e.g. with suitable radionuclides, will facilitate the visualization of even small amounts of activated $OX40^+$ T cells. Due to beneficial pharmacokinetics, it is conceivable that these Nbs further will enable earlier imaging timepoints and therefore, the usage of shorter-lived isotopes, e.g., ^{18}F, thereby reducing patients' radiation exposure and allowing more longitudinal imaging to assess dynamic changes in the T cell composition within the TME, IME and the lymphatic organs. In perspective, the hOX40-Nbs can not only be used to detect activated T cells in cancer lesions, but also for the applications in the diagnosis of IMIDs like rheumatoid arthritis (41) or graft-versus-host disease (40).

Materials and methods

Expression constructs

hOX40-encoding DNA (GenBank accession: NM_003327.3) was synthesized and cloned into NheI and EcoRI site of pcDNA3.1(+) by GenScript Biotech. The vector backbone was changed by cutting with the restriction enzymes EcoRI and BstBI into a backbone comprising an internal ribosomal entry site (IRES) and genes for eGFP as reporter and Blasticidin S deaminase for antibiotics resistance from the expression construct as described previously (16). For the generation of hOX40 domain deletion mutant expression constructs hOX40ΔD1 (aa 66-277), hOX40ΔD1-2 (aa 108-277), hOX40ΔD1-3 (aa 127-277) of UniProtKB P43489, respective fragments were amplified (Supplementary Table S3) and genetically fused N-terminally to a SPOT-Tag (69). DNA encoding

for murine OX40 (mOX40) was purchased from Sino Biological (Catalog Number MG50808-NM).

Stable cell line generation and culturing

U2OS cells (ATCC) were cultured according to standard protocols in Dulbecco's modified Eagle's medium (DMEM), supplemented with 10% (v/v) FCS and 1% (v/v) penicillin/streptomycin (all Thermo Fisher Scientific). Cultivation conditions were 37°C and 5% CO_2 atmosphere in a humidified incubator and passaged using 0.05% trypsin-EDTA (Thermo Fisher Scientific). Transfection of plasmid DNA (0.8 µg per 24 well plate well) was performed using Lipofectamine 2000 (Thermo Fisher Scientific) according to the manufacturer's protocol. To generate U2OS cells stably overexpressing hOX40 on their surface (U2OS-hOX40), 24 h after transfection, selection pressure by 5 µg/mL Blasticidine S (Sigma Aldrich) was applied for a period of two weeks. After single cell separation, monoclonal cells were analyzed for hOX40 expression using live-cell fluorescence microscopy.

Animal immunization and hOX40-Nb library generation

The alpaca immunization was performed with the approval of the Government of Upper Bavaria (approval number: 55.2-1-54-2532.0-80-14). Two alpacas (*Vicugna pacos*) were immunized using the extracellular part of recombinant hOX40 (hOX40 AA Leu 29 – Ala 216) produced in human HEK293 cells (Acrobiosystems). During a period of 91 days, the animals were vaccinated six times at day 0, 21, 28, 35, 49, 87. The initial vaccination was performed with 560 µg followed by five booster injections each consisting of 280 µg hOX40 with Adjuvant F (Gebru). After the 91-day period, lymphocytes were isolated from ~200 mL of blood performing Ficoll gradient centrifugation with lymphocyte separation medium (Carl Roth) and total RNA was extracted by NucleoSpin® RNA II (Macherey&Nagel). The mRNA was subsequently transcribed into cDNA by the First Strand cDNA Synthesis Kit (GE Healthcare). The Nb repertoire was isolated as described in three subsequent PCR reactions using the following primer combinations: (1) CALL001 and CALL002, (2) forward primers FR1-1, FR1-2, FR1-3, FR1-4, and reverse primer CALL002, and (3) forward primers FR1-ext1 and FR1-ext2 and reverse primers FR4-1, FR4-2, FR4-3, FR4-4, FR4-5, and FR4-6 introducing SfiI and NotI restriction sites (16) (Supplementary Table S3). This enables subcloning of Nb library into the pHEN4 phagemid vector (70).

Nb screening

The selection of hOX40-specific Nbs was performed by two consecutive rounds of phage display against immobilized recombinant antigen. For this purpose, electrocompetent TG1 *E. coli* bacteria were transformed with the hOX40-Nb library in pHEN4 and infected with M13K07 helper phages leading to the generation of hOX40-Nb presenting phages. 1 x 10^{11} phages were enriched by adsorption to streptavidin or neutravidin plates (Thermo Fisher Scientific) coated with hOX40 (5 µg/mL), biotinylated by Sulfo-NHS-LC-LC-Biotin (Thermo Fisher Scientific) in 5 molar excess at ambient temperature for 30 min and purified using Zeba™ Spin Desalting Columns 7 K MWCo 0.5 mL (Thermo Fisher Scientific) according to manufacturer's protocol. Antigen and phage blocking was performed with 5% milk in PBS-T during the first round or BSA in the second. Washing stringency was increased with each panning round and elution of bound phages was performed by 100 mM triethylamine pH 10 (TEA, Roth), followed by neutralization with 1 M Tris/HCl pH 7.4. For phage rescue, TG1 bacteria were infected with the eluted phages during their exponential growth phase, spread on selection plates for subsequent selection rounds and incubated at 37°C overnight. Enrichment of antigen-specific phages was monitored by counting colony forming units (CFUs).

Whole-cell phage ELISA

Monoclonal phage ELISA was executed in a whole cell setting. Individual clones were picked, and phage production was induced as described above. For antigen presentation U2OS-hOX40 cells or wild type (wt) U2OS for background determination were seeded in a density of 2 × 10^4 cells per well in 100 µL in 96-well cell culture plates (Corning) coated with poly-L-lysine (Sigma Aldrich) and grown overnight. The next day, 70 µL of phage supernatant was added to each cell type and incubated at 4°C for 3 h. Cells were washed 5 × with 5% FCS in PBS, followed by incubation with M13-HRP-labeled detection antibody (Progen, 1:2000 Dilution) for 1 h and washed again 3 × with 5% FCS in PBS. For the final detection, Onestep ultra TMB 32048 ELISA substrate (Thermo Fisher Scientific) was added to each well and incubated until the color changed. The reaction was stopped with 100 µL of 1 M H_2SO_4 and the signal was detected with the Pherastar plate reader at 450 nm. Phage ELISA-positive clones were defined by a 2-fold signal above U2OS-WT control cells.

Protein expression and purification

For production, hOX40-Nbs were cloned into pHEN6 vector (70), expressed in XL-1 and purified using immobilized metal affinity chromatography (IMAC) and size exclusion chromatography according to standard procedures as previously described (16). Sortase A pentamutant (eSrtA) in pET29 was a gift from David Liu (Addgene plasmid # 75144) and expressed and purified as published (71). The quality of all purified proteins was analyzed via standard SDS-PAGE under denaturizing and reducing conditions (5 min, 95°C in 2x SDS-sample buffer containing 100 mM Tris/HCl, pH 6.8; 2% (w/v) SDS; 5% (v/v) 2-mercaptoethanol, 10% (v/v) glycerol, 0.02% bromphenole blue). Proteins were visualized by InstantBlue Coomassie (Expedeon) staining or alternatively by immunoblotting transferring proteins to nitrocellulose membrane (GE Healthcare, Chicago, IL, USA) and

detection using a primary anti-Penta-His antibody (Qiagen) and secondary donkey anti-mouse AF647 antibody (Invitrogen) on a Typhoon Trio scanner (GE-Healthcare, excitation 633 nm, emission filter settings 670 nm BP30).

Biolayer interferometry

The binding kinetics analysis of hOX40-Nbs was performed using the Octet RED96e system (Sartorius) applying manufacturer's recommendations. Therefore, 5 µg/mL of biotinylated hOX40-Nbs diluted in Octet buffer (PBS, 0.1% BSA, 0.02% Tween20) were immobilized on streptavidin coated biosensor tips (SA, Sartorius) for 30 s and unbound Nb was washed away. For the association step, a dilution series of hOX40 ranging from 0.2 nM – 320 nM were applied for 300 s followed by dissociation in Octet buffer for 720 s. Each concentration was normalized to a reference applying Octet buffer only for association. Data were analyzed using the Octet Data Analysis HT 12.0 software applying the 1:1 ligand-binding model and global fitting. For epitope binning 5 µg/mL of each Nb, except O7 due to its inappropriate dissociation behavior, was immobilized to SA tips and the association was performed with a premixture of OX40 (100 nM) and an excess of unbiotinylated second Nb (1000 nM). By analyzing the binding behavior of the premixture, conclusions about shared epitopes were drawn. To determine a potential competition of Nbs with the natural OX40 ligand OX40L, OX40L was biotinylated and 10 µg/mL were immobilized to the SA tips. Premixture of hOX40 with a ten-time molar excess of each Nb was applied for the association step.

Live-cell immunofluorescence

U2OS-hOX40 cells, U2OS-WT or U2OS cells transiently expressing hOX40 domain deletion mutants or murine OX40 were plated at a density of 1 x 10^4 cells per well in 100 µL of a µClear 96-well plate (Greiner Bio One, cat. #655090) and cultivated overnight at standard conditions. The next day, cells were stained with 2 µg/mL Hoechst33258 (Sigma Aldrich) for nuclear staining in live-cell visualization medium DMEMgfp-2 (Evrogen, cat. #MC102) supplemented with 10% FCS for 30 min at 37°C. Afterwards 10 -1000 nM fluorescently labeled hOX40-Nbs, a non-binding PEP-Nb (Nb Ctrl.) or an OX40 antibody (positive control) were added and incubated for 30 min at 4°C. Staining solution was replaced by live-cell visualization medium DMEMgfp-2 with 10% FCS and images were acquired with a MetaXpress Micro XL system (Molecular Devices) at 20 x magnification.

Affinity determination by flow cytometry

For cell-based affinity determination, U2OS-hOX40 cells were detached using enzyme-free cell dissociation buffer (Gibco) and resuspended in FACS buffer (PBS containing 0.02% sodium azide, 2 mM EDTA, 2% FBS). For each staining condition, 200,000 cells were incubated with suitable dilution series (O12 and O18: starting from 2.5 µM; O7 and O19 starting from 10 µM) of AF647-labeled hOX40-Nbs at 4°C for 30 min. After two washing steps, samples were resuspended in 200 µL FACS buffer and analyzed on the same day using a LSRFortessa™ flow cytometer (Becton Dickinson) equipped with the DIVA Software (Becton Dickinson). Final data analysis was performed using the FlowJo10® software (Becton Dickinson).

Stability analysis

To assess the thermal stability of the Nbs, nanoscale differential scanning fluorimetry (nanoDSF) with the Prometheus NT.48 device (Nanotemper) was performed. Freshly thawed hOX40-Nbs were diluted to 0.25 mg/mL in PBS and measured at time point d0 and after an incubation period of ten days at 37°C (d10) using standard capillaries. A thermal gradient ramping from 20°C to 95°C was applied while measuring fluorescence ratios (F350/F330) and light scattering. Using PR. ThermControl v2.0.4 the melting (T_M) and aggregation (T_{Agg}) temperatures were determined.

Fluorescent labeling of nanobodies

For sortase A based coupling of 50 µM Nb were added to 250 µM sortase peptide (H-Gly-Gly-Gly-propyl-azide synthesized by Intavis AG) and 10 µM sortase A both dissolved in sortase buffer (50 mM Tris, and 150 mM NaCl, pH 7.4 at 4°C) and reaction was started by adding 10 mM $CaCl_2$ for 4 h at 4°C. To avoid reverse sortase reaction, sortase A and uncoupled Nb were removed by Ni-NTA affinity chromatography. The coupled Nbs were concentrated and residual peptide was depleted using Amicon ultra-centrifugal filters MWCO 3 kDa. Taking advantage of SPAAC (strain-promoted azide-alkyne cycloaddition) click chemistry reaction fluorescent labeling was performed by incubating azide-coupled Nbs with 2-fold molar excess of DBCO-AF647 (Jena Bioscience) for 2 h at room temperature. Subsequent dialysis (GeBAflex-tube, 6-8 kDa, Scienova) led to removal of excess of DBCO-AF647. As final polishing step a hydrophobic interaction chromatography (HIC, HiTrap Butyl-S FF, Cytiva) was performed to deplete unlabeled Nb. The final products were analyzed via SDS-PAGE and spectrophotometry.

OX40 bioassay

The OX40 bioassay kit (Promega) was used to determine a potential agonistic activity of Nbs O12, O18 and O19 according to manufacturer´s instructions. On the day before assay, thaw-and-use OX40 effector cells (Promega) were thawed and seeded into the inner 60 wells of two white 96 well assay plates cultured in assay buffer (RPMI1640 with 5% FBS) at standard conditions overnight. The next day OX40L and Nbs were serially diluted (OX40L: 50 – 0.0008 nM; Nbs: 2000-0.3 nM) in assay buffer, and 20 µL of the diluted recombinant proteins were added to the assay plate. The assay plate was incubated at 37°C, 5% CO_2 for 5 h. Afterwards, the assay plate was equilibrated to ambient temperature for 10 min. For

detection of agonistic function, 75 µL of Bio-GloReagent was added to all wells. The assay plate was incubated at room temperature for 5 min, and luminescence was measured using a Tecan M2000 plate reader. The average relative luminescence unit (RLU) was calculated for each dilution. The average RLU data were plotted against the different concentrations of OX40L and hOX40-Nbs Nbs. To test antagonistic properties of the Nbs, the OX40 bioassay was transformed into a competition assay. For this purpose, the cells were pre-incubated with a serial dilution of hOX40-Nbs (0.13 µM to 0.002 nM) for one hour, followed by a 5 h incubation period with 0.12 µM OX40L. All experiments were performed in three independent replicates.

Peripheral blood mononuclear cells isolation and start of culture

Human peripheral blood mononuclear cells (hPBMCs) were isolated as described in (16). In brief, fresh mononuclear blood cell concentrates were obtained from healthy volunteers at the ZKT Tübingen gGmbH. Participants gave informed written consent and the studies were approved by the ethical review committee of the University of Tübingen, projects 156/2012BO1 and 713/2018BO2. Blood products were diluted with PBS 1x (homemade from 10x stock solution, Lonza, Switzerland) and PBMCs were isolated by density gradient centrifugation with Biocoll separation solution (Biochrom, Germany). PBMCs were washed twice with PBS 1x, counted with a NC-250 cell counter (Chemometec, Denmark), resuspended in heat-inactivated (h.i.) fetal bovine serum (FBS) (Capricorn Scientific, Germany) containing 10% DMSO (Merck) and frozen in aliquots using a freezing container before transfer to nitrogen for long term storage. For the experiments, cells were thawed in Iscove´s Modified Dulbecco´s Medium (IMDM + L-Glutamin + 25 mM HEPES; Thermo Fisher Scientific) supplemented with 2.5% h.i. FBS (Thermo Fisher Scientific), 1% P/S (Sigma-Aldrich), and 50 µM β-mercaptoethanol (β-ME; Merck), washed once, counted, and rested for 1 h at 37°C 5% CO_2 in T cell medium (TCM, IMDM + 2% h.i. FBS + 1x P/S + 50 µM β-ME) supplemented with 1 µg/mL DNase I (Sigma-Aldrich). After resting, cells were washed once again, counted and used for subsequent analysis.

Validation of hOX40-Nb binding to activated T cells

For the validation of Nb binding to activated T cells, hPBMCs were stained before and after stimulation for 24 h with 5 µg/mL PHA-L and 50 U/mL IL-2 in TCM at 37°C 5% CO_2. For flow cytometry analysis $2x10^5$ cells per staining condition in FACS buffer (PBS containing 0.02% sodium azide, 2 mM EDTA, 2% h.i. FBS) were used. Extracellular staining was performed with AF647-labeled hOX40-Nbs or the non-binding PEP-Nb [Nb Ctrl (50)] (each 200 nM), phycoerythrin (PE)-labeled anti-hOX40 mAb (Ber-Act35, BioLegend), CD3 Ab APC-Cy7 (HIT3a, BioLegend), dead cell marker Zombie Violet (BioLegend) and isotype control Abs (BioLegend) each in pretested optimal concentrations by incubation for 30 min at 4°C. Cells were washed twice with FACS buffer and acquired on the same day using a LSRFortessa™ flow cytometer (Becton Dickinson) equipped with the DIVA Software (Becton Dickinson). Final data analysis was performed using the FlowJo10® software (Becton Dickinson). Geometric mean fluorescence intensity (MFI) for the four Nbs was determined using the FlowJo10® software (Becton Dickinson) and normalized to the non-binding PEP-Nb control.

hOX40-Nb binding to distinct T cell populations

To assess Nb binding to T cell subpopulations, hPBMCs were stained after stimulation for 24 h with 5 µg/mL PHA-L and 50 U/mL IL-2 in TCM at 37°C 5% CO_2. For flow cytometry analysis, $4x10^5$ cells per staining condition in FACS buffer were used. Extracellular staining was performed with AF647-labeled hOX40-Nbs or the non-binding PEP-Nb [Nb Ctrl (50)] (each 400 nM), phycoerythrin (PE)-labeled anti-hOX40 mAb (Ber-Act35, BioLegend), CD3 Ab PE-Cy5.5 (SK7, eBioscience), CD4 Ab APC-Cy7 (RPA-T4, BD), CD8 Ab BV605 (RPA-T8, BioLegend), CD25 Ab or isotype control PE-Cy7 (BC96 or MOPC-21, BioLegend), dead cell marker Zombie aqua (BioLegend) each at pretested optimal concentrations by incubation for 20 min at 4°C and washed. Afterwards, cells were fixed and permeabilized (Intracellular Fixation & Permeabilization Buffer Set, eBioscience) and intracellular staining with anti-FoxP3 Ab FITC or isotype control Ab (PCH101 or eBR2a, respectively, both from eBioscience) was performed according to the manufacturer´s instructions for 20 min at RT. Cells were washed twice with permeabilization buffer, resuspended in FACS buffer and acquired on the same day using a LSRFortessa™ flow cytometer (Becton Dickinson) equipped with the DIVA Software (Becton Dickinson). Final data analysis was performed using the FlowJo10® software (Becton Dickinson).

T cell proliferation assay

The proliferation behavior of T cells was assessed using a carboxyfluorescein succinimidyl ester (CFSE) based approach. Up to $1×10^8$ cells were labeled with 2.5 µM CFSE (BioLegend) in 1 ml PBS for 20 min according to the manufacturer's protocol. The cells were washed twice in medium containing 10% h.i. FBS to stop CFSE labeling and stimulated for 24 h with 5 µg/mL PHA-L in TCM at 37°C 5% CO_2 in a 48-well cell culture plate with $1.6–2.5×10^6$ cells/well. Induced OX40 expression was validated via flow cytometry. Subsequent to the stimulation, hPBMCs were treated with 0.5 µM of OX40 specific Nbs O12, O18 and O19, a non-binding PEP-Nb (Ctrl. Nb), OX40L or left untreated and cultured at 37°C and 5% CO_2. Concentrations were chosen in a large excess than the expected concentration during clinical application. On days 3, 5 and 7, 2 ng/mL recombinant human IL-2 (R&D, USA) were added. One-third of the culture on day 4, one half of the culture on days 6 and 8, and

the remaining cells on day 12 were harvested and counted. Cells from each condition were washed twice with FACS buffer (PBS containing 0.02% sodium azide, 2 mM EDTA, 5% h.i. FBS). Extracellular staining was performed with CD3 Ab APC-Cy7 (HIT3a, BioLegend), dead cell marker Zombie Violet (BioLegend) and isotype control Abs (BioLegend) each in pretested optimal concentrations by incubation for 30 min at 4°C. Cells were washed two times with FACS buffer and acquired on the same day using a LSRFortessaTM flow cytometer (Becton Dickinson) equipped with the DIVA Software (Becton Dickinson). Final data analysis was performed using the FlowJo10® software (Becton Dickinson). The percentage of proliferating T cells was determined by assessment of CFSE negative cells.

Cytokine release assay

For cytokine release analysis, a set of in-house developed Luminex-based sandwich immunoassays was used. Supernatants after 24, 72 and 168 hours post Nb treatment of the proliferation assay were frozen at -80°C until cytokine measurements. Levels of IL-1b, IL-1Rα, IL-4, IL-6, IL-8, IL-10, IL-12p70, IL-13, granulocyte-macrophage colony-stimulating factor (GM-CSF), IFN-γ, macrophage chemotactic protein (MCP)-1, macrophage inflammatory protein (MIP)-1b, TNFα, and vascular endothelial growth factor (VEGF) were determined using a those immunoassays each consisting of commercially available capture and detection antibodies and calibrator proteins. All assays were thoroughly validated ahead of the study with respect to accuracy, precision, parallelism, robustness, specificity, and sensitivity (72, 73). Samples were diluted at least 1:4 or higher. After incubation of the prediluted samples or calibrator protein with the capture coated microspheres, beads were washed and incubated with biotinylated detection antibodies. Streptavidin-phycoerythrin was added after an additional washing step for visualization. For control purposes, calibrators and quality control samples were included on each microtiter plate. All measurements were performed on a Luminex FlexMap® 3D analyzer system using Luminex xPONENT® 4.2 software (Luminex, USA). For data analysis, MasterPlex QT, version 5.0, was employed. Standard curve and quality control samples were evaluated according to internal criteria adapted to the Westgard Rules (74) to ensure proper assay performance.

hOX40-Nbs for *in vivo* optical imaging

For optical *in vivo* imaging, we labeled the Nb O18 with the fluorophore AlexaFluor647 ($O18_{AF647}$) by sortase-mediated attachment of an azide group followed by click-chemistry addition of DBCO-AF647. To establish $hOX40^+$ expressing tumors, 5 x 10^6 HT1080 cells stably expressing human OX40 (HT1080-hOX40) or 5 x 10^6 wild type HT1080 (HT1080-WT) cells serving as negative control were resuspended in 50% Matrigel (BD) and 50% PBS and subcutaneously injected into the right upper flank of 7-week-old CD1 nude mice (Charles River Laboratories). When the tumors reached a size of 50 - 100 mm^3, HT1080-hOX40 (n=3) or HT1080-WT (n=3) bearing mice were *i.v.* injected with 5 µg of Nb $O18_{AF647}$ and noninvasively *in vivo* investigated by optical imaging (OI). For the *in vivo* measurements, the mice were anaesthetized with 1.5% isoflurane and the body temperature was kept constant at 37°C using a heating mat. The mice were imaged over the course of 6 h and were sacrificed after the last imaging time point before tumors were explanted for *ex vivo* OI analysis. A bright field image and an image of the fluorescence signal (excitation 640 nm/emission 680 nm) were recorded using an IVIS Spectrum OI System (PerkinElmer, Waltham, MA, USA). The fluorescence intensities were quantified by drawing regions of interest around the tumor borders and were expressed as average radiant efficiency (photons/s)/(µW/cm^2) subtracted by the background fluorescence signal using the Living Image software 4.4 (Perkin Elmer). Statistical analyses using an unpaired t-test, corrected for multiple comparisons using the Holm-Sidak method, were conducted with graph pad prism, Version 10. All mouse experiments were performed according to the German Animal Protection Law and were approved by the local authorities (Regierungspräsidium Tübingen).

Data availability statement

The original contributions presented in the study are included in the article/Supplementary Material. Further inquiries can be directed to the corresponding author.

Ethics statement

The studies involving human samples were approved by the ethical review committee of the University of Tübingen, projects 156/2012BO1 and 713/2018BO2, Participants gave informed written consent. The studies were conducted in accordance with the local legislation and institutional requirements. The studies for the immunization of the animals (*Vicugna pacos*) were approved by the Government of Upper Bavaria (approval number: 55.2-1-54-2532.0-80-14). All mouse experiments were performed according to the German Animal Protection Law and were approved by the local authorities (Regierungspräsidium Tübingen). The studies were conducted in accordance with the local legislation and institutional requirements and in accordance with the German Animal Welfare Act.

Author contributions

DF: Conceptualization, Data curation, Investigation, Methodology, Project administration, Visualization, Writing – original draft. SB: Formal analysis, Investigation, Visualization, Writing – review & editing. TW: Investigation, Writing – review & editing. PK: Investigation, Methodology, Writing – review & editing. BT: Investigation, Writing – review & editing. MF: Formal analysis, Investigation, Writing – review & editing. MJ: Formal

analysis, Investigation, Methodology, Writing – review & editing. AS: Investigation, Resources, Writing – review & editing. SN: Investigation, Resources, Writing – review & editing. NS-M: Formal analysis, Methodology, Writing – review & editing. CG: Methodology, Resources, Writing – review & editing. MK: Conceptualization, Supervision, Writing – review & editing. BP: Conceptualization, Supervision, Writing – review & editing. DS: Formal analysis, Investigation, Methodology, Writing – review & editing. UR: Conceptualization, Funding acquisition, Project administration, Supervision, Writing – original draft.

Funding

The author(s) declare that financial support was received for the research, authorship, and/or publication of this article. This work received financial support from the State Ministry of Baden-Wuerttemberg for Economic Affairs, Labour and Tourism (Grant: Predictive diagnostics of immune-associated diseases for personalized medicine. FKZ: 35-4223.10/8) and by the Federal Ministry for Economic Affairs and Climate Action and the European Social Fund as part of the EXIST program (03EFVBW253 – REVELICE). This work was further supported by the Deutsche Forschungsgemeinschaft (DFG, German Research Foundation, Germany´s Excellence Strategy-EXC2180-390900677) and the Werner Siemens-Foundation. We acknowledge support by Open Access Publishing Fund of University of Tuebingen.

Conflict of interest

DF, DS, MK, BP, TW, BT, PK, and UR are named as inventors on a patent application claiming the use of the described nanobodies for diagnosis and therapeutics filed by the Natural and Medical Sciences Institute, the Werner Siemens Imaging Center and the University of Tuebingen.

The remaining authors declare that the research was conducted in the absence of any commercial or financial relationships that could be construed as a potential conflict of interest.

Publisher's note

Supplementary material

The Supplementary Material for this article can be found online at: https://www.frontiersin.org/articles/10.3389/fimmu.2024.1480091/full#supplementary-material

References

1. Twomey JD, Zhang B. Cancer immunotherapy update: FDA-approved checkpoint inhibitors and companion diagnostics. *AAPS J*. (2021) 23:39. doi: 10.1208/s12248-021-00574-0

2. Ghobadinezhad F, Ebrahimi N, Mozaffari F, Moradi N, Beiranvand S, Pournazari M, et al. The emerging role of regulatory cell-based therapy in autoimmune disease. *Front Immunol*. (2022) 13:1075813. doi: 10.3389/fimmu.2022.1075813

3. Liu C, Yang M, Zhang D, Chen M, Zhu D. Clinical cancer immunotherapy: Current progress and prospects. *Front Immunol*. (2022) 13:961805. doi: 10.3389/fimmu.2022.961805

4. Chasov V, Zmievskaya E, Ganeeva I, Gilyazova E, Davletshin D, Khaliulin M, et al. Immunotherapy strategy for systemic autoimmune diseases: betting on CAR-T cells and antibodies. *Antibodies*. (2024) 13:10. doi: 10.3390/antib13010010

5. Wierstra P, Sandker G, Aarntzen E, Gotthardt M, Adema G, Bussink J, et al. Tracers for non-invasive radionuclide imaging of immune checkpoint expression in cancer. *EJNMMI Radiopharm Chem*. (2019) 4:29. doi: 10.1186/s41181-019-0078-z

6. Russano M, Napolitano A, Ribelli G, Iuliani M, Simonetti S, Citarella F, et al. Liquid biopsy and tumor heterogeneity in metastatic solid tumors: the potentiality of blood samples. *J Exp Clin Cancer Res*. (2020) 39:95. doi: 10.1186/s13046-020-01601-2

7. Schwenck J, Sonanini D, Cotton JM, Rammensee HG, la Fougere C, Zender L, et al. Advances in PET imaging of cancer. *Nat Rev Cancer*. (2023) 23:474–90. doi: 10.1038/s41568-023-00576-4

8. Tavare R, Escuin-Ordinas H, Mok S, McCracken MN, Zettlitz KA, Salazar FB, et al. An effective immuno-PET imaging method to monitor CD8-dependent responses to immunotherapy. *Cancer Res*. (2016) 76:73–82. doi: 10.1158/0008-5472.CAN-15-1707

9. Farwell MD, Gamache RF, Babazada H, Hellmann MD, Harding JJ, Korn R, et al. CD8-targeted PET imaging of tumor-infiltrating T cells in patients with cancer: A phase I first-in-humans study of (89)Zr-df-IAB22M2C, a radiolabeled anti-CD8 minibody. *J Nucl Med*. (2022) 63:720–6. doi: 10.2967/jnumed.121262485

10. Wang Y, Wang C, Huang M, Qin S, Zhao J, Sang S, et al. Pilot study of a novel nanobody (68) Ga-NODAGA-SNA006 for instant PET imaging of CD8(+) T cells. *Eur J Nucl Med Mol Imaging*. (2022) 49:4394–405. doi: 10.1007/s00259-022-05903-9

11. Sriraman SK, Davies CW, Gill H, Kiefer JR, Yin J, Ogasawara A, et al. Development of an (18)F-labeled anti-human CD8 VHH for same-day immunoPET imaging. *Eur J Nucl Med Mol Imaging*. (2023) 50:679–91. doi: 10.1007/s00259-022-05998-0

12. Ogasawara A, Kiefer JR, Gill H, Chiang E, Sriraman S, Ferl GZ, et al. Preclinical development of ZED8, an (89)Zr immuno-PET reagent for monitoring tumor CD8 status in patients undergoing cancer immunotherapy. *Eur J Nucl Med Mol Imaging*. (2023) 50:287–301. doi: 10.1007/s00259-022-05968-6

13. De Groof TWM, Lauwers Y, De Pauw T, Saxena M, Vincke C, Van Craenenbroeck J, et al. Specific imaging of CD8 + T-Cell dynamics with a nanobody radiotracer against human CD8beta. *Eur J Nucl Med Mol Imaging*. (2024). doi: 10.1007/s00259-024-06896-3

14. Oh DY, Kwek SS, Raju SS, Li T, McCarthy E, Chow E, et al. Intratumoral CD4(+) T cells mediate anti-tumor cytotoxicity in human bladder cancer. *Cell*. (2020) 181:1612–25.e13. doi: 10.1016/j.cell.2020.05.017

15. Richardson JR, Schöllhorn A, Gouttefangeas C, Schuhmacher J. CD4+ T cells: multitasking cells in the duty of cancer immunotherapy. *Cancers*. (2021) 13:596. doi: 10.3390/cancers13040596

16. Traenkle B, Kaiser PD, Pezzana S, Richardson J, Gramlich M, Wagner TR, et al. Single-domain antibodies for targeting, detection, and *in vivo* imaging of human CD4 (+) cells. *Front Immunol*. (2021) 12:799910. doi: 10.3389/fimmu.2021.799910

17. Freise AC, Zettlitz KA, Salazar FB, Lu X, Tavare R, Wu AM. ImmunoPET imaging of murine CD4(+) T cells using anti-CD4 cys-diabody: effects of protein dose on T cell function and imaging. *Mol Imaging Biol*. (2017) 19:599–609. doi: 10.1007/s11307-016-1032-z

18. Gondry O, Xavier C, Raes L, Heemskerk J, Devoogdt N, Everaert H, et al. Phase I study of [(68)Ga]Ga-anti-CD206-sdAb for PET/CT assessment of protumorigenic macrophage presence in solid tumors (MMR phase I). *J Nucl Med*. (2023) 64:1378–84. doi: 10.2967/jnumed.122.264853

19. Wagner TR, Blaess S, Leske IB, Frecot DI, Gramlich M, Traenkle B, et al. Two birds with one stone: human SIRPalpha nanobodies for functional modulation and *in vivo* imaging of myeloid cells. *Front Immunol*. (2023) 14:1264179. doi: 10.3389/fimmu.2023.1264179

20. Lutje S, Feldmann G, Essler M, Brossart P, Bundschuh RA. Immune checkpoint imaging in oncology: A game changer toward personalized immunotherapy? *J Nucl Med*. (2020) 61:1137–44. doi: 10.2967/jnumed.119.237891

21. Ge S, Jia T, Li J, Zhang B, Deng S, Sang S. Molecular imaging of immune checkpoints in oncology: Current and future applications. *Cancer Lett*. (2022) 548:215896. doi: 10.1016/j.canlet.2022.215896

22. Xiao Z, Mayer AT, Nobashi TW, Gambhir SS. ICOS is an indicator of T-cell-mediated response to cancer immunotherapy. *Cancer Res*. (2020) 80:3023–32. doi: 10.1158/0008-5472.CAN-19-3265

23. Edwards KJ, Chang B, Babazada H, Lohith K, Park DH, Farwell MD, et al. Using CD69 PET imaging to monitor immunotherapy-induced immune activation. *Cancer Immunol Res*. (2022) 10:1084–94. doi: 10.1158/2326-6066.CIR-21-0874

24. Larimer BM, Wehrenberg-Klee E, Dubois F, Mehta A, Kalomeris T, Flaherty K, et al. Granzyme B PET imaging as a predictive biomarker of immunotherapy response. *Cancer Res*. (2017) 77:2318–27. doi: 10.1158/0008-5472.CAN-16-3346

25. Zhao N, Bardine C, Lourenço AL, Wang Y-h, Huang Y, Cleary SJ, et al. *In vivo* measurement of granzyme proteolysis from activated immune cells with PET. *ACS Cent Sci*. (2021) 7:1638–49. doi: 10.1021/acscentsci.1c00529

26. Vetto JT, Lum S, Morris A, Sicotte M, Davis J, Lemon M, et al. Presence of the T-cell activation marker OX-40 on tumor infiltrating lymphocytes and draining lymph node cells from patients with melanoma and head and neck cancers. *Am J Surg*. (1997) 174:258–65. doi: 10.1016/S0002-9610(97)00139-6

27. Croft M, So T, Duan W, Soroosh P. The significance of OX40 and OX40L to T-cell biology and immune disease. *Immunol Rev*. (2009) 229:173–91. doi: 10.1111/j.1600-065X.2009.00766.x

28. Ge W, Dong Y, Deng Y, Chen L, Chen J, Liu M, et al. Potential biomarkers: Identifying powerful tumor specific T cells in adoptive cellular therapy. *Front Immunol*. (2022) 13:1003626. doi: 10.3389/fimmu.2022.1003626

29. Poloni C, Schonhofer C, Ivison S, Levings MK, Steiner TS, Cook L. T-cell activation-induced marker assays in health and disease. *Immunol Cell Biol*. (2023) 101:491–503. doi: 10.1111/imcb.12636

30. Sako MO, Larimer BM. Imaging of activated T cells. *J Nucl Med*. (2023) 64:30–3. doi: 10.2967/jnumed.122.264097

31. Mallett S, Fossum S, Barclay AN. Characterization of the MRC OX40 antigen of activated CD4 positive T lymphocytes–a molecule related to nerve growth factor receptor. *EMBO J*. (1990) 9:1063–8. doi: 10.1002/embj.1990.9.issue-4

32. Calderhead DM, Buhlmann JE, van den Eertwegh AJ, Claassen E, Noelle RJ, Fell HP. Cloning of mouse Ox40: a T cell activation marker that may mediate T-B cell interactions. *J Immunol (Baltimore Md: 1950)*. (1993) 151:5261–71. doi: 10.4049/jimmunol.151.10.5261

33. Sugamura K, Ishii N, Weinberg AD. Therapeutic targeting of the effector T-cell co-stimulatory molecule OX40. *Nat Rev Immunol*. (2004) 4:420–31. doi: 10.1038/nri1371

34. Stuber E, Neurath M, Calderhead D, Fell HP, Strober W. Cross-linking of OX40 ligand, a member of the TNF/NGF cytokine family, induces proliferation and differentiation in murine splenic B cells. *Immunity*. (1995) 2:507–21. doi: 10.1016/1074-7613(95)90031-4

35. Ohshima Y, Tanaka Y, Tozawa H, Takahashi Y, Maliszewski C, Delespesse G. Expression and function of OX40 ligand on human dendritic cells. *J Immunol (Baltimore Md: 1950)*. (1997) 159:3838–48. doi: 10.4049/jimmunol.159.8.3838

36. Weinberg AD, Wegmann KW, Funatake C, Whitham RH. Blocking OX-40/OX-40 ligand interaction *in vitro* and *in vivo* leads to decreased T cell function and amelioration of experimental allergic encephalomyelitis. *J Immunol (Baltimore Md: 1950)*. (1999) 162:1818–26. doi: 10.4049/jimmunol.162.3.1818

37. Weinberg AD, Rivera M-M, Prell R, Morris A, Ramstad T, Vetto JT, et al. Engagement of the OX-40 receptor *in vivo* enhances antitumor immunity. *J Immunol*. (2000) 164:2160–9. doi: 10.4049/jimmunol.164.4.2160

38. Alam IS, Mayer AT, Sagiv-Barfi I, Wang K, Vermesh O, Czerwinski DK, et al. Imaging activated T cells predicts response to cancer vaccines. *J Clin Invest*. (2018) 128:2569–80. doi: 10.1172/JCI98509

39. Nobashi TW, Mayer AT, Xiao Z, Chan CT, Chaney AM, James ML, et al. Whole-body PET imaging of T-cell response to glioblastoma. *Clin Cancer Res*. (2021) 27:6445–56. doi: 10.1158/1078-0432.CCR-21-1412

40. Alam IS, Simonetta F, Scheller L, Mayer AT, Murty S, Vermesh O, et al. Visualization of activated T cells by OX40-ImmunoPET as a strategy for diagnosis of acute graft-versus-host disease. *Cancer Res*. (2020) 80:4780–90. doi: 10.1158/0008-5472.CAN-20-1149

41. Wen G, Lei H, Qi B, Duan S, Xiao Z, Han C, et al. Noninvasive imaging OX40(+) activated T cells provides early warning of rheumatoid arthritis. *Mol Imaging Biol*. (2023) 25:621–9. doi: 10.1007/s11307-023-01819-4

42. Freise AC, Wu AM. *In vivo* imaging with antibodies and engineered fragments. *Mol Immunol*. (2015) 67:142–52. doi: 10.1016/j.molimm.2015.04.001

43. Rashidian M, Ploegh H. Nanobodies as non-invasive imaging tools. *Immuno-Oncol Technol*. (2020) 7:2–14. doi: 10.1016/j.iotech.2020.07.001

44. Hamers-Casterman C, Atarhouch T, Muyldermans S, Robinson G, Hamers C, Songa EB, et al. Naturally occurring antibodies devoid of light chains. *Nature*. (1993) 363:446–8. doi: 10.1038/363446a0

45. Lecocq Q, De Vlaeminck Y, Hanssens H, D'Huyvetter M, Raes G, Goyvaerts C, et al. Theranostics in immuno-oncology using nanobody derivatives. *Theranostics*. (2019) 9:7772–91. doi: 10.7150/thno.34941

46. Berland L, Kim L, Abousaway O, Mines A, Mishra S, Clark L, et al. Nanobodies for medical imaging: about ready for prime time? *Biomolecules*. (2021) 11:637. doi: 10.3390/biom11050637

47. Yang E, Liu Q, Huang G, Liu J, Wei W. Engineering nanobodies for next-generation molecular imaging. *Drug Discovery Today*. (2022) 27:1622–38. doi: 10.1016/j.drudis.2022.03.013

48. Chakravarty R, Goel S, Cai W. Nanobody: the "magic bullet" for molecular imaging? *Theranostics*. (2014) 4:386–98. doi: 10.7150/thno.8006

49. Voo KS, Bover L, Harline ML, Vien LT, Facchinetti V, Arima K, et al. Antibodies targeting human OX40 expand effector T cells and block inducible and natural regulatory T cell function. *J Immunol (Baltimore Md: 1950)*. (2013) 191:3641–50. doi: 10.4049/jimmunol.1202752

50. Traenkle B, Segan S, Fagbadebo FO, Kaiser PD, Rothbauer U. A novel epitope tagging system to visualize and monitor antigens in live cells with chromobodies. *Sci Rep*. (2020) 10:14267. doi: 10.1038/s41598-020-71091-x

51. Croft M. Control of immunity by the TNFR-related molecule OX40 (CD134). *Annu Rev Immunol*. (2009) 28:57–78. doi: 10.1146/annurev-immunol-030409-101243

52. Linch SN, McNamara MJ, Redmond WL. OX40 agonists and combination immunotherapy: putting the pedal to the metal. *Front Oncol*. (2015) 5:34. doi: 10.3389/fonc.2015.00034

53. Petty JK, He K, Corless CL, Vetto JT, Weinberg AD. Survival in human colorectal cancer correlates with expression of the T-cell costimulatory molecule OX-40 (CD134). *Am J Surg*. (2002) 183:512–8. doi: 10.1016/S0002-9610(02)00831-0

54. Ladányi A, Somlai B, Gilde K, Fejös Z, Gaudi I, Tímár J. T-cell activation marker expression on tumor-infiltrating lymphocytes as prognostic factor in cutaneous Malignant melanoma. *Clin Cancer Res*. (2004) 10:521–30. doi: 10.1158/1078-0432.CCR-1161-03

55. Massarelli E, Lam VK, Parra ER, Rodriguez-Canales J, Behrens C, Diao L, et al. High OX-40 expression in the tumor immune infiltrate is a favorable prognostic factor of overall survival in non-small cell lung cancer. *J immunother cancer*. (2019) 7:351. doi: 10.1186/s40425-019-0827-2

56. Yokouchi H, Nishihara H, Harada T, Amano T, Ohkuri T, Yamazaki S, et al. Prognostic significance of OX40+ lymphocytes in tumor stroma of surgically resected small-cell lung cancer. *OncoImmunology*. (2021) 10:1971430. doi: 10.1080/2162402X.2021.1971430

57. James NE, Valenzuela AD, Emerson JB, Woodman M, Miller K, Hovanesian V, et al. Intratumoral expression analysis reveals that OX40 and TIM-3 are prominently expressed and have variable associations with clinical outcomes in high grade serous ovarian cancer. *Oncol Lett*. (2022) 23:188. doi: 10.3892/ol

58. Webb GJ, Hirschfield GM, Lane PJ. OX40, OX40L and autoimmunity: a comprehensive review. *Clin Rev Allergy Immunol*. (2016) 50:312–32. doi: 10.1007/s12016-015-8498-3

59. Keyaerts M, Xavier C, Heemskerk J, Devoogdt N, Everaert H, Ackaert C, et al. Phase I study of 68Ga-HER2-nanobody for PET/CT assessment of HER2 expression in breast carcinoma. *J Nucl Med*. (2016) 57:27–33. doi: 10.2967/jnumed.115.162024

60. Keyaerts M, Xavier C, Everaert H, Vaneycken I, Fontaine C, Decoster L, et al. 85TiP - Phase II trial of HER2-PET/CT using 68Ga-anti-HER2 VHH1 for characterization of HER2 presence in brain metastases of breast cancer patients. *Ann Oncol*. (2019) 30:iii25–iii6. doi: 10.1093/annonc/mdz095.081

61. Harmand TJ, Islam A, Pishesha N, Ploegh HL. Nanobodies as *in vivo*, non-invasive, imaging agents. *RSC Chem Biol*. (2021) 2:685–701. doi: 10.1039/D1CB00023C

62. Barakat S, Berksöz M, Zahedimaram P, Piepoli S, Erman B. Nanobodies as molecular imaging probes. *Free Radic Biol Med*. (2022) 182:260–75. doi: 10.1016/j.freeradbiomed.2022.02.031

63. Wagner TR, Ostertag E, Kaiser PD, Gramlich M, Ruetalo N, Junker D, et al. NeutrobodyPlex-monitoring SARS-CoV-2 neutralizing immune responses using nanobodies. *EMBO Rep*. (2021) 22:e52325. doi: 10.15252/embr.202052325

64. Duhen R, Ballesteros-Merino C, Frye AK, Tran E, Rajamanickam V, Chang S-C, et al. Neoadjuvant anti-OX40 (MEDI6469) therapy in patients with head and neck squamous cell carcinoma activates and expands antigen-specific tumor-infiltrating T cells. *Nat Commun*. (2021) 12:1047. doi: 10.1038/s41467-021-21383-1

65. Davis EJ, Martin-Liberal J, Kristeleit R, Cho DC, Blagden SP, Berthold D, et al. First-in-human phase I/II, open-label study of the anti-OX40 agonist INCAGN01949 in patients with advanced solid tumors. *J immunother cancer*. (2022) 10:e004235. doi: 10.1136/jitc-2021-004235

66. Rashidian M, Ingram JR, Dougan M, Dongre A, Whang KA, LeGall C, et al. Predicting the response to CTLA-4 blockade by longitudinal noninvasive monitoring of CD8 T cells. *J Exp Med*. (2017) 214:2243–55. doi: 10.1084/jem.20161950

67. Gibson HM, McKnight BN, Malysa A, Dyson G, Wiesend WN, McCarthy CE, et al. IFNgamma PET imaging as a predictive tool for monitoring response to tumor immunotherapy. *Cancer Res*. (2018) 78:5706–17. doi: 10.1158/0008-5472.CAN-18-0253

68. Persson J, Puuvuori E, Zhang B, Velikyan I, Aberg O, Muller M, et al. Discovery, optimization and biodistribution of an Affibody molecule for imaging of CD69. *Sci Rep*. (2021) 11:19151. doi: 10.1038/s41598-021-97694-6

69. Virant D, Traenkle B, Maier J, Kaiser PD, Bodenhöfer M, Schmees C, et al. A peptide tag-specific nanobody enables high-quality labeling for dSTORM imaging. *Nat Commun*. (2018) 9:930. doi: 10.1038/s41467-018-03191-2

70. Arbabi Ghahroudi M, Desmyter A, Wyns L, Hamers R, Muyldermans S. Selection and identification of single domain antibody fragments from camel heavy-chain antibodies. *FEBS Lett.* (1997) 414:521–6. doi: 10.1016/S0014-5793(97)01062-4

71. Chen I, Dorr BM, Liu DR. A general strategy for the evolution of bond-forming enzymes using yeast display. *Proc Natl Acad Sci U S A.* (2011) 108:11399–404. doi: 10.1073/pnas.1101046108

72. FDA. *Bioanalytical Method Validation: Guidance for Industry*. Silver Spring, Rockville: US Department of Health and Human Services, Food and Drug Administration, Center for Drug Evaluation and Research, Center for Veterinary Medicine (2018).

73. EMEA. *Guideline on Bioanalytical Method Validation*. London: European Medicines Agency; Comittee for Medicinal Products for Human Use (CHMP (2013).

74. Westgard JO, Barry PL, Hunt MR, Groth T. A multi-rule Shewhart chart for quality control in clinical chemistry. *Clin Chem.* (1981) 27:493–501. doi: 10.1093/clinchem/27.3.493

frontiers | Frontiers in Immunology

TYPE Original Research
PUBLISHED 29 November 2024
DOI 10.3389/fimmu.2024.1513076

OPEN ACCESS

EDITED BY
Jinhwan Kim,
University of California, Davis, United States

REVIEWED BY
Shuai Ren,
Affiliated Hospital of Nanjing University of Chinese Medicine, China
Myeongsoo Kim,
Georgia Institute of Technology, United States

*CORRESPONDENCE
Jian-Guo Zhou
jianguo.zhou@zmu.edu.cn

†These authors have contributed equally to this work and share first authorship

‡These authors have contributed equally to this work and share last authorship

RECEIVED 17 October 2024
ACCEPTED 12 November 2024
PUBLISHED 29 November 2024

CITATION
Miao Y, Dong M, Zhou Q, Thiel J, Li N, Cai Y, Yuan D, Wang H, Jin S-H, Yang H, Wang J, Frey B, Gaipl US, Ma H and Zhou J-G (2024) Single-cell RNA-seq reveals *FGF12* as a prognostic biomarker in low-grade endometrial stromal sarcoma. *Front. Immunol.* 15:1513076. doi: 10.3389/fimmu.2024.1513076

Single-cell RNA-seq reveals *FGF12* as a prognostic biomarker in low-grade endometrial stromal sarcoma

Yu Miao[1,2†], Meng Dong[3†], Qiyin Zhou[4†], Julia Thiel[3], Na Li[5], Ying Cai[1], Dan Yuan[6], Haitao Wang[7], Su-Han Jin[8], Hua Yang[9], Jinjing Wang[6], Benjamin Frey[10,11,12], Udo S. Gaipl[10,11,12], Hu Ma[1‡] and Jian-Guo Zhou[1,10,11,12*‡]

[1]Department of Oncology, The Second Affiliated Hospital of Zunyi Medical University, Zunyi, China, [2]Institute of Biomedical Research, Henan Academy of Sciences, Zhengzhou, China, [3]Dr. Margarete Fischer-Bosch Institute of Clinical Pharmacology and University of Tübingen, Stuttgart, Germany, [4]Department of Obstetrics and Gynecology, Yanhe County People's Hospital, Tongren, Guizhou, China, [5]Department of Obstetrics and Gynecology, The Second Affiliated Hospital of Zunyi Medical University, Zunyi, Guizhou, China, [6]Department of Pathology, The Affiliated Hospital of Zunyi Medical University, Zunyi, China, [7]Thoracic Surgery Branch, Center for Cancer Research, National Cancer Institute (NCI), NIH, Bethesda, MD, United States, [8]Department of Orthodontics, Affiliated Stomatological Hospital of Zunyi Medical University, Zunyi, China, [9]Department of Pathology, The Second Affiliated Hospital of Zunyi Medical University, Zunyi, China, [10]Translational Radiobiology, Department of Radiation Oncology, Universitätsklinikum Erlangen, Friedrich-Alexander-Universität Erlangen-Nürnberg, Erlangen, Germany, [11]Comprehensive Cancer Center Erlangen, European Metropolitan Region Nuremberg, Erlangen, Germany, [12]FAU Profile Center for Immunomedicine, Friedrich-Alexander-Universität Erlangen-Nürnberg, Erlangen, Germany

Background: Low-grade endometrial stromal sarcoma (LG-ESS) is a rare uterine malignancy characterized by its complex tumor microenvironment (TME) and high recurrence rates, posing challenges to accurate prognosis and effective treatment. Identifying prognostic biomarkers is essential for improving patient stratification and guiding therapeutic strategies.

Methods: Using single-cell transcriptome analysis combined with H&E and multiplex immunofluorescence staining, we identified a subpopulation of tumor cells in LG-ESS and further validated the association of this subpopulation and its characteristic genes with LG-ESS prognosis by molecular characterization and bulk transcriptome data.

Results: Our analysis reveals multiple cellular subpopulations within the tumor tissue, particularly a tumor cell subpopulation among them which is associated with poor prognosis. Originating from normal stromal fibroblasts, this subpopulation appears to play a crucial role in TME remodeling, smooth muscle cell behavior, and potentially in tumorigenesis and metastasis. Of particular interest in this subpopulation is the highly expressed *FGF12* gene, which is significantly associated with a shortened survival in ESS, highlighting its potential as a prognostic biomarker.

Conclusion: Our study reveals the complexity of TME within the LG-ESS and highlights the role that tumor cell subpopulations play in disease progression and patient prognosis. The identification of *FGF12* as a prognostic biomarker suggests a new approach for the personalized treatment and prognosis monitoring of patients.

KEYWORDS

scRNA-seq, *FGF12*, low-grade endometrial stromal sarcoma, tumor microenvironments, prognostic biomarker

Introduction

Endometrial stromal sarcoma (ESS) is a rare uterine malignancy originating from endometrial mesenchymal cells (1), accounting for less than 1% of all uterine tumors (2). ESS was classified by the World Health Organization into four types in 2020 based on clinical and pathologic features and progress in molecular genetic studies: endometrial stromal nodule (ESN), low-grade ESS (LG-ESS), high-grade ESS (HG-ESS), and undifferentiated uterine sarcoma (UUS) (3). Although LG-ESS is usually slow-growing and has a relatively good prognosis (5-year overall survival rate of more than 80%) (4, 5), its recurrence and late mortality rates are still not negligible, approximately 60% and 15%-25%, respectively (6, 7). Due to its variable behavior and limited understanding of its pathobiology, LG-ESS represents a significant therapeutic challenge (4, 8, 9). In addition, the lack of distinctive clinical manifestations makes preoperative imaging difficult to diagnose, necessitating reliance on postoperative pathologic assessments (10, 11). However, this reliance inadvertently increases the risk of misdiagnosis and underdiagnosis, potentially impacting patient management and prognostic outcomes.

Current therapeutic strategies for LG-ESS generally follow the approaches used for other sarcomas, including surgery, hormonal therapy, radiotherapy, and chemotherapy (4, 12, 13). However, despite the generally favorable prognosis in early-stage cases, LG-ESS tends to recur, and advanced or recurrent disease remains difficult to treat with the current therapeutic options (14–16). The rarity of LG-ESS, coupled with the dearth of detailed insights into its molecular foundations and comprehensive molecular profiling, has impeded the advancement of innovative therapeutic strategies, including targeted therapies that are pivotal in modern precision medicine (17).

Despite advances in the understanding of uterine malignancies, the precise molecular and cellular mechanisms driving LG-ESS remain elusive. While hormone receptor expression (18–20) and the presence of chromosomal rearrangements, such as *JAZF1-SUZ12* and *JAZF1-PHF1* fusions (21), have been implicated in the pathogenesis of LG-ESS, the specific cellular subpopulations responsible for tumor initiation, progression, and recurrence have not been comprehensively characterized. As a result, there is a critical need to delineate the molecular characterization of LG-ESS to identify potential therapeutic vulnerabilities and improve treatment outcomes for patients.

In addition, predicting the clinical course of LG-ESS remains challenging, and the risk of recurrence is high. Currently, prognostic biomarkers for LG-ESS are largely based on clinical and pathological characteristics such as tumor size, stage at diagnosis, and hormone receptor status. While these factors provide some predictive value, they are insufficient for accurately identifying patients at high risk for recurrence or poor prognosis. Identifying molecular markers that can accurately predict patient outcomes will not only improve treatment planning but also enhance the overall management of this rare and challenging malignancy. A reliable prognostic biomarker for LG-ESS would allow clinicians to stratify patients into different risk categories, guiding treatment decisions accordingly. Patients with a higher risk of recurrence or poor survival outcomes could benefit from more aggressive treatment strategies, such as adjuvant therapy or closer post-surgical monitoring, while those with a lower risk could avoid unnecessary interventions.

Tumors are not homogenous entities but rather complex ecosystems composed of diverse cell types, with each contributing differently to tumor progression, immune evasion, and therapeutic resistance. For LG-ESS, exploring this heterogeneity is especially critical given the limited understanding of its stromal origin and how the tumor microenvironment may influence its behavior. Advances in single-cell transcriptomics have provided unprecedented insights into the heterogeneity of cellular populations within the tumor immune microenvironment (TME), enabling the identification of subpopulations that may contribute to tumorigenesis, disease progression, and therapeutic resistance (22). The application of these technologies to LG-ESS research holds promise for unveiling the intricate cellular composition and deepening our understanding of the molecular drivers of tumor behavior. The identification of unique molecular signatures in tumor cell subpopulations could lead to the discovery of novel biomarkers and therapeutic targets, potentially revolutionizing the treatment landscape for LG-ESS.

This study aims to characterize LG-ESS using single-cell transcriptomics to describe the cellular composition, molecular

characteristics and identify potential prognostic biomarkers. The insights gained from this study are expected to lay the cornerstone for a new paradigm in the personalized treatment of endometrial stromal sarcomas.

Methods

Sample collection and sequencing

A sample of LG-ESS was collected immediately after surgery, some of which were fixed with 10% formalin fixation, and some were snap frozen. The formalin fixed sample was further embedded in paraffin for immunohistochemical staining. The snap frozen sample was digested and dispersed to form a single-cell suspension. Single cell capture, reverse transcription, amplification, and library construction were performed using the 10X Genomics platform according to the manufacturer's instructions. Libraries were then sequenced, and data was processed using CellRanger software to generate a single cell transcriptome data matrix. The study was approved by the Ethics Committee of Zunyi Medical University (No. 2020-1-013), with informed consent obtained from all participants.

Data collection

Single-cell transcriptome sequencing data for five healthy control (HC) endometrial samples (raw fastq files) were downloaded from the NCBI SRA database, accession number SRP349751 (23). Bulk transcriptomic datasets used for validation were sourced from the GEO database (GSE128630, GSE119041, and GSE85383). The GSE128630 dataset encompasses 75 ESS cases (24). GSE119041 includes 13 leiomyosarcoma (LMS), 16 ESS, 26 UUS, and three YWHAE-FAM22 endometrial stromal sarcomas (YFAM) samples, along with 14 benign leiomyoma controls (LM) (25). GSE85383 contains 9 LG-ESS, 4 HG-ESS, 8 UUS, and 4 uterine LMS (26). The clinical characteristics of these samples were extracted from the corresponding publications.

Identification and removal of doublets

DoubletFinder (version 2.0.3) (27) was used for each sample to identify and remove doublets, with the doublet rate set to 0.03 for 10x genomic sequencing.

Data preprocessing

Data integration of Seurat objects after doublet removal was performed using the Seurat (R package,version 4.4.0) (28), filtering out abnormal cells (mito_percent < 15% & nFeature > 200 & nFeature < 6000) and logarithmizing the UMIcount matrix. In order to eliminate experimental batch effects, the harmony package (version 1.0.3) was used for the integration of the data (29).

Cell type identification

The top 2000 highly variable genes were selected for principal component analysis (PCA), with principal components determined through the JackStraw procedure. After determining the selected number of principal components (dims = 1:30) during the integration process, we clustered the cells with a resolution of 1 and performed dimensionality reduction with t-SNE for visualization. Cell subpopulations were named based on SingleR (version 2.2.0) annotation and classic marker expression (23, 30).

RNA velocity analysis

We performed RNA velocity analysis based on bam files generated from *CellRanger* Count (version 7.2.0) analysis using the *scVelo* software (version 0.2.5) (31). scVelo infers temporal dynamic changes in gene expression by estimating splicing dynamics and unspliced/spliced ratios of individual cells. Finally, based on the RNA velocity results, we can reveal the dynamic changes in cell status and their potential differentiation pathways in the LG-ESS tumor sample.

Trajectory analysis

For trajectory analysis, Monocle 2 (version 2.18.0) (32) was used to investigate dynamic changes in cell states based on the expression of variable genes in the target population (cells expressing ≥10 genes with an average expression >0.5). Genes with significant temporal variation were identified using the differentialGeneTest function. Dimensionality reduction was performed with the DDRTree algorithm, and a minimum spanning tree was constructed using the plot_cell_trajectory function. To visualize gene expression changes along pseudotime, the top 100 dynamically expressed genes were clustered using the plot_pseudotime_heatmap function. Functional enrichment analysis for each gene cluster was conducted using KOBAS 3.0.

Analysis of intercellular communication

In order to investigate the interactions between different cell types in the tumor microenvironment of LG-ESS, we performed intercellular communication analysis using CellPhoneDB2 (database version v2.0.0) (33), a Python-based computational analysis tool, to identify interaction networks.

Estimation of cell proportions in samples of bulk transcriptome

To quantify the cell type composition within our bulk transcriptome samples, we utilized the BisqueRNA (version 1.0.5) algorithm (34). This tool allowed us to leverage the gene expression profiles derived from identified subpopulations in single-cell RNA

sequencing data. Through this deconvolution approach, we were able to infer the relative abundances of different cell types present in the mixed tissue samples.

Enrichment analysis

We performed gene set enrichment analysis (GSEA) and Kyoto Encyclopedia of Genes and Genomes (KEGG) enrichment analysis on the differential gene expression results using the clusterProfiler (version 4.8.3) (35) and kobas (version 3.0) software, respectively.

Survival analysis and Cox regression analysis

Survival analysis: We used the cutoff values (median expression or best cutoff value) of the expression of specific genes in the GSE128630 cohort and the GSE119041 cohort to divide the cohort into two groups and used the survival package to compare the differences in survival rates between the groups and to plot Kaplan-Meier (KM) curves.

Univariate Cox regression analysis: Cox regression modeling was performed using the survival package of the R software, and one-way Cox regression was performed with the expression of the gene of interest as a covariate.

Multivariate Cox regression analysis: Cox regression modeling was performed using the survival package in R software, incorporating relevant clinical factors such as age at diagnosis, tumor grade, and BMI, alongside the expression levels of *FGF12* and *KLHL29* as covariates. This approach allowed us to assess the independent prognostic significance of *FGF12* and *KLHL29* while adjusting for the effects of these clinical variables.

H&E staining

The paraffin-embedded tissue samples (FFPE) are cut into 3-5 micron sections. For H&E staining, the sections are stained in an acid hematoxylin solution for about 8 minutes and then in an eosin solution for about 2.5 minutes using a slide stainer.

Multiplex immunofluorescence (mIF) staining

A 7-color multiplex immunofluorescence staining was performed using the OPAL™ multiplexing method. The staining protocol for FFPE tissue sections was optimized for the simultaneous detection of 6 antibodies and DAPI as a nuclear stain. The fixed tissues were cut into 4μm sections by Rotary Microtome (Leica RM2255, Germany). The sections were deparaffinized, rehydrated, subjected to heat-induced epitope retrieval and incubated with primary and secondary antibodies. The antibodies were visualized using the fluorescent tyramide from the Opal 6-Plex Manual Detection Kit (NEL861001KT, Akoya Biosciences). The process of epitope retrieval and staining was repeated sequentially for different primary antibodies and fluorescent tyramide combinations. The following primary antibodies with different dilutions were used: CD10 (#110M-16, Cell Marque) with 1:40 dilution, Desmin (#243M-14, Cell Marque) with 1:50 dilution, CD4 (#104R-14, Cell Marque) with 1:100 dilution, CD8 (#108R-14, Cell Marque) with 1:75 dilution, CD68 (#168M-94, Cell Marque) with 1:75 dilution, FOX-P3 (#14-4777-82, eBioscience). Antibodies were visualized with the following tyramide dyes from the Opal Detection kit (NEL861001KT, Akoya Biosciences): Opal Polaris 480, Opal 520, Opal 570, Opal 620, Opal 690, and DIG-Opal 780. Sections were mounted with ProLong® Diamond Antifade Mountant (P36961, Thermo Fisher Scientific). Multiplex-stained slides were imaged using a PhenoImager Fusion system (Akoya Biosciences).

Statistical analysis

The log-rank test was used for survival analysis. For other intergroup comparisons, the Wilcoxon rank-sum test was used. $P<0.05$ is considered to be statistically significant.

Result

Altered gene expression profiles in multiple subpopulations of LG-ESS

To investigate the cellular composition of LG-ESS, we collected a fresh tissue sample from an LG-ESS patient during surgery and performed single-cell transcriptomic sequencing. Concurrently, we rigorously curated and integrated this dataset with single-cell transcriptomic data from five healthy controls (HCs) sourced from a public database, ensuring stringent quality control throughout the analysis (Figure 1A).

Following batch correction (Supplementary Figure S1A), we dimensionally reduced and clustered 38,288 cells, identifying 12 primary cell subpopulations (Figure 1B): non-ciliated epithelial cells (Epi, $EPCAM^{+}$ $SNTN^{-}$), ciliated epithelial cells (Cili_Epi, $EPCAM^{+}$ $SNTN^{+}$), Str (stromal fibroblasts, DCN^{+} MME^{+} LUM^{+}), smooth muscle cells (Smooth_muscle_cell, $ACTA2^{+}$), proliferative stromal cells (pStr, $MKI67^{+}$), pericytes (Peri, $NOTCH3^{+}$ $RGS5^{+}$), endothelial cells (Endo, $PECAM1^{+}$), lymphatic endothelial cells (Lymph, $CCL21^{+}$), macrophages (Mac, $CD163^{+}$), T cells (Tcell, $CD3D^{+}$), natural killer cells (NK, $GNLY^{+}$), and mast cells (Mast_cell, $TPSB2^{+}$) (Figure 1C). Supplementary Figure S1B displays the top five highly expressed genes in each cell subpopulation, and Supplementary Figure S1C shows the quantification of all cell subpopulations from each sample. Furthermore, differential gene analysis of all subpopulations between LG-ESS and HC revealed that multiple subpopulations exhibited significant differences in gene expression, particularly within the Str subpopulation (Figure 1D). We speculate that changes in the gene expression profile of this subpopulation may be intricately linked to the pathogenesis of LG-ESS.

10.3389/fimmu.2024.1513076

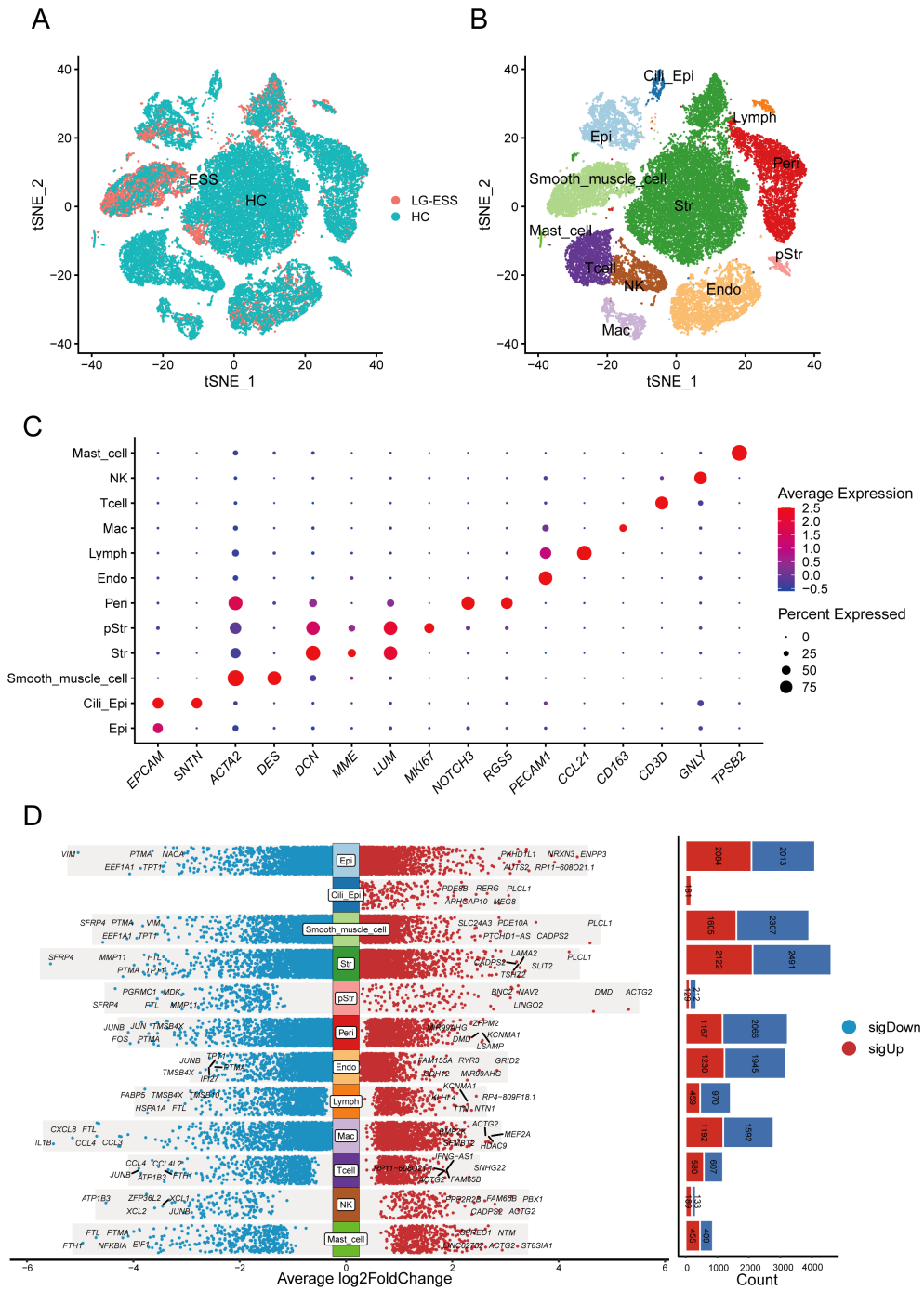

FIGURE 1
Single-cell transcriptome analysis reveals altered gene expression profiles in multiple cellular subpopulations in LG-ESS. **(A)** Scatterplot showing the overall distribution of cell subpopulations in HC and LG-ESS. **(B)** t-SNE plot showing the major cell types identified from HC and LG-ESS groups in different colors. **(C)** Scatterplot showing the expression of representative marker genes in different cell types. **(D)** Differential genes between different cell subpopulations of HC and LG-ESS, red color indicates genes up-regulated in LG-ESS, blue color indicates genes down-regulated in LG-ESS, and the bar graph on the right side shows the number of differential genes.

The tumor cell subpopulation, Str1, significantly associated with poor prognosis of LG-ESS

Previous studies have indicated that most LG-ESS exhibit positive expression of CD10 (protein of MME gene) and WT1, with elevated levels of estrogen receptor expression (20, 36, 37). Through H&E staining (Figure 2A) and multiplex immunofluorescence (mIF) staining (Figures 2B, C; Supplementary Figure S2A) of adjacent tissue sections, we found that the tumor cell-rich regions of the LG-ESS sample displayed positive CD10 expression (Figure 2B, right middle) and were located adjacent to smooth muscle cell populations

(α-SMA$^+$ DES$^+$) (Figure 2B). Additionally, the tumor sample contained various other cell types, including epithelial cells (EPCAM$^+$), pStr (MKI67$^+$) CD4$^+$T cells (CD4$^+$), CD8$^+$ T cells (CD8A$^+$), macrophages (CD68$^+$), and regulatory T cells (FOXP3$^+$), which were further validated by our single-cell data (Figure 2D). Unlike most epithelial-derived solid tumors (including endometrial carcinoma (22)), LG-ESS originates from mesenchymal fibroblasts rather than endometrial epithelial cells (4). Consistent with this notion, we found that MME$^+$(CD10) was predominantly expressed in the Str subpopulation, with almost no expression in epithelial cells.

To explore the functional roles of tumor cell subpopulations in LG-ESS, we re-clustered the Str subpopulation (Figure 2E), resulting in eight distinct clusters. We observed that Cluster2 and Cluster4 were primarily composed of LG-ESS, and notably, LG-ESS tumor cells (MME$^+$) were mainly located in Cluster4 (Figure 2F). Consequently, we independently clustered the LG-ESS samples and further differentiated the Str subpopulation into two subgroups: Str1, characterized by MME$^+$ tumor cells (predominantly in Cluster4), and Str2, defined by MME- cells (predominantly in Cluster3) (Figures 2G, H). KEGG enrichment analysis indicated that the highly expressed genes in the Str1 tumor cell subgroup were significantly enriched in several classic cancer-related pathways, including focal adhesion, choline metabolism in cancer, Wnt signaling pathway, and PI3K-Akt signaling pathway (Figure 2I). This aligns with previous findings demonstrating significant activation of the Wnt signaling pathway in LG-ESS (38).

Subsequently, we utilized BisqueRNA to estimate the proportions of cells in a large number of transcriptomic samples based on the top 50 most highly expressed genes across all LG-ESS cell subpopulations, and we explored the relationship between subpopulation proportions and the prognosis of LG-ESS. We found that an increased proportion of Str1 in LG-ESS was significantly associated with shorter overall survival and progression-free survival of patients (Supplementary Figure S2B). At the same time, we observed no significant differences in the proportion of Str1 across different sarcoma types (Supplementary Figure S2C).

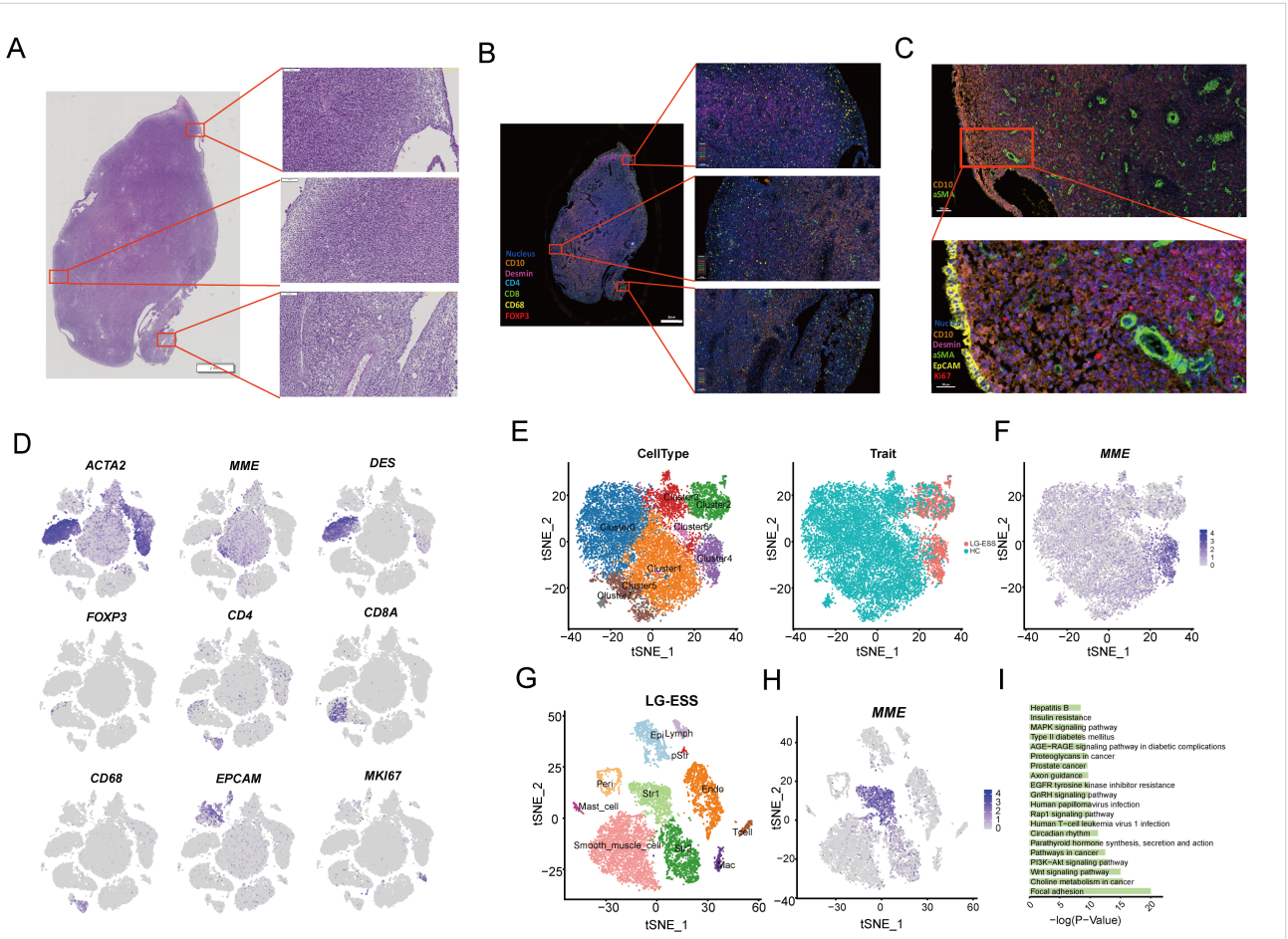

FIGURE 2
Characterization and functional analysis of LG-ESS tumor cell subpopulations. **(A)** H&E staining result of the LG-ESS tissue sample, highlighting the overall tissue architecture at low magnification, with higher magnification images of selected regions showing cellular morphology. **(B, C)** miF staining result of LG-ESS sample. CD10, desmin, and other markers are used to distinguish different cell populations within the tumor, with magnified views focusing on specific regions of interest. The scale in figure **(B)** represents 2 mm and 100 μm, while in figure **(C)** it represents 100 μm and 30 μm. **(D)**. Expression of key marker genes from the single-cell RNA sequencing data corresponding to the same LG-ESS sample. These markers (e.g., *ACTA2*, *MME*, *DES*, *FOXP3*, *CD4*, *CD8A*) help identify distinct cell types within the tumor microenvironment. **(E)** t-SNE plots showing the clustering of cell subpopulations (left) in the LG-ESS sample and their distribution in HC and LG-ESS tissue (right). **(F)** Featureplot demonstrating the expression of the CD10 (MME) gene in different subgroups of Str. **(G)** t-SNE plot highlighting the main cell types present in LG-ESS, identified by distinct colors. **(H)** MME expression across all cell types in the LG-ESS sample, with Str1 cells showing prominent expression. **(I)** Results of KEGG enrichment analysis of genes highly expressed in Str1.

Tumor cells in LG-ESS derive from normal stromal fibroblasts rather than MME$^-$ Str subpopulation

To further elucidate the origins of the Str1 tumor cell subpopulation in LG-ESS, we conducted RNA velocity analysis on both Str1 and Str2 subpopulations to determine their lineage relationships. Surprisingly, our findings indicated that Str1 and Str2 may share a common ancestral origin, contradicting our initial hypothesis that Str1 arose from Str2 (Figure 3A).

To validate this finding, we utilized the Str subpopulation from HC as a normal reference and performed RNA velocity analysis on all Str cells from both HC and LG-ESS samples. We discovered that Str1 (predominantly corresponding to Cluster4) and Str2 (primarily corresponding to Cluster2) indeed originated from the same ancestral cluster, Cluster3. Moreover, Cluster4 originating from Cluster3 through the intermediate Cluster6 (Figure 3B). Simultaneously, we conducted pseudo-time analysis on Clusters3, Clusters4, and Clusters6 using Monocle2. Consistent with the RNA velocity analysis, our results confirmed that Cluster4, which primarily comprises the Str1 tumor cell subpopulation in LG-ESS, predominantly develops from Cluster3 and Cluster6 (Figure 3C).

To explore the characteristic changes occurring during the differentiation of tumor cells, we clustered the genes that exhibited significant changes throughout the differentiation process (Figure 3D). KEGG enrichment analysis revealed that genes that were significantly upregulated during differentiation were primarily associated with common cancer-related pathways, such as focal adhesion, proteoglycans in cancer, Wnt signaling pathway, and Jak-STAT signaling pathway. Conversely, genes that were significantly downregulated during differentiation were predominantly linked to metabolic processes and oxidative phosphorylation pathways (Figure 3E).

High expression of *FGF12* is significantly associated with poor prognosis of LG-ESS

Upon investigating the biological alterations within tumor cell subpopulations of ESS as compared to HC, our enrichment analyses of differentially expressed genes (LG-ESS *vs.* HC) within the Str-Cluster4 subpopulation (Figure 2E) indicated significant gene expression modifications. These modifications predominantly clustered around pathways integral to oncogenesis and tumor progression, including growth hormone synthesis, secretion, and action, along with cell cycle regulation, focal adhesion, Wnt, and MAPK signaling pathways (Figure 4A). To investigate the underlying drivers of these pathways, we performed Cox regression and survival analysis on these significantly differentially expressed genes based on the gene expression data of ESS patients from the GEO database, focusing on genes uniquely expressed in Str1 (Figure 4B). Notably, high expression of *FGF12* and *KLHL29* in ESS was significantly associated with shorter overall and progression-free survival (Figures 4C-E). Through multivariate cox regression analysis, we found that FGF12 and KLHL29 remain important independent prognostic factors affecting overall survival (Supplementary Figure S3A) and progression-free survival (Supplementary Figure S3B). In addition, an independent cohort of patients further validated the association between high *FGF12* gene expression and shortened overall survival (OS) in uterine sarcoma patients (Supplementary Figure S3C), suggesting that *FGF12* could potentially be a prognostic biomarker for ESS.

Moreover, a comparative analysis of *FGF12* and *KLHL29* expression across different sarcoma subtypes and leiomyosarcomas (LMS) revealed a significant difference in *KLHL29* expression between HG-ESS and LG-ESS and LMS. In contrast, *FGF12* expression showed no significant difference. This indicates that *KLHL29* may serve as a potential biomarker for distinguishing HG-ESS from LG-ESS (Supplementary Figure S3D).

To further elucidate the biological functions of *FGF12* and *KLHL29* in ESS, we categorized ESS samples into high- and low-expression groups based on their gene expression levels and conducted GSEA enrichment analysis. We observed that the MYOGENESIS pathway was significantly activated in both the *FGF12*^{high} and *KLHL29*^{high} groups. Conversely, immune-related pathways, such as the INFLAMMATORY RESPONSE and INTERFERON GAMMA RESPONSE, were notably suppressed in the *FGF12*^{high} group, while the ESTROGEN RESPONSE EARLY pathway was significantly suppressed in the *KLHL29*^{high} group (Figures 4F, G).

Functional aberrations in cell subpopulations influenced by tumor cells in LG-ESS

Previous studies have shown that in epithelial-derived tumors, fibroblasts within the tumor microenvironment may be induced into cancer-associated fibroblasts (CAFs) through interactions with tumor cells (39, 40), and macrophages may undergo M2 polarization under the influence of tumor-derived factors (41). These phenotypic and functional changes in stromal and immune cells within the tumor microenvironment, in turn, contribute to tumor progression.

Through intercellular communication analysis, we identified a strong interaction between Str1 and Str2 as well as smooth muscle cell subpopulations in LG-ESS, particularly mediated by secreted growth factors (Figures 5A, B). We hypothesize that these interactions may lead to functional alterations in the subpopulations, thereby promoting tumor progression. To further explore these potential functional changes, we performed KEGG enrichment analysis on the highly expressed genes in the Str2 and smooth muscle cell subpopulations in LG-ESS. Interestingly, the genes predominantly clustered in pathways associated with tumorigenesis and metastasis, such as focal adhesion, proteoglycans in cancer, PI3K-Akt signaling, and ECM-receptor interactions (Figures 5C, D). Differential gene expression analysis between LG-ESS and healthy controls further supported these findings, indicating that the functions of Str2 and smooth muscle cells in LG-ESS are altered under the influence of tumor cells (Figures 5E, F).

10.3389/fimmu.2024.1513076

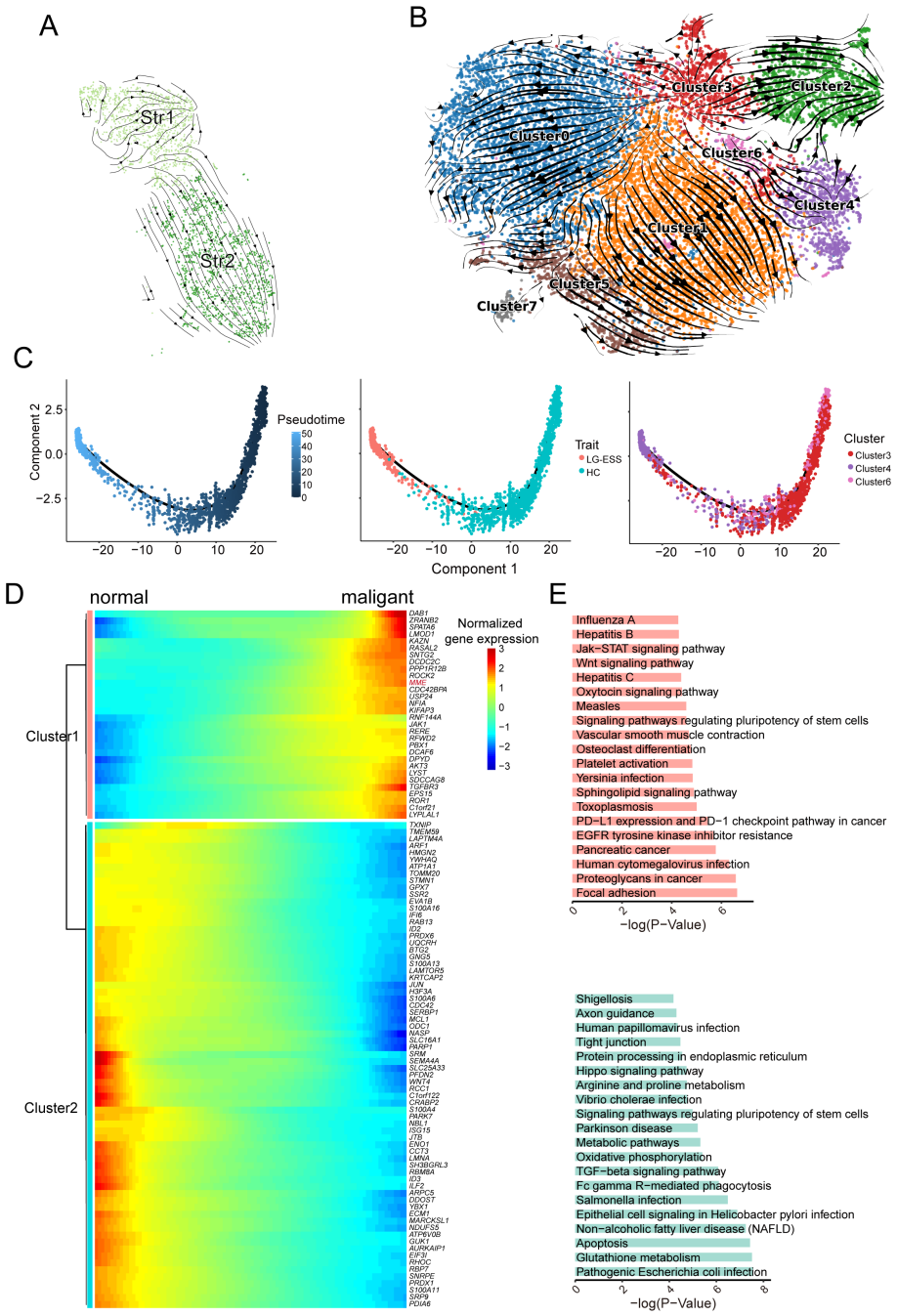

FIGURE 3
Origin of Str1 tumor cell subpopulations in LG-ESS. **(A)** RNA velocity analysis of Str1 and Str2 subpopulations in LG-ESS, illustrating their potential shared ancestral origin. **(B)** RNA velocity analysis of Str subpopulations from HC and LG-ESS samples, showing lineage relationships between clusters. **(C)** Pseudotime analysis of Cluster3, 4, and 6, demonstrating differentiation paths in Str cell subpopulations. **(D)** Heatmap of gene expression changes during the differentiation of normal stromal fibroblasts to malignant cells. **(E)** Results of KEGG enrichment analysis of significantly upregulated (top) and downregulated (below)pathways during tumor cell differentiation.

Discussion

LG-ESS is a rare uterine malignancy with a high recurrence rate, posing significant challenges for prognosis and treatment. Understanding the molecular characteristics and identifying prognostic biomarkers for LG-ESS is crucial for improving patient stratification and guiding personalized treatment. In this study, we used scRNA-seq to uncover the molecular characterization of tumor cell subpopulations within LG-ESS and their association with clinical outcomes. Our primary goal was to explore potential biomarkers linked to poor prognosis, offering new insights into disease progression.

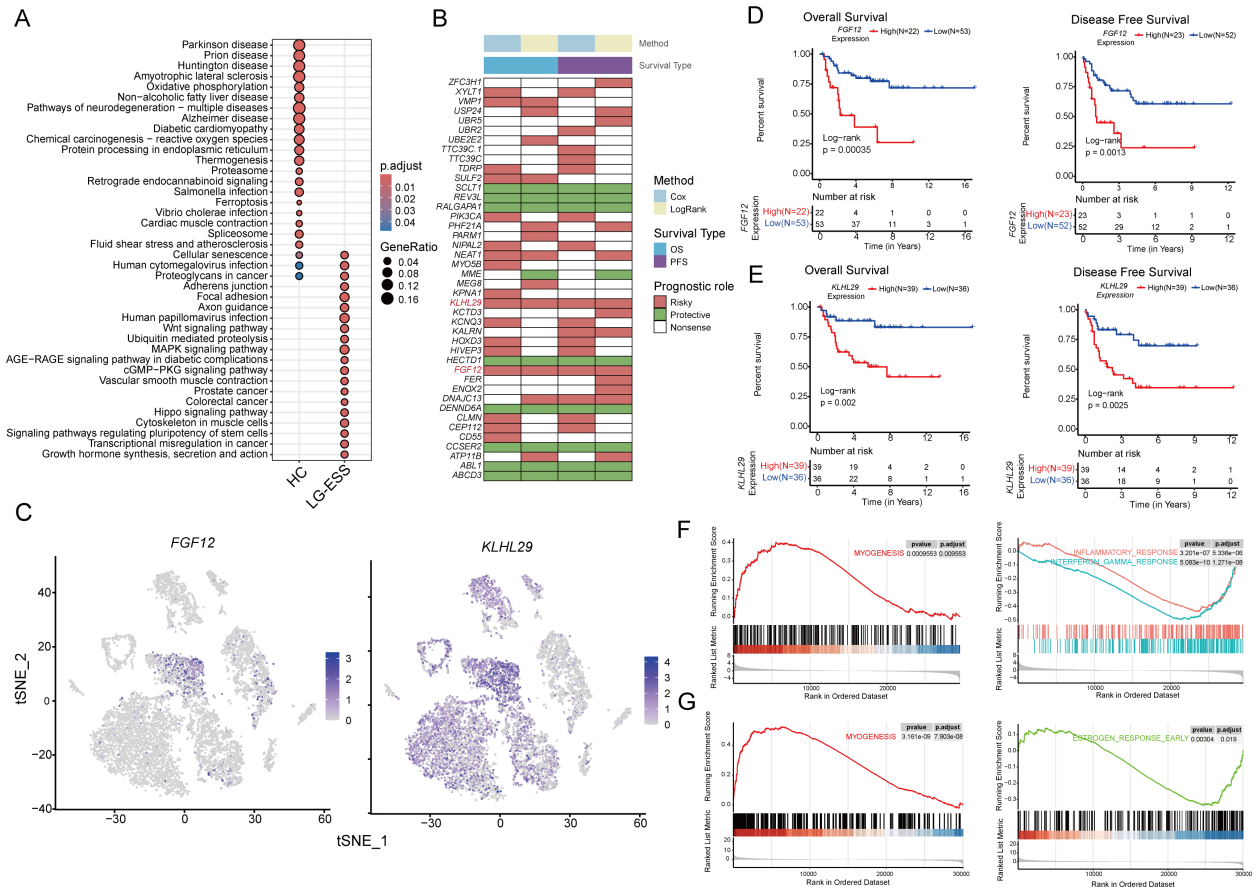

FIGURE 4
FGF12 and *KLHL29* expression correlates with poor prognosis and tumor progression in ESS. **(A)** Scatterplot demonstrating the results of KEGG enrichment analysis of differentially expressed genes of Str1 between LG-ESS and HC. **(B)** Heatmap demonstrating the results of Cox regression analysis and survival analysis for specific genes based on bulk transcriptome data of ESS patients. **(C)** Featureplot demonstrating the expression of *FGF12* and *KLHL29* genes in different cellular subpopulations of LG-ESS. **(D, E)** Results of survival analysis based on *FGF12* **(D)** and *KLHL29* **(E)** expression in ESS patients, with overall survival on the left and progression-free survival on the right (GSE128630). **(F, G)** Results of GSEA enrichment analysis after differentiating patients into high and low expression groups based on *FGF12* **(F)** and *KLHL29* **(G)** gene expression in ESS patients, with significantly activated pathways in the high expression group on the left and significantly inhibited pathways on the right.

Through the integration of single-cell transcriptomic data from LG-ESS patients and HC, we delineated 12 major cell subpopulations, highlighting the complexity of the tumor microenvironment and its potential role in the pathogenesis of LG-ESS. Among these subpopulations, the Str in particular displayed substantial gene expression changes, underscoring their involvement in LG-ESS tumorigenesis. The identification of two distinct stromal subgroups, Str1 (MME^+ tumor cells) and Str2 (MME^- stromal fibroblasts), through reclustering of the Str subpopulation, has shed light on their divergent roles in LG-ESS. Our KEGG enrichment analysis revealed that Str1 is significantly enriched in pathways associated with oncogenesis, including Wnt signaling, focal adhesion, and PI3K-Akt signaling. The association between the abundance of Str1 and poor patient prognosis further accentuates the clinical relevance of this subpopulation. This suggests that Str1, characterized by their expression of MME, may play a central role in the malignant transformation and progression of LG-ESS.

Using RNA velocity analysis, we demonstrated that Str1 and Str2 cells share a common ancestral origin, suggesting that the differentiation of Str1 from normal stromal fibroblasts may be a key event in LG-ESS pathogenesis. This finding contradicts our initial hypothesis that Str1 arose directly from Str2, instead indicating a more complex tumorigenic process. Our pseudo-time analysis further confirmed that Str1 cells develop from an ancestral fibroblast population, highlighting the dynamic nature of tumor evolution in LG-ESS. Functional analysis of the gene expression changes during the differentiation of Str1 tumor cells further demonstrated the activation of key oncogenic pathways. Genes that were upregulated during the progression from normal fibroblasts to Str1 cells were enriched in pathways linked to cancer cell migration, proliferation, and extracellular matrix remodeling, all of which are hallmarks of tumor progression. Conversely, the downregulation of metabolic pathways, such as oxidative phosphorylation, suggests that tumor cells may undergo metabolic reprogramming as they acquire malignant characteristics.

10.3389/fimmu.2024.1513076

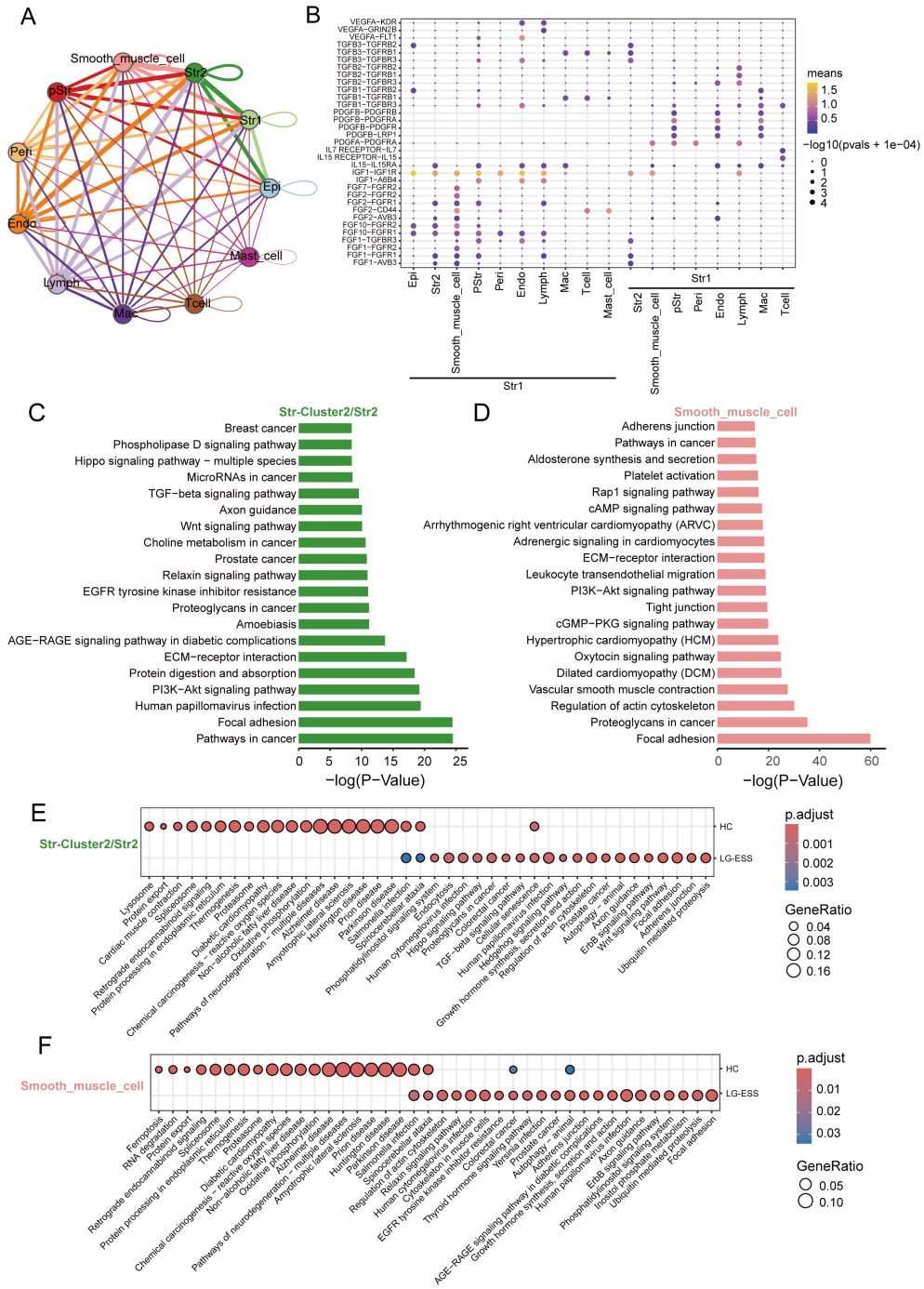

FIGURE 5
The functions of the Str2 and smooth muscle cells in the LG-ESS were altered. **(A)** Intercellular communication capacity between different cell types in LG-ESS. The color and thickness of the lines are used to distinguish the cellular origin and number of interacting ligands, and the circular lines indicate autocrine circuits. **(B)** Scatterplot indicating the interaction between Str1 and other cell subpopulations in LG-ESS via growth factor ligand-receptors. **(C, D)** Results of KEGG enrichment analysis of genes highly expressed in Str2 **(C)** and smooth muscle cells **(D)** in LG-ESS. **(E, F)** Scatter plots showing the results of KEGG enrichment analysis of differentially expressed genes in Str2 **(E)** and smooth muscle cells **(F)** in LG-ESS and compared to HC.

These observations are consistent with the metabolic changes often seen in cancer cells, which shift from oxidative phosphorylation to glycolysis to support rapid proliferation and survival in hypoxic environments.

Previous studies have indicated that the Wnt signaling pathway is significantly activated in LG-ESS (21, 38). Additionally, other research has found that FGF signaling plays a crucial role in Wnt-regulated cell proliferation (42), with FGF inhibition negating Wnt-

mediated cell proliferation (43). In our study, *FGF12* and *KLHL29* were found to be significantly overexpressed in Str1 cells, and their high expression levels were associated with shorter overall survival and progression-free survival. It is worth noting that the overexpression of *FGF12* was also observed in an independent cohort of uterine sarcoma patients and was significantly associated with a decrease in patient survival, further confirming its prognostic significance.

While *FGF12* serves as a prognostic biomarker associated with poor outcomes in LG-ESS, *KLHL29* also emerged as a potentially significant marker in this context. Our analysis revealed that *KLHL29* expression levels vary across different sarcoma subtypes, which may help distinguish between high-grade and low-grade ESS and LMS. This differential expression suggests that *KLHL29* could be valuable for clinical stratification of ESS patients, providing insights into tumor behavior and treatment responses. While *FGF12* may reflect the aggressiveness of the tumor microenvironment, *KLHL29*'s varying expression levels among different sarcoma types highlight its potential as a biomarker for distinguishing tumor subtypes. The synergistic evaluation of both *FGF12* and *KLHL29* may enhance our understanding of LG-ESS progression and guide more tailored therapeutic strategies.

In tumors, FGF is essential for maintaining endothelial integrity, promoting angiogenesis, and supporting tumor proliferation, survival, and metastasis (44, 45). Abnormal FGF signaling accelerates tumor growth by enhancing the formation of new blood vessels, which makes FGF inhibitors a promising therapeutic strategy (46–48). The association between the tumor cell subpopulation Str1 and its marker *FGF12* with poor prognosis in ESS suggests that targeting the FGF signaling pathway could be a promising therapeutic approach. Furthermore, their abundance/expression levels show no significant differences across different ESS subtypes, indicating that despite the clinical variations among ESS subtypes, they may share some key molecular characteristics that lead to similar prognostic outcomes. The relative stability of Str1 and *FGF12* may reflect their importance within the tumor microenvironment, particularly in promoting tumor cell survival and proliferation. Therefore, specific *FGF12*-targeted therapies, including selective FGFR inhibitors and neutralizing antibodies, could potentially be developed to inhibit FGF-mediated cell proliferation across all ESS subtypes. FGF receptor inhibitors, such as FGFR tyrosine kinase inhibitors (49), have shown efficacy in various cancers with aberrant FGF signaling and may represent a potential treatment avenue for ESS patients with high *FGF12* expression. However, developing FGF inhibitors presents certain challenges, as the FGF/FGFR signaling axis is vital for many normal biological processes, raising concerns about potential toxicity and necessitating careful dosage management (48). Furthermore, overcoming resistance may require combining FGF inhibitors with other therapeutic agents to enhance treatment efficacy (50).

The functional consequences of *FGF12* and *KLHL29* overexpression were further explored through gene set enrichment analysis (GSEA). Our results showed that high expression of both genes was associated with the activation of the MYOGENESIS pathway, a process often linked to tissue remodeling and cancer progression. In contrast, immune-related pathways such as the inflammatory response and interferon-gamma response were suppressed in the $FGF12^{high}$ group, implying that *FGF12* may contribute to immune evasion in LG-ESS. Similarly, $KLHL29^{high}$ tumors exhibited downregulation of the estrogen response early pathway, which may reflect an altered hormonal milieu in these tumors. This suggests that *FGF12* and *KLHL29* may play functional roles in promoting LG-ESS progression through different biological pathways.

Our study also emphasizes the broader impact of tumor cells on the surrounding stromal and immune compartments within the LG-ESS microenvironment. We observed strong intercellular interactions between Str1 tumor cells and smooth muscle cell subpopulations, particularly through growth factor-mediated signaling. These interactions are likely to drive functional changes in both stromal and smooth muscle cells, as evidenced by our KEGG analysis, which revealed enrichment of genes related to tumorigenesis and metastasis in these cell types. This indicates that stromal fibroblasts and smooth muscle cells within the tumor microenvironment can undergo phenotypic and functional alterations that promote tumor growth and invasion. The activation of CAFs and M2 macrophage polarization in epithelial tumors serves as a parallel example of how tumor cells can reshape their surrounding microenvironment to facilitate malignancy. Our findings suggest that a similar mechanism may be at play in LG-ESS, where tumor-derived factors drive the reprogramming of stromal and immune cells, ultimately contributing to disease progression.

While our study provides valuable insights into the biology of LG-ESS, several limitations should be acknowledged. First, given the rarity of LG-ESS, our single-cell RNA sequencing analysis was conducted on a sample from one LG-ESS patient. Although this single-sample design constrains generalizability, we addressed this limitation by integrating publicly available transcriptomic datasets and validating key findings—such as the prognostic significance of *FGF12*—within independent cohorts. These steps strengthen the reliability of our observations, yet additional studies with larger patient cohorts are essential to validate our findings and to capture the full spectrum of LG-ESS heterogeneity. Additionally, our study identified the tumor cell subgroup Str1, characterized by MME^{+} (gene of CD10 protein) expression, through a combination of H&E and miF staining. A minor population of cells in the Str2 subgroup also exhibited diffuse CD10 expression. However, since CD10 is expressed in both normal endometrial stromal cells and LG-ESS tumor cells (36, 37), CD10 alone cannot reliably distinguish malignant cells. This suggests that while some Str2 cells may have undergone malignant transformation, further marker studies are required to confirm their tumorigenic nature. Moreover, while we focused on stromal fibroblasts and their role in tumor progression, other cellular components of the tumor microenvironment, such as immune cells, were not analyzed in depth. Given the importance of immune-stromal crosstalk in tumor biology, further exploration of the interactions between tumor cells, stromal fibroblasts, and immune cells will be critical.

In conclusion, our study highlights the heterogeneity of stromal fibroblasts in LG-ESS and their critical role in tumor progression. The identification of Str1 as a poor prognostic factor and the discovery of *FGF12* as a prognostic biomarker opens new avenues for understanding and treating this rare form of uterine sarcoma.

Data availability statement

The datasets presented in this study can be found in online repositories. The names of the repository/repositories and accession number(s) can be found below: https://zenodo.org/records/, 13946278.

Ethics statement

The studies involving humans were approved by the Ethics Committee of Zunyi Medical University. The studies were conducted in accordance with the local legislation and institutional requirements. The participants provided their written informed consent to participate in this study.

Author contributions

YM: Formal Analysis, Visualization, Writing – original draft, Writing – review & editing. MD: Visualization, Validation, Writing – review & editing, Funding acquisition. QZ: Writing – review & editing. JT: Visualization, Writing – review & editing. NL: Writing – review & editing. YC: Writing – review & editing. DY: Writing – review & editing. HW: Writing – review & editing. S-HJ: Writing – review & editing. HY: Writing – review & editing. JW: Writing – review & editing. BF: Writing – review & editing. UG: Writing – review & editing. HM: Writing – review & editing. J-GZ: Funding acquisition, Resources, Writing – review & editing, Validation.

Funding

The author(s) declare that financial support was received for the research, authorship, and/or publication of this article. This work was supported by the National Natural Science Foundation of China (Grant No. 82060475), National Science and Technology Major Project of National Health Commission of China (Grant No. 2023ZD0502105), Chunhui program of the MOE (Ministry of Education in China) (Grant No. HZKY20220231), MOE Liberal arts and Social Sciences Foundation (Grant No. 24YJCZH462), the Natural Science Foundation of Guizhou Province (Grant No. ZK2022-YB632), Youth Talent Project of Guizhou Provincial Department of Education (Grant No. QJJ2022-224), Excellent Young Talent Cultivation Project of Zunyi City (Zunshi Kehe HZ (2023) 142), Future Journal Pre-proof Science and Technology Elite Talent Cultivation Project of Zunyi Medical University (ZYSE 2023-02), the Key Program of the Education Sciences Planning of Guizhou Province (Grant No.7), Collaborative Innovation Center of MOE (Grant No. 2020-39), Robert Bosch Stiftung (Grant No. 481).

Acknowledgments

We thank Kerstin Willecke for her excellent technical assistance. We gratefully acknowledge Prof. Steven Johnsen and the Robert Bosch Center for Tumor Diseases (RBCT) at the Bosch Health Campus for sharing the Akoya PhenoImager Fusion system.

Conflict of interest

The authors declare that the research was conducted in the absence of any commercial or financial relationships that could be construed as a potential conflict of interest.

The author(s) declared that they were an editorial board member of Frontiers, at the time of submission. This had no impact on the peer review process and the final decision.

Generative AI statement

The author(s) declare that no Generative AI was used in the creation of this manuscript.

Publisher's note

Supplementary material

The Supplementary Material for this article can be found online at: https://www.frontiersin.org/articles/10.3389/fimmu.2024.1513076/full#supplementary-material

SUPPLEMENTARY FIGURE 1
Results of removing batch effects for data from different sources and number of cells in all subpopulations. **(A)** Scatterplot plot showing the well-corrected batch effect (harmony) of different sources of HC and LG-ESS patient data. **(B)** Heatmap showing the expression levels of highly expressed top5 genes in all subpopulations. **(C)** The table shows the number of cells from all samples in each subpopulation.

SUPPLEMENTARY FIGURE 2
Elevated Proportion of Str1 in ESS Correlates with Reduced Survival. **(A)** miF staining result of LG-ESS sample. CD10, desmin,α-SMA, and other markers are used to distinguish different cell populations within the tumor, with magnified views focusing on specific regions of interest. The scale bars represent 100μm and 30μm. **(B)** Survival analysis results of the proportion of Str1 in ESS patients, with the left panel representing overall survival and the right panel depicting progression-free survival (GSE128630). **(C)** Variations in the proportion of Str1 among different subtypes of uterine sarcoma patients (GSE85383). (Wilcoxon rank-sum test; ns, non-significant)

SUPPLEMENTARY FIGURE 3
FGF12 has potential as a prognostic biomarker for sarcoma. **(A, B)** Multivariate Cox regression analysis for overall survival **(A)** and progression-free survival **(B)** in LG-ESS patients. The analysis included relevant clinical factors, such as age at diagnosis, tumor grade, and BMI, alongside the expression levels of *FGF12* and *KLHL29*. Hazard ratios (HR) and 95% confidence intervals (CI) are shown for each factor. **(C)** Survival analysis outcomes based on the expression of *FGF12* (left) and *KLHL29* (right) genes in uterine sarcoma patients (GSE119041), focusing on overall survival. **(D)** Differential expression of *FGF12* and *KLHL29* genes among various subtypes of uterine sarcoma patients. (Wilcoxon rank-sum test; $*P < 0.05$; $**P < 0.01$; ns, non-significant)

References

1. Stewart LE, Beck TL, Giannakopoulos NV, Rendi MH, Isacson C, Goff BA. Impact of oophorectomy and hormone suppression in low grade endometrial stromal sarcoma: A multicenter review. *Gynecol Oncol*. (2018) 149(2):297–300. doi: 10.1016/j.ygyno.2018.03.008

2. Rauh-Hain JA, Del Carmen MG. Endometrial stromal sarcoma: a systematic review. *Obstet Gynecol*. (2013) 122(3):676–83. doi: 10.1097/AOG.0b013e3182a189ac

3. Höhn AK, Brambs CE, Hiller GGR, May D, Schmoeckel E, Horn LC. 2020 WHO classification of female genital tumors. *Geburtshilfe Frauenheilkd*. (2021) 81(10):1145–53. doi: 10.1055/a-1545-4279

4. Gadducci A, Multinu F, De Vitis LA, Cosio S, Carinelli S, Aletti GD. Endometrial stromal tumors of the uterus: Epidemiology, pathological and biological features, treatment options and clinical outcomes. *Gynecol Oncol*. (2023) 171:95–105. doi: 10.1016/j.ygyno.2023.02.009

5. Kikuchi A, Yoshida H, Tsuda H, Nishio S, Suzuki S, Takehara K, et al. Clinical characteristics and prognostic factors of endometrial stromal sarcoma and undifferentiated uterine sarcoma confirmed by central pathologic review: A multi-institutional retrospective study from the Japanese Clinical Oncology Group. *Gynecol Oncol*. (2023) 176:82–9. doi: 10.1016/j.ygyno.2023.07.002

6. Desar IME, Ottevanger PB, Benson C, van der Graaf WTA. Systemic treatment in adult uterine sarcomas. *Crit Rev Oncol Hematol*. (2018) 122:10–20. doi: 10.1016/j.critrevonc.2017.12.009

7. Dessources K, Miller KM, Kertowidjojo E, Da Cruz Paula A, Zou Y, Selenica P, et al. ESR1 hotspot mutations in endometrial stromal sarcoma with high-grade transformation and endocrine treatment. *Mod Pathol*. (2022) 35(7):972–8. doi: 10.1038/s41379-021-01003-5

8. Chu MC, Mor G, Lim C, Zheng W, Parkash V, Schwartz PE. Low-grade endometrial stromal sarcoma: hormonal aspects. *Gynecol Oncol*. (2003) 90(1):170–6. doi: 10.1016/S0090-8258(03)00258-0

9. Yamaguchi M, Erdenebaatar C, Saito F, Motohara T, Miyahara Y, Tashiro H, et al. Long-term outcome of aromatase inhibitor therapy with letrozole in patients with advanced low-grade endometrial stromal sarcoma. *Int J Gynecol Cancer*. (2015) 25(9):1645–51. doi: 10.1097/IGC.0000000000000557

10. Yamamoto M, Tsujikawa T, Yamada S, Kurokawa T, Shinagawa A, Chino Y, et al. 18F-FDG/18F-FES standardized uptake value ratio determined using PET predicts prognosis in uterine sarcoma. *Oncotarget*. (2017) 8(14):22581–9. doi: 10.18632/oncotarget.15127

11. Zhao Z, Yoshida Y, Kurokawa T, Kiyono Y, Mori T, Okazawa H. 18F-FES and 18F-FDG PET for differential diagnosis and quantitative evaluation of mesenchymal uterine tumors: correlation with immunohistochemical analysis. *J Nucl Med*. (2013) 54(4):499–506. doi: 10.2967/jnumed.112.113472

12. Ali SI, Sayyed RH, Bakar MA, Sadaf T, Syed AA. A retrospective study of endometrial stromal sarcoma: an institutional review. *J Pak Med Assoc*. (2020) 70(5):926–9. doi: 10.5455/JPMA.299808

13. Bai H, Yang J, Cao D, Huang H, Xiang Y, Wu M, et al. Ovary and uterus-sparing procedures for low-grade endometrial stromal sarcoma: a retrospective study of 153 cases. *Gynecol Oncol*. (2014) 132(3):654–60. doi: 10.1016/j.ygyno.2013.12.032

14. Wu J, Zhang H, Li L, Hu M, Chen L, Xu B, et al. A nomogram for predicting overall survival in patients with low-grade endometrial stromal sarcoma: A population-based analysis. *Cancer Commun (Lond)*. (2020) 40(7):301–12. doi: 10.1002/cac2.12067

15. Seagle BL, Shilpi A, Buchanan S, Goodman C, Shahabi S. Low-grade and high-grade endometrial stromal sarcoma: A National Cancer Database study. *Gynecol Oncol*. (2017) 146(2):254–62. doi: 10.1016/j.ygyno.2017.05.036

16. Barney B, Tward JD, Skidmore T, Gaffney DK. Does radiotherapy or lymphadenectomy improve survival in endometrial stromal sarcoma? *Int J Gynecol Cancer*. (2009) 19(7):1232–8. doi: 10.1111/IGC.0b013e3181b33c9a

17. Kang N, Zhang Y, Guo S, Chen R, Kong F, Wang S, et al. Genomic and transcriptomic characterization revealed the high sensitivity of targeted therapy and immunotherapy in a subset of endometrial stromal sarcoma. *Cancer Res Treat*. (2023) 55(3):978–91. doi: 10.4143/crt.2022.1647

18. Sylvestre VT, Dunton CJ. Treatment of recurrent endometrial stromal sarcoma with letrozole: a case report and literature review. *Horm Cancer*. (2010) 1(2):112–5. doi: 10.1007/s12672-010-0007-9

19. Conklin CM, Longacre TA. Endometrial stromal tumors: the new WHO classification. *Adv Anat Pathol*. (2014) 21(6):383–93. doi: 10.1097/PAP.0000000000000046

20. Kim GW, Baek SK, Han JJ, Kim HJ, Sung JY, Maeng CH. Pulmonary metastasizing low-grade endometrial stromal sarcoma: case report and review of diagnostic pitfalls. *Diagnost (Basel)*. (2022) 12(2). doi: 10.3390/diagnostics12020271

21. Micci F, Heim S, Panagopoulos I. Molecular pathogenesis and prognostication of "low-grade" and "high-grade" endometrial stromal sarcoma. *Genes Chromosomes Cancer*. (2021) 60(3):160–7. doi: 10.1002/gcc.22907

22. Miao Y, Konno Y, Wang B, Zhu L, Zhai T, Ihira K, et al. Integrated multi-omics analyses and functional validation reveal TTK as a novel EMT activator for endometrial cancer. *J Transl Med*. (2023) 21(1):151. doi: 10.1186/s12967-023-03998-8

23. Ren X, Liang J, Zhang Y, Jiang N, Xu Y, Qiu M, et al. Single-cell transcriptomic analysis highlights origin and pathological process of human endometrioid endometrial carcinoma. *Nat Commun*. (2022) 13(1):6300. doi: 10.1038/s41467-022-33982-7

24. Gotoh O, Sugiyama Y, Takazawa Y, Kato K, Tanaka N, Omatsu K, et al. Clinically relevant molecular subtypes and genomic alteration-independent differentiation in gynecologic carcinosarcoma. *Nat Commun*. (2019) 10(1):4965. doi: 10.1038/s41467-019-12985-x

25. Gultekin O, Gonzalez-Molina J, Hardell E, Moyano-Galceran L, Mitsios N, Mulder J, et al. FOXP3+ T cells in uterine sarcomas are associated with favorable prognosis, low extracellular matrix expression and reduced YAP activation. *NPJ Precis Oncol*. (2021) 5(1):97. doi: 10.1038/s41698-021-00236-6

26. Przybyl J, Kowalewska M, Quattrone A, Dewaele B, Vanspauwen V, Varma S, et al. Macrophage infiltration and genetic landscape of undifferentiated uterine sarcomas. *JCI Insight*. (2017) 2(11). doi: 10.1172/jci.insight.94033

27. Mcginnis CS, Murrow LM, Gartner ZJ. DoubletFinder: doublet detection in single-cell RNA sequencing data using artificial nearest neighbors. *Cell Syst*. (2019) 8(4):329–37.e4. doi: 10.1016/j.cels.2019.03.003

28. Hao Y, Hao S, Andersen-Nissen E, Mauck WM, Zheng S, Butler A, et al. Integrated analysis of multimodal single-cell data. *Cell*. (2021) 184(13). doi: 10.1016/j.cell.2021.04.048

29. Korsunsky I, Millard N, Fan J, Slowikowski K, Zhang F, Wei K, et al. Fast, sensitive and accurate integration of single-cell data with Harmony. *Nat Methods*. (2019) 16(12):1289–96. doi: 10.1038/s41592-019-0619-0

30. Lv H, Zhao G, Jiang P, Wang H, Wang Z, Yao S, et al. Deciphering the endometrial niche of human thin endometrium at single-cell resolution. *Proc Natl Acad Sci U.S.A*. (2022) 119(8). doi: 10.1073/pnas.2115912119

31. La Manno G, Soldatov R, Zeisel A, Braun E, Hochgerner H, Petukhov V, et al. RNA velocity of single cells. *Nature*. (2018) 560(7719):494–8. doi: 10.1038/s41586-018-0414-6

32. Qiu X, Mao Q, Tang Y, Wang L, Chawla R, Pliner HA, et al. Reversed graph embedding resolves complex single-cell trajectories. *Nat Methods*. (2017) 14(10):979–82. doi: 10.1038/nmeth.4402

33. Efremova M, Vento-Tormo M, Teichmann SA, Vento-Tormo R. CellPhoneDB: inferring cell-cell communication from combined expression of multi-subunit ligand-receptor complexes. *Nat Protoc*. (2020) 15(4):1484–506. doi: 10.1038/s41596-020-0292-x

34. Jew B, Alvarez M, Rahmani E, Miao Z, Ko A, Garske KM, et al. Accurate estimation of cell composition in bulk expression through robust integration of single-cell information. *Nat Commun*. (2020) 11(1):1971. doi: 10.1038/s41467-020-15816-6

35. Yu G, Wang LG, Han Y, He QY. clusterProfiler: an R package for comparing biological themes among gene clusters. *Omics*. (2012) 16(5):284–7. doi: 10.1089/omi.2011.0118

36. Mccluggage WG, Sumathi VP, Maxwell P. CD10 is a sensitive and diagnostically useful immunohistochemical marker of normal endometrial stroma and of endometrial stromal neoplasms. *Histopathology*. (2001) 39(3):273–8. doi: 10.1046/j.1365-2559.2001.01215.x

37. Akaev I, Yeoh CC, Rahimi S. Update on endometrial stromal tumours of the uterus. *Diagnost (Basel)*. (2021) 11(3). doi: 10.3390/diagnostics11030429

38. Przybyl J, Kidzinski L, Hastie T, Debiec-Rychter M, Nusse R, van de Rijn M. Gene expression profiling of low-grade endometrial stromal sarcoma indicates fusion protein-mediated activation of the Wnt signaling pathway. *Gynecol Oncol*. (2018) 149(2):388–93. doi: 10.1016/j.ygyno.2018.03.007

39. Mao X, Xu J, Wang W, Liang C, Hua J, Liu J, et al. Crosstalk between cancer-associated fibroblasts and immune cells in the tumor microenvironment: new findings and future perspectives. *Mol Cancer*. (2021) 20(1):131. doi: 10.1186/s12943-021-01428-1

40. Kennel KB, Bozlar M, De Valk AF, Greten FR. Cancer-associated fibroblasts in inflammation and antitumor immunity. *Clin Cancer Res*. (2023) 29(6):1009–16. doi: 10.1158/1078-0432.CCR-22-1031

41. Zhao S, Mi Y, Guan B, Zheng B, Wei P, Gu Y, et al. Tumor-derived exosomal miR-934 induces macrophage M2 polarization to promote liver metastasis of colorectal cancer. *J Hematol Oncol*. (2020) 13(1):156. doi: 10.1186/s13045-020-00991-2

42. Ten Berge D, Brugmann SA, Helms JA, Nusse R. Wnt and FGF signals interact to coordinate growth with cell fate specification during limb development. *Development*. (2008) 135(19):3247–57. doi: 10.1242/dev.023176

43. Tang D, He Y, Li W, Li H. Wnt/β-catenin interacts with the FGF pathway to promote proliferation and regenerative cell proliferation in the zebrafish lateral line neuromast. *Exp Mol Med*. (2019) 51(5):1–16. doi: 10.1038/s12276-019-0247-x

44. Zhou Y, Tao L, Qiu J, Xu J, Yang X, Zhang Y, et al. Tumor biomarkers for diagnosis, prognosis and targeted therapy. *Signal Transduct Target Ther*. (2024) 9(1):132. doi: 10.1038/s41392-024-01823-2

45. Presta M, Dell'era P, Mitola S, Moroni E, Ronca R, Rusnati M. Fibroblast growth factor/fibroblast growth factor receptor system in angiogenesis. *Cytokine Growth Factor Rev*. (2005) 16(2):159–78. doi: 10.1016/j.cytogfr.2005.01.004

46. Mashreghi M, Azarpara H, Bazaz MR, Jafari A, Masoudifar A, Mirzaei H, et al. Angiogenesis biomarkers and their targeting ligands as potential targets for tumor angiogenesis. *J Cell Physiol*. (2018) 233(4):2949–65. doi: 10.1002/jcp.v233.4

47. Yashiro M, Matsuoka T. Fibroblast growth factor receptor signaling as therapeutic targets in gastric cancer. *World J Gastroenterol*. (2016) 22(8):2415–23. doi: 10.3748/wjg.v22.i8.2415

48. Brooks AN, Kilgour E, Smith PD. Molecular pathways: fibroblast growth factor signaling: a new therapeutic opportunity in cancer. *Clin Cancer Res*. (2012) 18(7):1855–62. doi: 10.1158/1078-0432.CCR-11-0699

49. Xie Y, Su N, Yang J, Tan Q, Huang S, Jin M, et al. FGF/FGFR signaling in health and disease. *Signal Transduct Target Ther*. (2020) 5(1):181. doi: 10.1038/s41392-020-00222-7

50. Dieci MV, Arnedos M, Andre F, Soria JC. Fibroblast growth factor receptor inhibitors as a cancer treatment: from a biologic rationale to medical perspectives. *Cancer Discovery*. (2013) 3(3):264–79. doi: 10.1158/2159-8290.CD-12-0362

frontiers | Frontiers in Immunology

TYPE Original Research
PUBLISHED 27 January 2025
DOI 10.3389/fimmu.2025.1492541

OPEN ACCESS

EDITED BY
Jinhwan Kim,
University of California, Davis, United States

REVIEWED BY
Zhiqing Long,
Sun Yat-sen University Cancer Center (SYSUCC), Guangzhou, China
Yunyoung Lee,
University of California, Davis, United States

*CORRESPONDENCE
Yu Lin
13580311726@163.com
Xiaoshan Hong
haifeng-1-1@163.com
Lv Deng
183027228@qq.com

†These authors have contributed equally to this work

RECEIVED 07 September 2024
ACCEPTED 07 January 2025
PUBLISHED 27 January 2025

CITATION
Huang Y, Li H, Wei Z, He W, Chen B, Cheng S, Zhao Z, Deng L, Chen X, Lin Y and Hong X (2025) Establishment of a prognostic signature and immune infiltration characteristics for uterine corpus endometrial carcinoma based on a disulfidptosis/ferroptosis-associated signature.
Front. Immunol. 16:1492541.
doi: 10.3389/fimmu.2025.1492541

Establishment of a prognostic signature and immune infiltration characteristics for uterine corpus endometrial carcinoma based on a disulfidptosis/ferroptosis-associated signature

Yong Huang[1†], Huibin Li[2†], Zhifu Wei[3†], Wanshan He[1], Bin Chen[1], Shuang Cheng[4], Zhifang Zhao[4], Lv Deng[5,6*], Xiaohua Chen[7], Yu Lin[8,9*] and Xiaoshan Hong[1,10*]

[1]Department of Gynecology, Guangdong Women and Children Hospital, Guangzhou, China, [2]Department of Pathology, Guangdong Women and Children Hospital, Guangzhou, China, [3]Department of Gynecology, The Affiliated Shunde Hospital of Jinan University, Foshan, China, [4]Department of Gastroenterology, Guizhou Provincial People's Hospital, Guiyang, China, [5]Department of Gastroenterology, People's Hospital of Rongjiang County, Rongjiang, China, [6]Department of Gastroenterology, People's Hospital of Nanhai District, Foshan, China, [7]Oncology Center, Southern Medical University Hospital of Integrated Traditional Chinese and Western Medicine, Southern Medical University, Guangzhou, China, [8]Nanfang Hospital, Southern Medical University, Guangzhou, China, [9]Department of Gastroenterology, Southern Medical University Hospital of Integrated Traditional Chinese and Western Medicine, Southern Medical University, Guangzhou, China, [10]Department of Gynecology, Qingxin District Hospital of Women and Children Healthcare, Qingyuan, China

Background: Disulfidptosis and ferroptosis are two different programmed cell death pathways, and their potential therapeutic targets have important clinical prospects. Although there is an association between the two, the role of genes associated with these two forms of cell death in the development of endometrial cancer remains unclear.

Methods: In this study, RNA sequencing (RNA-seq) and clinical data were obtained from public databases, and comprehensive analysis methods, including difference analysis, univariate Cox regression, and Least Absolute Shrinkage and Selection Operator (LASSO) analysis were used to construct a disulfidptosis/ferroptosis-related genes (DFRGs) prognostic signature. To further explore this new feature, pathway and functional analyses were performed, and the differences in gene mutation frequency and the level of immune cell infiltration between the high- and low-risk groups were studied. Finally, we validated the prognostic gene expression profile in clinical samples.

Results: We identified five optimal DFRGs that were differentially expressed and associated with the prognosis of uterine corpus endometrial carcinoma (UCEC). These genes include CDKN2A, FZD7, LCN2, ACTN4, and MYH10. Based on these DFRGs, we constructed a robust prognostic model with significantly lower overall survival in the high-risk group than in the low-risk group, with differences in tumor burden and immune invasion between the different risk groups. The expression of two key genes, ACTN4 and LCN2, was verified by immunohistochemistry and RT-qPCR.

Conclusion: This study established a clinical prognostic model associated with disulfidptosis/ferroptosis-related genes, and the expression characteristics of key genes were validated in clinical samples. The comprehensive assessment of disulfidptosis and ferroptosis provides new insights to further guide patient clinical management and personalized treatment.

KEYWORDS

UCEC, uterine corpus endometrial carcinoma, disulfidptosis, ferroptosis, prognostic signature, immune infiltration

1 Introduction

Uterine corpus endometrial carcinoma (UCEC) is a common malignant gynecological disease, and the prevalence rate of UCEC has increased by 132% in the past three decades (1). Currently, the key to the diagnosis of endometrial cancer is the pathological evaluation of endometrial tissue, but this invasive test is only useful for patients who have undergone endometrial biopsy or ultrasound and who exhibit endometrial thickening. Despite treatment guidelines from the European Society of Gynecologic Oncology, which are based on clinical staging and molecular subtyping, there are differences in the prognoses of patients with endometrial cancer according to risk group (2). Approximately 15% of patients with urothelial carcinoma (UCEC) are at an advanced stage at the time of diagnosis. In addition, approximately 15 to 20% of patients are at risk of recurrence after initial surgical treatment (3, 4), and the prognosis for this subset of patients remains poor (5). Research on the early diagnosis of endometrial cancer and its prognostic risk factors is still in its infancy. Currently, no feasible clinical prognostic model has been developed, which limits the effective formulation of personalized treatment strategies. Disulfidptosis is a unique type of cell death pathway identified in recent biological studies (6). Excessive cystine induces rapid apoptosis due to the increase in disulfide bond pressure, which has extraordinary potential value in predicting the end of cells and the effectiveness of immunotherapy. Ferroptosis, a specific form related to iron-dependent cell death, has received extensive attention in the treatment of drug-resistant endometrial cancer in recent years (7–9)and some articles have reported that some ferroptosis-related genes have important value in predicting the prognostic status of endometrial cancer patients (10, 11).

Although disulfidptosis and ferroptosis are two different forms of cell death, they share a common regulator plasma carrier family 7 member11 (SLC7A11). Cancer cells rely on SLC7A11 cystine input to maintain redox balance and cell survival, which can inhibit the occurrence of ferroptosis, and SLC7A11 downregulation and methylation can induce ferroptosis in endometrial cancer cells (12, 13), however, when the SLC7A11 gene is overexpressed and glucose deprivation occurs, disulfidptosis death is triggered. Therefore, this exploratory work is the first to link disulfidptosis with ferroptosis. By analyzing large-scale public data resources, we screened genes related to these two phenomena (disulfidptosis/ferroptosis-related genes, (DFRGs)) and established a prognostic model of their coexistence. This model provides a comprehensive perspective for understanding the composite effects of DFRGs on UCEC. After careful screening, we identified five genes associated with survival probability (CDKN2A, FZD7, LCN2, ACTN4, and MYH10) as useful biomarkers for disease identification and prognostic assessment. Based on the risk ratings of these genes, we subdivided UCEC patients into several different prognostic classes. We subsequently compared the differences between the higher- and lower-risk categories in terms of immune score, and immune cell penetration, and initially confirmed them in actual clinical tissue samples. The aim of this study was to determine the feasibility of a personalized medical protocol for UCEC patients, with the expectation of optimizing their postoperative recovery prospects.

2 Materials and methods

2.1 Dataset information

RNA sequencing data (HTSeq-FPKM) and clinical prognostic information on UCEC patients were obtained from the TGCA database (https://portal.gdc.cancer.gov/). A total of 589 cases were included in the analysis, including 554 endometrial cancer samples and 35 normal tissue samples. (Supplementary Figure S1). Out of these, 560 cases included clinical information. we implemented the following preprocessing steps to ensure data quality: (1) Cases with a reported survival time of zero or those lacking survival time information were excluded from our analysis, resulting in the removal of 16 cases. (2) In instances of missing clinical data other than survival time, we applied appropriate imputation methods where feasible or documented exclusions to maintain data integrity and transparency.

We screened 512 ferroptosis-associated genes (FAGs) through a comprehensive review of the FerrDb database (14) (http://zhounan.org/ferrdb/legacy/index.html, July 1, 2023), which is a curated resource focused on genes and molecules associated with

ferroptosis. The identification of the disulfidptosis-related genes mainly referenced the protein-protein interaction network of the proteins with disulfide bonds, reported by Liu et al. (15). We applied a filter to include only those genes that had at least two supporting studies cited in the literature. This led to the inclusion of the following key genes: NADPH, INF2, SLC7A11, CD2AP, DLIM1, MYH9, ACTN4, IQGAP1, MYH10, FLNB, FLNA, MYL6, TLN1, DSTN, CAPZB and ACTB.

2.2 Differential analysis of disulfidptosis-related and ferroptosis-associated genes

In this study, a preliminary collation of the RNA-seq dataset and associated clinical information was performed to eliminate incomplete records. First, the "Limma" R software package was used to screen the differentially expressed disulfidptosis/ferroptosis-related genes (DE-DFRGs) using the criteria of $|\log2FC| > 0.5$ and FDR < 0.05. This selection was made to capture potential candidate genes that may play a role in cancer prognosis to the greatest extent possible, balancing sensitivity and specificity. The correlation between disulfidptosis and ferroptosis was calculated via the Spearman method using the "psych" R software, and a Holm-adjusted significance test was performed with P value correction to generate a network showing the association between the two.

2.3 Construction of the DFRG prognostic model and validation

To explore the DE-DFRGs associated with disease prognosis, we first partitioned the dataset into a training set (70%) and a validation set (30%). In the training set, we performed Cox proportional hazard model analysis on the independent variables and identified differentially expressed genes that were considered significantly associated with the survival period. Subsequently, Least Absolute Shrinkage and Selection Operator (LASSO)-Cox regression analysis was performed to filter out genes with strong collinearity, aiming to identify genes that are critical for prognosis. Specifically, we performed variance inflation factor (VIF) analysis prior to applying LASSO-Cox regression, predictors with VIF values greater than 5 were considered indicative of multicollinearity and were either removed or combined where appropriate. Additionally, we have included details on the optimization of the regularization parameter using 10-fold cross-validation, which helps to minimize the overfitting risk and determine the most appropriate lambda value. The predictive models were established using the "GLMnet" and "Survival" packages in R software. The prognostic risk score of the TCGA-UCEC cohort was estimated using the "Model Predictions" R package, and patients were classified into different prognostic classes according to the median risk score (low -risk or high -risk). The Kaplan-Meier method, stratified Cox regression, multivariate Cox regression, and ROC curve analysis were used to confirm the validity and reliability of the prognostic model. Calibration curves were generated via a canonical graph model to produce a prognostic graph depicting the survival of patients with endometrial cancer at 1-, 3-, and 5- years. Additionally, we conducted external validation using two independent transcriptomic datasets from the GEO database (GSE21882 and GSE115810). Applying our prognostic model to these cohorts, we compared risk factors associated with different 5-year survival outcomes and tumor differentiation levels.

2.4 GO, KEGG and mi-RNA regulatory relationship

Gene ontology (GO) and Kyoto Encyclopedia (KEGG) enrichment analyses were used to further explore the biological processes and pathways associated with the DFRGs, via 'Cluster Profiler' R software (version 3.14.3). Due to the high number of tests performed in enrichment analysis, we utilized the Benjamini-Hochberg (BH) method to control the false discovery rate (FDR), thereby improving the reliability of the findings. In addition, the UCEC miRNA sequence data were obtained from the TCGA database. The "Limma" package of R was used to explore the differences in miRNA expression. Prognostic miRNAs were screened via a univariate Cox regression model. We employed Pearson or Spearman correlation coefficients to assess the relationships between miRNAs and their target genes, depending on the distribution of the data.

2.5 Tumor mutational burden analysis

After the analysis, single nucleotide polymorphism (SNP) information for UCEC was extracted from the TCGA database, which is helpful for exploring the associations between prognosis and cancer. Through the "maftools" R software package, the TMB value of each patient was calculated. Only non-synonymous variants in coding regions were considered for the TMB calculation, as these are more likely to have functional implications in tumor biology. Previous studies have shown that using the median is a common practice in TMB analysis, ensuring that our approach aligns with established conventions in the field. Accordingly, all patients were subsequently divided into two groups based on the median TMB value: one group included samples with high TMB values, and the other included samples with low TMB values. We identified the top variant genes with significant differences when high and low -risk categories were compared and explored the correlation between the TMB and risk score.

2.6 Immune infiltration of the disulfidptosis/ferroptosis-related prognostic model

We obtained the abundance of infiltrating immune cells through various algorithms adopted by the TIMER 2.0 (http://

timer.cistrome.Org/) database. To account for potential batch effects and noise in the immune infiltration data, we utilized the ComBat method from the "sva" package in R, which adjusts for batch effects in the data. Twenty-two immune cell infiltrates between different risk groups were evaluated via the CIBERSORT algorithm, and the results were visualized via the "vioplot" R package. The prognostic differences between different immune infiltration profiles were subsequently analyzed.

2.7 Expression levels of key prognostic genes in biological samples

In this study, we collected postoperative biological samples and paraffin-fixed sections from patients treated at Guangdong Women and Children's Hospital from January 2023 to August 2023. The patients signed a consent form before surgery for the donation of their excised tissue, which was stored in our pathology laboratory, for scientific research. After the model was constructed, this study submitted a clinical sample use application to the Ethics Committee of Guangdong Women and Children Hospital according to standard procedures and received ethical approval (Approval No. 202301078). Five endometrial cancer tissue samples and sections were approved for key gene validation, one of which was used for preexperiments (clinical information is detailed in Appendix File 2).

During the sample application process, the samples were reviewed by pathology experts and labeled as tumor tissue or adjacent tissue. Fresh tissue indicated a sample retained for rapid pathological testing during surgery and was stored in liquid nitrogen, a -80°C environment or a dry ice transport box until it was used for detection. The mRNA expression levels of CDKN2A, FZD7, LCN2, ACTN4 and MYH10 were quantitatively analyzed via real-time quantitative polymerase chain reaction (RT–qPCR). We specified that all experiments were performed in triplicate and included information on the assessment of technical variability. Each sample was analyzed in at least three independent biological replicates to account for biological variability. we employed the ΔΔCt method for relative quantification of gene expression. The statistical methods used to analyze the RT-qPCR results included a paired t-test for comparing expression levels between tumor and adjacent normal tissues when analyzing matched samples.

RNA was extracted from the tumor samples and normal tissues via TRIzol reagent (Ambion, USA). A quantitative reverse transcription kit (Promega, USA) was subsequently used to reverse transcribe the products into cDNA. Quantitative PCR (qPCR) is a technique for measuring the DNA content of a sample in real time. The SYBR-Green reagent of the Vazyme Company was used to carry out real-time fluorescence quantitative qPCR detection, and the expression level of each sample was corrected and standardized to the expression level of actin. The primers used are detailed in Appendix S3.

All the slides were processed by first incubating them at 60°C for 20 minutes, deparaffinizing them in xylene, and rehydrating them in gradient ethanol. After incubation with 3% hydrogen peroxide for 10 min, the slides were soaked in 0.01 M citrate buffer (pH 6.0) to recover the antigen for 30 min. The slides were incubated overnight at 4°C with their corresponding antibodies after being blocked with 5% bovine serum albumin. Then, another biotinylated antibody was added at room temperature for one hour. The progress of immunohistochemical staining was monitored by using diaminobenzidine as the reaction medium, and restraining was performed with hematoxylin.

2.8 Statistical analysis

In this study, we adopted a series of analytical validation methods for bioinformatics and statistical analysis. Differentially expressed gene screening and model construction are primarily performed using R software (4.2.0), which is derived from publicly available versions in CRAN and Bioconductor. For differential expression analysis, we utilized the DESeq2 package, using the DESeq() function to normalize and analyze RNA-seq data. For survival analysis, the survival package was used, specifically the coxph() function to fit Cox proportional hazards models, and analysis of survival curves was conducted using the survfit() function. For LASSO-Cox regression, we implemented the glmnet package, utilizing the cv.glmnet() function for cross-validation and lambda optimization. For immune infiltration analysis with CIBERSORT, we utilized custom R scripts compatible with the CIBERSORT algorithm to process RNA-seq data. Enrichment analysis for GO and KEGG was performed using the clusterProfiler package with functions such as enrichGO and enrichKEGG. The t test and Wilcoxon rank sum test were performed to analyze the differences between two sample groups, whereas the Kruskal–Wallis test was used to analyze the differences between two or more sample groups. We set the threshold for statistical significance to $p<0.05$, and all data analysis was performed via R software.

3 Results

3.1 Differential expression of disulfidptosis-related and ferroptosis-associated genes in UCEC

We analyzed the differential expression of 16 disulfidptosis-related genes and 512 ferroptosis-related genes in the TCGA-UCEC cohort (Supplementary Figure S1). DE-DFRGs were identified via the "limma" R package, and expression heatmaps were generated for normal versus tumor tissues (Figures 1A, B). Finally, 10 genes associated with disulfidptosis (Figure 1C) and 41 genes associated with ferroptosis (Figure 1D) were screened and mapped to volcanoes. In addition, we explored the correlation between the differential genes related to disulfidptosis and ferroptosis and found that there was a significant positive correlation between the expression of disulfidptosis genes and the expression of most ferroptosis genes (Figure 1E, Appendix File 4).

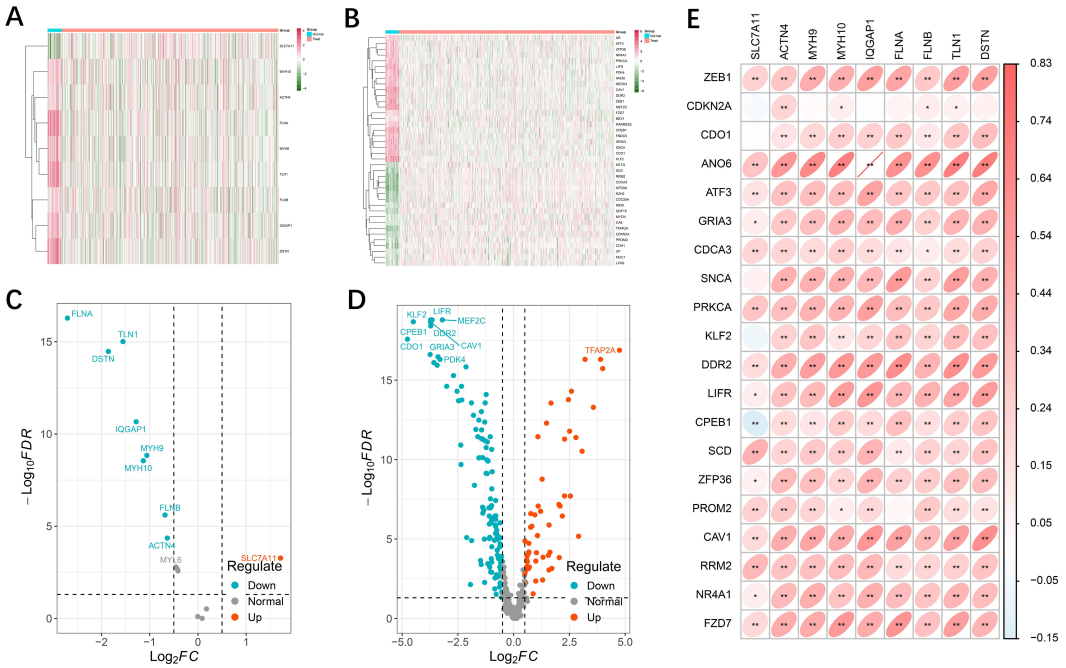

FIGURE 1
Differential expression of disulfidptosis- and ferroptosis-related genes. **(A, B)** Heatmap showing the disulfidptosis- and ferroptosis-related genes in tumor and normal adjacent tissues. Green represents downregulation, and red represents upregulation of the gene. **(C, D)** Volcano map of 9 differential disulfidptosis-related genes and 178 differential ferroptosis-related genes. **(E)** Interactive correlation heatmap between differential disulfidptosis-related genes and ferroptosis-related genes (p <0.01 = **, and p < 0.05 = *).

3.2 Establishment of the DFRG model

To further screen DFRG genes related to survival prognosis, we first performed univariate Cox regression on the differential genes associated with disulfidptosis and ferroptosis, calculated the relationships between the changes in the expression of individual genes and the prognostic characteristics of patients (Supplementary Figure S2), followed by further screening of the common differential genes via a LASSO regression model (Figures 2A, B). Finally, a prognostic risk model based on five genes was constructed with the following formula: risk score = [CDKN2A expression × (1.3412)] + [FZD7 expression × (0.7441)] + [LCN2 expression × (-0.5069)] + [ACTN4 × (0.7265)] + [MYH10 expression × (-0.7140)]. Using the median risk score as a criterion for differentiation, we subdivided UCEC patients into high- and low-risk groups (Figure 2C). The statistical distributions of the five different DE-DFRG expression patterns are illustrated below (Figure 2D). The data from the KM curve revealed that overall survival was significantly lower in the high-risk group than in the low-risk group (Figure 2E).

3.3 Validation of model accuracy

Time-based ROC curve analysis was performed to determine the predictive efficacy of the signal, and the area under the operating characteristic curve (AUC) of the observed object was 0.689 at 365 days; at 1905 and 1825 days, the values were 0.652 and 0.727, respectively (Figure 3A). We then constructed a model for predicting one-, three-, and five-year survival in patients with UCEC based on relevant prognostic indicators, which showed significant accuracy in predicting the outcome (Figure 3B). We evaluated the risk signature regard to pathological features (tumor stage), high risk was significantly associated with more severe stages (Figures 3C, D). We included two additional analyses to further validate our prognostic model. we compared the risk scores for patients those who survived to five years with those who did not (GSE21882 from GEO dataset), and the risk scores between normal/G1 stage tumors with G2/G3 stage tumors (GSE115810 from GEO dataset). The results indicated that patients with poorer 5-year survival outcomes (Figure 3E) and lower tumor differentiation (Figure 3F) had significantly higher risk scores.

3.4 Functional enrichment analysis and correlation analysis of microRNA

To explore the hidden biological attributes related to risk assessment indicators, this study analyzed the KEGG and GO functions of differentially expressed genes (DEGs) in high- and low-risk categories. The results revealed that the pathways involved in glycosphingolipid biosynthesis, extracellular mechanism interactions, and signaling are diverse and complex (Figures 4A, B). In addition, through deep mining of the TCGA-

10.3389/fimmu.2025.1492541

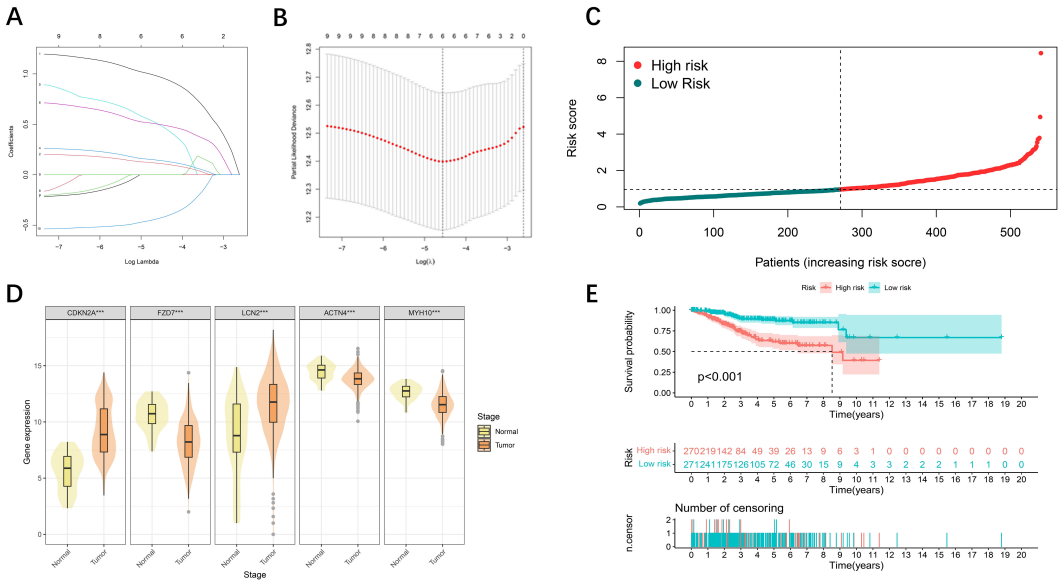

FIGURE 2
Development of prognostic features of the DE-DFRG model. **(A, B)** Lasso-Cox regression analysis revealed 5 DE-DFRGs. **(C)** Risk score curve graph. The green curves indicate the low-risk group, and the red curves indicate the high-risk group. **(D)** Expression of 5 DE-DFRGs between the UCEC samples and normal samples (***p < 0.001). **(E)** Kaplan-Meier survival curves. Survival time was shorter in the high-risk group in the TCGA-UCEC cohort.

UCEC RNA-Seq sequence data, we identified a total of 16,877 microRNAs (miRNAs) and analyzed them via univariate Cox regression models to confirm whether these miRNAs are associated with the survival risk of patients with UCEC (Supplementary Figure S3). An exploration of the associations between the expression of key genes and miRNAs associated with survival revealed that hsa−mir−4758 was significantly associated with five key genes (Figures 4C–G).

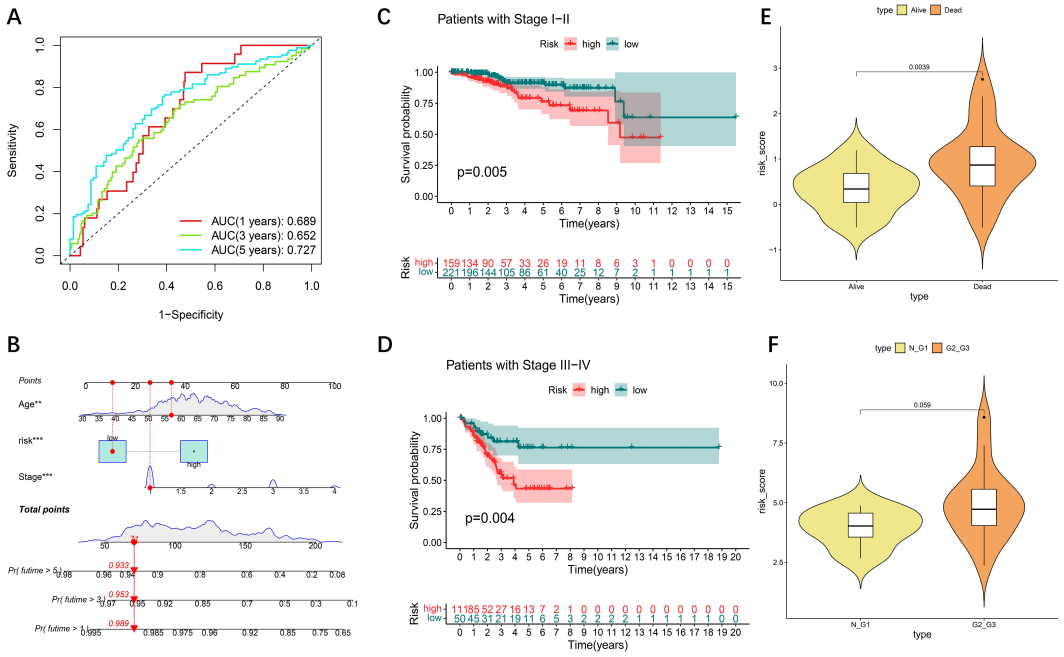

FIGURE 3
Internal validation of the DE-DFRG model by TCGA-UCEC. **(A)** Time-dependent ROC curve and AUC of the prognostic signature in UCEC patients from TCGA. **(B)** Nomogram for the prediction of 1-, 3-, and 5-year overall survival. **(C, D)** Kaplan-Meier survival curves of patients with clinical stage I-II and III-IV disease. **(E)** Violin plot of risk scores between patients who survived for five years and those who did not. **(F)** Violin plot of risk scores between normal/G1 stage tumors to G2/G3 stage tumors.

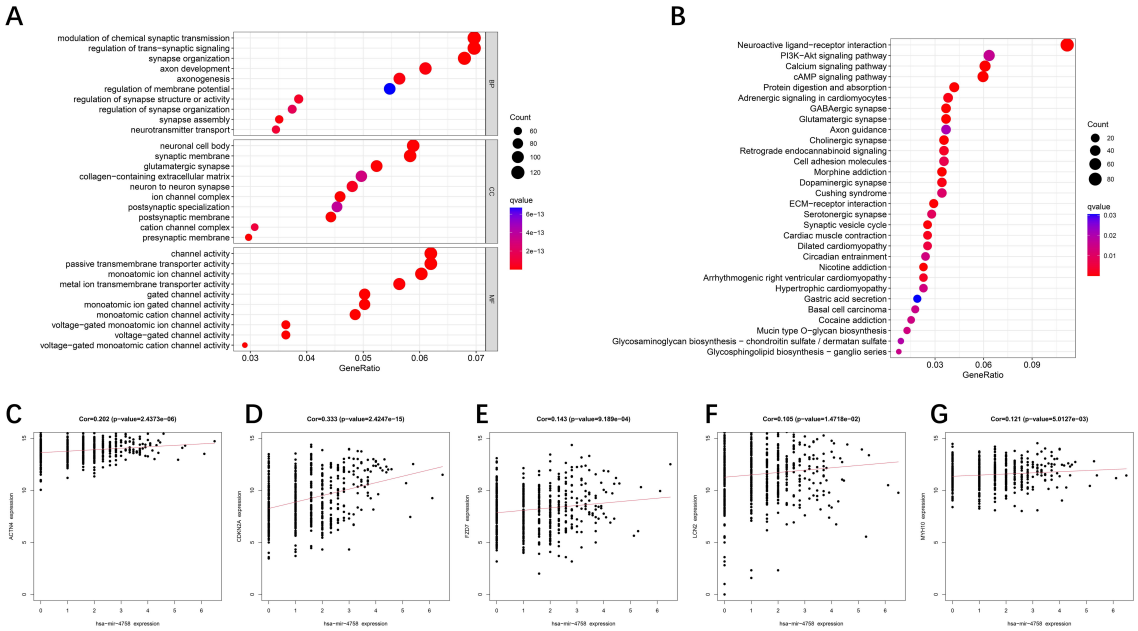

FIGURE 4
GO/KEGG enrichment analysis of DE-DFRGs and miRNA correlation analysis. **(A, B)** GO and KEGG functional enrichment analyses of the differentially expressed genes. **(C–G)** Relationships between miRNAs and the expression of 5 DE-DFRGs in the model.

3.5 Relationship between the tumor mutational burden and the risk model

The genetic variant density of a tumor, defined as the number of variants found per megabase (MutS per MB), has been associated with the quality of life and prognosis of cancer patients. High levels of tumor genetic variant density (TMB-H) indicate that patients may benefit more from immunotherapy. To more thoroughly explore the role of the risk-prognosis model in predicting the extent of tumor progression, this study explored the association between the model and TMB. First, we performed a Kaplan-Meier analysis on survival data from patients with varying TMB levels and found that patients with higher TMB exhibited better survival rates (Figure 5A), which aligns with current perspectives in the field. Subsequently, we analyzed the correlation between TMB and risk scores, revealing that lower risk scores were associated with higher mutation rates (Figure 5B), indicating a better prognosis. Figure 5C illustrates the differences in gene mutation characteristics between low-risk and high-risk groups, suggesting that variations at the gene level may be key factors contributing to differing prognoses:PTEN (65%), PIK3CA (49%), ARID1A (46%), TP53 (38%) and TTN (38%) were the top five mutated genes.

3.6 Signaling-related immune infiltration and LMRG-FAG based immune response

Recent studies have revealed two key structural changes in the tumor microenvironment, the dissociation of disulfidptosis and ferroptosis, which are closely related to the immune response of tumors. Using the CIBERSORT algorithm tool, we aimed to estimate the distribution of twenty-two immune cell classes in patients with UCEC (Figure 6A), and the Violin plot revealed significant differences in the expression levels of regulatory T cells (Tregs), monocytes, macrophages, and neutrophils in different risk classes (Figure 6B). Thereafter, we calculated the infiltration scores for 22 types of immune cells and grouped the UCEC patients based on the median scores. A Kaplan-Meier analysis was performed in conjunction with survival data, and the results indicated that higher immune infiltration scores were associated with better patient prognosis (Figures 6C–E). Significant heterogeneity in patient survival was observed in the infiltration of several types of immune cells (NK cells, CD8+ T cells, regulatory T cells and highly invasive cells).

3.7 Immunohistochemistry and RT-qPCR validation of key prognostic genes

We subsequently confirmed the expression of prognostically relevant genes in clinical samples via real-time quantitative reverse transcription polymerase chain reaction (RT–qPCR) and immunohistochemistry. The experimental data revealed the expression levels of several genes in tumor samples via real-time quantitative polymerase chain reaction (RT–qPCR). Specifically, ACTN4, FZD7, and MYH10 were expressed at low levels in these tumors, whereas LCN2 and CDKN2A were expressed at high levels (Figures 7A–E). This finding is in accordance with transcriptional data from The Cancer Genome Atlas (TCGA) based on urothelial cancer (UCEC) samples. The results revealed that the expression of ACTN4 and LCN2 was positive in the cytoplasm and partly in the nucleus and that the expression level of ACTN4 was low

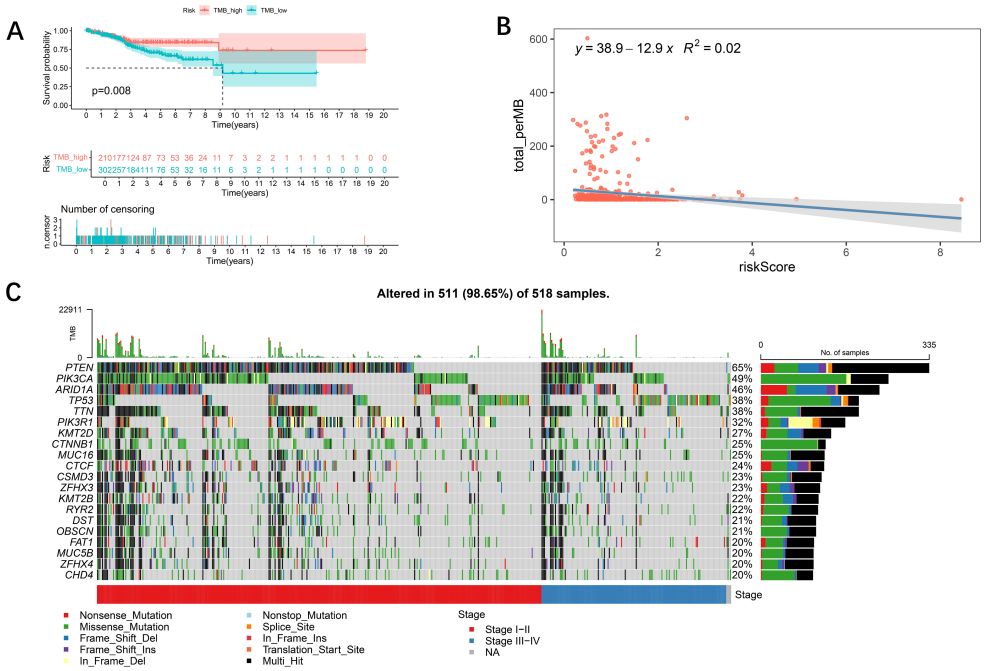

FIGURE 5
Relationships between the tumor mutational burden (TMB) and the risk model. **(A)** K–M analysis showing the difference in overall survival between the low- and high-TMB groups. In addition, patients with a high TMB had a better prognosis ($p < 0.05$). **(B)** Relationships between TMB and the risk score. TMB was negatively associated with the risk score (R = –12.9, R2 = 0.02). **(C)** Waterfall plot showing the mutation information on the top 20 genes in each UCEC sample.

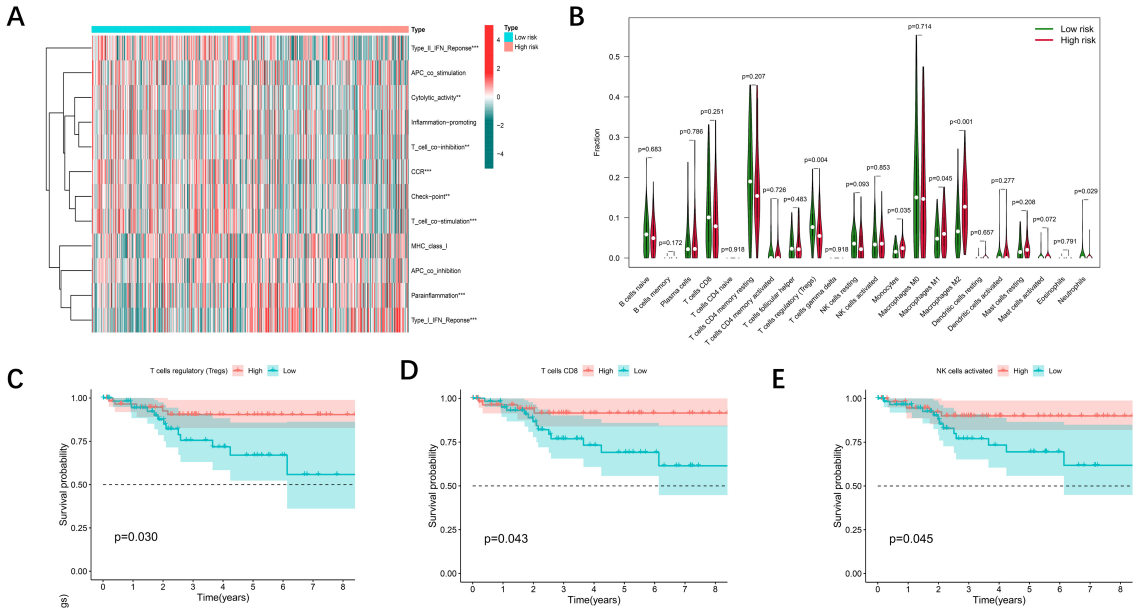

FIGURE 6
Immune cell infiltration associated with the DE-DFRG model. **(A)** Heatmap showing the comparison of immune-related functions in the high- and low-risk groups. **(B)** The differences in 22 infiltrating immune cells in the TCGA-UCEC cohort between the high- and low-risk groups were analyzed via the Wilcoxon test ($p < 0.05$). **(C-E)** Kaplan-Meier survival curves illustrating the differences in overall survival between the low and high immune cell infiltration groups.

10.3389/fimmu.2025.1492541

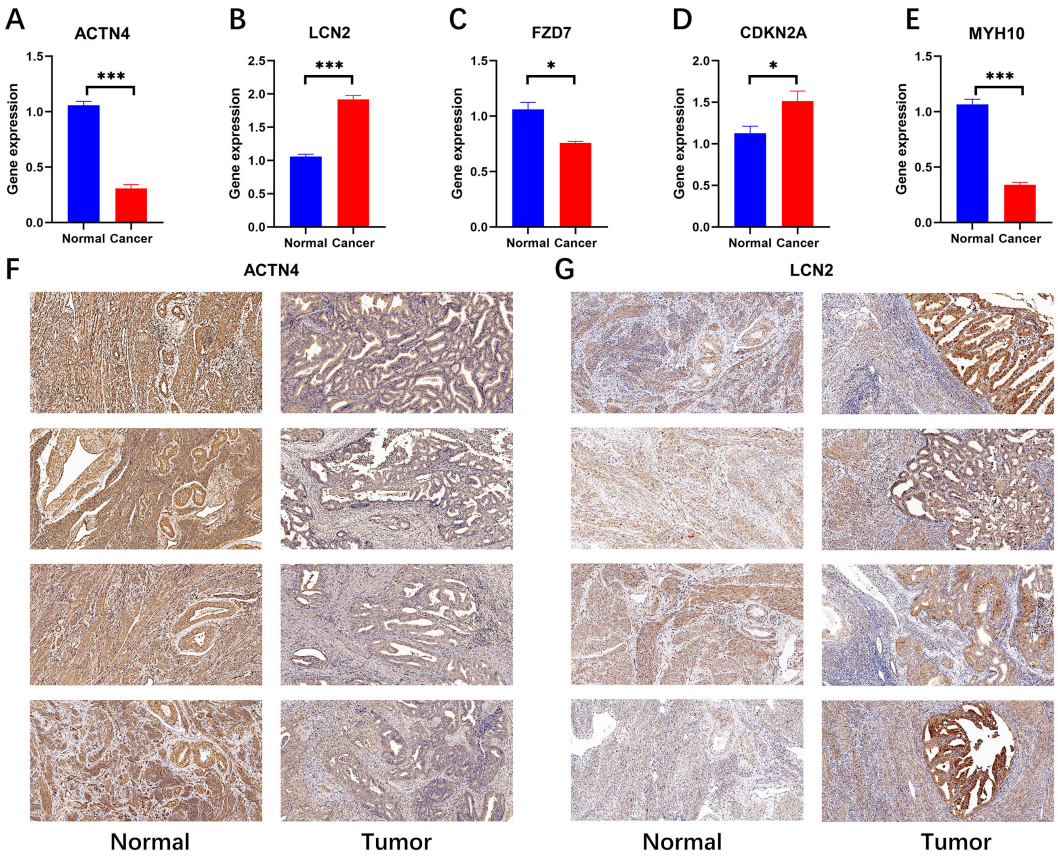

FIGURE 7
RT–qPCR (N=4) validation and immunohistochemical validation (N=4, x10) of key prognostic genes. **(A-E)** RT–qPCR results revealed that ACTN4, FZD7 and MYH10 were expressed at low levels in cancer tissues and that LCN2 and CDKN2A were highly expressed in cancer tissues (*p < 0.05, and ***p < 0.001). **(F, G)** Immunohistochemical results revealed that ACTN4 was expressed at low levels in cancer tissues and that LCN2 was highly expressed in cancer tissues.

(Figure 7F), whereas the expression level of LCN2 was high in tumor tissue (Figure 7G). This finding was also confirmed by real-time quantitative polymerase chain reaction (RT–qPCR) data. (Photos with higher magnification are detailed in Appendix File 5).

4 Discussion

UCEC is a common malignant disease of female reproductive organs, and its prevalence has increased in recent years. For patients, the precise determination of disease stage has a significant effect on the treatment efficacy and patient prognosis. For the first time, the International Federation of Gynecology and Obstetrics (FIGO) has included molecular subtypes in its revised staging guidelines for endometrial cancer in 2023, aiming to provide a more accurate assessment of the prognosis of patients with UCEC. Therefore, the study of new molecular markers and cell communication pathways will provide key theoretical support for interdisciplinary treatment strategies for endometrial cancer. Currently, several ferroptosis-related models have been developed to predict the prognosis of UCEC patients, which are based on a single variable and do not fully consider the complexity of the tumor microenvironment (16, 17). Recent findings indicate a close relationship between ferroptosis and disulfidptosis. Disulfidptosis and ferroptosis are two forms of regulated cell death that share some biochemical pathways and mechanisms. Both processes involve the accumulation of reactive oxygen species (ROS) and perturbations in cellular redox homeostasis, leading to oxidative damage. Recent studies suggest that disulfidptosis may act in concert with ferroptosis, where the oxidative stress from disulfide accumulation can potentially promote ferroptosis (18). In our exploration, we comprehensively considered the correlation between disulfidptosis and ferroptosis. First, we revealed ferroptosis-disulfidptosis differential genes by dissecting gene transcription in tumor and normal tissues. The Lasso algorithm was subsequently applied to filter out the most influential predictor variables, and we constructed a prognostic assessment model consisting of five key genes. Through the analysis of Kaplan–Meier curves, ROC curves and calibration curves the stability, accuracy and reliability of the model were verified.

Recent studies have revealed a strong association between disulfide metabolism and tumor development. In fact, many tumor cells are subjected to oxidative stress, which causes

abnormalities in disulfide metabolism, thereby significantly affecting the survival and proliferation of cancer cells (19, 20). The metabolic activity of tumor cells, especially the formation of disulfide bonds, is associated with various biological characteristics of tumors, such as resistance to antibiotics, tumor spread, and immune system evasion (21, 22). Recent studies have shown that specific long noncoding RNAs associated with disulfide dysregulation can provide significant prognostic information for UCEC patients (23). Ferroptosis is caused by the combined effects of intracellular oxidative stress and membrane lipid peroxidation, which leads to the destruction of cells and the termination of life activities. Ferroptosis-related genes and long noncoding RNA coding genes in endometrial carcinomatous tissues are often mutated and epigenetically modulated in contrast to those in conventional tissues (9), resulting in their differential expression in regulating the viability, migration, and invasion of endometrial cancer cells (7, 12). Although a direct association between these genes and endometrial cancer has not yet been established, ferroptosis gene markers play a key role in assessing the prognosis of endometrial cancer patients and formulating targeted treatments. To deepen the research in the field of cancer therapy, explore the interaction between disulfidptosis and ferroptosis signal transduction pathways, reveal the internal relationship between them, and translate this insight into innovative strategies for anticancer therapy, we must build a closer bridge between them.

A recent study revealed that UCEC is one of the two cancer types with the highest mutation rates in disulfidptosis-related genes, whereas mutations in the ACTN4 and MYH10 genes are closely linked to poor survival (18). In the actin-binding protein family, the ACTN4 protein, which was described by Honda and other researchers in the early stage and is considered a nonmuscle α-actinin closely linked to the migration ability of tumor cells, has attracted much attention (24). ACTN4 influences the cell cycle and cell motility and plays a key role in the development and spread of cancer (25), and some studies have shown that ACTN4 behaves differently in endometriotic lesions than in the normal endometrium (26). The MYH10 gene is responsible for the production of nonmuscle myosin IIB (NMIIB), a protein that plays a crucial role in cell adhesion. It also plays a key role in many tumor processes, including promoting cancer cell migration, invasion of surrounding tissues, synthesis of the extracellular matrix (ECM), and triggering the transformation of epithelial cells into mesenchymal cells. CDKN2A is considered to play a key clinical role in assessing various prognostic mechanisms of endometrial cancer (16, 27, 28), possibly related to cell cycle dysregulation caused by CDKN2A deletion (29). Lipocarin 2 (LCN2), a new member of the lipocarin family, is closely related to immune function. Studies have shown that the expression level of LCN2 is increased in many malignant tumors. including lung cancer, breast cancer, prostate cancer, pancreatic cancer and esophageal cancer. Moreover, studies indicate that LCN2 induced ferroptosis is closely related to tumor progression (30). LCN2 serum levels play an important role in the diagnosis of endometrial cancer (31), and upregulation of LCN2 expression promotes drug resistance in endometrial cancer cells and inhibits the ferroptosis process (32). One of the receptors of Wnt signaling, Frizzled 7 (FZD7), plays a key role in the canonical and atypical Wnt pathways. Abnormal activation of the Wnt/β-catenin signaling pathway is closely related to endometrial hyperplasia and its related carcinogenesis (33), and plays a vital role in promoting the spread and migration of tumor cells. Studies have revealed that FZD7 gene expression often increases when ovarian cancer tissues are resistant to platinum-based drugs (34). This increased gene expression increases the sensitivity of tumor cells to ferroptosis.

MicroRNAs(miRNAs) have been shown to coordinate various biological processes and diseases, including the occurrence and progression of cancer (35). Research has shown that miRNAs not only control mRNA expression but also target long noncoding RNAs (36). In recent years, abnormal expression of miRNAs has been reported to be associated with the occurrence of various cancers, and abnormal expression of miRNAs can also induce different epigenetic changes. After screening key prognostic genes, our study further identified hsa-mir-4758 as co-associated with disulfidptosis/ferroptosis-related genes. A comprehensive transcriptome analysis revealed that hsa-mir-4758 is associated with hormone-dependent cancer risk (37). A miRNA-based prognostic model for endometrial cancer also suggested that high expression of hsa-mir-4758 in EC tissue is associated with poor prognosis and a lower survival rate in patients with endometrial cancer (38). This finding may suggest the significant potential value of hsa-mir-4758 in the occurrence and prognosis of endometrial cancer (39).

The characteristic of disulfidptosis is the accumulation of disulfide bonds and the subsequent cellular stress. Cancer cells undergoing disulfidptosis can release a variety of cytoplasmic contents and inflammatory factors, triggering a robust immune response by promoting immune cell infiltration and reprogramming the immunosuppressive tumor microenvironment (TME). This process can activate immune cells and facilitate the occurrence of inflammatory responses (40). On the other hand, ferroptosis is primarily induced by lipid peroxidation caused by iron overload, during which reactive oxygen species (ROS) are generated that can also influence immune cell function. This may alter the recruitment and activation of immune cells within the tumor microenvironment (41). Different forms of regulated cell death can modulate immune infiltration in the tumor microenvironment, thereby affecting therapeutic efficacy against tumors and the overall progression of cancer (42). Immune cells play crucial roles in the stroma of tumors, and they have a significant impact on tumor progression and prognosis (43). Therefore, we performed an in-depth analysis of the immune cell composition in patients with different prognostic grades. The performance of regulatory T cells (Tregs), monocytes, macrophages, and neutrophils varies significantly across risk classes. These observations suggest that patients at lower risk may be more sensitive to immunotherapy, suggesting that they may benefit more from immunotherapy.

However, it must be recognized that our study has inherent limitations. First, our data are based on transcriptome data, so there remains a considerable journey ahead from our research conclusions to their application in a clinical setting. Specifically, understanding how risk stratification derived from our signature could influence the selection between standard therapies and novel treatments requires substantial evidence-based research. Follow-up studies (both prospective and retrospective) are essential to confirm the accuracy of our model. In addition, we need to pay attention to the consistency of samples of various ethnic groups. Moreover, the results of the analysis of the tumor mutation burden and immune invasion profile were only from the TCGA, and more prospective experimental data are needed to confirm these conclusions. Finally, further exploration of the molecular mechanism of UCEC-related risk genes is necessary to explore effective therapeutic targets.

Nonetheless, we believe that our study holds significant value in the exploration of prognosis in endometrial cancer. It underscores the importance of collaboration among oncologists, pathologists, and bioinformaticians to effectively implement our prognostic features in clinical practice. To this end, we are committed to conducting further research at both the foundational and clinical levels to validate our findings and enhance their applicability in real-world settings.

5 Conclusions

In summary, by selecting five genes associated with disulfidptosis/ferroptosis-related genes, we created a predictive model of the clinical outcome for UCEC patients based on the TCGA database and validated it internally. In addition, this study explored the mutation burden and immune cell infiltration level of tumors in different prognostic risk groups, which provided possible biomarkers and preliminary evidence for the development of personalized treatment.

Data availability statement

The original contributions presented in the study are included in the article/Supplementary Materials, further inquiries can be directed to the corresponding author/s.

Ethics statement

The studies involving humans were approved by Ethics Committee of Guangdong Women and Children Hospital. The studies were conducted in accordance with the local legislation and institutional requirements. The participants provided their written informed consent to participate in this study.

Author contributions

YH: Writing – original draft. HL: Writing – review & editing. ZW: Writing – review & editing. WH: Conceptualization, Investigation, Writing – review & editing. BC: Conceptualization, Investigation, Writing – review & editing. SC: Conceptualization, Investigation, Writing – review & editing. ZZ: Conceptualization, Investigation, Writing – review & editing. LD: Conceptualization, Investigation, Writing – review & editing. XC: Writing – review & editing. YL: Data curation, Supervision, Writing – review & editing. XH: Conceptualization, Project administration, Supervision, Writing – review & editing.

Funding

The author(s) declare that financial support was received for the research, authorship, and/or publication of this article. The present work was funded by Guangdong Medical Science and Technology Research Fund (B2024003) and Guizhou Provincial Science and Technology Projects ZK (2024)455.

Acknowledgments

We would like to express our gratitude to our colleagues at Pathology laboratory of Guangdong Women and Children Hospital.

Conflict of interest

The authors declare that the research was conducted in the absence of any commercial or financial relationships that could be construed as a potential conflict of interest.

Publisher's note

Supplementary material

The Supplementary Material for this article can be found online at: https://www.frontiersin.org/articles/10.3389/fimmu.2025.1492541/full#supplementary-material

References

1. Gu B, Shang X, Yan M, Li X, Wang W, Wang Q, et al. Variations in incidence and mortality rates of endometrial cancer at the global, regional, and national levels 1990-2019. *Gynecol Oncol*. (2021) 161:573–80. doi: 10.1016/j.ygyno.2021.01.036

2. Concin N, Matias-Guiu X, Vergote I, Cibula D, Mirza MR, Marnitz S, et al. ESGO/ESTRO/ESP guidelines for the management of patients with endometrial carcinoma. *Int J Gynecol Cancer*. (2021) 31:12–39. doi: 10.1136/ijgc-2020-002230

3. Crosbie EJ, Kitson SJ, McAlpine JN, Mukhopadhyay A, Powell ME, Singh N. Endometrial cancer. *Lancet*. (2022) 399:1412–28. doi: 10.1016/S0140-6736(22)00323-3

4. Lu KH, Broaddus RR. Endometrial cancer. *N Engl J Med*. (2020) 383:2053–64. doi: 10.1056/NEJMra1514010

5. Connor EV, Rose PG. Management strategies for recurrent endometrial cancer. *Expert Rev Anticancer Ther*. (2018) 18:873–85. doi: 10.1080/14737140.2018.1491311

6. Zheng P, Zhou C, Ding Y, Duan S. Disulfidptosis: a new target for metabolic cancer therapy. *J Exp Clin Cancer Res*. (2023) 42:103. doi: 10.1186/s13046-023-02675-4

7. Wang Y, Wang C, Guan X, Ma Y, Zhang S, Li F, et al. PRMT3-mediated arginine methylation of METTL14 promotes Malignant progression and treatment resistance in endometrial carcinoma. *Adv Sci (Weinh)*. (2023) 10:e2303812. doi: 10.1002/advs.202303812

8. Wang Z, Shu W, Zhao R, Liu Y, Wang H. Sodium butyrate induces ferroptosis in endometrial cancer cells via the RBM3/SLC7A11 axis. *Apoptosis*. (2023) 28:1168–83. doi: 10.1007/s10495-023-01850-4

9. Zalyte E. Ferroptosis, metabolic rewiring, and endometrial cancer. *Int J Mol Sci*. (2023) 25. doi: 10.3390/ijms25010075

10. Liu S, Zhang Q, Liu W, Huang X. Prediction of prognosis in patients with endometrial carcinoma and immune microenvironment estimation based on ferroptosis-related genes. *Front Mol Biosci*. (2022) 9:916689. doi: 10.3389/fmolb.2022.916689

11. Qin J, Shao X, Wu L, Du H. Identification of the ferroptosis-associated gene signature to predict the prognostic status of endometrial carcinoma patients. *Comput Math Methods Med*. (2021) 2021:9954370. doi: 10.1155/2021/9954370

12. Chen SJ, Zhang J, Zhou T, Rao SS, Li Q, Xiao LY, et al. Epigenetically upregulated NSUN2 confers ferroptosis resistance in endometrial cancer via m(5)C modification of SLC7A11 mRNA. *Redox Biol*. (2024) 69:102975. doi: 10.1016/j.redox.2023.102975

13. Murakami H, Hayashi M, Terada S, Ohmichi M. Medroxyprogesterone acetate-resistant endometrial cancer cells are susceptible to ferroptosis inducers. *Life Sci*. (2023) 325:121753. doi: 10.1016/j.lfs.2023.121753

14. Zhou N, Yuan X, Du Q, Zhang Z, Shi X, Bao J, et al. FerrDb V2: update of the manually curated database of ferroptosis regulators and ferroptosis-disease associations. *Nucleic Acids Res*. (2023) 51:D571–d582. doi: 10.1093/nar/gkac935

15. Liu X, Nie L, Zhang Y, Yan Y, Wang C, Colic M, et al. Actin cytoskeleton vulnerability to disulfide stress mediates disulfidptosis. *Nat Cell Biol*. (2023) 25:404–14. doi: 10.1038/s41556-023-01091-2

16. Jin W, Zhuang X, Lin Y, Zhao X. Integrating ferroptosis-related genes (FRGs) and prognostic models to enhance UCEC outcome prediction and therapeutic insights. *J Appl Genet*. (2023) 64:723–35. doi: 10.1007/s13353-023-00779-3

17. Weijiao Y, Fuchun L, Mengjie C, Xiaoqing Q, Hao L, Yuan L, et al. Immune infiltration and a ferroptosis-associated gene signature for predicting the prognosis of patients with endometrial cancer. *Aging (Albany NY)*. (2021) 13:16713–32. doi: 10.18632/aging.203190

18. Liu H, Tang T. Pan-cancer genetic analysis of disulfidptosis-related gene set. *Cancer Genet*. (2023) 278-279:91–103. doi: 10.1016/j.cancergen.2023.10.001

19. Daly EB, Wind T, Jiang XM, Sun L, Hogg PJ. Secretion of phosphoglycerate kinase from tumour cells is controlled by oxygen-sensing hydroxylases. *Biochim Biophys Acta*. (2004) 1691:17–22. doi: 10.1016/j.bbamcr.2003.11.004

20. Hogg PJ. Biological regulation through protein disulfide bond cleavage. *Redox Rep*. (2002) 7:71–7. doi: 10.1179/135100002125000299

21. Chen C, Shen M, Liao H, Guo Q, Fu H, Yu J, et al. A paclitaxel and microRNA-124 coloaded stepped cleavable nanosystem against triple negative breast cancer. *J Nanobiotechnology*. (2021) 19:55. doi: 10.1186/s12951-021-00800-z

22. Wang Y, Jiang Y, Wei D, Singh P, Yu Y, Lee T, et al. Nanoparticle-mediated convection-enhanced delivery of a DNA intercalator to gliomas circumvents temozolomide resistance. *Nat BioMed Eng*. (2021) 5:1048–58. doi: 10.1038/s41551-021-00728-7

23. Li B, Li X, Ma M, Wang Q, Shi J, Wu C. Analysis of long non-coding RNAs associated with disulfidptosis for prognostic signature and immunotherapy response in uterine corpus endometrial carcinoma. *Sci Rep*. (2023) 13:22220. doi: 10.1038/s41598-023-49750-6

24. Honda K, Yamada T, Endo R, Ino Y, Gotoh M, Tsuda H, et al. Actinin-4, a novel actin-bundling protein associated with cell motility and cancer invasion. *J Cell Biol*. (1998) 140:1383–93. doi: 10.1083/jcb.140.6.1383

25. Tentler D, Lomert E, Novitskaya K, Barlev NA. Role of ACTN4 in tumorigenesis, metastasis, and EMT. *Cells*. (2019) 8. doi: 10.3390/cells8111427

26. Honda H, Barrueto FF, Gogusev J, Im DD, Morin PJ. Serial analysis of gene expression reveals differential expression between endometriosis and normal endometrium. Possible roles for AXL and SHC1 in the pathogenesis of endometriosis. *Reprod Biol Endocrinol*. (2008) 6:59. doi: 10.1186/1477-7827-6-59

27. Fang F, Wang P, Huang H, Ye M, Liu X, Li Q. m(6)A RNA methylation regulator-based signature for prognostic prediction and its potential immunological role in uterine corpus endometrial carcinoma. *BMC Cancer*. (2022) 22:1364. doi: 10.1186/s12885-022-10490-x

28. Wang Y, Ren F, Chen P, Liu S, Song Z, Ma X. Identification of a six-gene signature with prognostic value for patients with endometrial carcinoma. *Cancer Med*. (2018) 7:5632–42. doi: 10.1002/cam4.2018.7.issue-11

29. Kreuger IZM, Slieker RC, van Groningen T, van Doorn R. Therapeutic strategies for targeting CDKN2A loss in melanoma. *J Invest Dermatol*. (2023) 143:18–25.e11. doi: 10.1016/j.jid.2022.07.016

30. Wang D, Li X, Jiao D, Cai Y, Qian L, Shen Y, et al. LCN2 secreted by tissue-infiltrating neutrophils induces the ferroptosis and wasting of adipose and muscle tissues in lung cancer cachexia. *J Hematol Oncol*. (2023) 16:30. doi: 10.1186/s13045-023-01429-1

31. Cymbaluk-Ploska A, Chudecka-Glaz A, Pius-Sadowska E, Machalinski B, Sompolska-Rzechula A, Kwiatkowski S, et al. The role of lipocalin-2 serum levels in the diagnostics of endometrial cancer. *Cancer biomark*. (2019) 24:315–24. doi: 10.3233/CBM-181942

32. Jiang J, Zhu J, Qiu P, Ni J, Zhu W, Wang X. HNRNPA2B1-mediated m6A modification of FOXM1 promotes drug resistance and inhibits ferroptosis in endometrial cancer via regulation of LCN2. *Funct Integr Genomics*. (2023) 24:3. doi: 10.1007/s10142-023-01279-7

33. Lan S, Zhang Z, Li Q. FZD7: A potential biomarker for endometriosis. *Med (Baltimore)*. (2023) 102:e35406. doi: 10.1097/MD.0000000000035406

34. Wang Y, Zhao G, Condello S, Huang H, Cardenas H, Tanner EJ, et al. Frizzled-7 identifies platinum-tolerant ovarian cancer cells susceptible to ferroptosis. *Cancer Res*. (2021) 81:384–99. doi: 10.1158/0008-5472.CAN-20-1488

35. Liu H, Wan J, Chu J. Long non-coding RNAs and endometrial cancer. *BioMed Pharmacother*. (2019) 119:109396. doi: 10.1016/j.biopha.2019.109396

36. Shetty A, Venkatesh T, Kabbekodu SP, Tsutsumi R, Suresh PS. LncRNA-miRNA-mRNA regulatory axes in endometrial cancer: a comprehensive overview. *Arch Gynecol Obstet*. (2022) 306:1431–47. doi: 10.1007/s00404-022-06423-5

37. Jayarathna DK, Renteria ME, Malik A, Sauret E, Batra J, Gandhi NS. Integrative transcriptome-wide analyses uncover novel risk-associated microRNAs in hormone-dependent cancers. *Front Genet*. (2021) 12:716236. doi: 10.3389/fgene.2021.716236

38. Ni L, Tang C, Wang Y, Wan J, Charles MG, Zhang Z, et al. Construction of a miRNA-based nomogram model to predict the prognosis of endometrial cancer. *J Pers Med*. (2022) 12. doi: 10.3390/jpm12071154

39. Wu S, Cai W, Li Y, Tan W, Yuan Y, Zhou Z, et al. SNHG3/hsa-miR-455-5p axis-mediated high expression of MTHFD2 correlates with tumor immune infiltration and endometrial carcinoma progression. *Int J Med Sci*. (2023) 20:1097–113. doi: 10.7150/ijms.81962

40. Jin XK, Zhang SK, Zhang SM, Liang JL, Yan X, Lin YT, et al. Disrupting intracellular homeostasis by copper-based nanoinducer with multiple enzyme-mimicking activities to induce disulfidptosis-enhanced pyroptosis for tumor immunotherapy. *Adv Mater*. (2024) 37(1):e2410957. doi: 10.1002/adma.202410957

41. Gao W, Wang X, Zhou Y, Wang X, Yu Y. Autophagy, ferroptosis, pyroptosis, and necroptosis in tumor immunotherapy. *Signal Transduct Target Ther*. (2022) 7:196. doi: 10.1038/s41392-022-01046-3

42. Jin M, Ni D, Cai J, Yang J. Identification and validation of immunity- and disulfidptosis-related genes signature for predicting prognosis in ovarian cancer. *Heliyon*. (2024) 10:e32273. doi: 10.1016/j.heliyon.2024.e32273

43. Hinshaw DC, Shevde LA. The tumor microenvironment innovately modulates cancer progression. *Cancer Res*. (2019) 79(18):4557–66. doi: 10.1158/0008-5472.CAN-18-3962

frontiers | Frontiers in Immunology

TYPE Original Research
PUBLISHED 28 January 2025
DOI 10.3389/fimmu.2025.1500792

OPEN ACCESS

EDITED BY
Kelsey P. Kubelick,
University of Virginia, United States

REVIEWED BY
Jessica Da Gama Duarte,
Olivia Newton-John Cancer Research Institute, Australia
Markus Germann,
Roche, Switzerland

*CORRESPONDENCE
P. Rod Dunbar
r.dunbar@auckland.ac.nz

†These authors have contributed equally to this work

RECEIVED 23 September 2024
ACCEPTED 02 January 2025
PUBLISHED 28 January 2025

CITATION
Munoz-Erazo L, Park SM, Lin S, Chen C-JJ, Zhou LYY, Rhodes JL, Jeon T, Fenton S, McCall JL, Kemp RA and Dunbar PR (2025) A novel approach to digital characterisation of Tertiary Lymphoid Structures in colorectal cancer.
Front. Immunol. 16:1500792.
doi: 10.3389/fimmu.2025.1500792

A novel approach to digital characterisation of Tertiary Lymphoid Structures in colorectal cancer

Luis Munoz-Erazo[1,2†], Saem Mul Park[1,2†], Shelly Lin[1,2], Chun-Jen J. Chen[1,2], Lisa Y. Y. Zhou[1,2], Janet L. Rhodes[2,3], Taesung Jeon[4], Sonya Fenton[5], John L. McCall[5], Roslyn A. Kemp[2,3] and P. Rod Dunbar[1,2*]

[1]School of Biological Sciences, The University of Auckland, Auckland, New Zealand, [2]Maurice Wilkins Centre, The University of Auckland, Auckland, New Zealand, [3]Department of Microbiology and Immunology, The University of Otago, Dunedin, New Zealand, [4]Department of Pathology, Korea University Guro Hospital, Korea University College of Medicine, Seoul, Republic of Korea, [5]Department of Surgical Sciences, The University of Otago, Dunedin, New Zealand

Introduction: Tertiary Lymphoid Structures (TLS) in cancer tissue are potential sites for the organisation of immune responses to cancer, and correlate positively with improved clinical outcomes for patients including in colorectal cancer (CRC). However it has proven challenging to standardise assessment of TLS due to the highly variable appearances of circumscribed domains of TLS within tissue sections. A recent three-dimensional reconstruction of TLS in CRC tissue showed that TLS are often large, multi-lobular structures, suggesting that assessing TLS across whole sections may be necessary to provide an accurate view of TLS activity in a patient's tumour.

Methods: We used whole-section scans of multiplexed immunofluorescence images to characterise TLS from 22 subjects with CRC. Multiplexed staining for CD20, CD3, CD8, Foxp3 and Ki-67 enabled us to identify B-cells, CD8+ T-cells, Foxp3– CD4 T-cells, and Foxp3+ CD4 Tcells in all sections, and quantify both the presence of these cell subsets in lymphocytic clusters and their degree of proliferation within those clusters.

Results: In total we identified 524 lymphocytic clusters with morphology consistent with TLS. TLS domains varied substantially between samples in size, morphology, cellular constituents, count (from 4 to 100), and proportion of total section area they occupied (0.2%-7.8%). We quantified proliferation of B-cells and T-cell subsets within TLS domains across entire sections and compared data to the canonical approach of counting and phenotyping individual TLS domains. The whole-slide approach proved simpler, generating digital summaries that readily identified patients with strikingly different levels of immune activity within their TLS. Strong correlations were observed between the proliferation of B-cells and T-cell subsets. The presence of non-proliferating Foxp3+ CD4 T-cells within TLS showed no correlation with the level of proliferation of other lymphocyte subsets.

Discussion: Whole-section digital quantification of immune cell activity within TLS has advantages over canonical approaches, and could accelerate research into correlations between TLS status and clinical outcomes, with potential to enable a standardised assay for clinical use.

KEYWORDS

tertiary lymphoid structure, colorectal cancer, quantitative multiplex immunohistochemistry, fluorescent multiplex IHC, digital pathology

Introduction

Tertiary Lymphoid Structures (TLS) are structured organisations of immune cells that develop in non-lymphoid tissues following persistent pathogen infection, or in inflammatory conditions associated with autoimmune disorders, allograft rejection, and cancer (1, 2). TLS are closely related to other organised collections of lymphoid cells within normal tissues such as Peyer's patches, and share many structural and organisational features with lymph nodes (LN). In sections of human tissue, TLS classically appear as circumscribed ovoid aggregates of lymphoid cells, centred around a B-cell follicle that may or may not contain a germinal centre (GC) comprising actively replicating B-cells. High endothelial venules (HEV) may be present within TLS, as well as peripheral T-cell zones with intercalating dendritic cells (1), though TLS lack other structural features of LN such as a capsule, with its connected hilum and trabeculae, or lymphatic sinuses.

In studies of cancer patients, correlations between TLS features and prognosis have been observed for several cancer types (1, 2) including colorectal cancer (CRC) (3, 4). The presence and characteristics of TLS in or around tumours have also been correlated with responses to immune therapy targeting the PD-1 pathway (5, 6), suggesting that TLS activity strongly influences the ability of T-cells to recognise and attack cancer cells.

Previous literature examining TLS features in cancer patients has typically sought to identify and characterise individual circumscribed zones within tissue sections that have features of TLS. Three classes of parameters have been extracted: the number and density of TLS within the section (7, 8); their location within the tumour with respect to cancer cells (9); and their cellular composition and functional state, especially their "maturity" (10). The manner in which all these parameters have been calculated and reported has been highly variable, making it challenging to compare TLS analysis in different clinical contexts.

Several previous studies set a threshold for the number of cells within a cluster needed to qualify as a TLS, though this threshold has varied (11–13). Other criteria for defining TLS have included cellular composition and architecture, such as the relative proportion of B-cells and T-cells within a cluster, and whether clear B- and T-cell zones are visible (4, 10, 11, 14, 15).

The location of TLS within tumours has also been variably reported. TLS are mostly found in peri-tumoural areas. In different human tumours, statistically significant correlations with prognosis have been found with both intra-tumoural TLS (16–18) and peri-tumoural/invasive margin TLS (10, 19). Hence, it remains unclear how TLS locations within tumours might impact prognosis.

Different criteria have been applied to classify the functional state of TLS. The presence of GCs and proliferating B-cells within B-cell follicles has often been used to describe TLS as "mature" and has been associated with improved prognosis (10, 20, 21). Some studies have also sought to sub-classify TLS according to the presence and density of particular cell types, such as follicular dendritic cells (FDC), CD8+ T-cells (22), and CD4+ T-cell subsets (23), including Foxp3+ CD4+ T-cells that are often regarded as "Tregs" (24), or the presence of HEVs (25). However, there is considerable heterogeneity in the cellular composition of TLS, even within a single tissue section (10, 23), and consensus has yet to emerge on how cellular composition might alter TLS function.

A large part of the variability in classifying TLS relates to the difficulty in assessing a dynamic three-dimensional (3D) structure from a single tissue section that effectively represents only a two-dimensional (2D) view. Recent 3D studies have begun to reveal human TLS as multi-lobular and interconnected (26) rather than discrete spheroidal entities. The appearance of TLS in a tissue section therefore depends on both the 3D shape of the TLS transected and the sectional plane, as illustrated in Figure 1. The sectional plane alters the shape and size of a circumscribed TLS domain in a tissue section (hereafter we use the term "TLS domain" to refer to this appearance in 2D). The sectional plane also changes the measurable cellular composition within a TLS domain, depending on whether it transects particular sub-structures such as GCs (Figure 1). Hence, the shape, size, and cellular composition of individual TLS domains within a tissue section are subject to the random interplay between the sectioning plane and TLS structures that might have highly variable multi-lobular shapes. This multi-lobular nature of human TLS (26) raises the possibility that instead of counting and classifying individual TLS domains, it might be preferable to characterise and summarise the totality of all these 2D cross-sections together. We therefore used multiplexed immunofluorescence (mIF) to image TLS across entire sections of

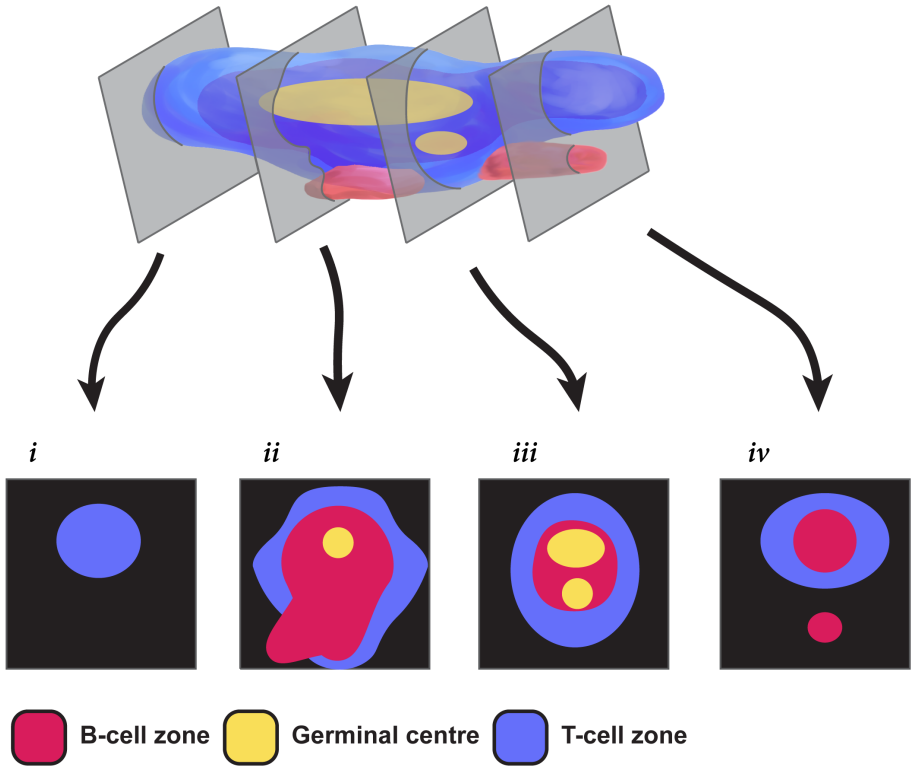

FIGURE 1
Challenges in extrapolating TLS structures from 2-dimensional sections. This pictorial representation shows how different a multi-GC TLS can appear in different 2-dimensional section planes. Section *i* shows only a T cell zone; sections *ii* & *iii* show differing relationships between T-cells, B-cells and the GC; section *iv* fails to capture a GC, and seems to show two TLS when the second is simply a protrusion from the same 3D structure.

tissue from 22 patients with colorectal cancer (CRC). As well as staining for B-cells and T-cell subsets, we stained for Ki-67 to quantify their proliferation. We first used a canonical approach to quantification, counting individual TLS domains within each sample, and quantifying the cell subsets and their proliferation within each individual TLS domain. We then tested an alternative global approach: measuring the total area of TLS domains across the tissue section, and quantifying B- and T- cell parameters across this combined total area. This simple whole-section approach was more efficient than the conventional method, yet still generated a similar ranking of patients for TLS activity. Our results suggest whole-section approaches to the digital characterisation of TLS will prove useful for comparative studies of large groups of cancer patients, and for future clinical applications.

Materials and methods

Patient selection

Formalin-fixed paraffin-embedded (FFPE) tissue blocks were obtained from 22 patients from the Dunedin Colorectal Cohort under ethical approval from the NZ Health and Disability Ethics Committee (HDEC 14/NTA/033). All samples were surgical samples excised prior to any adjuvant treatment. Previous H&E staining of these tissue blocks had revealed at least 3 highly-defined immune aggregates in each sample. Patient characteristics are shown in Table 1.

Tissue processing and imaging

5µm sections were derived from these blocks by the Histology Services Unit at the University of Otago. Sections were deparaffinised, antigen retrieved (AR6 solution, Akoya Bioscience) and blocked with 10% human serum (ThermoFisher). Slides were stained for markers using the 7-plex Opal Polaris kit (Akoya Biosciences) according to the manufacturer's instructions, using the primary antibodies and Opal dyes listed in Table 2; Foxp3 was stained with a cocktail of two antibodies as shown. Slides were mounted and imaged with the PhenoImager HT instrument (Akoya Biosciences).

Due to the variable staining patterns of CD4, observed across a range of cell types including myeloid and epithelial cells that express varying levels of CD4, we did not quantify CD4 expression. In CRC, double positive or negative T-cells are present in low frequencies (27), which include NKT cells (~0.7%) (28) and γδ T-cells [~0.5% of all CD3+ cells (29)] in cancer-associated TLS. In the absence of confirmation of CD4 positivity, we defined CD3+CD8- cells as 'most likely' representing CD4+ T cells. Hence our analysis utilised 5 markers in addition to the nuclear stain DAPI: CD3, CD8, Foxp3, CD20, Ki-67.

TABLE 1 List of patient characteristics.

Age at resection	
Range	46-99
Median	71
Sex	
Female	13
Male	9
Tumour site	
Ascending	4
Descending	1
Caecum	2
Hepatic flexure	1
Recto-sigmoid	4
Rectum	6
Sigmoid	2
Splenic flexure	1
Transverse	1
AJCC stage	
I	4
II	8
III	8
IV	1

AJCC, American Joint Committee on Cancer.

TABLE 2 List of antibodies used in this experiment and the Opal dyes assigned to them.

Antibody	Manufacturer	Catalogue #	OPAL dye assigned
CD20	Cell Marque	120M-84	Opal 480
CD3	Cell Marque	103R-95	Opal 520
Foxp3	Biolegend	320102	Opal 570
Foxp3	Abcam	ab450	Opal 570
CD4	Novus	NBP2-46149	Opal 620
Ki-67	Cell Marque	275R-15	Opal 690
CD8	Cell Marque	108M-94	Opal 780
			DAPI (nuclei)

The order of the antibodies listed is the order that the antibodies were added used in the cyclical staining procedure Opal procedure.

For H&E images, slides were deparaffinised and stained with Gills haematoxylin (Merck/Sigma Aldrich) counterstained with Eosin Y, aqueous (Merck/Sigma Aldrich) before dehydration and mounting with Eukitt Quick-hardening mounting medium (Merck/Sigma Aldrich).

Image analysis

Image unmixing, cell segmentation and positive channel marker thresholding were undertaken using the InForm (version 2.6 AKOYA BioSciences) program. Phenotyping and analysis of InForm-derived data was undertaken using R (version 4.0.4) in conjunction with custom analysis pipelines and the phenoptr package (version 0.3.2).

To improve comprehension of our results, we classified CD3+ CD8- cells as CD4 T-cells, since almost all T-cells present in CRC are single positive for either CD8 or CD4 (27, 28). Lymphocytes were therefore classified into 4 groups: B cells (CD20+ CD3–); CD8 T-cells (CD3+ CD8+); Foxp3– CD4 cells (CD3+ CD8– Foxp3–); Foxp3+ CD4 cells (CD3+ CD8– Foxp3+). Each of these 4 cell subsets were then sub-classified as Ki-67+ or Ki-67– to generate counts of 8 cell classifications for each TLS. A ninth category of cells shown in some analyses is "undefined" – cells that did not fall into the aforementioned categories, the vast majority of which were negative for all markers with the exception of their DAPI+ status.

TLS quantification

Our strategy to determine TLS from other non-TLS lymphoid aggregates for downstream analyses is outlined in Supplementary Figure S1. Lymphoid aggregates were initially identified in images by two researchers; where B-cell aggregates were close to each other and were connected by strands of lymphocytes (e.g. Figure 2J; Supplementary Figure S2E) these were considered as a single aggregate. The two researchers then re-assessed each other's selections to determine which aggregates met defined criteria for classification as TLS domains. Cellular composition of each aggregate was phenotyped as described above, and only aggregates of ≥250 cells comprising >50% B-cells and/or T-cells were included as TLS domains.

Given the lack of consistency in the literature in how the peri-tumoural region is defined (1), TLS domains were not further sub-classified according to their distance from tumour margins, although all TLS domains analysed were either intra-tumoural or within ≈10mm of cancer cells.

Area measurement

Total tissue area measurements were made on Qupath (30) (version, 0.4.2) using the pixel classifier thresholder function. Briefly, the average of all channels were prefiltered (Gaussian) and a threshold was chosen that coved the tissue region. Tumour

area measurements were made manually, aided by H&E stained sections from the same tumour annotated by a pathologist (T. Jeon). TLS tissue measurements used the pixel classifier thresholder function using CD3 and CD20 channels. Manual adjustments were made to the region where required.

Statistical analyses

Statistical analysis on individual TLS data was performed in R using the R package lme4 (v1.1-29) to apply a generalised linear mixed model with REML/residual maximum likelihood to account for grouping effects. The p-values were calculated with lmerTest (v3.1-3) using Satterthwaite's method. For the whole TLS tissue analysis, a linear regression with Spearmann's correlation test was implemented using the stats package on R (v4.0.4). Values scaled in log10.

TLS with fewer than 50 cells of the assessed phenotypes were removed from analysis when performing correlation analyses, to ensure each datapoint was based on robust sample sizes.

Results

TLS domains in tissue sections from patients with CRC show highly diverse morphology

We examined FFPE tissue sections from the tumours of 22 patients with CRC; patient characteristics are described in Table 1. We used the criteria shown in Methods to identify 524 TLS domains in these combined tissue sections (Supplementary Figure S1).

TLS domains stained for the B-cell marker CD20, with variable staining for the T-cell markers CD3, CD8 (Figure 2) and Foxp3 (Supplementary Figures S2A–D). Subsets of both B-cells and T-cells stained for Ki-67 (Figure 2). Most TLS domains were outside the tumour zones, with a minority in the peri-tumoural zones within 1mm from the invasive margin, and even fewer within the tumours (data not shown); however, in this study we did not quantify location of TLS domains with respect to cancer cells.

In images of these TLS domains, some resembled the canonical descriptions of mature TLS (1), with a well-defined GC surrounded

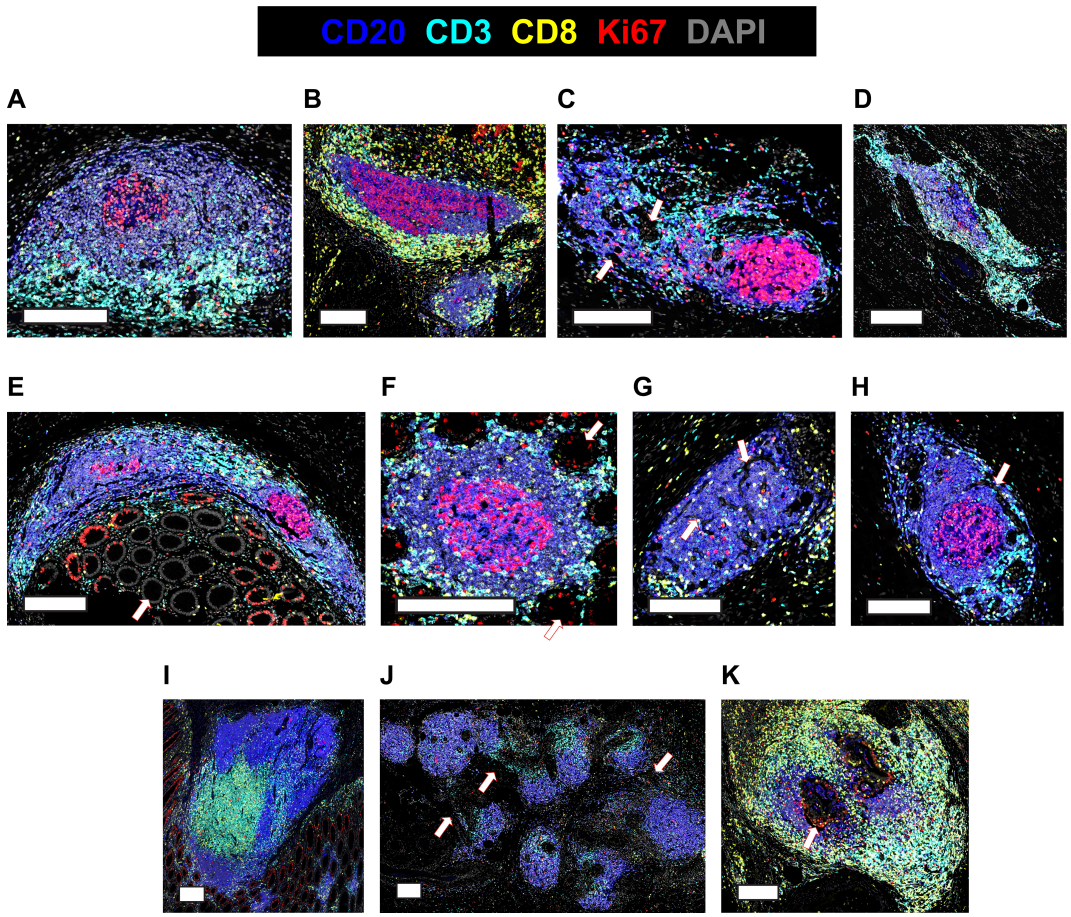

FIGURE 2
Diverse appearances of TLS in CRC. **(A-K)** Selected microscopic images of TLS imaged in the 22-patient cohort, highlighting the different visual appearances. Slides were stained for CD3, CD20, Ki-67, CD8, DAPI and Foxp3 (not shown), imaged on the Akoya PhenoImager HT instrument. Scale bars are 200µm. Arrows are used to highlight **(C)** non-lymphocytic regions **(E, F)** epithelial crypts **(G, H)** channels **(J)** lymphocytic strands connecting discrete B-cell follicles **(K)** a Ki-67+ non-lymphocyte region encased by TLS.

by a compact, mostly ovoid-shaped B-cell zone and an associated T-cell zone (Figure 2A). However, many TLS domains displayed other geometries. TLS domains were not always ovoid (Figures 2B, D) and both the B-cell zones (Figure 2B) and T-cell zones (Figure 2C) adjacent to GCs varied in shape, with non-lymphoid cells and ECM often intercalated (Figure 2C, arrows). Local tissue architecture such as epithelial crypts also impacted TLS domain morphology (Figures 2D–F), while channels and holes sometimes led to perforated appearances, probably due to blood or lymphatic vasculature (Figures 2G, H).

Some TLS domains were large and contained multiple B-cell regions (Figure 2I), consistent with the section plane passing through large multi-lobular TLS (26). Other TLS domains appeared in close proximity, connected by strands of lymphocytes (Figure 2J, arrows and Supplementary Figure S2E), raising the possibility that they might be part of the same TLS in 3D. Occasional TLS domains surrounded Ki-67+ proliferating cells that were negative for CD3 and CD20 (Figure 2K, highlighted by arrow).

Collectively, our results show that TLS domains do not usually appear as classical ovoid structures and often lack well defined T-cell zones within the sectioning plane, even when GCs are clearly present (Figures 2B, C, E, F, H).

TLS domains show significant heterogeneity between and within CRC patients

We sought to quantify and classify individual TLS domains within each CRC tissue sample, by counting circumscribed TLS domains and phenotyping their cellular constituents. The counts of TLS domains within each tissue sample varied greatly (Figure 3A). The lowest and highest TLS domain counts were 4 and 100, respectively, with a mean of 24.

The cellular composition of each TLS domain was analysed by digitally quantifying four different lymphocyte subsets, and the proportions of each of these subsets that expressed Ki-67 (Figure 3A). The proportion of B-cells expressing Ki-67 within TLS domains ranged from 0% to 94% (Figure 3A). Within each patient's sample, the Ki-67+ proportion of B-cells also varied considerably (Figure 3A). However, when comparing the results between patients across their TLS domains, differences between patients become apparent. Some patients had higher proportions of Ki-67+ B-cells in most B-cell zones (Figure 3A, upper row), while others had consistently low proportions of Ki-67+ B-cells (Figure 3A, lower row). Hence, despite the variation in Ki-67 expression by B-cells in different TLS domains within individual

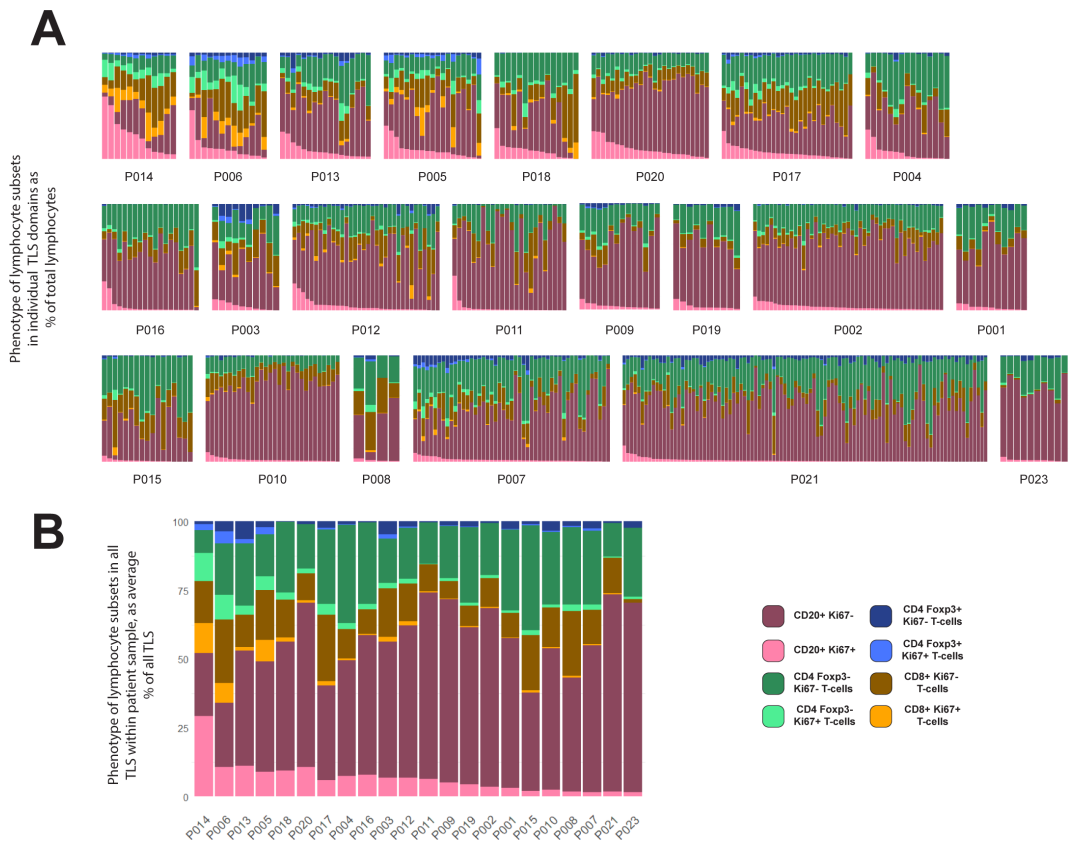

FIGURE 3
Variation within and between patients in lymphocyte composition of TLS domains. **(A, B)** 524 TLS domains across 22 patients with CRC were segmented and phenotyped, and lymphocyte subsets counted in each TLS. Data shown represent % of total lymphocytes occupied by each of the 4 lymphocyte types shown, with each lymphocyte subset sub-plotted for expression of Ki-67 (pale colours Ki-67+, dark colour Ki-67-). Patient identity codes are shown on the x-axis, and patients are ranked left to right according to average B-cell Ki-67+ % across all TLS within each patient. **(A)** Data from all individual TLS domains, grouped by patient. **(B)** Averages across all TLS domains in each patient.

patient samples, patients clearly differed in their B-cell proliferation once all their TLS domains were taken into account. Averaging the proportion of proliferating B-cells within all TLS domains in a tissue section allowed patients to be ranked for B-cell proliferation within their tissue sample (Figure 3B; Supplementary Figure S4A; this ranking was also used to order patients in Figure 3A).

Previous studies have suggested CRC patients with higher TLS numbers as well as those with a higher proportion of mature TLS have a better prognosis compared with patients with lower proportions (10, 23, 31). The numbers of TLS domains varied substantially even within the patients with the highest levels of B-cell proliferation (Figure 3A, top row). Additionally, patients among those with the lowest B-cell activation also had some of highest TLS domain counts (such as P007, P010 and P021). Taken together, these observations confirm that counts of TLS domains from 2D sections do not adequately summarise TLS activity.

Ki-67+ status of B-cells is correlated with Ki-67+ status of T-cells, including Foxp3+ CD4+ T cells

Patients that ranked highest for the proportion of Ki-67+ B-cells also exhibited high Ki-67 expression in T-cell subsets (Figure 3B), suggesting a potential correlation between B-cell proliferation and that of certain T-cell subsets. We therefore compared the Ki-67 expression in B-cells with that in different T-cell subsets within individual TLS domains across all patients (Figure 4A). This analysis confirmed a correlation between the proportion of B-cells expressing Ki-67 within each TLS domain and the Ki-67 expression of both Foxp3– CD4 T-cells and CD8+ T-cells (Figure 4A).

Foxp3+ CD4 T cells also expressed Ki-67 frequently, and this expression correlated with that in B-cells, CD8+ T-cells and Foxp3– CD4 T-cells (Figure 4B). Hence individual TLS domains with high proportions of Ki-67+ B-cells also had higher proportions of proliferation in all T-cell subpopulations, including Foxp3+ CD4 cells.

To test whether non-proliferating (Ki-67–) Foxp3+ CD4 T-cells might suppress T-cell proliferation, we plotted the correlation between the presence of this population (represented by their proportion of all lymphocytes within the TLS domain) and the Ki-67 expression in the other T-cell subsets (Figure 4C). The proportion of non-proliferating Foxp3+ CD4 cells per TLS domain did not show an inverse correlation with the presence of Ki-67 on other T-cell populations (nor B-cells) suggesting they were not suppressing T-cell proliferation within TLS.

Assessing TLS area across entire tissue sections

Accurate measures of the total quantity of TLS within tumour sections might generate clinically-informative parameters, given that parameters such as T-cell counts within CRC tissue correlate with increased survival (32). The striking variation in the area of individual TLS domains (e.g. Figure 2), and the multi-lobular nature

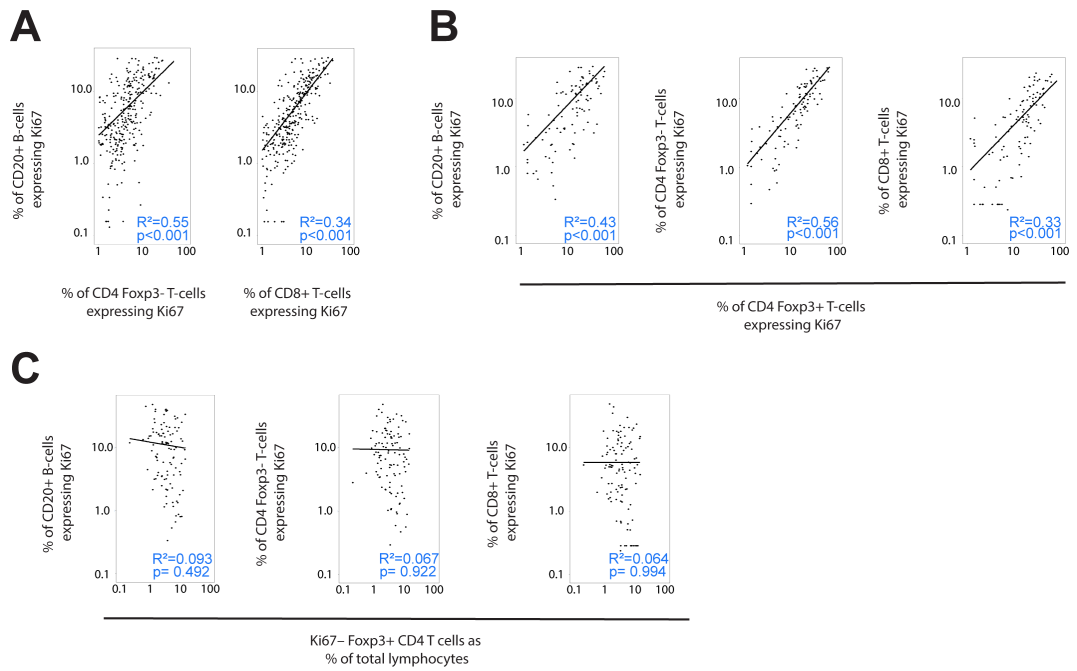

FIGURE 4
(A–C) Correlation of Ki-67 expression between lymphocyte subsets. Scatterplots showing the correlation between Ki-67 expression in different lymphocyte subsets within individual TLS domains. **(A)** Ki-67 expression in B-cells (y-axes) plotted against that in Foxp3– CD4 T-cells and CD8+ T-cells (x-axes) **(B)** Ki-67 expression in Foxp3+ CD4 T-cells (x-axes) plotted against that in B-cells, Foxp3- CD4 T-cells and CD8+ T-cells (y-axes) **(C)** Presence of Foxp3+ CD4 T-cells that are not proliferating (Ki-67–) in each TLS domain (x-axes) plotted against Ki-67 expression in CD20+ B-cells, Foxp3– CD4 T-cells and CD8+ T-cells. Note log scaling of all scatterplots.

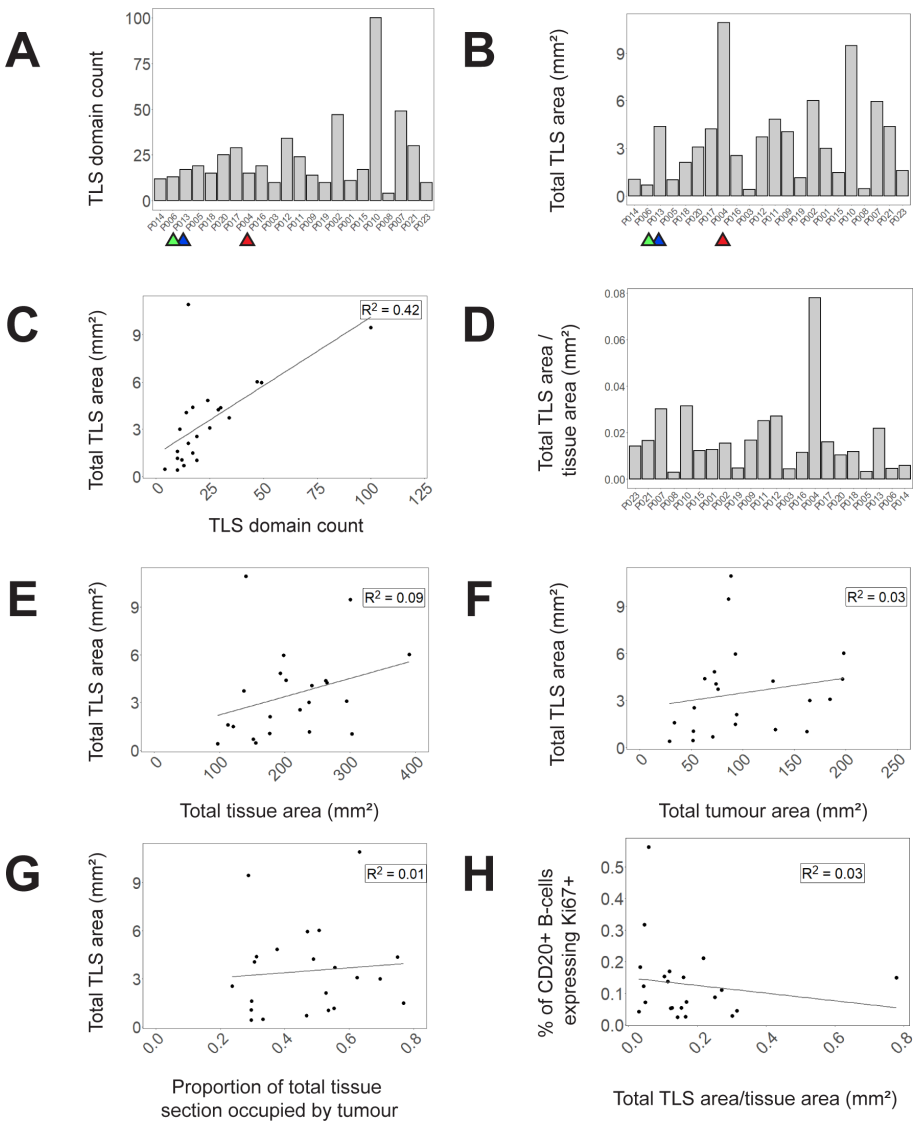

FIGURE 5
TLS domain density and correlation with other spatial measures. **(A)** Counts of circumscribed TLS domains in each tissue section **(B)** Total area of TLS domains in each tissue section **(C)** A scatterplot of total TLS area against TLS domain counts **(D)** and a bar graph demonstrating proportion of total tissue area occupied by TLS domains. **(E–G)** Correlations of total TLS area across all tissue samples to **(E)** total tissue area **(F)** total tumour area **(G)** proportion of total tissue area occupied by tumour. **(H)** Correlation of B-cell Ki-67 expression (averaged across TLS domains within each sample) with the proportion of tissue section occupied by TLS in that tissue section. Selected samples are highlighted by coloured arrows in (**A–C**) corresponding to P006 (green), P013 (blue) and P004 (red).

of TLS in at least some CRC samples (e.g. Figure 2J), suggested that TLS count would poorly represent the total area of the TLS domains within a complete section. We therefore measured the total area of TLS within each section and compared this parameter with the canonical approach of counting the number of TLS domains.

Our data show that the count of TLS domains (Figure 5A) does not always reflect total TLS area within the section (Figure 5B). When the two parameters are compared against each other in a scatterplot, a weak correlation is observed with notable outliers (Figure 5C). For example, although P006, P013 and P004 are very similar in terms of TLS count (Figure 5A, highlighted samples) they have very dissimilar total TLS area (Figure 5B) due to different average TLS domain areas, as is clearly evident in images from these subjects (Supplementary Figure S3). Hence measuring total TLS area across an entire section provides an alternative measure of the total quantity of TLS domains that accounts for the substantial variation in area of individual TLS domains, which TLS domain counts alone do not.

Assessing total TLS area within a section needs to take account of total section size, and the proportion of the section that is occupied by tumour. Within our 22 samples, the proportion of the total tissue area occupied by TLS varied substantially (Figure 5D) and there was no correlation between total section area and the area occupied by TLS (Figure 5E). Total TLS area did not correlate with total tumour area (Figure 5F) nor the proportion of the total section occupied by tumour (Figure 5G). Hence total

TLS area varied independently of tissue section size and the degree of tumour infiltration.

To compare whether the area of TLS within a section might correlate with TLS activation, we plotted the proportion of total section area occupied by TLS against the average proportion of B-cells expressing Ki-67 in each TLS domain (Figure 5H). No correlation was observed suggesting that the level of TLS activation represented by B-cell proliferation is not dependent on TLS area.

Assessing sum of B- and T-cell proliferation vs averaged individual TLS composition

Measurement of activation or proliferation of B- and T-cells across entire tissue sections may help correct for the failure of the section plane to transect structures such as GCs, while also simplifying analysis. We therefore re-analysed our data by combining data from all TLS domains identified within each section, and then ranking patients by the proportion of cell subsets across all TLS. When compared with the previous method based on identifying individual circumscribed TLS (Figures 3A, B), this whole-section approach led to broadly similar rankings of patient TLS activity (Figure 6A), with the same 8 subjects top-ranked, but with significant re-positioning of some patients with low to moderate levels of B-cell proliferation (Supplementary Figure S4). Plotting the proportions of B-cells expressing Ki-67 against the Ki-67+ proportions of T-cell subsets showed improved correlations based on this whole-section aggregated data compared with the previous method based on individual TLS zones (Figure 6B compared with Figures 4A, B). This simpler whole-section analysis confirmed that proliferation of B-cells is highly correlated with proliferation of all T-cell subsets.

Discussion

The goal of this study was to create and evaluate a simple workflow to study TLS composition across entire sections of CRC tissue. We used multiplexed immunofluorescence to stain CRC tissue, then digitally quantified the major lymphocyte populations in each TLS domain. These quantitative data differed substantially between individual TLS domains within each sample, consistent with the wide range of appearances in our images. Aggregating data from the cellular phenotypes within all TLS prior to analysis enabled facile comparison between specimens, such as ranking patients according to lymphocyte proliferation, without needing to laboriously compare the constituents of individual TLS.

We stained for Ki-67 to identify proliferating lymphocytes. B-cells within GCs frequently expressed Ki-67, so the quantification of B-cell Ki-67 across whole tissue sections we performed might prove a much simpler measure of total GC formation within TLS than counting individual GCs. However we did note that in some TLS domains with high proportions of proliferating B-cells, the cells were not clustered into GCs (data not shown). Digital detection of B-cell clustering as well as B-cell proliferation might be necessary to accurately quantify GCs, though co-staining for other GC features, such as the presence of FDCs, may also prove useful in future.

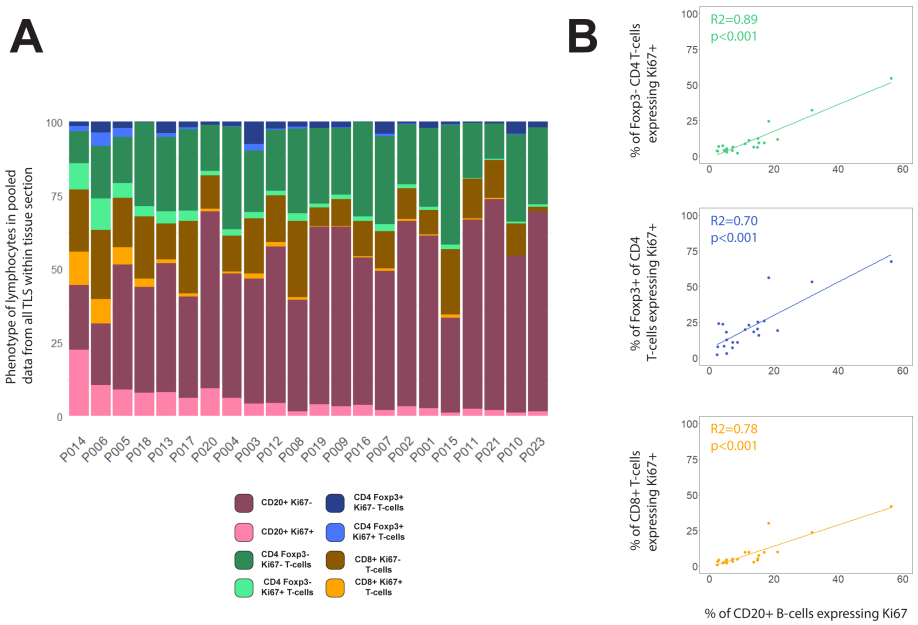

FIGURE 6
Compositions of total TLS area within each tissue section. **(A)** Lymphocyte phenotype data from all TLS domains within each tissue section were pooled before plotting % of each phenotype across the entire section. Patients were ranked by the proportion of B-cells expressing Ki-67. **(B)** Scatterplots showing the correlations between % of B-cells expressing Ki67+ with the Ki-67+ % for Foxp3– CD4 T-cells (green), Foxp3+ CD4 T-cells (blue) and CD8+ T-cells (orange). Spearman's correlation test on all slopes were p<0.001.

We found Ki-67 staining to be particularly informative because it simultaneously reads out both B- and T-cell proliferation. When assessed across entire sections, proliferation of all T-cell subsets correlated with B-cell proliferation, despite the highly variable T-cell content observed within individual TLS domains. This raises that possibility that quantifying T-cell parameters as well as B-cell parameters within any structure that might be part of a TLS may add to predictive power for clinical outcomes, compared with approaches where analysis is restricted to only those lymphocyte clusters that contain both cell types juxtaposed.

Foxp3+ CD4 T-cells are sometimes considered to be regulatory T-cells with potential to suppress activation and proliferation of other T-cell subsets. To check whether the non-proliferating Foxp3+ CD4 T-cells might exert a negative effect on the proliferation of the other subsets, we tested the correlation between the presence of these cells in TLS and the Ki-67 signal in all T-cell subsets: no correlation – either positive or negative – was found. In contrast, we found a positive correlation between the proportions of Foxp3+ CD4 T-cells expressing Ki-67, and the proliferation of both CD4 and CD8+ T-cells, suggesting Foxp3+ CD4 T-cells had often been activated to proliferate within TLS alongside Foxp3– CD4 T-cells and CD8+ T-cells. These data are consistent with the concept that the presence of Foxp3+ CD4 T cells within CRC tissue does not suppress proliferation of other T-cell subsets. This result might seem inconsistent with the immunosuppressive activity ascribed to Foxp3+ CD4 T-cells in some human cancers, where their presence within tumours has been associated with poor outcomes (33, 34). However while Foxp3 is often used as a marker of Treg cells, in humans, many Foxp3+ T-cells are not Tregs (35, 36) and may even be activated effector/memory cells (37, 38). Indeed the presence of CD4+ CD45RA– effector/memory T-cells expressing low levels of Foxp3+ has been associated with improved prognosis in CRC (36). Hence our data reinforce the concept that the expression of Foxp3 by CD4 T-cells does not necessarily correlate with immunosuppressive activity.

Our study suggests measures of total TLS area are likely to better represent the quantity of TLS within a patient sample than counts of individual TLS domains. The average area of individual TLS domains varied substantially between patients, so that the number of discrete TLS domains did not accurately reflect the proportion of the total section occupied by TLS. Our study also showed no correlation between this TLS area and the presence of proliferating lymphocytes within the TLS, suggesting TLS area and activation are independent. In future clinical studies it would therefore be valuable to report TLS area parameters separately from activation parameters in order to tease out correlations with clinical features.

We can already envisage several potential improvements to whole slide analysis of TLS that are worthy of further investigation:

Firstly we suggest that whole-slide approaches incorporating cancer cell markers might give a better index of overall proximity of TLS to cancer cells than merely marking tumour boundaries in 2D, given the complexity of the 3D spatial relationship between TLS and tumours. We did not formally assess the spatial relationships of TLS to cancer cells, but in addition to occasional intra-tumoural TLS we did note some TLS domains wrapped around isolated tumour buds (e.g. Figure 2K). Such TLS may be functionally similar to intra-tumoural TLS given the direct access TLS-resident immune cells will have to cancer cell macromolecules (14). It may therefore be useful to quantify the area of TLS that is in contact with any cancer cells, no matter where they are located with respect to the main tumour body.

Secondly we recognise that further investigation of the constituents of immune cell clusters within CRC tissue may enable new classifications of clusters that could be independently quantified across entire sections. In this study we took a relatively broad view of immune cell clusters that might comprise parts of TLS within the tissue section, consistent with the 3D structure of human TLS (26). However use of additional markers that can distinguish other cell types, such as myeloid cell subsets, might reveal distinctive subtypes of clusters. We did not attempt to distinguish between TLS and other gut-associated lymphoid tissue (GALT), in the absence of markers that can distinguish pre-existing GALT structures from induced TLS (39). Should such specific markers emerge it would be useful to include these in future whole slide analysis.

In conclusion, we have shown that whole section analysis of TLS activity in aggregate efficiently averages the highly variable appearance of complex TLS structures within a single 2D section plane. Quantification of molecular markers such as Ki-67 in TLS lymphocytes across entire sections greatly reduced the complexity of canonical approaches based on counting and characterising individual TLS domains, and may potentially improve accuracy. These novel methods can now be tested against clinical parameters in large cohorts of patients, potentially with automated detection of TLS domains, and inclusion of cancer cell markers to enable quantification of TLS proximity to cancer cell zones.

Data availability statement

The raw data supporting the conclusions of this article will be made available by the authors upon reasonable request, dependent on ethical constraints associated with consent.

Ethics statement

The studies involving humans were approved by Health and Disability Ethics Committee (NZ Ministry of Health). The studies were conducted in accordance with the local legislation and institutional requirements. The human samples used in this study were acquired from The Dunedin Colorectal Cohort (DNCRC) biobank. Written informed consent for participation in research that adhered to the aims of the DNCRC was obtained from the participants or the participants' legal guardians/next of kin by the DNCRC.

Author contributions

LM: Conceptualization, Data curation, Formal analysis, Investigation, Methodology, Validation, Visualization, Writing – original draft, Writing – review & editing. SP: Conceptualization, Data curation, Formal analysis, Investigation, Methodology,

Supervision, Validation, Visualization, Writing – review & editing, Writing – original draft. SL: Formal analysis, Investigation, Methodology, Software, Validation, Visualization, Writing – review & editing. CC: Methodology, Resources, Validation, Writing – review & editing. LZ: Formal analysis, Writing – review & editing. JR: Data curation, Writing – review & editing. TJ: Data curation, Validation, Writing – review & editing. SF: Resources, Writing – review & editing. JM: Project administration, Resources, Writing – review & editing. RK: Funding acquisition, Investigation, Methodology, Project administration, Resources, Supervision, Writing – review & editing. PRD: Conceptualization, Funding acquisition, Investigation, Project administration, Resources, Supervision, Writing – original draft, Writing – review & editing.

Funding

The author(s) declare financial support was received for the research, authorship, and/or publication of this article. Funding for reagents, salaries and equipment use was provided by the Maurice Wilkins Centre under its Precision Immuno-oncology programme, by the Health Research Council (grant numbers 22-432 and 19/081), and by the University of Auckland.

Conflict of interest

The authors declare that the research was conducted in the absence of any commercial or financial relationships that could be construed as a potential conflict of interest.

Publisher's note

Supplementary material

The Supplementary Material for this article can be found online at: https://www.frontiersin.org/articles/10.3389/fimmu.2025.1500792/full#supplementary-material

References

1. Munoz-Erazo L, Rhodes JL, Marion VC, Kemp RA. Tertiary lymphoid structures in cancer - considerations for patient prognosis. *Cell Mol Immunol*. (2020) 17:570–5. doi: 10.1038/s41423-020-0457-0

2. Zhao Z, Ding H, Lin ZB, Qiu SH, Zhang YR, Guo YG, et al. Relationship between tertiary lymphoid structure and the prognosis and clinicopathologic characteristics in solid tumors. *Int J Med Sci*. (2021) 18:2327–38. doi: 10.7150/ijms.56347

3. Coppola D, Nebozhyn M, Khalil F, Dai H, Yeatman T, Loboda A, et al. Unique ectopic lymph node-like structures present in human primary colorectal carcinoma are identified by immune gene array profiling. *Am J Pathol*. (2011) 179:37–45. doi: 10.1016/j.ajpath.2011.03.007

4. Di Caro G, Bergomas F, Grizzi F, Doni A, Bianchi P, Malesci A, et al. Occurrence of tertiary lymphoid tissue is associated with T-cell infiltration and predicts better prognosis in early-stage colorectal cancers. *Clin Cancer Res*. (2014) 20:2147–58. doi: 10.1158/1078-0432.CCR-13-2590

5. Jiang Q, Tian C, Wu H, Min L, Chen H, Chen L, et al. Tertiary lymphoid structure patterns predicted anti-PD1 therapeutic responses in gastric cancer. *Chin J Cancer Res*. (2022) 34:365–82. doi: 10.21147/j.issn.1000-9604.2022.04.05

6. Vanhersecke L, Brunet M, Guegan JP, Rey C, Bougouin A, Cousin S, et al. Mature tertiary lymphoid structures predict immune checkpoint inhibitor efficacy in solid tumors independently of PD-L1 expression. *Nat Cancer*. (2021) 2:794–802. doi: 10.1038/s43018-021-00232-6

7. Pfannstiel C, Strissel PL, Chiappinelli KB, Sikic D, Wach S, Wirtz RM, et al. The tumor immune microenvironment drives a prognostic relevance that correlates with bladder cancer subtypes. *Cancer Immunol Res*. (2019) 7:923–38. doi: 10.1158/2326-6066.CIR-18-0758

8. Kim A, Lee SJ, Ahn J, Park WY, Shin DH, Lee CH, et al. The prognostic significance of tumor-infiltrating lymphocytes assessment with hematoxylin and eosin sections in resected primary lung adenocarcinoma. *PloS One*. (2019) 14:e0224430. doi: 10.1371/journal.pone.0224430

9. Sofopoulos M, Fortis SP, Vaxevanis CK, Sotiriadou NN, Arnogiannaki N, Ardavanis A, et al. The prognostic significance of peritumoral tertiary lymphoid structures in breast cancer. *Cancer Immunol Immunother*. (2019) 68:1733–45. doi: 10.1007/s00262-019-02407-8

10. Posch F, Silina K, Leibl S, Mündlein A, Moch H, Siebenhüner A, et al. Maturation of tertiary lymphoid structures and recurrence of stage II and III colorectal cancer. *Oncoimmunology*. (2018) 7:e1378844. doi: 10.1080/2162402X.2017.1378844

11. Barmpoutis P, Di Capite M, Kayhanian H, Waddingham W, Alexander DC, Jansen M, et al. Tertiary lymphoid structures (TLS) identification and density assessment on H&E-stained digital slides of lung cancer. *PloS One*. (2021) 16:e0256907. doi: 10.1371/journal.pone.0256907

12. Karjula T, Niskakangas A, Mustonen O, Puro I, Elomaa H, Ahtiainen M, et al. Tertiary lymphoid structures in pulmonary metastases of microsatellite stable colorectal cancer. *Virchows Arch*. (2023) 483:21–32. doi: 10.1007/s00428-023-03577-8

13. Kasikova L, Rakova J, Hensler M, Lanickova T, Tomankova J, Pasulka J, et al. Tertiary lymphoid structures and B cells determine clinically relevant T cell phenotypes in ovarian cancer. *Nat Commun*. (2024) 15:2528. doi: 10.1038/s41467-024-46873-w

14. Schumacher TN, Thommen DS. Tertiary lymphoid structures in cancer. *Science*. (2022) 375:eabf9419. doi: 10.1126/science.abf9419

15. Werner F, Wagner C, Simon M, Glatz K, Mertz KD, Laubli H, et al. A standardized analysis of tertiary lymphoid structures in human melanoma: disease progression- and tumor site-associated changes with germinal center alteration. *Front Immunol*. (2021) 12:675146. doi: 10.3389/fimmu.2021.675146

16. Calderaro J, Petitprez F, Becht E, Laurent A, Hirsch TZ, Rousseau B, et al. Intra-tumoral tertiary lymphoid structures are associated with a low risk of early recurrence of hepatocellular carcinoma. *J Hepatol*. (2019) 70:58–65. doi: 10.1016/j.jhep.2018.09.003

17. Wu YH, Wu F, Yan GR, Zeng QY, Jia N, Zheng Z, et al. Features and clinical significance of tertiary lymphoid structure in cutaneous squamous cell carcinoma. *J Eur Acad Dermatol Venereol*. (2022) 36:2043–50. doi: 10.1111/jdv.18464

18. Hiraoka N, Ino Y, Yamazaki-Itoh R, Kanai Y, Kosuge T, Shimada K. Intratumoral tertiary lymphoid organ is a favourable prognosticator in patients with pancreatic cancer. *Br J Cancer*. (2015) 112:1782–90. doi: 10.1038/bjc.2015.145

19. Hayashi Y, Makino T, Sato E, Ohshima K, Nogi Y, Kanemura T, et al. Density and maturity of peritumoral tertiary lymphoid structures in oesophageal squamous cell carcinoma predicts patient survival and response to immune checkpoint inhibitors. *Br J Cancer*. (2023) 128:2175–85. doi: 10.1038/s41416-023-02235-9

20. Silina K, Soltermann A, Attar FM, Casanova R, Uckeley ZM, Thut H, et al. Germinal centers determine the prognostic relevance of tertiary lymphoid structures and are impaired by corticosteroids in lung squamous cell carcinoma. *Cancer Res*. (2018) 78:1308–20. doi: 10.1158/0008-5472.CAN-17-1987

21. Ling Y, Zhong J, Weng Z, Lin G, Liu C, Pan C, et al. The prognostic value and molecular properties of tertiary lymphoid structures in oesophageal squamous cell carcinoma. *Clin Transl Med*. (2022) 12:e1074. doi: 10.1002/ctm2.v12.10

22. Kuwabara S, Tsuchikawa T, Nakamura T, Hatanaka Y, Hatanaka KC, Sasaki K, et al. Prognostic relevance of tertiary lymphoid organs following neoadjuvant chemoradiotherapy in pancreatic ductal adenocarcinoma. *Cancer Sci*. (2019) 110:1853–62. doi: 10.1111/cas.2019.110.issue-6

23. Yamaguchi K, Ito M, Ohmura H, Hanamura F, Nakano M, Tsuchihashi K, et al. Helper T cell-dominant tertiary lymphoid structures are associated with disease relapse of advanced colorectal cancer. *Oncoimmunology*. (2020) 9:1724763. doi: 10.1080/2162402X.2020.1724763

24. Gobert M, Treilleux I, Bendriss-Vermare N, Bachelot T, Goddard-Leon S, Arfi V, et al. Regulatory T cells recruited through CCL22/CCR4 are selectively activated in lymphoid infiltrates surrounding primary breast tumors and lead to an adverse clinical outcome. *Cancer Res*. (2009) 69:2000–9. doi: 10.1158/0008-5472.CAN-08-2360

25. Zhan Z, Shi-Jin L, Yi-Ran Z, Zhi-Long L, Xiao-Xu Z, Hui D, et al. High endothelial venules proportion in tertiary lymphoid structure is a prognostic marker and correlated with anti-tumor immune microenvironment in colorectal cancer. *Ann Med*. (2023) 55:114–26. doi: 10.1080/07853890.2022.2153911

26. Lin JR, Wang S, Coy S, Chen YA, Yapp C, Tyler M, et al. Multiplexed 3D atlas of state transitions and immune interaction in colorectal cancer. *Cell*. (2023) 186:363–81 e19. doi: 10.1016/j.cell.2022.12.028

27. Di J, Liu M, Fan Y, Gao P, Wang Z, Jiang B, et al. Phenotype molding of T cells in colorectal cancer by single-cell analysis. *Int J Cancer*. (2020) 146:2281–95. doi: 10.1002/ijc.32856

28. Vayrynen JP, Haruki K, Lau MC, Vayrynen SA, Ugai T, Akimoto N, et al. Spatial organization and prognostic significance of NK and NKT-like cells via multimarker analysis of the colorectal cancer microenvironment. *Cancer Immunol Res*. (2022) 10:215–27. doi: 10.1158/2326-6066.CIR-21-0772

29. Giacomelli M, Monti M, Pezzola DC, Lonardi S, Bugatti M, Missale F, et al. Immuno-contexture and immune checkpoint molecule expression in mismatch repair proficient colorectal carcinoma. *Cancers (Basel)*. (2023) 15. doi: 10.3390/cancers15123097

30. Bankhead P, Loughrey MB, Fernandez JA, Dombrowski Y, McArt DG, Dunne PD, et al. QuPath: Open source software for digital pathology image analysis. *Sci Rep*. (2017) 7:16878. doi: 10.1038/s41598-017-17204-5

31. Trajkovski G, Ognjenovic L, Karadzov Z, Jota G, Hadzi-Manchev D, Kostovski O, et al. Tertiary lymphoid structures in colorectal cancers and their prognostic value. *Open Access Maced J Med Sci*. (2018) 6:1824–8. doi: 10.3889/oamjms.2018.341

32. Grivennikov SI, Greten FR, Karin M. Immunity, inflammation, and cancer. *Cell*. (2010) 140:883–99. doi: 10.1016/j.cell.2010.01.025

33. Fu J, Xu D, Liu Z, Shi M, Zhao P, Fu B, et al. Increased regulatory T cells correlate with CD8 T-cell impairment and poor survival in hepatocellular carcinoma patients. *Gastroenterology*. (2007) 132:2328–39. doi: 10.1053/j.gastro.2007.03.102

34. Plitas G, Konopacki C, Wu K, Bos PD, Morrow M, Putintseva EV, et al. Regulatory T cells exhibit distinct features in human breast cancer. *Immunity*. (2016) 45:1122–34. doi: 10.1016/j.immuni.2016.10.032

35. Miyara M, Yoshioka Y, Kitoh A, Shima T, Wing K, Niwa A, et al. Functional delineation and differentiation dynamics of human CD4+ T cells expressing the Foxp3 transcription factor. *Immunity*. (2009) 30:899–911. doi: 10.1016/j.immuni.2009.03.019

36. Saito T, Nishikawa H, Wada H, Nagano Y, Sugiyama D, Atarashi K, et al. Two FOXP3(+)CD4(+) T cell subpopulations distinctly control the prognosis of colorectal cancers. *Nat Med*. (2016) 22:679–84. doi: 10.1038/nm.4086

37. Sakaguchi S, Mikami N, Wing JB, Tanaka A, Ichiyama K, Ohkura N. Regulatory T cells and human disease. *Annu Rev Immunol*. (2020) 38:541–66. doi: 10.1146/annurev-immunol-042718-041717

38. Allan SE, Crome SQ, Crellin NK, Passerini L, Steiner TS, Bacchetta R, et al. Activation-induced FOXP3 in human T effector cells does not suppress proliferation or cytokine production. *Int Immunol*. (2007) 19:345–54. doi: 10.1093/intimm/dxm014

39. Fenton TM, Jorgensen PB, Niss K, Rubin SJS, Morbe UM, Riis LB, et al. Immune profiling of human gut-associated lymphoid tissue identifies a role for isolated lymphoid follicles in priming of region-specific immunity. *Immunity*. (2020) 52:557–70.e6. doi: 10.1016/j.immuni.2020.02.001

frontiers | Frontiers in Immunology

TYPE Original Research
PUBLISHED 11 March 2025
DOI 10.3389/fimmu.2025.1540013

OPEN ACCESS

EDITED BY
Kelsey P. Kubelick,
University of Virginia, United States

REVIEWED BY
Alessio Vagliasindi,
Oncological Center of Basilicata (IRCCS), Italy
Xi Wang,
The Chinese University of Hong Kong, China

*CORRESPONDENCE
Shi Yin
yinshi2021@njtech.edu.cn
Cheng Gong
xxwkgongcheng@163.com
Bin Wang
wangbin1987@suda.edu.cn

RECEIVED 05 December 2024
ACCEPTED 20 February 2025
PUBLISHED 11 March 2025

CITATION
Liu H, Bai Y, Wang Z, Yin S, Gong C and Wang B (2025) Multimodal deep learning for predicting PD-L1 biomarker and clinical immunotherapy outcomes of esophageal cancer.
Front. Immunol. 16:1540013.
doi: 10.3389/fimmu.2025.1540013

Multimodal deep learning for predicting PD-L1 biomarker and clinical immunotherapy outcomes of esophageal cancer

Hui Liu[1], Yinpu Bai[1], Zhidong Wang[2], Shi Yin[1*], Cheng Gong[2*] and Bin Wang[2*]

[1]College of Computer and Information Engineering, Nanjing Tech University, Nanjing, Jiangsu, China, [2]Department of Cardiothoracic Surgery, the Third Affiliated Hospital of Soochow University, Changzhou, Jiangsu, China

Although the immune checkpoint inhibitors (ICIs) have demonstrated remarkable anti-tumor efficacy in solid tumors, the proportion of ESCC patients who benefit from ICIs remains limited. Current biomarkers have assisted in identifying potential responders to immunotherapy, yet they all have inherent limitations. In this study, two ESCC cohorts were established from the Third Affiliated Hospital of Soochow University in China. One cohort included 220 patients with PD-L1 expression levels determined by immunohistochemistry, and the other cohort included 75 patients who underwent immunotherapy. For each patient in both cohorts, we curated multimodal data encompassing Hematoxylin and Eosin-stained pathology images, longitudinal computed tomography (CT) scans, and pertinent clinical variables. Next, we introduced a novel multimodal deep learning model that integrated pathological features, radiomic features, and clinical information to predict PD-L1 levels, immunotherapy response, and overall survival. Our model achieved an AUC value of 0.836 for PD-L1 biomarker prediction, and 0.809 for immunotherapy response prediction. Furthermore, our model also achieved an AUC value of 0.8 in predicting overall survival beyond one or three years. Our findings confirmed that the multimodal integration of pathological, radiomic, and clinical features offers a powerful means to predict PD-L1 biomarker levels and immunotherapy response in esophageal cancer.

KEYWORDS

esophageal squamous cell carcinoma, PD-L1 biomarker, multi-modal deep learning, immunotherapy response, pathology image, CT imaging

1 Introduction

Esophageal cancer is one of the most prevalent cancers and a leading cause of cancer-related mortality worldwide (1), accounting for more than 500,000 deaths each year (2). Esophageal squamous cell carcinoma (ESCC) is the main histological subtype that has distinct epidemiological and clinical characteristics. It is prone to lymphatic spread and associated with poor prognosis (3). Immune checkpoint inhibitors (ICIs) have demonstrated remarkable anti-tumor efficacy in ESCC patients. However, the proportion of ESCC patients who benefit from ICIs remains limited.

In current clinical practice, the choice of immunotherapy is mainly guided by the levels of PD-L1 biomarker within tumor tissue (4). Elevated levels of PD-L1 are often indicative of favorable response to immunotherapy (5). Nonetheless, the assessment of PD-L1 biomarker via immunohistochemistry (IHC), commonly quantified as the combined positive score (CPS) or tumor proportion score (TPS) (6), is both resource-intensive and time-consuming (7). The variability in PD-L1 quantification is also substantial, influenced by the staining method and antibody employed (8). Some studies have reported a low rate of reproducibility for PD-L1 assessment by certified pathologists (9, 10). Besides, its nontrivial interpretation, coupled with the absence of a universal expert consensus, exacerbates the challenges in clinical decision-making (11).

Hematoxylin and eosin (H&E) staining is a routine examination of clinical specimens, facilitating the visual inspection of malignant cells (12). Pathologists rely on H&E staining for tumor diagnosis, including the determination of tumor subtype and grade. Recent advancements in computational pathology have achieved performance on par with that of pathologists in tasks such as tumor diagnosis and grade classification (13). Deep learning methodologies can capture information from H&E images beyond human visual capability, thereby offering new potential for pathology slides. For instance, Shamai et al. demonstrated that the expression levels of molecular biomarkers could be predicted from H&E whole slide images of breast cancer (7). Jin et al. introduced a multiple instance learning method for pan-cancer PD-L1 level prediction from histopathology slides, highlighting its potential to identify diverse histological patterns indicative of molecular levels (14). Despite these advancements, there is currently no evidence supporting the use of H&E slide analysis for predicting PD-L1 levels in esophageal cancer.

Moreover, radiomic features derived from regions of interest (ROIs) of radiographic imaging, such as lesion shape, size, voxel intensity, and texture, have demonstrated strong correlations with transcriptional and protein expression of clinical biomarkers in solid tumors (4, 15–18). For instance, Tian et al. proposed a deep learning framework based on CT images to non-invasively assess PD-L1 expression and immunotherapy response in NSCLC patients (15). Mu et al. developed a residual deep network utilizing pre-treatment PET/CT images to predict PD-L1 expression, as well as the durable clinical benefit, progression-free survival (PFS), and overall survival (OS) in advanced-stage NSCLC patients (4). However, radiomic features have not yet been explored for predicting the immunotherapy response of ESCC patients.

Currently, ESCC cohorts containing both H&E-stained slides and CT images with corresponding PD-L1 levels remain limited. In this paper, we invested our effort to construct two multimodal datasets in this retrospective study: a PD-L1 cohort and an immunotherapy cohort. For each patient, we manually collected the H&E whole-slide images, pre-treatment and early on-treatment CT images, as well as clinical variables. With the joint efforts of expert pathologists and computerized tools designed for rapid annotation, we successfully annotated the H&E slides and regions of interest (ROIs) in CT images. We think the esophageal cancer cohorts with manually curated immunotherapy response and multimodal data are valuable to the biomedical community. Next, we introduced a multimodal deep learning model to predict PD-L1 biomarker level and immunotherapy response. For H&E-stained slides, we employed deep convolutional networks to extract pathological tissue features. For CT images, we extracted radiomic features from the ROIs. When combined with clinical variables, these features demonstrated high predictive power for both PD-L1 levels and immunotherapy outcomes.

2 Materials and methods

2.1 Ethical review approval

This study was approved by the Institutional Review Boards of the Third Affiliated Hospital of Soochow University (Approval number: 2024-KD139) and was performed in accordance with the Declaration of Helsinki.

2.2 Patient cohorts

For the task of PD-L1 level prediction, we retrospectively curated a PD-L1 cohort of ESCC patients who underwent esophagectomy. The inclusion criteria were: (a) histologically confirmed ESCC; (b) treatment by surgery; (c) availability of complete clinical records. The exclusion criteria were: (a) receipt of neoadjuvant therapy before surgery; (b) baseline contrast-enhanced chest CT images of poor quality or with unmeasurable lesions; (c) poor-quality H&E images. The clinical variables include: age, sex, BMI, smoking history, drinking history, hypertension, tumor node metastasis (TNM) stage, grade, neurovascular invasion, tumor size, adjuvant radiotherapy and chemotherapy. The clinical endpoint of interest was overall survival, defined as the time from the treatment of esophagectomy to death from any cause or the latest follow-up. The latest follow-up period ended on 1 January 2024. As a result, the PD-L1 cohort included 220 patients, and the detailed summary is presented in Table 1. The PD-L1 levels were examined by immunohistochemistry assay on formalin-fixed, paraffin-embedded samples, using PD-L1 22C3 antibody on the Dako Link 48 platform (RRID: AB 2889976). The PD-L1 levels were reported in the form of combined positive scores (CPS) that fall in [0–100]. Two pathologists independently evaluated the ESCC slides to determine the PD-L1 expression in both tumor cells and immune cells, including lymphocytes and macrophages.

10.3389/fimmu.2025.1540013

TABLE 1 Demographic and clinical variables of ESCC PD-L1 cohort.

	ESCC PD-L1 cohort		
	All	PD-L1<50% (N=188)	PD-L1≥ 50% (N=32)
Age (years)			
Mean ± SD	66.5 ± 8.1	66.7 ± 8.1	65.4 ± 7.0
Gender, n (%)			
Female	45 (20.5)	37 (19.7)	8 (25.0)
Male BMI	175 (79.5)	151 (80.3)	24 (75.0)
Mean ± SD	22.56 ± 3.31	22.53 ± 3.28	22.76 ± 3.51
Smoking history, n (%)			
No	127 (57.7)	109 (58.0)	18 (56.2)
Yes	93 (42.3)	79 (42.0)	14 (43.8)
Drinking history, n (%)			
No	136 (61.8)	115 (61.2)	21 (65.6)
Yes	84 (38.2)	73 (38.8)	11 (34.4)
Hypertension, n (%)			
No	124 (56.4)	106 (56.4)	18 (56.2)
Yes	96 (43.6)	82 (43.6)	14 (43.8)
TNM Stage, n (%)			
I	19 (8.6)	16 (8.5)	3 (9.4)
II	95 (43.2)	83 (44.1)	12 (37.5)
III	94 (42.7)	78 (41.5)	16 (50.0)
IV	12 (5.5)	11 (5.9)	1 (3.1)
Grade, n (%)			
G1	20 (9.1)	15 (8.0)	5 (15.6)
G2	139 (63.2)	124 (66.0)	15 (46.9)
G3	61 (27.7)	49 (26.1)	12 (37.5)
Neurovascular invasion, n (%)			
No	123 (55.9)	104 (55.3)	19 (59.4)
Yes	97 (44.1)	84 (44.7)	13 (40.6)
Tumor size			
Mean ± SD	12.31 ± 9.48	12.21 ± 9.76	12.89 ± 7.74
Adjuvant radiotherapy, n (%)			
No	135 (61.4)	117 (62.2)	18 (56.2)
Yes	85 (38.6)	71 (37.8)	14 (43.8)
Adjuvant chemotherapy, n (%)			
No	121 (55.0)	107 (56.9)	14 (43.8)
Yes	99 (45.0)	81 (43.1)	18 (56.2)
Overall survival (months)			
Median	24.65	24.43	26.03

For immunotherapy response prediction, we built an immunotherapy cohort of patients who received immune checkpoint inhibitors (Tislelizumab, Camrelizumab, and Sintilimab) alone or in combination with chemotherapy. The inclusion criteria were: (a) histologically confirmed ESCC via endoscope; (b) stage III/IV; (c) receipt of immunotherapy alone or in combination with chemotherapy; (d) availability of contrast-enhanced chest CT within 2 months before the start of immunotherapy; and (e) completion of 2-4 cycles of treatment with follow-up CT images available for response evaluation. The exclusion criteria were: (a) receipt of surgery or radiotherapy during immunotherapy; (b) incomplete clinical records; and (c) poor-quality CT and H&E images. Immunotherapy response was independently evaluated by two experienced radiologists and one oncologist according to RECIST version 1.1 (19, 20). The immunotherapy cohort included 75 patients, and the clinical variables are presented in Table 2. We also provided the clinical and radiomics features collected before treatment for both the PD-L1 and immunotherapy cohorts (Supplementary Table S6), and the radiomics features after treatment for the immunotherapy cohort (Supplementary Table S7).

2.3 Multimodal learning framework

Our learning framework leveraged self-supervised contrastive learning and multimodal fusion techniques. Unlike previous studies that utilized only WSIs or CT images, our method integrated multimodal features across multiple prediction tasks, thereby achieving better performance. Overall, the framework consisted of three stages (Figure 1). First, the WSIs were segmented and tessellated into patches, which were labeled as tumor or non-tumor based on pathologist annotations. All CT images were delineated to identify regions of interest (ROI), from which radiomic features were extracted. Second, we trained a contrastive learning model on a large number of unlabeled patches, thereby extracting expressive patch-level features for downstream tasks. Finally, we used LASSO to select important features from the radiomic features and clinical variables. These selected features were then aggregated with the pathological features of tumor patches through an attention mechanism. The multimodal features were used for downstream tasks, including PD-L1 level assessment, immunotherapy response prediction, and prognosis evaluation.

2.4 Data preprocessing and annotation

The preprocessing of WSIs involved tissue segmentation and tiling. For each slide, we used OpenSlide to read it into memory and then converted it from RGB to HSV color space (21). To identify tissue regions (foreground), a binary mask was generated by thresholding the saturation channel in HSV space. The edges were smoothed, and morphological closure was applied to fill small gaps and holes, effectively segmenting the slide into tissue

TABLE 2 Demographic and clinical variables of ESCC immunotherapy response cohort.

	ESCC immunotherapy cohort		
	All	Non-responder (N=39)	Responder (N=36)
Age (years)			
Mean ± SD	67.04 ± 8.56	68.23 ± 8.73	65.75 ± 8.31
Gender, n (%)			
Female	10 (13.33)	4 (10.26)	6 (16.67)
Male BMI	65 (86.67)	35 (89.74)	30 (83.33)
Mean ± SD	21.98 ± 2.88	21.93 ± 2.95	22.02 ± 2.86
Smoking history, n (%)			
No	49 (65.33)	28 (71.79)	21 (58.33)
Yes	26 (34.67)	11 (28.21)	15 (41.67)
Drinking history, n (%)			
No	55 (73.33)	30 (76.92)	25 (69.44)
Yes	20 (26.67)	9 (23.08)	11 (30.56)
Hypertension, n (%)			
No	49 (65.33)	27 (69.23)	22 (61.11)
Yes	26 (34.67)	12 (30.77)	14 (38.89)
TNM Stage, n (%)			
III	49 (65.33)	25 (64.10)	24 (66.67)
IV	26 (34.67)	14 (35.90)	12 (33.33)
Treatment strategy, n (%)			
Immunotherapy	4 (5.33)	4 (10.26)	0 (0.00)
Immunotherapy +Chemotherapy	71 (94.67)	35 (89.74)	36 (100.00)
PD-L1/PD-1 inhibitor, n (%)			
Sintilimab	59 (78.67)	30 (76.92)	29 (80.56)
Camrelizumab	10 (13.33)	4 (10.26)	6 (16.67)
Tislelizumab	6 (8.00)	5 (12.82)	1 (2.78)
Progression-free survival (months)			
Median	14.27	13.33	14.42
(95%CI)	(11.97-16.56)	(9.64-17.03)	(11.76-17.08)

and non-tissue regions. Following segmentation, each WSI was split into 256×256 pixel patches within the foreground region at 20x magnification. As a result, we obtained 742,978 patches, with an average of 3,377 patches per WSI.

Patches were filtered to exclude those with insufficient tissue content, using a threshold where pixel values greater than 210 were considered white. Two pathologists with more than 10 years of clinical experience independently annotated the tumor regions on each slide. Patches overlapping the annotated tumor regions were labeled as tumor, and non-tumor otherwise.

All preoperative contrast-enhanced chest CT images from both cohorts were independently reviewed by 2 cardiothoracic surgeons who had 10 years of clinical experience. They manually delineated the region of interest (ROI) using the open-source software 3D Slicer (https://www.slicer.org/) to perform image segmentation.

2.5 Contrastive learning for pathological feature extraction

Given a large number of unlabeled patches, we leveraged contrastive learning to train an encoder to extract the intrinsic features of each patch (22, 23). The main idea of contrastive learning is to bring positive samples close to each other in the latent space and push negative samples to be far apart, by setting a pretext task. In our practice, we generated two views of a patch via image augmentation as positive pairs, while the augmentations of other patches in a mini-batch were regarded as negative samples. We employed a diverse range of image augmentations, including random proportion cropping and scaling, random color jittering, random Gaussian blurring, and random flipping. The ResNet50 CNN network pre-trained on ImageNet (24) was used as the encoder backbone f, which yields a 1024-dimensional latent representation h_i for an input patch x_i, namely, $h_i = f(x_i)$. Next, a projection head g transforms the latent representation into embedding z_i. Formally, we have $z_i = g(h_i)$, and the contrastive loss of the input patch x_i is defined as:

$$L = -log \frac{exp(sim(z_i, z_i^{'})/\tau)}{exp(sim(z_i, z_i^{'})/\tau) + \sum_{j=1}^{N} exp(sim(z_i, z_j)/\tau)}$$

where z_i and $z_i^{'}$ represent the embeddings of a pair of positive samples regarding the input patch x_i, $sim()$ is the cosine similarity obtained by dot product of two embeddings after L2 normalization. N is the size of the negative sample queue, z_j refers to the embedding of a negative sample and τ is the temperature parameter. The size and the quality of negative samples greatly affect the performance of contrastive learning. Inspired by our previous work (22), we adopted the adversarial contrastive learning method AdCo (25) to pre-train the encoder. It treats negative samples as learnable weights and alternately updates adversarial samples to generate the most challenging negative samples.

After the contrastive learning finished, the encoder was used to extract the patchlevel features. To extend the applicability of our model, we used the features of the labeled patches (tumor vs. non-tumor) to train a classifier with only one fullyconnected layer to identify tumor patches. The classifier achieved an AUC value of 0.903.

2.6 Multimodal feature fusion

Following the extraction of pathological features, we used the Python package PyRa-diomics (26) to extract radiomics features from the ROIs that were manually annotated by physicians. For each CT image, 118 features were extracted, including first-order

statistical features, as well as shape and texture features. The clinical variables listed in Tables 1 and 2 were also taken into account.

Next, we employed the Least Absolute Shrinkage and Selection Operator (LASSO) algorithm (27) to select important radiomic and clinical features for prediction tasks. The selected features were then concatenated with the pathological features of tumor patches, resulting in a comprehensive set of fused features. These fused features were input into a self-attention module to adjust their weights according to the prediction tasks. Finally, average pooling was applied to yield patient-level features for downstream prediction tasks.

2.7 Prediction task for PD-L1 level

Given the fused multimodal features, a network with two fully-connected layers was used to predict PD-L1 levels. Based on the PD-L1 levels measured by immunohisto-chemistry, we divided the 220 patients into two groups: a high-level group (PD-L1≥50, n=32) and a low-level group (PD-L1<50, n=188). The patients in the high-level group were labeled as 1, and 0 otherwise. As a result, we formulated the prediction task as a binary classification problem. The cross-entropy loss function was used:

$$\mathcal{L} = -\sum_i y_i \log p_i + (1 - y_i) \log (1 - p_i)$$

where y_i is the ground-truth label of PD-L1, p_i is the predicted probability. In this task, we excluded the clinical variables during the feature fusion stage, as clinical information contributed less to predicting PD-L1 levels.

We trained our model using the Adam optimizer for a total of 50 epochs. The initial learning rate was set to 1e-5, with the learning rate multiplied by 0.1 every 15 epochs. The weight decay was set to 1e-2. We employed five-fold cross-validation to verify the performance of our model and reported the average AUC value.

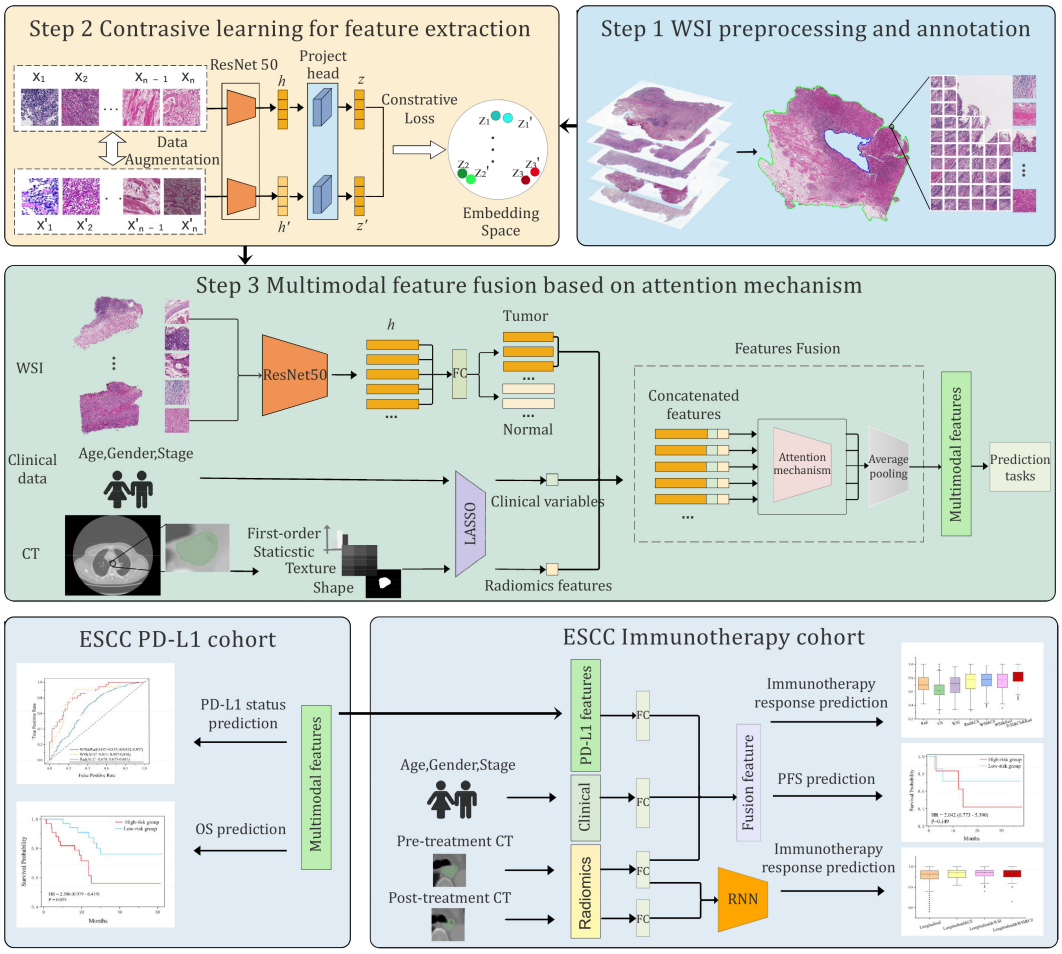

FIGURE 1
Overview of the proposed multimodal deep learning framework. The framework involved three steps: preprocessing and annotation of whole slide images (WSIs) and CT images, pretraining of a contrastive learning model to extract patch-level features, and integration of multimodal features by attention mechanism. The multimodal features were applied for PD-L1 level and immunotherapy response prediction, as well as prognosis.

2.8 Prediction task for overall survival

For overall survival (OS) prediction, the patients in the PD-L1 cohort were divided into two groups based on their OS using a threshold of 12 months or 36 months. With the 12-month threshold, patients were categorized into a high-risk group (OS<12 months, n=24) and a low-risk group (OS≥12 months, n=196). Using the 36-month threshold, patients were also categorized into a high-risk group (OS<36 months, n=67) and a low-risk group (OS≥36 months, n=153). The patients in the high-risk group were labeled as 1, and 0 otherwise. Similarly, the binary cross-entropy loss function was used for the OS prediction task.

2.9 Prediction task for immunotherapy response

For the 75 patients in the immunotherapy cohort, we categorized patients with partial response (PR) and complete response (CR) as responders (n=36, labeled as 1), and those with stable disease (SD) as non-responders (n=39, labeled as 0). We were also interested in the prediction of progression-free survival (PFS). For this task, the patients with PFS less than 12 months were classified into a low-PFS group (n=27, PFS<12 months), and others were classified into a high-PFS group (n=48, PFS≥12 months). The prediction task was formulated as a binary classification task, utilizing the cross-entropy loss function.

Since the expression level of PD-L1 is closely related to immunotherapy response (28, 29), with high PD-L1 levels generally indicating a favorable response to immunotherapy, we incorporated the features derived from the PD-L1 level prediction model into the immunotherapy response prediction task. Specifically, the 512-dimensional features, transferred from the final layer of the trained PD-L1 prediction model, were concatenated with 8-dimensional radiomic features and 8-dimensional clinical variables selected by the Lasso algorithm. The combined features were fed into a single fully-connected layer to predict immunotherapy response.

2.10 Integration of longitudinal CT images

To further enhance the predictive performance for immunotherapy response, we introduced a recurrent neural network (RNN) module (30) into the multimodal framework to effectively exploit the longitudinal CT images. First, we used the Pyradiomics package to extract radiomic features from the baseline and the early on-treatment CT images. These radiomic features were then converted into 64-dimensional embeddings through a fully-connected network. The embeddings were stacked over time to form a sequence of input features for the RNN module. Finally, we concatenated the pathological features, longitudinal CT features, and clinical variables into a 128-dimensional fused feature, which was subsequently used to predict the immunotherapy response.

2.11 Feature importance assessment

We used the Shapley Additive Explanations (SHAP) method to evaluate the importance of features (31–33). The SHAP value measures the impact of each feature on the predictions of a machine learning model for a single input. The average SHAP value across a dataset quantifies the overall importance of an input feature. The Kernel Explainer function of SHAP was used to assess the importance of clinical variables and deep learning-derived features. Bar plots were utilized to depict the average SHAP value magnitudes of top variables for each class. For each variable group, total importance is defined as the sum of the importance across all variables in that group (e.g., all clinical variables or deep learning features). To enhance interpretability for deep learning features, the class activation map (CAM) (34) was employed to visualize the most important features.

3 Results

3.1 Multimodal fusion enhanced PD-L1 level prediction

For PD-L1 level prediction, our multimodal model achieves superior performance in distinguishing high-level and low-level cases at the threshold 50 CPS (AUC=0.836 ± 0.0003, Figure 2a). To further demonstrate the effectiveness of the multimodal model, we built a few variant models that used only H&E images or CT images. The results showed that the multimodal model surpassed the H&E-only model (AUC=0.81 ± 0.0051) and the CT-only model (AUC=0.678 ± 0.0105). Also, we compared our H&E-only model to previously published methods that are also built solely on H&E slides (Figure 2b), including ResNet50 (35), CLAM (36), and TransMIL (37). We found that our H&E-only model remarkably outperformed ResNet50 (AUC=0.66 ± 0.0086), CLAM (AUC=0.61 ± 0.0009), and TransMIL (AUC=0.74 ± 0.0150).

Furthermore, we used the multimodal model to perform regression analysis on PD-L1 levels. For this regression task, the PD-L1 levels were normalized into the [0, 1] range, and the Pearson correlation coefficient (r) (38) was reported as a performance metric. As a result, our multimodal model showed notable performance (Figure 2c), and we observed a significant positive correlation between the actual and predicted values across five-fold cross-validation (r=0.52, p-value=1.55e-12).

To explore the impact of patch-level features on the PD-L1 prediction, we evaluated the importance of each patch by calculating the ratio of the predicted probabilities with and without the inclusion of each patch's feature. This ratio reflected the importance of each patch and enabled us to generate a heatmap for each slide. We presented two representative H&E slides randomly selected from the PD-L1 cohort, along with the corresponding heatmaps and several patches with high and low importance scores (Figure 2d–g). Visual inspection of these patches revealed significant differences, suggesting close association

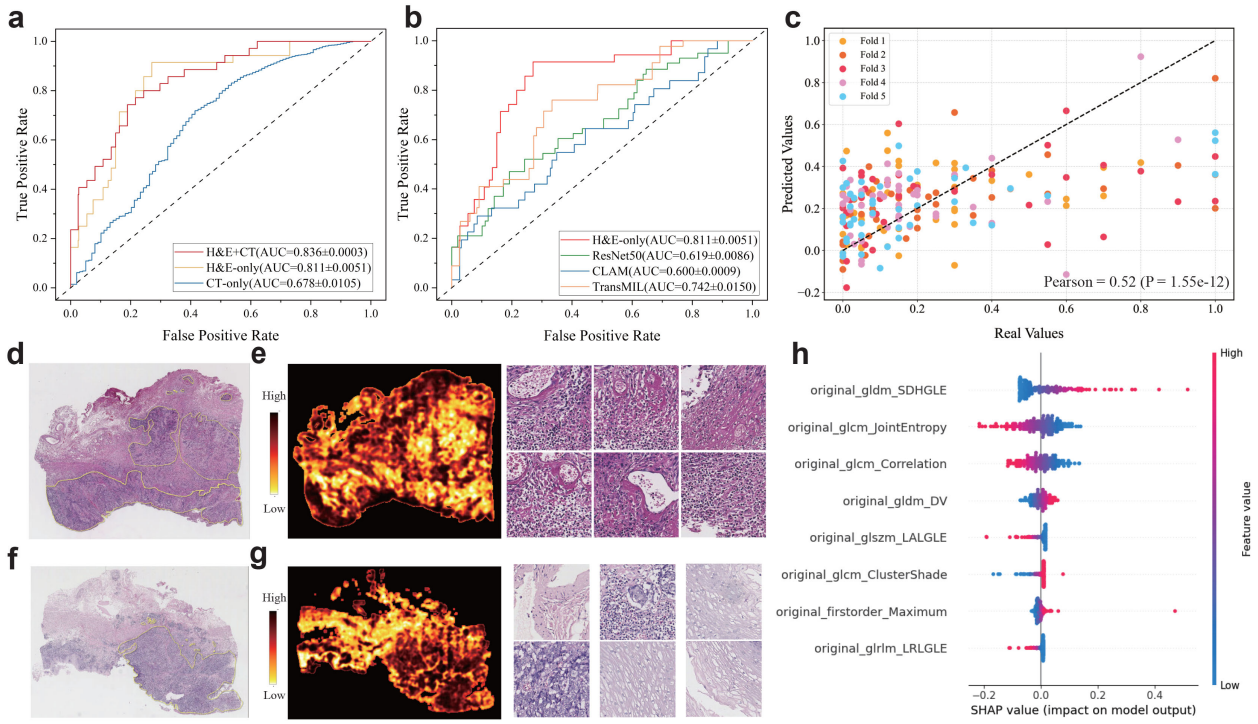

FIGURE 2
Multimodal prediction of PD-L1 levels in ESCC cohort. **(a, b)** ROC curves for the prediction of PD-L1 level (high: CPS≥50 vs low: CPS<50) using the multimodal and ablated models. **(b)** ROC curves for performance comparison between our image-only model and comparative methods. **(c)** Scatter plots of the predicted and actual expression levels of PD-L1. **(d-g)** Representative H&E slides associated to the specimens with low and high PD-L1 levels assessed by immunohistochemistry (upper: low PD-L1 and bottom: high PD-L1), as well as the heatmaps generated by predicted scores and exemplar patches. **(h)** SHAP values of top predictive features for PD-L1 levels. The features are ranked by the sum of SHAP value magnitudes over all samples.

between the PD-L1 levels and histological morphology. Furthermore, we highlighted the important radiomic features evaluated by SHapley Additive exPlanation (SHAP) (31–33) values (Figure 2h) that contribute significantly to PD-L1 prediction.

3.2 Multimodal prediction of overall survival

We further evaluated the multimodal model in predicting overall survival. For the high-and low-risk groups defined by a 1-year threshold, we compared the multimodal model with variant models built on different subsets of features (Figure 3a). Although the model using only clinical variables (AUC=0.785 ± 0.0103) performed better than the H&E-only model (AUC=0.761 ± 0.014) or the CT-only model (AUC=0.705 ± 0.015), the multimodal fusion achieved the highest performance (AUC=0.802 ± 0.014), which also outperformed the clinical+CT model (AUC=0.756 ± 0.015), the clinical+H&E model (AUC=0.751 ± 0.023), and the H&E+CT model (AUC=0.766 ± 0.005). Furthermore, based on the multimodal model predicted scores, we categorized the patients into low-risk and high-risk groups and conducted survival analysis (Figure 3b, Supplementary Figure S1). The Kaplan–Meier curves showed that the high-risk group had a poorer prognosis compared to the low-risk group (HR=2.10, p-value=0.055), where HR represents the hazard ratio between the high-risk and low-risk groups, indicating the relative risk of an event occurring in the high-risk group. However, the stratification by H&E-only model and other ablated models did not show statistical significance (Figure 3c, Supplementary Figure S1).

Using the 3-year threshold, the H&E-only model (AUC=0.741 ± 0.004) outperformed the model using only clinical variables (AUC=0.735 ± 0.008) or the model using radiomics features (AUC=0.670 ± 0.008) (Figure 3d). The multimodal model demonstrated superior performance (AUC=0.802 ± 0.004), compared to the clinical+CT model (AUC=0.758 ± 0.007), H&E +clinical model (AUC=0.774 ± 0.097), and H&E+CT model (AUC=0.782 ± 0.098). Similarly, the survival analysis based on the predicted scores by the multimodal model showed that the high-risk group had a poorer prognosis than the low-risk group (HR=2.460, p-value=0.045), while all other ablated models did not yield statistical significance (Figures 3e, f, Supplementary Figure S2).

Furthermore, the multimodal model also demonstrated superior performance in the PFS prediction task (Figures 3g–i). The patients were classified into high- and low-PFS groups using a threshold of 12 months. As a result, the clinical-only model achieved better performance (AUC=0.820 ± 0.004) than the H&E-only model (AUC=0.713 ± 0.021) and the CT-only model (AUC=0.698 ± 0.028). The multimodal model showed the best performance (AUC=0.875 ± 0.010), which is better than the clinical

+CT model (AUC=0.857 ± 0.009), H&E+clinical model (AUC=0.856 ± 0.006), and H&E+CT model (AUC=0.757 ± 0.027).

To reveal key features with prognostic values, we computed SHAP values of multi-modal features in prediction of OS (Supplementary Figure S3). Some radiomic features associated with tumor shape and first-order statistics contributed significantly to OS. Quite a few clinical variables, such as hypertension, hemoglobin, and stage, played a key role in OS prediction. Moreover, we presented four representative H&E slides, which were randomly selected from the low-risk and high-risk patients for 1-year OS and 3-year OS. For visual inspection, we generated their corresponding heatmaps and presented a few representative patches for each slide (Figures 4a–d). After careful examination, pathologists concluded that the high-risk slides were characterized by lack of keratin pearls, numerous mitotic figures, increased tumor cellularity and intensity. In contrast, the slides from the low-risk group exhibited formation of keratin pearls and intercellular bridges.

3.3 Multimodal prediction of immunotherapy response

To highlight the significance of multimodal data in predicting immune therapy response, we initially developed predictive models using basic features and assessed their performance. We then progressively fused features from diverse modalities to improve model performance. Specifically, we initially predicted immunotherapy response using only H&E and CT feature, achieving

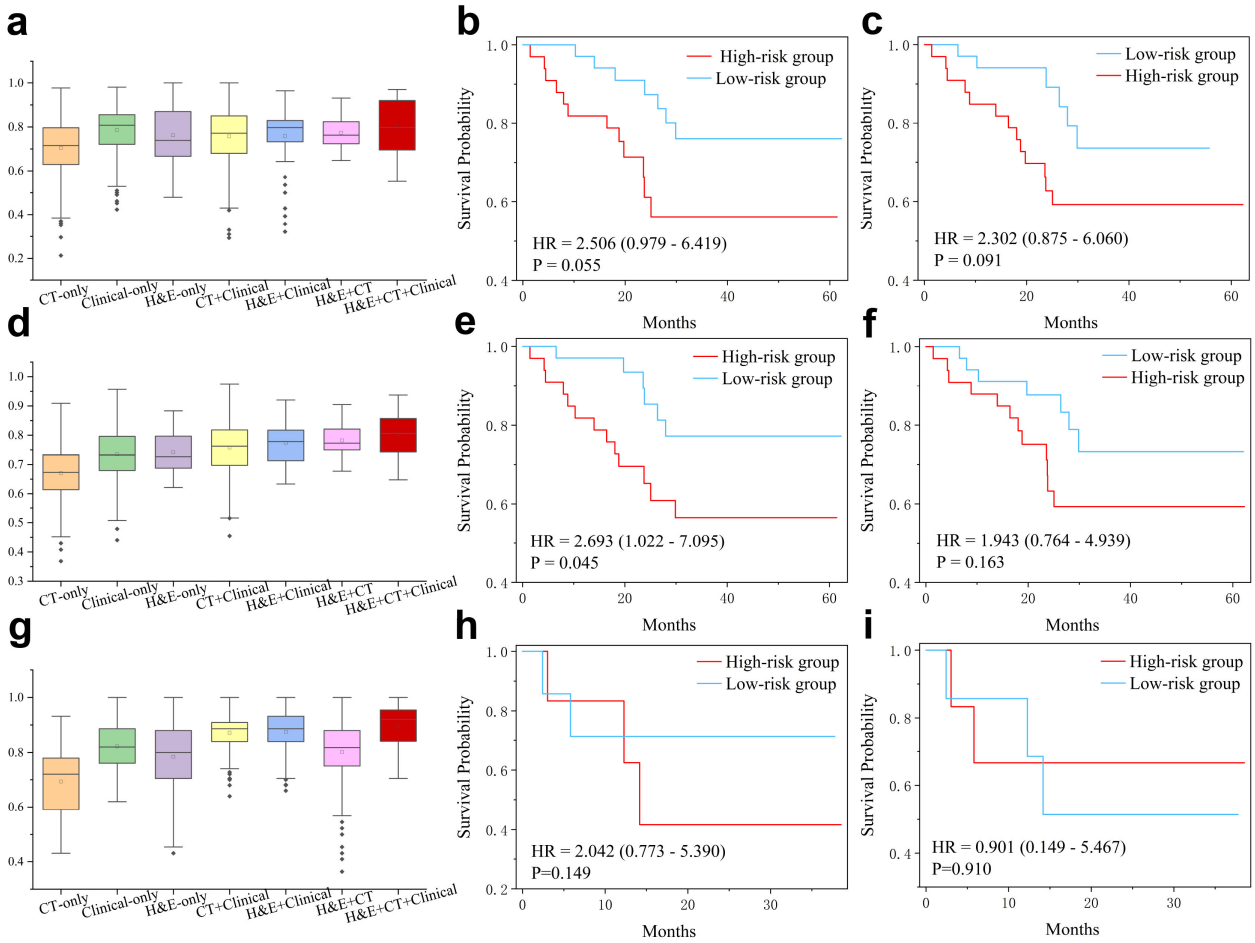

FIGURE 3
Multimodal features for prediction of overall survival (OS) and progression-free survival (PFS). **(a)** AUC values in prediction of high-risk (OS<12 months) and low-risk (OS≥12 months) patients of the PD-L1 cohort. Note that statistical significance has been conduced by two-sided *t*-test and the results are presented in the Supplementary Table S1. **(b, c)** Kaplan-Meier curves for hig-hand low-risk (cutoff=12m) patients predicted by the multimodal and H&E-only models, respectively. **(d)** AUC values in prediction of high-risk (OS<36 months) and low-risk (OS≥36 months) patients of the PD-L1 cohort. Statistical significance (two-sided *t*-test) has been presented in the Supplementary Table S2. **(e, f)** Kaplan-Meier curves for high- and low-risk (cutoff=36m) patients predicted by the multimodal and H&E-only models, respectively. **(g)** AUC values in prediction of high- and low-PFS (cutoff=12m) patients of immunotherapy cohort. Statistical significance (two-sided *t*-test) has been presented in the Supplementary Table S3. **(h, i)** Kaplan-Meier curves for high- and low-PFS (cutoff=12m) patients of immunotherapy cohort, predicted by the multimodal model and pre-trained model on PD-L1 cohort, respectively.

a suboptimal performance with an AUC of 0.65. After integrating the pathological features extracted from H&E for predicting PD-L1 level, the AUC improved to 0.70. When these fused features were further combined with clinical variables, the AUC increased to 0.75. Finally, the incorporation of radiomics features resulted in a further improvement, achieving an AUC of 0.80 (Figure 5a).

To investigate the interpretability of our model, we computed SHAP values to assess the contribution of the clinical variables, H&E features, and radiomic features to the final prediction (Figure 5b). Several clinical variables, such as smoking history, age, and hemoglobin (Hb) levels, significantly contributed to the prediction of immunotherapy response. Importantly, some radiomic features, originally transferred from the PD-L1 prediction task, also played a significant role in influencing the immunotherapy response. For example, the GLSZM LAHGLE feature, which quantifies the proportion of the joint distribution of larger zones with higher grey-level values within the tumor, often reflects the tumor intratumoural heterogeneity associated with the response to treatment. Moreover, the NGTDM strength feature was notably related to the treatment response. The responders exhibited significantly lower NGTDM strength values compared to non-responders (Figure 5c, p-value=0.01). Further analysis of two representative cases (Figures 5d, e) revealed that the case with high NGTDM strength (right, non-responder) showed well-defined boundaries and a uniform internal structure, in contrast to the case with low NGTDM strength (left, responder). Examination of corresponding H&E slides (Figures 5f, g) indicated that the non-responder slide was characterized by a lack of keratin pearl formation, high mitotic figures, increased tumor cellularity, and intensity. In addition, the clinical variables such as smoking history, triglyceride, hemoglobin, and age also contributed significantly to the immunotherapy response prediction.

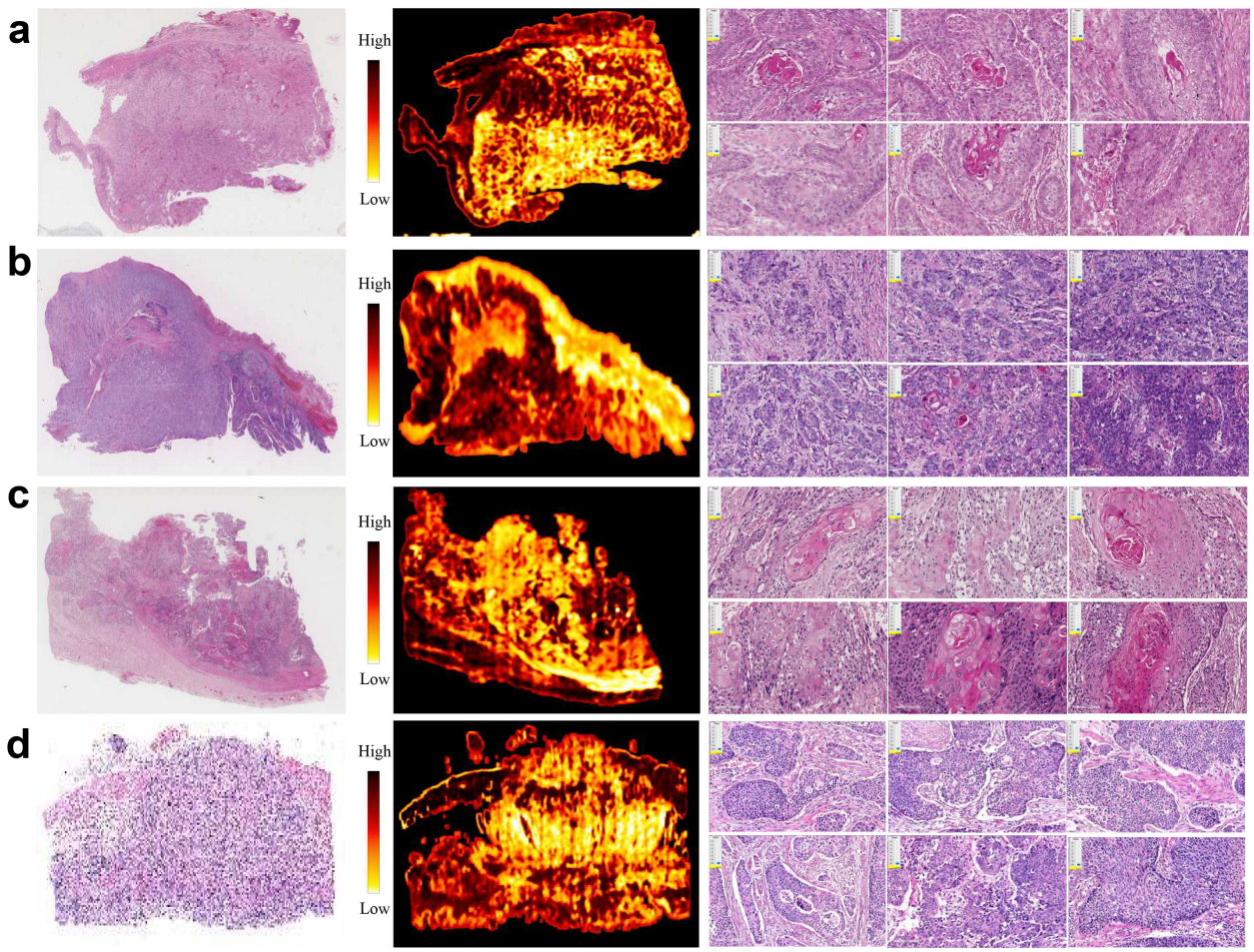

FIGURE 4
Representative H&E slides from PD-L1 cohort, and corresponding heatmaps generated using patch-level attention scores, as well as exemplar patches. **(a, b)** H&E slides, heatmaps and exemplar patches randomly selected from patients with high- and low-risk prognosis by threshold 12 months, respectively. **(c, d)** H&E slides, heatmaps and exemplar patches randomly selected from patients with high- and low-risk prognosis by threshold 36 months, respectively.

3.4 Early on-treatment CT enhanced prediction performance

Although the multimodal model achieved an AUC of 0.8 in the prediction of immunotherapy response, there remains a significant gap for clinical practice. We further tested whether the first follow-up CT after treatment could enhance predictive performance. Our findings indicate that by integrating longitudinal CT features with H&E and clinical features, the multimodal model achieved an AUC of 0.937 ± 0.002 (Supplementary Figure S4A). Treatment with immune checkpoint inhibitors typically lasted between 2 and 6 months, with an average duration of 4 months. The first follow-up CT is usually conducted around 1-2 months after the start of treatment. Our study verified that the incorporation of the early on-treatment CT scans remarkably improved the predictive performance, suggesting that longitudinal CT effectively captured the changes in characteristics of lesions induced by immunotherapy.

To explore the important features, we employed the SHAP method to assess the contribution of each clinical and deep learning feature to the model prediction (Supplementary Figure S4B). It was found that the radiomic features extracted from longitudinal CT scans accounted for the top 20 most important features. In contrast, clinical variables such as smoking history, triglyceride, hemoglobin, and age contributed less significantly to the immunotherapy response prediction.

4 Discussion

The PD-L1 level has gained attention as a predictive biomarker for immunotherapy response. Previous deep learning-based studies focus on predicting PD-L1 biomarker from H&E-stained slides across several cancer types. For instance, one study achieved a weighted average AUC of 0.74 on formalin-fixed specimens across nine types of

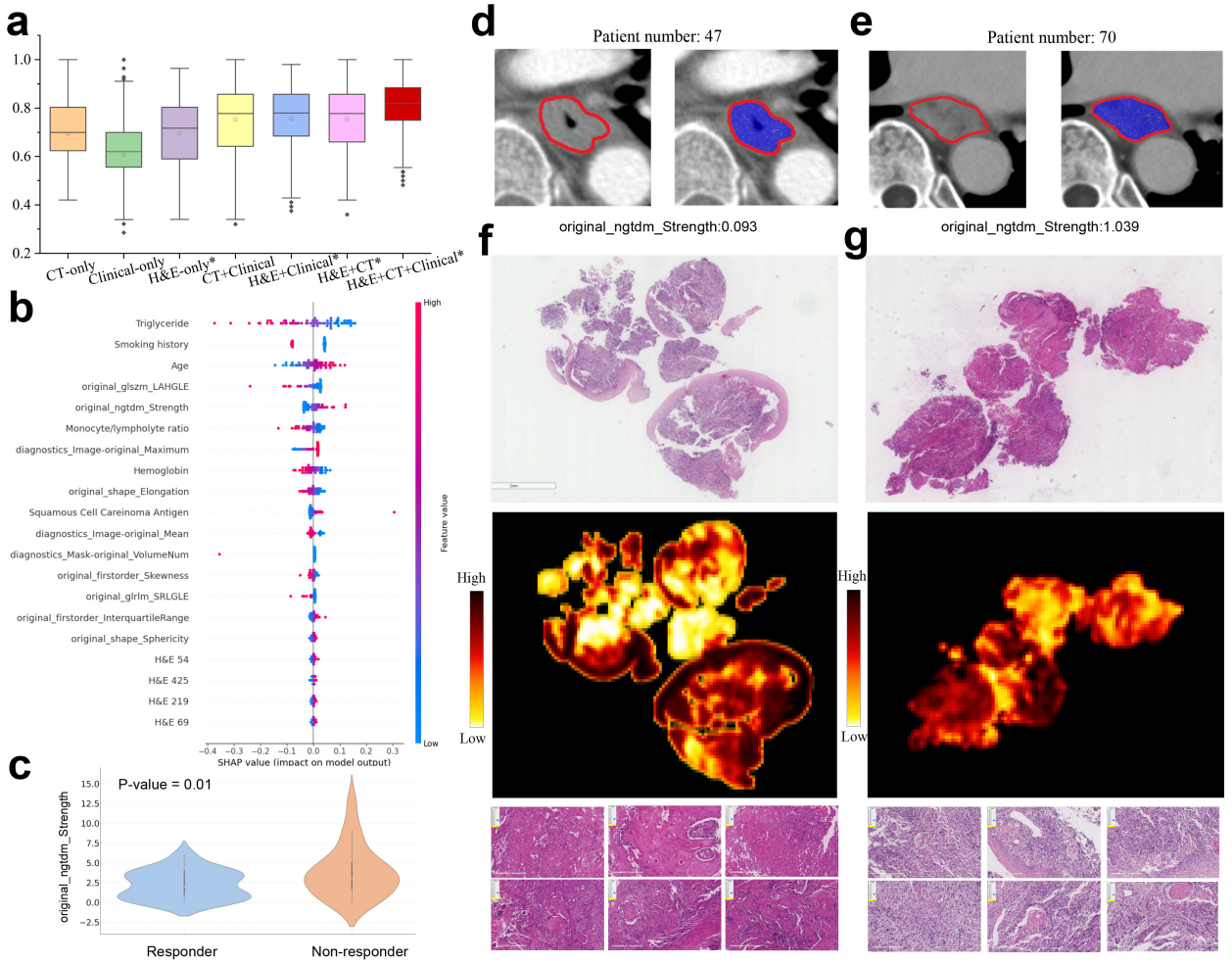

FIGURE 5
Multimodal prediction of immunotherapy response. **(a)** AUC values in prediction of responsive and non-responsive to immunotherapy by multimodal and ablated models. The models marked with an asterisk use the pathological features learned in PD-L1 prediction task. Statistically significant differences are detailed in theSupplementary Table S4. **(b)** Top 20 multimodal features ranked by SHAP values for predicting immunotherapy response. **(c)** Violin plot of the radiomic feature original ngtdm Strength in responders and non-responders. **(d, e)** CT images with annotated tumor regions came from two patients having low and high original ngtdm Strength feature values. **(f, g)** Representative H&E slides came from responders and non-responders to immunotherapy (left column: responsive, right column: non-responsive), as well as the corresponding heatmaps and exemplar patches.

tumors where PD-L1 is an established biomarker (14). However, the use of CT images for PDL1 level prediction has been less explored. A pioneering study proposed a deep learning model to predict PD-L1 expression using CT images in non-small cell lung cancer (NSCLC) patients, achieving AUCs of 0.71 (95% CI: 0.59-0.81) and 0.76 (95% CI: 0.66-0.85) in the validation and test cohorts (4). Despite these efforts, the performance of such studies has not been satisfactory. In contrast, our multimodal deep learning model achieved 0.836 AUC value in predicting PD-L1 levels of ESCC patients. Our study demonstrated that H&E staining and CT imaging are highly indicative of PD-L1 expression, and these predictive signatures can be effectively learned by an adequately trained deep learning model based on unannotated samples. From a clinical practice perspective, our multimodal model offers a cost-effective and efficient alternative to traditional immunohistochemistry (IHC) techniques.

Our model successfully stratified patients who underwent surgery into low- and high-risk groups in terms of overall survival. For the prediction of 1-year and 3-year survival times, our model achieved AUC values exceeding 0.80, underscoring the robustness of the proposed model. Compared to previous studies that relied primarily on single-modal data, such as the H&E slides (39, 40) or CT images (41), our multimodal model demonstrated superior performance. Previous studies have utilized tumor characteristics (e.g., location, size, differentiation, TNM stage) and pathology features (e.g., lymphovascular invasion), as well as hematology test results (e.g., leukocyte and platelet counts) to predict clinical outcomes of ESCC patients (41). However, CT images or clinical variables alone are insufficient to fully reflect the complexity of clinical outcomes. In contrast, our multimodal model, which integrated diverse data sources, provided complementary information that enhanced predictive capability in a clinical setting.

We also evaluated our multimodal model for predicting immunotherapy response on a separate ESCC immunotherapy cohort, entirely independent from the PD-L1 cohort. Notably, we found that the multimodal features extracted by the encoder, trained on the PD-L1 cohort for PD-L1 level prediction, significantly enhanced the predictive performance for immunotherapy response. This finding aligned with previous reports indicating that higher PD-L1 levels are often associated with a more favorable response to immunotherapy (5). The cross-cohort experiments confirmed that our model captures features pertinent to the prediction tasks, rather than merely memorizing the samples. Consequently, our multimodal model achieved an AUC value exceeding 0.8 in predicting immunotherapy response, demonstrating its efficacy in stratifying patients likely to benefit from immunotherapy.

One limitation of this study is that the current model is restricted to binary classification, whereas immunotherapy response is typically categorized into four distinct types: complete response, partial response, stable disease, and progressive disease. Furthermore, the sample size of ESCC patients in the cohorts is relatively small, which may affect the robustness and generalizability of the model. In addition, incorporating multi-omics data, such as genetic alterations and epigenetic modifications, could potentially enhance the model's performance in predicting clinical outcomes.

5 Conclusion

We propose a multimodal deep learning model designed to predict PD-L1 biomarker level and immunotherapy response in patients with esophageal squamous cell carcinoma. Our approach integrates multimodal features derived from Hematoxylin and Eosin (H&E) stained slides and CT images, alongside clinical variables. The integrated features are highly indicative of PD-L1 expression levels, immunotherapy response, and overall survival. Furthermore, our findings reveal that extracted features predictive of PD-L1 expression are also significantly associated with immunotherapy response. Notably, the inclusion of longitudinal CT images enhances the predictive accuracy of immunotherapy response.

Data availability statement

The datasets presented in this study can be found in online repositories. The names of the repository/repositories and accession number(s) can be found in the article/Supplementary Material.

Ethics statement

The studies involving humans were approved by Third Affiliated Hospital of Soochow University (Approval number: 2024-KD139). The studies were conducted in accordance with the local legislation and institutional requirements. The participants provided their written informed consent to participate in this study.

Author contributions

HL: Conceptualization, Methodology, Resources, Visualization, Writing – review & editing. YB: Formal analysis, Investigation, Visualization, Writing – original draft. ZW: Data curation, Resources, Validation, Writing – original draft. SY: Methodology, Supervision, Validation, Writing – original draft. CG: Resources, Supervision, Writing – original draft, Writing – review & editing. BW: Project administration, Resources, Writing – original draft, Funding acquisition.

Funding

The author(s) declare that financial support was received for the research, authorship, and/or publication of this article. This work was supported by National Natural Science Foundation of China

(No. 62372229), Natural Science Foundation of Jiangsu Province (No. BK20231271). This work was also supported by the funding granted from Young Talent Development plan of Changzhou Health Commission (CZQM2020034, CZQM2020004), Top Talent of Changzhou "14th Five-Year Plan" High-level Health Personnel Training Project (KY20221388).

Acknowledgments

We are very grateful to Dr. Meihua Wang from the Department of Pathology at Changzhou Cancer Hospital, Jiangsu, China. Thanks for his work on the annotations of the pathology images used in this study.

Conflict of interest

The authors declare that the research was conducted in the absence of any commercial or financial relationships that could be construed as a potential conflict of interest.

Generative AI statement

The author(s) declare that no Generative AI was used in the creation of this manuscript.

Publisher's note

All claims expressed in this article are solely those of the authors and do not necessarily represent those of their affiliated organizations, or those of the publisher, the editors and the reviewers. Any product that may be evaluated in this article, or claim that may be made by its manufacturer, is not guaranteed or endorsed by the publisher.

Supplementary material

The Supplementary Material for this article can be found online at: https://www.frontiersin.org/articles/10.3389/fimmu.2025.1540013/full#supplementary-material

References

1. Sung H, Ferlay J, Siegel RL, Laversanne M, Soerjomataram I, Jemal A, et al. Global cancer statistics 2020: Globocan estimates of incidence and mortality worldwide for 36 cancers in 185 countries. *CA: Cancer J Clin*. (2021) 71:209–49. doi: 10.3322/caac.21660

2. Sheikh M, Roshandel G, McCormack V, Malekzadeh R. Current status and future prospects for esophageal cancer. *Cancers*. (2023) 15:765. doi: 10.3390/cancers15030765

3. Li M, Zhang Z, Wang Q, Yi Y, Li B. Integrated cohort of esophageal squamous cell cancer reveals genomic features underlying clinical characteristics. *Nat Commun*. (2022) 13:5268. doi: 10.1038/s41467-022-32962-1

4. Mu W, Jiang L, Shi Y, Tunali I, Gray JE, Katsoulakis E, et al. Non-invasive measurement of pd-l1 status and prediction of immunotherapy response using deep learning of pet/ct images. *J immunother Cancer*. (2021) 9. doi: 10.1136/jitc-2020-002118

5. Mu C-Y, Huang J-A, Chen Y, Chen C, Zhang X-G. High expression of pd-l1 in lung cancer may contribute to poor prognosis and tumor cells immune escape through suppressing tumor infiltrating dendritic cells maturation. *Med Oncol*. (2011) 28:682–8. doi: 10.1007/s12032-010-9515-2

6. Doroshow DB, Bhalla S, Beasley MB, Sholl LM, Kerr KM, Gnjatic S, et al. Pd-l1 as a biomarker of response to immune-checkpoint inhibitors. *Nat Rev Clin Oncol*. (2021) 18:345–62. doi: 10.1038/s41571-021-00473-5

7. Shamai G, Livne A, Polónia A, Sabo E, Cretu A, Bar-Sela G, et al. Deep learning-based image analysis predicts pd-l1 status from h&e-stained histopathology images in breast cancer. *Nat Commun*. (2022) 13:6753. doi: 10.1038/s41467-022-34275-9

8. Pang J-MB, Castles B, Byrne DJ, Button P, Hendry S, Lakhani SR, et al. Sp142 pd-l1 scoring shows high interobserver and intraobserver agreement in triple-negative breast carcinoma but overall low percentage agreement with other pd-l1 clones sp263 and 22c3. *Am J Surg Pathol*. (2021) 45:1108–17. doi: 10.1097/PAS.0000000000001701

9. Hoda RS, Brogi E, D'Alfonso TM, Grabenstetter A, Giri D, Hanna MG, et al. Interobserver variation of pd-l1 sp142 immunohistochemistry interpretation in breast carcinoma: a study of 79 cases using whole slide imaging. *Arch Pathol Lab Med*. (2021) 145:1132–7. doi: 10.5858/arpa.2020-0451-OA

10. Reisenbichler ES, Han G, Bellizzi A, Bossuyt V, Brock J, Cole K, et al. Prospective multi-institutional evaluation of pathologist assessment of pd-l1 assays for patient selection in triple negative breast cancer. *Modern Pathol*. (2020) 33:1746–52. doi: 10.1038/s41379-020-0544-x

11. Wang X, Wang L, Bu H, Zhang N, Yue M, Jia Z, et al. How can artificial intelligence models assist pd-l1 expression scoring in breast cancer: results of multi-institutional ring studies. *NPJ Breast Cancer*. (2021) 7:61. doi: 10.1038/s41523-021-00268-y

12. Gamble M, Wilson I. The hematoxylins and eosin. *Theory Pract histol techniques*. (2008) 6:121–34. doi: 10.1016/B978-0-443-10279-0.50016-6

13. Srinidhi CL, Ciga O, Martel AL. Deep neural network models for computational histopathology: A survey. *Med image Anal*. (2021) 67:101813. doi: 10.1016/j.media.2020.101813

14. Jin D, Liang S, Shmatko A, Arnold A, Horst D, Grünewald TG, et al. Teacher-student collaborated multiple instance learning for pan-cancer pdl1 expression prediction from histopathology slides. *Nat Commun*. (2024) 15:3063. doi: 10.1038/s41467-024-46764-0

15. Tian P, He B, Mu W, Liu K, Liu L, Zeng H, et al. Assessing pd-l1 expression in non-small cell lung cancer and predicting responses to immune checkpoint inhibitors using deep learning on computed tomography images. *Theranostics*. (2021) 11:2098. doi: 10.7150/thno.48027

16. He B, Dong D, She Y, Zhou C, Fang M, Zhu Y, et al. Predicting response to immunotherapy in advanced non-small-cell lung cancer using tumor mutational burden radiomic biomarker. *J immunother Cancer*. (2020) 8. doi: 10.1136/jitc-2020-000550

17. Coroller TP, Agrawal V, Narayan V, Hou Y, Grossmann P, Lee SW, et al. Radiomic phenotype features predict pathological response in non-small cell lung cancer. *Radiother Oncol*. (2016) 119:480–6. doi: 10.1016/j.radonc.2016.04.004

18. Khorrami M, Jain P, Bera K, Alilou M, Thawani R, Patil P, et al. Predicting pathologic response to neoadjuvant chemoradiation in resectable stage iii non-small cell lung cancer patients using computed tomography radiomic features. *Lung Cancer*. (2019) 135:1–9. doi: 10.1016/j.lungcan.2019.06.020

19. Eisenhauer EA, Therasse P, Bogaerts J, Schwartz LH, Sargent D, Ford R, et al. New response evaluation criteria in solid tumours: revised recist guideline (version 1.1). *Eur J Cancer*. (2009) 45:228–47. doi: 10.1016/j.ejca.2008.10.026

20. Schwartz LH, Litière S, De Vries E, Ford R, Gwyther S, Mandrekar S, et al. Recist 1.1—update and clarification: From the recist committee. *Eur J Cancer*. (2016) 62:132–7. doi: 10.1016/j.ejca.2016.03.081

21. Bradski G. The opencv library. dr dobb's j softw tools. The OpenCV Library. *Dr Dobb's J Softw Tools*. (2000) 25:120–5.

22. Liu H, Zhang Y, Luo J. Contrastive learning-based histopathological features infer molecular subtypes and clinical outcomes of breast cancer from unannotated whole slide images. *Comput Biol Med*. (2024) 170:107997. doi: 10.1016/j.compbiomed.2024.107997

23. Liu H, Xie X, Wang B. Deep learning infers clinically relevant protein levels and drug response in breast cancer from unannotated pathology images. *NPJ Breast Cancer*. (2024) 10:18. doi: 10.1038/s41523-024-00620-y

24. Deng J, Dong W, Socher R, Li L-J, Li K, Fei-Fei L. (2009). Imagenet: A large-scale hierarchical image database, in: *2009 IEEE Conference on Computer Vision and Pattern Recognition*, Miami, Florida, USA: IEEE. pp. 248–55.

25. Hu Q, Wang X, Hu W, Qi G-J. (2021). Adco: Adversarial contrast for efficient learning of unsupervised representations from self-trained negative adversaries, in: *Proceedings of the IEEE/CVF Conference on Computer Vision and Pattern Recognition*, Nashville, TN, USA: IEEE. pp. 1074–83.

26. Van Griethuysen JJ, Fedorov A, Parmar C, Hosny A, Aucoin N, Narayan V, et al. Computational radiomics system to decode the radiographic phenotype. *Cancer Res*. (2017) 77:104–7. doi: 10.1158/0008-5472.CAN-17-0339

27. Ranstam J, Cook JA. Lasso regression. *J Br Surg*. (2018) 105:1348–8. doi: 10.1002/bjs.10895

28. Kollmann D, Ignatova D, Jedamzik J, Chang Y-T, Jomrich G, Baierl A, et al. Pd-l1 expression is an independent predictor of favorable outcome in patients with localized esophageal adenocarcinoma. *Oncoimmunology*. (2018) 7:1435226. doi: 10.1080/2162402X.2018.1435226

29. Chen K, Wang X, Yang L, Chen Z. The anti-pd-1/pd-l1 immunotherapy for gastric esophageal cancer: a systematic review and meta-analysis and literature review. *Cancer Control*. (2021) 28:1073274821997430. doi: 10.1177/1073274821997430

30. Grossberg S. Recurrent neural networks. *Scholarpedia*. (2013) 8:1888. doi: 10.4249/scholarpedia.1888

31. Lundberg SM, Lee S-I. A unified approach to interpreting model predictions. *Adv Neural Inf Process Syst*. (2017) 30:4768–77. doi: 10.5555/3295222.3295230

32. Lundberg SM, Nair B, Vavilala MS, Horibe M, Eisses MJ, Adams T, et al. Explainable machine-learning predictions for the prevention of hypoxaemia during surgery. *Nat Biomed Eng*. (2018) 2:749–60. doi: 10.1038/s41551-018-0304-0

33. Lundberg SM, Erion G, Chen H, DeGrave A, Prutkin JM, Nair B, et al. From local explanations to global understanding with explainable ai for trees. *Nat Mach Intell*. (2020) 2:56–67. doi: 10.1038/s42256-019-0138-9

34. Zhou B, Khosla A, Lapedriza A, Oliva A, Torralba A. (2016). Learning deep features for discriminative localization, in: *Proceedings of the IEEE Conference on Computer Vision and Pattern Recognition*, Las Vegas, NV, USA: IEEE. pp. 2921–9.

35. He K, Zhang X, Ren S, Sun J. (2016). Deep residual learning for image recognition, in: *Proceedings of the IEEE Conference on Computer Vision and Pattern Recognition*, Las Vegas, NV, USA: IEEE. pp. 770–8.

36. Lu MY, Williamson DF, Chen TY, Chen RJ, Barbieri M, Mahmood F. Data-efficient and weakly supervised computational pathology on whole-slide images. *Nat Biomed Eng*. (2021) 5:555–70. doi: 10.1038/s41551-020-00682-w

37. Shao Z, Bian H, Chen Y, Wang Y, Zhang J, Ji X, et al. Transmil: Transformer based correlated multiple instance learning for whole slide image classification. *Adv Neural Inf Process Syst*. (2021) 34:2136–47. doi: 10.5555/3540261.3540425

38. Cohen I, Huang Y, Chen J, Benesty J, Benesty J, Chen J, et al. Pearson correlation coefficient. *Noise reduct speech Process*. (2009) 1–4. doi: 10.1007/978-3-642-00296-0_5

39. Li B, Qin W, Yang L, Li H, Jiang C, Yao Y, et al. From pixels to patient care: deep learning-enabled pathomics signature offers precise outcome predictions for immunotherapy in esophageal squamous cell cancer. *J Trans Med*. (2024) 22:195. doi: 10.1186/s12967-024-04997-z

40. Chen Y, Gao R, Jing D, Shi L, Kuang F, Jing R. Classification and prediction of chemoradiotherapy response and survival from esophageal carcinoma histopathology images. *Spectrochimica Acta Part A: Mol Biomol Spectrosc*. (2024) 312:124030. doi: 10.1016/j.saa.2024.124030

41. Cui Y, Li Z, Xiang M, Han D, Yin Y, Ma C. Machine learning models predict overall survival and progression free survival of non-surgical esophageal cancer patients with chemoradiotherapy based on ct image radiomics signatures. *Radiat Oncol*. (2022) 17:212. doi: 10.1186/s13014-022-02186-0

frontiers | Frontiers in Immunology

TYPE Opinion
PUBLISHED 16 May 2025
DOI 10.3389/fimmu.2025.1609606

OPEN ACCESS

EDITED BY
Kelsey P. Kubelick,
University of Virginia, United States

REVIEWED BY
Myeongsoo Kim,
Georgia Institute of Technology, United States

*CORRESPONDENCE
Dawei Zhang
zdw170320@163.com
Shuhong Dai
shuhong0404@163.com

†These authors have contributed equally to this work

RECEIVED 10 April 2025
ACCEPTED 25 April 2025
PUBLISHED 16 May 2025

CITATION
Zhang X, Cheng C, Qu X, Wang P, Zhang D and Dai S (2025) Spatiotemporal imaging of immune dynamics: rethinking drug efficacy evaluation in cancer immunotherapy. *Front. Immunol.* 16:1609606. doi: 10.3389/fimmu.2025.1609606

Spatiotemporal imaging of immune dynamics: rethinking drug efficacy evaluation in cancer immunotherapy

Xiaowei Zhang[1†], Cheng Cheng[2†], Xiaoyang Qu[3], Pengyun Wang[1], Dawei Zhang[1*] and Shuhong Dai[2*]

[1]Department of Orthopedics, Zibo Central Hospital, Zibo, China, [2]Department of Cardiology, Zibo Central Hospital, Zibo, China, [3]Department of Infectious Diseases, Zibo Central Hospital, Zibo, China

KEYWORDS

tumor immune microenvironment, spatiotemporal imaging, immunotherapy evaluation, in vivo imaging, multiplexed tissue imaging

1 Introduction: the need for a new paradigm in drug efficacy evaluation

The evaluation of drug efficacy remains a central pillar in the development and clinical application of immunotherapies. Traditionally, therapeutic success has been assessed using static and endpoint-based biomarkers, such as tumor size reduction, survival extension, or changes in a limited set of immune markers (e.g., PD-L1 expression or circulating cytokine levels) (1–3). While these metrics have guided many clinical decisions, they often fail to capture the full complexity and heterogeneity of dynamic immune responses, particularly in the context of immuno-oncology, where therapeutic effects can be delayed, indirect, or spatially restricted (4).

Recent advances in immunotherapy, including immune checkpoint inhibitors, CAR-T cells, and tumor vaccines, demand a new framework for evaluating drug efficacy—one that accounts for the spatiotemporal dynamics of immune responses (5, 6). Immune cells may transiently infiltrate tumors, reorganize spatially, or engage in local interactions that are critical for therapeutic outcomes but remain undetectable using conventional assays. Conventional assays typically employed for immune response assessment include IHC, enzyme-linked immunosorbent assay (ELISA), flow cytometry, and quantitative polymerase chain reaction (qPCR). Although informative, these assays provide endpoint measurements and generally lack the resolution to detect transient, spatially restricted, or dynamic interactions of immune cells within the tumor microenvironment (TME) (4). The immune landscape is not static, and responses can evolve rapidly over time and vary widely between tumor regions (7).

In this evolving therapeutic landscape, emerging imaging technologies—ranging from multiplexed spatial imaging at the tissue level to real-time *in vivo* imaging platforms—offer a transformative opportunity (6). Emerging imaging technologies that are significantly enhancing our understanding of the tumor-immune microenvironment include Multiplexed Ion Beam Imaging (MIBI), Imaging Mass Cytometry (IMC), Cyclic Immunofluorescence (CycIF), CO-Detection by Indexing (CODEX), Positron Emission

Tomography (PET), Single-Photon Emission Computed Tomography (SPECT), Magnetic Resonance Imaging (MRI), and Intravital Microscopy. These advanced methods provide detailed spatial, temporal, and molecular resolution, enabling visualization of immune cell dynamics and interactions within the tumor microenvironment at levels previously unattainable by conventional assays (4, 8, 9). These tools allow researchers and clinicians to visualize immune activity where it happens and as it unfolds. By directly observing how drugs engage their targets, modulate the immune microenvironment, and impact immune cell behavior, imaging can provide a richer and more accurate representation of therapeutic efficacy (9).

This opinion article argues that drug efficacy evaluation must shift beyond static biomarkers toward integrated, image-guided approaches that combine spatial, temporal, and functional insights. Such a paradigm shift could greatly enhance precision medicine and improve therapeutic outcomes in immunotherapy.

2 The rise of multiplex and spatial imaging for tissue-level analysis

Tissue-level drug efficacy evaluation has historically relied on basic histological techniques and immunohistochemistry (IHC), offering limited information on the complex spatial relationships that define immune response (10). While traditional biomarkers like PD-L1 or $CD8^+$ T cell counts remain clinically relevant, they offer a static and often incomplete snapshot (11). As our understanding of tumor–immune dynamics deepens, the ability to analyze immune responses in spatial context has become indispensable.

Multiplexed spatial imaging technologies have emerged as powerful tools to overcome these limitations (8). Techniques such as Imaging Mass Cytometry (IMC), Multiplexed Ion Beam Imaging (MIBI), Cyclic Immunofluorescence (CycIF), and CO-Detection by Indexing (CODEX) allow simultaneous visualization of 30 to over 60 proteins within intact tissue sections, preserving spatial architecture (12–14). The multiplex spatial imaging pipeline is illustrated in Figure 1, which includes both the experimental workflow (top panel) and a representative imaging output (bottom panel). The workflow begins with tissue preparation steps including paraffin removal and antigen retrieval, followed by iterative rounds of antibody staining and image acquisition (4). Each cycle involves the application of a primary antibody and a fluorescently labeled secondary antibody, after which the tissue is imaged and the signal is chemically stripped. This process is repeated multiple times (Cycle 1 to Cycle N), each targeting a distinct set of protein markers.

Once imaging is complete, all cycle images are computationally registered to produce a high-dimensional, spatially resolved composite image. The bottom panel shows an example of such a multiplex image, highlighting distinct cell types and structures within the TME. Markers such as DNA, pan-cytokeratin, αSMA, PDGFRβ, CD20, CD45, CD4, CD8, vimentin, and collagen reveal a rich tissue architecture that includes epithelial structures, stromal fibroblasts, immune infiltrates, and extracellular matrix components. Additional single-channel panels demonstrate high-resolution staining of over 20 individual markers, facilitating the detailed classification of immune and stromal subtypes and their spatial distribution.

Building upon workflows like the one shown in Figure 1, these technologies offer unprecedented resolution into the tumor immune microenvironment (TIME), revealing how immune cells are distributed relative to tumor cells, vasculature, and each other. For example, the presence of tertiary lymphoid structures (TLS), spatial clustering of CD8+ T cells near tumor nests, or exclusion of effector T cells from tumor cores are spatial features that have all been correlated with response or resistance to immune checkpoint inhibitors (15). Such findings underscore the need to incorporate spatial biomarkers into drug evaluation pipelines. Moreover, spatial imaging enables retrospective evaluation of clinical trial specimens, helping explain heterogeneous responses. In trials where traditional biomarkers fail to predict outcomes, spatial immune phenotypes—such as myeloid-rich immunosuppressive niches or immune deserts—can offer mechanistic insights and support patient stratification strategies (16). Emerging applications also include the study of therapeutic interventions themselves, such as evaluating immune infiltration post-vaccination or CAR-T cell localization after infusion. Multiplex imaging allows researchers to quantify how drugs reshape the TIME, revealing shifts in cell phenotypes, activation states, or the emergence of suppressive cell types (17).

Despite their promise, integration of these technologies into clinical workflows remains limited due to high cost, labor intensity, and analytical complexity. Nonetheless, advances in automation, cloud-based analysis platforms, and machine learning-driven interpretation are making spatial imaging increasingly accessible. When paired with clinical endpoints, spatial imaging offers not only correlative insights but the potential for spatial biomarker-driven patient selection and real-time therapy monitoring.

In sum, multiplex and spatial imaging have redefined how immune activity within tissues can be visualized, quantified, and interpreted. They offer a much-needed bridge between molecular data and tissue-level functional context, laying the foundation for more nuanced and effective immunotherapy evaluation.

3 *In vivo* and real-time imaging: capturing immune dynamics beyond the slide

The evaluation of drug efficacy in immunotherapy has traditionally relied on static biomarkers and endpoint assessments, which often fail to capture the dynamic nature of immune responses (18). Recent advancements in *in vivo* and real-time imaging technologies have revolutionized our ability to monitor immune dynamics, providing deeper insights into therapeutic mechanisms and facilitating the development of more effective treatment strategies (19, 20).

10.3389/fimmu.2025.1609606

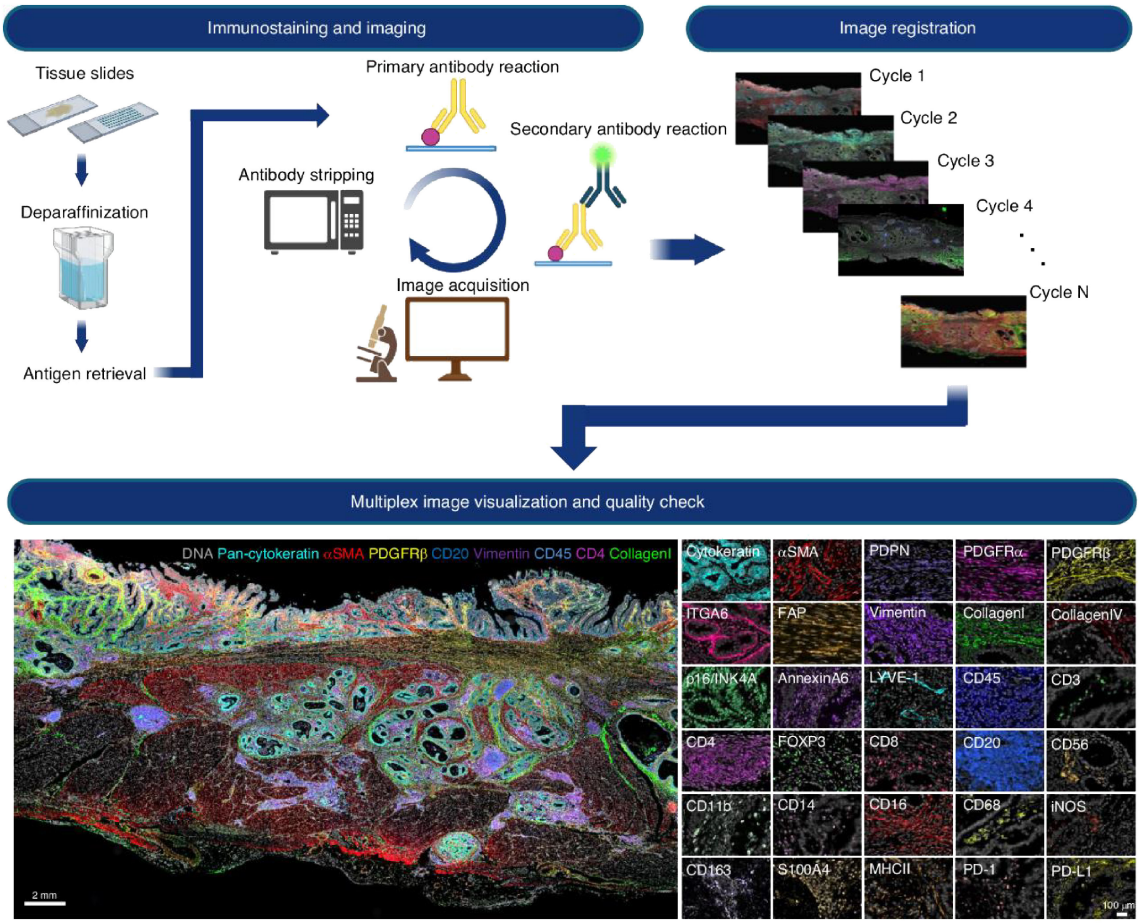

FIGURE 1
Cyclic multiplex immunofluorescence imaging workflow and representative results. Top panel: Iterative imaging process begins with formalin-fixed paraffin-embedded (FFPE) tissue slides undergoing deparaffinization and antigen retrieval. Each cycle consists of primary and secondary antibody labeling, image acquisition, and fluorophore stripping. The resulting images from multiple cycles are computationally aligned (registered) to generate a spatially resolved dataset containing dozens of protein markers. Bottom panel: Composite visualization of a multiplex image from tumor tissue, displaying color-coded spatial expression of markers such as DNA (blue), pan-cytokeratin (cyan), αSMA (red), PDGFRβ (green), CD20, CD45, CD4, CD8, vimentin, and collagen. The right side presents selected single-marker images (e.g., ITGA6, CD3, CD8, MHC-II, PD-L1), enabling detailed analysis of immune cell subsets and structural compartments within the tumor microenvironment. Reproduced with permission from ref (4).

3.1 Advancements in *in vivo* and real-time imaging technologies

In vivo imaging techniques have evolved to allow non-invasive visualization of immune cells within their native environments, enabling the study of cellular behaviors and interactions over time (21, 22). Table 1 provides an overview of key imaging modalities employed in immunotherapy research, highlighting their spatial and temporal resolution, primary applications, as well as their respective advantages and limitations. Key technologies include intravital microscopy, positron emission tomography (PET), single-photon emission computed tomography (SPECT), and magnetic resonance imaging (MRI). These modalities offer unique advantages in tracking immune cell migration, activation, and function in response to immunotherapies.

3.2 Intravital microscopy

Intravital microscopy provides high-resolution, real-time visualization of cellular processes in live animals (23). This technique has been instrumental in elucidating the dynamics of T cell infiltration into tumors, mechanisms of cancer cell killing, and the role of myeloid cells in tumor progression. For instance, Intravital microscopy uniquely enables direct visualization of dynamic immune cell behaviors such as T-cell migration patterns, stable versus transient interactions with tumor cells, and their real-time cytotoxic effects *in vivo*. For instance, studies using intravital imaging have illustrated how stable, long-lasting interactions between cytotoxic T lymphocytes (CTLs) and tumor cells correlate with enhanced tumor cell apoptosis, providing mechanistic insights that static assays fail to capture (24, 25).

Conversely, transient interactions may indicate ineffective immune responses and tumor evasion strategies (26).

3.3 Positron emission tomography and single-photon emission computed tomography

PET and SPECT generate imaging contrast through the use of radiolabeled probes. In PET imaging, positron-emitting isotopes such as ^{18}F, ^{68}Ga, or ^{89}Zr emit positrons upon decay, which interact with electrons to produce gamma photons detectable by the PET scanner. SPECT imaging utilizes gamma-emitting isotopes like ^{99}mTc or ^{111}In, directly detecting gamma photons via gamma cameras. These radiotracers can be conjugated to antibodies, peptides, or metabolic substrates, enabling the specific visualization of immune cells, tumor markers, or molecular processes non-invasively with high sensitivity (27, 28). PET and SPECT imaging utilize radiolabeled tracers to detect specific molecular targets, offering whole-body insights into immune cell distribution and activity (29). These modalities have been employed to monitor the expression of immune checkpoints, such as PD-1/PD-L1, and to assess the biodistribution of therapeutic antibodies. For example, PET imaging with radiolabeled anti-PD-L1 antibodies has enabled the non-invasive assessment of PD-L1 expression in tumors, providing valuable information for patient stratification and treatment planning (30).

3.4 Magnetic resonance imaging and cancer vaccine imaging: tracking immune activation *in vivo*

MRI offers high-resolution anatomical imaging with excellent soft-tissue contrast, making it suitable for tracking labeled immune cells *in vivo* (31, 32). Superparamagnetic iron oxide (SPIO) nanoparticles have been used to label various immune cell populations, allowing their migration and accumulation in tumors to be visualized. SPIO nanoparticles label immune cells through *ex vivo* incubation followed by reinfusion or via antibody-mediated targeting of surface markers *in vivo*. Upon administration, SPIO-labeled cells disturb local magnetic fields detectable by MRI, producing contrast enhancement in images. However, the inherent limitation is the passive accumulation of SPIO nanoparticles in tumors via the enhanced permeability and retention (EPR) effect, which may obscure the precise identification of specific immune populations. Recent advances involve coupling SPIO nanoparticles with specific antibodies or ligands to improve targeting specificity, reducing nonspecific tumor uptake, and enhancing cellular resolution in MRI (33, 34). This approach has been applied to monitor the recruitment of cytotoxic T lymphocytes (CTLs) and regulatory T cells (Tregs) following immunotherapy, providing insights into the mechanisms underlying therapeutic responses (35).

Moreover, the efficacy of cancer vaccines relies on the activation and recruitment of antigen-specific T cells to tumor sites (36). *In vivo* imaging has been employed to monitor these processes, providing insights into vaccine-induced immune responses. MRI tracking of SPIO-labeled dendritic cells, used as vaccine adjuvants, has demonstrated successful migration to lymph nodes and subsequent T cell activation, correlating with tumor regression in preclinical models (37). Together, these applications illustrate how MRI serves as a powerful platform to visualize and quantify immune activation triggered by cancer vaccines, complementing conventional biomarker-based evaluation.

3.5 Tracking CAR T-cell therapy

Chimeric antigen receptor (CAR) T-cell therapy has shown promise in treating certain hematologic malignancies (38, 39). *In vivo* imaging has been pivotal in tracking the migration, expansion, and persistence of CAR T cells post-infusion. For instance, PET imaging using ^{89}Zr-labeled CAR T cells has allowed researchers to monitor the trafficking of these cells to tumor sites, correlating their accumulation with therapeutic outcomes (40). While CAR T cell expansion and persistence can indeed be quantitatively monitored through blood sampling, imaging modalities such as PET, SPECT, or MRI provide complementary insights into spatial biodistribution, trafficking, and infiltration of CAR T cells into solid tumor masses or sanctuary sites not readily accessible via peripheral blood analysis. Imaging approaches thus are invaluable for assessing CAR T cell targeting efficacy, understanding resistance mechanisms, and optimizing therapy regimens, especially in scenarios involving solid tumors or metastatic niches beyond hematologic contexts (41, 42).

3.6 Assessing immune checkpoint inhibitor therapy

Immune checkpoint inhibitors targeting PD-1/PD-L1 and CTLA-4 have revolutionized cancer treatment. *In vivo* imaging has facilitated the evaluation of these therapies by enabling the visualization of dynamic changes in immune cell infiltration and activation within the tumor microenvironment (43). For example, PET imaging with radiolabeled PD-1 antibodies has been used to assess PD-1 expression levels in tumors, aiding in the prediction of patient responses to checkpoint blockade therapies (44).

3.7 From technical barriers to imaging innovation

Despite the advancements, several challenges hinder the widespread clinical adoption of *in vivo* immune imaging. Technical limitations, such as the need for highly specific and sensitive imaging agents, and the potential for tracer-induced

TABLE 1 Key imaging modalities for drug efficacy evaluation in immunotherapy.

Imaging Modality	Spatial Resolution	Temporal Resolution	Key Applications	Strengths	Limitations
CycIF	High (single-cell)	Static (tissue-based)	Immune cell phenotyping, spatial context	High multiplexing; preserved tissue architecture	Labor-intensive; ex vivo only
IMC	High	Static	Deep profiling of TIME	>30 markers simultaneously; metal-tagged antibodies	Costly; limited throughput
PET (e.g., anti-PD-L1 tracer)	Whole-body	Real-time	Monitoring checkpoint expression, cell trafficking	Non-invasive; whole-body coverage	Limited resolution; radiation exposure
Intravital Microscopy	Very high	Real-time	T cell–tumor interactions, vascular dynamics	Direct observation of live processes	Invasive; preclinical only
MRI (e.g., SPIO-labeled cells)	Moderate	Real-time	Immune cell tracking	High soft-tissue contrast; clinical-grade	Low sensitivity for some targets

alterations in cell behavior, must be addressed (45). Additionally, standardization of imaging protocols and data interpretation is essential to ensure reproducibility and comparability across studies (20).

Future research should focus on developing novel imaging probes with enhanced specificity for immune cell subsets and activation states. Combining multiple imaging modalities, such as PET/MRI, could leverage the strengths of each technique, providing comprehensive insights into immune dynamics. Furthermore, integrating *in vivo* imaging data with other biomarkers and clinical parameters may enhance predictive models for treatment responses, ultimately guiding personalized immunotherapy strategies (46).

In summary, *in vivo* and real-time imaging technologies have significantly advanced our ability to monitor immune dynamics beyond traditional histological methods. By providing spatiotemporal insights into immune responses, these techniques offer valuable tools for evaluating and optimizing immunotherapies, paving the way for more effective and personalized cancer treatments.

4 Challenges and integration into clinical practice

Despite the significant promise of advanced imaging technologies in drug efficacy evaluation, several critical challenges continue to limit their widespread adoption in clinical settings. These challenges span technical, operational, analytical, and regulatory domains (47). One of the foremost technical challenges lies in the development and standardization of imaging agents and protocols. Many imaging platforms, especially *in vivo* real-time modalities such as PET, SPECT, and intravital microscopy, rely on customized tracers, labeled antibodies, or nanoparticles that require rigorous validation. These reagents often lack regulatory approval for routine human use and may suffer from variability in synthesis, stability, or immunogenicity (45). Additionally, achieving sufficient resolution, sensitivity, and specificity in a clinical setting—while maintaining patient safety—remains an ongoing challenge, particularly in deep-tissue imaging.

From an operational perspective, the infrastructure required for advanced imaging is substantial. High-end platforms such as imaging mass cytometry, multiplexed ion beam imaging, or hybrid PET/MRI systems are costly to install and maintain. Furthermore, the execution of multi-modal imaging studies demands highly skilled personnel, cross-disciplinary coordination (e.g., pathology, radiology, immunology), and extended processing times, all of which strain hospital resources and reduce scalability. Data analysis and interpretation pose further hurdles. Imaging datasets are large, multidimensional, and complex, requiring bioinformatics expertise, machine learning pipelines, and standardized analytic workflows. Currently, there is a lack of consensus on how to translate spatial or dynamic imaging findings into clinical decisions. While some spatial biomarkers have shown predictive power in trials, few have undergone prospective validation or regulatory qualification as companion diagnostics (48).

To successfully integrate these technologies into clinical immunotherapy practice, several steps are needed. These include the development of standardized imaging protocols, harmonization of analysis tools across platforms, and validation of predictive imaging biomarkers in large, multicenter cohorts. Moreover, regulatory frameworks must evolve to accommodate dynamic and spatial biomarkers, with pathways for the approval of imaging-based diagnostics and clinical decision tools. With strategic investment and collaboration, imaging can shift from an academic asset to a routine pillar of personalized cancer care.

5 Outlook and future perspectives

As immunotherapy continues to reshape the oncology landscape, there is a growing consensus that traditional, static methods of drug efficacy assessment are no longer sufficient. The future of immunotherapy evaluation lies in integrating imaging technologies that can provide comprehensive spatial, temporal, and functional information—enabling a more dynamic and nuanced understanding of immune responses at both tissue and whole-body levels. The convergence of tissue-level multiplex imaging and *in vivo* real-time imaging marks a major step forward. Multiplex platforms like CODEX and IMC offer unprecedented granularity in characterizing the tumor immune microenvironment, while non-

invasive modalities such as PET, MRI, and intravital microscopy allow longitudinal monitoring of immune activity and therapeutic impact. Together, these technologies offer the potential to build a unified, high-resolution view of drug–immune system interactions that can guide real-time clinical decisions.

Looking ahead, the integration of these platforms with computational tools—particularly artificial intelligence (AI) and machine learning—will be key. These approaches can help process vast, multidimensional datasets to identify predictive patterns, generate response signatures, and even forecast resistance. Additionally, combining imaging data with other omics layers (e.g., genomics, transcriptomics, proteomics) will further enhance our ability to stratify patients and tailor therapies.

To fully realize this potential, future efforts must focus on standardization, scalability, and clinical validation. Imaging protocols should be harmonized across institutions, and regulatory frameworks must evolve to recognize imaging-based spatial and functional biomarkers as legitimate endpoints in clinical trials. Equally important is the development of user-friendly analytical platforms that can democratize access to high-content imaging, even in resource-limited settings. In conclusion, imaging technologies are poised to transition from passive diagnostic tools to active drivers of precision immunotherapy. Their ability to visualize immune dynamics in space and time offers a powerful avenue to improve therapeutic evaluation, optimize patient selection, and ultimately enhance clinical outcomes in cancer immunotherapy.

Author contributions

XZ: Writing – original draft, Writing – review & editing. CC: Writing – original draft. XQ: Writing – original draft. PW: Writing – original draft. DZ: Writing – original draft, Writing – review & editing. SD: Writing – original draft, Writing – review & editing.

Funding

The author(s) declare that financial support was received for the research and/or publication of this article. This study was supported by Natural Science Foundation of Shandong Province (ZR2021QH032) and The Medical and Health Science and Technology Project of Shandong Province (202304070941).

Conflict of interest

The authors declare that the research was conducted in the absence of any commercial or financial relationships that could be construed as a potential conflict of interest.

Generative AI statement

The author(s) declare that no Generative AI was used in the creation of this manuscript.

Publisher's note

References

1. Maleki Vareki S, Garrigs C, Duran I. Biomarkers of response to PD-1/PD-L1 inhibition. *Crit Rev Oncology/Hematology*. (2017) 116:116–24. doi: 10.1016/j.critrevonc.2017.06.001

2. Li H, van der Merwe PA, Sivakumar S. Biomarkers of response to PD-1 pathway blockade. *Br J Cancer*. (2022) 126:1663–75. doi: 10.1038/s41416-022-01743-4

3. Zhong Y, Zhang W, Liu D, Zeng Z, Liao S, Cai W, et al. Screening biomarkers for Siogrengaos Syndrome by computer analysis and evaluating the expression correlations with the levels of immune cells. *Front Immunol*. (2023) 14:1023248. doi: 10.3389/fimmu.2023.1023248

4. Semba T, Ishimoto T. Spatial analysis by current multiplexed imaging technologies for the molecular characterisation of cancer tissues. *Br J Cancer*. (2024) 131:1737–47. doi: 10.1038/s41416-024-02882-6

5. Wang B, Yu W, Jiang H, Meng X, Tang D, Liu D. Clinical applications of STING agonists in cancer immunotherapy: current progress and future prospects. *Front Immunol*. (2024) 15:1485546. doi: 10.3389/fimmu.2024.1485546

6. Lv Y, Luo X, Xie Z, Qiu J, Yang J, Deng Y, et al. Prospects and challenges of CAR-T cell therapy combined with ICIs. *Front Oncol*. (2024) 14:1368732. doi: 10.3389/fonc.2024.1368732

7. Sun K, Tempia S, Kleynhans J, von Gottberg A, McMorrow ML, Wolter N, et al. P.-C.g. the, Rapidly shifting immunologic landscape and severity of SARS-CoV-2 in the Omicron era in South Africa. *Nat Commun*. (2023) 14:246. doi: 10.1038/s41467-022-35652-0

8. de Souza N, Zhao S, Bodenmiller B. Multiplex protein imaging in tumour biology. *Nat Rev Cancer*. (2024) 24:171–91. doi: 10.1038/s41568-023-00657-4

9. Rabiee N. Super-resolution microscopy for protein imaging: Unraveling cellular architecture and function. *TrAC Trends Analytical Chem*. (2025) 184:118140. doi: 10.1016/j.trac.2025.118140

10. Giesen C, Wang HAO, Schapiro D, Zivanovic N, Jacobs A, Hattendorf B, et al. Highly multiplexed imaging of tumor tissues with subcellular resolution by mass cytometry. *Nat Methods*. (2014) 11:417–22. doi: 10.1038/nmeth.2869

11. He Y, Ren T, Ji C, Zhao L, Wang X. The baseline hemoglobin level is a positive biomarker for immunotherapy response and can improve the predictability of tumor mutation burden for immunotherapy response in cancer, Frontiers in Pharmacology 15. (2024). doi: 10.3389/fphar.2024.1456833

12. Scuiller Y, Hemon P, Rochais M, Pers J-O, Jamin C, Foulquier N. YOUPI: Your powerful and intelligent tool for segmenting cells from imaging mass cytometry data. *Front Immunol*. (2023) 14:1072118. doi: 10.3389/fimmu.2023.1072118

13. Baharlou H, Canete NP, Cunningham AL, Harman AN, Patrick E. Mass cytometry imaging for the study of human diseases Applications and data analysis strategies. *Front Immunol*. (2019) 10:02657. doi: 10.3389/fimmu.2019.02657

14. Lin J-R, Fallahi-Sichani M, Chen J-Y, Sorger PK. Cyclic immunofluorescence (CycIF), A highly multiplexed method for single-cell imaging. *Curr Protoc Chem Biol*. (2016) 8:251–64. doi: 10.1002/9780470559277.2016.8.issue-4

15. Gobbini E, Hubert M, Doffin A-C, Eberhardt A, L.o. Hermet D, Duplouye LP, et al. The spatial organization of cDC1 with CD8+ T cells is critical for the response to immune checkpoint inhibitors in patients with melanoma. *Cancer Immunol Res*. (2025) 13:517–26. doi: 10.1158/2326-6066.CIR-24-0421

16. Binnewies M, Roberts EW, Kersten K, Chan V, Fearon DF, Merad M, et al. Understanding the tumor immune microenvironment (TIME) for effective therapy. *Nat Med*. (2018) 24:541–50. doi: 10.1038/s41591-018-0014-x

17. Reinhard K, Rengstl B, Oehm P, Michel K, Billmeier A, Hayduk N, et al. An RNA vaccine drives expansion and efficacy of claudin-CAR-T cells against solid tumors. *Science*. (2020) 367:446–53. doi: 10.1126/science.aay5967

18. van de Donk PP, Kist de Ruijter L, Lub-de Hooge MN, Brouwers AH, van der Wekken AJ, Oosting SF, et al. Molecular imaging biomarkers for immune checkpoint inhibitor therapy. *Theranostics*. (2020) 10:1708–18. doi: 10.7150/thno.38339

19. Abdulreda MH, Faleo G, Molano RD, Lopez-Cabezas M, Molina J, Tan Y, et al. High-resolution, noninvasive longitudinal live imaging of immune responses. *Proc Natl Acad Sci*. (2011) 108:12863–8. doi: 10.1073/pnas.1105002108

20. Hor JL, Germain RN. Intravital and high-content multiplex imaging of the immune system. *Trends Cell Biol*. (2022) 32:406–20. doi: 10.1016/j.tcb.2021.11.007

21. Liu J, Cheng P, Xu C, Pu K. Molecular probes for *in vivo* optical imaging of immune cells, Nature Biomedical Engineering. (2025). doi: 10.1038/s41551-024-01275-7

22. Heaton AR, Rehani PR, Hoefges A, Lopez AF, Erbe AK, Sondel PM, et al. ingle cell metabolic imaging of tumor and immune cells *in vivo* in melanoma bearing mice. *Front Oncol*. (2023) 13:1110503. doi: 10.3389/fonc.2023.1110503

23. Pittet MJ, Weissleder R. Intravital imaging. *Cell*. (2011) 147:983–91. doi: 10.1016/j.cell.2011.11.004

24. B.a. Breart F, Celli LS, Bousso P. Two-photon imaging of intratumoral CD8+ T cell cytotoxic activity during adoptive T cell therapy in mice. *J Clin Invest*. (2008) 118:1390–7. doi: 10.1172/JCI34388

25. Nolz JC, Hill AB. Strength in numbers: visualizing CTL-mediated killing *in Vivo*. *Immunity*. (2016) 44:207–8. doi: 10.1016/j.immuni.2016.01.026

26. Boissonnas A, Fetler L, Zeelenberg IS, Hugues S, Amigorena S. *In vivo* imaging of cytotoxic T cell infiltration and elimination of a solid tumor. *J Exp Med*. (2007) 204:345–56. doi: 10.1084/jem.20061890

27. Weissleder R, Pittet MJ. Imaging in the era of molecular oncology. *Nature*. (2008) 452:580–9. doi: 10.1038/nature06917

28. Wierstra P, Sandker G, Aarntzen E, Gotthardt M, Adema G, Bussink J, et al. Tracers for non-invasive radionuclide imaging of immune checkpoint expression in cancer. *EJNMMI Radiopharmacy Chem*. (2019) 4:29. doi: 10.1186/s41181-019-0078-z

29. Jiemy WF, Heeringa P, Kamps JAAM, van der Laken CJ, Slart RHJA, Brouwer E. Positron emission tomography (PET) and single photon emission computed tomography (SPECT) imaging of macrophages in large vessel vasculitis: Current status and future prospects. *Autoimmun Rev*. (2018) 17:715–26. doi: 10.1016/j.autrev.2018.02.006

30. Bansal A, Barham W, Liu X, Harrington S, Lucien-Matteoni F, Dong H, et al. PET imaging of PD-L1 using anti-PD-L1-B11 antibody in breast cancer tumor model. *J Nuclear Med 62(supplement*. (2021) 1):1486.

31. Zhao Y, Ding Y, Lau V, Man C, Su S, Xiao L, et al. Whole-body magnetic resonance imaging at 0.05 Tesla. *Science*. (2024) 384:eadm7168.

32. Zhang C, Hsu P, Wang D, Zhang W, Zhang C, Guo S, et al. Superparamagnetic iron oxide (SPIO) nanoparticles labeled endothelial progenitor cells (EPCs) administration inhibited heterotopic ossification in rats. *Nanomedicine: Nanotechnology Biol Med*. (2019) 21:102078. doi: 10.1016/j.nano.2019.102078

33. Cho EC, Glaus C, Chen J, Welch MJ, Xia Y. Inorganic nanoparticle-based contrast agents for molecular imaging. *Trends Mol Med*. (2010) 16:561–73. doi: 10.1016/j.molmed.2010.09.004

34. Daldrup-Link HE. Ten things you might not know about iron oxide nanoparticles. *Radiology*. (2017) 284:616–29. doi: 10.1148/radiol.2017162759

35. Beer AJ, Holzapfel K, Neudorfer J, Piontek G, Settles M, Krinig H, et al. Visualization of antigen-specific human cytotoxic T lymphocytes labeled with superparamagnetic iron-oxide particles. *Eur Radiol*. (2008) 18:1087–95. doi: 10.1007/s00330-008-0874-4

36. Zhou H, Ma Y, Liu F, Li B, Qiao D, Ren P, et al. Current advances in cancer vaccines targeting NY-ESO-1 for solid cancer treatment. *Front Immunol*. (2023) 14. doi: 10.3389/fimmu.2023.1255799

37. Xu Y, Wu C, Zhu W, Xia C, Wang D, Zhang H, et al. Superparamagnetic MRI probes for in vivo tracking of dendritic cell migration with a clinical 3T scanner. *Biomaterials*. (2015) 58:63–71. doi: 10.1016/j.biomaterials.2015.04.016

38. Butler SE, Hartman CJ, Huang YH, Ackerman ME. Toward high-throughput engineering techniques for improving CAR intracellular signaling domains. *Front Bioengineering Biotechnol*. (2023) 11:1101122. doi: 10.3389/fbioe.2023.1101122

39. Requejo Cier CJ, Valentini N, Lamarche C. Unlocking the potential of Tregs: innovations in CAR technology. *Front Mol Biosci*. (2023) 10:1267762. doi: 10.3389/fmolb.2023.1267762

40. Lee SH, Soh H, Chung J, Cho E, Lee S, Ju J-M, et al. Feasibility of real-time *in vivo* Zr-DFO-labeled CAR T-cell trafficking using PET imaging. *PloS One*. (2020) 15:e0223814.

41. Van Hoeck J, Vanhove C, De Smedt SC, Raemdonck K. Non-invasive cell-tracking methods for adoptive T cell therapies. *Drug Discov Today*. (2022) 27:793–807. doi: 10.1016/j.drudis.2021.10.012

42. Sakemura R, Cox MJ, Bansal A, Roman CM, Hefazi M, Vernon CJ, et al. Dynamic imaging of chimeric antigen receptor T cells with Tetrafluoroborate positron emission tomography/computed tomography. *JoVE*. (2022) 180):e62334.

43. Heskamp S, Hobo W, Molkenboer-Kuenen JDM, Olive D, Oyen WJG, Dolstra H, et al. Noninvasive imaging of tumor PD-L1 expression using radiolabeled anti PD-L1 antibodies. *Cancer Res*. (2015) 75:2928–36. doi: 10.1158/0008-5472.CAN-14-3477

44. England CG, Ehlerding EB, Hernandez R, Rekoske BT, Graves SA, Sun H, et al. Preclinical pharmacokinetics and biodistribution studies of -labeled pembrolizumab. *J Nuclear Med*. (2017) 58:162. doi: 10.2967/jnumed.116.177857

45. Kircher MF, Hricak H, Larson SM. Molecular imaging for personalized cancer care. *Mol Oncol*. (2012) 6:182–95. doi: 10.1016/j.molonc.2012.02.005

46. Turley SJ, Cremasco V, Astarita JL. Immunological hallmarks of stromal cells in the tumour microenvironment. *Nat Rev Immunol*. (2015) 15:669–82. doi: 10.1038/nri3902

47. Rowe SP, Pomper MG. Molecular imaging in oncology: Current impact and future directions. *CA: A Cancer J Clinicians*. (2022) 72:333–52. doi: 10.3322/caac.21713

48. Kwok SJJ, Martino N, Dannenberg PH, Yun S-H. Multiplexed laser particles for spatially resolved single-cell analysis. *Light: Sci Appl*. (2019) 8:74. doi: 10.1038/s41377-019-0183-5

frontiers | Frontiers in Immunology

TYPE Review
PUBLISHED 22 May 2025
DOI 10.3389/fimmu.2025.1473969

OPEN ACCESS

EDITED BY
Kelsey P. Kubelick,
University of Virginia, United States

REVIEWED BY
Jichang Han,
Washington University in St. Louis, United States
Jinhwan Kim,
University of California, Davis, United States

*CORRESPONDENCE
Emese Zsiros
emese.zsiros@roswellpark.org

†These authors share first authorship

RECEIVED 31 July 2024
ACCEPTED 24 April 2025
PUBLISHED 22 May 2025

CITATION
Varghese A, Hess SM, Chilakapati S, Conejo-Garcia JR, McGray AJR and Zsiros E (2025) Tertiary lymphoid structures: exploring opportunities to improve immunotherapy in ovarian cancer. *Front. Immunol.* 16:1473969. doi: 10.3389/fimmu.2025.1473969

Tertiary lymphoid structures: exploring opportunities to improve immunotherapy in ovarian cancer

Aaron Varghese[1,2†], Suzanne M. Hess[1†], Shanmuga Chilakapati[1,3], Jose R. Conejo-Garcia[4], A.J. Robert McGray[1,5] and Emese Zsiros[1*]

[1]Department of Gynecologic Oncology, Roswell Park Comprehensive Cancer Center, Buffalo, NY, United States, [2]Department of Obstetrics and Gynecology, University of Rochester Medical Center, Rochester, NY, United States, [3]Department of Pharmaceutical Sciences, Northeastern University, Boston, MA, United States, [4]Department of Integrative Immunobiology, Duke University School of Medicine, Durham, NC, United States, [5]Department of Immunology, Roswell Park Comprehensive Cancer Center, Buffalo, NY, United States

Tertiary lymphoid structures (TLS) are organized ectopic lymphoid clusters of immune cells that develop in non-lymphoid tissue to promote antigen presentation, drive cytotoxic immune responses, and enhance humoral immunity via B cell clonal expansion. Their presence within the tumor microenvironment (TME) correlates with increased patient survival and an improved response to immune checkpoint inhibitors (ICIs), positioning TLS as potential predictive and prognostic biomarkers. Despite the widespread use of ICIs across various cancers, their effectiveness remains limited in gynecological malignancies, including ovarian cancer (OC), a notably challenging disease characterized by poor responses to both single and combination ICI therapies. Interestingly, the infiltration of T cells into the OC TME is linked to enhanced progression-free survival (PFS) and overall survival (OS), yet an immunosuppressive TME frequently impedes therapeutic efficacy, suggesting cell activity within localized immune niches can impact antitumor immunity. This review explores the roles of TLS, their maturity, functionality, identification, and related gene signatures; specific immune cells and cytokines that play a role in TLS formation and antitumor response; and other modifiable elements, including gut microbiota, that may drive improving OC survival by leveraging a TLS-driven antitumor response to bolster immunotherapy outcomes.

KEYWORDS

tertiary lymphoid structures, ovarian cancer, immunotherapy, tumor microenvironment, gut microbiome, biomarkers

Introduction

Ovarian cancer (OC) represents the most lethal gynecologic malignancy in the United States, underscoring the need for innovative therapeutic strategies (1). OC is predominantly diagnosed at an advanced stage, where cytoreductive surgery and chemotherapy rarely produce curative benefit. The clinical trajectory for most patients is characterized by cycles of remission and relapse, with each remission period becoming progressively shorter until the disease develops resistance to chemotherapy or until significant toxicity arises (2). Given the limited clinical benefits of second line and subsequent therapies, a critical and ongoing need exists to develop novel therapeutic approaches.

Extensive evidence suggests OC is an immunogenic tumor that the host immune system can recognize. A higher infiltration of cytotoxic T cells within OC tumor islets is associated with significantly improved survival rates (3, 4). Tumor-specific T cell responses against multiple antigens overexpressed by OC, including folate receptor alpha (FRα), New York Esophageal Squamous Cell Carcinoma 1 (NY-ESO-1), p53, human epidermal growth factor receptor 2/neu (HER-2/neu), survivin, sperm surface protein 17 (Sp17), Wilms' tumor 1 (WT1), transmembrane glycoprotein mucin 1 (MUC1), and melanoma-associated antigen-3 (MAGE-3), are quantifiable and highlight the potential for immunotherapy in treating OC (5–12). However, effective immunotherapy depends on the successful homing of functional tumor-specific cytotoxic T lymphocytes (CTLs) into tumors and chemotactic gradients within the tumor microenvironment (TME) (13–15) that support persistent immune cell infiltration or inflammatory function (8).

Even with the immunogenic nature of OC, immune checkpoint inhibitors (ICIs) show limited effectiveness in the relapsed/refractory setting, achieving response rates of only 8-15% (16–18). Currently, ICIs are approved solely for mismatch repair deficient (MMRd) OC or have high microsatellite instability (MSI) due to their inadequate effectiveness as single agents (19). While trials testing single agent antibodies targeting programmed cell death protein 1/program death-ligand 1(PD-1/PD-L1) or other ICIs in OC cancer patients have been disappointing (20), in a recent triple combination therapy clinical trial in advanced OC patients testing pembrolizumab, bevacizumab, and oral cyclophosphamide, one third of patients had a durable clinical benefit (DCB) (21–23). Comprehensive molecular, immunological, microbiome, and metabolic profiling analyses were performed on these patients' biospecimens to assess response to this regimen. Increased T and B cell clusters and distinct microbial patterns with lipid and amino acid metabolism were linked to these patients with exceptional responses (23), compared to those with limited clinical benefit (LCB). Identifying reliable predictive biomarkers and who may benefit from immunotherapy would greatly contribute to patient selection for future immunotherapy clinical trials (21, 24–26).

Immunosuppression in ovarian cancer

Despite successful CTL infiltration, tumor heterogeneity and an immunosuppressive microenvironment often undermine the antitumor immune response, with increased recruitment of immunosuppressive cells, including regulatory T cells (Tregs), tumor associated macrophages (TAMs) and myeloid derived stem cells (MDSCs), indicative of poor survival outcomes in OC (27–29). Low tumor mutational burden (TMB) and neoantigen (NA) load (30), downregulation of major histocompatibility complex (MHC)-1 in tumor cells (31), lysophosphatidic acid inhibition of type 1 interferon (32), an immunosuppressive environment in the ascites (33–36), immune evasion promoted by cancer driver mutations, including TP53 and phosphatase and tensin homolog deleted on chromosome ten (PTEN) (37), and aberrant oncogenic signaling pathways, all contribute to ICI resistance across various cancers (38). High metabolic demands of rapidly proliferating cancer cells also exhaust key nutrients needed for immune cell function. Elevated glycolysis rates in tumor cells lead to metabolic exhaustion in effector T cells, while lactate accumulation inhibits natural killer (NK) cell activation. Furthermore, increased expression of indoleamine-2,3-dioxygenase in tumor cells depletes tryptophan levels, impairing cytotoxic T cell proliferation, and inducing T cell exhaustion through kynurenine production (39–42).

Tumor-extrinsic factors also play a significant role in dampening antitumor immunity. Inadequate infiltration of lymphocytes into tumor islets is often due to abnormal vasculature and chemokine gradients (43), as well as compensatory mechanisms like upregulating inhibitory immune checkpoint receptor signaling, including cytotoxic T-lymphocyte associated protein 4 (CTLA-4) and lymphocyte activation gene 3 (LAG-3) (44, 45). Most recently, tertiary lymphoid structures (TLS) or organized ectopic lymphoid structures, that serve as hubs at sites of inflammation and support interactions between B and T lymphocytes and antigen-presenting cells (APCs) (46), has proved to be a major area of investigation (47). While the presence of TLS appears to be essential for coordinating robust antitumor responses, their absence impedes the integration of the humoral and cellular components of adaptive immunity, both of which have been deemed to be important for response to therapy. This limits immune activation and T-cell priming, thus underscoring the important role of TLS in effective tumor control. Given the critical role of TLS in enhancing antitumor immunity, this review will focus on presence and maturity of TLS, their significance on ICI efficacy and clinical trial outcomes, and the impact the gut microbiome and other factors have on antitumor immunity and TLS formation, especially in OC.

Tertiary lymphoid structures

TLS support interactions where specialized formations of B cells, $CD4^+$ and $CD8^+$ T cells, and antigen presenting dendritic cells (DC) come together, along with high endothelial venule cells (HEV), in a coordinated manner, supported by a stromal infrastructure (48). TLS were initially described in autoimmune diseases, chronic infections, solid tumors, age-related diseases, and graft rejection (49–52), and have roles in local autoantibody formation, antibody-mediated immune responses in infected organs, and allograft rejection. TLS

do not exist under physiological conditions which contrasts with primary (bone marrow and thymus) or secondary lymphoid organs (SLO). SLO are embryonic in nature and involve encapsulated lymph nodes (LN), the spleen, Peyer's Patches, as well as tonsils, the human appendix, and mucosal-associated lymphoid tissues. SLOs are dependent on specialized Lymphoid Tissue inducer (LTi) cells that help to drive embryonic mesenchymal tissue organizing cells into follicular dendritic cells (FDC) and fibroblast reticular cells (FRC), driven by CXCL13 and CCL19/CCL21, respectively. TLS are generated after birth by specific cells involved in the immune response at sites of inflammation and are not associated with a specific organ. Both SLO and TLS are involved in generation of antigen-specific immune responses, antigen recognition, and activation of B and T cells (46), as well as involvement with HEV, specialized structures which help facilitate movement of lymphocytes from the blood into tissue. Due to TLS being sites or hubs of inflamed tissue without encapsulation, they are exposed to tumor antigens (TA), cytokines, and other inflammatory signals, which prompt a humoral and cellular immune response.

The presence of TLS correlate with favorable disease outcomes in a variety of cancers, while in autoimmune and chronic age-related disease, TLS are associated with worse, more severe outcomes (52). TLS formation has been observed in almost all organ specific human autoimmune diseases including Sjogren syndrome (SjS) (53), lupus nephritis (54), type I Diabetes (55), Crohn's disease (56) and rheumatoid arthritis (57), however the prevalence of TLS is variable (52). Understanding the involvement of TLS in chronic diseases, including cancer, is therefore important regarding how they are formed and mature to determine potential strategies to aid in disease management.

The autoimmune SjS has been used as a model to derive a spatial and cellular map of key components involved in the formation and function of TLS. Single cell RNA, tissue transcriptomics, and spatial proteomics have been used on salivary glands from SjS patients (58). It has been shown that TLS formation and maturation including a Germinal Center (GC) correlates with autoimmunity, a pathological humoral response, B cell hyperactivity, and development of B cell lymphoma. Results from these studies suggest a complex cellular landscape of TLS, an immunomodulatory pericyte population in SjS, and significant fibroblast diversity, including presence of tissue-resident fibroblasts (immunofibroblasts) that have features like FRC in SLOs. There are different signals involved in the production of CCL21 and CCL19 cytokines in fibroblasts vs. pericytes, as well as distinct properties related to GC in SLO vs TLS. Transcriptomic and proteomic analysis between the SLO and TLS revealed differences in lymphoid structures and enrichment of certain cell types in mature TLS (mTLS), including genes involved in inflammatory cell recruitment, inflammatory pathways, and co-stimulation (58).

These specialized stroma derived fibroblasts have been determined to be crucial for the structure of TLS (59). Fibroblasts have been shown to exhibit plasticity and specialization under inflammatory conditions (48). While TLS are primarily composed of lymphocytes and DC, TLS are also supported by a complex network of additional stromal cells, including endothelial cells, lymphatic vessels, nerves, and immunofibroblasts. Immunofibroblast progenitors have been shown to be present at sites where TLS are established. A mouse model of TLS has shown that under chronic inflammatory conditions, tissue resident fibroblasts can acquire an immunofibroblast phenotype, including expression of lymphoid chemokines, adhesion molecules, and lymphocyte factors which sustain B and T cell survival in tissue. This process includes 1. priming by tumor necrosis factor (TNF) and interferon (INF) family members, interleukin (IL)-13, IL-1 family cytokines, IL-17, and IL-22, resulting in upregulation of intercellular adhesion molecule 1 (ICAM-1), vascular cell adhesion molecule (VCAM1), and podoplanin-posititve (PDPN); 2. expansion (fibroblast proliferation); and 3. maturation (stable expression of lymphoid cytokines CXCL13, CCL19, CCL21, and lymphocyte survival factors, IL-7 or B cell activating factor) of the immunofibroblast network (48). Upregulation of cell adhesion molecules-ICAM1 and VCAM1 also appear to facilitate network interactions.

A variety of cell types are associated with TLS (Figure 1). These organized structures are composed of B cell-containing GCs and DC-lysosome-associated membrane glycoprotein-positive dendritic cells $(DC\text{-}LAMP)^+$ for antigen presentation (60). TLS are also marked by peripheral T cell zones with $CD4^+/CD8^+/T^{fc}$ cells and peripheral node addressin ($PNAd^+$) HEVs (60–62). B lymphocytes which play an active role, express activation-induced deaminase, an enzyme vital to class switch recombination and somatic hypermutation, which leads to the production of antigen-specific antibodies (63). Inflammatory factors are directly implicated in TLS formation and released from activated T cells, macrophages (MP), and DCs in TLS (64, 65).

TLS maturity

TLS maturation stage is a key determinant of TLS function and mTLS have been linked to improved survival and sensitivity to ICI in several cancers. Discussions are ongoing regarding how TLS are defined, their maturity, their increased levels of organization and complexity, and the involvement of immune cells to drive antitumor immunity more effectively, compared to loose immune aggregates of T and B cells observed in immature or "early" TLS. (66–68). As such, the careful classification of TLS and how their presence/location can impact patient outcome or treatment response represents active areas of ongoing investigation. For example, it has been proposed that B cells that accumulate in immature TLS can develop into regulatory B cells with immunosuppressive features that support tumor progression. In contrast, B cells found in mTLS associated with GC are activated and proliferate, undergo affinity maturation, as well as isotype switching, resulting in plasma cells (PC), which produce tumor-specific antibodies, resulting in improved survival and immunotherapy response (66).

At least three levels of organization for TLS have been described: Lymphoid aggregates with minimal organization and occasional DCs; Immature DCs with an organized T and B cell presence, a network of FDCs, no GC, and possibly HEVs; and mTLS

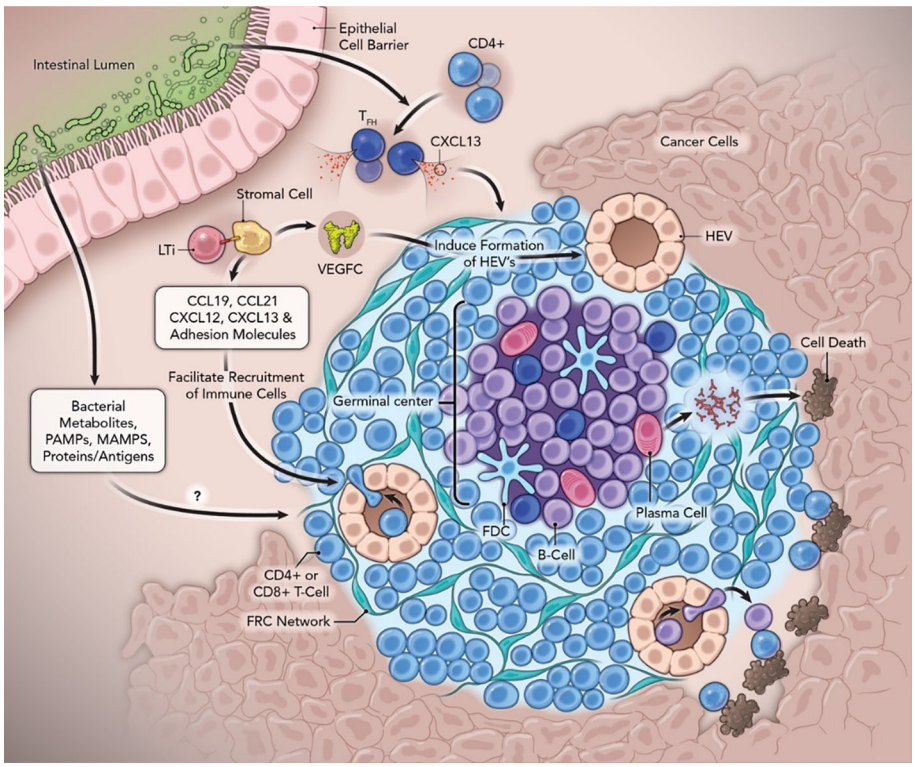

FIGURE 1
Neogenesis and function of tertiary lymphoid structures with the contribution of the gut microbiome in anti-cancer immunity. Abbreviations: FDC, follicular dendritic cells; Tfh, follicular helper T cells; FRC, fibroblastic reticular cells; GC, Germinal Centers; HEV, high endothelial venules; LTi, lymphoid tissue inducer cells; LTβR, lymphotoxin-β receptor; MAMPs, microbe-associated molecular patterns; PAMPs, pathogen-associated molecular patterns; PC, Plasma Cells; SHM, somatic hypermutation; TLS, tertiary lymphoid structure; VEGFC, vascular endothelial growth factor C.

with active GC and HEV, and full B and T cell zones for activation of cell proliferation and recruitment of immune cells (69). Vanhersecke has proposed a standardized method to screen mTLS in cancer samples using hematoxylin-eosin-saffron (HES) staining and immunohistochemistry (IHC) that can be applied to all specimens (70). Vanhersecke has previously defined only two TLS categories, including mTLS (secondary follicle-like TLS) with TLSs containing either a visible GC on HES staining or CD23+ FDC or immature TLS (including early aggregation and primary follicle-like TLS) (68, 70). Of note, the clinical specimen used for TLS detection (surgical vs. biopsy vs. metastatic) had an impact, with TLS identification more prevalent in larger tissue samples.

In gynecological cancers, including OC, Zhang et al. (71) classified these heterogenous TLS into 3 different categories: a very diffuse group of lymphoid aggregate cells containing stomal, dendritic, memory B, follicular B and T cells, and CD4+ and CD8+ T cells; an immature TLS, with more organization including follicular B cells and a CD4+ and CD8+ T cell zone surrounding them with HEV at the periphery, and finally, mTLS consisting of mainly B cell follicles with GC in a B cell zone with networks of CD21+FDCs near an adjacent T cell zone of CD4+ and CD8+ cells, surrounded by stromal and fibroblast cells, PC, and HEV (71).

The organization and maturity of TLS also appears to play a significant role in response to ICI in OC. High-grade serous ovarian cancer (HGSOC) have a low density of follicular helper T (Tfh) cells resulting in a limited number of mTLS, with accumulation of TIM3+PD-1+, rather than TCF1+PD1+ CD8+ T cells, which may at least in part promote ICI resistance in HGSOC patients (72). The quality of TLS, i.e., how well they are formed, have also recently been implicated in OC relapse (73). In addition to changes in T cell localization and increased glycoprotein PDPN+ cancer associated fibroblasts (CAF), which help regulate tumor development and activity of immune cells, malformed TLS-like aggregates and some lymphoid aggregates were associated with spatial patterns of early OC relapse, with PC allocated into compartments associated with TLS-like aggregates and CAFs, potentially accounting for context-dependent roles for PC in HGSOC. In addition, PDPN+ CAFs were frequently associated with partially organized immune cells.

TLS formation

It was thought TLS formation was similar to SLO induction involving LTi cells, hematopoietic cells with a critical immune function during embryonic development (74), which express lymphotoxin-$\alpha_1\beta_2$ ligand and interact with the lymphotoxin-β receptor (LTβR) on lymphoid tissue organizer (LTo) cells to form aggregates. LTi cells interact with LTβR-expressing stromal cells, producing homeostatic chemokines, which are essential for an organization phase. TLS-associated cells are regulated during each

phase of TLS formation by several categories of cytokines/chemokines that participate in stromal cell activation, LiTi cell aggregation, the loop between LTi and LTo, expansion of HEV and recruitment of lymphocytes, formation of T and B cell compartments, and GC formation with differentiation of B cells (63). These chemokines recruit B cells and T cells (via CXCL13, CCL19, CCL21) to form distinct immunological zones (75, 76). LTβR signaling also induces the production of VCAM-1, mucosal vascular addressin cell adhesion molecule-1, and ICAM-1, which further promote lymphangiogenesis (77).

It is now proposed T and B cells are surrogate LTi cells in TLS attracted to the inflammatory site by CXCL13 and IL-7 which activate LTo cells including stromal or immune cells via the TNF family receptor (78). LTo produce chemokines (CCL19 and CCL21 and CXCL10 and CXCL13) to attract immune cells near the site of immune activation and vascularization by establishing gradients which help guide the cells to the lymphoid structures. Adhesion molecules VCAM-1, ICAM-1, MAdCAM-1, and PNAd help circulating immune cells get from HEV to tissue and survival factors BAFF and IL-7 aid in B and T cell maturation and survival. It is thought that in OC, CD4+ T cells and DCs secrete cytokines as potential LTo cells (79).

In contrast to the pathway mentioned above, an alternative mechanistic pathway of lymphangiogenesis that generates TLS involves TNF superfamily member 14 (TNFSF14)/LIGHT, a cytokine produced by activated T cells (80, 81). LIGHT fused to a vascular targeting peptide has been found to normalize tumor blood vessels, activate $CD4^+$/$CD8^+$ T cells, and triggers TLS formation in immunotherapy-resistant pancreatic adenocarcinoma (64). Here, TLS were also found intratumorally instead of at the conventional tumor periphery, which could be due to vessel stabilization in deep tumor parenchyma and relocation of macrophages and effector T cells into the TME (64). In contrast, Tfh tumor-infiltrating lymphocytes (TILs), which secrete LIGHT, IL-21, and CXCL13, are sufficient to initiate TLS assembly, but at peritoneal tumor beds in OC murine models (82, 83)

Analysis of chemokine profiles in HGSOC supports the role of B cells in recruitment of DC-$LAMP^+$, the latter which function in TA uptake and presentation for effective T cell priming (84). B cell clonal expansion correlates with an immunologic response in OC where $CD20^+$ B cells that infiltrate tumors possess qualities of APCs, including surface expression of MHC class I/II, CD80, and CD86 (85, 86). Nielsen et al. suggested $CD20^+$ TILs could serve as APCs to cytolytic $CD8^+$ TILs, and the simultaneous presence of both B- and T-TIL subsets contribute to improved survival in OC patients (86). Montfort and colleagues demonstrated TLS present in OC omental specimens had an upregulated class-switched, memory B cell phenotype after neoadjuvant chemotherapy, suggesting that chemotherapy can regulate B cell functional status within TLS (84).

Detection of TLS

Several methods, including pathological diagnosis, to detect, characterize, and quantify TLS as a predictive and prognostic biomarker have been used including H&E, multiplex IHC and immunofluorescence, and transcriptomic means, however, a consensus method has not yet been determined. While H&E staining is easy, affordable, and widely accepted, there are some concerns including potential for bias, reproducibility among pathologists, and underrepresentation of TLS structures (71). Several markers have been used to identify and quantify key immunological players in TLS through IHC with mTLS identified by markers of T cells (CD3, CD8), B cells (CD20), CD21(B cell), PNAd (HEV), CD208 (DC), CD79A (B cells), PC (CD138), proliferation (Ki67), and cytokines (CXCL13/BCL6). Early and immature phenotypes include CD20, CD3, CD79A, CD8, and PNAd markers, while aggregates include CD20 and CD3 and CD68 MP (87). Additional methods, including IHC and immunofluorescence, are used to identify TLS through staining methods and spatial detection and visualization, respectively, of target proteins in the TLS.

Newer approaches have been used to automate and detect TLS. Multi-resolution deep learning based on HookNet-TLS, has been shown to automate TLS quantification, and identify GC in H&E- stained digital pathology slides. This approach was recently shown to characterize TLS and their prognostic relevance in lung squamous cell carcinoma, muscle invasive bladder cancer, and clear cell renal cell carcinoma (ccRCC). While TCGA slides for OC were not initially used to develop this tool, its availability may provide opportunities to validate it in the OC patient population (88). Multi-plexed whole specimen tissue imaging, 3D reconstruction, spatial statistics, and machine learning was used in a colorectal cancer (CRC) model to determine relevant morphological features associated with diagnostic and prognostic significance, including TLS (89). TLS were commonly interconnected, formed larger 3D structures or TLS networks, had graded molecular properties, and were found in patients' samples at various locations.

Identifying new ways to effectively image TLS in the TME will be invaluable in advancing this field of study and may involve the use of multiple spatial -omic technologies including spatial transcriptomics, proteomics, and metabolomics (90) to identify TLS. Imaging-based approaches will also be important for identifying spatial patterns of TLS that may be associated with early relapse, presence of CAFs (73), risk stratification (91) or assessing recurrence of cancers through flow cytometry and co-detection by indexing (CODEX) (92). Li et al. have suggested several biomaterials that may be suitable for monitoring TLS (93), while three-dimensional imaging may also be an option to characterize TLS (94). Positron emission tomography (PET) using18-F-fluoro-2-deoxy-D-glucose (18F-FDG)(PET/FDG) tail vein injections, combined with computed tomography (CT) for anatomical localization and single photon emission computed tomography (SPECT) by intraperitoneal injection of 99mTC labeled Albumin Nanocoll (99mTC-Nanocoll), has been explored in murine models of systemic lupus erythematosus (SLE) to detect early kidney changes and TLS presence. While TLS were detected in pancreas and not kidney, future studies using new PET/SPECT tracer administration sites, together with more specific tracers in combination with magnetic resonance imaging (MRI), may make it possible to detect formation of TLS and LN for pre-clinical studies. This may be relevant in OC due to different sites of origin of OC. Additional opportunities may include CT-based

radiomic models to non-invasively predict intratumoral TLS (iTLS) as demonstrated for hepatocellular carcinoma (HCC) (95) and invasive pulmonary adenocarcinoma (96), as well as the transfer learning radiomic model, an MRI-based model to detect iTLS in HCC which was found to correlate with favorable prognosis and responsiveness to combination therapy in the context of higher model scores (97).

Genomic signatures of TLS

Gene expression signatures have been used to identify TLS in a variety of cancers and determine their association to survival. A three-gene expression signature including IL-7, LTB, and CXCL13 was associated with LN neogenesis in human oral cancer, where higher grades of TLS were associated with improved disease-free survival (DFS) and overall survival (OS) (98). A unique 12-chemokine (CK) gene expression signature enriched for immune- and inflammation-related genes in primary CRC (99), identified TLS, and found an association with better patient survival independent of tumor staging. This gene signature has been used to confirm the presence of TLS in a variety of cancers including melanoma (100), breast (101), and bladder (102). A 12-gene signature associated with TLS derived from melanoma patient samples treated with ICI predicted clinical outcomes associated with B cells, immune cells, and $CD8^+$ T cell-specific genes, including CXCL13 (103).

Recent OC studies have determined more involvement of TLS in immunotherapy responses. The presence of TLSs in OC and their potential clinical significance was also determined using the 12-CK signature (CCL2, CCL3, CCL4, CCL5, CCL8, CCL18, CCL19, CCL21, CXCL9, CXCL10, CXCL11, and CXCL13) previously identified (91). A 9-gene signature for TLS using a TCGA dataset was constructed and validated in the GSE140082 dataset (104). High expression of this gene signature (CETP, CCR7, SELL, LAMP3, CCL19, CXCL9, CXCL10, CXCL11, CXCL13) positively correlated with developed immune infiltration, and reduced immune escape with TLS associated with favorable responses to ICI in HGSOC patients. High-TLS clusters were characterized by better clinical prognosis, higher immune infiltration, more biological pathways, a higher TMB score, and higher expression of immune checkpoint (71). TLS strongly correlated with the immune-responsive microenvironment and were a favorable prognostic factor independent of other clinical characteristics. While the 12-gene CK signature associated with OC compares to TLS gene signatures from other cancers, additional genes appeared to be unique in the 9-gene signature, including CETP, CCR7, SELL, and LAMP 3. Using this signature, Lu et al. (105), showed TLS-high HGSOC tumors associated with better PFS, B cell maturation, and cytotoxic tumor-specific T cell activation and proliferation.

Recently, Chen et al. explored relevance of the 12-CK gene signature in gynecologic cancers and found it resonated most with cervical cancer, then endometrial cancer (EC), and finally OC (67). In addressing TLS in EC in biobanked samples from the PORTEC study, TLS associated with prognosis in only 2 of 4 EC subtypes: an *excellent* prognosis was associated with the ultra-mutated EC with DNA-polymerase epsilon exonuclease domain mutations (*POLE* mut), and an *intermediate* prognosis with hypermutated EC with MMRd (103, 106). TLSs were also found to assess recurrence with lower 5-year recurrence risk by 4-fold in EC patients (32.6% without TLS vs. 7.2% with TLS) (106). Mature TLS, presence of naïve-B, cycling/GC B cells, and antibody-secreting cells were also associated with L1CAM expression, a cell adhesion molecule independent of tumor expression, and what appears to be a specific biomarker for GC cells in mTLS. This might be a potential biomarker in OC, as well as EC. Note, in OC, TLS loss/dysfunction was linked to chromosome 4q deletion/DCAF15 amplification, whose copy number loss of IL15 and CXCL10 may limit TLS formation (105).

Overall, TLS related gene signatures may be relevant for OC patient stratification to different immunotherapies or responses. Specific gene signatures may not only predict the presence of TLS, involvement of immune markers, and clinical outcomes in different cancers, but may also select patients for specific immunotherapies based on molecular profiling of intratumoral lymphoid aggregates (65). Additional TLS-cancer-specific gene signatures may be forthcoming with artificial intelligence (AI)-driven assessment of large cancer-based datasets and further validation.

Clinical value of TLS

TLS have been identified in a variety of tumor models with characterizations of pro- and anti-tumorigenicity (46), however, the potential for TLS to serve as predictive ICI-based biomarkers is strengthened through clinical trials of solid tumors assessing TLS in immunological, pathological, and clinically relevant outcomes (Table 1), and serve as a potential model for OC. While there is a limited amount of OC clinical trials performed where TLS has been accessed as a biomarker, several studies have shown promising results (Table 2), including those that also indicate the importance B cells in survival and the anti-tumor response (61, 63, 107, 108). Immune and stromal transcriptomic profiles for melanoma patients who respond to neoadjuvant ICI therapy reveal TLS clusters with the highest B cell signature have significantly longer survival (109, 110). Additionally, co-occurrence of tumor-associated $CD8^+$ T cells and $CD20^+$ B cells improves survival in metastatic melanoma patient samples, where TLS in $CD8^+CD20^+$ tumors stained for CXCL13, CXCR5, and CD20, and B cell-enriched tumors had increased TCF-7 naive and/or memory T cell levels (111).

Pembrolizumab monotherapy was assessed in soft tissue sarcoma where one out of 5 sarcoma immune classes were characterized by high immune, TLS, and B cell lineage expression which significantly improved OS and overall response rate (ORR) (112). Sarcoma patients treated with pembrolizumab with low-dose cyclophosphamide had three times greater PFS in the TLS-enriched populations vs. all-comers (113), while NSCLC tumors from patients treated with either the PD-L1 inhibitor atezolizumab or chemotherapy showed B cells associated with extended OS following PD-L1 blockade. B cells and PC were also associated with TLS and organized lymphoid aggregates, with

TABLE 1 Relevant cancer clinical trials with tertiary lymphoid structure involvement in outcomes.

Author, Year, [Ref]	Cancer Type	Clinical Trial NCT Number Phase	Patients	Therapy	Endpoint	Outcomes and TLS Involvement
Garaud et al., 2018 (169)	Breast	N/A	66 primary BC patients.	91-Ag microarray, IgG & IgA.	Analysis of autoantibodies & tumor features.	ex vivo IgA autoantibodies only reactive to BC-associated Ag. Linked with GC and early memory B cell maturation & TLS, suggesting TIL-B activated in the TME.
Maldonado et al., 2014 (142)	Cervical	NCT00788164 Phase 1	12 patients with HPV 16 + CIN.	IM vaccine targeting HPV16 E6/E7.	Safety, tolerability, feasibility, immuno-genicity. Dose and side effect efficacy +/- imiquimod.	Post-vac cervical tissue immune infiltrates included organized stromal TLLS. Increased expression of genes associated with immune activation (CXCR3), effector function (Tbet & IFNβ) & immunologic signature in the overlying dysplastic epithelium. TCR-seq of unmanipulated specimens identified clonal expansions in tissue not detectable in peripheral blood. Vaccination to HPV antigens can induce a robust tissue-localized effector immune response.
Horeweg et al., 2022 (106)	Endo-metrioid	NCT00411138 PORTEC 3 Phase 3	Stage IA G3/II-III endometrioid or stage I-III serous CC endometrial AC.	Chemo XRT + 4 C chemo vs XRT.	Primary outcome, OS, failure free survival. 411 EC slides analyzed.	Chemo XRT + Chemo no improved OS. TLS associated in POLE hypermutated and MMRd & is a prognostic factor. L1CAM identified as a potential TLS biomarker.
Ho et al., 2021 (120)	Hepato-cellular carcinoma (HCC)	NCT03299946 Single arm Phase 1b	15 patients with locally advanced HCC including patients outside of traditional resection criteria.	Feasibility of neo -cabozantinib and nivolumab.	Primary outcomes, DFS, ORR, OS; Secondary outcomes, AE, pre-op to surgery mPR, CRP.	80% of patients had successful margin negative resection; 42% had major pathologic responses. Enrichment in T effector cells, & TLS, CD138+ PC; TLS found in R. Spatial arrangement of B cells in R only, indicating an orchestrated B cell contribution to antitumor immunity in HCC.
Li K et al., 2020 (98)	Oral	NA	65 pts. with oral cancer.	Oral cancer pts. treated by surgical resection.	Determine gene expression profile & DSF & OS.	Identified up-regulated cytokine & chemokine genes (IL7, LTB & CXCL13) responsible for LN neogenesis correlated with oral cancer-TLS. Improved DFS & OS in patients with higher grades of TLSs. Positive intratumoral (33.8%) and peritumoral (75.4%) TLS detection rates found with intratumoral TLSs significantly associated with decreased P53 & Ki67 scores.
Lutz et al., 2014 (141)	Pancreatic ductal adeno-carcinoma (PDAC)	NCT00727441 Phase 2 Randomized 3-arm vaccine trial	39 PDAC pts. who underwent surgical resection.	GM-CSF secreting allogeneic vaccine (GVAX) +/- IV oral cyclo-phosphamide.	Safety, feasibility, & toxicity. ICB alterations of TME.	Histologic evidence of TLS in 85% of specimens post vs. pre-vac. Improved post-vac responses. Involved in 5 immune-cell activation and trafficking signaling pathways. Suppressed Treg pathway & enhanced Th17 pathway associated with improved survival, enhanced post-vac mesothelin-specific T-cell responses, & increased intratumoral Teff: Treg ratios. Infiltration of T cells & TLS development was in TME. Post-GVAX T-cell infiltration &

(Continued)

TABLE 1 Continued

Author, Year, [Ref]	Cancer Type	Clinical Trial NCT Number Phase	Patients	Therapy	Endpoint	Outcomes and TLS Involvement
						aggregate formation resulted in upregulation of PD-1-PD-L1 pathway.
Ryan et al., 2020 (170)	Prostate (PCa)	NCT01804712 Pilot/Phase 1, open label, single arm	8 high risk PCa patients.	Neo anti-CD-20 immuno-therapy with Rituximab.	Primary outcome histological ORR after 1 C; secondary, PSA, PB B cell, CXCL13 serum levels.	Mean CD20 density in tumor of treated group significantly lower than control. Mean CD3 density in tumors was significantly decreased in treated group. Neo rituximab was well-tolerated & decreased B- & T-cell density within high-risk PCa tumors. CD20, CD3 & PD-L1 staining primarily occurred in TLS. Rituximab reduced tumor infiltrating B & T-cell density in TLSs denoting inter-dependence between PCa B & T cells.
Helmink et al., 2020 (110)	Melanoma	NCT02519322 Phase 2	Patients with stage IIIB-IV melanoma.	Neo nivolumab (anti-PD-1) +/- ipi (anti-CTLA-4) or relatimab (anti-LAG-3).	Primary outcome, PR. Secondary, OR immuno-logical response, RR. AE, Biomarker & 3 MICs.	Higher RR in tumors enriched with higher expression of B cell-related genes. MIC with the highest expression of B cells exhibited higher OS. CD20+ B cells localized in TLS of R & promoted T-cell activity in the TME.
Cottrell et al., 2018 (171)	Non-small cell lung cancer (NSCLC)	NCT02259621 Phase 2	20 Pts with stage I-IIIA NSCLC.	Neo nivo.	Safety, feasibility, AE, radiographic response	Two (10%) had a pCR, seven (35%) had a pPR, and four (20%) had a pNR. Of the total 9 patients with a major pathologic response, 7 (78%) exhibited TLS.
Campbell et al., 2021 (118)	Metastatic renal cell carcinoma (mRCC)	NCT02626130 Pilot	18 patients with CC & 11 patients with non-CC histologies.	anti-PD-1 or nivo + Ipi.	Primary endpoint, safety; secondary endpoints, ORR, PFS, & immune monitoring.	Trem + cryoablation is feasible, modulates the immune microenvironment, & leads to significant increase in immune cell infiltration in CC. TLS is observed in CC, but not non-CC mRCC in cryoablation plus Trem therapy.
Carril-Ajuria et al., 2022 (119)	Metastatic clear cell renal cell carcinoma (mccRCC)	NIVOREN Phase II (Correlative analysis) GETUG-AFU 26 study	44 mccRCC treated with nivolumab.	Trem (anti-CTLA-4) (n = 15) or without (n = 14) cryoablation in patients with mRCC.	Primary outcome, safety; secondary outcome, best overall response, AE, & association of biomarkers, with OS, PFS, and response.	Baseline unswitched memory B cells (NSwM) enriched in R & associated with improved OS and PFS. Tfh cells inversely correlated with IL-6 & CXCL13. BAFF significantly associated with worse OS in discovery & validation cohorts. R were enriched in circulating Tfh cells and TLS. Circulating NSwM B cells positively correlated with Tfh, TLS, and $CD20^{+}$ B cells at the tumor center & inversely correlated with CXCL13 and BAFF.
Petitprez et al., 2020 (112)	Soft tissue sarcoma	NCT02301039 SARC 028 Phase 2	608 tumors across sarcoma tissue types analyzed.	Nivolumab in patients with mccRCC.	MCP-counter was used to establish 5 different SICs.	SICs Identified. Immune low (A,B), immune high (D, E), and highly vascularized (C). High expression of B cell lineage & association with TLS based on the elevated expression of CXCL13 had the highest ORR and PFS.

(Continued)

TABLE 1 Continued

Author, Year, [Ref]	Cancer Type	Clinical Trial NCT Number Phase	Patients	Therapy	Endpoint	Outcomes and TLS Involvement
						Group E had TLS containing T cells, follicular DCs, and B cells.
Italiano et al., 2022 (113)	Sarcomas	NCT02406781 PEMBRO-SARC Multiple centers Multi-cohort basket trial 6 parallel single-arm Phase 2 trials	240 patient specimens. LMS, UPS, other STS, GIST, osteosarcoma.	Pembro in soft tissue sarcoma.	Primary outcome, efficacy & safety of Pembro & low dose cyclo-phosphamide.	20% had TLS (700 + CD3+/CD20+ cells) & 73% were included. Median follow-up was 15.6 months. The 6-month PFS was 4.9 (TLS-enriched) vs 1.5 months (all-comer population). 6-month NPR was 40% vs. 4.9% favoring TLS population. TLS potential predictive biomarker in advanced STS to improve patients' selection for pembrolizumab treatment.
Gao et al., 2020 (115)	Urothelial cancers	NCT02812420 Pilot Phase 1 Neo trial	24-Cisplatin-ineligible patients with UC with high-risk features (bulky tumors, LVSI, variant histology, HG disease, and hydro-nephrosis.	Pembro with low-dose cyclo-phosphamide in independent populations.	Primary endpoint, safety, AE, toxicity.	Higher density TLS found in pretreatment tumor specimens of R vs. NR & associated with longer RFS and OS. Pretreatment samples of CD40+ cells had a significantly higher density of B, CD4+, and CD8+ in pretreatment samples. Higher expression of POU2AF1, a gene that defines TLS, and plays a role in GC initiation. pCR achieved in 37.5%.
van Dijk et al., 2020 (116)	Urothelial cancer	NCT03387761 NABUCCO trial Phase 1B feasibility trial	24 patients with stage III UC.	Neo durvalumab (anti-PD-L1) plus Trem (anti-CTLA-4).	Primary endpoint, feasibility to resect within 12 wks., safety, and efficacy.	Eleven (46%) of patients had a pCR. No correlation between TLS quantity & response. Immature TLS formation higher in tumor specimen without a CR. TLS induction observed in R. TLS presence does not predict response to IMTX.
van Dijk et al., 2021 (117)	Urothelial cancer	NCT03387761 NABUCCO trial Phase 1B	24 patients with stage III UC.	Two doses of neo/ipi (anti-CTLA-4) & nivo (anti-PD-1).	MIF analyzed immune cells in tumors +/-pre-op anti-PD1/CTLA-4.	Specific TLS clusters identified based on immune subset densities (CD3, CD8, FoxP3, CD68, CD20, PanCK, DAPI). Tumors not responsive to IMTX enriched for FoxP3+ T-cell-low TLS clusters after treatment. TLS with low MPs significantly higher after pre-op IMTX compared to untreated tumors. Submucosal TLS had more Th cells & enrichment of early TLS than TLS located in deeper tissue & displayed a lower fraction of secondary follicle like TLS than deeper TLS.

AC, Adenocarcinoma; Ag, Antigen; BAFF, B cell activating Factor; CAF, Cancer-associated fibroblasts; CC, clear cell; CBR, clinical benefit or response; CR, complete response; CIN, Cervical Intraepithelial Neoplasia; CTLA-4, cytotoxic-T-lymphocyte-associated protein 4; C, cycle; DFS, disease free survival; FACS, fluorescence-activated cell sorting; GIST, gastrointestinal stromal tumor; GM-CSF, granulocyte-macrophage colony-stimulating factor; GVAX, GM-CSF-secreting, allogeneic PDAC vaccine; HG, high grade; ICB, immune checkpoint blockade; ICI, Immune checkpoint inhibition; IMTX, immunotherapy; IM, intramuscular; ipi, ipilimumab; HTS, High Throughput Sequencing; LAG-3, lymphocyte-activation gene 3; LINE1, Long-interspersed element 1; LMS, leiomyosarcoma; LVSI, lymphovascular space invasion; MPs, macrophages; mccRCC, metastatic clear cell renal cell carcinoma; MCP, microenvironment cell populations; MIC, melanoma immune class; MIF, multiplex immunofluorescence; MMRd, mismatch repair deficient; mRCC, metastatic Renal Cell Carcinoma; Neo, Neo-adjuvant; Nivo, nivolumab; NPR, non-progression rate; NR, non-responders; NSCLC, non-small cell lung cancer; NSMP, no specific molecular profile; NSwM B cells; Baseline unswitched memory B cells; OC, Ovarian cancer; ORR, Overall Response Rate; OS, overall survival; PBMC, Peripheral Blood Mononuclear Cells; pCR, pathologic complete response; PD-1, programmed cell death protein 1; PFS, progression free survival; pNR, pathological non-response; pPR, pathologic partial response; PR, Partial response; Pembro, Pembrolizumab; POLE, DNA polymerase epsilon; Post-vac, Post-vaccination; Pre-vac, pre-vaccination; PC, Prostate cancer; Pts, Patients; R, responders; RFS, recurrence-free survival; RR, Response rate; SD, Stable Disease; SIC, sarcoma immune class; STS, soft tissue sarcoma; TCGA, The Cancer Genome Atlas; T_{eff}, effector T-cell; TLLS, Tertiary lymphoid-like structures; TLS, tertiary lymphoid structures; Tfh, T follicular helper; TME, tumor microenvironment; TX, Treatment; T_{reg}, regulatory T cell; Trem, tremelimumab; UC, urothelial carcinoma; UPS, undifferentiated pleomorphic sarcoma; wks., weeks. PubMed search through April 2024.

TABLE 2 Tertiary lymphoid structure involvement in ovarian cancer.

Author, Year, [Ref]	Goal/Intervention	Patients/Methods	Relevant Results	TLS Involvement and Conclusions
Kroeger et al., 2016 (172)	Determine colocalization patterns, phenotypes, & gene expression profiles of tumor associated T & B lineage cells in HGSOC.	Multicolor IHC, flow cytometry & bioinformatic analysis of gene expression data from TCGA.	T-and B- cells colocalized in four types of lymphoid aggregate, ranging from small, diffuse clusters to large, well-organized TLS resembling activated LN. PCs associated with the highest levels of CD8+, CD4+ & CD20+ TIL, & numerous cytotoxicity-related gene products. CD8+ TIL carried prognostic benefit only in the presence of PCs & these other TIL subsets. PCs were independent of mutation load, BRCA1/2 status, & differentiation Ags but positively associated with CTA.	B and T cells co-localize in 4 lymphoid patterns, including large, well- organized TLS. TLS frequently surrounded by dense infiltrates of PC, comprising up to 90% of tumor stroma. Tumor infiltrating-PC expressed mature, oligoclonal IgG transcripts indicative of Ag-specific responses & are associated with TLS, cytolytic T-cell responses, & superior prognosis in OC.
Yang et al., 2021 (124)	Determine therapeutic effect of CXCL13 & PD-1 blockade.	264 HGSOC patients/2 cohorts & 340 HGSOC TCGA cases used. Survival compared in pt. subsets (Kaplan-Meier analysis). Therapeutic effect of CXCL13 & PD-1 blockade, validated in murine models & human HGSOC tumors. Spatial correlation between CXCL13, CXCR5, CD8, & CD20 evaluated by IHC & IF.	CXCL13 associated with CD20+ B cells predicted better patient survival. Combination of CD8+ T cells, CXCL13, & CXCR5 was an independent predictor for survival. Tumors with high CXCL13 expression had increased infiltration of activated and CXCR5 expressing CD8+ T cells. Murine studies: CXCL13 & anti-PD1 therapy showed a CD8+ T cell dependent retarded tumor growth with increased infiltration of cytotoxic CD8+ T cells & CXCR5-CD8+ T cells.	CXCL13 colocalizing with TLSs shapes anti-tumor microenvironment by maintenance of CXCR5+CD8+ T cells in TLS. TLS prognostic benefit is only relevant in the presence of CXCL13. High CXCL13 expression associated with prolonged survival. Supports a new CXCL13 & PD-1 blockade clinical trial in HGSOC.
Chen S, 2022 (122) NCT02901899	Determine if hypomethylating agent guadecitabine in a phase II study improves ICI in platinum-resistant OC.	35 platinum-resistant OC patients (normal organ function, measurable disease, up to 5 prior treatments). Primary endpoint: ORR. Secondary endpoints: CBR, PFS, & Toxicity.	3 patients had PR, 8 had SD, CBR of 31.4%. Median duration of clinical benefit was 6.8 mo. Anti-tumor immunity activated in post-treatment biopsies as seen with methylomic & transcriptomic analyses. PBMCs showed higher frequency of naive &/or central memory CD4+ T cells and classical monocytes in patients with a durable CBR.	A higher baseline density of CD8+ T cells & CD20+ B cells & the presence of TLS in tumors were associated with a durable CBR.
Gaulin, 2022 (22) NCT02853318 (21)	Determine factors contributing to durable response in R.	40 advanced OC patients with previous multiple lines of therapy treated with Pembro, Beva, and Cytoxan therapy (21). Improved PFS & OS.	Transcriptomic assessment indicative of a more favorable immune signature with B & T cells, CD40, Ag presenting, cytokine, & TLS, at baseline & during treatment. Immunoproteins are upregulated intratumorally. Immune cells move from stroma into the TME.	Multi-omics assessment of R and NR pt. samples indicative of cellular and humoral response, including TLS signature, in R who have a durable response to Pembro, Beva, and Cytoxan therapy.
Ozmadenci et al., PNAS 2022 (148)	Determined the effects of tumor intrinsic genetic or oral small molecule FAK inhibitor (FAKi; VS-4718) *in vivo*.	Used the Kras, Myc, FAK (KMF) syngeneic ovarian tumor mouse model containing spontaneous FAK/PTK2 gene gains.	Blocking FAK activity decreased tumor burden, suppressed ascites KMF-associated CD155/PVR levels, & increased peritoneal TILs.	FAKi + 1B4 TIGIT blocking antibody maintained elevated TIL levels, reduced TIGIT+ T reg cell levels, prolonged host survival, increased CXCL13 levels, & led to the formation of omental TLS. These results support FAK & TIGIT targeting as a rational immunotherapy combination for HGSOC.
Ukita, M et al., 2022 (79)	Determine TLS distribution in TME in relation to TILs &	Used OC cases registered in TCGA.	CXCL13 gene expression correlated T & B cells infiltration. CXCL13 was a favorable prognostic	CXCL13 gene expression correlated with TLS presence. CXCL13-producing CD4+ T cells are

(Continued)

TABLE 2 Continued

Author, Year, [Ref]	Goal/Intervention	Patients/Methods	Relevant Results	TLS Involvement and Conclusions
	related gene expression in HGSOC specimens.	TCGA-RNA seq used, & KOV microarray data.	factor. CD8+ T cells and B cell lineages in TME significantly improved the prognosis of HGSOC & correlated with presence of TLS. CXCL13 expression coincident with CD4+ T cells in TLS & CD8+ T cells in TILs & shifted from CD4+ T cells to CD21+ follicular DCs as TLS matured.	involved in the early stage of TLS formation. TLS formation was associated with CXCL13-producing CD4+ T cells & TLS facilitated the coordinated anti-tumor response of cellular & humoral immunity in OC.
Hou, Y et al., 2023 (104)	Determine related gene signature of TLS in OC.	TLS gene signature constructed in TCGA dataset & validated in the GSE140082 dataset.	High expression of gene signatures positively correlated with developed immune infiltration & reduced immune escape. Quantified TILs (CD20+ B cells & CD8+ T cells) in OC patients. PD-L1 proved predictive value of immunotherapy for gene signature. Signature showed a better correlation between TMB & classical checkpoint genes.	OC TLS gene signature (CETP, CCR7, SELL, LAMP3, CCL19, CXCL9, CXCL10, CXCL11, CXCL13) identified & validated. Signature predicts prognosis & immunotherapy benefit. Confirmed improved survival values of TLS & TLS play an important role in tumor immunity. Gene signature proposed as prognostic biomarker & means to guide immunotherapy in OC.
Zhang K., et al., 2023 (71)	Determine presence of TLSs, their potential clinical significance & association with TME, & immunotherapy response in HGSOC.	HGSOC TCGA cohort of 376 pts with RNA seq data, 74 with H&E; 212 with microarray data (GEO cohort). TLS pathological sections with TLS number assessed by 12-chemokine transcriptomic signature.	TLSs located mainly in stroma & invasive margin of tumor (H&E). HGSOC patients are divided into a low-TLS & high-TLS cluster. Expression of 12 chemokines significantly higher in samples abundant with TLSs.	TLS associated with favorable response to ICI & are a favorable independent prognostic factor in HGSOC. High-TLS cluster had better clinical prognosis, higher immune infiltration and TMB score, more biological pathways, & higher immune checkpoint expression. TLSs strongly correlated with the immune-responsive microenvironment.
Lu, H et al., 2023 (105)	Determine if tumor & local lymphoid tissue interaction decide prognosis in HCSOC.	Immunogenomic analysis of 242 HGSOC cases.	TLS associated with B & T cell activation in OC & predict survival. TLS loss/dysfunction linked to chromosome 4q deletion/ DCAF15 amplification.	Presence of TLS in HGSOC tumors associated with B cell maturation & cytotoxic tumor-specific T cell activation & proliferation. Copy-number loss of IL15 & CXCL10 may limit TLS formation in HGSOC.
Feng et al., 2023 (147)	Determine the mechanism cdk4/ 6i promotes TLS formation & if TLS affect OC prognosis.	Mouse model & HTS used to explore potential mechanisms.	After CDK4/6i treatment, TLS observed & associated with favorable OC prognosis. CDK4/6i promoted TLS formation, enhanced immunotherapeutic effect of anti-PD-1, & may be modulated through SCD1, ATF3, & CCL4.	TLS associated with favorable OC prognosis following CDK4/6i. CDK4/6i may be a therapeutic option for OC, alone & in combination with anti-PD-1 therapy.
Kasilova et al., 2024 (72)	Determine distinct immune aggregate patterns, organization, & maturity associated with HGSOC.	FFPE OC & LC cohorts, IHC, flow, & RNAseq.	mTLS formed in limited HGSOC with high TMB & are associated with increased intratumoral density of CD8+ effector T cells. An ICI-resistant TIM3+PD1+ phenotype is more prevalent in HGSOC & supported by less mTLS.	TLS and B cells determine clinically relevant T cell phenotypes in OC. OC associated with low density of Tfh cells, low mTLS that might not preserve an ICI-sensitive TCF1+PD1+ CD8+ T cell phenotype.
Xu et al., 2024 (73)	Determine how spatial heterogeneity contributes to HGSOC progression & early relapse.	Profiled an HGSOC tissue microarray of 42 patients matched longitudinally.	Spatial patterns associated with early relapses (Changes in T cell location, malformed TLS-like aggregates, & increased podoplanin-positive CAFs). PC distribute to 2 different compartments associated with TLS-like aggregates & CAFs.	Poorly formed TLS-like aggregates play a role in early relapses (<15 mo.) of HGSOC patients. TLS-like aggregates appear to associate with PCs in compartments with distinct microenvironments.

(Continued)

TABLE 2 Continued

Author, Year, [Ref]	Goal/Intervention	Patients/Methods	Relevant Results	TLS Involvement and Conclusions
Lanickova et al., 2024 (168)	Determine if neoadjuvant chemotherapy paclitaxel-carboplatin had impact on immunological configuration of paired primary and metastatic HGSOC biopsies.	Used transcriptomic, spatial, and functional assays.	TLS maturation is associated with increased intratumoral density of ICI sensitive TCF+PD1+CD8+T cells. Chemotherapy + PD-1 targeting ICI provides a survival benefit. Increase in effector CD8+ T (Teff) cells, B cells, DC, and TLS-associated cells, such as follicular helper T cells, which collectively contribute to cancer cell killing also observed.	Neoadjuvant chemotherapy promotes TLS formation, adaptive immunity, and maturation in metastatic HCSOC lesions. Intracellular calreticulin (CALR) expression within cancer cells, a marker of endoplasmic reticulum stress and potential cell death, was increased. Suggests clinical trial with chemo + ICI.
Zhang L et al., 2024 (173)	Determine antibody-secreting B lymphocytes from OC patients.	Profiled stably maintained cell lines with flow, and B cell receptor sequencing. Tumor samples used for spatial profiling with chip cytometry.	Presence of EBV proteins Original tumors had high frequency of tumor infiltrating B cells present as lymphoid aggregates or TLS.	Antigens recognized coil-coil domain containing protein 155 (CCDC155), growth factor receptor-bound protein 2 (GRB2), and pyruvate dehydrogenase phosphatase 2 (PDP2).
MacFawn et al., 2024 (125)	Determine TLS in various locations of OC development.	Spatial analytes used. Spatial transcriptomics Digital Spatial Profiling.	Pro-tumorigenic stroma could limit TLS formation. Cancer-educated Mesenchymal Stem Cells (CA-MSC) could decrease antitumor efficacy.	TLS less developed in tumors originating in ovary tumor vs FT or OM. Immune cell activity increases when residing in more developed TLS and produces a prognostic, spatially derived signature from HGSOC tumors. CA-MSC may contribute to more suppressive TME in ovary limiting TLS, T and B cell and antibody infiltration, and overall decreased anti-tumor activity.
Rosario et al., 2024 (23) NCT02853318 (21)	Multi-omics assessment of durable clinical benefit (DCB) vs. limited clinical benefit (LCB) patients.	40 pts accrued. Bulk RNA seq, metabolomics, microbiome, immune studies, and DSP performed.	Infiltration of immune cells from stroma to tumor. Coordinated increase and movement of T and B cell infiltrates. Additional immune cell signatures associated with CD40 Ag, Ag presentation, cytokine presence, and indications of TLS	Identification of Tumor-Immune-Gut Axis. Presence of TLS signatures and humoral and cellular involvement of TLS, humoral and cellular anti-tumor responses, and metabolomic pathways in DCB vs. LCB patients.
Westbom-Fremer et al., 2025 (174)	Investigated mTLS, iTLS & LA in PTs & pMets of HGSC.	Whole H&E slides interrogated for mTLS and LA in a cohort of 130 cases with stage III-IV HGSC. Immune cell tumor infiltration evaluated using TMA on cases with single chromogenic IHC. MIF further performed on select PT and pMet samples.	mTLS more common in pMets than in PTs but did not have an independent prognostic impact on overall or PFS. mTLS presence correlated with intratumoral infiltration of CD8+ cytotoxic T cells, FOXP3+ Tregs and PD-1+ lymphocytes in pMets only. mTLS cell composition similar between PTs and pMets, but outer zones of mTLS in PTs were more immune cell rich. No iTLS identified.	Differences in TLS presence and cellular elements between PTs and synchronous pMets important for understanding mechanisms of immune evasion and initiation of tumor targeted immunity. Could not deduce an independent prognostic impact of mTLS and LA in this case cohort. Suggests anatomical site relevant for modulation of immune landscape especially in recurrent setting.

Ag, Antigen; ATF3, Activating transcription factor 3; Beva, Bevacizumab; CCL4, chemokine ligand 4; Cdk4/6i, Cyclin dependent kinase 4 and 6 inhibitor; CAF, Cancer-associated fibroblasts; CBR, clinical benefit rate/response; CR, complete response; CTA, Cancer testis antigen; DC, Dendritic Cells; FAK, Focal adhesion kinase; FAKi, Focal adhesion kinase inhibitor; FFPE, formalin fixed paraffin embedded; FT, Fallopian Tube; H&E, Hematoxylin and Eosin; HGSC, High grade serous cancer; HGSOC, High grade serous ovarian cancer; HTS, High throughput screens; ICI, Immune checkpoint inhibition; IF, Immunofluorescence; IgG, Immunoglobulin G; IHC, Immunohistochemistry; iTLS, immature Tertiary lymphoid structures; KMF, Kras, Myc, FAK syngeneic mouse; LN, Lymph node; LA, Lymphoid aggregates; LC, Lung cancer; MIF, multiplex immunofluorescence; mTLS, mature tertiary lymphoid structure; NR, non-responders; OC, Ovarian cancer; OM, Omentum; ORR, Overall Response Rate; OS, overall survival; PBMC, Peripheral Blood Mononuclear Cells; PD-1, programmed cell death protein 1; PD-L1, Programmed death-ligand 1; PFS, progression free survival; PR, Partial response; Pembro, Pembrolizumab; PTs, primary adnexal tumors; pMets, omental/peritoneal metastases; PVR, Polio virus receptor; R, responders; SCD1, Stearoyl-CoA desaturase 1; SD, Stable Disease; TCGA, The Cancer Genome Atlas; TIGIT, T cell immunoglobulin and ITIM domain; TMA, tissue microarray; TLS, tertiary lymphoid structures; Tfh, T follicular helper cell; TME, tumor microenvironment; TIL, Tumor infiltrating lymphocyte; T_{reg}, regulatory T cell; TMB, Tumor mutational burden; wks., weeks. PubMed search (tertiary lymphoid structures and ovarian and cancer) through January 2025.

increased PC signatures predictive of OS in patients treated with atezolizumab only (114).

Combination immunotherapy trials have shown improved outcomes in some solid tumor cancers. Neoadjuvant anti-PD-L1 (durvalumab) plus anti-CTLA-4 (tremelimumab) treatment of cisplatin-ineligible patients with urothelial cancer (UC) had higher density TLS in pretreatment tumor specimens of responders (R) associated with longer recurrence-free survival

(RFS) and OS (115). In previous neoadjuvant ipilimumab (anti-CTLA-4) and nivolumab (anti-PD-1) studies prior to surgical resection, while no correlation was observed between TLS quantity, TLS induction was seen in R, with immature TLSs higher in patient tumor specimens that did not have a complete response (CR) (116). Enriched FoxP3$^+$ T cell-low TLS clusters were observed after anti-PD-1/CTLA-4 immunotherapy in unresponsive tumors in another study, while submucosal TLS had more pronounced T-helper cells, enrichment of early TLS, and displayed a lower fraction of secondary follicle-like TLS than TLS located in deeper tissue (117).

Other combination therapy, including immunotherapy, had varied results in smaller trials. Cryoablation plus tremelimumab modulated the immune microenvironment with increased immune cell infiltration in patients with clear cell (CC) metastatic renal cell carcinoma (mRCC); however, TLS were only observed in CC mRCC patients and not non-CC (118). An enhanced immune response was observed in R in a second trial where CC mRCC patients treated with nivolumab were enriched in circulating Tfh cells, TLS, and baseline NSwM B cells, and were also associated with improved OS and PFS (119). In a small single arm phase 1b study in 15 HCC patients testing neoadjuvant cabozantinib, a tyrosine kinases inhibitor, and nivolumab, TLS were found in R, with an enrichment in T effector cells, TLS, and CD138$^+$ PC. Here, a distinctive spatial arrangement of B cells contributed to antitumor immunity in R vs. Non-responders (NR) (120).

Tertiary lymphoid structures in ovarian cancer

Several studies, including data collected through The Cancer Genome Atlas (TCGA), confirm a connection between TLS, B and T cells, and OC (Table 2). Increased patient survival was observed between tumor-infiltrating B cells and CD8$^+$ T cells, offering possible mechanisms for B cell involvement in cellular immunity, including secreting polarized cytokines, serving as APCs, or organizing centers for TLS (121). B cells colocalized to large, well-organized TLS, while dense infiltrates of PC surrounded TLS, which are associated with the highest levels of CD8$^+$, CD4$^+$, and CD20$^+$ TIL, as well as cytotoxicity-related gene products. TLS also correlated with CXCL13 gene expression, infiltration of T cells and B cells, and improved prognosis for HGSOC (79). The coexistence of CD8$^+$ T cells and B cell lineages in the TME significantly improved the prognosis of HGSOC and correlated with the presence of TLS. CXCL13 expression predominantly coincided with CD4$^+$ and CD8$^+$ T cells in TILs, shifting from CD4$^+$ T cells to CD21$^+$ FDCs as TLS matured.

A phase II clinical trial with the hypomethylating agent guadecitabine and the anti-PD1 inhibitor pembrolizumab resulted in a clinical benefit rate (CBR) of 31.4% (8.6% partial responders and 22.9% stable disease) (122). Naive and/or central memory CD4$^+$ T cells and classical monocytes were observed at a higher frequency in patients with a durable CBR, while TLS present in tumors were associated with a durable CBR and higher baseline density of CD8$^+$ T cells and CD20$^+$ B cells. Updated efficacy and OS survival data for an open-label single-arm nonrandomized phase 2 trial (NCT02853318) by Zsiros et al. (21) was presented in 2022 (22) for a triple combination therapy (pembrolizumab, bevacizumab, and oral metronomic cyclophosphamide) conducted in a heavily pre-treated OC patient population. Originally, an ORR of 47.5% was obtained, along with a median PFS of 10 months, which was over 4 times better than ORR (8%) or PFS (2.1 mo.) in single-agent ICI, and better than bevacizumab and cyclophosphamide combination therapy (25). Thirty percent of patients had disease control, with 95% having a clinical benefit, with limited toxicity and good quality of life (QoL) reported. Some exceptional R survived more than three years, and one up to five, with multi-omics performed on collected biospecimens from this study (23) suggesting involvement of TLS, humoral and cellular anti-tumor responses, and metabolomic pathways in DCB vs. LCB patients. These results contributed to changes in NCCN guidelines (123).

Additionally, in studies to predict immunotherapy response to PD-1 blockade, HGSOC samples from two patient cohorts and an HGSOC cohort from TCGA were analyzed to assess the relationship between TME and follicular cytotoxic CXCR5-CD8$^+$ T cells. Again, high expression of CXCL13 was associated with prolonged survival, and, combined with CXCR5 and CD8$^+$ cells, was an independent predictor for survival. CXCL13 also carried prognostic benefit, but only with TLS, and was also associated with CD20$^+$ B cell clusters, predicting better patient survival when both were present (124). Along with the 9-gene and 12-gene CK signatures, the combinations of immune cell markers, as well as CXCL13, are the strongest biomarker front runners for prolonged survival in combination with mTLS.

Recently, MacFawn et al. (125), using spatial transcriptomics and multiplex immunofluorescence, demonstrated TLS in HGSOC differ significantly by anatomical site resulting in altered TLS activity and patient prognosis. Composition, function, activity, and number of TLS are distinct between OC originating in the ovary (OV) compared to the fallopian tube (FT) and omentum (OM) and this directly impacts TLS activity, immune function, and survival. Ovarian tumors originating from the FT and OM had more TLS that are more functionally active compared to OV, which are less mature and fewer in number, as well as have a reduced B to T cell ratio, fewer HEVs, and less GC, thus reduced antitumor immunity. Not only were B cells markedly reduced in OV compared to OM or FT, but there are decreased markers (MZB1 +) of antibody production in OV. The TLS 12 CK-gene signature associated with improved survival was observed in FT and OM but indicated poor survival in OV. Another major finding was the impact of stromal cells in the OV TME (126). Cancer educated mesenchymal stem cells (CA-MSC) have been identified in the OV, where the CA-MSC signature appears to override the benefit of the TLS signature (125). These cells previously have been associated with reduced survival and metastasis (127). mTLS differences were also observed in adnexal tumors (PTs) and synchronous omental/peritoneal metastases (pMets) in HGSOC. pMets had more mTLS and immune components (CD8+ cytotoxic T cells, FOXP3+ Tregs and PD-1+ lymphocytes) than PT, but an independent prognostic

impact of mTLS could not be obtained. A more immune cell rich outer zone of mTLS was observed in PTs, but not pMets. This suggests the anatomical site, as well as deciphering what is involved in immune response and evasion, are relevant when considering what signals to modulate to improve the antitumor response. TLS have also been assessed in HGSOC progression & early relapses using spatial heterogeneity. Spatial patterns associated with early relapses included changes in T cell location, TLS-like aggregates which appear malformed, and an increased presence of PDPN-CAFs. These poorly formed TLS aggregates are potential indicators of early relapse in HGSOC (73). Figure 2 summarizes factors that impact TLS in OC and identifies potential pathways or strategies that may be manipulated or explored that may increase TLS formation and improve therapeutic outcomes.

While this review has predominantly focused on the role of TLS in the context of ICI, additional immunotherapeutic approaches and treatment strategies are in development for OC where TLS are likely to also play a functional role. Given that OC is readily infiltrated by T and NK cells, leveraging these cell subsets may represent particularly attractive therapeutic opportunities. This includes adoptive T cell therapies (ACT) or T cell activating modalities, such as the delivery of expanded TILs, or vaccine-primed T cells, infusion of engineered TCR-T or CAR-T cell therapies, as well as treatment with BiTEs to redirect T cells for tumor targeting (128, 129). A major focus of ACT-based modalities hinges on successful target identification, which includes in OC MUC 16, FRα, B7H3, mesothelin, and TAG72 (130), to name a few, as well as strategies to overcome inherent limitations of antitumor T cell responses, including lack of T cell persistence, tumor heterogeneity, loss of functionality, and impaired trafficking towards the TME, all of which may benefit from the presence of TLS. A recent publication from our group addressed some of these barriers to magnify therapeutic responses by using BiTE-secreting T cells targeting FRα present on most OC cells. Engineered T cells secreting FR-alpha engagers (FR-B T cells) not only effectively killed targeted OC cells but also redirected endogenous host T-cells to kill tumor cells (131). Follow up studies are currently underway to understand how TLS may influence the local organization of both transferred FR-B T cells and endogenous immune cells in the TME in orchestrating the antitumor response.

Other ACT strategies include using NK cells, which can kill cancer cells without prior sensitization and are not antigen dependent. Several studies have been conducted using murine models (132–134) to explore improving cytotoxicity and longevity of NK cells. One example, addition of cytokines IL-2, IL-15, and IL-18, promotes activation and proliferation of NK cells, as well as secretion of INF gamma and inhibition of OC cells (135). This strategy generated cytokine-induced memory-like NK cells.

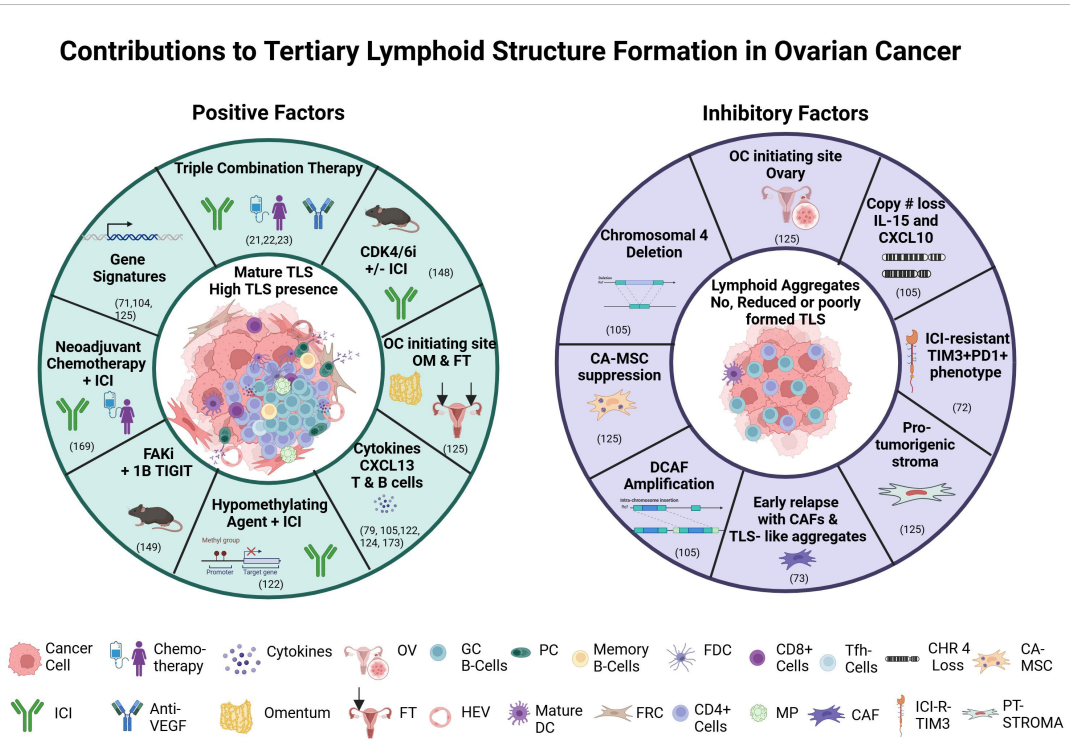

FIGURE 2
Factors contributing to or inhibiting tertiary lymphoid structure formation. Abbreviations: anti-PD-L1, Programmed death ligand 1; CDK 4/6i, cyclin dependent kinase 4/6 inhibitor; CAF, cancer associated fibroblasts; CA-MSC, cancer-educated mesenchymal stem cell; CHR 4, chromosome 4 loss; DC, dendritic cell; FAKi, focal adhesion kinase inhibitor; FDC, follicular dendritic cell; FRC, fibroblastic reticular cell; FT, fallopian tube; GC B-cells, germinal center B cells; HEV, high endothelial venule; ICI, immune checkpoint inhibitor; ICI-R-TIM3, ICI-Resistant TIM3; MP, macrophage; OM, omentum; OC, ovarian cancer; OV, ovary; PC, plasma cell; PT-STOMA, pro-tumorigenic stroma; TIGITi, T cell immunoreceptor with Ig and ITIM domain inhibitor; TIM3, T cell immunoglobulin and mucin domain 3;TLS, tertiary lymphoid structures; VEGF, vascular endothelial growth factor. Figure generated with BioRender.com.

Additional IL-15 or IL-15 super agonist complexes (N-803 or ALT-803) also promoted proliferation of NK cells with additional secreted factors including TNFα, CXCL10, and CD107a, which may enhance the function of NK cells (132, 136, 137). Only a limited number of OC patients have been treated clinically with NK ACT (138, 139), with some patients achieving stable disease with mild side effects (139). Several pre-clinical NK studies propose strategies to maximize effects of NK ACT including genetic modifications, combination therapy with ICI, targeted therapies, cytokines, and CAR-NK constructs, which currently are in early phase clinical trials (140)

Therapeutic strategies to induce TLS

Because TLS appears to play a major role in the anti-tumor response, identifying ways to induce TLS appears to be an important strategy. Vaccination contributes to induction of TLS and T cell infiltration as evidenced in pancreatic and cervical cancer. For example, in pancreatic adenocarcinoma patients with GM-CSF secreting allogeneic vaccine (GVAX) +/- a single IV dose of daily oral cyclophosphamide, eighty-five percent of post-vaccination tumor specimens contained histologic evidence of TLS formation not observed pre-vaccination. T cell infiltration and TLS development occurred in TME, with five signaling pathways involved in regulating immune-cell activation and trafficking associated with improved postvaccination responses differentially expressed, including genes encoding integrins, chemokines/chemokine receptors, and members of the ubiquitin-proteasome system and NK-kappa B pathway (141). In cervical cancer patients, intramuscular injection of a vaccine against HPV16E6/E7 induced TLS (142). This suggests that TLS formation may be needed for optimal vaccine response, since cancer vaccines often have limited efficacy, but also vaccination may be a strategy to induce TLS formation.

Oncolytic virotherapy has been proposed to induce TLS especially with immune checkpoint blockade (ICB) to amplify antitumor immune responses to patients with cancer (143). Because many tumors do not form functional TLS structures, “designer LN” have been proposed via injection of genetically modified immune cells in biomaterial scaffolds (65). The success of bioengineered lymph structures may depend on cellular properties for effective migration, hydrostatic fluid pressures for regulation of lymph flow and extravasation, as well as safety for cancer patients (144).

TLS in murine models

Several murine models suggest key players and potential strategies for the induction of TLS or new therapeutic strategies +/- immunotherapy. He et al., 2022 (145) have shown an oncolytic adenovirus carrying mIL-15 effectively facilitated activation and infiltration of DC, T, and NK cells into the TME, and induced TLS and vascular normalization. This mechanism appears to be through induced activation of the STING-TBK1-IRF3 pathway in DCs, and not traditional pathways of TLS induction. IKZF1, a gene related to the development of OC, melanoma, breast, and liver cancer, has been proposed to be a key driver of the formation of immature TLS (146). Using CRISPR/Cas9 gene editing to generate novel ID8 derivatives that harbor single and double suppressor gene mutations ($Trp53^{-/-}$ or $Trp53^{-/-}$; $Brca2^{-/-}$) in HGSOC, slower orthotopic tumor growth was observed in the double mutant compared to $Trp53^{-/-}$, with rich intra-tumoral TLS in $CD3^+$ T cells (146). TGF-Beta mediated silencing of genomic organizer SATB1 promoted Tfh cell differentiation and formation of intra-tumoral TLS, providing additional insight into how TLS are generated within tumors (82). Accumulated tumor antigen-specific $LIGHT^+CXCL13^+IL\text{-}21^+$ Tfh cells and TLS decreased tumor growth in a $CD4^+$ T cell and CXCL13-dependent manner (82).

Finally, two murine studies that are TLS-driven may offer new therapeutic strategies for OC patients. Cdk4/6 inhibitors (CDK4/6i) promoted TLS formation and enhanced the immunotherapeutic effect of anti-PD-1 when used in combination. TLS were associated with a favorable prognosis following CDK4/6i treatment, which may provide a therapeutic option for OC patients when used either alone, or in combination with anti-PD-1 therapy (147). A second study used an oral, small molecule focal adhesion kinase (FAK) inhibitor, FAKi (VS-4718), alone, and in combination with a blocking antibody to the checkpoint protein T cell immunoglobulin and ITIM domain (TIGIT), an inhibitory receptor expressed on lymphocytes that interacts with CD155 expressed on APC or tumor cells to down-regulate T cell and NK cell functions. Using a Kras, Myc, FAK (KMF) syngeneic ovarian tumor mouse model, decreased tumor burden, suppressed ascites KMF-associated CD155/Polio Virus Receptor (PVR) levels, and increased peritoneal TILs were observed with blocked FAK activity. FAKi combined with the 1B4 TIGIT blocking antibody maintained elevated TIL levels, reduced $TIGIT^+$ T reg cell levels, prolonged host survival, increased CXCL13 levels, and led to omental TLS formation. These results provide a rationale, especially considering different anatomical sites of OC origin playing a role in humoral and cellular immunity, conducting a FAKi/TIGIT blocking antibody pilot in HGSOC patients (148).

Influence of the gut microbiome on TLS formation and generation of antitumor immunity

Another inducer of TLS is the gut microbiome, which appears to play a role in modulating the host response to ICI. The microbiome, comprised of trillions of microorganisms lives in a symbiotic relationship with human hosts (149), and actively regulates aspects of host physiology, including immunity (150). The human gut microbiome appears to be associated with TLS, B cells, and the antitumor response (151–153), although the exact mechanism still needs to be elucidated. Advances in identifying potential important bacteria in the microbiome are due to culture-independent genomic sequencing (e.g., 16S rRNA sequencing) at the species and strain level (154). Recently, *Helicobacter hepaticus*, a single immunogenic commensal bacterium, controlled growth in a

carcinogen-induced orthotopic CRC mouse model, challenging the premise multiple immune-potentiating microbes are required to shift the host immune system towards potent antitumor immune responses. Generated bacteria-specific $CD4^+$ Tfh cells stimulated TLS formation within the tumor and surrounding areas, leading to increased tumor immune infiltration and reduced tumor burden (155). This manipulation at a single taxa level was sufficient to generate robust anti-tumor immunity and TLS formation. TLS induction has also been found in a retrospective study of 60 HCC cases which showed that in an intratumoral TLS group, Lachnoclostridium, Hungatella, Blautia, Gusobacterium, and Clostridium were increased (156).

The gut microbiome is also associated with clinical responses to anti-PD-1 immunotherapy in a variety of cancers (155, 157–163), however, no common overall microbial signal or metabolomic profile has been identified, even within cancers, indicating additional factors must be at play. Higher alpha diversity associated with longer PFS (151) (157) (162), and abundance of specific species has been observed. In melanoma, higher microbial community richness is associated with longer PFS, and abundance of specific Bacteroides species (Ruminococcus gnavus), while the Blautia producta strain is related to shorter PFS (162). PFS also correlated to metatranscriptomic expression of risk-associated pathways of L-rhamnose degradation, guanosine nucleotide biosynthesis, and B vitamin biosynthesis. Higher relative abundance of Ruminococcaceae family of bacteria were also found in melanoma R, as well as anabolic pathway enrichment and enhanced systemic and antitumor immunity, mediated by increased antigen presentation and improved effector T-cell function in the periphery and TME (151).

In two NSCLC studies, patients with high microbiome diversity at baseline (and throughout), had significantly prolonged PFS compared to those with low diversity, and also had a greater frequency of unique memory $CD8^+$ T cell and NK cell subsets in the periphery, suggesting a strong association between gut microbiome diversity and specific immune-related systemic populations (157). In clinical response to anti-PD-1/PD-L1 in advanced-stage gastrointestinal (GI) cancer, an elevated Prevotella/Bacteroides ratio was observed in R. A differential abundance of pathways related to nucleoside and nucleotide biosynthesis, lipid biosynthesis, sugar metabolism, and fermentation to short-chain fatty acids (SCFA) was identified in patients' samples exhibiting differential responses. Gut bacteria associated with SCFA production, including Eubacterium, Lactobacillus, and Streptococcus, were positively associated with anti-PD-1/PD-L1 response across different GI cancer types (161).

The gut microbiome of durable R was enriched for *Akkermansia muciniphila* and *Ruminococcaceae* species in HCC patients treated with anti-PD-1 therapy. In hepatobiliary cancers, seventy-four specific taxa, including Lachnospiraceae bacterium-GAM79 and Alistipes sp Marseille-P5997, were significantly enriched in the CBR group, which achieved longer PFS and OS than patients with lower bacterial abundance (158) and the CBR group was associated with energy metabolism. These bacterial, metabolomic, and immune signatures are potential biomarkers to explore in OC patients treated with immunotherapy. Recently, specific bacteria were identified, including Intestinimonas butyriciproducens and Anaerotignum propionicum (Clostridium propionicum), that were highly abundant both before and after treatment for OC patients that achieved DCB following a triple combination therapy (23). These butyrate-producing bacteria have previously been associated with an enhanced response to immunotherapy (164), and increases of these bacteria in the triple combination therapy were also linked to increased immune and TLS changes in the TME. These results may generate signatures for R and NR of specific combination therapies.

While such findings are encouraging, additional studies, including an improved understanding of the microbiome and metabolic pathways, are needed to delineate nuances of a patient's likelihood to respond to ICI therapy (163), as well as to drive TLS formation. Opportunities exist for immunomodulation through dietary and gut microbial interventions (165). Manipulating the presence of different bacterial species or metabolic pathways/metabolites, with interventions such as fecal transplants, probiotic use, microbial antigens or proteins, and selective antibiotics, may generate TLS and more favorable patient outcomes using immunotherapeutic approaches.

Conclusion and future directions

Understanding the complex roles of TLS within the TME is vital for improving therapeutic outcome for cancer patients, especially for those with limited treatment options at late-stage disease, as is the case with OC patients. Unlike SLO which develop during embryogenesis, TLS develop in response to chronic inflammation and cancer, playing a crucial role in antitumor immunity by enhancing both humoral and cellular responses. Their presence, especially in intratumoral areas, has been linked to better outcomes following immunotherapy, indicating their potential as a predictive biomarker for treatment success. Determining how these biomarkers may be mechanistically linked to therapeutic response likely depends on several factors including the type of therapeutic intervention (chemotherapy, ICI, radiation, vaccine-based, ACT-based, chemokine strategies, etc.), single agent or combination therapies, sequence of combination drug administration, timepoints for biospecimen collection (Baseline, on treatment, end of treatment), TLS location and density, anatomical site, and specific cancer type. Further, these factors may differ between preclinical models and real-world settings, further complicating data interpretation and integration. Therefore, additional studies to validate TLS as a reliable biomarker for therapeutic response in OC will provide additional insights and guide future applications.

In the case of OC, several factors recently have been implicated that contribute to the complexity of the role of TLS. The anatomical site of origin of OC may contribute to not only the role that TLS play, but their potential as a biomarker for response to therapy. Cancers that develop in the OV appear to have less TLS, less B cells, and a reduced antitumor response, while TLS that originate in the FT or OM have increased TLS and more B cells, suggestive that the TME is more supportive of TLS formation and indicative of an

antitumor response (125). These results not only suggest the importance of B cells in the antitumor response, but also suggest the OV has a more suppressive TME. In fact, CA-MSC present in the OV negatively impacts adaptive immunity and survival. This poses an important area for future studies to identify ways to mitigate their impact and improve TLS formation, function, and antitumor response.

Research into TLS has highlighted their influence on the balance between promoting and inhibiting tumor growth, driven by factors such as patient demographics, tumor characteristics, environmental exposures, and previous treatments. The dynamic interplay between these factors and therapeutic interventions, as well as the gut microbiome's impact, points to the complexity of harnessing TLS for cancer therapy. While several means to induce TLS have been proposed, modulation of the microbiome through diet or probiotic efforts may be a low-cost way to affect immunity and response to ICI. Continued studies that assess fecal microbiome transplants may also be a viable option to enhance efficacy of ICI as more potential beneficial bacteria or pathways that contribute to OS in OC are identified (166).

Analysis of patients' samples who achieved a DCB in a triple combination therapy, which included pembrolizumab, uncovered a tumor-immune-gut axis influencing immunotherapy outcomes in OC (23). Assessment of fecal biospecimens revealed several metabolites were altered in samples from DCB and LCB patients. Metabolic alterations were observed in pathways that impact immune cell function. For example, fatty acids, amino acids, indole, and purine biosynthetic pathways were altered (23). While this study had only 40 patients (21), it suggests the immune milieu and host-microbiome can be leveraged to improve antitumor response in future immunotherapy trials. Omics results identified a target, CD40 (23), that is currently in clinical trial (NCT05231122) using a CD40 agonist in combination with pembrolizumab and bevacizumab. It also suggests that strategically combining different therapies (immunotherapy, chemotherapy, PARP inhibitors, adoptive cell therapies, targeted therapies) may lead to generation of TLS and improved OS. Radiation therapy and chemotherapy have been shown to generate TLS as well. Radiation impacts infiltration of T cells and maturation of DC cells which can help drive TLS formation and reshape the TME (167). A study has shown encouraging results where neoadjuvant chemotherapy (paclitaxel and carboplatin) induced TLS formation in HGSOC suggesting that it may be used in combination with ICI to drive an anti-tumor response with increased TLS formation (168).

Several next step options to drive TLS may be through promising OC murine pre-clinical models such as the combination of cdki with ICI or use of FAK inhibitors +/- ICI. Additionally, combination therapies (ICI, chemotherapy, targeted therapy) that may modulate different components of the immune system may stimulate both the cellular and humoral response and provide a more robust DCB, as well as identify new therapeutic targets or pathways, potentially through multi-omics means. Vaccination strategies that may prime the immune response may also bolster an enhanced response through TLS generation as has been observed for PANC GM-CSF (GVAX) vaccination and HPV vaccination. CXCL13 approaches to introduce this powerful cytokine to drive TLS formation may also be a viable option in combination with ACT approaches. Finally, transcriptional assessment of different genes that may drive TLS formation may also prove to be beneficial in predicting a patient's response by biospecimen analysis at baseline or over the course of treatment.

Advancing our knowledge of TLS, particularly in OC, and the factors affecting therapeutic response is critical. Future efforts focusing on exploiting TLS to improve immune infiltration, boost anti-tumor responses, and enhance patient responses to treatment, promise significant impact on cancer therapy optimization.

Author contributions

AV: Writing – review & editing, Writing – original draft. SH: Writing – review & editing. SC: Writing – original draft, Writing – review & editing. JC-G: Conceptualization, Writing – review & editing. AM: Writing – review & editing. EZ: Conceptualization, Methodology, Supervision, Writing – review & editing.

Funding

The author(s) declare that no financial support was received for the research and/or publication of this article.

Acknowledgments

Figure 1 printed with permission from the Roswell Park Comprehensive Cancer Center, ATLAS Program. Figure 2 was created using BioRender.com and has been included under publication license granted to Suzanne M. Hess, PhD.

Conflict of interest

The authors declare that the research was conducted in the absence of any commercial or financial relationships that could be construed as a potential conflict of interest.

Publisher's note

References

1. Lehrer EJ, Stoltzfus KC, Jones BM, Gusani NJ, Walter V, Wang M, et al. Trends in diagnosis and treatment of metastatic cancer in the United States. *Am J Clin Oncol.* (2021) 44:572–9. doi: 10.1097/COC.0000000000000866

2. Armstrong DK, Alvarez RD, Backes FJ, Bakkum-Gamez JN, Barroilhet L, Behbakht K, et al. NCCN guidelines(R) insights: ovarian cancer, version 3. *2022. J Natl Compr Canc Netw.* (2022) 20:972–80. doi: 10.6004/jnccn.2022.0047

3. Zhang L, Conejo-Garcia JR, Katsaros D, Gimotty PA, Massobrio M, Regnani G, et al. Intratumoral T cells, recurrence, and survival in epithelial ovarian cancer. *N Engl J Med.* (2003) 348:203–13. doi: 10.1056/NEJMoa020177

4. Sato E, Olson SH, Ahn J, Bundy B, Nishikawa H, Qian F, et al. Intraepithelial CD8 + tumor-infiltrating lymphocytes and a high CD8+/regulatory T cell ratio are associated with favorable prognosis in ovarian cancer. *Proc Natl Acad Sci U S A.* (2005) 102:18538–43. doi: 10.1073/pnas.0509182102

5. Kalli KR, Krco CJ, Hartmann LC, Goodman K, Maurer MJ, Yu C, et al. An HLA-DR-degenerate epitope pool detects insulin-like growth factor binding protein 2-specific immunity in patients with cancer. *Cancer Res.* (2008) 68:4893–901. doi: 10.1158/0008-5472.CAN-07-6726

6. Knutson KL, Krco CJ, Erskine CL, Goodman K, Kelemen LE, Wettstein PJ, et al. T-cell immunity to the folate receptor alpha is prevalent in women with breast or ovarian cancer. *J Clin Oncol.* (2006) 24:4254–61. doi: 10.1200/JCO.2006.05.9311

7. Reuschenbach M, von Knebel Doeberitz M, Wentzensen N. A systematic review of humoral immune responses against tumor antigens. *Cancer Immunol Immunother.* (2009) 58:1535–44. doi: 10.1007/s00262-009-0733-4

8. Milne K, Barnes RO, Girardin A, Mawer MA, Nesslinger NJ, Ng A, et al. Tumor-infiltrating T cells correlate with NY-ESO-1-specific autoantibodies in ovarian cancer. *PLoS One.* (2008) 3:e3409. doi: 10.1371/journal.pone.0003409

9. Zhao J, Xu Z, Liu Y, Wang X, Liu X, Gao Y, et al. The expression of cancer-testis antigen in ovarian cancer and the development of immunotherapy. *Am J Cancer Res.* (2022) 12:681–94.

10. Takai N, Miyazaki T, Nishida M, Nasu K, Miyakawa I. Expression of survivin is associated with Malignant potential in epithelial ovarian carcinoma. *Int J Mol Med.* (2002) 10:211–6. doi: 10.3892/ijmm.10.2.211

11. Wang L, Ma J, Liu F, Yu Q, Chu G, Perkins AC, et al. Expression of MUC1 in primary and metastatic human epithelial ovarian cancer and its therapeutic significance. *Gynecol Oncol.* (2007) 105:695–702. doi: 10.1016/j.ygyno.2007.02.004

12. Vermeij R, de Bock GH, Leffers N, Ten Hoor KA, Schulze U, Hollema H, et al. Tumor-infiltrating cytotoxic T lymphocytes as independent prognostic factor in epithelial ovarian cancer with wilms tumor protein 1 overexpression. *J Immunother.* (2011) 34:516–23. doi: 10.1097/CJI.0b013e31821e012f

13. Motz GT, Santoro SP, Wang LP, Garrabrant T, Lastra RR, Hagemann IS, et al. Tumor endothelium FasL establishes a selective immune barrier promoting tolerance in tumors. *Nat medicine.* (2014) 20:607–15. doi: 10.1038/nm.3541

14. Mukai S, Kjaergaard J, Shu S, Plautz GE. Infiltration of tumors by systemically transferred tumor-reactive T lymphocytes is required for antitumor efficacy. *Cancer Res.* (1999) 59:5245–9.

15. Springer TA. Traffic signals for lymphocyte recirculation and leukocyte emigration: the multistep paradigm. *Cell.* (1994) 76:301–14. doi: 10.1016/0092-8674(94)90337-9

16. Brahmer JR, Tykodi SS, Chow LQ, Hwu WJ, Topalian SL, Hwu P, et al. Safety and activity of anti-PD-L1 antibody in patients with advanced cancer. *N Engl J Med.* (2012) 366:2455–65. doi: 10.1056/NEJMoa1200694

17. Hamanishi J, Mandai M, Ikeda T, Minami M, Kawaguchi A, Murayama T, et al. Safety and antitumor activity of anti-PD-1 antibody, nivolumab, in patients with platinum-resistant ovarian cancer. *J Clin Oncol.* (2015) 33:4015–22. doi: 10.1200/JCO.2015.62.3397

18. Matulonis UA, Shapira-Frommer R, Santin AD, Lisyanskaya AS, Pignata S, Vergote I, et al. Antitumor activity and safety of pembrolizumab in patients with advanced recurrent ovarian cancer: results from the phase II KEYNOTE-100 study. *Ann Oncol.* (2019) 30:1080–7. doi: 10.1093/annonc/mdz135

19. Gonzalez-Martin A, Sanchez-Lorenzo L. Immunotherapy with checkpoint inhibitors in patients with ovarian cancer: Still promising? *Cancer.* (2019) 125 Suppl 24:4616–22. doi: 10.1002/cncr.v125.s24

20. Ghisoni E, Morotti M, Sarivalasis A, Grimm AJ, Kandalaft L, Laniti DD, et al. Immunotherapy for ovarian cancer: towards a tailored immunophenotype-based approach. *Nat Rev Clin Oncol.* (2024) 21(11):801–7. doi: 10.1038/s41571-024-00937-4

21. Zsiros E, Lynam S, Attwood KM, Wang C, Chilakapati S, Gomez EC, et al. Efficacy and safety of pembrolizumab in combination with bevacizumab and oral metronomic cyclophosphamide in the treatment of recurrent ovarian cancer: A phase 2 nonrandomized clinical trial. *JAMA Oncol.* (2021) 7:78–85. doi: 10.1001/jamaoncol.2020.5945

22. Gaulin N, Chilakapati SR, Zsiros E. Turning cold into hot: combination of pembrolizumab with bevacizumab and oral metronomic cyclophosphamide increases immune cell migration into the tumor microenvironment in responding patients with recurrent ovarian cancer (090). *Gynecologic Oncology.* (2022) 166:S61. doi: 10.1016/S0090-8258(22)01316-6

23. Rosario SR, Long MD, Chilakapati S, Gomez EC, Battaglia S, Singh PK, et al. Integrative multi-omics analysis uncovers tumor-immune-gut axis influencing immunotherapy outcomes in ovarian cancer. *Nat Commun.* (2024) 15:10609. doi: 10.1038/s41467-024-54565-8

24. Liu JF, Herold C, Gray KP, Penson RT, Horowitz N, Konstantinopoulos PA, et al. Assessment of combined nivolumab and bevacizumab in relapsed ovarian cancer: A phase 2 clinical trial. *JAMA Oncol.* (2019) 5:1731–8. doi: 10.1001/jamaoncol.2019.3343

25. Garcia AA, Hirte H, Fleming G, Yang D, Tsao-Wei DD, Roman L, et al. Phase II clinical trial of bevacizumab and low-dose metronomic oral cyclophosphamide in recurrent ovarian cancer: a trial of the California, Chicago, and Princess Margaret Hospital phase II consortia. *J Clin Oncol.* (2008) 26:76–82. doi: 10.1200/JCO.2007.12.1939

26. Walsh CS, Kamrava M, Rogatko A, Kim S, Li A, Cass I, et al. Phase II trial of cisplatin, gemcitabine and pembrolizumab for platinum-resistant ovarian cancer. *PLoS One.* (2021) 16:e0252665. doi: 10.1371/journal.pone.0252665

27. Curiel TJ, Coukos G, Zou L, Alvarez X, Cheng P, Mottram P, et al. Specific recruitment of regulatory T cells in ovarian carcinoma fosters immune privilege and predicts reduced survival. *Nat medicine.* (2004) 10:942–9. doi: 10.1038/nm1093

28. Kryczek I, Wei S, Zhu G, Myers L, Mottram P, Cheng P, et al. Relationship between B7-H4, regulatory T cells, and patient outcome in human ovarian carcinoma. *Cancer Res.* (2007) 67:8900–5. doi: 10.1158/0008-5472.CAN-07-1866

29. Garlisi B, Lauks S, Aitken C, Ogilvie LM, Lockington C, Petrik D, et al. The complex tumor microenvironment in ovarian cancer: therapeutic challenges and opportunities. *Curr Oncol.* (2024) 31:3826–44. doi: 10.3390/curroncol31070283

30. Yarchoan M, Hopkins A, Jaffee EM. Tumor mutational burden and response rate to PD-1 inhibition. *N Engl J Med.* (2017) 377:2500–1. doi: 10.1056/NEJMc1713444

31. Cornel AM, Mimpen IL, Nierkens S. MHC class I downregulation in cancer: underlying mechanisms and potential targets for cancer immunotherapy. *Cancers (Basel).* (2020) 12(7):1760–91. doi: 10.3390/cancers12071760

32. Chae CS, Sandoval TA, Hwang SM, Park ES, Giovanelli P, Awasthi D, et al. Tumor-derived lysophosphatidic acid blunts protective type I interferon responses in ovarian cancer. *Cancer Discov.* (2022) 12:1904–21. doi: 10.1158/2159-8290.CD-21-1181

33. Singel KL, Emmons TR, Khan ANH, Mayor PC, Shen S, Wong JT, et al. Mature neutrophils suppress T cell immunity in ovarian cancer microenvironment. *JCI Insight.* (2019) 4(5):e122311. doi: 10.1172/jci.insight.122311

34. Emmons TR, Giridharan T, Singel KL, Khan ANH, Ricciuti J, Howard K, et al. Mechanisms driving neutrophil-induced T-cell immunoparalysis in ovarian cancer. *Cancer Immunol Res.* (2021) 9:790–810. doi: 10.1158/2326-6066.CIR-20-0922

35. Song M, Sandoval TA, Chae CS, Chopra S, Tan C, Rutkowski MR, et al. IRE1alpha-XBP1 controls T cell function in ovarian cancer by regulating mitochondrial activity. *Nature.* (2018) 562:423–8. doi: 10.1038/s41586-018-0597-x

36. Kelleher RJ Jr., Balu-Iyer S, Loyall J, Sacca AJ, Shenoy GN, Peng P, et al. Extracellular vesicles present in human ovarian tumor microenvironments induce a phosphatidylserine-dependent arrest in the T-cell signaling cascade. *Cancer Immunol Res.* (2015) 3:1269–78. doi: 10.1158/2326-6066.CIR-15-0086

37. Walton J, Blagih J, Ennis D, Leung E, Dowson S, Farquharson M, et al. CRISPR/cas9-mediated trp53 and brca2 knockout to generate improved murine models of ovarian high-grade serous carcinoma. *Cancer Res.* (2016) 76:6118–29. doi: 10.1158/0008-5472.CAN-16-1272

38. Kobayashi Y, Lim SO, Yamaguchi H. Oncogenic signaling pathways associated with immune evasion and resistance to immune checkpoint inhibitors in cancer. *Semin Cancer Biol.* (2020) 65:51–64. doi: 10.1016/j.semcancer.2019.11.011

39. Johnson RL, Cummings M, Thangavelu A, Theophilou G, de Jong D, Orsi NM. Barriers to immunotherapy in ovarian cancer: metabolic, genomic, and immune perturbations in the tumour microenvironment. *Cancers (Basel).* (2021) 13(24):6231–79. doi: 10.3390/cancers13246231

40. Husain Z, Huang Y, Seth P, Sukhatme VP. Tumor-derived lactate modifies antitumor immune response: effect on myeloid-derived suppressor cells and NK cells. *J Immunol.* (2013) 191:1486–95. doi: 10.4049/jimmunol.1202702

41. Amobi-McCloud A, Muthuswamy R, Battaglia S, Yu H, Liu T, Wang J, et al. IDO1 expression in ovarian cancer induces PD-1 in T cells via aryl hydrocarbon receptor activation. *Front Immunol.* (2021) 12:678999. doi: 10.3389/fimmu.2021.678999

42. Mellor AL, Munn DH. Tryptophan catabolism and T-cell tolerance: immunosuppression by starvation? *Immunol Today.* (1999) 20:469–73. doi: 10.1016/s0167-5699(99)01520-0

43. Schaaf MB, Garg AD, Agostinis P. Defining the role of the tumor vasculature in antitumor immunity and immunotherapy. *Cell Death Dis.* (2018) 9:115. doi: 10.1038/s41419-017-0061-0

44. Kandalaft LE, Odunsi K, Coukos G. Immunotherapy in ovarian cancer: are we there yet? *J Clin Oncol*. (2019) 37:2460–71. doi: 10.1200/JCO.19.00508

45. Huang RY, Francois A, McGray AR, Miliotto A, Odunsi K. Compensatory upregulation of PD-1, LAG-3, and CTLA-4 limits the efficacy of single-agent checkpoint blockade in metastatic ovarian cancer. *Oncoimmunology*. (2017) 6: e1249561. doi: 10.1080/2162402X.2016.1249561

46. Colbeck EJ, Ager A, Gallimore A, Jones GW. Tertiary lymphoid structures in cancer: drivers of antitumor immunity, immunosuppression, or bystander sentinels in disease? *Front Immunol*. (2017) 8:1830. doi: 10.3389/fimmu.2017.01830

47. Sun G, Liu Y. Tertiary lymphoid structures in ovarian cancer. *Front Immunol*. (2024) 15:1465516. doi: 10.3389/fimmu.2024.1465516

48. Asam S, Nayar S, Gardner D, Barone F. Stromal cells in tertiary lymphoid structures: Architects of autoimmunity. *Immunol Rev*. (2021) 302:184–95. doi: 10.1111/imr.v302.1

49. Buckley CD, Barone F, Nayar S, Bénézech C, Caamaño J. Stromal cells in chronic inflammation and tertiary lymphoid organ formation. *Annu Rev Immunol*. (2015) 33:715–45. doi: 10.1146/annurev-immunol-032713-120252

50. Mauri C, Menon M. The expanding family of regulatory B cells. *Int Immunol*. (2015) 27:479–86. doi: 10.1093/intimm/dxv038

51. Pitzalis C, Jones GW, Bombardieri M, Jones SA. Ectopic lymphoid-like structures in infection, cancer and autoimmunity. *Nat Rev Immunol*. (2014) 14:447–62. doi: 10.1038/nri3700

52. Sato Y, Silina K, van den Broek M, Hirahara K, Yanagita M. The roles of tertiary lymphoid structures in chronic diseases. *Nat Rev Nephrol*. (2023) 19:525–37. doi: 10.1038/s41581-023-00706-z

53. Pers JO, Le Pottier L, Devauchelle V, Saraux A, Youinou P. B lymphocytes in Sjogren's syndrome. *Rev Med Interne*. (2008) 29:1000–6. doi: 10.1016/j.revmed.2008.01.018

54. Chang A, Henderson SG, Brandt D, Liu N, Guttikonda R, Hsieh C, et al. *In situ* B cell-mediated immune responses and tubulointerstitial inflammation in human lupus nephritis. *J Immunol*. (2011) 186:1849–60. doi: 10.4049/jimmunol.1001983

55. Korpos E, Kadri N, Loismann S, Findeisen CR, Arfuso F, Burke GW 3rd, et al. Identification and characterisation of tertiary lymphoid organs in human type 1 diabetes. *Diabetologia*. (2021) 64:1626–41. doi: 10.1007/s00125-021-05453-z

56. Gomez-Nguyen A, Gupta N, Sanaka H, Gruszka D, Pizarro A, DiMartino L, et al. Chronic stress induces colonic tertiary lymphoid organ formation and protection against secondary injury through IL-23/IL-22 signaling. *Proc Natl Acad Sci U S A*. (2022) 119:e2208160119. doi: 10.1073/pnas.2208160119

57. Takemura S, Braun A, Crowson C, Kurtin PJ, Cofield RH, O'Fallon WM, et al. Lymphoid neogenesis in rheumatoid synovitis. *J Immunol*. (2001) 167:1072–80. doi: 10.4049/jimmunol.167.2.1072

58. Nayar S, Turner JD, Asam S, Fennell E, Pugh M, ColaFrancesco S, et al. Molecular and spatial analysis of tertiary lymphoid structures in Sjogren's syndrome. *Nat Commun*. (2025) 16:5. doi: 10.1038/s41467-024-54686-0

59. Nayar S, Campos J, Smith CG, Iannizzotto V, Gardner DH, Mourcin F, et al. Immunofibroblasts are pivotal drivers of tertiary lymphoid structure formation and local pathology. *Proc Natl Acad Sci U S A*. (2019) 116:13490–7. doi: 10.1073/pnas.1905301116

60. Ruddle NH. High endothelial venules and lymphatic vessels in tertiary lymphoid organs: characteristics, functions, and regulation. *Front Immunol*. (2016) 7:491. doi: 10.3389/fimmu.2016.00491

61. Sautes-Fridman C, Verneau J, Sun CM, Moreira M, Chen TW, Meylan M, et al. Tertiary Lymphoid Structures and B cells: Clinical impact and therapeutic modulation in cancer. *Semin Immunol*. (2020) 48:101406. doi: 10.1016/j.smim.2020.101406

62. Zhao L, Jin S, Wang S, Zhang Z, Wang X, Chen Z, et al. Tertiary lymphoid structures in diseases: immune mechanisms and therapeutic advances. *Signal Transduct Target Ther*. (2024) 9:225. doi: 10.1038/s41392-024-01947-5

63. Sautès-Fridman C, Petitprez F, Calderaro J, Fridman WH. Tertiary lymphoid structures in the era of cancer immunotherapy. *Nat Rev Cancer*. (2019) 19:307–25. doi: 10.1038/s41568-019-0144-6

64. Johansson-Percival A, He B, Li ZJ, Kjellén A, Russell K, Li J, et al. *De novo* induction of intratumoral lymphoid structures and vessel normalization enhances immunotherapy in resistant tumors. *Nat Immunol*. (2017) 18:1207–17. doi: 10.1038/ni.3836

65. Zhu G, Falahat R, Wang K, Mailloux A, Artzi N, Mulé JJ. Tumor-associated tertiary lymphoid structures: gene-expression profiling and their bioengineering. *Front Immunol*. (2017) 8:767. doi: 10.3389/fimmu.2017.00767

66. Fridman WH, Siberil S, Pupier G, Soussan S, Sautes-Fridman C. Activation of B cells in Tertiary Lymphoid Structures in cancer: Anti-tumor or anti-self? *Semin Immunol*. (2023) 65:101703. doi: 10.1016/j.smim.2022.101703

67. Chen Y, Wu Y, Yan G, Zhang G. Tertiary lymphoid structures in cancer: maturation and induction. *Front Immunol*. (2024) 15:1369626. doi: 10.3389/fimmu.2024.1369626

68. Vanhersecke L, Brunet M, Guegan JP, Rey C, Bougouin A, Cousin S, et al. Mature tertiary lymphoid structures predict immune checkpoint inhibitor efficacy in solid tumors independently of PD-L1 expression. *Nat Cancer*. (2021) 2:794–802. doi: 10.1038/s43018-021-00232-6

69. Teillaud JL, Houel A, Panouillot M, Riffard C, Dieu-Nosjean MC. Tertiary lymphoid structures in anticancer immunity. *Nat Rev Cancer*. (2024) 24:629–46. doi: 10.1038/s41568-024-00728-0

70. Vanhersecke L, Bougouin A, Crombe A, Brunet M, Sofeu C, Parrens M, et al. Standardized pathology screening of mature tertiary lymphoid structures in cancers. *Lab Invest*. (2023) 103:100063. doi: 10.1016/j.labinv.2023.100063

71. Zhang K, Xie X, Zheng SL, Deng YR, Liao D, Yan HC, et al. Tertiary lymphoid structures in gynecological cancers: prognostic role, methods for evaluating, antitumor immunity, and induction for therapy. *Front Oncol*. (2023) 13:1276907. doi: 10.3389/fonc.2023.1276907

72. Kasikova L, Rakova J, Hensler M, Lanickova T, Tomankova J, Pasulka J, et al. Tertiary lymphoid structures and B cells determine clinically relevant T cell phenotypes in ovarian cancer. *Nat Commun*. (2024) 15:2528. doi: 10.1038/s41467-024-46873-w

73. Xu AM, Haro M, Walts AE, Hu Y, John J, Karlan BY, et al. Spatiotemporal architecture of immune cells and cancer-associated fibroblasts in high-grade serous ovarian carcinoma. *Sci Adv*. (2024) 10:eadk8805. doi: 10.1126/sciadv.adk8805

74. van de Pavert SA. Lymphoid Tissue inducer (LTi) cell ontogeny and functioning in embryo and adult. *BioMed J*. (2021) 44:123–32. doi: 10.1016/j.bj.2020.12.003

75. Randall TD, Carragher DM, Rangel-Moreno J. Development of secondary lymphoid organs. *Annu Rev Immunol*. (2008) 26:627–50. doi: 10.1146/annurev.immunol.26.021607.090257

76. van de Pavert SA, Mebius RE. New insights into the development of lymphoid tissues. *Nat Rev Immunol*. (2010) 10:664–74. doi: 10.1038/nri2832

77. Honda K, Nakano H, Yoshida H, Nishikawa S, Rennert P, Ikuta K, et al. Molecular basis for hematopoietic/mesenchymal interaction during initiation of Peyer's patch organogenesis. *J Exp Med*. (2001) 193:621–30. doi: 10.1084/jem.193.5.621

78. Schumacher TN, Thommen DS. Tertiary lymphoid structures in cancer. *Science*. (2022) 375:eabf9419. doi: 10.1126/science.abf9419

79. Ukita M, Hamanishi J, Yoshitomi H, Yamanoi K, Takamatsu S, Ueda A, et al. CXCL13-producing CD4+ T cells accumulate in the early phase of tertiary lymphoid structures in ovarian cancer. *JCI Insight*. (2022) 7(12):e157215. doi: 10.1172/jci.insight.157215

80. Lee Y, Chin RK, Christiansen P, Sun Y, Tumanov AV, Wang J, et al. Recruitment and activation of naive T cells in the islets by lymphotoxin beta receptor-dependent tertiary lymphoid structure. *Immunity*. (2006) 25:499–509. doi: 10.1016/j.immuni.2006.06.016

81. Lu TT, Browning JL. Role of the lymphotoxin/LIGHT system in the development and maintenance of reticular networks and vasculature in lymphoid tissues. *Front Immunol*. (2014) 5:47. doi: 10.3389/fimmu.2014.00047

82. Chaurio RA, Anadon CM, Lee Costich T, Payne KK, Biswas S, Harro CM, et al. TGF-beta-mediated silencing of genomic organizer SATB1 promotes Tfh cell differentiation and formation of intra-tumoral tertiary lymphoid structures. *Immunity*. (2022) 55:115–28.e9. doi: 10.1016/j.immuni.2021.12.007

83. Conejo-Garcia JR, Biswas S, Chaurio R, Rodriguez PC. Neglected no more: B cell-mediated anti-tumor immunity. *Semin Immunol*. (2023) 65:101707. doi: 10.1016/j.smim.2022.101707

84. Montfort A, Pearce O, Maniati E, Vincent BG, Bixby L, Bohm S, et al. A strong B-cell response is part of the immune landscape in human high-grade serous ovarian metastases. *Clin Cancer Res*. (2017) 23:250–62. doi: 10.1158/1078-0432.CCR-16-0081

85. Biswas S, Mandal G, Payne KK, Anadon CM, Gatenbee CD, Chaurio RA, et al. IgA transcytosis and antigen recognition govern ovarian cancer immunity. *Nature*. (2021) 591:464–70. doi: 10.1038/s41586-020-03144-0

86. Nielsen JS, Sahota RA, Milne K, Kost SE, Nesslinger NJ, Watson PH, et al. CD20 + tumor-infiltrating lymphocytes have an atypical CD27- memory phenotype and together with CD8+ T cells promote favorable prognosis in ovarian cancer. *Clin Cancer Res*. (2012) 18:3281–92. doi: 10.1158/1078-0432.CCR-12-0234

87. Khanal S, Wieland A, Gunderson AJ. Mechanisms of tertiary lymphoid structure formation: cooperation between inflammation and antigenicity. *Front Immunol*. (2023) 14:1267654. doi: 10.3389/fimmu.2023.1267654

88. van Rijthoven M, Obahor S, Pagliarulo F, van den Broek M, Schraml P, Moch H, et al. Multi-resolution deep learning characterizes tertiary lymphoid structures and their prognostic relevance in solid tumors. *Commun Med (Lond)*. (2024) 4:5. doi: 10.1038/s43856-023-00421-7

89. Lin JR, Wang S, Coy S, Chen YA, Yapp C, Tyler M, et al. Multiplexed 3D atlas of state transitions and immune interaction in colorectal cancer. *Cell*. (2023) 186:363–81.e19. doi: 10.1016/j.cell.2022.12.028

90. Walsh LA, Quail DF. Decoding the tumor microenvironment with spatial technologies. *Nat Immunol*. (2023) 24:1982–93. doi: 10.1038/s41590-023-01678-9

91. Gan X, Dong W, You W, Ding D, Yang Y, Sun D, et al. Spatial multimodal analysis revealed tertiary lymphoid structures as a risk stratification indicator in combined hepatocellular-cholangiocarcinoma. *Cancer Lett*. (2024) 581:216513. doi: 10.1016/j.canlet.2023.216513

92. Weed DT, Zilio S, McGee C, Marnissi B, Sargi Z, Franzmann E, et al. The tumor immune microenvironment architecture correlates with risk of recurrence in head and neck squamous cell carcinoma. *Cancer Res*. (2023) 83:3886–900. doi: 10.1158/0008-5472.CAN-23-0379

93. Li H, Lin WP, Zhang ZN, Sun ZJ. Tailoring biomaterials for monitoring and evoking tertiary lymphoid structures. *Acta Biomater*. (2023) 172:1–15. doi: 10.1016/j.actbio.2023.09.028

94. Yang M, Che Y, Li K, Fang Z, Li S, Wang M, et al. Detection and quantitative analysis of tumor-associated tertiary lymphoid structures. *J Zhejiang Univ Sci B*. (2023) 24:779–95. doi: 10.1631/jzus.B2200605

95. Xu Y, Li Z, Yang Y, Li L, Zhou Y, Ouyang J, et al. A CT-based radiomics approach to predict intra-tumoral tertiary lymphoid structures and recurrence of intrahepatic cholangiocarcinoma. *Insights Imaging*. (2023) 14:173. doi: 10.1186/s13244-023-01527-1

96. Yu Y, Yang T, Ma P, Zeng Y, Dai Y, Fu Y, et al. Determining the status of tertiary lymphoid structures in invasive pulmonary adenocarcinoma based on chest CT radiomic features. *Insights Imaging*. (2025) 16:28. doi: 10.1186/s13244-025-01906-w

97. Long S, Li M, Chen J, Zhong L, Dai G, Pan D, et al. Transfer learning radiomic model predicts intratumoral tertiary lymphoid structures in hepatocellular carcinoma: a multicenter study. *J Immunother Cancer*. (2025) 13(3):e011126. doi: 10.1136/jitc-2024-011126

98. Li K, Guo Q, Zhang X, Dong X, Liu W, Zhang A, et al. Oral cancer-associated tertiary lymphoid structures: gene expression profile and prognostic value. *Clin Exp Immunol*. (2020) 199:172–81. doi: 10.1111/cei.13389

99. Coppola D, Nebozhyn M, Khalil F, Dai H, Yeatman T, Loboda A, et al. Unique ectopic lymph node-like structures present in human primary colorectal carcinoma are identified by immune gene array profiling. *Am J Pathol*. (2011) 179:37–45. doi: 10.1016/j.ajpath.2011.03.007

100. Messina JL, Fenstermacher DA, Eschrich S, Qu X, Berglund AE, Lloyd MC, et al. 12-Chemokine gene signature identifies lymph node-like structures in melanoma: potential for patient selection for immunotherapy? *Sci Rep*. (2012) 2:765. doi: 10.1038/srep00765

101. Prabhakaran S, Rizk VT, Ma Z, Cheng CH, Berglund AE, Coppola D, et al. Evaluation of invasive breast cancer samples using a 12-chemokine gene expression score: correlation with clinical outcomes. *Breast Cancer Res*. (2017) 19:71. doi: 10.1186/s13058-017-0864-z

102. Zhang C, Kang Y, Miao P, Chang D. A novel genes-based signature with prognostic value and predictive ability to select patients responsive to Atezolizumab treatment in bladder cancer: an analysis on data from real-world studies. *Transl Cancer Res*. (2023) 12:2063–70. doi: 10.21037/tcr-23-220

103. Li R, Berglund A, Zemp L, Dhillon J, Putney R, Kim Y, et al. The 12-CK score: global measurement of tertiary lymphoid structures. *Front Immunol*. (2021) 12:694079. doi: 10.3389/fimmu.2021.694079

104. Hou Y, Qiao S, Li M, Han X, Wei X, Pang Y, et al. The gene signature of tertiary lymphoid structures within ovarian cancer predicts the prognosis and immunotherapy benefit. *Front Genet*. (2022) 13:1090640. doi: 10.3389/fgene.2022.1090640

105. Lu H, Lou H, Wengert G, Paudel R, Patel N, Desai S, et al. Tumor and local lymphoid tissue interaction determines prognosis in high-grade serous ovarian cancer. *Cell Rep Med*. (2023) 4:101092. doi: 10.1016/j.xcrm.2023.101092

106. Horeweg N, Workel HH, Loiero D, Church DN, Vermij L, Leon-Castillo A, et al. Tertiary lymphoid structures critical for prognosis in endometrial cancer patients. *Nat Commun*. (2022) 13:1373. doi: 10.1038/s41467-022-29040-x

107. Fridman WH, Meylan M, Petitprez F, Sun CM, Italiano A, Sautes-Fridman C. B cells and tertiary lymphoid structures as determinants of tumour immune contexture and clinical outcome. *Nat Rev Clin Oncol*. (2022) 19:441–57. doi: 10.1038/s41571-022-00619-z

108. Peyraud F, Guegan JP, Vanhersecke L, Brunet M, Teyssonneau D, Palmieri LJ, et al. Tertiary lymphoid structures and cancer immunotherapy: From bench to bedside. *Med*. (2025) 6:100546. doi: 10.1016/j.medj.2024.10.023

109. Amaria RN, Reddy SM, Tawbi HA, Davies MA, Ross MI, Glitza IC, et al. Neoadjuvant immune checkpoint blockade in high-risk resectable melanoma. *Nat Med*. (2018) 24:1649–54. doi: 10.1038/s41591-018-0197-1

110. Helmink BA, Reddy SM, Gao J, Zhang S, Basar R, Thakur R, et al. B cells and tertiary lymphoid structures promote immunotherapy response. *Nature*. (2020) 577:549–55. doi: 10.1038/s41586-019-1922-8

111. Cabrita R, Lauss M, Sanna A, Donia M, Skaarup Larsen M, Mitra S, et al. Tertiary lymphoid structures improve immunotherapy and survival in melanoma. *Nature*. (2020) 577:561–5. doi: 10.1038/s41586-019-1914-8

112. Petitprez F, de Reynies A, Keung EZ, Chen TW, Sun CM, Calderaro J, et al. B cells are associated with survival and immunotherapy response in sarcoma. *Nature*. (2020) 577:556–60. doi: 10.1038/s41586-019-1906-8

113. Italiano A, Bessede A, Pulido M, Bompas E, Piperno-Neumann S, Chevreau C, et al. Pembrolizumab in soft-tissue sarcomas with tertiary lymphoid structures: a phase 2 PEMBROSARC trial cohort. *Nat Med*. (2022) 28:1199–206. doi: 10.1038/s41591-022-01821-3

114. Patil NS, Nabet BY, Muller S, Koeppen H, Zou W, Giltnane J, et al. Intratumoral plasma cells predict outcomes to PD-L1 blockade in non-small cell lung cancer. *Cancer Cell*. (2022) 40:289–300.e4. doi: 10.1016/j.ccell.2022.02.002

115. Gao J, Navai N, Alhalabi O, Siefker-Radtke A, Campbell MT, Tidwell RS, et al. Neoadjuvant PD-L1 plus CTLA-4 blockade in patients with cisplatin-ineligible operable high-risk urothelial carcinoma. *Nat Med*. (2020) 26:1845–51. doi: 10.1038/s41591-020-1086-y

116. van Dijk N, Gil-Jimenez A, Silina K, Hendricksen K, Smit LA, de Feijter JM, et al. Preoperative ipilimumab plus nivolumab in locoregionally advanced urothelial cancer: the NABUCCO trial. *Nat Med*. (2020) 26:1839–44. doi: 10.1038/s41591-020-1085-z

117. van Dijk N, Gil-Jimenez A, Silina K, van Montfoort ML, Einerhand S, Jonkman L, et al. The tumor immune landscape and architecture of tertiary lymphoid structures in urothelial cancer. *Front Immunol*. (2021) 12:793964. doi: 10.3389/fimmu.2021.793964

118. Campbell MT, Matin SF, Tam AL, Sheth RA, Ahrar K, Tidwell RS, et al. Pilot study of Tremelimumab with and without cryoablation in patients with metastatic renal cell carcinoma. *Nat Commun*. (2021) 12:6375. doi: 10.1038/s41467-021-26415-4

119. Carril-Ajuria L, Desnoyer A, Meylan M, Dalban C, Naigeon M, Cassard L, et al. Baseline circulating unswitched memory B cells and B-cell related soluble factors are associated with overall survival in patients with clear cell renal cell carcinoma treated with nivolumab within the NIVOREN GETUG-AFU 26 study. *J Immunother Cancer*. (2022) 10(5):e004885. doi: 10.1136/jitc-2022-004885

120. Ho WJ, Zhu Q, Durham J, Popovic A, Xavier S, Leatherman J, et al. Neoadjuvant cabozantinib and nivolumab converts locally advanced HCC into resectable disease with enhanced antitumor immunity. *Nat Cancer*. (2021) 2:891–903. doi: 10.1038/s43018-021-00234-4

121. Nielsen JS, Nelson BH. Tumor-infiltrating B cells and T cells: Working together to promote patient survival. *Oncoimmunology*. (2012) 1:1623–5. doi: 10.4161/onci.21650

122. Chen S, Xie P, Cowan M, Huang H, Cardenas H, Keathley R, et al. Epigenetic priming enhances antitumor immunity in platinum-resistant ovarian cancer. *J Clin Invest*. (2022) 132(14):e158800. doi: 10.1172/JCI158800

123. Liu J, Berchuck A, Backes FJ, Cohen J, Grisham R, Leath CA, et al. NCCN guidelines(R) insights: ovarian cancer/fallopian tube cancer/primary peritoneal cancer, version 3.2024. *J Natl Compr Canc Netw*. (2024) 22:512–9. doi: 10.6004/jnccn.2024.0052

124. Yang M, Lu J, Zhang G, Wang Y, He M, Xu Q, et al. CXCL13 shapes immunoactive tumor microenvironment and enhances the efficacy of PD-1 checkpoint blockade in high-grade serous ovarian cancer. *J Immunother Cancer*. (2021) 9(1):e001136. doi: 10.1136/jitc-2020-001136

125. MacFawn IP, Magnon G, Gorecki G, Kunning S, Rashid R, Kaiza ME, et al. The activity of tertiary lymphoid structures in high grade serous ovarian cancer is governed by site, stroma, and cellular interactions. *Cancer Cell*. (2024) 42(11):1864–81.e5. doi: 10.1016/j.ccell.2024.09.007

126. Bod L. Finding the right friends: Stromal composition influences TLS formation in ovarian cancer. *Cancer Cell*. (2024) 42:1811–2. doi: 10.1016/j.ccell.2024.10.004

127. Fan H, Atiya HI, Wang Y, Pisanic TR, Wang TH, Shih IM, et al. Epigenomic reprogramming toward mesenchymal-epithelial transition in ovarian-cancer-associated mesenchymal stem cells drives metastasis. *Cell Rep*. (2020) 33:108473. doi: 10.1016/j.celrep.2020.108473

128. Gitto SB, Ihewulezi CJN, Powell DJ Jr. Adoptive T cell therapy for ovarian cancer. *Gynecol Oncol*. (2024) 186:77–84. doi: 10.1016/j.ygyno.2024.04.001

129. Mittica G, Capellero S, Genta S, Cagnazzo C, Aglietta M, Sangiolo D, et al. Adoptive immunotherapy against ovarian cancer. *J Ovarian Res*. (2016) 9:30. doi: 10.1186/s13048-016-0236-9

130. Wala JA, Hanna GJ. Chimeric antigen receptor T-cell therapy for solid tumors. *Hematol Oncol Clin North Am*. (2023) 37:1149–68. doi: 10.1016/j.hoc.2023.05.009

131. McGray AJR, Chiello JL, Tsuji T, Long M, Maraszek K, Gaulin N, et al. BiTE secretion by adoptively transferred stem-like T cells improves FRalpha+ ovarian cancer control. *J Immunother Cancer*. (2023) 11(6):e006863. doi: 10.1136/jitc-2023-006863

132. Felices M, Chu S, Kodal B, Bendzick L, Ryan C, Lenvik AJ, et al. IL-15 super-agonist (ALT-803) enhances natural killer (NK) cell function against ovarian cancer. *Gynecol Oncol*. (2017) 145:453–61. doi: 10.1016/j.ygyno.2017.02.028

133. Geller MA, Knorr DA, Hermanson DA, Pribyl L, Bendzick L, McCullar V, et al. Intraperitoneal delivery of human natural killer cells for treatment of ovarian cancer in a mouse xenograft model. *Cytotherapy*. (2013) 15:1297–306. doi: 10.1016/j.jcyt.2013.05.022

134. Uppendahl LD, Dahl CM, Miller JS, Felices M, Geller MA. Natural killer cell-based immunotherapy in gynecologic Malignancy: A review. *Front Immunol*. (2017) 8:1825. doi: 10.3389/fimmu.2017.01825

135. Uppendahl LD, Felices M, Bendzick L, Ryan C, Kodal B, Hinderlie P, et al. Cytokine-induced memory-like natural killer cells have enhanced function, proliferation, and *in vivo* expansion against ovarian cancer cells. *Gynecol Oncol*. (2019) 153:149–57. doi: 10.1016/j.ygyno.2019.01.006

136. Hoogstad-van Evert JS, Maas RJ, van der Meer J, Cany J, van der Steen S, Jansen JH, et al. Peritoneal NK cells are responsive to IL-15 and percentages are correlated with outcome in advanced ovarian cancer patients. *Oncotarget*. (2018) 9:34810–20. doi: 10.18632/oncotarget.26199

137. Van der Meer JMR, Maas RJA, Guldevall K, Klarenaar K, de Jonge P, Evert JSH, et al. IL-15 superagonist N-803 improves IFNgamma production and killing of leukemia and ovarian cancer cells by CD34(+) progenitor-derived NK cells. *Cancer Immunol Immunother*. (2021) 70:1305–21. doi: 10.1007/s00262-020-02749-8

138. Hou Y, Zhao X, Nie X. Enhancing the therapeutic efficacy of NK cells in the treatment of ovarian cancer (Review). *Oncol Rep*. (2024) 51(3):50. doi: 10.3892/or.2024.8709

139. Hoogstad-van Evert JS, Bekkers R, Ottevanger N, Jansen JH, Massuger L, Dolstra H. Harnessing natural killer cells for the treatment of ovarian cancer. *Gynecol Oncol*. (2020) 157:810–6. doi: 10.1016/j.ygyno.2020.03.020

140. Rezvani K. Adoptive cell therapy using engineered natural killer cells. *Bone Marrow Transplant*. (2019) 54:785–8. doi: 10.1038/s41409-019-0601-6

141. Lutz ER, Wu AA, Bigelow E, Sharma R, Mo G, Soares K, et al. Immunotherapy converts nonimmunogenic pancreatic tumors into immunogenic foci of immune regulation. *Cancer Immunol Res*. (2014) 2:616–31. doi: 10.1158/2326-6066.CIR-14-0027

142. Maldonado L, Teague JE, Morrow MP, Jotova I, Wu TC, Wang C, et al. Intramuscular therapeutic vaccination targeting HPV16 induces T cell responses that localize in mucosal lesions. *Sci Transl Med*. (2014) 6:221ra13. doi: 10.1126/scitranslmed.3007323

143. Houel A, Foloppe J, Dieu-Nosjean MC. Harnessing the power of oncolytic virotherapy and tertiary lymphoid structures to amplify antitumor immune responses in cancer patients. *Semin Immunol*. (2023) 69:101796. doi: 10.1016/j.smim.2023.101796

144. Aoyama S, Nakagawa R, Mule JJ, Mailloux AW. Inducible tertiary lymphoid structures: promise and challenges for translating a new class of immunotherapy. *Front Immunol*. (2021) 12:675538. doi: 10.3389/fimmu.2021.675538

145. He T, Hao Z, Lin M, Xin Z, Chen Y, Ouyang W, et al. Oncolytic adenovirus promotes vascular normalization and nonclassical tertiary lymphoid structure formation through STING-mediated DC activation. *Oncoimmunology*. (2022) 11:2093054. doi: 10.1080/2162402X.2022.2093054

146. Yin S, Zhang C, Gao F. Immature tertiary lymphoid structure formation was increased in the melanoma tumor microenvironment of IKZF1 transgenic mice. *Transl Cancer Res*. (2022) 11:2388–97. doi: 10.21037/tcr-22-1759

147. Feng W, Jiang D, Xu Y, Li Y, Chen L, Zhao M, et al. CDK4/6i enhances the antitumor effect of PD1 antibody by promoting TLS formation in ovarian cancer. *Heliyon*. (2023) 9:e19760. doi: 10.1016/j.heliyon.2023.e19760

148. Ozmadenci D, Shankara Narayanan JS, Andrew J, Ojalill M, Barrie AM, Jiang S, et al. Tumor FAK orchestrates immunosuppression in ovarian cancer via the CD155/TIGIT axis. *Proc Natl Acad Sci U S A*. (2022) 119:e2117065119. doi: 10.1073/pnas.2117065119

149. Lynch SV, Pedersen O. The human intestinal microbiome in health and disease. *N Engl J Med*. (2016) 375:2369–79. doi: 10.1056/NEJMra1600266

150. Zheng D, Liwinski T, Elinav E. Interaction between microbiota and immunity in health and disease. *Cell Res*. (2020) 30:492–506. doi: 10.1038/s41422-020-0332-7

151. Gopalakrishnan V, Spencer CN, Nezi L, Reuben A, Andrews MC, Karpinets TV, et al. Gut microbiome modulates response to anti-PD-1 immunotherapy in melanoma patients. *Science*. (2018) 359:97–103. doi: 10.1126/science.aan4236

152. Routy B, Le Chatelier E, Derosa L, Duong CPM, Alou MT, Daillere R, et al. Gut microbiome influences efficacy of PD-1-based immunotherapy against epithelial tumors. *Science*. (2018) 359:91–7. doi: 10.1126/science.aan3706

153. Sivan A, Corrales L, Hubert N, Williams JB, Aquino-Michaels K, Earley ZM, et al. Commensal Bifidobacterium promotes antitumor immunity and facilitates anti-PD-L1 efficacy. *Science*. (2015) 350:1084–9. doi: 10.1126/science.aac4255

154. Mas-Lloret J, Obon-Santacana M, Ibanez-Sanz G, Guino E, Pato ML, Rodriguez-Moranta F, et al. Gut microbiome diversity detected by high-coverage 16S and shotgun sequencing of paired stool and colon sample. *Sci Data*. (2020) 7:92. doi: 10.1038/s41597-020-0427-5

155. Overacre-Delgoffe AE, Bumgarner HJ, Cillo AR, Burr AHP, Tometich JT, Bhattacharjee A, et al. Microbiota-specific T follicular helper cells drive tertiary lymphoid structures and anti-tumor immunity against colorectal cancer. *Immunity*. (2021) 54:2812–24.e4. doi: 10.1016/j.immuni.2021.11.003

156. Zhao R, Li J, Chen B, Zhao J, Hu L, Huang K, et al. The enrichment of the gut microbiota Lachnoclostridium is associated with the presence of intratumoral tertiary lymphoid structures in hepatocellular carcinoma. *Front Immunol*. (2023) 14:1289753. doi: 10.3389/fimmu.2023.1289753

157. Jin Y, Dong H, Xia L, Yang Y, Zhu Y, Shen Y, et al. The diversity of gut microbiome is associated with favorable responses to anti-programmed death 1 immunotherapy in chinese patients with NSCLC. *J Thorac Oncol*. (2019) 14:1378–89. doi: 10.1016/j.jtho.2019.04.007

158. Mao J, Wang D, Long J, Yang X, Lin J, Song Y, et al. Gut microbiome is associated with the clinical response to anti-PD-1 based immunotherapy in hepatobiliary cancers. *J Immunother Cancer*. (2021) 9(12):e003334. doi: 10.1136/jitc-2021-003334

159. Matson V, Fessler J, Bao R, Chongsuwat T, Zha Y, Alegre ML, et al. The commensal microbiome is associated with anti-PD-1 efficacy in metastatic melanoma patients. *Science*. (2018) 359:104–8. doi: 10.1126/science.aao3290

160. Newsome RC, Gharaibeh RZ, Pierce CM, da Silva WV, Paul S, Hogue SR, et al. Interaction of bacterial genera associated with therapeutic response to immune checkpoint PD-1 blockade in a United States cohort. *Genome Med*. (2022) 14:35. doi: 10.1186/s13073-022-01037-7

161. Peng Z, Cheng S, Kou Y, Wang Z, Jin R, Hu H, et al. The gut microbiome is associated with clinical response to anti-PD-1/PD-L1 immunotherapy in gastrointestinal cancer. *Cancer Immunol Res*. (2020) 8:1251–61. doi: 10.1158/2326-6066.CIR-19-1014

162. Peters BA, Wilson M, Moran U, Pavlick A, Izsak A, Wechter T, et al. Relating the gut metagenome and metatranscriptome to immunotherapy responses in melanoma patients. *Genome Med*. (2019) 11:61. doi: 10.1186/s13073-019-0672-4

163. Zheng Y, Wang T, Tu X, Huang Y, Zhang H, Tan D, et al. Gut microbiome affects the response to anti-PD-1 immunotherapy in patients with hepatocellular carcinoma. *J Immunother Cancer*. (2019) 7:193. doi: 10.1186/s40425-019-0650-9

164. Dizman N, Meza L, Bergerot P, Alcantara M, Dorff T, Lyou Y, et al. Nivolumab plus ipilimumab with or without live bacterial supplementation in metastatic renal cell carcinoma: a randomized phase 1 trial. *Nat Med*. (2022) 28:704–12. doi: 10.1038/s41591-022-01694-6

165. McKenzie ND, Ahmad S, Awada A, Kuhn TM, Recio FO, Holloway RW. Prognostic features of the tumor microenvironment in high-grade serous ovarian cancer and dietary immunomodulation. *Life Sci*. (2023) 333:122178. doi: 10.1016/j.lfs.2023.122178

166. Kang YB, Cai Y. Faecal microbiota transplantation enhances efficacy of immune checkpoint inhibitors therapy against cancer. *World J Gastroenterol*. (2021) 27:5362–75. doi: 10.3748/wjg.v27.i32.5362

167. Li S, Chen K, Sun Z, Chen M, Pi W, Zhou S, et al. Radiation drives tertiary lymphoid structures to reshape TME for synergized antitumour immunity. *Expert Rev Mol Med*. (2024) 26:e30. doi: 10.1017/erm.2024.27

168. Lanickova T, Hensler M, Kasikova L, Vosahlikova S, Angelidou A, Pasulka J, et al. Chemotherapy drives tertiary lymphoid structures that correlate with ICI-responsive TCF1+CD8+ T cells in metastatic ovarian cancer. *Clin Cancer Res*. (2024) 31(1):164–80. doi: 10.1158/1078-0432.CCR-24-1594

169. Garaud S, Zayakin P, Buisseret L, Rulle U, Silina K, de Wind A, et al. Antigen specificity and clinical significance of igG and igA autoantibodies produced in *situ* by tumor-infiltrating B cells in breast cancer. *Front Immunol*. (2018) 9:2660. doi: 10.3389/fimmu.2018.02660

170. Ryan ST, Zhang J, Burner DN, Liss M, Pittman E, Muldong M, et al. Neoadjuvant rituximab modulates the tumor immune environment in patients with high risk prostate cancer. *J Transl Med*. (2020) 18:214. doi: 10.1186/s12967-020-02370-4

171. Cottrell TR, Taube JM. PD-L1 and emerging biomarkers in immune checkpoint blockade therapy. *Cancer J*. (2018) 24:41–6. doi: 10.1097/PPO.0000000000000301

172. Kroeger DR, Milne K, Nelson BH. Tumor-infiltrating plasma cells are associated with tertiary lymphoid structures, cytolytic T-cell responses, and superior prognosis in ovarian cancer. *Clin Cancer Res*. (2016) 22:3005–15. doi: 10.1158/1078-0432.CCR-15-2762

173. Zhang L, Strange M, Elishaev E, Zaidi S, Modugno F, Radolec M, et al. Characterization of latently infected EBV+ antibody-secreting B cells isolated from ovarian tumors and Malignant ascites. *Front Immunol*. (2024) 15:1379175. doi: 10.3389/fimmu.2024.1379175

174. Westbom-Fremer S, Tran L, Ebbesson A, Martin de la Fuente L, Jonsson JM, Kannisto P, et al. Tertiary lymphoid structures in high-grade serous tubo-ovarian carcinoma: anatomical site matters. *Cancer Immunol Immunother*. (2025) 74:56. doi: 10.1007/s00262-024-03911-2

frontiers | Frontiers in Immunology

TYPE Original Research
PUBLISHED 19 June 2025
DOI 10.3389/fimmu.2025.1578243

OPEN ACCESS

EDITED BY
Jinhwan Kim,
University of California, Davis, United States

REVIEWED BY
Ahmed Elsayed Noreldin,
Damanhour University, Egypt
Junmeng Li,
Henan Provincial People's Hospital, China
Maoshu Bai,
Dazhou Integrated Traditional Chinese Medicine and Western Medicine Hospital, China

*CORRESPONDENCE
Bingwei Zeng
zbwsnow@qq.com

†These authors have contributed equally to this work and share first authorship

RECEIVED 17 February 2025
ACCEPTED 06 June 2025
PUBLISHED 19 June 2025

CITATION
Zheng J, Lin N, Huang B, Wu M, Xiao L and Zeng B (2025) Comprehensive analysis of RFC4 as a potential biomarker for regulating the immune microenvironment and predicting immune therapy response in lung adenocarcinoma.
Front. Immunol. 16:1578243.
doi: 10.3389/fimmu.2025.1578243

Comprehensive analysis of RFC4 as a potential biomarker for regulating the immune microenvironment and predicting immune therapy response in lung adenocarcinoma

Jianqing Zheng[1†], Na Lin[2†], Bifen Huang[3†], Min Wu[1], Lihua Xiao[1] and Bingwei Zeng[2*]

[1]Department of Radiation Oncology, The Second Affiliated Hospital of Fujian Medical University, Quanzhou, Fujian, China, [2]Department of Pathology, The Second Affiliated Hospital of Fujian Medical University, Quanzhou, Fujian, China, [3]Department of Obstetrics and Gynecology, People's Hospital Affiliated of Quanzhou Medical College, Quanzhou, Fujian, China

Background: Replication factor C subunit 4 (RFC4) is crucial for initiating DNA replication via DNA polymerase δ and ε and is overexpressed in various cancers. However, its relationship with the tumor immune microenvironment (TIME), and immunotherapy response in lung adenocarcinoma (LUAD) remains unclear. This study aimed to determine whether overexpressed RFC4 impacts survival in patients with LUAD and to explore potential mechanisms of RFC4 in regulating the TIME using integrated bioinformatics.

Methods: LUAD gene expression data were downloaded from the Cancer Genome Atlas (TCGA) database and used for exploratory analysis. Differential expression of RFC4 was validated using gene expression data from the Gene Expression Omnibus (GEO). Clinical data with survival information from TCGA and GEO were use to explore and validate the prognostic value of RFC4. The relationship between RFC4 and TIME was studied by Cell-type identification by estimating relative subsets of RNA transcripts (CIBERSORT) and Estimation of Stromal and Immune cells in Malignant Tumor tissues using Expression data (ESTIMATE). Tumor Immune Dysfunction and Exclusion (TIDE) was used to predict the therapeutic response of RFC4 to immune checkpoint inhibitors. We validated the differential expression of RFC4 in LUAD and adjacent tissues using immunohistochemical staining in a real-world cohort from the Second Affiliated Hospital of Fujian Medical University.

Results: RFC4 was significantly over-expressed in LUAD at both the RNA and protein levels. High RFC4 expression levels were associated with poor prognosis in LUAD, both in TCGA and GEO. High RFC4 levels were significantly associated with immunostimulators and immune cells infiltration in LUAD tissues. Correlation analysis revealed a significant relationship between the RFC4 and ESTIMATE scores. A high RFC4 expression level was associated with a lower TIDE

score, indicating a stronger therapeutic response to immunotherapy. Functional prediction of RFC4 suggested that RFC4 mainly participated in DNA replication and repair, and reshaped the TIME.

Conclusions: RFC4 proved to be a promising biomarker for tumorigenesis and could effectively predict immunotherapy response in LUAD. RCF4 altered tumor prognosis by reshaping the TIME, and targeted inhibition of RCF4 may be a promising new strategy for treating LUAD.

KEYWORDS

lung adenocarcinoma, replication factor C subunit 4 (RFC4), immune regulatory factors, tumor immune microenvironment, immune therapy response

1 Introduction

Lung cancer (LC) is the leading cause of cancer-related deaths worldwide (1), with lung adenocarcinoma (LUAD) is the predominant histological subtype, accounting for approximately 40%-50% of all LC cases (2, 3). Most patients with LUAD are diagnosed at an advanced stage or have cancer metastasis, which results in a poor prognosis with a 5-year overall survival (OS) of <20% (4, 5). Recent significant progress has been made in immunotherapy with immune checkpoint inhibitors (ICIs) for LUAD, resulting in significantly reduced mortality rates (6). Owing to significant improvements in the clinical efficacy of immunotherapy for advanced LC, immunotherapy has become the preferred treatment mode for advanced LC (7). Several biomarkers have been widely used to predict immunotherapy response (IMTR) in clinical sets, including programmed death-ligand 1 (PD-L1) expression and tumor mutation burden (8). However, these biomarkers do not fully reflect the heterogeneity of the tumor microenvironment (TME) or the tumor immune microenvironment (TIME), and immunotherapy can only achieve remarkable clinical benefits in a few patients with cancer (9). Therefore, new biomarkers for predicting the prognosis and therapeutic efficacy of immunotherapy need to be identified.

The replication factor C subunit 4 (RFC4) gene encodes a highly conserved protein that is involved in many cellular processes related to DNA repair and DNA replication (10). RFC4 is necessary for DNA polymerase δ and DNA polymerase ε to extend primer DNA templates (11, 12). The RFC family (RFCs) plays a clamp loader role in DNA synthesis, loading proliferating cell nuclear antigen (PCNA) onto DNA through adenosine triphosphate (ATP)-dependent processes (13). During the S phase of DNA replication, RFC participates in cell cycle checkpoint control by activating polymerase assembly (14). After DNA damage occurs, they activate their mismatch and excision repair mechanisms by forming complexes with PCNA (15). Therefore, RFCs play a crucial role in DNA repair after DNA damage. RFC4 may play a crucial role in cancer cell survival, and because of its significant ability to regulate cell division and proliferation, it may be a promising target for cancer therapy (16, 17). Although emerging evidence has demonstrated that RFC4 plays an oncogene role in many human cancers, its expression patterns and functions in LUAD remain unclear. In this study, various bioinformatics tools were used to analyze RFC4 as a potential oncogene and therapeutic target in LUAD. The future development direction of this field is also discussed to provide evidence that is more in line with RFC4 as a promising biomarker in immunotherapy for LUAD.

Abbreviations: GEO, Gene expression omnibus; TCGA, The cancer genome atlas; DEGs, differentially expressed genes; GO, Gene Ontology; KEGG, Kyoto Encyclopedia of Genes and Genomes; TME, Tumor microenvironment; OS, Overall survival.

2 Materials and methods

2.1 Data collection of LUAD samples

RNA sequencing (RNA-seq) data and clinical data were downloaded from the Cancer Genome Atlas (TCGA) (https://portal.gdc.cancer.gov/) and Gene Expression Omnibus (https://www.ncbi.nlm.nih.gov/geo/, GEO). A total of 586 samples were collected in the TCGA database, of which 527 were cancerous tissues and 59 were normal tissues. RNA-seq data was processed using standard bioinformatics procedures and used for subsequent analysis. The study flowchart is shown in Figure 1.

We validated the exploration results of TCGA with the GEO data. The inclusion criteria of the GEO data in our study were as follows: (1) datasets involving LUAD samples; (2) datasets with RNA-seq or gene microarrays from any type of sequencing platform; (3) datasets with normal tissues, which can be used to verify the differential expression of RFC4; and (4) datasets with clinical survival information, which can be used to verify the prognostic value of RFC4. The exclusion criteria for the GEO datasets were as follows: (1) datasets containing non-LUAD samples and (2) datasets without survival data and normal

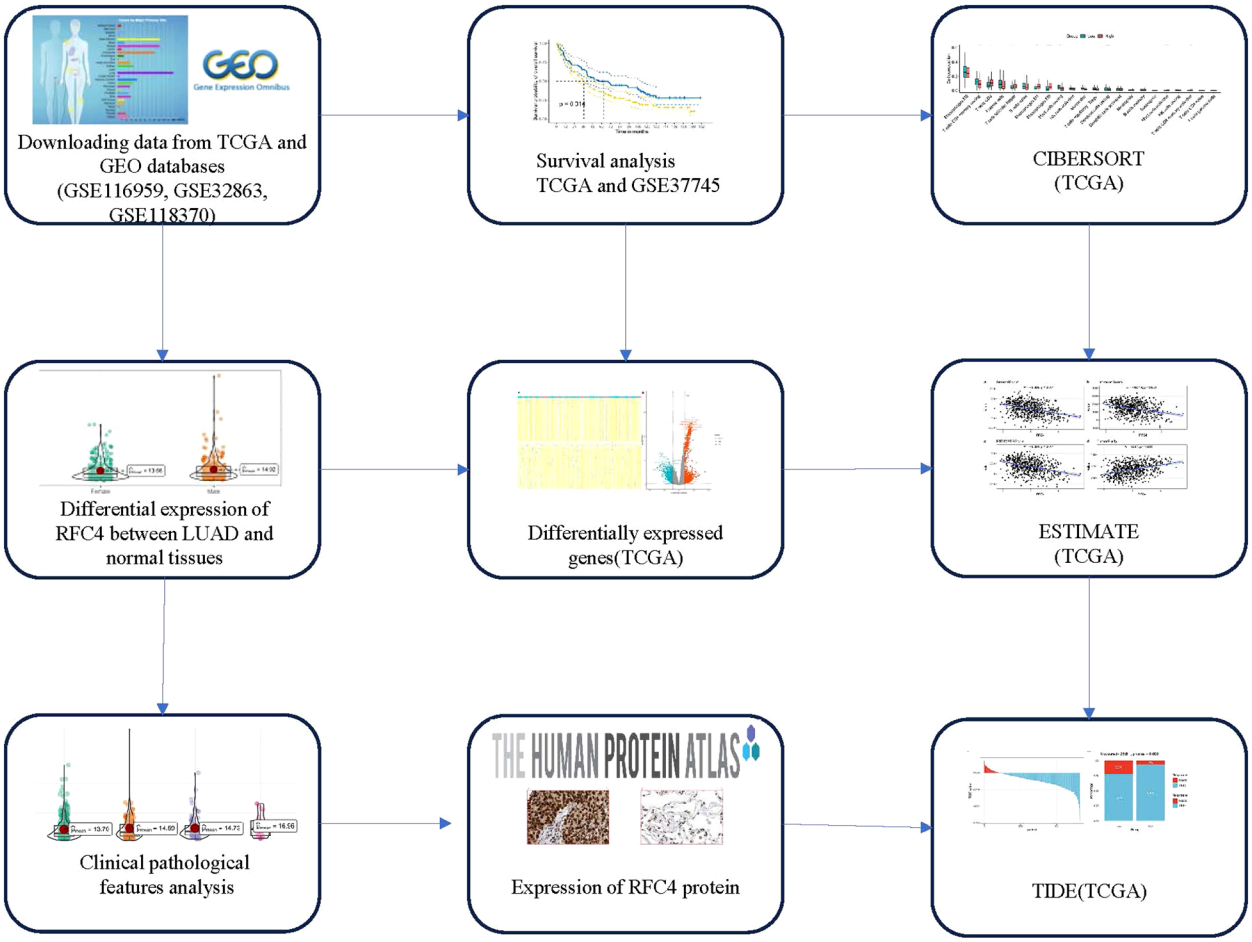

FIGURE 1
Flow chart of study design. TCGA, The cancer genome atlas; GEO, Gene expression omnibus; LUAD, lung adenocarcinoma; CIBERSORT, Cell-type identification by estimating relative subsets of RNA transcripts; ESTIMATE, Estimation of Stromal and Immune cells in Malignant Tumor tissues using Expression data; TIDE, Tumor Immune Dysfunction and Exclusion.

tissues. Finally, three external cohorts downloaded from GEO database were used to further validate the differential expression of RFC4: GSE116959 (18), GSE32863 (19), GSE118370 (20). One external cohort, GSE37745 (21), was used to further validate the prognostic efficacy of RFC4.

2.2 Differential expressions of RFC4 mRNA and protein between LUAD tissues and adjacent tissues or normal lung tissues

The Wilcox test was used to compare differential expression of RFC4 mRNA between LUAD tissues and adjacent tissues or normal lung tissues in TCGA and GEO datasets. Subsequently, we applied the "ggplot2" R package to show the results. The Human Protein Atlas (HPA, http://www.proteinatlas.org) was used to explore the protein expression levels of RFC4.

2.3 Survival analysis and clinical correlation analysis of RFC4

Clinicopathological features and survival data were extracted from the TCGA and GEO datasets (GSE37745). The relationship between RFC4 mRNA and different clinicopathological characteristics, such as survival status, cancer status, age, gender, race, and clinical stage, was explored using an independent sample Wilcox test or one-way analysis of variance. Using the best cutoff value of RFC4 mRNA in cancer tissues, patients with LUAD were divided into high expression ($RFC4^{High}$) and low expression ($RFC4^{Low}$) groups. The Kaplan-Meier method was used to plot the OS curves of the two groups, and log-rank test was used to compare difference. Next, survival results were further validated in patients with LUAD and then divided using the same method. Survival was analyzed using the "survival," "survminer," and "forestplot" packages.

2.4 Screening and functional analysis of RFC4 related differentially expressed genes in LUAD

Using the median value of RFC4 mRNA in TGCA, the patients were divided into high expression ($RFC4^{High}$) and low expression ($RFC4^{Low}$) groups. Subsequently, the "limma" package was used to identify DEGs in cancer tissues between the $RFC4^{High}$ and the $RFC4^{Low}$ groups. The top 50 DEGs closest to RFC4 were selected, and a heatmap was plotted using the "pheatmap" package. RFC4-related DEGs were selected to perform Gene Ontology (GO) and Kyoto Encyclopedia of Genes and Genomes (KEGG) analysis using the R package "clusterProfiler". GO analysis of cell composition, biological processes, and molecular function was performed using the enrichGO function in the "clusterProfiler" R package. KEGG analysis was performed using the enrichKEGG function in the "clusterProfiler" R package. Pathways with $P < 0.05$ were considered significantly enriched.

2.5 Immune cell infiltration analysis and gene set variation analysis

The correlation between RFC4 expression and various infiltrating immune cells in the TIME was explored and analyzed by Spearman correlation analysis. Significance was set at $P<0.05$. Gene sets of immune-regulatory factors, including immunoinhibitors and immunostimulators, were screened from previously reported references (22–24). Correlation analyses between various immunoregulatory factors and RFC4 expression were displayed using lollipop plots. To simplify interpretation, we separately analyzed immunoinhibitors and immunostimulators using the "GSVA" package.

Cell-type identification by estimating relative subsets of RNA transcripts (CIBERSORT) was used to analyze the infiltration of immune cells between the $RFC4^{High}$ and the $RFC4^{Low}$ groups (25). CIBERSORT can obtain the infiltrating characteristics of 22 immune cell types with gene expression profiles and provide changes in characteristics of TIME in different cancer tissues.

2.6 Estimation of stromal and immune scores

The Estimation of Stromal and Immune cells in Malignant Tumor tissues using Expression data (ESTIMATE) was used to predict tumor purity and stromal/immune cell infiltration (26), which assess levels of stromal and immune cell infiltration using expression profiles by the "estimate" R package. Stromal, immune, ESTIMATE, and tumor purity scores were calculated using RNA sequencing data from TCGA cohort. A Wilcoxon test was then performed to compare scores between the two groups.

2.7 Immunotherapy response prediction

Tumor Immune Dysfunction and Exclusion (TIDE) (http://tide.dfci.harvard.edu/) was used to predict response to immune checkpoint blockade therapy. The Wilcoxon test was performed to compare TIDE scores between the two groups.

2.8 RFC4 protein expression in LUAD

The RFC4 protein expression in LUAD tissues was evaluated by immunohistochemical staining in both cancer tissues and normal tissues, and the data was retrieved and downloaded from the Human Protein Atlas database (HPA, http://www.proteinatlas.org/).

To verify the differential expression of RFC4 protein, we recruited 31 patients with LUAD who underwent surgical treatment at the Second Affiliated Hospital of Fujian Medical University between January 2021 and May 2024. Postoperative cancer tissues were donated by the patient or their family members, and written informed consent was obtained. This study has been approved by the Ethics Committee of the Second Affiliated Hospital of Fujian Medical University (2025-001). RFC4 rabbit polyclonal antibody was purchased from Wuhan Sanying Company. Immunohistochemical (IHC) staining was conducted by Na Lin, and the results were interpreted by two members of the research team (Bingwei Zeng and Jianqing Zheng).

2.9 Statistical analysis

Statistical analysis of the association between RFC4 and clinicopathological parameters was performed using independent sample t-test, Wilcoxon test, chi-square test, or Fisher's exact test. For survival variables, Kaplan-Meier curves were plotted as well as log-rank tests. The prognostic value of RFC4 was analyzed using the Cox proportional risk model via "survminer" and "survival" R package. Significance was set at $P<0.05$. The above analyses were performed using the R software (version 4.3.1).

3 Results

3.1 Expression of RFC4 mRNA in LUAD tissues

The differential expression of RFC4 mRNA between LUAD cancer and normal tissue samples is shown in Figures 2A-D. RFC4 expression level was significantly higher in LUAD tissues than normal tissues in TCGA samples($P<0.001$). The differential expression of RFC4 in LUAD was further validated using the GEO dataset. Consistent results in the exploration and validation sets indicated that RFC4 mRNA expression was significantly elevated in LUAD samples, suggesting the involvement of RFC4 in LUAD tumorigenesis.

3.2 Relationship between RFC4 and clinical characteristics of patients

We divided the TCGA samples into different groups based on the following clinical characteristics, survival status (alive: patients

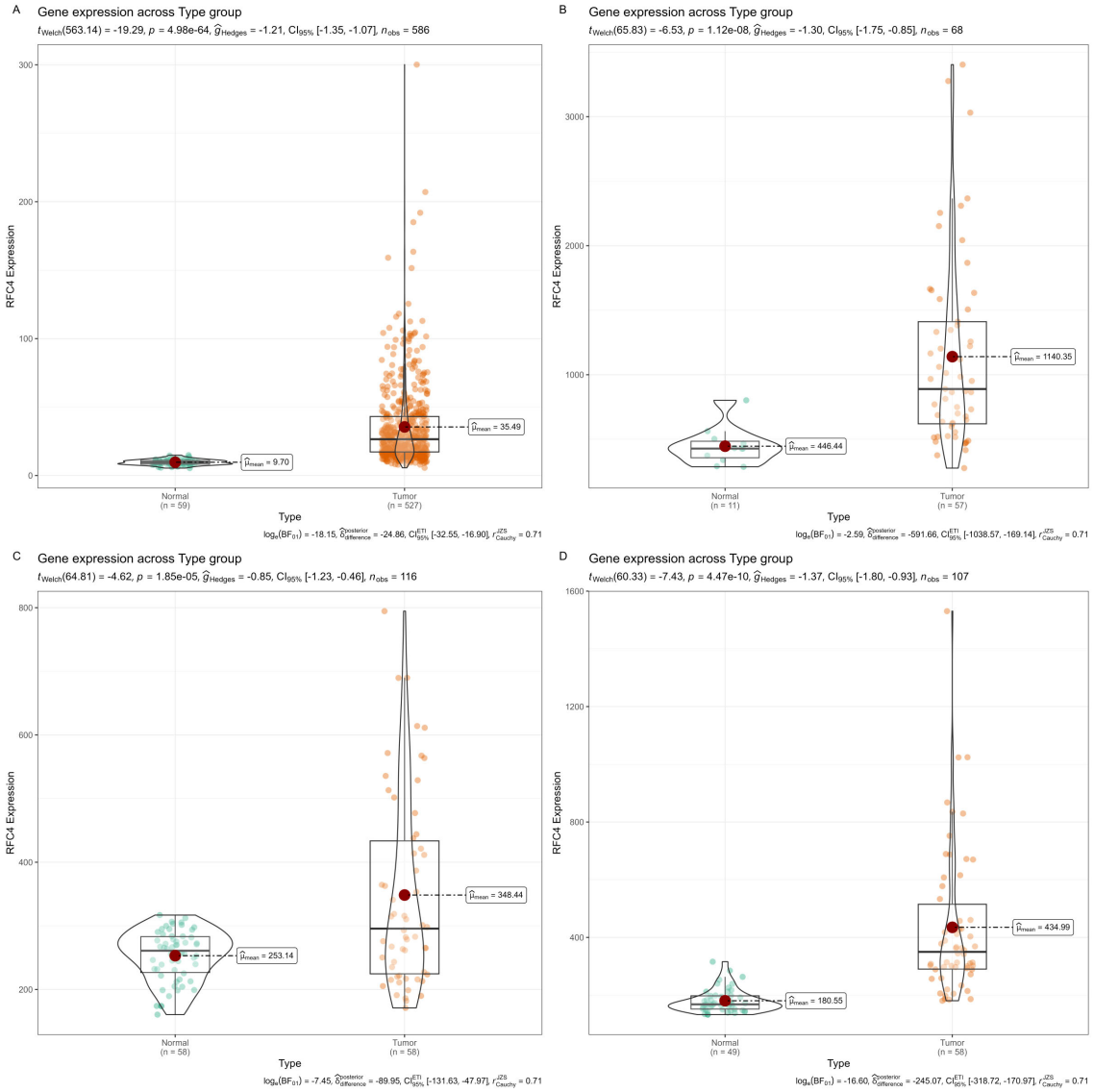

FIGURE 2
Expression of RFC4 mRNA in LUAD tissues from TCGA and GEO. **(A)** Expression of RFC4 mRNA between cancer tissues and normal tissue in TCGA cohort. **(B)** Expression of RFC4 mRNA between cancer tissues and normal tissue in GSE116959 cohort. **(C)** Expression of RFC4 mRNA between cancer tissues and normal tissue in GSE32863 cohort. **(D)** Expression of RFC4 mRNA between cancer tissues and normal tissue in GSE118370 cohort.

who still lived in the TCGA samples. dead: patients who have died in the TCGA samples.), cancer status (WithTumor: patients who still lived or died with tumor. TumorFree: patients who still lived or died without tumor), gender (males and females), age (younger: <60 years old, older:≥60 years old), race (white and non-white), smoking status (smoker and never smoked), clinical stage (stage I, stage II, stage III, and stage IV). According to the Response Evaluation Criteria in Solid Tumors (RECIST), the samples were divided into complete response, partial response, progressive disease and stable disease groups. The results of the RFC4 expression in LUAD samples from different groups are shown in Figures 3A–K. Only survival status demonstrated a significant relationship with RFC4 expression.

3.3 Relationship between RFC4 and prognosis of patients with LUAD

Using best cutoff value of 7.16, patients with LUAD in the TCGA database were divided into the $RFC4^{High}$ group (n=344) and $RFC4^{Low}$ group (n=136). Kaplan-Meier survival analysis showed that patients with high RFC4 expression levels had significantly worse OS than those with low RFC4 expression levels (hazard ratio [HR] =1.83; 1.25-2.68, *P*=0.002) (Figure 4A). The 5-year survival rate was 54.95% (42.39%-71.23%) in the $RFC4^{Low}$ group and 41.25% (33.68%-50.51%) in the $RFC4^{High}$ group, respectively. Using best cutoff value of 9.31, patients with LUAD in the GSE37745 dataset were divided into the $RFC4^{High}$ group (n=112)

10.3389/fimmu.2025.1578243

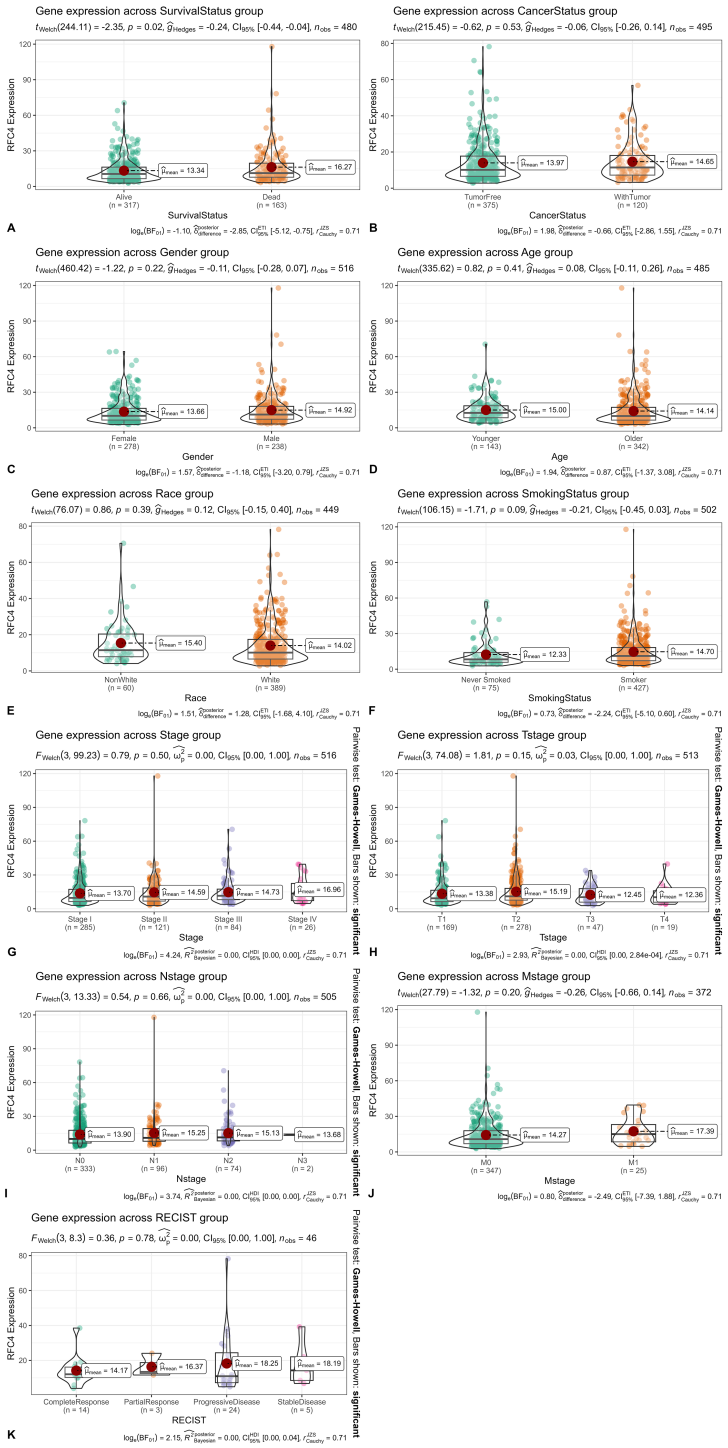

FIGURE 3
Relationship between RFC4 mRNA and clinical characteristics of patients. **(A)** Expression of RFC4 mRNA with different survival status (Alive: Patients who still lived in the TCGA samples. Dead: Patients who have died in the TCGA samples.). **(B)** Expression of RFC4 mRNA with different cancer status (WithTumor: Patients who still lived or died with tumor. TumorFree: Patients who still lived or died without tumor). **(C)** Expression of RFC4 mRNA with different gender. **(D)** Expression of RFC4 mRNA with different survival status. **(A)** Expression of RFC4 mRNA with different age (Younger: <60 years old, Older:≥60 years old). **(E)** Expression of RFC4 mRNA with different race (white and non-white). **(F)** Expression of RFC4 mRNA with different smoking status (smoker and never smoked). **(G)** Expression of RFC4 mRNA with different clinical stage. **(H)** Expression of RFC4 mRNA with different T stage. **(I)** Expression of RFC4 mRNA with different N stage. **(J)** Expression of RFC4 mRNA with different M stage. **(K)** Expression of RFC4 mRNA with different RECIST status.

and RFC4^{Low} group (n=84). Kaplan-Meier survival analysis showed that patients with high RFC4 expression had worse overall survival than those with low RFC4 expression levels had significantly worse OS than those with low RFC4 expression levels (HR = 1.52; 1.09–2.13, *P*=0.015) (Figure 4B). 5-year survival rate was 50.00% (40.37%-61.92%) in the RFC4^{Low} group, and 35.71% (27.86%-45.79%) in RFC4 ^{High} group, respectively.

To verify whether RFC4 has an independent prognostic value, multivariate analysis was conducted. Univariate analysis showed that the RFC4 expression, clinical stage, cancer status and residual tumor were potential factors for the OS of patients with LUAD (*P*<0.05), as shown in Table 1. A multivariate COX regression analysis based on the abovementioned four positive variables was performed, and the results were presented in Table 2. In the stepwise regression multivariate model, RFC4.AutoCut significantly affected the OS (HR=1.52, 95%CI: 1.09-2.12, *P*=0.007), thus suggesting the independent prognostic value of RFC4 in LUAD.

3.4 Analysis of DEGs and functional enrichment related to RFC4

Using the median expression value of RFC4, patients with LUAD in the TCGA database were divided, and a differential expression analysis was conducted. Using the absolute value of log fold change≧1 and *P* <0.05 as screening criteria, a total of 1346 DEGs were identified, of which 746 genes were highly expressed and 600 genes were lowly expressed. Detailed information of DEGs were listed in Supplementary Table S1. Heatmaps and volcano maps are provided in Figures 5A, B, respectively.

All DEGs that showed significant differences between the RFC4^{High} and RFC4^{Low} groups were screened and selected for functional enrichment analyses. The biological processes were mainly enriched in nuclear division, chromosome segregation, organelle fission, nuclear chromosome segregation, mitotic nuclear division, mitotic sister chromatid segregation, sister chromatid segregation, regulation of mitotic nuclear division, DNA-templated DNA replication, and regulation of nuclear division. The cellular composition was mainly enriched in condensed chromosomes, chromosomal regions, chromosomes, centromeric regions, condensed chromosomes, centromeric regions, kinetochores, outer kinetochores, CMG complexes, DNA replication pre-initiation complexes, spindles, and mitotic spindles. The molecular functions were mainly enriched for microtubule motor activity, microtubule binding, cytoskeletal motor activity, single-stranded DNA helicase activity, hormone activity, tubulin binding, serine-type endopeptidase activity, sodium-ion transmembrane transporter activity, peptidase inhibitor activity, and DNA helicase activity. The KEGG pathways were mainly enriched in the cell cycle, neuroactive ligand–receptor interaction, motor proteins, bile secretion, pancreatic secretion, Fanconi anemia pathway, cytokine–cytokine receptor interaction, drug metabolism-cytochrome P450, oocyte meiosis, and the cAMP signaling pathway. The results of the functional enrichment analysis are shown in Figures 6A–D. Detailed information on the functional enrichment analysis is provided in Supplementary Table S2.

3.5 Correlation analysis between RFC4 and immunostimulators and immunoinhibitors

The detail results of the correlation analysis between RFC4 and the immunostimulators were listed in Supplementary Table S3 and shown in Figure 7A. In our study, 43 immunostimulators were selected for correlation analysis. RFC4 expression was positively correlated with 14 immunostimulatory factors and negatively correlated with 13 immunostimulatory factors. We used GSVA to evaluate the correlation between RFC4 and immunostimulators and provided a correlation coefficient indicator called GSVA.Meta, which reflects the GSVA results. The GSVA results showed that RFC4 was negatively correlated with GSVA.Meta (rho=−0.164, *P*<0.001). Based on these results, we inferred that RFC4 mainly altered the TIME by suppressing the expression of immune-stimulatory factors.

Similarly, 23 immunoinhibitors were selected for the correlation analysis. The detail results were listed in Supplementary Table S4 and

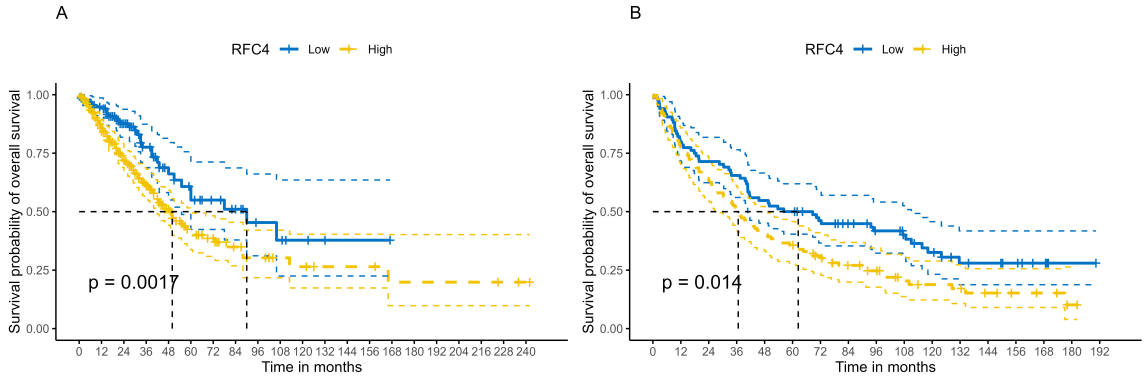

FIGURE 4
Kaplan–Meier survival analysis of RFC4 expression on survival in LUAD. **(A)** Overall survival from TCGA. **(B)** Validation result of survival from GSE37745 dataset.

10.3389/fimmu.2025.1578243

TABLE 1 Univariate analysis of the prognostic ability of RFC4 in patients with LUAD.

Characteristics	Levels	Beta	SE	HR (95% CI for HR)	Statistics (Z value)	P
RFC4		0.01	0.01	1.01 (1.00, 1.02)	2.496	0.013
RFC4.Median	Low					
	High	0.27	0.15	1.30 (0.97, 1.76)	1.731	0.083
RFC4.AutoCut	Low					
	High	0.56	0.17	1.75 (1.26, 2.43)	3.360	<0.001
CancerStatus	TumorFree					
	WithTumor	1.45	0.15	4.28 (3.16, 5.80)	9.412	<0.001
Gender	Female					
	Male	0.06	0.15	1.06 (0.79, 1.44)	0.403	0.687
Age_group	Younger					
	Older	0.11	0.17	1.12 (0.80, 1.56)	0.673	0.501
SmokingStatus	Never Smoked					
	Smoker	-0.03	0.21	0.97 (0.64, 1.47)	-0.140	0.889
TumorSite	L-Lower					
	L-Upper	0.08	0.25	1.08 (0.67, 1.75)	0.316	0.752
	R-Lower	0.24	0.25	1.27 (0.77, 2.08)	0.949	0.343
	R-Middle	0.24	0.46	1.27 (0.52, 3.11)	0.531	0.595
	R-Upper	-0.12	0.24	0.89 (0.56, 1.42)	-0.500	0.617
ResidualTumor	R0					
	R1/R2	1.43	0.26	4.19 (2.54, 6.93)	5.593	<0.001
	Rx	0.27	0.37	1.31 (0.64, 2.68)	0.736	0.462
Stage	Stage I					
	Stage II	0.96	0.19	2.62 (1.79, 3.83)	4.966	<0.001
	Stage III	1.38	0.20	3.98 (2.71, 5.85)	7.024	<0.001
	Stage IV	1.50	0.28	4.47 (2.56, 7.80)	5.271	<0.001

TABLE 2 Multivariate analysis of prognostic ability of RFC4 in patients with LUAD.

Characteristics	Levels	Beta	SE	HR (95% CI for HR)	Statistics (Z value)	P
RFC4.AutoCut	Low					
	High	0.42	0.17	1.52 (1.09,2.12)	2.444	0.015
CancerStatus	TumorFree					
	WithTumor	1.16	0.17	3.18 (2.28,4.42)	6.854	<0.001
ResidualTumor	R0					
	R1/R2	0.73	0.28	2.07 (1.21,3.56)	2.650	0.008
	Rx	-0.09	0.37	0.92 (0.45,1.89)	0.238	0.812
Stage	Stage I					
	Stage II	0.68	0.20	1.96 (1.33,2.90)	3.399	0.001
	Stage III	1.11	0.20	3.04 (2.05,4.52)	5.505	<0.001
	Stage IV	0.66	0.30	1.93 (1.06,3.50)	2.166	0.030

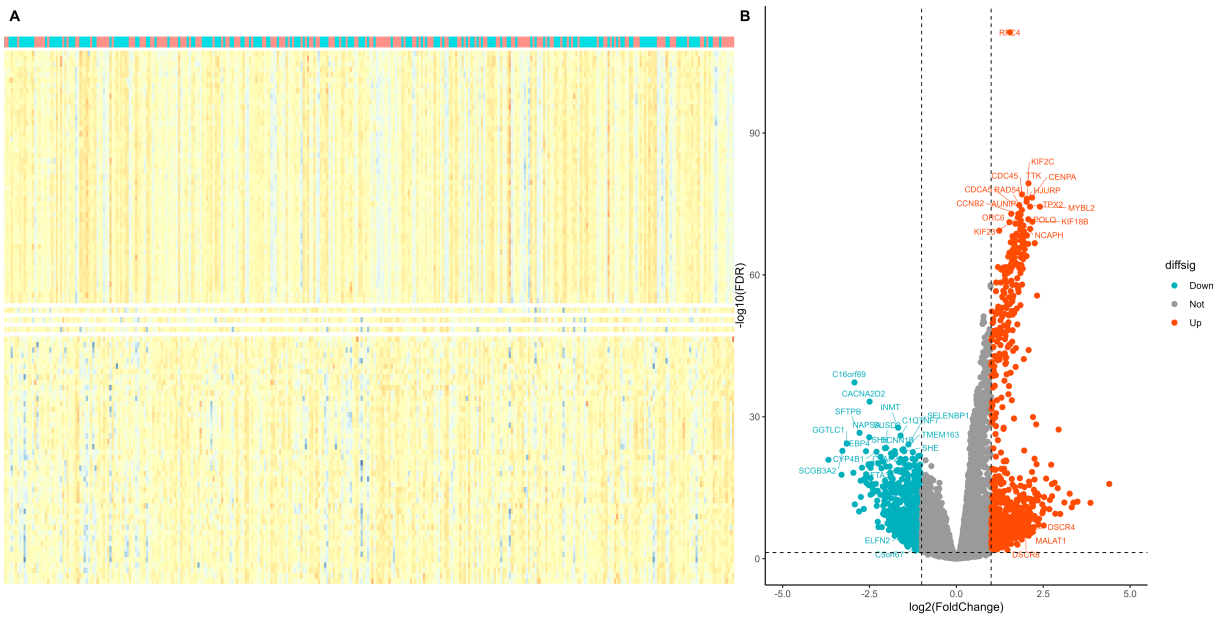

FIGURE 5
Screening of differentially expressed genes in different RFC4 status in LUAD cohort. **(A)** Heatmap. The figure shows 50 genes with the most significant upregulation, 50 genes with the most significant downregulation. **(B)** volcano plot. Differentially expressed genes were selected to labelled.

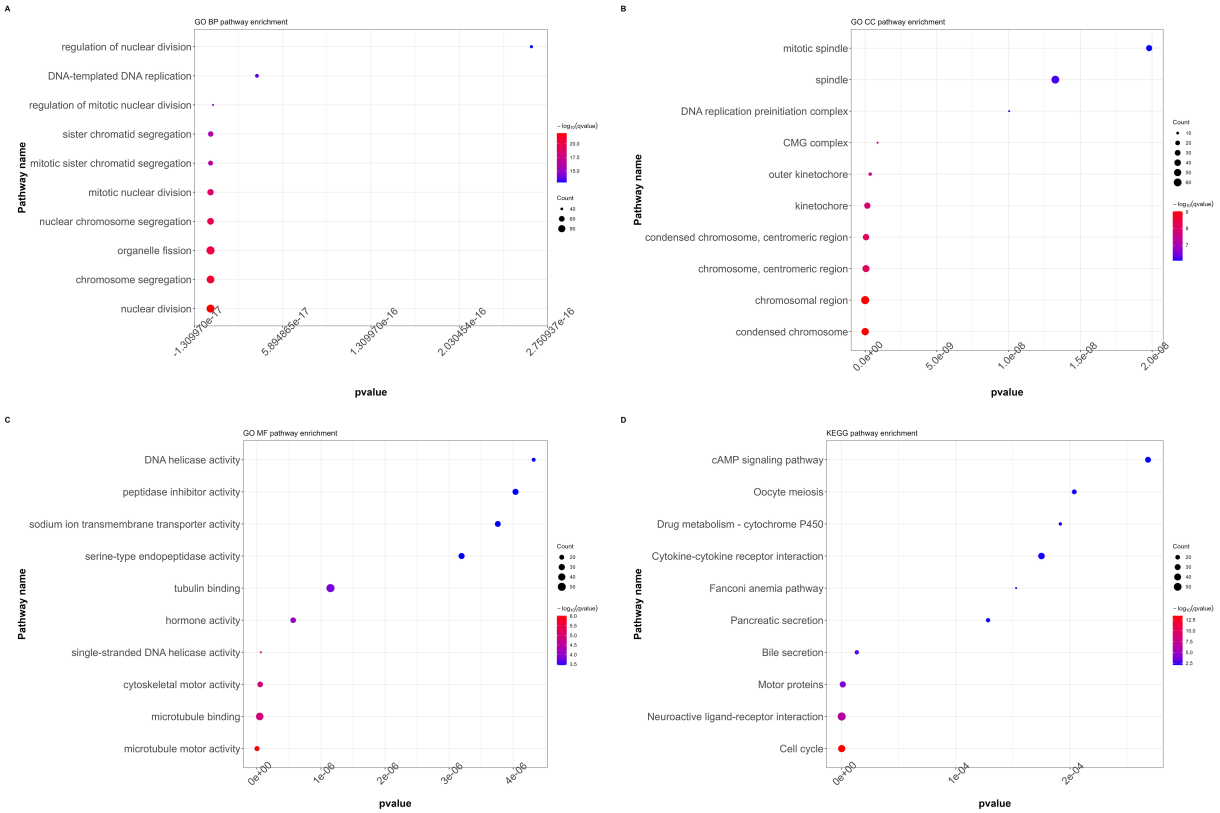

FIGURE 6
Functional annotation and pathway enrichment analysis of differentially expressed genes in LUAD cohort. **(A)** GO functional annotation (BP, biological processes). **(B)** GO functional annotation (CC, cellular composition). **(C)** GO functional annotation (MF, Molecular functions). **(D)** KEGG pathway enrichment. (GO, Gene Ontology; KEGG, Kyoto Encyclopedia of Genes and Genomes).

shown in Figure 7B. RFC4 expression was positively correlated with the expression of 10 immunosuppressive factors and negatively correlated with the expression of two immunosuppressive factors. The GSVA results showed that RFC4 was negatively correlated with GSVA.Meta, with no statistical significance (rho=−0.068, *P*=0.122).

3.6 Relationship between RFC4 and immune cell infiltration

To evaluate the discriminative potential of RFC4 for TIME and its applicability in immunotherapy in patients with LUAD, a correlation analysis between 22 immune cells and RFC4 was conducted using CIBERSORT, and results were shown in Figure 8A; Supplementary Table S5. Among them, T cells CD4 memory resting, mast cells resting, dendritic cells resting, monocytes, macrophages M2, and plasma cells were negatively correlated with RFC4 gene with significance, while T cells gamma delta, mast cells activated, T cells CD4 memory activated, macrophages M0, T cells follicular helper, T cells CD8, macrophages M1 were positively correlated with RFC4 gene with significance. The infiltration of 22 types of immune cells between $RFC4^{High}$ group and $RFC4^{Low}$ group was shown in Figure 8B. With median expression value of RFC4, our results showed that NK cells resting, macrophages M0, macrophages M1, mast cells activated, T cells CD4 memory activated, T cells CD8 and T cells follicular helper had more infiltration in the $RFC4^{High}$ group, while plasma cells, dendritic cells resting, mast cells resting, monocytes and T cells CD4 memory resting had more infiltration in the $RFC4^{Low}$ group. Furthermore, we regrouped immune cells into four categories, and dendritic cells, macrophages and mast cells showed the most significant differences between the $RFC4^{High}$ group and $RFC4^{Low}$ group, as shown in Figure 8C. Immune cell infiltration in different RFC4 groups and LUAD samples is shown in Supplementary Figures S1A, S1B.

The ESTIMATE analysis revealed that cancer tissues in the $RFC4^{High}$ group had lower stromal scores, lower immune scores, lower ESTIMATE scores, and higher tumor purity than those in the $RFC4^{Low}$ group, as shown in Figures 9A–D. Correlation analyses between RFC4 expression levels and stromal, immune, ESTIMATE, and tumor purity from ESTIMATE are shown in Figure 9E. Among them, stromal, immune and ESTIMATE scores were negatively correlated with RFC4 expression, whereas tumor purity was positively correlated with RFC4 expression.

3.7 Potential function prediction of RFC4

We downloaded 14 gene sets with common cancer-related functions from CancerSEA (http://biocc.hrbmu.edu.cn/CancerSEA/goDownload) and used GSVA to predict the RFC4

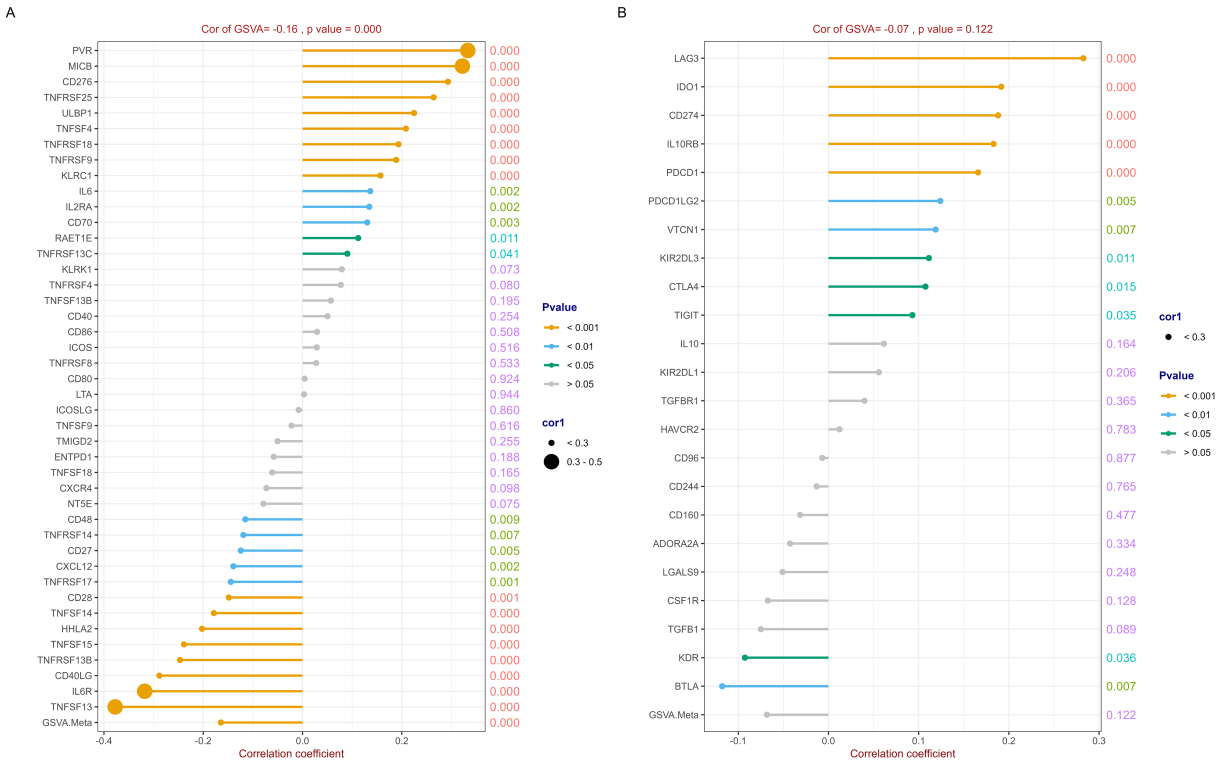

FIGURE 7
Correlation analysis between RFC4 and immunostimulators and immunoinhibitors. **(A)** Correlation analysis of 43 immunostimulators with RFC4. **(B)** Correlation analysis of 23 immunoinhibitors with RFC4. (Correlation analysis was conducted using Pearson's method. The numbers on the right side of each line represent the statistical significance of the correlation coefficient, that is, the P value. cor1: the abbreviation of the correlation coefficient).

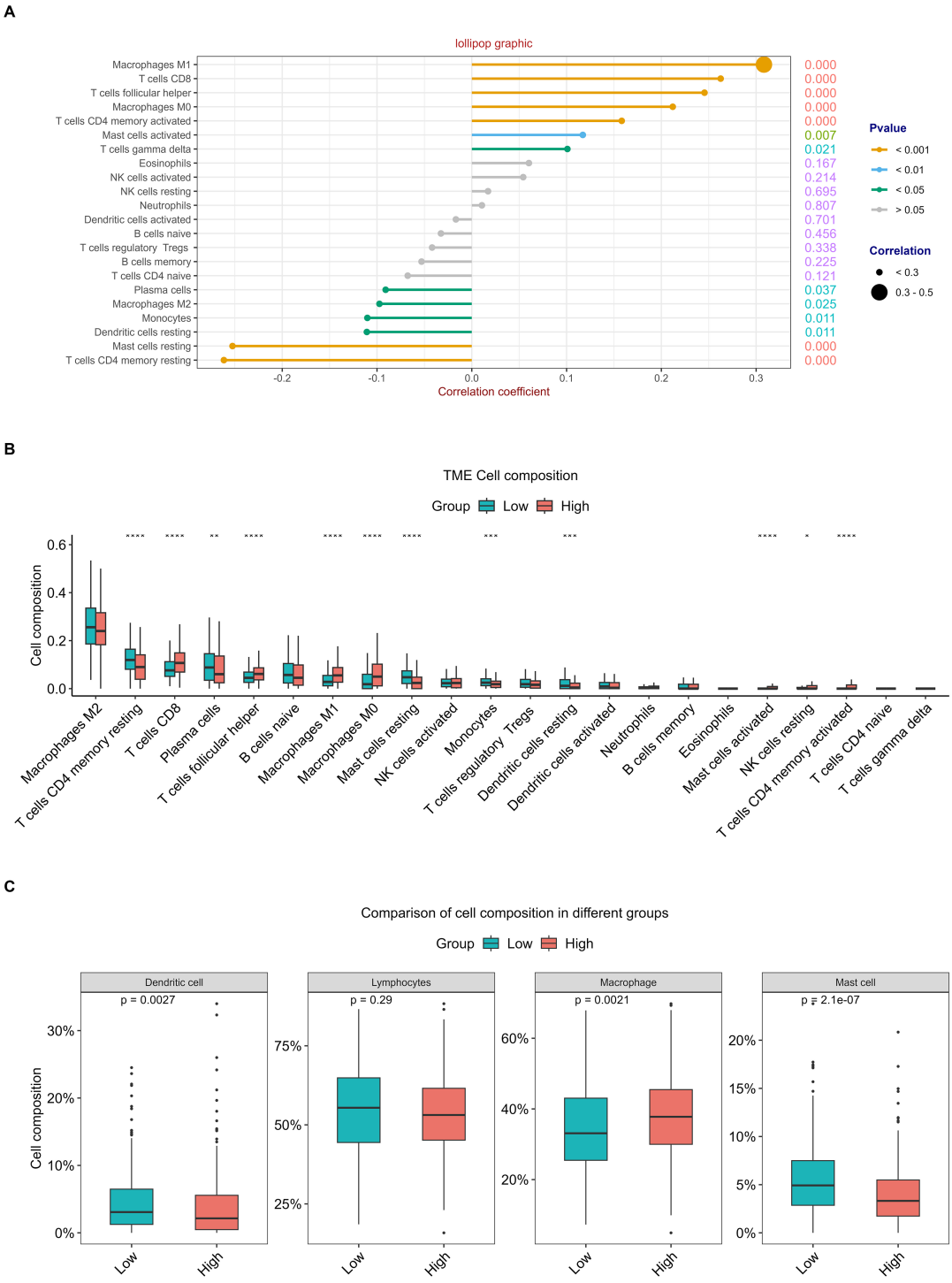

FIGURE 8
Analysis of tumor-infiltrating immune cells changes in different RFC4 status in LUAD cohort via CIBERSORT. **(A)** Correlation analysis of 22 immune cells with RFC4. **(B)** Differential analysis of immune cell infiltration between $RFC4^{High}$ group and $RFC4^{Low}$ group. **(C)** Four categories tumor-infiltrating immune cells between $RFC4^{High}$ group and $RFC4^{Low}$ group. (Correlation analysis was conducted using Pearson's method. The numbers on the right side of each line represent the statistical significance of the correlation coefficient, that is, the P value. cor1: the abbreviation of the correlation coefficient). "*":<0.05, "**":<0.01, "***":<0.001 and "****":<0.0001.

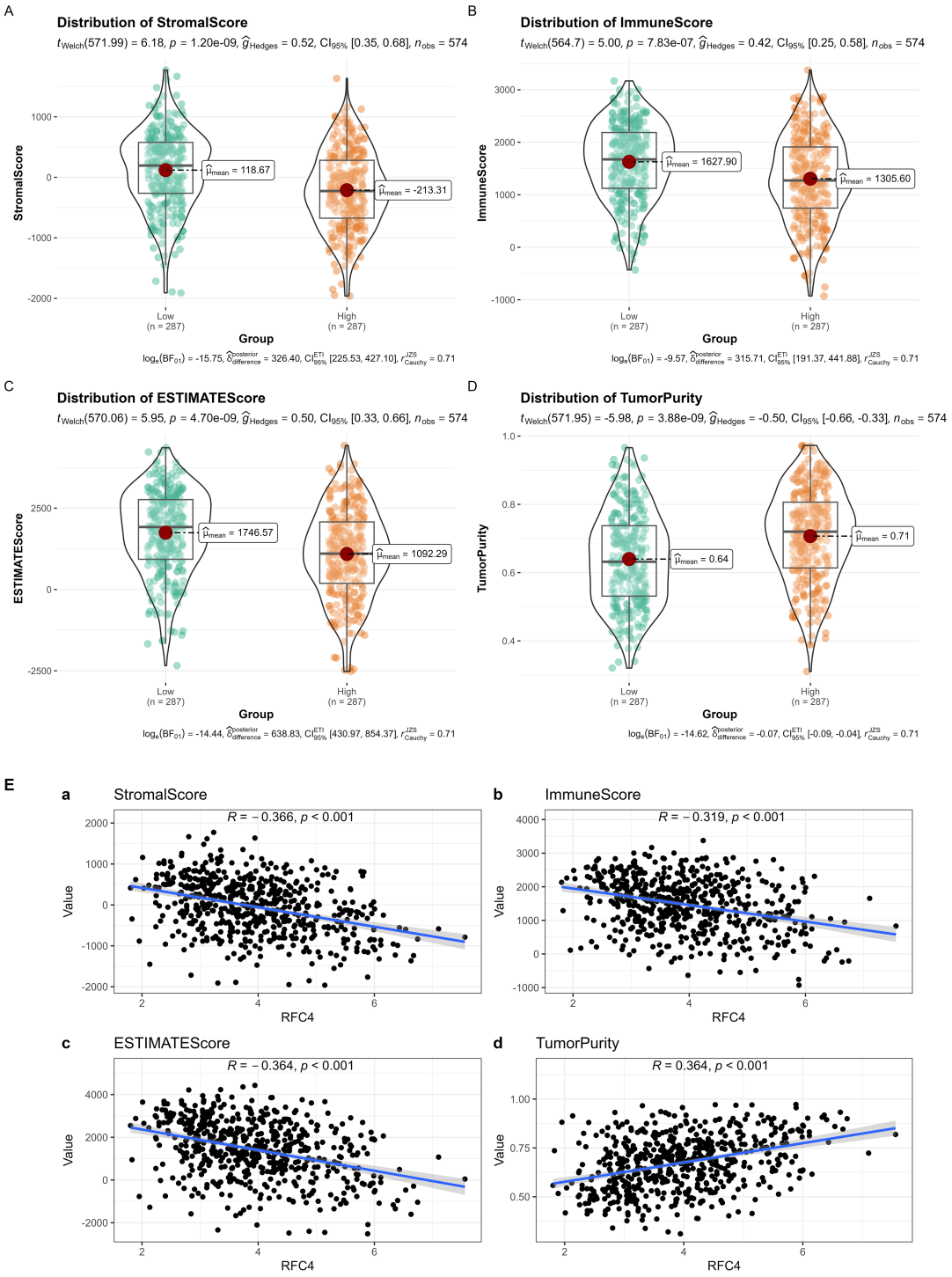

FIGURE 9
Analysis of tumor-infiltrating immune cells changes between RFC4^{High} group and RFC4^{Low} group in LUAD cohort via ESTIMATE. **(A)** Stromal scores. **(B)** immune scores. **(C)** ESTIMATE scores. **(D)** Tumor purity. **(E)** Correlation analysis between RFC4 and stromal scores **(a)**, immune scores **(b)**, ESTIMATE scores **(c)** and tumor purity **(d)**. Independent sample t-tests were used for the analysis of differences between groups in **(A–D)**. Correlation analysis was conducted using Pearson's method in **(E)**.

function (27). Except epithelial-mesenchymal transition (EMT) and metastasis, RFC4 was widely involved in other biological processes, including angiogenesis, apoptosis, cell cycle, differentiation, DNA damage, DNA repair, hypoxia, inflammation, invasion, proliferation, quiescence and stemness, as shown in Figure 10. Among them, RFC4 has the strongest positive relationship with cell cycle, DNA repair and DNA damage, indicating that RFC4 was mainly involved in these biological processes.

3.8 Prediction of immunotherapy efficacy of RFC4 in LUAD

TIDE predicted the efficacy of RFC4 in immunotherapy, as shown in Figures 11A–D. The $RFC4^{High}$ group showed a higher response rate to immune therapy than the $RFC4^{Low}$ group. Lower TIDE scores were observed in the $RFC4^{High}$ group, indicating higher immune sensitivity and increased patient benefit from ICIs treatment. Moreover, high RFC4 expression levels were correlated with lower dysfunction and higher exclusion. Furthermore, high RFC4 expression levels were correlated with higher MDSC, higher CAF, higher CD8 scores and lower TAM.M2 and lower IFNG scores. Thus, high RFC4 expression levels were correlated with better immunotherapy sensitivity in patients with LUAD.

3.9 RFC4 protein expression in LUAD

To verify RFC4 protein expression in LUAD tissues, we analyzed IHC images from the HPA database. RFC4 protein exhibited moderate-to-strong expression in 83.33% (25/30) cases of LUAD tissues and 22.22% (2/9) case of normal tissues, and the difference was statistically significant (χ^2 = 12.56, P=0.002). The IHC schematic of RFC4 protein in LUAD and normal lung tissues from the HPA database is shown in Figures 12A, B.

In our real-world cohort, among 31 cases of LUAD tissue, 24 cases had a strong positive RFC4 expression, 7 cases had a weak positive expression, and no cases demonstrated a negative expression. In adjacent tissues, only six cases showed strong positive RFC4 expression, 10 cases showed a weak positive expression, and 15 cases showed a negative expression. Thus, the strong positive expression rate of RFC4 in LUAD tissues was 77.42% (24/31), whereas that in adjacent tissues was 19.35% (6/31), and the difference was statistically significant (χ^2 = 26.329, P<0.001). An IHC schematic of RFC4 protein in LUAD and normal lung tissues from our real-world cohort is shown in Figures 13A–D.

4 Discussion

This study has made several important discoveries. First, both RFC4 mRNA and protein are overexpressed in LUAD cancer tissues, indicating a strong correlation between RFC4 and occurrence of LUAD cancer. Second, high RFC4 expression levels were associated with poor prognosis in patients with LUAD. Third, a relationship between the expression status of RFC4 and TIME remodeling was identified. Finally, patients with LUAD with high RFC4 expression levels may be more likely to benefit from immunotherapy.

In the past two decades, cancer research has significantly progressed, with targeted and immunotherapy drugs being constantly updated. The emergence of ICIs, used alone or in combination with chemotherapy, marks a milestone in the treatment of advanced LUAD (28). With the application of an increasing number of ICIs against PD-1, PD-L1, and CTLA-4, more treatment options are available and prognoses in patients with advanced LUAD has significantly improved (29). However, the current effective of immunotherapy for LUAD is still <40% (30).

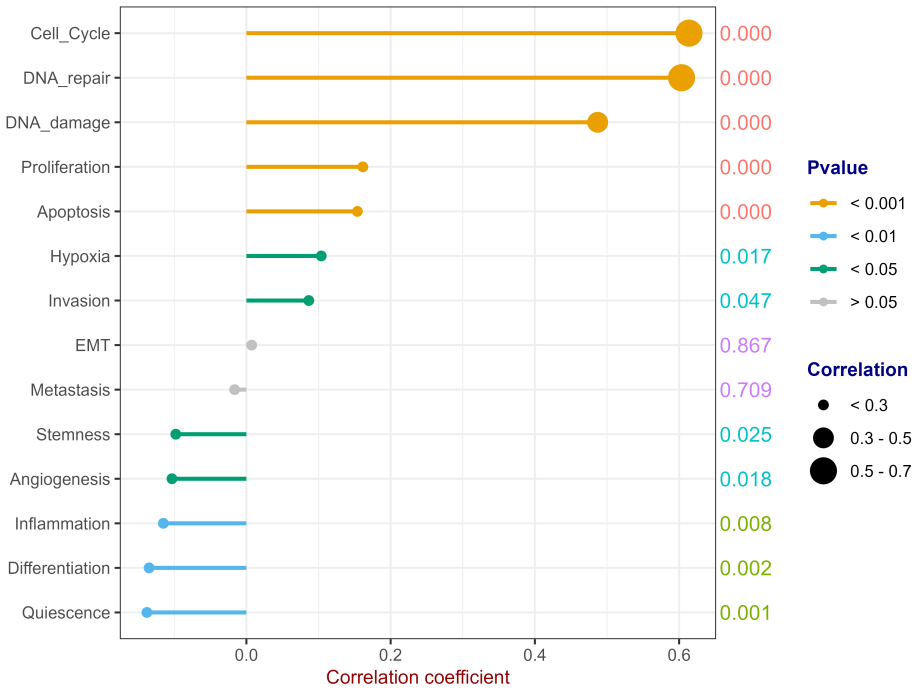

FIGURE 10
Potential Function Prediction of RFC4. (Correlation analysis was conducted using Pearson's method. The numbers on the right side of each line represent the statistical significance of the correlation coefficient, that is, the P value. cor1: the abbreviation of the correlation coefficient).

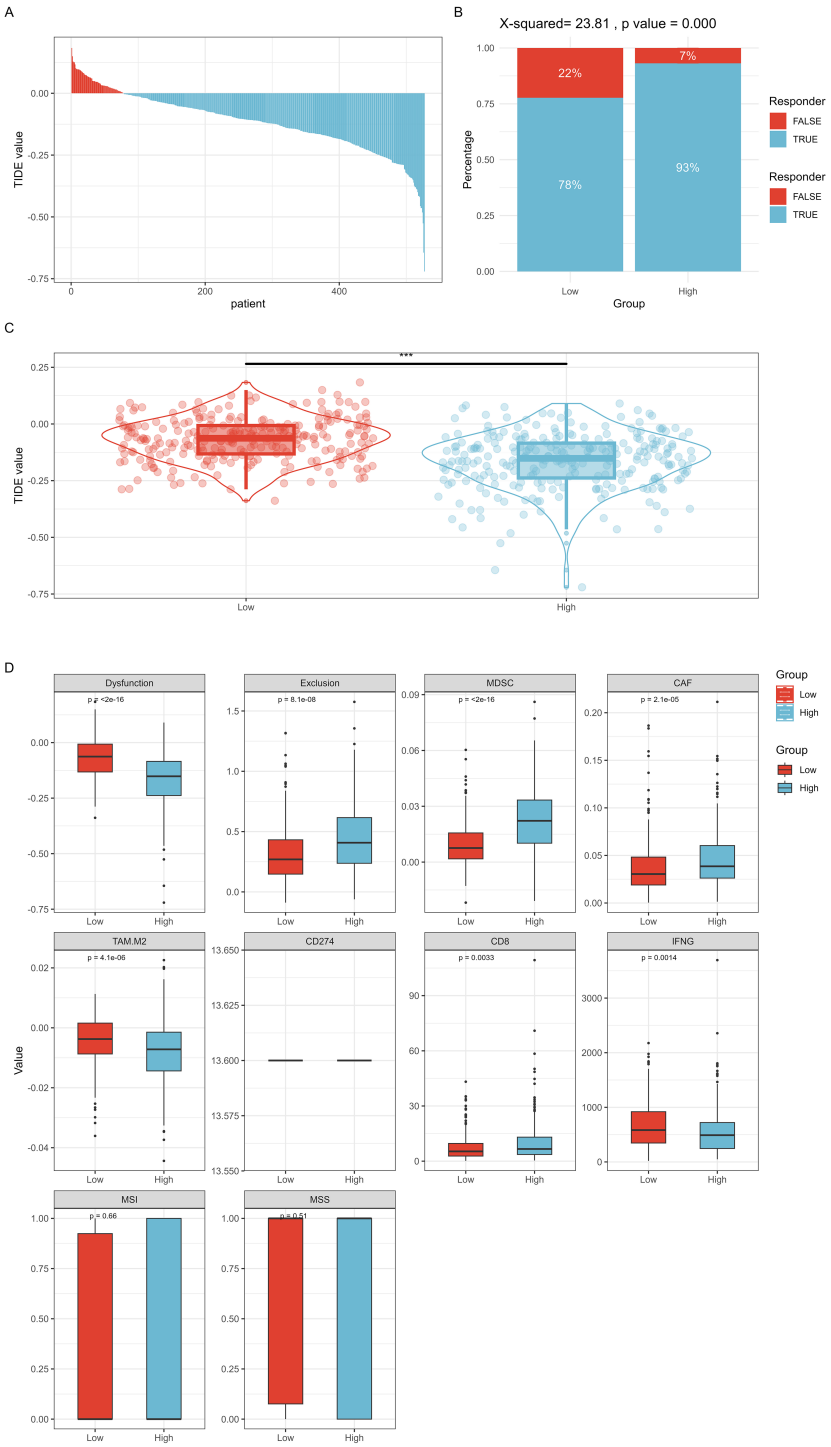

FIGURE 11
TIDE method predicted the efficacy of RFC4 in immunotherapy. **(A)** TIDE value of all TCGA samples. **(B)** Comparison of immune therapy response rates at different RFC4 expression levels. **(C)** Comparison of TIDE scores at different RFC4 expression levels. **(D)** Other immune therapy response prediction scores. "***":<0.001.

The response of LUAD to these therapies varies greatly, from patients with complete and long-term remission of metastatic diseases to those who rapidly progress and die from cancer despite the use of the latest ICIs. Thus, if patients with LUAD are not effectively selected, many will receive unnecessary and ineffective immunotherapy (31, 32). Unfortunately, biomarkers for predicting the effectiveness of immunotherapy in human cancer are currently lacking. Therefore, new robust markers still need to be explored to guide clinical treatment decisions about ICIs.

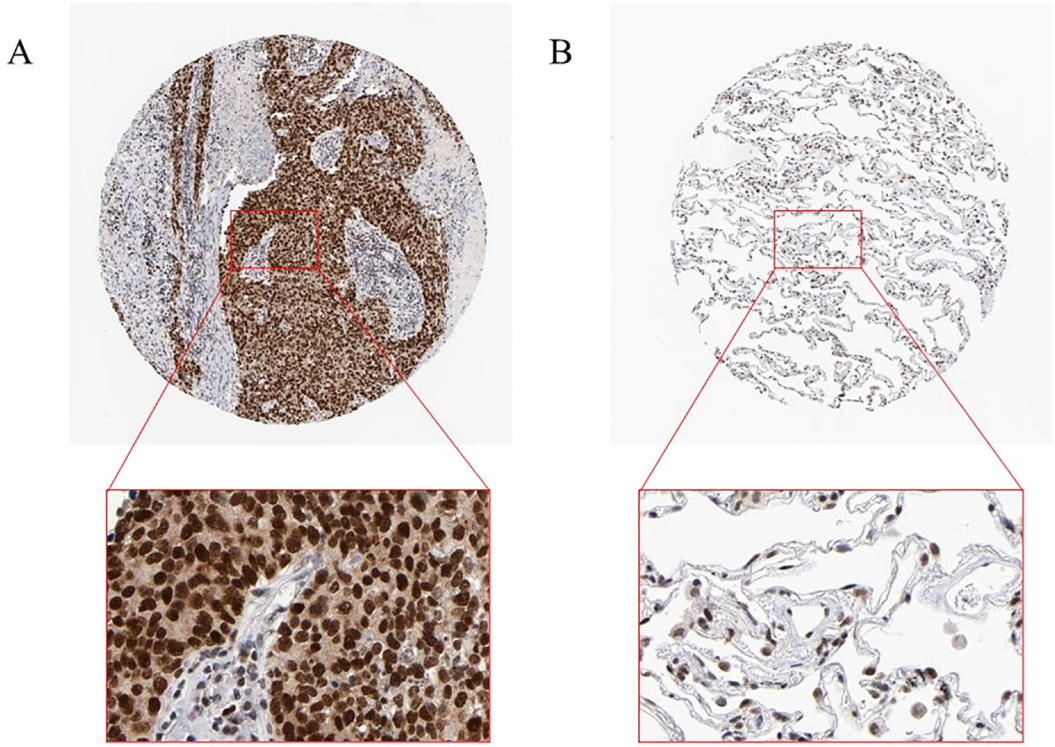

FIGURE 12
Interpretation of RFC4 in immunohistochemical staining. **(A)** High expression of RFC4 in LUAD cancer tissue. **(B)** Low expression of RFC4 in normal tissue.

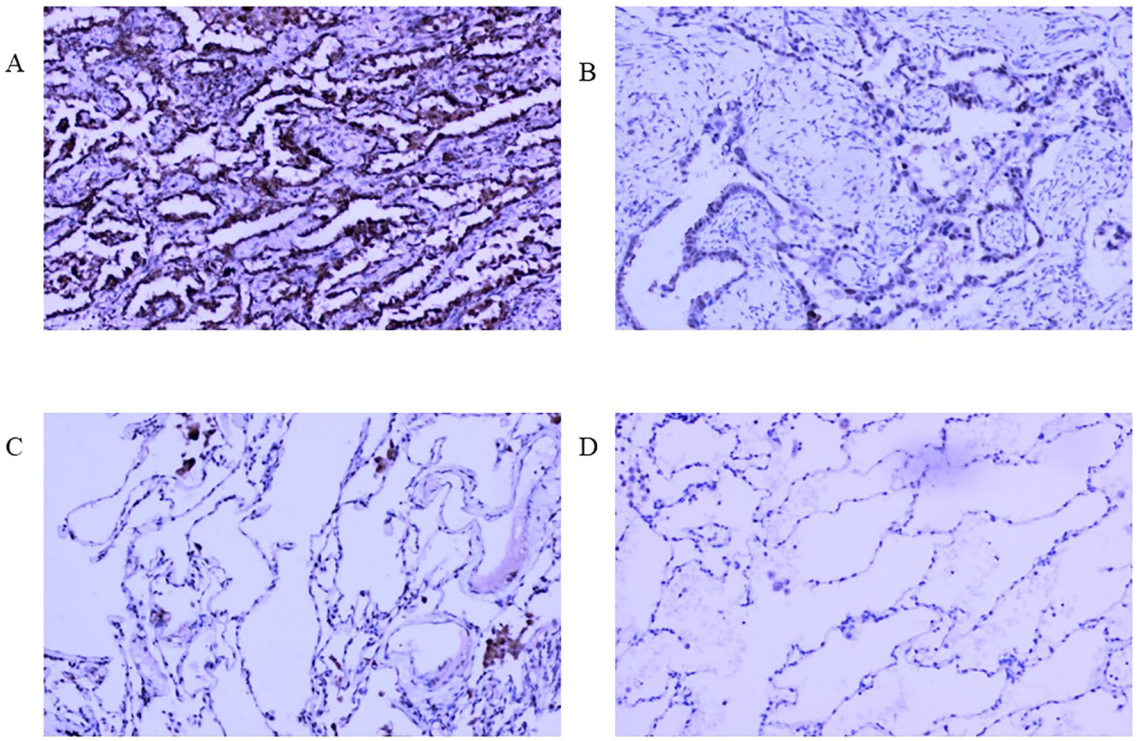

FIGURE 13
Interpretation of RFC4 in immunohistochemical staining from real-world cohort. **(A)** High expression of RFC4 in LUAD cancer tissue. **(B)** Low expression of RFC4 in LUAD cancer tissue. **(C)** Positive expression of RFC4 in normal lung tissue. **(D)** Negative expression of RFC4 in normal lung tissue.

RFCs are composed of the following five subunits: RFC1, RFC2, RFC3, RFC4, and RFC5 (16). RFCs not only increase the affinity between DNA polymerase and primer ends, but also reduce the number of PCNAs required to activate DNA polymerase (33). The RFCs exhibit DNA-dependent ATPase activity, which is necessary to activate DNA polymerase (33). The RFC complex contains a new 5′ DNA binding site responsible for transferring the 9-1–1 heterotrimeric clamp onto DNA, playing a role in DNA break repair (34). The role of RFCs in cancer progression has attracted increasing attention (10, 35). RFCs exhibit biological activities in various malignant tumors and may play important roles in the proliferation, progression, invasion, and metastasis of cancer cells (36, 37). Until recently, the role of RFC4 in cancer progression remained underexplored or unclear. Many studies have shown that RFC4 can promote tumor progression and metastasis in lung, nasopharyngeal, hepatocellular and colorectal cancers (16, 17, 36, 37). RFC4 is a regulatory protein that is primarily present in the nucleus (38). RFC4 exists mainly in the RFC complex of DNA and participates in the formation of DNA replication complexes to initiate the replication process of DNA. RFC4 is also involved in various important cellular processes, including DNA strand extension, DNA repair, and the other important signaling pathways (39). To elucidate the mechanism of RFC4 in LUAD, we used a series of bioinformatics methods to comprehensively analyze the gene expression and clinical characteristics of RFC4 in LUAD as well as the relationship between RFC4 expression and survival, microsatellite instability, and immune infiltration.

To the best of our knowledge, this study is the first to investigate the expression levels of RFC4 in cancer and normal tissues using the TCGA, GEO, and HPA databases. RFC4 expression was significantly upregulated in LUAD, which is consistent with its expression in other cancers (10, 16, 36). Thus, RFC4 may be involved in LUAD development and may be an important genetic diagnostic marker for LUAD. Interestingly, the increase in RFC4 expression was highly correlated with the mortality status of patients with LUAD, with RFC4 expression significantly elevated in deceased patients. Further survival analysis suggested that a high RFC4 expression level was an important prognostic factor. Unfortunately, we did not observe any correlation between RFC4 expression levels and tumor staging, nor were they associated with clinical features such as gender, age, and smoking status. Based on these results, RFC4 may be a potential prognostic biomarker of LUAD, providing a new targeted therapy strategy for the treatment of LUAD.

Changes in TIME are important features of tumors, which are highly correlated not only with cancer prognosis but also with tumor response to immunotherapy (40, 41). Several types of immunotherapies, including adoptive cell transfer and ICIs, have achieved long-lasting clinical responses, with the core mechanism of reshaping the TIME, enhancing tumor response to immunotherapy, and promoting tumor cell apoptosis (41). However, the high heterogeneity and dynamism of TIME hinder the precise isolation of immune cells within tumors, making it difficult to comprehensively analyze cancer prognosis. To further investigate the potential value of RFC4 in LUAD, we explored the correlation between RFC4 expression, immune cell infiltration and immunomodulators.

Among the selected immunostimulators, RFC4 expression was positively associated with 14 immunostimulatory factors and negatively correlated with 13 immunostimulatory factors. These results hindered the understanding of the role of RFC4 as an immunostimulator. Therefore, to clarify and summarize the results, we used GSVA to predict the gene set of immunostimulators. The GSVA results showed that RFC4 was negatively correlated with GSVA.Meta (rho=-0.164, P<0.001). The same method was applied to immune inhibitors. The GSVA result showed that RFC4 was negatively correlated with GSVA.Meta with no statistical significance (rho=-0.068, P=0.122). Based on these results, we inferred that RFC4 mainly alters the TIME by suppressing the expression of immune stimulatory factors. The dual positive/negative correlations between RFC4 and immunostimulators (as shown in Figure 7A) suggest that the mechanism by which RFC4 regulates the TIME is very complex. TIME is a complex system with highly precise regulatory mechanisms, and complex crosstalk with stromal components may be key to maintaining the orderly operation of these complex components (42, 43). A focused study on how RFC4 simultaneously suppress and activate immune pathways is required.

In addition, although the bioinformatics results were robust, the biological implications of RFC4 overexpression in LUAD remain unexplored. The present study is an exploratory study; therefore, we cannot yet determine the mechanism by which RFC4 affects the TME, which requires further research. In our preliminary results, RFC4 expression was positively correlated with PD-L1(CD274, as shown in Figure 7B), but not with CTLA-4 expression. We speculated that RFC4 might be related to PD1/PD-L1 pathway. Although the GO/KEGG analyses highlight the association of RFC4 with DNA repair and cell cycle pathways, direct mechanistic links to immune evasion (e.g., via PD-L1 regulation or antigen presentation) remain speculative. Therefore, our future study will verify the effect of RFC4 on PD-L1 expression through overexpression or knockdown, demonstrate the direction of gene regulation, and clarify whether RFC4 is a driver or consequence of immune evasion. The RFC4/NOTCH1 signal feedback loop was identified and revealed the mechanism of RFC4 promoting NSCLC metastasis and stemness, indicating its therapeutic and diagnostic/prognostic potential for NSCLC treatment (17).

With breakthroughs in tumor-related immunosuppressants and immunostimulants, ICIs have been widely used in tumor immunotherapy and have achieved significant and encouraging results. ICIs targeting PD-1/PD-L1 have been approved for the treatment of various malignant tumors, including melanoma, lymphoma, LC, and many other cancers. Therefore, speculating that RFC4 expression may regulate the infiltration level of tumor immune cells and the immune response, ultimately affecting the prognosis of patients with cancer, is reasonable. To verify this hypothesis, we employed two methods to explore the impact of RFC4 expression on immune cell infiltration into the TME. Using the CIBERSORT algorithm, we found that T cells CD4 memory resting, mast cells resting, dendritic cells resting, monocytes, macrophages M2, and plasma cells were negatively correlated with RFC4 gene with significance, whereas T cells gamma delta, mast cells activated, T cells CD4 memory activated, macrophages

M0, T cells follicular helper, T cells CD8, macrophages M1 were positively correlated with RFC4 gene. Using the ESTIMATE algorithm, we observed that cancer tissues in the $RFC4^{High}$ group had lower stromal and immune scores, lower ESTIMATE scores, and higher tumor purity. Based on the above analysis results, we confirmed that RFC4 played an important role in reshaping TIME. Therefore, the targeted regulation of RFC4 expression may alter the TIME of patients with LUAD and achieve better immunotherapy outcomes. Immunotherapy predictions further confirmed our hypothesis. In the TIDE algorithm, lower TIDE scores were observed in the $RFC4^{High}$ group, indicating higher immune sensitivity and increased patient benefit from ICI treatment. Moreover, high RFC4 expression levels were correlated with lower dysfunction and higher exclusion. Furthermore, high RFC4 expression levels were correlated with higher MDSC, CAF, and CD8 scores and lower TAM.M2 and IFNG scores. In tumors with a high infiltration of immune cells, dysfunctional effector toxic T cells can effectively kill tumor cells; however, their function is suppressed for some situation. Lower dysfunction and higher exclusion indicated that the cancer environment is more suitable for immunotherapy.

Our study also predicted the impact of RFC4 on 14 biological functions in common cancers. RFC4 is widely involved in other biological processes, including angiogenesis, apoptosis, cell cycle, differentiation, DNA damage, DNA repair, hypoxia, inflammation, invasion, proliferation, quiescence and stemness. According to previous reports, RFC4 is mainly related to DNA replication and repair, and our research yielded similar results, indicating that our prediction results have highly accurate (11, 37, 39). The manner by which RFC4-driven DNA replication/repair processes intersect with immune evasion requires further investigation. In most cancer tissues, the expression of DNA replication/repair genes is high (44), which may reflect the proliferative properties of cancers. High expression of DNA replication/repair genes is commonly a passive physiological state, although it is crucial for maintaining genomic stability. Genomic instability is a hallmark of cancer cell differentiation from normal cells (45). Genomic instability is an important genetic feature of changes in the TIME (46). In the presence of ATP, RFC4 can assemble PCNA and DNA polymerase δ onto a template using primers, thereby effectively extending the DNA replication strand. This process is essential for DNA replication and repair. Therefore, RFC4 expression was highly correlated with DNA repair.

Our findings strengthen the idea that high RFC4 expression levels were associated with poor prognosis in patients with LUAD. From the perspective of bioinformatics analysis, RCF4 alters tumor prognosis by reshaping the TIME, and targeted inhibition of RCF4 may be a promising new strategy for the treatment of LUAD. Our study has some limitations. First, our study was based only on the TCGA and GEO databases and should be validated in clinical cohorts in the future. Second, our study relied on TIDE scores to predict immunotherapy response but lacked experimental validation. In the future, a real-world cohort should be collected to verify whether RFC4 expression correlates with immunotherapy responses. Third, our study identified RFC4 as a potential therapeutic target but did not provide functional validation. In the future, silencing (shRNA/CRISPR) or overexpression of RFC4 in LUAD cell lines could be used to examine its impact on tumor growth, immune evasion, drug sensitivity, and cytokine expression. Fourth, the biological function of RFC4 protein expression in LUAD cells should be experimentally validated. Further exploration of the factors and upstream and downstream signaling pathways that regulate RFC4 *in vivo* is required. Finally, the biomarkers currently established, such as PD-L1 expression and tumor mutation burden, have shown very optimistic predictive value in immunotherapy (47, 48). It is still unclear whether RFC4 can provide additional predictive value compared with PD-L1 expression and tumor mutation burden. Further exploration is required in real-world cohorts.

5 Conclusion

RFC4 may be a promising biomarker for tumorigenesis and could effectively predict immunotherapy response in LUAD. RCF4 altered tumor prognosis by reshaping the TIME, and targeted inhibition of RCF4 may be a promising new strategy for the treatment of LUAD.

Data availability statement

The original contributions presented in the study are included in the article/Supplementary Material. Further inquiries can be directed to the corresponding author.

Ethics statement

The studies involving humans were approved by the Ethics Committee of the Second Affiliated Hospital of Fujian Medical University. The studies were conducted in accordance with the local legislation and institutional requirements. The participants provided their written informed consent to participate in this study.

Author contributions

JZ: Data curation, Funding acquisition, Methodology, Software, Writing – original draft. NL: Resources, Validation, Writing – original draft. BH: Data curation, Formal Analysis, Funding acquisition, Software, Writing – original draft. MW: Resources, Software, Writing – review & editing. LX: Data curation, Methodology, Writing – review & editing. BZ: Data curation, Validation, Writing – review & editing.

Funding

The author(s) declare that financial support was received for the research and/or publication of this article. The author(s) declare that financial support was received for the research and/or publication of this article. This study was supported by Fujian Provincial Natural and Scientific Foundation (Grant No:

2024J01671, to JZ), the Joint Funds for the Innovation of Science and Technology, Fujian Province (Grant No: 2024Y9358 to JZ), Science and technology projects of Quanzhou city (Grant No: 2023NS010 to JZ), Science and technology projects of Quanzhou city (Grant No: 2025QZNG056 to BH) and School-level Project of Quanzhou Medical College (Grant No: XJK2402A, to BH).

Conflict of interest

The authors declared that the research was conducted in the absence of any commercial or financial relationships that could be construed as a potential conflict of interest.

Generative AI statement

The author(s) declare that no Generative AI was used in the creation of this manuscript.

Publisher's note

Supplementary material

The Supplementary Material for this article can be found online at: https://www.frontiersin.org/articles/10.3389/fimmu.2025.1578243/full#supplementary-material

SUPPLEMENTARY FIGURE 1
Analysis of tumor-infiltrating immune cells changes in different RFC4 status in LUAD cohort via CIBERSORT. **(A)** Cell proportion of 22 immune cells between RFC4High group and RFC4Low group. **(B)** Cell proportion of 22 immune cells in all LUAD cancer samples.

References

1. Siegel RL, Miller KD, Fuchs HE, Jemal A. Cancer statistics, 2021. *CA Cancer J Clin*. (2021) 71:7–33. doi: 10.3322/caac.21654

2. Torre LA, Siegel RL, Jemal A. Lung cancer statistics. *Adv Exp Med Biol*. (2016) 893:1–19. doi: 10.1007/978-3-319-24223-1_1

3. Zheng R, Zhang S, Wang S, Chen R, Sun K, Zeng H, et al. Lung cancer incidence and mortality in China: Updated statistics and an overview of temporal trends from 2000 to 2016. *J Natl Cancer Cent*. (2022) 2:139–47. doi: 10.1016/j.jncc.2022.07.004

4. Duma N, Santana-Davila R, Molina JR. Non-small cell lung cancer: epidemiology, screening, diagnosis, and treatment. *Mayo Clin Proc*. (2019) 94:1623–40. doi: 10.1016/j.mayocp.2019.01.013

5. Alexander M, Kim SY, Cheng H. Update 2020: management of non-small cell lung cancer. *Lung*. (2020) 198:897–907. doi: 10.1007/s00408-020-00407-5

6. Jasper K, Stiles B, McDonald F, Palma DA. Practical management of oligometastatic non-small-cell lung cancer. *J Clin Oncol*. (2022) 40:635–41. doi: 10.1200/jco.21.01719

7. Patel SA, Weiss J. Advances in the treatment of non-small cell lung cancer: immunotherapy. *Clin Chest Med*. (2020) 41:237–47. doi: 10.1016/j.ccm.2020.02.010

8. Song P, Li W, Guo L, Ying J, Gao S, He J. Identification and validation of a novel signature based on NK cell marker genes to predict prognosis and immunotherapy response in lung adenocarcinoma by integrated analysis of single-cell and bulk RNA-sequencing. *Front Immunol*. (2022) 13:850745. doi: 10.3389/fimmu.2022.850745

9. Sharma P, Hu-Lieskovan S, Wargo JA, Ribas A. Primary, adaptive, and acquired resistance to cancer immunotherapy. *Cell*. (2017) 168:707–23. doi: 10.1016/j.cell.2017.01.017

10. Yu L, Li J, Zhang M, Li Y, Bai J, Liu P, et al. Identification of RFC4 as a potential biomarker for pan-cancer involving prognosis, tumour immune microenvironment and drugs. *J Cell Mol Med*. (2024) 28:e18478. doi: 10.1111/jcmm.18478

11. Li X, Burgers PM. Cloning and characterization of the essential Saccharomyces cerevisiae RFC4 gene encoding the 37-kDa subunit of replication factor C. *J Biol Chem*. (1994) 269:21880–4. doi: 10.1016/S0021-9258(17)31884-7

12. Zhou Y, Hingorani MM. Impact of individual proliferating cell nuclear antigen-DNA contacts on clamp loading and function on DNA. *J Biol Chem*. (2012) 287:35370–81. doi: 10.1074/jbc.M112.399071

13. Cullmann G, Fien K, Kobayashi R, Stillman B. Characterization of the five replication factor C genes of Saccharomyces cerevisiae. *Mol Cell Biol*. (1995) 15:4661–71. doi: 10.1128/mcb.15.9.4661

14. Wu G, Zhou J, Zhu X, Tang X, Liu J, Zhou Q, et al. Integrative analysis of expression, prognostic significance and immune infiltration of RFC family genes in human sarcoma. *Aging (Albany NY)*. (2022) 14:3705–19. doi: 10.18632/aging.204039

15. Corrette-Bennett SE, Borgeson C, Sommer D, Burgers PM, Lahue RS. DNA polymerase delta, RFC and PCNA are required for repair synthesis of large looped heteroduplexes in Saccharomyces cerevisiae. *Nucleic Acids Res*. (2004) 32:6268–75. doi: 10.1093/nar/gkh965

16. Guan S, Feng L, Wei J, Wang G, Wu L. Knockdown of RFC4 inhibits the cell proliferation of nasopharyngeal carcinoma *in vitro* and in *vivo*. *Front Med*. (2023) 17:132–42. doi: 10.1007/s11684-022-0938-x

17. Liu L, Tao T, Liu S, Yang X, Chen X, Liang J, et al. An RFC4/Notch1 signaling feedback loop promotes NSCLC metastasis and stemness. *Nat Commun*. (2021) 12:2693. doi: 10.1038/s41467-021-22971-x

18. Moreno Leon L, Gautier M, Allan R, Ilié M, Nottet N, Pons N, et al. The nuclear hypoxia-regulated NLUCAT1 long non-coding RNA contributes to an aggressive phenotype in lung adenocarcinoma through regulation of oxidative stress. *Oncogene*. (2019) 38:7146–65. doi: 10.1038/s41388-019-0935-y

19. Selamat SA, Chung BS, Girard L, Zhang W, Zhang Y, Campan M, et al. Genome-scale analysis of DNA methylation in lung adenocarcinoma and integration with mRNA expression. *Genome Res*. (2012) 22:1197–211. doi: 10.1101/gr.132662.111

20. Xu L, Lu C, Huang Y, Zhou J, Wang X, Liu C, et al. SPINK1 promotes cell growth and metastasis of lung adenocarcinoma and acts as a novel prognostic biomarker. *BMB Rep*. (2018) 51:648–53. doi: 10.5483/BMBRep.2018.51.12.205

21. Botling J, Edlund K, Lohr M, Hellwig B, Holmberg L, Lambe M, et al. Biomarker discovery in non-small cell lung cancer: integrating gene expression profiling, meta-analysis, and tissue microarray validation. *Clin Cancer Res*. (2013) 19:194–204. doi: 10.1158/1078-0432.Ccr-12-1139

22. Zhang C, Berndt-Paetz M, Neuhaus J. A comprehensive bioinformatics analysis of notch pathways in bladder cancer. *Cancers (Basel)*. (2021) 13:1–33 doi: 10.3390/cancers13123089

23. Gao Y, Chen Y, Liu M, Zeng D, Tan F, Wan H, et al. SLC17A9 as a prognostic biomarker correlated with immune infiltrates in human non-small cell lung cancer. *Am J Cancer Res*. (2023) 13:3963–82.

24. Li J, Hu K, He D, Zhou L, Wang Z, Tao Y. Prognostic value of PLXND1 and TGF-β1 coexpression and its correlation with immune infiltrates in hepatocellular carcinoma. *Front Oncol*. (2020) 10:604131. doi: 10.3389/fonc.2020.604131

25. Chen B, Khodadoust MS, Liu CL, Newman AM, Alizadeh AA. Profiling tumor infiltrating immune cells with CIBERSORT. *Methods Mol Biol*. (2018) 1711:243–59. doi: 10.1007/978-1-4939-7493-1_12

26. Yoshihara K, Shahmoradgoli M, Martínez E, Vegesna R, Kim H, Torres-Garcia W, et al. Inferring tumour purity and stromal and immune cell admixture from expression data. *Nat Commun*. (2013) 4:2612. doi: 10.1038/ncomms3612

27. Yuan H, Yan M, Zhang G, Liu W, Deng C, Liao G, et al. CancerSEA: a cancer single-cell state atlas. *Nucleic Acids Res*. (2019) 47:D900–d8. doi: 10.1093/nar/gky939

28. Kawachi H, Yamada T, Tamiya M, Negi Y, Goto Y, Nakao A, et al. Concomitant proton pump inhibitor use with pembrolizumab monotherapy vs immune checkpoint inhibitor plus chemotherapy in patients with non-small cell lung cancer. *JAMA Netw Open*. (2023) 6:e2322915. doi: 10.1001/jamanetworkopen.2023.22915

29. Shiravand Y, Khodadadi F, Kashani SMA, Hosseini-Fard SR, Hosseini S, Sadeghirad H, et al. Immune checkpoint inhibitors in cancer therapy. *Curr Oncol*. (2022) 29:3044–60. doi: 10.3390/curroncol29050247

30. Tang S, Qin C, Hu H, Liu T, He Y, Guo H, et al. Immune checkpoint inhibitors in non-small cell lung cancer: progress, challenges, and prospects. *Cells*. (2022) 11:1–27. doi: 10.3390/cells11030320

31. Sholl LM. Biomarkers of response to checkpoint inhibitors beyond PD-L1 in lung cancer. *Mod Pathol*. (2022) 35:66–74. doi: 10.1038/s41379-021-00932-5

32. Wu B, Lu S. The effect of PD-L1 categories-directed pembrolizumab plus chemotherapy for newly diagnosed metastatic non-small-cell lung cancer: a cost-effectiveness analysis. *Transl Lung Cancer Res*. (2020) 9:1770–84. doi: 10.21037/tlcr-19-605

33. Liu X, Gaubitz C, Pajak J, Kelch BA. A second DNA binding site on RFC facilitates clamp loading at gapped or nicked DNA. *Elife*. (2022) 11:e77483. doi: 10.7554/eLife.77483

34. Li H, O'Donnell M, Kelch B. Unexpected new insights into DNA clamp loaders: Eukaryotic clamp loaders contain a second DNA site for recessed 5' ends that facilitates repair and signals DNA damage: Eukaryotic clamp loaders contain a second DNA site for recessed 5' ends that facilitates repair and signals DNA damage. *Bioessays*. (2022) 44:e2200154. doi: 10.1002/bies.202200154

35. Bermúdez-Guzmán L. Pan-cancer analysis of non-oncogene addiction to DNA repair. *Sci Rep*. (2021) 11:23264. doi: 10.1038/s41598-021-02773-3

36. Yang WX, Pan YY, You CG. CDK1, CCNB1, CDC20, BUB1, MAD2L1, MCM3, BUB1B, MCM2, and RFC4 may be potential therapeutic targets for hepatocellular carcinoma using integrated bioinformatic analysis. *BioMed Res Int*. (2019) 2019:1245072. doi: 10.1155/2019/1245072

37. Wang XC, Yue X, Zhang RX, Liu TY, Pan ZZ, Yang MJ, et al. Genome-wide RNAi screening identifies RFC4 as a factor that mediates radioresistance in colorectal cancer by facilitating nonhomologous end joining repair. *Clin Cancer Res*. (2019) 25:4567–79. doi: 10.1158/1078-0432.Ccr-18-3735

38. Maga G, Mossi R, Fischer R, Berchtold MW, Hübscher U. Phosphorylation of the PCNA binding domain of the large subunit of replication factor C by Ca2+/calmodulin-dependent protein kinase II inhibits DNA synthesis. *Biochemistry*. (1997) 36:5300–10. doi: 10.1021/bi962809n

39. Krause SA, Loupart ML, Vass S, Schoenfelder S, Harrison S, Heck MM. Loss of cell cycle checkpoint control in Drosophila Rfc4 mutants. *Mol Cell Biol*. (2001) 21:5156–68. doi: 10.1128/mcb.21.15.5156-5168.2001

40. Binnewies M, Roberts EW, Kersten K, Chan V, Fearon DF, Merad M, et al. Understanding the tumor immune microenvironment (TIME) for effective therapy. *Nat Med*. (2018) 24:541–50. doi: 10.1038/s41591-018-0014-x

41. Zhang Y, Zhang Z. The history and advances in cancer immunotherapy: understanding the characteristics of tumor-infiltrating immune cells and their therapeutic implications. *Cell Mol Immunol*. (2020) 17:807–21. doi: 10.1038/s41423-020-0488-6

42. Mavatkar AD, Naidu CM, Prabhu JS, Nair MG. The dynamic tumor-stromal crosstalk: implications of 'stromal-hot' tumors in the process of epithelial-mesenchymal transition in breast cancer. *Mol Biol Rep*. (2023) 50:5379–93. doi: 10.1007/s11033-023-08422-4

43. Du W, Pasca di Magliano M, Zhang Y. Therapeutic potential of targeting stromal crosstalk-mediated immune suppression in pancreatic cancer. *Front Oncol*. (2021) 11:682217. doi: 10.3389/fonc.2021.682217

44. Suzuki M, Takahashi T. Aberrant DNA replication in cancer. *Mutat Res*. (2013) 743-744:111–7. doi: 10.1016/j.mrfmmm.2012.07.003

45. Li H, Zimmerman SE, Weyemi U. Genomic instability and metabolism in cancer. *Int Rev Cell Mol Biol*. (2021) 364:241–65. doi: 10.1016/bs.ircmb.2021.05.004

46. Bakhoum SF, Cantley LC. The multifaceted role of chromosomal instability in cancer and its microenvironment. *Cell*. (2018) 174:1347–60. doi: 10.1016/j.cell.2018.08.027

47. Luchini C, Bibeau F, Ligtenberg MJL, Singh N, Nottegar A, Bosse T, et al. ESMO recommendations on microsatellite instability testing for immunotherapy in cancer, and its relationship with PD-1/PD-L1 expression and tumour mutational burden: a systematic review-based approach. *Ann Oncol*. (2019) 30:1232–43. doi: 10.1093/annonc/mdz116

48. Ricciuti B, Wang X, Alessi JV, Rizvi H, Mahadevan NR, Li YY, et al. Association of high tumor mutation burden in non-small cell lung cancers with increased immune infiltration and improved clinical outcomes of PD-L1 blockade across PD-L1 expression levels. *JAMA Oncol*. (2022) 8:1160–8. doi: 10.1001/jamaoncol.2022.1981

frontiers | Frontiers in Immunology

TYPE Mini Review
PUBLISHED 25 June 2025
DOI 10.3389/fimmu.2025.1611861

OPEN ACCESS

EDITED BY
Kelsey P. Kubelick,
University of Virginia, United States

REVIEWED BY
Khan M. Imran,
University of North Carolina at Chapel Hill, United States
Alex Blair,
The Ohio State University, United States

*CORRESPONDENCE
Sean J. Judge
sjjudge@ucdavis.edu

RECEIVED 14 April 2025
ACCEPTED 04 June 2025
PUBLISHED 25 June 2025

CITATION
Purl MC, Shick A, Canter RJ and Judge SJ (2025) Tracking cellular therapies to optimize homing against liver metastases.
Front. Immunol. 16:1611861.
doi: 10.3389/fimmu.2025.1611861

Tracking cellular therapies to optimize homing against liver metastases

Megan C. Purl[1], Alexandria Shick[1], Robert J. Canter[1,2] and Sean J. Judge[1,2]*

[1]University of California Davis Health, Division of Surgical Oncology, Department of Surgery, Sacramento, CA, United States, [2]Comprehensive Cancer Center, University of California, Davis, Sacramento, CA, United States

Novel cellular therapies have shown practice changing results in a range of hematologic malignancies, though success against solid tumors has been limited. Key factors limiting success of these therapies against solid tumors are homing to the site(s) of disease, engraftment, maintenance of function, and persistence. The inhospitable tumor microenvironment appears to provide barriers at every step of this process. The liver, a unique organ with diverse immunoregulatory functions, is a common site for metastatic disease from solid cancers of the gastrointestinal (GI) tract. Although the complex interplay between hepatocytes, circulatory and tissue resident immune cells, and the enterohepatic circulation has been investigated for some time, many unanswered questions about the immunobiology of the liver remain. More so, novel imaging techniques provide unparalleled insight into these interactions and shed light on these complex processes that can lead to an improved understanding of the tumor microenvironment in the liver and opportunities for improving homing of cellular therapy against liver tumors. In this review, we will provide a focused assessment of this burgeoning field and focus on the emerging tools for studying homing of these therapies and how they may be enhanced to better treat liver metastases.

KEYWORDS

cancer immunotherapy, cellular therapy, immune cell tracking, chimeric antigen receptor, liver metastases, regional therapy

1 Introduction

The use of autologous chimeric antigen receptor (CAR) T cells has revolutionized the treatment of select hematologic malignancies. The success of CAR T therapy in these B-cell malignancies has sparked investigation into their use in solid tumors. Among gastrointestinal tumors, CAR T cells targeting claudin 18.2 has arisen as one of the most promising therapies against advanced or metastatic disease. Recent long-term results from a Phase I/II clinical trial investigating CAR T cells against claudin 18.2 for advanced GI tumors showed a 39% overall response rate among the 98 patients treated, though there

were different cohorts undergoing different treatment sequencing and immunotherapy adjuncts. However, it is notable that the investigators detected significantly worse outcomes in patients with liver metastases (median PFS 3.9 months versus 7.1 months) (1). This observation may highlight unique features of the liver and show how CAR cell therapy may function differently within this organ. Several clinical trials are underway (Table 1) aiming to treat advanced GI malignancies with cellular therapy and with different augmentation strategies.

The liver contains a diverse repertoire of immune and non-immune cells including liver sinusoid endothelial cells (LSEC), hepatic stellate cells, hepatocytes, Kupffer cells (KCs), monocyte-derived macrophages, myeloid-derived suppressor cells (MDSCs), natural killer (NK) cells, neutrophils, and T lymphocytes. These cell populations have broad and often opposing roles within the context of liver metastases. For example, Kupffer cells and monocyte-derived macrophages can demonstrate anti-tumor effects through direct phagocytosis of cancer cells, the production and pro-inflammatory cytokines such as TNF-a and the recruitment of cytotoxic T lymphocytes and NK cells (2). However, these same cells also demonstrate pro-tumorigenic actions. KCs have been shown to participate in the pre-metastatic niche formation (3), production of various cytokines and tumorigenic growth factors including IL-6, hepatocyte growth factor (HGF), vascular endothelial growth factor (VEGF), and matrix metalloproteinases (MMP) (2, 4), while monocyte-derived macrophages can be polarized to M2 where they also secrete growth factors such as VEGF (5), and induce regulatory T cells which can inhibit cytotoxic T cells via IL-10 and TGF-b (6). This diverse and highly complex environment is further complicated in the context of cellular therapies such as CAR T, where the interplay between these therapeutic cells and the liver milieu are less understood. Given the limited ability of CAR T cell therapy to successfully treat solid tumors metastatic to the liver, further insights into the unique

TABLE 1 Ongoing clinical trials investigating cellular therapies for advanced gastrointestinal malignancies.

Cell therapies for advanced GI malignancies		
	NCT Number	Study Title
Systemic CAR T	NCT05239143	P-MUC1C-ALLO1 Allogeneic CAR-T Cells in the Treatment of Subjects with Advanced or Metastatic Solid Tumors
	NCT05583201	NKG2D/CLDN18.2 CAR-T(KD-496) in the Treatment of Advanced NKG2DL +/CLDN18.2+ Solid Tumors
	NCT05089266	Study of αPD1-MSLN-CAR T Cells to Evaluate the Safety, Tolerability, and Effectiveness for Patients With MSLN-positive Advanced Solid Tumors
	NCT06912152	MT027 in Patients With Advanced Peritoneal Malignancies or Abdominal Metastatic Solid Tumors
	NCT05538195	Safety and Efficacy of CEA-targeted CAR-T for CEA-positive Advanced Malignant Solid Tumors
	NCT03874897	Chimeric Antigen Receptor T Cells Targeting claudin18.2 in Solid Tumors
	NCT05605197	U87 CART in Treatment of Advanced Solid Tumor
	NCT05947487	CD70 Targeted CAR-T Cells in CD70 Positive Advanced/Metastatic Solid Tumors
	NCT05120271	BOXR1030 T Cells in Subjects With Advanced GPC3-Positive Solid Tumors
	NCT06937567	CDH17 CAR-T Therapy in Advanced Malignant Solid Tumors
Regional CAR T	NCT02850536	CAR-T Hepatic Artery Infusions or Pancreatic Venous Infusions for CEA-Expressing Liver Metastases or Pancreas Cancer
	NCT02862704	A Study of MG7 Redirected Autologous T Cells for Advanced MG7 Positive Liver Metastases(MG7-CART)
	NCT03370198	Hepatic Transarterial Administrations of NKR-2 in Patients With Unresectable Liver Metastases From Colorectal Cancer
	NCT03818165	Phase 1b Study of CAR2Anti-CEA CAR-T Cell Hepatic Infusions for Pancreatic Carcinoma Patients With CEA+ Liver Metastases
	NCT04037241	Study of Anti-CEA CAR-T + Chemotherapy VS Chemotherapy Alone in Patients With CEA+Pancreatic Cancer & Liver Metastases
	NCT04952272	Intratumor CpG-ODN Injection Boosters Immune Killing Against in Situ Tumor Antigen Release for Advanced Solid Tumors
	NCT02416466	CAR-T Hepatic Artery Infusions and Sir-Spheres for Liver Metastases

(Continued)

10.3389/fimmu.2025.1611861

TABLE 1 Continued

Cell therapies for advanced GI malignancies		
NCT Number		Study Title
Systemic CAR T + cytokines	NCT02498912	Cyclophosphamide Followed by Intravenous and Intraperitoneal Infusion of Autologous T Cells Genetically Engineered to Secrete IL-12 and to Target the MUC16ecto Antigen in Patients With Recurrent MUC16ecto+ Solid Tumors
	NCT03932565	Interventional Therapy Sequential With the Fourth-generation CAR-T Targeting Nectin4/FAP for Malignant Solid Tumors
	NCT04377932	Interleukin-15 Armored Glypican 3-specific Chimeric Antigen Receptor Expressed in T Cells for Pediatric Solid Tumors
	NCT04715191	Interleukin-15 and -21 Armored Glypican-3-specific Chimeric Antigen Receptor Expressed in T Cells for Pediatric Solid Tumors
	NCT05035407	T Cell Receptor Gene Therapy Targeting KK-LC-1 for Gastric, Breast, Cervical, Lung and Other KK-LC-1 Positive Epithelial Cancers
	NCT05103631	Interleukin-15 Armored Glypican 3-specific Chimeric Antigen Receptor Expressed in Autologous T Cells for Solid Tumors
	NCT05393986	Claudin18.2-redirected Chimeric Antigen Receptor T Cells With Co-expression of Cytokines in Solid Tumors
	NCT06198296	Immunotherapy for Adults with GPC3-Positive Solid Tumors Using IL-15 and IL-21 Armored GPC3-CAR T Cells
	NCT05605197	U87 CART in Treatment of Advanced Solid Tumor
Systemic ACT + cytokines	NCT01868490	The Adoptive Immunotherapy for Solid Tumors Using Modified Autologous CIK Cells
	NCT01914263	Safety Study of Cord Blood-derived Cytokine-induced Killer Cells in Patients With Solid Tumor After Radical Resection
	NCT02757391	CD8+ T Cell Therapy and Pembrolizumab in Treating Patients With Metastatic Gastrointestinal Tumors
	NCT03610490	Autologous Tumor Infiltrating Lymphocytes MDA-TIL in Treating Patients With Recurrent or Refractory Ovarian Cancer, Colorectal Cancer, or Pancreatic Ductal Adenocarcinoma
	NCT06626256	STIL101 for Injection for the Treatment of Locally Advanced, Metastatic or Unresectable Pancreatic Cancer, Colorectal Cancer, Renal Cell Cancer, Cervical Cancer and Melanoma
Systemic ACT + RT	NCT04765462	Allogeneic γδT T Cell Therapy for the Treatment of Solid Tumors
	NCT03992326	Adoptive Transfer Of Autologous Tumor-Infiltrating Lymphocytes in Solid Tumors
	NCT06069570	Safety Study for a Gamma Delta T Cell Product Used With Low Dose Radiotherapy in Patients With Locally Advanced or Metastatic NSCLC or Solid Tumors With Bone Metastases
Regional CAR T + RT	NCT02416466	CAR-T Hepatic Artery Infusions and Sir-Spheres for Liver Metastases

GI, gastrointestinal; CAR T, chimeric antigen receptor T cells; ACT, adoptive cell transfer; RT, radiation therapy.

nature of liver metastases and how CAR cells may, or may not, be homing and functioning within the tumor-bearing liver are needed.

2 Liver metastases from gastrointestinal cancers

Malignancies of the GI tract represent some of the most common cancers in the United States and globally (7, 8). These include malignancies of the colon, esophagus, pancreas, rectum, and stomach with the most common histology being adenocarcinoma. Similar across these disease sites is the prevalent rate of liver metastases from the primary tumor (9). Observational data from the SEER database indicate that about 5% of patients present with synchronous liver metastases at the time of their diagnosis. Malignancies with the highest rate of synchronous liver metastases are cancers of the pancreas (36%), colon and rectum (27%), small bowel (15%), stomach (14%), and esophagus (14%) (10). Among all age groups, the highest incidence of liver metastases at diagnosis was among patients with cancers of the pancreas, colon and rectum. Better treatment of liver metastases is therefore a critical and urgent unmet need.

The current approach to treating liver metastases from GI cancers is mainly based on the primary cancer site. Treatment may include systemic therapy, radiation, or resection, though this depends on the extent of disease. In colorectal cancer, management of isolated liver metastases focuses on resection or other regional therapies such as radiofrequency ablation, arterial directed therapies, and selective internal radiation. Results from a large, multi-centered randomized clinical trial showed no improvement in overall survival (OS) when adding systemic chemotherapy to resection compared to resection alone in the management of colorectal liver metastases (median OS 61.3 months vs. 54.3 months) (11). This is in contrast to pancreas cancer where systemic chemotherapy is standard for patients with metastatic disease, and small case series investigating the role of simultaneous pancreas and liver resection in well-selected patients with low volume liver metastases identified no difference in OS compared to patients receiving palliative bypass without curative surgery and adjuvant chemotherapy (12). Apart from systemic therapy, and unique to the management of liver metastases, is the role of liver-directed, regional therapies. This was recently highlighted in the management of pancreatic cancer with limited liver or lung metastases where patients were randomized to chemotherapy or chemotherapy with targeted radiation to the metastatic sites and investigators detected improved PFS in the group receiving metastasis-directed RT (13). More so, these investigators analyzed patient peripheral blood and identified changes in circulating immune cells and cytokines that were positively associated with better PFS, highlighting the role of the immune system as a putative mediator of the anti-tumor effects following regional RT.

3 Liver homing of systemic cellular therapies

In the initial report of the clinical efficacy of the autologous CD19 CAR T therapy, CTL019 (tisaganleucel), for CD19+ lymphoid malignancies (14), responders had a median peak expansion of the cell therapy product at 8 days and 14/16 responders had consistently detectable levels of CTL019 DNA in their peripheral blood between 6 and 24 months after infusion. While peripheral blood is frequently the source for measuring CAR cell persistence in hematologic malignancies, peripheral blood may not be the most representative source for CAR cell persistence and function in the setting of solid tumors. Detecting the presence of CAR cells within a tumor-bearing solid organ is a challenging clinical issue and is either completed using a biopsy or requires investigation at autopsy. An earlier Phase I safety trial evaluating a second-generation CD19 CAR T cell therapy against B-cell leukemias investigated CAR T cell presence in other tissue sites following patient death. In a patient with CLL, researchers evaluated tumor contained within the lymph nodes, liver and bone marrow and identified the presence of these modified cells 44 hours after CAR T infusion (15). These data suggest that CAR T cells can home to sites of disease when given systemically. However, although CAR T cells can traffic to solid organs and tissues, it is not clear what effect infiltration into solid organs and tumors has on CAR T cell function. While there is an association between persistence of the cell therapy product and improved long term clinical outcomes (16), this does not appear necessary to prevent disease relapse. Additionally, relapse can still occur in the presence of persisting CAR T cells. In a recent review investigating long-term outcomes after CAR T therapy for hematologic malignancies, researchers cite various examples where durable responses have occurred in patients with no long-term evidence of CAR T persistence, and the setting where disease recurs while CAR T cells remain detectable (17). Using techniques to maximize homing of the cell therapy to sites of disease may lead to increased function and persistence by placing the CAR in proximity to the intended antigen. While these data show that systemically administered CAR cells can home to the liver, the larger question is whether this represents passive circulation of the CAR T cells through a highly vascular organ, or rather an active process where the CAR T cells preferentially traffic to the liver based on antigen recognition, chemokine or cytokine gradients, or some other pro-infiltrative signal.

4 PET imaging for tracking cellular therapies

Positron emission tomography (PET) is a nuclear medicine imaging technique that utilizes radioactive tracers to track both typical and atypical metabolic activity. PET/CT is commonly used for staging, assessment of therapeutic responses, and surveillance for different cancer types, including GI malignancies (18). The most commonly used PET radiotracer is 2-deoxy-2-[^{18}F] fluorodeoxyglucose ([^{18}F]FDG) which identified tissues with elevated glycolysis by radiotracer uptake. PET imaging can also be used to track cellular therapies *in vivo*. Techniques for tracking CAR cell therapy have been driven in large part due to advances in novel PET imaging probes. These technologies have allowed researchers to evaluate the variables of time and dose as a function of CAR homing and persistence, however these studies can be limited by the short half-life of these tracers. In one such study, investigators used CD19-tPSMA CAR T cells tagged with 18-fluorinated-DCFPyL against an acute lymphoblastic leukemia (ALL) mouse model to characterize CAR T durability and persistence (19). While the CAR T cells homed to tumor and had a profound anti-tumor effect, CAR T infiltration into tumor did not correlate with the concentration of CAR T cells within the peripheral blood or bone marrow, suggesting that peripheral blood levels may not represent what's occurring within the sites of disease. These results highlight the challenges in using peripheral blood as a surrogate in solid tumors.

Other PET-based imaging modalities are also being investigated to track cellular therapies *in vivo*. Immuno-positron emission tomography (ImmunoPET) is increasingly used in cellular therapies by combining the specificity of monoclonal antibodies with the high sensitivity and resolution of PET through utilizing radiolabeled antibodies and antibody fragments. These immunoPET probes such as the ^{89}Zr-DFO anti-ICOS tracer have been used to track human CAR T cells *in vivo* (20). Other strategies

include Immuno-PET/SPECT imaging which combines immunoPET with single-photon emission computed tomography (SPECT) to track CAR T cell therapies within solid tumors. This method has also been demonstrated to detect CAR T distribution, engraftment, and clearance within the setting of solid tumors (21). While these antibody-based imaging strategies have shown to be quite advantageous, the choice of antibody conjugation strategy and radionuclide half-life can determine the effectiveness of these methods and are important considerations when designing these experiments. The goal of these imaging techniques is to further enhance our understanding of cellular therapy in the setting of solid tumors and give insight into how to better improve these therapies. Various avenues have been investigated in order to improve these cellular therapies including route of administration, as well as enhancement with immunomodulatory agents such as radiation therapy and cytokines.

5 Regional administration to enhance liver homing

In clinical practice certain regional therapies have exploited the unique vasculature of the liver. This is most notable with the use of hepatic artery infusion therapy that utilizes high potency chemotherapeutics instilled directly into the hepatic artery to target liver metastases. Since the chemotherapy undergoes rapid first-pass metabolism in the liver, the agents can deliver targeted doses of chemotherapy to the liver before entering the systemic circulation via hepatic venous outflow as an inert chemotherapy byproduct. Several prior studies have clearly demonstrated that liver metastases are preferentially fed by the hepatic arterial system, as compared to the portal venous system. More so, pre-clinical studies have shown that higher concentrations of active chemotherapy are detected within liver tumors when the chemotherapy is administered via the hepatic artery compared to the portal vein (22). While these observations make a clear case for utilizing the hepatic arterial system for infusion of high potency chemotherapy, portal venous infusion appears to be the preferred route of administration for islet cell transplantation for the treatment and prevention of diabetes (23). While the reason for this observation remains unknown, those prior investigators posited that it may be related to relative ischemia at the end arterioles limiting islet cell survival and persistence. Nonetheless, there appears to be relevant differences between these two vascular systems in how the inflow arrives and is metabolized within the liver parenchyma, and this may be especially true when dealing with a cellular therapy.

5.1 Hepatic artery and portal vein delivery

Hepatic artery infusion therapy has been used for decades with favorable results (24). While this platform is most frequently utilized to deliver high-dose chemotherapy directly to liver tumors, new treatment options have arisen with the advent of novel therapies, including immunotherapy and cellular therapy. More recently, CAR T cells targeting the CEA antigen have been administered via the hepatic artery without or with systemic interleukin (IL)-2 support to target GI cancers metastatic to the liver. In a phase I trial of 8 patients, investigators showed the safety and feasibility of CAR T infusion into the hepatic arterial system for unresectable liver metastases from diverse GI malignancies (25). Investigators also collected a targeted and non-targeted liver biopsy at the time of the third CAR T infusion and evaluated the persistence of the product. The authors noted that nearly 1% of the normal liver mononuclear cells were CAR+ and 6.6% of the intratumoral mononuclear cells were CAR+, suggesting at least some preferential homing to the site of disease. Additionally, in four of the patients CAR T cells were not detectable in peripheral blood, suggesting that either the cell therapy product does not consistently enter systemic circulation, or that there is poor persistence of the cells within the periphery.

While most current CAR T or CAR NK studies are not utilizing regional therapy, prior investigators examined the effect of infusing lymphokine activated killer (LAK) cells into the liver for treating metastases from various primary sources. Using peripheral blood mononuclear cells exposed to IL-2 *in vitro*, LAK cells were generated and administered. Investigators delivered LAK cells into either the portal vein or hepatic arterial system in patients with liver metastases from melanoma (26). In a subset of patients, these LAK cells were radio-labelled and followed *in vivo* with imaging. *In vivo* distribution was monitored 24 and 120 hours after infusion and showed that over 80% of the radioactivity remained in the liver while the remainder of the radioactivity was in the spleen. This observation was noted to be similar between portal venous and hepatic arterial administration at both timepoints. The authors did not report a difference in anti-tumor effect between these two routes. While these results do not show a difference in homing between the route of regional delivery, it does support regional delivery as a technique to maximize cellular engraftment into the liver when targeting liver metastases.

5.2 Technique and safety of regional delivery

The dual blood supply to the liver allows administration of regional therapies via either the hepatic arterial or portal venous systems. For both routes, direct and indirect access are possible. Access to the portal vein is commonly performed via either image-guided percutaneous venous access (often trans-hepatic) or direct needle cannulation at the time of surgery. Access to the hepatic arterial system is commonly performed via selective cannulation following peripheral arterial access, image-guided percutaneous arterial access, or through a hepatic arterial infusion device placed during a surgical procedure. For percutaneous portal vein access, most experience is from trans-jugular intrahepatic portosystemic shunt (TIPS) and islet cell transplantation. In a large series from Japan investigating complications after transhepatic portal vein access, the overall complication rate was 16.5% (bleeding, pleural effusion, bile leak, liver dysfunction), highlighting that bleeding is

the most common complication (27). In a more contemporary series of surgical portal vein access for islet cell transplantation following total pancreatectomy, investigators measured a post-operative portal vein thrombosis rate of 6.6% (12/183), with most resolving after anti-coagulation therapy (28). This low thrombosis rate may be related to the large size and high flow volumes of the portal vein and support the safety of direct access during surgery.

Hepatic arterial access is most often completed using selective cannulation or through placement of a hepatic arterial infusion (HAI) device. Selective cannulation is a common technique and is most often utilized for trans-arterial embolization (TAE) for primary liver tumors. In one large study of nearly 5000 hepatic artery catheterizations for TAE, the incidence of arterial dissection of the celiac or its major branches was only 1.3% (61/4791) (29). This approach appears safe, but typically only allows for single treatment sessions. HAI therapy, where a permanent catheter is placed into a major hepatic arterial branch, allowing for continuous infusions and has been used for decades. In a large single-center series evaluating complications in HAI pump placement, the overall complication rate was 22% (120/544) with hepatic arterial thrombosis having occurred in 33 patients (6% total rate) (30), Notably, this thrombosis rate is similar to the portal venous thrombosis rate in the prior study. These results highlight the overall safety of these interventions however, it is important to note that these low complication rates were reported in high-volume centers with significant institutional experience in these procedures.

6 Radiation and cytokines to enhance liver homing

Radiation therapy (RT) has well established benefits in the multimodality management of solid tumors. RT has also been shown to demonstrate a variety of immunomodulatory effects on tumors and is now being investigated for its ability to enhance the engraftment and function of CAR therapies (31, 32). While there are currently few clinical studies investigating the combination of RT with CAR therapies, there is good evidence demonstrating the synergistic effects and enhanced antitumor efficacy with other immunotherapies such as PD-1/PD-L1 blockade (33). RT represents an additional locoregional strategy to improve cellular therapy against solid tumors, specifically cancers of the GI tract.

It has recently been shown that RT has a variety of immunomodulatory effects including direct effects on the tumor microenvironment (34, 35). It has also been shown to improve immune cell homing into the tumor via modulation of endothelial adhesion molecules intracellular adhesion molecule 1 (ICAM-1) and vascular-cell adhesion molecule 1 (VCAM-1), facilitating increased adherence and extravasation of lymphocytes out of circulation and into the tumor (36, 37). RT has also been shown to mediate increased T cell infiltration by inducing T cell attracting chemokines such as CXCL9, CXCL11, CCL5, and CCL8 in tumor cells (38, 39). Furthermore, the combination of RT with CAR T therapy has demonstrated increased CAR T infiltration into tumors with increased efficacy in a number of preclinical studies of GI malignancies. Amit and colleagues demonstrated that proton radiation boosts efficacy of CAR T therapy against pancreatic cancer. Using an orthotopic pancreatic cancer model, investigators treated mice with RT and subsequently injected mesothelin targeted CAR T cells (40). Not only did they observe an increase of CAR T infiltration into tumors but also saw an increase in tumor mesothelin expression following RT, further augmenting CAR-mediated antitumor responses. In a similar pancreatic cancer model, investigators showed that RT in combination with CAR T therapy increased CAR T efficacy and increased antigen-negative tumor susceptibility to CAR therapy (41). Jin and colleagues exploited radiation-induced IL-8 expression from tumors by utilizing CAR T cells expressing IL-8 receptors (CXCR1 or CXCR2). This resulted in enhanced migration and persistence of the CAR T cells in the tumor and was accompanied by tumor regression in pre-clinical models of pancreatic cancer (42). These pre-clinical studies demonstrate that combining RT with CAR T could enhance CAR T trafficking and have synergistic antitumor effects. In the context of GI liver metastases, RT can be directed specifically towards the liver and represents a promising modality to enhance the efficacy of cellular therapy towards solid tumors.

Cytokines represent an additional strategy by which to enhance the homing, engraftment, function, and persistence of CAR T therapy within solid GI tumors. While cytokine administration, namely IL-2, has historically been shown to have anti-tumor activity on their own (43), they are becoming increasingly used within the context of cellular immunotherapy, either via systemic administration or encoded within the cellular product to enhance therapeutic efficacy. In the context of CAR T therapy, 4th generation CARs or TRUCKs (T cell Redirected Universal Cytokine-mediated Killing) are being developed that secrete cytokines to signal in an autocrine fashion for increased efficacy and anti-tumor activity (44). Examples of cytokines currently under investigation include IL-2, IL-7, IL-12, IL-15, IL-18, IL-21, among others (45–50). There are also a number of clinical trials that are investigating cytokine-armored CAR T therapies for solid GI malignancies including IL-12, IL-15/IL-21, IL-7, CCL19 (NCT02498912, NCT06198296, NCT05035407). Allen and colleagues engineered CAR T cells with a synthetic Notch receptor which secrets IL-2 upon tumor recognition. In orthotopic PDAC models using immunocompetent mice, these authors demonstrated that the addition of the IL-2 circuit to the CAR T not only enhanced anti-tumor efficacy but specifically increased the infiltration of CAR T cells into the tumors, demonstrating the importance of cytokines in CAR T infiltration into solid tumors (46). Chemokine gradients have also been investigated to enhance the trafficking of CAR T therapies to solid tumors. Wang and colleagues developed an anti-mesothelin CAR T that co-expresses the chemokine receptor CCR2b for treatment of preclinical models of non-small-cell lung carcinoma

which demonstrated superior tumor infiltration compared to the Msln-CAR alone (51). This demonstrates translational potential to liver tumors as CCR2 has been shown to be involved in multiple stages of liver pathology including tumor progression (52). Thus, cytokines represent a promising strategy for enhancing the trafficking and function of CAR T therapy to solid tumors, specifically GI malignancies. While combination of CAR T therapy with strategies such as RT and cytokines do represent great promise for enhancing the efficacy of CAR T therapy against solid tumors, it is important to acknowledge the limitations of these strategies, primarily the safety of these methods. CAR T therapy alone has well documented risks of cytokine release syndrome and neurotoxicity and when combined with RT and/or cytokines which also have individual risks of toxicities, it's important to be cognizant of these risks and develop strategies that aim to mitigate these toxicities.

7 Conclusion

Chimeric antigen receptor therapies have revolutionized the treatment of hematological malignancies, but there is still much work to be done in optimizing these therapies for solid tumors. Several techniques are being investigated to optimize cell therapy function (Figure 1). Fundamental barriers to their success in solid tumors include homing, engraftment and persistence within the organ of disease. The liver is a common site of metastasis of GI malignancies and provides a unique opportunity to investigate the

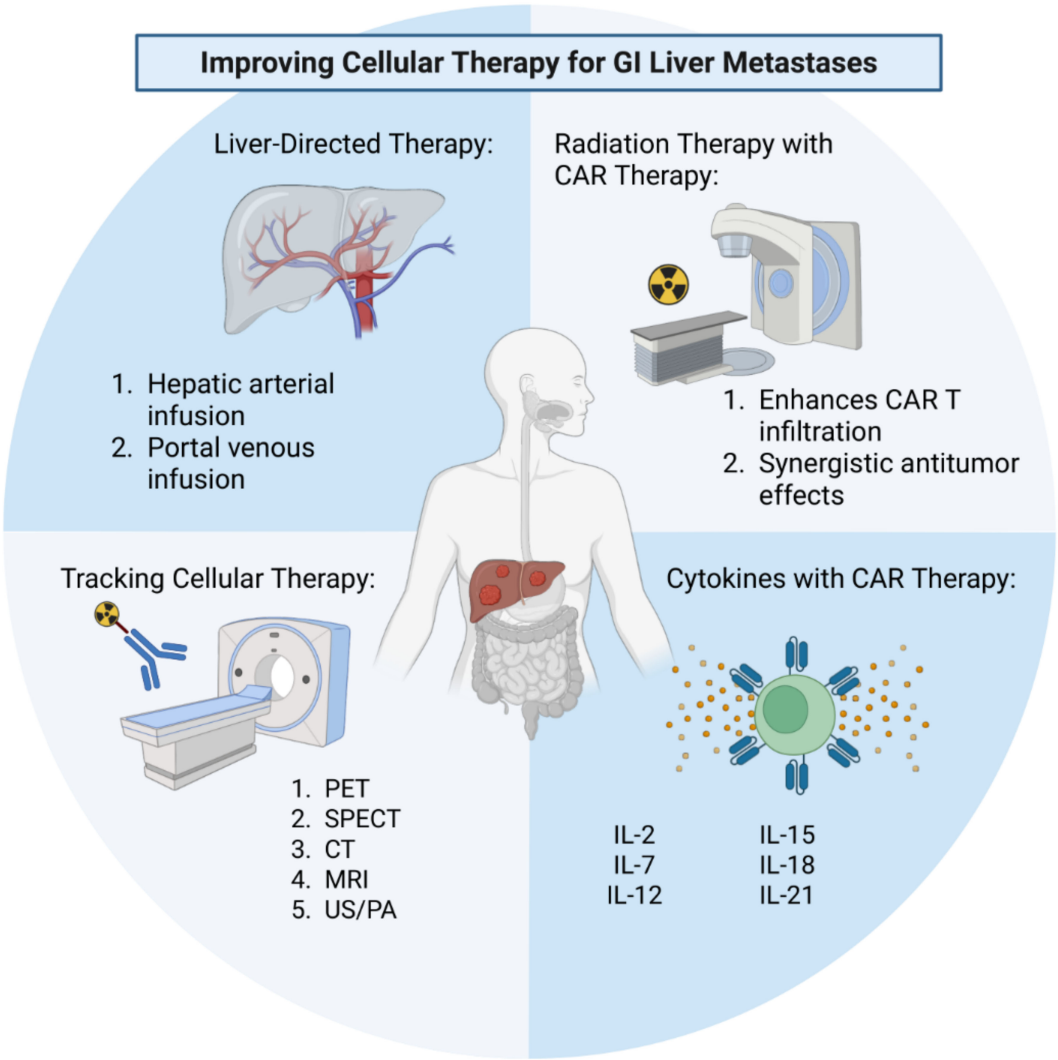

FIGURE 1
Strategies and techniques to improve cellular therapy for liver metastases of gastrointestinal (GI) origin. These include liver-directed regional therapies, combinations with external beam radiation therapy, augmenting CAR therapy with cytokines, and tracking CAR therapy using modern imaging modalities and novel probes. CAR, chimeric antigen receptor; PET, positron emission tomography; SPECT, single-photon emission computed tomography; CT, computed tomography; MRI, magnetic resonance imaging; US/PA, ultrasound/photoacoustic imaging. Created in BioRender. Purl, M. (2025) https://BioRender.com/4givi1o.

complex interactions between the host immune system, tumor microenvironment and cellular therapies. Novel liver-directed therapies are needed to improve cellular therapies in the context of GI liver metastases. Locoregional delivery of cellular therapies via hepatic arterial infusion or portal venous infusion represent two strategies for enhancing the homing, engraftment, and persistence of cellular therapy in the liver. While these strategies have long been tested in the application of chemotherapy, they represent a promising avenue for use in the setting of cellular therapy, specifically CAR T therapy for liver-directed treatments. Radiation therapy represents a second promising approach to enhancing the engraftment of CAR T therapy into solid tumors, specifically the liver. Studies investigating the combination of RT with CAR T therapy continue to emerge and have demonstrated promising success in the preclinical setting as a method of enhancing CAR T engraftment into solid GI malignancies. Utilizing cytokines in combination with CAR T therapy represents an additional strategy for enhancing homing and function of CAR T therapy into solid tumors. Lastly, tracking cellular therapy in real time is crucial in furthering our understanding of cellular therapy in the setting of solid tumors so that we may improve our approaches. Positron emission tomography, specifically immunoPET, has emerged as an innovative method to track CAR T therapy and has potential to provide vital information regarding the successes and failures of CAR T therapy. These tools can be utilized together to shed light on the complex interactions between host immunity, cellular therapy and the tumor microenvironment thus leading to improved cellular therapy against solid tumors.

Author contributions

MP: Conceptualization, Data curation, Visualization, Writing – original draft, Writing – review & editing. AS: Writing – original draft, Writing – review & editing. RC: Conceptualization, Writing – original draft, Writing – review & editing. SJ: Conceptualization, Supervision, Visualization, Writing – original draft, Writing – review & editing.

Funding

The author(s) declare that financial support was received for the research and/or publication of this article. This work was supported by the V Foundation and the following National Institutes of Health/National Cancer Institute Grants: R03CA270854, R03CA252793, and NIH Training Grant 1T32CA251007. SJJ is supported in part by the UC Davis Paul Calabresi Career Development Award for Clinical Oncology as funded by the National Cancer Institute/National Institutes of Health through grant #5K12-CA138464.

Acknowledgments

The authors would like to thank all members of the lab for their thoughtful feedback on this manuscript.

Conflict of interest

The authors declare that the research was conducted in the absence of any commercial or financial relationships that could be construed as a potential conflict of interest.

Generative AI statement

The author(s) declare that no Generative AI was used in the creation of this manuscript.

Publisher's note

References

1. Qi C, Liu C, Gong J, Liu D, Wang X, Zhang P, et al. Claudin18.2-specific CAR T cells in gastrointestinal cancers: phase 1 trial final results. *Nat Med*. (2024) 30:2224–34. doi: 10.1038/s41591-024-03037-z

2. Brodt P. Role of the microenvironment in liver metastasis: from pre- to prometastatic niches. *Clin Cancer Res*. (2016) 22:5971–82. doi: 10.1158/1078-0432.CCR-16-0460

3. Costa-Silva B, Aiello NM, Ocean AJ, Singh S, Zhang H, Thakur BK, et al. Pancreatic cancer exosomes initiate pre-metastatic niche formation in the liver. *Nat Cell Biol*. (2015) 17:816–26. doi: 10.1038/ncb3169

4. Dey A, Allen J, Hankey-Giblin. PA. Ontogeny and polarization of macrophages in inflammation: blood monocytes versus tissue macrophages. *Front Immunol*. (2014) 5:683. doi: 10.3389/fimmu.2014.00683

5. Mills CD. Anatomy of a discovery: M1 and M2 macrophages. *Front Immunol*. (2015) 6:212. doi: 10.3389/fimmu.2015.00212

6. Mills CD, Lenz LL, Harris. RA. A breakthrough: macrophage-directed cancer immunotherapy. *Cancer Res*. (2016) 76:513–165. doi: 10.1158/0008-5472.CAN-15-1737

7. Siegel RL, Miller KD, Wagle NS, Jemal. A. Cancer statistics 2023. *CA: A Cancer J Clin*. (2023) 73:17–485. doi: 10.3322/caac.21763

8. Sung H, Ferlay J, Siegel RL, Laversanne M, Soerjomataram I, Jemal A, et al. Global cancer statistics 2020: GLOBOCAN estimates of incidence and mortality worldwide for 36 cancers in 185 countries. *CA: A Cancer J Clin*. (2021) 71:209–495. doi: 10.3322/caac.21660

9. Tsilimigras DI, Brodt P, Clavien P-A, Muschel RJ, D'Angelica MI, Endo I, et al. Liver metastases. *Nat Rev Dis Primers*. (2021) 7:275. doi: 10.1038/s41572-021-00261-6

10. Horn SR, Stoltzfus KC, Lehrer EJ, Dawson LA, Tchelebi L, Gusani NJ, et al. Epidemiology of liver metastases. *Cancer Epidemiol*. (2020) 67:101760. doi: 10.1016/j.canep.2020.101760

11. Nordlinger B, Sorbye H, Glimelius B, Poston GJ, Schlag PM, Rougier P, et al. Perioperative FOLFOX4 chemotherapy and surgery versus surgery alone for resectable liver metastases from colorectal cancer (EORTC 40983): long-term results of a randomised, controlled, phase 3 trial. *Lancet Oncol.* (2013) 14:1208–15. doi: 10.1016/S1470-2045(13)70447-9

12. Gleisner AL, Assumpcao L, Cameron JL, Wolfgang CL, Choti MA, Herman JM, et al. Is resection of periampullary or pancreatic adenocarcinoma with synchronous hepatic metastasis justified? *Cancer*. (2007) 110:2484–925. doi: 10.1002/cncr.23074

13. Ludmir EB, Sherry AD, Fellman BM, Liu S, Bathala T, Haymaker C, et al. Addition of metastasis-directed therapy to systemic therapy for oligometastatic pancreatic ductal adenocarcinoma (EXTEND): A multicenter, randomized phase II trial. *J Clin Oncol*. (2024) 42:32. doi: 10.1200/JCO.24.00081

14. Schuster Stephen J, Jakub S, Chong Elise A, Nasta Sunita D, Mato Anthony R, Özlem A, et al. Chimeric antigen receptor T cells in refractory B-cell lymphomas. *N Engl J Med*. (2017) 377:2545–54. doi: 10.1056/NEJMoa1708566

15. Brentjens RJ, Rivière I, Park JH, Davila ML, Wang X, Stefanski J, et al. Safety and persistence of adoptively transferred autologous CD19-targeted T cells in patients with relapsed or chemotherapy refractory B-cell leukemias. *Blood*. (2011) 118:4817–28. doi: 10.1182/blood-2011-04-348540

16. Melenhorst JJ, Chen GM, Wang M, Porter DL, Chen C, Collins MA, et al. Decade-long leukaemia remissions with persistence of CD4+ CAR T cells. *Nature*. (2022) 602:503–9. doi: 10.1038/s41586-021-04390-6

17. Cappell KM, Kochenderfer. JN. Long-term outcomes following CAR T cell therapy: what we know so far. *Nat Rev Clin Oncol*. (2023) 20:359–715. doi: 10.1038/s41571-023-00754-1

18. Mulgaonkar A, Udayakumar D, Yang Y, Harris S, Öz OK, Geethakumari PR, et al. Current and potential roles of immuno-PET/-SPECT in CAR T-cell therapy. *Front Med*. (2023) 10:1199146. doi: 10.3389/fmed.2023.1199146

19. Minn Il, Huss DJ, Ahn H-H, Chinn TM, Park A, Jones J, et al. Imaging CAR T cell therapy with PSMA-targeted positron emission tomography. *Sci Adv*. (2019) 5: eaaw5096. doi: 10.1126/sciadv.aaw5096

20. Simonetta F, Alam IS, Lohmeyer JK, Sahaf B, Good Z, Chen W, et al. Molecular imaging of chimeric antigen receptor T cells by ICOS-immunoPET. *Clin Cancer Res*. (2021) 27:1058–68. doi: 10.1158/1078-0432.CCR-20-2770

21. Hu Y, Huang J. The chimeric antigen receptor detection toolkit. *Front Immunol*. (2020) 11:1770. doi: 10.3389/fimmu.2020.01770

22. Archer SG, Gray. BN. Comparison of portal vein chemotherapy with hepatic artery chemotherapy in the treatment of liver micrometastases. *Am J Surg*. (1990) 159:325–295. doi: 10.1016/S0002-9610(05)81228-0

23. Hirshberg B, Montgomery S, Wysoki MG, Xu H, Tadaki D, Lee J, et al. Pancreatic islet transplantation using the nonhuman primate (Rhesus) model predicts that the portal vein is superior to the celiac artery as the islet infusion site. *Diabetes*. (2002) 51:2135–40. doi: 10.2337/diabetes.51.7.2135

24. Datta J, Narayan RR, Kemeny NE, D'Angelica. MI. Role of hepatic artery infusion chemotherapy in treatment of initially unresectable colorectal liver metastases: A review. *JAMA Surg*. (2019) 154:768–5. doi: 10.1001/jamasurg.2019.1694

25. Katz SC, Burga RA, McCormack E, Wang LJ, Mooring W, Point GR, et al. Phase I hepatic immunotherapy for metastases study of intra-arterial chimeric antigen receptor–modified T-cell therapy for CEA+ Liver metastases. *Clin Cancer Res*. (2015) 21:3149–59. doi: 10.1158/1078-0432.CCR-14-1421

26. Keilholz U, Scheibenbogen C, Maclachlan D, Brado B, Hunstein W, Brado M, et al. Regional adoptive immunotherapy with interleukin-2 and lymphokine-activated killer (LAK) cells for liver metastases. *Eur J Cancer*. (1994) 30:103–5. doi: 10.1016/S0959-8049(05)80028-0

27. Ohta M, HashizumeME M, Kawanaka H, Akazawa K, Ueno K, Tomikawa M, et al. Complications of percutaneous transhepatic catheterization of the portal venous system in patients with portal hypertension. *J Gastroenterol Hepatol*. (1996) 11:630–345. doi: 10.1111/j.1440-1746.1996.tb00305.x

28. Robbins AJ, Skube ME, Bellin MD, Dunn TB, Chapman SA, Berry KL, et al. Portal vein thrombosis after total pancreatectomy and islet autotransplant: prophylaxis and graft impact. *Pancreas*. (2019) 48(10):1329–33. doi: 10.1097/MPA.0000000000001421

29. Yoon DY, Park JH, Chung JW, Han JK, Han. MC. Iatrogenic dissection of the celiac artery and its branches during transcatheter arterial embolization for hepatocellular carcinoma: outcome in 40 patients. *Cardiovasc Intervent Radiol*. (1995) 18:16–195. doi: 10.1007/BF02807349

30. Allen PJ, Nissan A, Picon AI, Kemeny N, Dudrick P, Ben-Porat L, et al. Technical complications and durability of hepatic artery infusion pumps for unresectable colorectal liver metastases: an institutional experience of 544 consecutive cases. *J Am Coll Surg*. (2005) 201:57–65. doi: 10.1016/j.jamcollsurg.2005.03.019

31. Quach HT, Skovgard MS, Villena-Vargas J, Bellis RY, Chintala NK, Amador-Molina A, et al. Tumor-targeted nonablative radiation promotes solid tumor CAR T-cell therapy efficacy. *Cancer Immunol Res*. (2023) 11:1314–31. doi: 10.1158/2326-6066.CIR-22-0840

32. Zhong L, Li Y, Achu TM, Wang. Y. "Combination of CAR–T cell therapy and radiotherapy: opportunities and challenges in solid tumors (Review). *Oncol Lett*. (2023) 26:2815. doi: 10.3892/ol.2023.13867

33. Gong J, Le TQ, Massarelli E, Hendifar AE, Tuli. R. Radiation therapy and PD-1/PD-L1 blockade: the clinical development of an evolving anticancer combination. *J ImmunoTher Cancer*. (2018) 6:46. doi: 10.1186/s40425-018-0361-7

34. Hovhannisyan L, Riether C, Aebersold DM, Medová M, Zimmer Y. CAR T cell-based immunotherapy and radiation therapy: potential, promises and risks. *Mol Cancer*. (2023) 22:825. doi: 10.1186/s12943-023-01775-1

35. Monjazeb AM, Schalper KA, Villarroel-Espindola F, Nguyen A, Shiao SL, Young K. Effects of radiation on the tumor microenvironment. *Semin Radiat Oncol*. (2020) 30:145–575. doi: 10.1016/j.semradonc.2019.12.004

36. Hallahan D, Kuchibhotla J, Wyble C. Cell adhesion molecules mediate radiation-induced leukocyte adhesion to the vascular endothelium. *Cancer Res*. (1996) 56:5150–55.

37. Krombach J, Hennel R, Brix N, Orth M, Schoetz U, Ernst A, et al. Priming anti-tumor immunity by radiotherapy: dying tumor cell-derived DAMPs trigger endothelial cell activation and recruitment of myeloid cells. *Oncoimmunology*. (2019) 8:e1523097. doi: 10.1080/2162402X.2018.1523097

38. Kohli K, Pillarisetty VG, Kim. TS. Key chemokines direct migration of immune cells in solid tumors. *Cancer Gene Ther*. (2022) 29:10–215. doi: 10.1038/s41417-021-00303-x

39. Dangaj D, Bruand M, Grimm AJ, Ronet C, Barras D, Duttagupta PA, et al. Cooperation between constitutive and inducible chemokines enables T cell engraftment and immune attack in solid tumors. *Cancer Cell*. (2019) 35:885–900.e10. doi: 10.1016/j.ccell.2019.05.004

40. Amit U, Uslu U, Verginadis II, Kim MM, Motlagh SAO, Diffenderfer ES, et al. Proton radiation boosts the efficacy of mesothelin-targeting chimeric antigen receptor T cell therapy in pancreatic cancer. *Proc Natl Acad Sci*. (2024) 121:e2403002121. doi: 10.1073/pnas.2403002121

41. DeSelm C, Palomba ML, Yahalom J, Hamieh M, Eyquem J, Rajasekhar VK, et al. Low-dose radiation conditioning enables CAR T cells to mitigate antigen escape. *Mol Ther: J Am Soc Gene Ther*. (2018) 26:2542–525. doi: 10.1016/j.ymthe.2018.09.008

42. Jin L, Tao H, Karachi A, Long Y, Hou AY, Na M, et al. CXCR1- or CXCR2-modified CAR T cells co-opt IL-8 for maximal antitumor efficacy in solid tumors. *Nat Commun*. (2019) 10:4016. doi: 10.1038/s41467-019-11869-4

43. Atkins MB, Lotze MT, Dutcher JP, Fisher RI, Weiss G, Margolin K, et al. High-dose recombinant interleukin 2 therapy for patients with metastatic melanoma: analysis of 270 patients treated between 1985 and 1993. *J Clin Oncol*. (1999) 17:2105–16. doi: 10.1200/JCO.1999.17.7.2105

44. Tang L, Pan S, Wei X, Xu X, Wei. Q. "Arming CAR-T cells with cytokines and more: innovations in the fourth-generation CAR-T development. *Mol Ther*. (2023) 31:3146–625. doi: 10.1016/j.ymthe.2023.09.021

45. Zhang Q, Hresko ME, Picton LK, Su L, Hollander MJ, Nunez-Cruz S, et al. A human orthogonal IL-2 and IL-2Rβ System enhances CAR T cell expansion and antitumor activity in a murine model of leukemia. *Sci Trans Med*. (2021) 13:eabg6986. doi: 10.1126/scitranslmed.abg6986

46. Allen GM, Frankel NW, Reddy NR, Bhargava HK, Yoshida MA, Stark SR, et al. Synthetic cytokine circuits that drive T cells into immune-excluded tumors. *Sci (New York NY)*. (2022) 378:eaba1624. doi: 10.1126/science.aba1624

47. Hurton LV, Singh H, Najjar AM, Switzer KC, Mi T, Maiti S, et al. Tethered IL-15 augments antitumor activity and promotes a stem-cell memory subset in tumor-specific T cells. *Proc Natl Acad Sci U S A*. (2016) 113:E7788–97. doi: 10.1073/pnas.1610544113

48. Chmielewski M, Abken H. CAR T cells transform to trucks: chimeric antigen receptor-redirected T cells engineered to deliver inducible IL-12 modulate the tumour stroma to combat cancer. *Cancer Immunol Immunother: CII*. (2012) 61:1269–775. doi: 10.1007/s00262-012-1202-z

49. He C, Zhou Y, Li Z, Farooq MA, Ajmal I, Zhang H, et al. Co-expression of IL-7 improves NKG2D-based CAR T cell therapy on prostate cancer by enhancing the expansion and inhibiting the apoptosis and exhaustion. *Cancers*. (2020) 12:1969. doi: 10.3390/cancers12071969

50. Štach M, Ptáčková P, Mucha M, Musil J, Klener P, Otáhal. P. "Inducible secretion of IL-21 augments anti-tumor activity of piggyBac-manufactured chimeric antigen receptor T cells. *Cytotherapy*. (2020) 22:744–545. doi: 10.1016/j.jcyt.2020.08.005

51. Wang Y, Wang J, Yang X, Yang J, Lu P, Zhao L, et al. Chemokine receptor CCR2b enhanced anti-tumor function of chimeric antigen receptor T cells targeting mesothelin in a non-small-cell lung carcinoma model. *Front Immunol*. (2021) 12:628906. doi: 10.3389/fimmu.2021.628906

52. She S, Ren L, Chen P, Wang M, Chen D, Wang Y, et al. Functional roles of chemokine receptor CCR2 and its ligands in liver disease. *Front Immunol*. (2022) 13:812431. doi: 10.3389/fimmu.2022.812431

frontiers | Frontiers in Immunology

TYPE Review
PUBLISHED 22 September 2025
DOI 10.3389/fimmu.2025.1621812

OPEN ACCESS

EDITED BY
Kelsey P. Kubelick,
University of Virginia, United States

REVIEWED BY
Pranita Sarangi,
Indian Institute of Technology Roorkee, India
Myeongsoo Kim,
Georgia Institute of Technology, United States

*CORRESPONDENCE
Yuanpei Li
lypli@health.ucdavis.edu

RECEIVED 01 May 2025
ACCEPTED 27 August 2025
PUBLISHED 22 September 2025

CITATION
Racacho KJ, Shiau Y-P, Villa R, Mahri S, Tang M, Lin T-Y and Li Y (2025) The tumor immune microenvironment: implications for cancer immunotherapy, treatment strategies, and monitoring approaches.
Front. Immunol. 16:1621812.
doi: 10.3389/fimmu.2025.1621812

The tumor immune microenvironment: implications for cancer immunotherapy, treatment strategies, and monitoring approaches

Kelsey Jane Racacho[1], Ya-Ping Shiau[1], Rodolfo Villa[1], Sohaib Mahri[1], Menghuan Tang[1], Tzu-Yin Lin[2] and Yuanpei Li[1]*

[1]Department of Biochemistry and Molecular Medicine, University of California, Davis, Sacramento, CA, United States, [2]Department of Internal Medicine, University of California, Davis, Sacramento, CA, United States

The tumor immune microenvironment (TIME) plays a pivotal role in cancer progression, detection, and response to cancer treatments. Current knowledge of the diverse and dynamic cellular components of the TIME underscores how the immune landscape evolves in response to immunotherapy. This review highlights the importance of understanding the TIME for advancing cancer immunotherapy by integrating insights from basic biology and clinical practice with recent advances in science and technology, paving the way for more personalized cancer therapies through modern medical innovations. The cellular and molecular compositions of the TIME and the cellular interactions will be explored. Next, we summarize how the TIME is shaped by immune activation and suppression through various mechanisms of action. Immunotherapies designed to enhance host immune function are discussed in detail to visualize and quantify cellular dynamics within the TIME once treated with immunotherapy. In particular, the integration of artificial intelligence (AI) has significantly enhanced early cancer detection and diagnostics by analyzing patient samples with greater precision. The topics are structured to explore core principles, immune activation and suppression, imaging methods, current and emerging therapies, and the broader influence of the TIME on diagnosis, monitoring, and treatment strategies.

KEYWORDS

tumor immune microenvironment, immune surveillance, immune activation, immunosuppressive, treatment, artificial intelligence

1 Introduction

The World Health Organization (WHO) has reported roughly 9.7 million cancer-related deaths around the world and nearly 20 million cancer-related incidences in 2022 (1). Globally, lung cancer was reported as the most common cancer type and the leading cause of cancer-related deaths in 2022. Among females, it was followed by breast cancer, colorectal cancer, prostate cancer, and stomach cancer, according to the WHO and the International Agency for Research on Cancer (2). Cancerous tumors arise from mutated cells that divide uncontrollably and can migrate to form new tumors—a process called metastasis that occurs in late-stage tumor development (3–5). Many cancer types form solid tumors, although some cancers, such as leukemias, form liquid tumors (6). Each tumor type has driver genes that promote tumorigenesis by supporting signaling pathways and creating a cancer-friendly environment, posing major challenges for treatment (7). Tumors create and sustain complex pro-tumorigenic environments called tumor immune microenvironments (TIME). TIME comprises host immune cells that can contribute to tumor progression by creating an immunosuppressive environment and facilitating tumor growth and expansion (8). TIME is a continuously evolving environment that best suits the specific tumor type, surrounding cells, and environment (8, 9). Due to the complexity of the TIME, monitoring and diagnostic tests have played an important role in cancer treatment to prevent progression and manage recurrence (10) We will discuss key cell types in the TIME - T lymphocytes (T cells), natural killer (NK cells), macrophages, and dendritic cells (DCs) - that help tumors evade the immune system and the complex interactions within the TIME presenting major challenges for effective cancer treatment (8). Current TIME-targeting treatments boost the immune system or directly attack tumor cells, using approaches like checkpoint inhibitors, adoptive cell therapy, and cancer vaccines (11, 12). Treating the TIME is challenged by its complexity, heterogeneity, and tumor immune evasion, leading to resistance and reduced efficacy, especially in solid tumors (13, 14). We will explore the complex immune landscape of the TIME, highlight key immune cell types and current immunotherapies, while addressing the challenges posed by tumor heterogeneity and immune evasion in cancer treatment.

1.1 Concepts of tumor immune microenvironment

TIME is a dynamic, multifaceted ecosystem composed of tumor cells, diverse immune populations—including tumor-infiltrating lymphocytes (TILs), macrophages, DCs, and myeloid-derived suppressor cells (MDSCs), as well as non-immune stromal components such as fibroblasts and endothelial cells, all of which work together to modulate anti-tumor immunity (15, 16). Tumor-host interactions shape the TIME as tumor-derived factors (tumor-derived cytokines, growth factors, and metabolites) promote tumor survival and remodel the microenvironment, while host immune and stromal cells provide nutrients and support that influence tumor progression (17, 18). Within the TIME, tumor cells mimic the host immune system to evade attacks and shape a specialized environment, while the host immune system continuously remodels the TIME through tumorigenesis and immune evasion, promoting chronic inflammation, a hallmark of cancer progression through the innate and adaptive immune response (8, 19, 20).

During immunosuppression, the immune system limits immune cell recruitment to the TIME by dampening the overall immune response (21). Immunotherapy can reshape the TIME by overcoming immune suppression and restoring the function of anti-tumor immune cells. The TIME is shaped by immunosuppressive cytokines, chemokines, and inflammatory growth factors, along with additional suppressive signals from lymphocytes, myeloid cells, macrophages, neutrophils, fibroblasts, and vascular-associated cells (18, 22, 23). The host immune system is responsible for identifying and neutralizing non-self-materials, such as foreign antigens. However, tumors can manipulate this system to shape the TIME by selectively promoting the survival of cancer cell variants that resist, evade, or suppress the anti-tumor immune response (20, 24). This host action can lead to the "escape phase," which is mediated by immune cell types such as regulatory T cells (Tregs) and MDSCs that are known to inhibit anti-tumor cells (3, 25). This section of the review will summarize the components of the TIME that contribute to tumor progression, including extracellular matrix (ECM) remodeling, cell recruitment, pH and hypoxic selectivity, immune suppressive environment through cytokine signaling, and shifting immune metabolism.

1.2 Extracellular matrix

Within the TIME, tumor and non-cancerous cells, immune cells, blood vessels, fibroblasts, cytokines, and growth factors all interact with the ECM to drive tumor development and progression (8, 23). The ECM provides a physical barrier for the TIME by preventing the recruitment of host immune cells into the tumor and influencing immune cell activation. The ECM density and stiffness can prevent the movement of T cells and other host immune cells from making contact with tumor cells (26). The polarization of macrophages has been shown to be influenced by the ECM, initiating either the tumor-suppressive (M1) or tumor-promoting (M2) macrophages (27). The ECM can influence cells through cell adhesion molecules (CAMs), such as integrins, which bind to ECM components (e.g., collagen, fibronectin, and laminin). This interaction plays a crucial role in regulating cell adhesion, migration, and signaling (28). Specific CAMs, such as integrins, play a key role in ECM remodeling. Integrins activate various cellular processes through signaling pathways like focal adhesion kinase (FAK), phosphatidylinositol 3-kinase (PI3K), and Rho GTPases (e.g., Rho, Rac, and Cdc42). These pathways are involved in regulating cell motility, proliferation, migration, adhesion dynamics, cellular morphology, and cancer progression (29, 30). While cadherins are calcium-dependent adhesion molecules essential for mainly cell-cell interactions and ECM remodeling (31).

The ECM also contributes to the recruitment of MDSCs primarily through chemokine signaling, including the pathways mentioned above, thereby enhancing ECM-driven suppression of the host immune response (27, 32, 33). Targeting the ECM is promising due to its role in tumor progression. Tumor heterogeneity and signaling pathways in the TIME drive ECM remodeling, hypoxia, angiogenesis, and immune evasion complicating therapies and promoting tumor growth and resistance (34).

1.3 Hypoxia

The high nutrient consumption in the TIME creates hypoxic conditions, leading tumors to shift their metabolism toward elevated glycolysis as their primary energy source, even in the presence of oxygen, a phenomenon known as the Warburg effect (35, 36). Rapid tumor growth and metabolism produce acidic byproducts like lactate and CO_2, creating toxic metabolites (ex. lactate, oxidized lipids, and adenosine) that suppress host immunity and promote tumor progression (37, 38). In the hypoxic conditions of the TIME, immune cell recruitment, the accumulation of immunosuppressive cells, and the upregulation of immunosuppressive molecules all contribute to tumor progression (39). Hypoxia-inducible factors (HIFs) are transcription factors that regulate tumor cell responses in a hypoxic environment by activating transcription of genes involved in tumor cell proliferation, angiogenesis, metabolism, and invasion (40, 41). Common HIFs are HIF-1α (HIF1A) and HIF-2α (HIF2A), both of which play key roles in tumor growth, and metastasis (42).

1.4 Abnormal tumor vasculature

One of the defining features of the TIME is its abnormal vasculature, which results from the inadequate oxygen supply to the tumor site (43). Once a tumor grows beyond a few millimeters, it releases growth factors, directing tumor and non-cancerous cells to grow, divide, differentiate, or undergo cell death (44). The tumor compensates for oxygen deprivation by inducing angiogenesis, a process of new blood vessel formation in response to increased oxygen demand (45), which is critical for tumor growth and vascularization (46, 47). The abnormal structure of blood vessels is often referred to as tumor vasculature and is associated with leaky barriers and cancer progression (48, 49). Disorganized vasculature hinders treatment delivery due to reduced blood flow throughout the tumor site and elevated fluid pressure, leading to uneven treatment distribution, creating a physical barrier for treatments, and impacting treatment efficacy (50). Irregular vasculature, acidosis, and high pressure hinder T-cell infiltration, promoting immune escape (49). Angiogenesis is also known to help regulate TIME by providing oxygen and manipulating various host cells, immune cells and nutrients using the irregular vasculature network to evade immune surveillance (51–54).

1.5 Tumor acidosis and immune modulation

The complexity of the TIME relies only on the increased use of host physiological supplies and nutrients and a tightly regulated pH of 6.7-7.1 and, specifically, a pH below 7.2 within the tumor site (55–57). The acidic environment suppresses and disrupts the host immune response by impairing their ability to proliferate, migrate, and produce cytokines (58–60). Acidity, specifically, lactic acid buildup in the TIME in an aerobic and anaerobic environment impairs lymphocytes and macrophages, especially during inflammation (61, 62). Acidosis impairs T cell function by reducing the production of key cytokines such as interferon-gamma (IFN-γ) and tumor necrosis factor-alpha (TNF-α), as well as cytotoxic molecules like perforin and granzyme. An acidic extracellular environment can influence cytotoxicity by modifying cell cycle kinetics, inhibiting cell death, and impairing cytotoxic functions (63, 64). Acidosis can significantly affect immune cell function by inhibiting DC maturation and altering macrophage polarization, specifically promoting M2 polarization, which can contribute to immunosuppression within the TIME (65, 66). A preclinical study showed that an acidic TIME promotes local invasion and metastasis in breast, colorectal, and colon cancers, supporting acid-mediated tumor progression in a colorectal mouse model (66, 67). The change in acidity stems from tumor cell metabolism increases acid production, lowering pH and creating a toxic environment that impairs immune cells, chemokines, and cytokines (60).

1.6 Immunosuppressive role of cytokines

Immune tolerance is maintained by suppressive cytokines that limit inflammation and prevent immune attacks, but tumor cells exploit this mechanism by reducing pro-inflammatory signals and weakening anti-tumor immunity (68, 69). However, dysregulation of immunosuppressive cytokines can lead to excessive or prolonged production of immunosuppressive cytokines, resulting in immunosuppression of the host (21). The immunosuppressive cytokine interleukin-10 (IL-10), produced by macrophages, monocytes, and T cells, can inhibit the production of pro-inflammatory cytokines and suppress the activation of T cells and NK cells (70). The accumulation of IL-10 can reduce the function of antigen-presenting cells, lowering the adaptive immune response (71). Another key cytokine is Interleukin-35 (IL-35), produced by regulatory T cells, inhibits the proliferation and function of effector T cells while promoting the development of immunosuppressive microenvironments (72). IL-35 inhibits pro-inflammatory cells and its cytokines while enhancing the production of anti-inflammatory cytokines such as IL-10 and transforming growth factor-beta (TGF-β). TGF-β, in turn, suppresses T cell proliferation and activation, reduces inflammatory cytokine production, and promotes regulatory T cell differentiation (73). IL-10 and IL-35 play critical roles in the development of TIME due to their significant role in

modulating the immune response, suppression of anti-tumor immunity and the promotion of tumor growth (74). Cytokines inhibit immune function in immunosuppression by regulating cell activation, differentiation, and metabolism (75).

Immune metabolism is a critical component that reflects the metabolism effects on the immune response, overall impacting tumor growth and development (76). Specifically, cytokines influence the activity of immune cells and also impact the metabolism by tailoring the energy and nutrients the cells use (77). The activation, differentiation, and function of immune cells are dependent on energy supply and metabolic transformation signaling (78). Tumor-intrinsic signaling fosters the exclusion and dysfunction of effective immune cells. Specifically, oncogenic drivers, including β-catenin, signal transducer and activator of transcription 3 (STAT3), phosphatidylinositol 3-kinase (PI3K), phosphatase and tensin homolog (PTEN), protein kinase B (AKT), mechanistic target of rapamycin (mTOR) (PI3K/PTEN/AKT/mTOR), p53, nuclear factor kappa-light-chain-enhancer of activated B cells (NF-κB), and Ras/Raf/mitogen-activated protein kinase (RAS/RAF/MAPK) signaling, are activated within the TIME and are critical for tumor development and metabolism (79). These oncogenic pathways reduce chemokine production, further hindering the recruitment of DCs, macrophages, T cells, and NK cells to the tumor site and promote the immunosuppression of host immune cells. Tumor-intrinsic signaling induces programmed cell death ligand 1 (PD-L1) expression, promoting T cell dysfunction and immune suppression, hindering tumor control and treatment (80).

2 Critical players for activating the immune system and suppressing tumor formation

The TIME is made up of diverse cell populations consisting of immune cells, cancerous and non-cancerous cells, each requiring optimal conditions to perform its specific function, collectively influencing tumor progression, Figure 1 (9). In early tumor development, dendritic cells (DCs) and macrophages recognize tumor-associated antigens and initiate inflammation by releasing pro-inflammatory cytokines (e.g., IL-6, TNF-α, IL-1β) and chemokines (e.g., CXCL2, CXCL9, CXCL10), which recruit immune cells to the tumor site to help prevent progression (81,

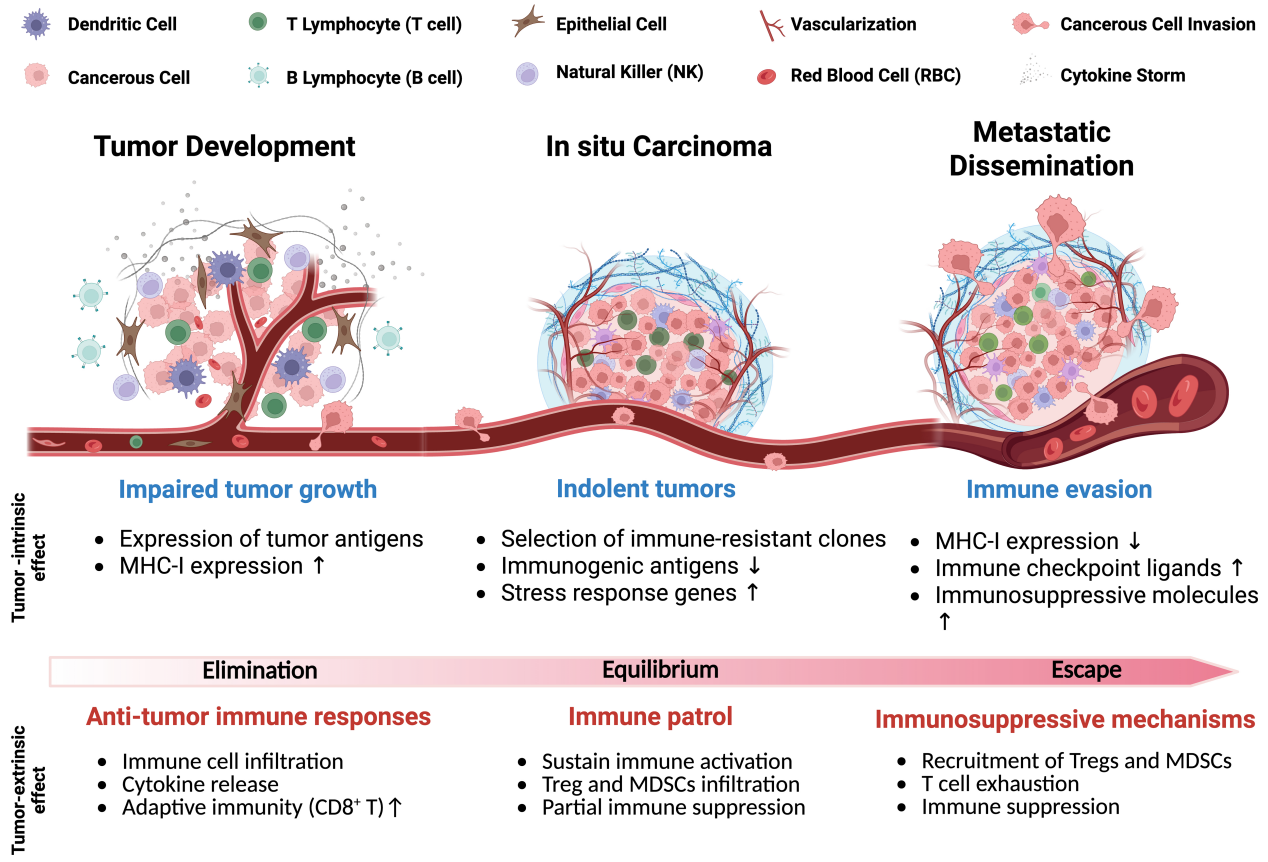

FIGURE 1
Schematic of tumor progression highlighting key physiological features and cell types. The gradient illustrates intrinsic and extrinsic factors driving the shift from anti-tumor immunity to immune evasion, including elimination and escape mechanisms used by tumors to suppress host immune responses.

82). Additionally, DCs and macrophages both are antigen-presenting cells (APCs), which process and present tumor antigens through MHC-I molecules by stimulating the proliferation of $CD8^+$ cytotoxic T cells for further tumor cell elimination (83, 84). In response, tumor cells experience immunological stress that temporarily slows their proliferation due to increased antigen expression and immune-mediated cytotoxicity (24). However, tumor cells adapt and evolve new mechanisms to evade immune detection by selecting immune-resistant clones, downregulating highly immunogenic antigens, and upregulating stress response genes, such as HIF-1α and STAT3, to compensate for host immune response (85, 86).

Stress response genes help tumor cells resist immune-induced apoptosis and survive inflammation by supporting protein refolding and degradation contributing to tumor cell survival from the hosts' immune system (87). Stress response genes can suppress the host immune system, impairing its ability to attack TIME. In turn, the TIME recruits MDSCs and Tregs, which further inhibit immune responses, promote immune evasion, and support tumor progression (88, 89). The immunosuppressive cells dampen immune activation, creating a tolerant microenvironment that weakens the host anti-tumor response (90). In the late stages of tumor development, the host immune system becomes progressively ineffective as tumor cells upregulate immune checkpoint ligands, such as PD-L1 and cytotoxic T lymphocyte-associated protein 4 (CTLA-4) (89, 91), which inhibit $CD8^+$ T cell-mediated cytotoxicity (21). Continuous activation of Tregs further suppresses effector T cell responses, which can reinforce an immune-tolerant state of the TIME (92). Under these conditions, tumor cells are primed for metastasis, acquiring the ability to invade surrounding tissues, migrate through the bloodstream, and colonize distant organs (92, 93). Here, we highlight key tumor-associated immune cells and their roles in modulating cancer progression Figure 2 and Table 1.

3 Characterizing immune activation within the TIME

The tumor immune microenvironment (TIME) is a dynamic ecosystem where cancer cells, stromal cells, cancer-associated

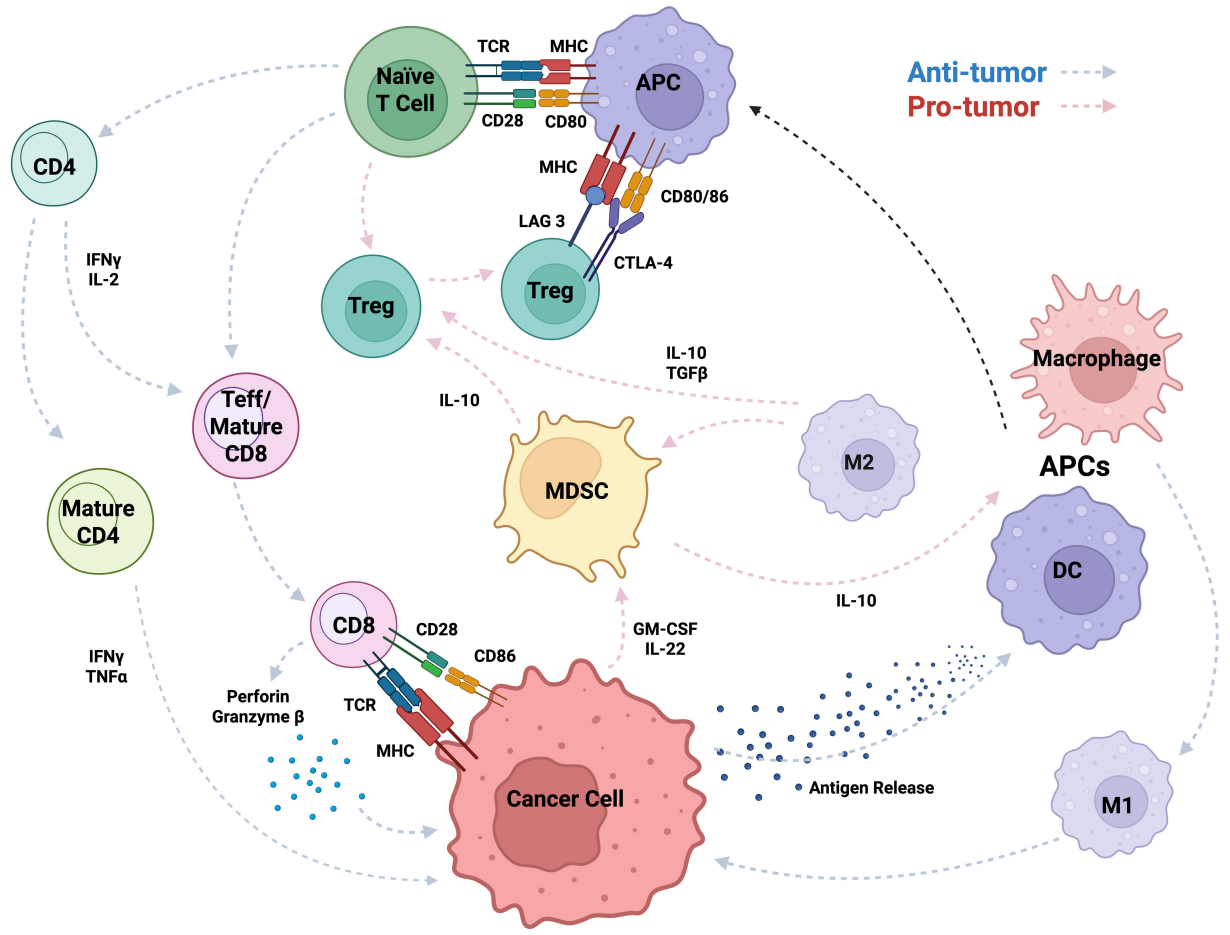

FIGURE 2
Immune cell crosstalk and regulatory mechanisms within the TIME, highlighting key cytokine signaling pathways and cellular functions. The schematic illustrates interactions among immune cells (e.g., T cells, APCs, MDSCs, macrophages, DCs, TAMs, Tregs, Teffs) through cytokines (e.g., IL-2/10/22, GM-CSF, TGF-β), molecules (e.g., perforin, granzyme B, IFN-γ), and receptors/ligands (e.g., TCR, MHC, CD28, CD80/86, LAG-3, CTLA-4), showing how signaling drives activation or suppression in the tumor microenvironment.

TABLE 1 Key cell types and receptors in the TIME and their roles.

Immune cells		Canonical Function	Anti-tumor Mechanisms	Pro-tumor Mechanisms	Targeted Therapeutic Strategies	Ref
Neutrophil (CD15)		• Innate responder to infection and inflammation.	• Tumor killing via ROS, MMP-9, H_2O_2, TRAIL, FasL/Fas, NETs, ADCC and cytokine production.	• Promotes angiogenesis (VEGF). • ECM remodeling. • Immunosuppression (ARG1). • Metastasis via NETs.	• Blocks CXCLR1/2 and C5aR to reduce neutrophil suppression. • NETosis inhibitors.	(94–98)
NK cells (CD56)		• Innate cytotoxic lymphocytes. • Regulate tumors and infections. • Control cell proliferation and limit tissue damage.	• Cytotoxicity via IFN-γ and perforin/granzyme, ADCC. • Promotes cell killing of MHC-presenting cells without prior sensitization.	• Dysfunction in TME due to hypoxia, TGF-β. • Reduced cytotoxicity and infiltration.	• CAR-NK therapies • Target exhaustion-related receptors (e.g., PD-1, TIM-3). • Modulate NK cell state to restore tumor-killing activity	(99–105)
T cells (CD3) ($CD4^+$ Th) ($CD8^+$ Tc)		• Adaptive immunity effects in both anti-tumor response and TIME protection.	• $CD8^+$ Tc cells suppress tumor growth and enhance host immune response. • $CD4^+$ Th1 cells enhance CTL and DC function.	• Treg cells promote tumor progression and metastasis. • Exhausted T cells lose effector function.	• ICIs (e.g., anti-CTLA4). • CAR-T cell therapy. • High T-cell infiltration, such as Fc-enhanced anti-CTLA4 antibodies (BMS-986218 and ONC-392). • Blocking other Treg markers along with CTLA4, such as CCR7 and TIGIT.	(106–111)
MDSCs ($CD11b^+Gr1^+$)		• Promotes immune evasion	• (minimal role) Potential antigen presentation	• Inhibit T cell, DCs and NK cells function via oxidative stress. • Promote Tregs, M2 macrophages.	• MDSC depletion, such as anti Gr-1 antibodies, CXCR1/2 or Src inhibitors and chemotherapy. • Suppress function using PDE5 and Galectin-3 inhibitors.	(25, 112–116)
APCs	DCs (CD11c)	• Antigen presentation via MHC I/II	• Activate $CD4^+$/$CD8^+$ T cells,by producing IL-12, TNF-α, IL-6.	• Upregulate PD-L1, IL-10, and TGF-β. • Promoting Treg expansion	• STING agonists. • DC vaccines. • Expand DCs (e.g., Flt3L and CHNPs).	(84, 117–120)
	Macrophage (CD68 M1) (CD163 M2)	• Phagocytosis • Both anti-tumor (M1-like) and pro-tumor (M2-like, TAM).	• M1-like macrophages support immune responses by producing IL12, TNF-α.	• M2-like TAMs promote angiogenesis, immune suppression, tissue remodeling, Treg expansion, and inhibit cytotoxic T cells.	• Reprogramming TAMs to M1, via CD40/TLR agonists. • TAM depletion via CSF1R inhibitors (e.g., Pexidartinib) and CCR2 inhibitors (e.g., PF-04136309). • CD47-SIRPα blockade enhances phagocytosis.	(121–125)

ADCC, antibody-dependent cellular cytotoxicity; ARG1, arginase 1; ATRA, all-trans retinoic acid; APCs, antigen presenting cells; CAR-NK, chimeric antigen receptor-natural killer cells; CAR-T, chimeric antigen receptor T cells; CHNP, cytotoxic hybrid neutrophil population; CSF1R, colony-stimulating factor 1 receptor; CTL, cytotoxic T lymphocyte; DCs, dendritic cells; ECM, extracellular matrix; Flt3L, fms-like tyrosine kinase 3 ligand; MDSC, myeloid-derived suppressor cell; NETs, neutrophil extracellular traps; NK cells, natural killer cells; PDE5, phosphodiesterase type 5; ROS, reactive oxygen species; STING, stimulator of interferon genes; TAMs, tumor-associated macrophages; TIM3, T cell immunoglobulin and mucin domain-containing protein 3; TME, tumor microenvironment; TRAIL, TNF-related apoptosis-inducing ligand; Treg, regulatory T cells; VEGF, vascular endothelial growth factor; VISTA, V-domain Ig suppressor of T cell activation.

10.3389/fimmu.2025.1621812

fibroblasts (CAFs), endothelial cells, and immune cells (including the extracellular matrix, ECM) engage in multifaceted interactions. These interactions contribute to tumor development, progression, and protection, ultimately shaping the tumor's fate and response to therapies (126, 127). Due to its modifiable immunosuppressive environment and potential to enhance immunotherapy effectiveness, TIME is a promising therapeutic target (128).

RNA sequencing and immunohistochemistry from the ORIENT-11 study to optimize a TIME classification model predicting non-small cell lung cancer (NSCLC) treatment outcomes. The TIME is classified into four types based on PD-L1 and TIL status. Patients with high PD-L1 and TIL benefit from combined chemo-immunotherapy, while those with low levels respond better to chemotherapy alone to avoid unnecessary toxicity. However, this model's efficacy lacks validation in large-scale randomized trials (129).

Additionally, tumor-associated immune cells can be classified into two categories: anti-tumor and tumor-promoting populations. Anti-tumor immune cells primarily include effector T cells (such as cytotoxic $CD8^+$ T cells and effector $CD4^+$ T cells), NK cells, DCs, and M1-polarized macrophages (127, 130). In contrast, anti-tumor immune cells are predominantly composed of Tregs, MDSCs, M2-polarized macrophages, N2-polarized neutrophils, type 2 natural killer T cells (NKT2), and innate lymphoid cells type 2 (ILC2s) (131). Figure 3 illustrates the dual roles of immune cells in the TIME, highlighting pro-tumoral and anti-tumoral functions in hot and cold tumors with key cellular interactions and cytokine effects. Furthermore, various metabolic and biochemical components within the tumor microenvironment significantly influence immune cell function (108).

Immunotherapy-induced changes in the TIME offer insights for improving combination treatments and patient outcomes. Targeting the TIME reveals cancer-specific responses and aids in detecting development and recurrence. Immune activation occurs when immune cells recognize tumor antigens, triggering responses against both tumor cells and the TIME (9). Targeted immunotherapies can utilize not only cell-based treatments but also immune-modulating treatments. These latter treatments consist of nanoparticles decorated with cell-specific ligands, antibodies, or peptides designed to actively bind to the cell surface of targeted cells. In combination with other therapies, nanoplatforms interact with the TIME, modulating tumor associated macrophages (TAMs) and Tregs, and directly activates immune cells, enhancing antigen presentation, and promoting immunological memory formation (132). Antibody-functionalized nanoparticles enable precise targeting. Such as, monoclonal antibody-coated magnetic nanoparticles (MgNPs) loaded with doxorubicin showed 1.8-fold greater accumulation in Met/HGFR-positive tumors than non-functionalized MgNPs, enhancing drug retention, reducing toxicity and demonstrating strong potential for targeted delivery (133).

3.1 Activation of the immune system

Immune activation overcomes the tumor's immunosuppressive microenvironment, transforming the TIME from resistant to responsive to cancer treatment by modifying its cellular and

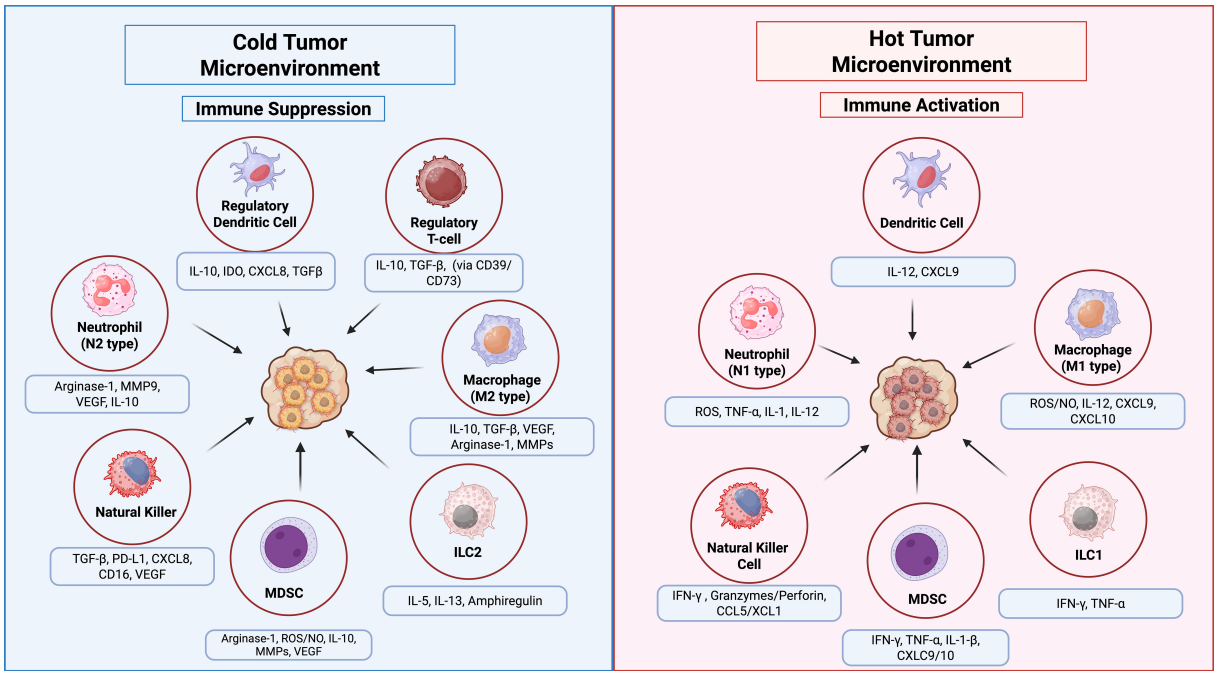

FIGURE 3
Innate immune cell functions in the TIME of hot vs. cold tumors. In hot tumors (right panel), high immune infiltration supports anti-tumor responses via NK cells, M1 macrophages, ILC1s, and N1 neutrophils through pro-inflammatory cytokines. In cold tumors (left panel), low immune infiltration and immunosuppressive cells, M2 macrophages, ILC2s, regulatory DCs, N2 neutrophils, MDSCs, and Tregs promote tumor growth. Arrows indicate key cellular interactions and cytokine effects.

molecular composition. This enhances the host immune system's ability to recognize and attack tumors, boosting T cell-mediated destruction, oncolytic viruses, cancer vaccines, and combination therapies (108). One critical route of cell death is immunogenic cell death (ICD), which is maintained and activated by the host's immune system. ICD is a form of cell death initiated by certain chemotherapeutic drugs, oncolytic viruses, physicochemical therapies, photodynamic therapy, and radiotherapies (134, 135). When ICD occurs in cancer, it promotes dying cells secreting damage-associated molecular patterns (DAMPs), which act as alarm signals that activate the immune system against tumor cells. This process effectively turns dying cancer cells into natural "vaccines," enhancing anti-tumor immunity. Key DAMPs such as surface-exposed calreticulin, secrete ATP, and the nuclear protein high-mobility group box 1 (HMGB1), increases tumor immunogenicity and attracts immune cells to the TIME (134, 136, 137). ICDs have mediated patterns that reveal immune microenvironment classification and immunotherapeutic responses in bladder cancer and many other cancer types. Fu et al., 2022, revealed a novel paradigm for characterizing the immune microenvironment and immunotherapeutic responses in bladder cancer, identifying two patterns of TIME and responses to immunotherapy of ICD within bladder cancer. The two patterns include an 'immune-inflamed' type, characterized by abundant activated immune cells and favorable immunotherapy response, and an 'immune-excluded' type, where immune cells are limited or localized to the tumor's outer regions, associated with less favorable outcomes. These TIME patterns help predict which patients are more likely to benefit from immunotherapeutic strategies like immune checkpoint inhibitors.

The main characterization found distinct clinical features of the TIME, exhibiting unique clinical and immune characteristics of an ICD cluster, despite being linked to a poor prognosis and high ICD score, demonstrated an immune-activated state. This activation was associated with a more favorable response to immunotherapy and ICD-inducing treatments leading to further investigation in ICD-related gene, *CALR*. *CALR* was significantly overexpressed in the T24 bladder cancer cell line compared to the control SV-HUC-1 cells. Experimental knockdown of *CALR* reduced T24 cell viability and triggered endoplasmic reticulum stress, highlighting its potential role in cancer cell survival, stress response, and activation of the immune system (138).

Chemotherapy induces ICD by exposing calreticulin, releasing ATP, and secreting HMGB1, which signals immune cells to recognize dying cancer cells (135). Treating NSCLC cells with 10 μM Crizotinib, an ICD-inducing tyrosine kinase inhibitor, enhances anticancer effects when combined with non-ICD chemotherapy like Cisplatin. This combination boosts tumor T cell infiltration and PD-1/PD-L1 expression, improving response to PD-1 immunotherapy. Removing T cells or blocking interferon-γ negates these effects, highlighting a promising strategy of chemotherapy plus Crizotinib followed by immune checkpoint inhibitors for NSCLC (139). One study compared the treatment method of preoperative neoadjuvant chemoradiotherapy (nCRT), a treatment using chemotherapy and radiation therapy before surgery to shrink a tumor (140). nCRT is used to potentially remove or increase the likelihood of a less invasive surgery which is the primary therapeutic strategy for patients with locally advanced rectal cancer (LARC). A Systematic Review and Meta-analysis revealed nCRT was associated with improved pathologic complete response rates and has a potential disease-free survival advantage compared to the standard CRT plus (140, 141). Huang et al. found that using a novel topoisomerase I inhibitor, Lipotecan (TLC388), induces ICD, leading to the release of damage-associated molecular patterns (DAMPs) such as HMGB1, ANXA1, and exposure of calreticulin. This process increases cancer immunogenicity and stimulates the host's anti-tumor response, promoting immune cell infiltration in the TIME of colorectal cancer. These findings suggest Lipotecan can reshape the TIME to boost neoCRT effectiveness in LARC patients (142).

3.2 Innate immune recruitment and activation in the TIME

In a healthy system, macrophages are generally of the M2-like subtype and produce anti-inflammatory cytokines such as IL-10 and TGF-β, which contribute to inflammation resolution and tissue regeneration (143, 144). Neutrophils also control tissue homeostasis by producing lipid mediators such as resolvins and lipoxins that tune the immune response (145, 146). Macrophages and neutrophils help maintain immune homeostasis through efferocytosis, the process of clearing apoptotic cells and cellular debris, promoting a controlled immune response essential for tissue repair and normal physiological function (147, 148). Moreover, both cells exhibit functional plasticity in the TIME by either promoting or suppressing tumors. Activated macrophages polarize into M1 and release pro-inflammatory cytokines (e.g. TNF-α and IL-12) and ROS to activate T cells and trigger tumor cell death (149). As tumors progress, the TIME often shifts to favor M2-like TAMs that secrete immunosuppressive factors such as IL-10 and TGF-β and suppress immune responses and support tumor growth (149). Similarly to macrophages, neutrophils in the TIME show plasticity, adopting anti-tumor (N1) or pro-tumor (N2) states based on cytokine signals. N1 neutrophils support anti-tumor immunity by releasing pro-inflammatory cytokines, activating T cells, and recruiting $CD8^+$ T cells to kill tumor cells (150). N2 neutrophils contribute to angiogenesis, immune suppression, and metastasis by the production of VEGF, arginase-1, and MMP9 (151). Neutrophils can influence almost every aspect of cancer progress, primary tumor growth, metastasis, cancer stem cell maintenance and therapeutic resistance (150). Neutrophils recruit macrophages and DCs via chemokines, creating a feedback loop that amplifies immune activation (152). Due to the important participation of innate immunity in TIME, it also influences dynamic neutrophil polarization. Specifically, TGF-β promotes N2 differentiation, while type I interferons or TGF-β blockade shift polarization toward the anti-tumor N1 phenotype (150, 152, 153).

3.3 Modulation of immune checkpoint activation

Immune checkpoints such as PD-1/PD-L1 and CTLA-4 help maintain immune homeostasis by balancing activating and

inhibitory signals to prevent excessive immune responses. PD-1, expressed on activated T cells, binds to PD-L1 on antigen-presenting or parenchymal cells, delivering inhibitory signals that suppress T cell proliferation, cytokine production (e.g., IFN-γ, IL-2), and cytotoxic activity (154). This interaction ensures autoreactive T cells do not attack healthy tissues by inducing functional exhaustion or apoptosis of self-reactive clones. Similarly, CTLA-4 competes with the costimulatory receptor CD28 for the ligands CD80/CD86, increases the naive T cell activation threshold and promotes Treg suppressive functions (155). These checkpoints also enforce peripheral tolerance through dual mechanism where PD-1/PD-L1 interactions directly inhibit effector T cell responses in tissues, whereas CTLA-4 modulates early T cell priming in lymph nodes and amplifies Treg-mediated suppression (91). In contrast to healthy cells, which dynamically regulate PD-L1 expression during inflammation to prevent collateral damage, the TIME hijacks this pathway by persistently overexpressing PD-L1 to evade immune responses. This dysregulation disrupts immune balance and promotes immune escape (156).

Immune checkpoint inhibitors (ICIs), for example, anti-PD-1/PD-L1 and anti-CTLA-4 antibodies, have revolutionized cancer therapy by restoring the function of exhausted T cells and renewing anti-tumor immunity. However, their efficacy varies widely across tumor types and is influenced by TIME factors such as T cell infiltration density, PD-L1 expression levels, and tertiary lymphoid structures (131). Despite their recent clinical success, resistance to ICIs remains a major challenge, frequently arising via compensatory upregulation of alternative inhibitory checkpoints (such as LAG-3 and TIM-3) and persistent epigenetic reprogramming of T cells within the TIME. Strategies to overcome this resistance include dual checkpoint blockade (e.g., targeting both PD-1 and LAG-3; see Table 2), as well as combining ICIs with therapies that target immunosuppressive components of the TIME, such as CSF-1R inhibitors that deplete tumor-associated macrophages (157).

DCs, key antigen-presenting cells, process tumor antigens via MHC and activate adaptive immunity by detecting pathogens through pattern recognition receptors (PRRs) like Toll-like receptors (TLRs) (158). The DC takes up the pathogen and then displays the antigens to T cells on MHC molecules, resulting in an immune response (159, 160). Activated DCs express moderate levels of costimulatory molecules like CD80 and CD86, enabling effective T cell activation, clonal expansion, and memory formation (161, 162). This maturation process enables T cells to receive the required signals for clonal expansion and the production of potent memory responses. Adaptive immune responses involve tumor-specific neoantigens that are released during immunogenic cell death (ICD). Processes involving DAMPs such as calreticulin, ATP, and HMGB1, also activate dendritic cells (DCs) and T cell priming to enhance anti-tumor immunity (163). This process allows for the recruitment and expansion of polyclonal cytotoxic and memory T cells and the establishment of systemic tumor-specific immunity and long-term immunological memory. In addition, DCs may also possess suppressive properties by inducing the activation of Tregs instead of effector T cells (164).

4 Characterizing immune suppression within the TIME

Tumors can evade the host immune system by creating an immunosuppressive microenvironment (165) One major mechanism involves impaired antigen presentation, typically through the downregulation of MHC molecules or other antigen-presenting proteins, which disrupts T cell recognition and weakens the antitumor immune response (166). Tumor cells may also mask their antigens with protective molecules, further preventing immune recognition, while the TIME releases factors that inhibit immune cells, such as, T cells, NK cells, and dendritic cells which promote immune tolerance and drive an unresponsive, immunosuppressive state (166, 167). Additionally, Tumor cells recruit immunosuppressive regulatory cells such as Tregs and exploit immune checkpoint pathways to suppress effector immune cell function. Cancer cells also develop cytoprotective mechanisms, like resistance to apoptosis, allowing them to evade immune-mediated death and modify the microenvironment to support their survival, growth, and continued immune evasion (68, 168). T cell exhaustion can also occur, leading to immune cell dysfunction and an inability to effectively target the tumor (169). To counteract these suppressive mechanisms, various clinical strategies have been developed to activate the TIME. These include dendritic cell activation, immune checkpoint blockade, therapeutic cancer vaccines, oncolytic virus therapy, vascular normalization, and combination therapies involving chemotherapy or radiotherapy with immune-stimulating agents (128).

4.1 Physical barriers to immune infiltration

Physical barriers in the TIME suppress immune responses by limiting immune cell access through poor vascularization, lack of T cell homing signals, ECM density, and cellular blockades. Tumor-altered ECM, enriched with collagen and fibronectin, becomes stiffer and more fibrotic, further hindering immune cell infiltration (170). CAFs in the TIME stroma promote tumor growth by secreting growth factors, cytokines, and chemokines, and by remodeling the ECM. Tumor-induced activation of CAFs and inflammation increases interstitial pressure and collagen deposition, leading to ECM stiffening and disorganization through elevated collagen-processing enzymes such as lysyl oxidases (127, 171). Tumors also express high levels of matrix metalloproteinases (MMPs) compared to non-cancerous epithelial cells, which can lead to increased ECM remodeling (172). Tumor cells influence the TIME by using CAFs by recruiting and activating them through paracrine signals such as TGFα, TGFβ, platelet-derived growth factor (PDGF), epidermal growth factor (EGF), and fibroblast growth factor 2 (FGF-2) (173, 174). Activated CAFs reorganize the TIME to promote metastasis, therapy resistance, dormancy, and reactivation. They contribute to the formation of physiological barriers by secreting both cellular and acellular components, thereby impeding drug penetration and treatment

efficacy (175) In preclinical mouse models, the TIME has shown a decrease in the monitoring effectiveness of drug delivery and treatment (176).

4.2 Reprogramming the immunosuppressive microenvironment

Healthy tissues maintain balanced cytokine levels and lack the hypoxia and acidosis found in the TIME, allowing immune cells to function without metabolic stress (177, 178). Unlike tumors, healthy tissues show a normal distribution of immune cells rather than an accumulation of immunosuppressive cells such as Tregs and MDSCs (179). The TIME contributes significantly to therapeutic resistance, making it a key target for enhancing immunotherapy. Among its key players, Tregs and MDSCs are major contributors to immune suppression. Tregs are characterized by the expression of FOXP3 and CD25, and they suppress effector T cell responses through the secretion of IL-10 and TGF-β, which inhibit T cell proliferation and function (179) Tregs are also highly expressed immune checkpoint molecules that express CTLA-4, PD-1, LAG-3, and TIM-3, and suppress T cell activation through inhibition of DC maturation and co-stimulation (180). Additionally, Tregs disrupt metabolic pathways by expressing CD39 and CD73. This process involves CD39 sequentially breaking down extracellular ATP into ADP and then AMP, while CD73 converts AMP into adenosine, creating an immunosuppressive environment that dampens effector T cell activity (181). Recent studies show activated CD8 T cells can produce adenosine via CD73-containing extracellular vesicles, revealing more complex adenosine pathway regulation than previously understood (182). MDSCs help sustain an immunosuppressive TIME by inhibiting T cells via arginase-1, nitric oxide, and ROS, promoting Treg expansion, and disrupting T cell trafficking through chemokine modulation (176). MDSCs suppress T cells by secreting IL-10, TGF-β, and checkpoint molecules such as PD-L1 and CTLA-4. They expand in response to inflammatory and tumor-derived signals and are divided into two main subtypes: polymorphonuclear (PMN-MDSCs) and monocytic (M-MDSCs), each with distinct mechanisms of action (32). The upregulation of PD-L1 in tumor cells is a hallmark of cancer progression and reflects oncogene-like behavior. This not only enables immune evasion but also supports more aggressive tumor growth and spread (183). Oncogene-driven pathways contribute to this by increasing PD-L1 expression through enhanced transcription, protein stabilization, and gene amplification. These changes help tumor cells avoid immune detection by elevating PD-L1 on their surface, thereby suppressing T cell responses (184).

4.3 Modulation of immune checkpoint suppression

Immune checkpoints serve as critical regulatory mechanisms for preventing excessive immune activation and autoimmunity (176). The PD-1/PD-L1 and CTLA-4 pathways are among the most studied immune checkpoints responsible for suppression of T cell activation within the TIME. However, tumors frequently exploit these pathways to suppress CTLs function and evade immune surveillance, thereby promoting tumor progression (185, 186) This PD-L1 binds to PD-1 on CTLs, inducing T cell exhaustion and impairing effector function (186). Similarly, CTLA-4, expressed on T cells, competes with the co-stimulatory receptor, CD28 for binding to CD80/CD86 on APCs, dampening early T cell activation and promoting immune tolerance (187). The TIME further amplifies checkpoint-mediated immunosuppression through metabolic reprogramming, for example, by inducing hypoxia-driven PD-L1 upregulation and recruiting immunosuppressive cell populations (188).

5 Stimulation of the immune system with immunotherapy therapy

The activation of the host immune system is crucial for effective targeting tumors, improving outcomes, and reducing treatment side effects (20). In cancer immunotherapy, various approaches have been developed to harness the patient's immune system to recognize and eliminate tumor cells. Some strategies involve extracting and modifying immune cells ex vivo, such as in CAR T cell therapy, to enhance their tumor-killing capacity (189) Other therapies rely on engineered antibodies to target tumor cells, or to stimulate the immune system to recognize and attack tumor cells using other modalities such as vaccines, cytokine or immune checkpoint inhibitors (190–192). Immunotherapies vary by cancer type and patient factors. This section reviews key treatments: monoclonal antibodies, immune checkpoint inhibitors, bispecific T cell engagers, CAR T cells, and cancer vaccines, focusing on their mechanisms and clinical studies (193).

5.1 Monoclonal antibodies

Monoclonal antibodies (mAbs) are immunoglobulins with a high level of specificity (mono-specificity) for a particular antigen or epitope of tumor interest. The mAbs bind to specific antigens or proteins on cell surfaces such as cancer cells and send a signal to the host immune system to destroy tumor cells (190, 194). Upon binding to their targets, mAbs can engage immune effector functions through their Fc region by activating Fc receptors on immune cells such as NK cells and macrophages. This leads to multiple cytotoxic mechanisms, including complement-dependent cytotoxicity (CDC), antibody-dependent cellular phagocytosis (ADCP), and antibody-dependent cellular cytotoxicity (ADCC) (195). MAbs are consist of different classes or origin, using murine, chimeric, humanized or fully human as well as varying in each function being naked conjugate or bispecific which are all dependent on the target (195), see Table 3. Fully human monoclonal antibodies targeting chitinase-3-like-1 (CHI3L1) have shown promise in suppressing tumor growth, fibrosis, angiogenesis, and immune remodeling across various cancers. CHI3L1 contributes to an immunosuppressive tumor microenvironment, supporting cancer progression and highlighting its potential as a therapeutic target (196). Su et al., 2024 developed fully human CHI3L1-neutralizing monoclonal antibodies (nAbs) were developed using phage display technology. These nAbs demonstrated high specificity and affinity for CHI3L1 across multiple cancer cell lines, including

lung, pancreatic, and colorectal cancers. Functionally, the antibodies reduced tumor-promoting signals, inhibited cancer cell proliferation and migration, and showed potential as therapeutic agents in an immunosuppressive TIME (196).

5.2 Immune checkpoint inhibitors

The TIME supports tumor growth by recruiting immune and stromal cells that supply nutrients to heterogeneous tumor cell populations. Specifically, T-cell activation targets threats, while Tregs suppress harmful immune responses (91). T cells express checkpoint receptors such as PD-1 and CTLA-4, which are targeted by FDA-approved immune checkpoint inhibitors (ICIs) including anti-CTLA-4, anti-PD-1, and anti-PD-L1 antibodies. These therapies harness cytotoxic $CD8^+$ T cells to induce durable anti-tumor responses and long-lasting remissions (91, 197). These immunotherapies block the interaction between immune cell proteins and their partners, called 'checkpoints,' which act as brakes on the immune system. ICIs allow the adaptive immune system to respond to tumors more effectively, creating a better treatment for TIME (198, 199). By inhibiting these checkpoints, ICIs enhance the ability of host T cells to more effectively recognize and attack cancer cells within the TIME (200).

Relatlimab is a LAG-3-blocking antibody, a lymphocyte-activation gene 3, and an FDA-approved ICI, see Table 2 for other ICIs. Relatlimab is a third checkpoint inhibitor shown to reduce T cell exhaustion and enhance anti-tumor activity when combined with nivolumab in previously treated melanoma patients (RELATIVITY-047, NCT03470922). ICI are also known for working well as combination therapy, specifically targeting LAG-3 and PD-1 shows greater progression-free survival than PD-1 inhibition alone in untreated metastatic or unresectable melanoma (201). LAG-3 is not cancer specific, although it has been shown to be associated with aggressive tumor progression (202, 203). LAG-3 is a promising immune checkpoint target; its inhibition can enhance anti-tumor immune responses and potentially overcome resistance to existing therapies. In the CheckMate 040 clinical trial, combining dual ICIs (Ipilimumab and Nivolumab) with the chemotherapy drug Sorafenib showed improved therapeutic efficacy in patients with advanced hepatocellular carcinoma. The combination of Ipilimumab (anti-

TABLE 2 Approved and emerging immune checkpoint inhibitors.

Approved Immune checkpoint inhibitors				
Drug	Target	Cells	Type	Approved indications
Atezolizumab (Tecentriq)	PD-L1	Tumor, APCs	mAb	NSCLC, SCLC, HCC, melanoma, breast cancer, urothelial cancer
Avelumab (Bavencio)	PD-L1	Tumor, APCs	mAb	Merkel cell carcinoma, urothelial carcinoma, renal cell carcinoma
Durvalumab (Imfinzi)	PD-L1	Tumor, APCs	mAb	NSCLC, urothelial carcinoma
Nivolumab (Opdivo)	PD-1	T cells	mAb	Melanoma, NSCLC, SCLC, HCC, HL, renal cell carcinoma, HNSCC, urothelial carcinoma, MSI-H/dMMR colorectal cancer.
Pembrolizumab (Keytruda)	PD-1	T cells	mAb	NSCLC, SCLC, HNSCC, HL, melanoma, urothelial carcinoma, MSI-H/dMMR CRC, MSI-H/dMMR cancers, gastric cancer, cervical cancer, HCC, Merkel cell carcinoma, renal cell carcinoma, esophageal carcinoma, endometrial cancer
Cemiplimab (Libtayo)	PD-1	T cells	mAb	Cutaneous squamous cell carcinoma (CSCC), NSCLC, basal cell carcinoma (BCC).
Nivolumab (Opdivo)	PD-1	T cells (CD8+)	mAb	Melanoma, NSCLC, SCLC, HCC, HL, renal cell carcinoma, HNSCC, urothelial carcinoma, MSI-H/dMMR colorectal cancer.
Toripalimab (Loqtorzi)	PD-1	T cells	mAb	Nasopharyngeal carcinoma, Melanoma.
Sintilimab (Tyvyt)	PD-1	T cells	mAb	HL, non-squamous and squamous NSCLC, HCC, esophageal squamous cell carcinoma, and gastric cancer.
Camrelizumab (AiRuiKa)	PD-1	T cells	mAb	HCC, HL, esophageal squamous cell carcinoma, and nasopharyngeal carcinoma.
Tislelizumab (Tevimbra)	PD-1	T cells	mAb	Esophageal squamous cell carcinoma, NSCLC, Gastric or gastroesophageal junction adenocarcinoma, HL.
Retifanlimab-dlwr (Zynyz)	PD-1	T cells	mAb	Merkel cell carcinoma.
Ipilimumab (Yervoy)	CTLA-4	Treg cells	mAb	Melanoma, metastatic, renal cell carcinoma, MSI-H/dMMR CRC.

(Continued)

TABLE 2 Continued

Approved Immune checkpoint inhibitors							
Drug	Target	Cells	Type	Approved indications			
Tremelimumab (Imjudo)	CTLA-4	T cells	mAb	Unresectable HCC, NSCLC.			
Relatlimab +Nivolumab (Opdualag)	LAG-3	Exhausted T cells	mAB	Melanoma.			
Immune checkpoint inhibitors in advanced clinical trials							
Drug	Target (T cells)	Type	Combination	Indications	Phase	Reference	
Favezelimab	LAG-3	mAb	Pembrolizumab/lenvatinib Egorafenib, TAS-102 Pembrolizumab Pembrolizumab Pembrolizumab.	cSCC, Endometrial Cancer CRC CRC cHL cHL,DLBCL,iNHL.	3 3 3 2/3	NCT06036836 NCT05600309 NCT05064059 NCT05508867 NCT03598608	
Eftilagimod alpha (efti)	LAG-3	Soluble LAG-3 fusion protein.	Paclitaxel Pembrolizumab.	Breast cancer cHL, DLBCL,iNH.L.	2/3 1/2	NCT05747794 NCT03598608	
Tebotelimab	PD-1 & LAG-3	Bispecific mAb.	Margetuximab/Chemotherapy	HER2+GC or GEJ.	2/3	NCT04082364	
Fianlimab	LAG-3	mAb.	Cemiplimab/Chemotherapy (Pemetrexed, Paclitaxel, Carboplatin, Cisplatin) Cemiplimab Cemiplimab.	NSCLC Metastatic melanoma Metastatic Melanoma Melanoma.	2/3 3	NCT05785767/ NCT05800015 NCT05352672 NCT06246916 NCT05608291 NCT06190951	
Botensilimab + Balstilimab	LAG-3 + PD-1	mAbs	- -	MSI/dMMR Esogastric Adenocarcinomas (CIME) dMMR and pMMR solid tumors	3 3	NCT06346197 NCT06279130	
Bispecific T-Cell Engagers (BiTEs)							
Drug	Target	Type	Indications			Year	
Blinatumomab (Blincyto)	CD19 x CD3	BITE	r/r B-cell precursor ALL, MRD-positive B-ALL			2014	
Mosunetuzumab (Lunsumio)	CD20 x CD3	BITE	FL			2022	
Teclistamab (Tecvayli)	BCMA X CD3	BITE	MM			2022	
Glofitamab (Columvi)	CD20 x CD3	BITE	DLBCL			2023	
Epcoritamab (Epkinly)	CD20 × CD3	BITE	DLBCL			2023	
Talquetamab (Talvey)	GPRC5D × CD3	BITE	MM.			2023	
Tebentafusp (Kimmtrak)	gp100 x CD3	BITE	Metastatic uveal melanoma.			2022	
Tarlatamab (Imdelltra)	DLL3 x CD3	BITE	Extensive-stage SCLC.			2024	

cHL, classical Hodgkin lymphoma; CRC, Colorectal Cancer; cSCC, Cutaneous Squamous Cell Carcinoma; DLBCL, diffuse large B-cell lymphoma; dMMR, Mismatch Repair Deficient; GC, Gastric cancer; GEJ, Gastroesophageal Junction; HCC, Hepatocellular Carcinoma; HL, Hodgkin's Lymphoma; HNSCC, Head and Neck Squamous Cell Carcinoma; iNHL, indolent non-Hodgkin lymphoma; LAG-3, Lymphocyte Activation Gene-3; mAb, monoclonal antibody; MSI-H, Microsatellite Instability-High; NSCLC, Non-Small Cell Lung Cancer; P, phase; pMMR, proficient mismatch repair; SCLC, Small Cell Lung Cancer.

TABLE 3 Approved monoclonal antibodies (mAbs).

Drug	Target	Type	Approved indications	Year
Brentuximab vedotin (Adcetris)	CD30	Chimeric IgG1 mAb (ADC)	HL, systemic ALCL	2011
Blinatumomab (Blincyto)	CD19	Bispecific T-cell engager (BITE)	B-cell precursor ALL	2014
Elotuzumab (Empliciti)	SLAMF7	Humanized IgG1 mAb	MM (in combination with lenalidomide and dexamethasone)	2015
Daratumumab (Darzalex)	CD38	Human IgG1k mAb	MM	2015
Gemtuzumab ozogamicin (Mylotarg)	CD33	Humanized IgG4 mAb (ADC)	AML	2017
Inotuzumab ozogamicin (Besponsa)	CD22	Humanized IgG4 mAb (ADC)	r/r B-cell precursor ALL	2017
Isatuximab (Sarclisa)	CD38	Human IgG1 mAb	r/r MM	2020
Mosunetuzumab (Lunsumio)	CD20	Bispecific T-cell engager (BITE)	r/r FL	2022
Teclistamab (Tecvayli)	BCMA	Bispecific T-cell engager (BITE)	r/r MM	2022
Epcoritamab (Epkinly)	CD20	Bispecific T-cell engager (BITE)	r/r DLBCL	2023

ADC, antibody-drug conjugate; ALCL, anaplastic large cell lymphoma; ALL, acute lymphoblastic leukemia; AML, acute myeloid leukemia; BCMA, B-cell maturation antigen; DLBCL, diffuse large B-cell lymphoma; FL, follicular lymphoma; HL, Hodgkin lymphoma; MM, multiple myeloma; r/r, relapsed/refractory.

CTLA-4) and Nivolumab (anti-PD-1), administered after prior treatment with Sorafenib, resulted in the most robust responses and the longest median overall survival (204).

5.3 Bispecific T cell engagers

Bispecific T cell engagers (BiTE) are engineered molecules of two single-chain variable fragments (scFv) linked by a flexible connector. Unlike the traditional antibodies that bind to a single antigen, BiTEs are designed to simultaneously target tumor-specific antigens on tumor cells and CD3 on T cells. Clinical-approved BiTEs target CD19 x CD3, BCMA x CD3, or CD20 x CD3 to promote cytotoxicity of T cells. One pair of the targets for BiTEs is scFv, a tumor-associated antigen (TAA) on the tumor cell and CD3 molecule on the T cell (205, 206). Since immune checkpoints and other immunosuppressive factors within the TIME result in a population of anergic T-cells, preventing their redirection to tumor killing and thereby limiting the effectiveness of BiTE therapy (206, 207). Blinatumomab is the first BiTE therapy that has shown to be an effective and long-lasting immunotherapy, blustering the host immune system by taking advantage of the flexibility of targeting multiple antigens simultaneously and potentially being used in a combination therapy (208). Using therapy constructs CD20 × CD3, showed a 37% overall response rate and 19% complete response rate in aggressive non-Hodgkin lymphoma, including CAR T–resistant or relapsed patients, demonstrating activity across multiple treatment lines. The successful clinical trial (NCT02500407) led to the FDA approval of mosunetuzumab-axgb (Lunsumio), see Table 2 for other BiTE therapies. BiTE-induced T-cell activation leads to cytokine release within the immune synapse, which diffuses to nearby cells and upregulates surface molecules, enhancing anti-tumor activity through a 'bystander effect (209). Despite their therapeutic potential, BiTEs can trigger cytokine storms, leading to cytokine release syndrome (CRS)—a potentially life-threatening condition marked by excessive cytokine release into the bloodstream (207, 210). Resistance to this immunotherapy has been associated with antigen loss and immunosuppressive factors within the TIME, including upregulated immune checkpoints and enhanced host immunosuppression via membrane trafficking (211, 212). BiTEs have a short half-life due to the engineered structure lacks the Fc region, preventing FcRn recycling. This leads to rapid clearance from circulation and necessitates continuous treatment to maintain therapeutic effectiveness (213, 214).

5.4 Chimeric antigen receptor T cell

Chimeric antigen receptor (CAR T) cell therapy is a personalized treatment that modifies patient T cells to help fight cancer. CAR Ts are synthetic receptors that redirect lymphocytes and primarily T cells, to recognize and eliminate cells expressing a specific target antigen (215). Traditionally, antigen-binding domains are constructed from the variable heavy (VH) and light (VL) chains of monoclonal antibodies, which are connected by a flexible peptide linker to form a single-chain variable fragment (scFv). CAR Ts binding to antigens on the cell surface occurs independently of the MHC receptor, resulting in robust T cell activation and potent anti-tumor responses. CAR Ts target the extracellular surface of cancer antigens using MHC-independent T cell activation (216). CAR T cell therapies have received FDA approval, see Table 4. Specifically CAR T cell therapy has been used for improving and treating progression-free survival in multiple myeloma, enhancing overall survival in large B-cell lymphoma, and achieving high remission rates in other hematologic cancers, including acute lymphoblastic leukemia, follicular lymphoma, and mantle cell lymphoma (217). Tisagenlecleucel an anti-CD19 CAR T cell therapy produced high rates of complete remission achieved complete response (CR) rates of 71–81% in multicenter clinical trials involving patients with relapsed or refractory B cell acute lymphoblastic leukemia (R/R B-ALL), and a group with limited treatment options (218, 219).

TABLE 4 Approved and emerging CAR T-cell therapies.

Approved CAR T-Cell Therapies			
Drug	Target	Approved indications	Year
Tisagenlecleucel (Kymriah)	CD19	- B-cell B-ALL - r/r LBCL - r/r FL	2017
Axicabtagene ciloleucel (Yescarta)	CD19	- r/r LBCL - r/r FL	2017
Brexucabtagene autoleucel (Tecartus)	CD19	- r/r MCL - r/r B-ALL	2020
Lisocabtagene maraleucel (Breyanzi)	CD19	- r/rLBCL - r/r CLL/SLL	2021
Idecabtagene vicleucel (Abecma)	BCMA	- r/r multiple myeloma (MM)	2021
Ciltacabtagene autoleucel (Carvykti)	BCMA	- r/r MM	2022
Equecabtagene autoleucel (Fucaso)	BCMA	-r/r MM	2023 (China)
Afamitresgene autoleucel = afami-cel (Tecelra)	CD30	-Synovial sarcoma	2024
obecabtagene autoleucel (Aucatzyl)	CD19	-B-cell ALL	2024

Emerging CAR T-Cell therapies				
Drug/Sponsor	Type/Target	Indication	P	Reference
BMS-986393	GPRC5D	r/r and Lenalidomide-refractory MM	3	NCT06615479
TanCAR19/20-T CAR-20/19-T IMPT-314 MBCART2019.1	CD19 & CD20	r/r NHL r/r B-cell malignancies r/r Aggressive B-cell NHL r/r aggressive CD20+ CD19+ B-NHL/CLL/SLL. r/r DLBCL	1/2	NCT03097770 NCT04186520 NCT05826535 NCT03870945 NCT04792489
PBCAR20A	CD20	r/r B-cell NHL or r/r CLL/SLL.	1/2	NCT04030195
bbT369	CD79a and CD20	r/r B Cell NHL	1/2	NCT05169489
CAR20(NAP)-T	CD20 (secrete NAP)	B-cell malignancies.	1/2	NCT06002659
HER2-CAR T	HER2	Metastatic rhabdomyosarcoma.	1	NCT00902044
PSCA-CAR T	PSCA	Prostate.	1/2	NCT02744287

ALL, acute lymphoblastic leukemia; BCMA, B-cell maturation antigen; CLL, chronic lymphocytic leukemia; FL, follicular lymphoma; LBCL, large B-cell lymphoma; MCL, mantle cell lymphoma; MM, Multiple myeloma; NAP, neutrophil-activating protein; NHL, non-Hodgkin lymphoma; P, phase; PSCA, prostate stem cell antigen; r/r, relapsed/refractory; SLL, small lymphocytic lymphoma.

CAR Ts can have cytokine-related toxicities due to host immune system recognition resulting in the implementation of human or humanized antibody fragments instead of the classical murine-derived CARs to lessen CAR T treatment immunogenicity (215, 220). CAR T therapy faces key challenges in treating solid tumors and blood cancers, including toxic off-target effects, modest anti-tumor efficacy, antigen loss by tumors, and an immunosuppressive TIME that blocks tumor clearance (215, 220). CAR T cell therapy can fail due to changes in tumor-associated antigens (TAAs), such as antigen loss or downregulation, which make cancer cells undetectable to CAR T cells (221). Additionally, poor trafficking and infiltration limit CAR T cell access to tumors, reducing treatment effectiveness. Limited CAR T cell expansion and short-term persistence, often caused by exhaustion from co-inhibitory pathways—also contribute to poor responses, posing a challenge for developing longer-lasting CAR T therapies (13).

5.5 Cancer vaccines

Cancer vaccines represent a vital component of immunotherapy, designed to either prevent or treat cancer using diverse platforms like cells, viruses, peptides, or nucleic acids, see Table 5 (222). The goal of cancer vaccines is to train the host immune system to recognize and attack tumor-associated and tumor cells by exposing them to specific cancer-associated molecules such as, antigens, of the tumor of interest (223). Some of the current cancer vaccines are targeting HPV- related cancers, melanoma and prostate cancer (224, 225), as well as other

TABLE 5 FDA-approved cancer vaccines.

Drug	Target	Type	Approved indications	Year
Bacillus Calmette Guérin (BCG) (Also TheraCys, branded form of BCG)	Urothelial carcinoma cells	Live attenuated bacterial	Treatment of early-stage non–muscle-invasive bladder cancer (NMIBC)	1990
HBV vaccine (Engerix-B, Recombivax HB, Heplisav-B, PreHevbrio)	Hepatitis B surface antigen (HBsAg)	Recombinant protein	Prevents hepatitis B virus and liver cancer	1989 onwards
Gardasil	HPV types 16, 18, 6, and 11	Virus-like particles	Prevents cervical cancer, anal cancer, vulvar, vaginal, and penile cancers	2006
Cervarix	HPV types 16 and 18	Virus-like particles	Prevents cervical cancers	2009
Sipuleucel-T (Provenge)	Prostatic acid phosphatase (PAP)	Autologous cellular	Treatment of asymptomatic or minimally symptomatic metastatic castration-resistant prostate cancer	2010
Gardasil-9	HPV types 6,11, 16, 18, 31, 33, 45, 52, and 58	Virus-like particles of 16, 18, 31, 33, 45, 52, and 58 proteins	Prevents cervical cancer, anal cancer, vulvar, vaginal, and penile cancers	2014
IMLYGIC (talimogene laherparepvec)	Herpes simplex virus (HSV-1)	Oncolytic virus	Treatment of unresectable melanoma (cutaneous, subcutaneous, and nodal lesions)	2015

HPV, human papillomavirus.

therapies under development for other cancers such as NSCLC, breast cancer and ovarian cancer (224–227). Each specificized cancer vaccine has different success rates, although, HPV-related vaccines are seen as highly effective, while other cancers vary the response rate and are often below 10% (228, 229).

DC vaccines are loaded with tumor-specific proteins and idiotypes, which target and treat specific cancers. Idiotypes produced by tumor cells help stimulate an immune response from the stimulated DC-based vaccine, which is then aimed at attacking the TIME (230). A study using idiotype protein-pulsed DC vaccines for multiple myeloma showed minimal side effects and boosted host immune responses, with patients exhibiting ID-specific immunity, indicating potential anti-myeloma effects (231). Unfortunately, DC-based vaccines have not achieved the strong clinical results initially expected, despite their promise in enhancing anti-tumor immune responses. However, recent studies suggest that combining DC vaccines with ICI, such as CTLA-4 and PD-1 blockers, may improve T cell responses and lead to better clinical outcomes (232–234).

Peptide-based vaccines stimulate T and B cell immunity by targeting specific epitopes, offering high specificity, improved efficacy, and fewer side effects compared to conventional cancer therapies (235, 236). Peptide-based vaccines are known to treat many cancer types such as, melanoma, lung cancer, breast cancer, pancreatic cancer, and even some brain tumors as FDA approved vaccines and vaccines in clinical trial (237–244). These vaccines offer benefits such as stability, safety, and the ability to elicit robust T cell responses, which enable direct monitoring of immune activity and support repeated booster doses (245, 246). An additional study using a HER-2/neu-derived peptide in combination with a linker peptides and Pan HLA-DR epitopes showed enhanced CD4+ and CD8+ T cell responses as well as a replicative result of increased IFN-γ production (247).

Virus-like particle vaccines, such as the widely used HPV vaccine, help prevent genital warts, respiratory papillomatosis, and cancers including cervical, anal, penile, vulvar, vaginal, and oropharyngeal (248, 249). Clinical trials show that adjuvant HPV vaccination significantly reduces the recurrence of CIN 1+ and CIN 2+ after surgical treatment (250). Repurposed antiviral subunit and mRNA vaccines are being studied to reshape the TIME by inducing cancer cell death, releasing tumor antigens, and enhancing immune cell activation for stronger anti-tumor responses (251).

Nucleic acid vaccines (NAVs) use cancer cell DNA and RNA to stimulate the immune system to target cancer cells and the tumor microenvironment by promoting tumor antigen production (252). DNA vaccines enter the nucleus to produce multiple mRNA copies, boosting antigen levels but risking delays and insertional mutations. mRNA vaccines act faster by translating in the cytoplasm without genome integration risk, though they typically yield fewer antigens (222). The Phase I Lipo-MERIT trial (NCT02410733) of the melanoma vaccine FixVac (BNT111) showed a favorable safety profile (225). Targeting four shared tumor-associated antigens, FixVac—alone or with PD-1 inhibitors—induced durable responses and strong CD4+/CD8+ T-cell immunity in advanced melanoma patients previously treated with ICIs, suggesting its promise as a potent RNA-based immunotherapy (225).

6 Incorporation of AI into TIME monitoring for cancer therapy

Recent advances in cancer therapy have seen AI become directly embedded within cutting edge technologies, from imaging to molecular analysis. AI-powered tools, such as deep learning algorithms integrated into MRI, PET/CT, and mass cytometry imaging, now enable precise detection of tumor-immune

interactions, automated identification and quantification of immune cell populations, and improved prediction of treatment outcomes (253, 254). Additionally, machine learning models are driving molecular data interpretation allowing for more rapid analysis of gene mutations, immune marker profiles, and recommendation of optimal personalized therapies for patients (255). Understanding the complex, heterogeneous TIME is crucial for improving cancer diagnostics and treatment, but its spatial and temporal variability challenges characterization and clinical use (15, 256, 257). To address these challenges, recent advancements have integrated cutting-edge imaging technologies, molecular assays, and computational tools, offering a more comprehensive and dynamic assessment of tumor-immune interactions (258). Imaging modalities have played a pivotal role in showing the TIME's spatial organization and functional dynamics. Fluorescence and bioluminescence imaging enable real-time tracking of immune cell infiltration, spatial distribution, and dynamic change in preclinical models (259–262). Multiplex immunohistochemistry (IHC) and imaging mass cytometry provide high-resolution spatial mapping of protein expression, allowing for precise characterization of immune cell phenotypes and their interactions with cancer cells (248, 263, 264). Multiplex ion beam imaging enables simultaneous detection of multiple biomarkers at subcellular resolution, revealing immune cell heterogeneity and spatial relationships across tumors (265, 266). A commonly used diagnostic scan in the medical field is the positron emission tomography-computed tomography (PET/CT) scan, which combines the PET and CT scans. A PET/CT scan can observe and record detailed body images to diagnose and treat diseases (267). This imaging technique is used to observe CAR T-cell treatment and many other cancerous mass treatments. Using PET/CT can also monitor tissue metabolism which helps provide more inclusive observations of the TIME (268, 269). Intravital microscopy (IVM) is an imaging technique that maps tumor-associated vessels, measures vessel density, and uses vital dyes to locate vessels within tumors (270). IVM has been used in clinical oncology to characterize superficial vessels in human melanoma tumors and to analyze tumor physiology, drug delivery, and immune cell trafficking (271). Aside from diagnostic imaging, MRI has recently been applied to treatment plans for individual cases. MRI uses strong magnetic fields to align protons in the body and measures their interactions, which are computationally processed to produce high-resolution anatomical images. Recently, MRI has been combined with nanoparticles to improve tumor detection, quantify tumor burden, and track the localization and accumulation of therapeutic agents (272). Additionally, photoacoustic imaging has emerged as a powerful, non-invasive technique, bridging optical and ultrasound imaging to provide high-contrast, deep-tissue visualization of tumor vascularization, metabolic activity, and immune cell infiltration (273, 274). Given the TIME's impact on current cancer therapies, there is a need for more effective screening, prevention, and treatment strategies to benefit patients.

Beyond imaging, molecular techniques like enzyme-linked immunosorbent assay, quantitative polymerase chain reaction, flow cytometry (FC), and IHC are vital for measuring immune markers and tumor-related biomolecules, enabling assessment of immune activation and therapy-induced changes in the TIME. AI integration further enhances accuracy, efficiency, and prediction in oncology diagnostics and treatment.

(143) Machine learning algorithms are increasingly employed for automated image analysis, enabling rapid identification of tumor-infiltrating lymphocytes, classification of histopathological features, and prediction of patient prognosis based on multi-modal data (70, 275, 276). AI-driven computational models also support treatment decision-making by analyzing vast datasets from genomic, transcriptomic, and proteomic studies, thereby identifying potential therapeutic targets and optimizing personalized medicine strategies (277).

6.1 AI-driven insights from biomarkers and liquid biopsies

Liquid biopsies and circulating tumor DNA (ctDNA) from blood samples offer a non-invasive way to assess cancer, monitor treatment response, and detect recurrence earlier than traditional imaging. In non-small cell lung cancer, biomarkers were used to predict immunotherapy outcomes independently of PD-L1 status (278). Biomarkers have become a great tool for screening and monitoring various cancer types and diseases by enabling clinicians to detect cancers at earlier stages, assess the effectiveness of therapies, and adjust treatment strategies based on individual patient responses (279). Many clinical trials have utilized predictive approaches using biomarkers like microsatellite instability (MSI), PD-L1, and tumor mutational burden (TMB) to predict patient response to ICI treatment of tumor types (280, 281). Combining biomarkers in panels offers the advantage of cross-confirmation and can detect changes independent of upregulated pathways, unlike single markers (256). Combining biomarkers like Alpha-Fetoprotein (AFP), a biomarker used to detect liver cancer (hepatocellular carcinoma) and germ cell tumors in the testicles or ovaries with cfDNA improving diagnostic accuracy and variety (282). Additional studies have found that combining different panels of biomarkers for breast cancer diagnosis improved performance over using cancer antigen 15-3 (CA15-3) or carcinoembryonic antigen (CEA) alone (30). Biomarkers detect gene mutations and tumor DNA to predict treatment response and safety, mainly identifying patients likely to benefit from immunotherapy. However, not all patients receive biomarker-based treatments due to tumor-specific factors (283–285).

The incorporation of AI models has successfully predicted patient survival and response to therapies by analyzing patient TIME and clinical data. AI empowers oncologists to develop personalized treatment plans tailored to each patient's genetic and molecular profile, Figure 4. This approach enhances the likelihood of successful treatment outcomes while reducing the risk of adverse side effects when treating the TIME (286). Integrating AI into monitoring and observing cancer progression has contributed significantly to the ongoing progress in biomedical cancer research, driving innovation and improvement in cancer treatment (287). The development of PERCEPTION (PERsonalized Single-Cell

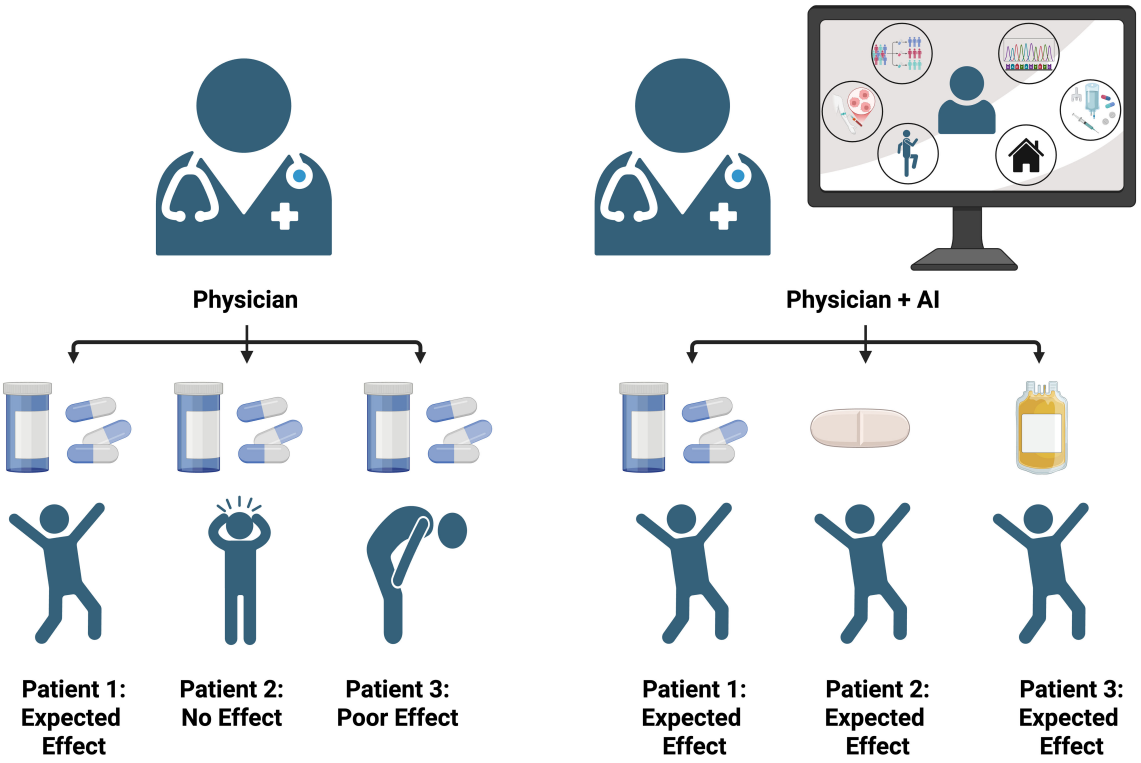

FIGURE 4
Comparison of patient outcomes with physician-only care versus integrated physician and AI-guided treatment. The AI-assisted approach leverages biomarkers, sequencing data, environmental factors, and treatment histories to personalize therapy, resulting in more consistent and optimized patient outcomes compared to physician evaluation alone.

Expression-Based Planning for Treatments In ONcology), a precision oncology computational pipeline, has produced promising results for prediction and diagnosis. This pipeline is based on publicly available matched bulk and single-cell expression profiles from large-scale cell-line drug screens from patients' single-cell tumor transcriptomics. The goal of PERCEPTION is to predict responses to targeted therapies in cultured and patient-tumor-derived primary cells from two clinical trials for multiple myeloma and breast cancer patients and the development of resistance to kinase inhibitors against lung cancer patients. The single-cell expression profiles have showcased patient stratification using tumor profiles and the available oncology tools to predict patient response and resistance to treatments (288). Biomarkers aid in detection and outcome management, though their clinical use can be complex. Integrating AI with biomarker data, particularly in liver cancer, shows promise in research and potential clinical applications. Studies have shown that using biomarkers using a predictive model for identifying the risk of hepatocellular carcinoma (HCC) one year in advance achieved an area under the receiver operating characteristic curve (AUROC) of 0.94, with a 95% confidence interval of 0.937 to 0.943. This model demonstrated a sensitivity of 0.869 and a specificity of 0.865. For predicting HCC at different time points, the AUROC values were as follows: 0.96 for 7 days, 0.94 for 6 months, 0.94 for 1 year, 0.91 for 2 years, and 0.91 for 3 years in advance (280, 289). Machine learning was used to develop a predictive model for diagnosing HCC, optimized with grid search to select the best hyperparameters. Trained on data from 539 HCC and 1,043 non-HCC patients, the gradient boosting model achieved the highest accuracy (87.34%) and an AUC of 0.940. Compared to single tumor markers, this approach significantly reduced misclassification, demonstrating the value of biomarker-based ML models (290, 291). AI and machine learning enable advanced models for cancer diagnosis and sub-classification using histopathology images, offering improved accuracy by handling population diversity and slide variability, enhancing patient sample analysis.

6.2 Enhanced tissue analysis: transforming immunohistochemistry and cancer evaluation

IHC is a method that uses tissue samples from patients from biopsy and processed where specific antibodies are selected to identify the presence of the target antigen (292). IHC slides are read by pathologists by analyzing the patient tissue samples by assessing cellular morphology, identifying cancer cells, evaluating treatment responses, and detecting specific cancer markers for tumor recognition and progression (293). AI and machine learning are used alongside pathologists to identify potential patterns and cancerous morphology in patient samples. These technologies help uncover additional findings, enhancing the accuracy of cancer cell identification and diagnosis. This collaborative approach is increasingly being implemented in cancer research and clinical settings. This technology

is called the Clinical Histopathology Imaging Evaluation Foundation (CHIEF) model, a general-purpose weakly supervised machine learning framework to extract pathology imaging features for systematic cancer evaluation. This technology uses two pretraining methods to extract diverse pathology representations from sample slides: unsupervised pretraining for tile-level identification and weakly supervised pretraining for whole–slide pattern recognition during training sessions. CHIEF was trained using 60,530 whole slide images using 16 different anatomical sites (294). This research underscores AI's significant potential to enhance the accuracy and reliability of biomarker detection, particularly in the context of liver cancer diagnosis and treatment.

Immune modulation has also become a focal point for AI integration due to the pivotal role immune therapy can provide for patients by using their immune system. AI is utilized to reveal underlying immune patterns associated with treatment responses, indirectly and directly; this approach predicts how patients will respond to immunotherapy. Including AI in analyzing high-throughput genetic sequences and medical imaging provides crucial insights for managing cancer immunotherapy. This analysis aids in selecting suitable patients, optimizing treatment strategies, and predicting personalized prognoses (295, 296).

6.3 Single-cell based analysis incorporating AI

FC is a widely adopted single-cell-based assay extensively used in cancer diagnostics. FC enables quantitative analysis of immune cells, tumor characterization, and treatment response assessment. It provides high-resolution insights into cell phenotypes and functions, allowing clinicians to monitor circulating tumor cells, cancer stem cells, tumor antigens, and immune subsets in blood, tissue, or bone marrow over time (297). Traditional methods for analyzing the TIME, such as manual assessment of TILs, are labor-intensive and subject to interobserver variability (298). Recent advancements have introduced AI-powered tools that enhance the precision and efficiency of TIME evaluation. For instance, an AI-based spatial analysis system has been developed to classify TIME into immune phenotypes: 'inflamed,' 'immune-excluded,' and 'immune-desert', which correlate with responses to immune checkpoint inhibitors in NSCLC patients (299). Additionally, deep learning frameworks like ImmunoAIzer have been utilized to characterize cell distribution and gene mutations within the tumor, facilitating a more comprehensive understanding of tumor-immune interactions (300). These AI-driven approaches enable high-throughput, objective, and reproducible analyses of the TIME, thereby informing treatment strategies and potentially improving patient outcomes.

6.4 Limitations of using AI in cancer diagnosis and therapy

Utilizing AI for cancer detection and therapy can provide complex multi-omics data, AI-powered models can uncover novel therapeutic targets and guide more precise, personalized treatment strategies. As AI continues to evolve and integrate into healthcare, its limitations and challenges must be carefully addressed, monitored, and managed to ensure safe and effective use. Although AI has potential in cancer diagnosis and therapy, its use also comes with drawbacks, such as the risk of inaccuracy and hallucinations. These issues often arise from outdated or poorly reviewed data, which can lead to misleading recommendations and suboptimal clinical decisions (301, 302). Data bias is a partially due to inaccuracy die to algorithms being trained in unrepresentative datasets that miss populations of patients, resulting in low accuracy of underrepresented groups, increasing the potential for health disparities in marginalized populations (302, 303). The use of AI in oncology raises concerns about patient privacy and data security, especially when handling sensitive genetic information. Additionally, as clinical practices evolve or data distributions shift, AI algorithms may experience performance degradation over time, leading to inconsistent or unreliable outcomes (302, 304). Health care and research can work to overcome these new and constantly evolving limitations by improving accuracy and reducing errors by stringently reinforcing the hybrid approaches that integrate AI predictions with clinician oversight which often referred to as 'human-in-the-loop' models. This approach helps reduce errors and build trust in AI-driven recommendations (305, 306). To reduce bias and reduce health disparities, mitigating bias and promoting equity through training AI algorithms on large, diverse, and representative datasets helps minimize bias and improve outcomes for underrepresented populations (307). Federated learning enables models to learn from data across multiple institutions without sharing raw patient information, thereby enhancing both data diversity and privacy (308, 309). In conclusion, overcoming the limitations of AI in cancer therapy requires a combined approach and leveraging technical solutions such as diverse datasets, explainable models, real-time monitoring, and federated learning, alongside systemic measures including workflow integration, regulatory clarity, data privacy, and cross-disciplinary collaboration—to support ethical, equitable, and effective clinical deployment.

6.5 Personalized care for patients

Personalized medicine (PM) refers to a medical approach that tailor's prevention, diagnosis, and treatment strategies based on an individual's unique biological characteristics, including genetic, epigenetic, proteomic, and metabolic profiles (310, 311). In oncology, PM uses molecular profiling of the patient and tumor to identify mutations and biomarkers, guiding targeted therapies that maximize efficacy and minimize side effects. For instance, breast cancer patients with HER2 overexpression benefit from HER2-targeted agents such as trastuzumab, while NSCLC patients harboring EGFR mutations or ALK rearrangements are treated with corresponding tyrosine kinase inhibitors. Adoptive Cell Transfer (ACT) therapy, including CAR T and tumor-infiltrating lymphocyte (TIL) therapy, represents a highly personalized approach to cancer treatment using a patient's immune cells to enhance their

anti-tumor response. CAR T-cells therapy involves engineering T cells to express synthetic receptors that recognize specific tumor antigens. In contrast, TIL therapy relies on expanding naturally occurring tumor-infiltrating lymphocytes that have already recognized cancer cells (312, 313). Using a patient's own immune cells, ACT offers high specificity with minimal rejection risk. It has shown strong efficacy in blood cancers, with CAR T-cell therapies targeting CD19 achieving high remission rates in leukemia and lymphoma (314–316). However, outcomes in solid tumors remain less impressive due to challenges such as tumor heterogeneity, antigen escape, and the immunosuppressive nature of TIME (317–319). Regulatory T cells, MDSCs, and inhibitory cytokines in the TIME can limit ACT by suppressing T-cell function. To enhance efficacy, strategies like combining ACT with immune checkpoint inhibitors help counter immunosuppression and prevent T-cell exhaustion (320). Additionally, approaches targeting the TIME itself, such as depleting immunosuppressive cell populations (321) or modulating the tumor vasculature (322), are being investigated to create a more favorable environment for ACT.

7 Discussion

The TIME coordinates cell behavior, shaping the tumor and immune environments both individually and collectively. This review highlights how these microenvironments adapt to evade current immunotherapies and treatments in patients and clinical trials.

Regulating the TIME by balancing activation and suppression is key to improving therapies that boost the host immune response reducing tumor burden and prevent immune evasion (9). Despite ongoing advancements in treatment development, a deeper understanding of the mechanisms by which the TIME adapts to therapies is still needed to overcome treatment resistance and improve therapeutic efficacy. Advances in science and AI have driven personalized cancer therapies by enabling tailored screening and early diagnostics from patient samples (258, 286). Understanding TIME behavior allows researchers and clinicians to combine immunotherapies, AI-driven early detection, and dual treatments to reduce tumor burden and counter immune suppression.

7.1 Current challenges caused by the TIME

A key challenge currently being explored by researchers and clinicians is how to monitor the complex and heterogeneous cell populations that comprise the TIME.

The TIME consists of diverse cell types including immune, fibroblasts, epithelial, endothelial and matrix components that interact with tumor vasculature to promote growth and invasion. Variations in cell composition across TIME regions create distinct functional profiles that impact treatment response (15). Tumor heterogeneity includes intratumoral heterogeneity, which refers to the diverse cancer cell populations within a single tumor that can exhibit distinct genetic, molecular, and phenotypic traits. In contrast, intertumoral heterogeneity refers to differences observed across tumors from different individuals, even when diagnosed with the same cancer type (323). The variation within the heterogenous population leads to various treatment responses which can lead to resistance highlighting the difficulties of using standard of care treatments compared to more targeted therapies in PM.

TAAs are the target for specialized CAR T cell therapies used to activate T cells and the destruction of tumor cells (315). Within the heterogeneity of an individual TIME, tumor antigenic heterogeneity will reduce and impair the therapeutic efficiency of adoptive cell therapies, CAR T cell therapy is known for having significant implications of antigen escape occurs within a patient undergoing treatment (324). This escape mechanism can lead to the antigen escape and potential tumor recurrence and immune therapy resistance due to the heterogeneous TIME having the ability to downregulate the targeted antigen of the adoptive cell therapy for treatment (325). Demonstrating that antigen escape driven by TIME heterogeneity has shown to be a predictor of resistance and recurrence, with implications for therapy design and or monitoring (324). A potential tool to overcome this escape mechanism is to target multiple TAAs using CAR T therapy to improve treatment, called 4dem CARs (TanCARs). The development of TanCARs is using a CAR construct with two antigen recognition domains to target two different TAAs simultaneously (326). TanCARs have shown promise in preclinical and clinical studies, demonstrating more durable responses and lower relapse rates compared to monospecific CARs, particularly in cancers prone to antigen escape. Additionally, certain TanCAR designs enhance safety by requiring engagement of both antigens for full activation, increasing specificity and potentially reducing off-target effects such as cytokine release syndrome (326, 327). In a 2020 study, Tong and colleagues developed a series of TanCARs targeting CD19 and CD20, demonstrating that TanCAR7 T cells provide dual antigen coverage and induce a potent, durable anti-tumor response—helping to prevent relapse due to antigen escape following CD19- or CD20-targeted therapies. Notably, no cases of grade 3 or higher CAR T-cell-related encephalopathy syndrome (CRES) were reported during treatment of relapsed/refractory non-Hodgkin lymphoma (r/rNHL) (13, 328). While TanCARs offer enhanced activation through bivalent engagement, this increased signaling strength can sometimes lead to T cell exhaustion, reduced persistence, or heightened toxicity. Their effectiveness also depends on a minimum threshold of antigen expression; if one or both target antigens are present at low levels, the therapeutic response may be diminished. Moreover, in rare cases, tumors may escape treatment by downregulating or losing both antigens, leading to potential resistance even with TanCAR therapy (13, 327). TanCARs are currently in development at various stages within clinical trials. One such trial is NCT07032129, which targets BCMA/GPRC5D in patients with relapsed/refractory multiple myeloma (BAH2573).

TIME can inhibit anti-tumor immune responses by attracting immunosuppressive cells, such as regulatory T cells and myeloid-derived suppressor cells, and by enhancing the expression of inhibitory molecules on immune cells. The TIME can cause tumor-infiltrating T cells to become exhausted, impairing their ability to recognize and destroy cancer cells effectively (21, 127). Additionally, the TIME can increase the expression of immune

checkpoint proteins, such as PD-1 and CTLA-4, on immune cells, further suppressing their activity. A study using the incorporation of doxorubicin with nivolumab showed a benefit, metastatic triple-negative breast cancer (TNBC) patients with a 23% objective response rate compared to PD-1/PD-L1 blockade in phase II clinical trial showed no benefit. This study also found that doxorubicin and cisplatin treatment induced the upregulation of genes involved in the T cell cytotoxicity pathway, establishing a link between the clinical activity of these agents and their capacity to regulate systemic immunity (329).

The potential barriers of the TIME have been linked to chemotherapy treatment and metabolic constraints, limiting the effectiveness of treatment and physical barriers created by the TIME (186). Decompression is another method used to reduce physiological pressure, improving oxygenation and reducing drug resistance (330). To overcome T cell exhaustion, strategies include blocking inhibitory receptors (e.g., PD-1, CTLA-4) and using epigenetic, transcriptional, metabolic, and cytokine-based therapies (331).

7.2 Future directions

Immunotherapies often work well with other therapies like surgery, chemotherapy, or radiation, which has become an effective treatment due to a simultaneous targeting mechanism that stimulates a host immune response to disrupt the TIME and overcome the immune suppression (332). This approach helps reduce drug resistance while offering multiple anti-cancer benefits, including slowing tumor growth, lowering metastatic potential, targeting mitotically active cells, decreasing cancer stem cell populations, and inducing apoptosis (333). However, the use of combination therapies has become a new line of treatment, due to the clinical benefits in certain cancers that previously had a poor prognosis (334, 335). Combination therapies tend to consist of one or more FDA-approved therapy agents that target similar pathways or mechanisms of cell death as they aim to improve patient outcomes. Combination therapy can reduce treatment costs through full or partial FDA-approved agents and repurposing existing drugs alongside novel therapies shows promise in reducing tumor burden (283). Nivolumab, a well-known immunotherapy and the first PD-1 inhibitor to be paired with classic chemotherapy, demonstrated superior overall and progression-free survival. The clinical trial showed benefits regarding an acceptable safety profile in combination with chemotherapy compared to chemotherapy alone and is now a new standard of first-line treatment for previously untreated patients with advanced gastric, gastro-esophageal junction, or esophageal adenocarcinoma (336).

The incorporation of AI into monitoring approaches for the TIME of cancer patients before, during, and after the treatment duration which can help prevent recurrence of various cancer types by detecting when tumor cells become less responsive to previous therapies in near real time (255). While traditional cancer monitoring remains standard, integrating early relapse detection, adaptive precision medicine, and real-time toxicity prevention can greatly improve outcomes. This requires better data interoperability and machine learning models that ensure privacy, explainability, safety, and accountability. With improved data integration and collaboration, AI can reduce treatment complications and enhance cancer care effectiveness. The use of immunotherapy in cancer treatment is rooted in significant advancements in understanding the key mechanisms behind T-cell activation and suppression. Innovative therapies, such as CAR T cells, CAR NK cells, and CAR M cells, are showing potential in effectively targeting solid tumors (312). The complex TIME poses significant challenges for developing universal cancer therapies and can lead to unintended side effects, such as immune-related adverse events, complicating treatment efforts. Our understanding of the TIME is still incomplete, with many aspects of its biology yet fully explored. These challenges underscore the importance of ongoing research to deepen our knowledge of the TIME and develop safer, more effective therapies.

Author contributions

KR: Conceptualization, Visualization, Writing – original draft, Writing – review & editing. YS: Visualization, Writing – original draft, Writing – review & editing. RV: Conceptualization, Visualization, Writing – original draft, Writing – review & editing. SM: Visualization, Writing – review & editing. MT: Visualization, Writing – review & editing. TL: Writing – review & editing. YL: Funding acquisition, Resources, Supervision, Writing – review & editing.

Funding

The author(s) declare financial support was received for the research and/or publication of this article. This study was financially supported by NIH/NCI (R01CA294557), NIH/NCI (R01CA232845), NIH/NIDCR (R01DE029237), NIH/NIBIB (R01EB033677), NIH/NIBIB (R01EB035416), T32 GM144303, and NIH/NCI (P30CA093373).

Conflict of interest

The authors declare that the research was conducted in the absence of any commercial or financial relationships that could be construed as a potential conflict of interest.

Generative AI statement

The author(s) declare that no Generative AI was used in the creation of this manuscript.

Any alternative text (alt text) provided alongside figures in this article has been generated by Frontiers with the support of artificial intelligence and reasonable efforts have been made to ensure accuracy, including review by the authors wherever possible. If you identify any issues, please contact us.

Publisher's note

References

1. Sung H, Ferlay J, Siegel RL, Laversanne M, Soerjomataram I, Jemal A, et al. Global cancer statistics 2020: GLOBOCAN estimates of incidence and mortality worldwide for 36 cancers in 185 countries. *CA A Cancer J Clin*. (2021) 71:209–49. doi: 10.3322/caac.21660

2. Global cancer burden growing, amidst mounting need for services. Available online at: https://www.who.int/news/item/01-02-2024-global-cancer-burden-growing–amidst-mounting-need-for-services. (Accessed April 23, 2025).

3. Dusek RL, Attardi LD. Desmosomes: new perpetrators in tumour suppression. *Nat Rev Cancer*. (2011) 11:317–23. Available online at: https://www.nature.com/articles/nrc3051. (Accessed February 19, 2025).

4. Martin TA, Ye L, Sanders AJ, Lane J, Jiang WG. Cancer invasion and metastasis: molecular and cellular perspective. In: *Madame Curie Bioscience Database*. Austin, Texas, USA: Landes Bioscience (2013). Available online at: https://www.ncbi.nlm.nih.gov/books/NBK164700/.

5. Brown JS, Amend SR, Austin RH, Gatenby RA, Hammarlund EU, Pienta KJ. Updating the definition of cancer. *Mol Cancer Res*. (2023) 21:1142–7. Available online at: https://aacrjournals.org/mcr/article/21/11/1142/729785/Updating-the-Definition-of-CancerUpdating-the. (Accessed February 19, 2025).

6. Connolly JL, Schnitt SJ, Wang HH, Longtine JA, Dvorak A, Dvorak HF. Tumor structure and tumor stroma generation. In: *Holland-Frei Cancer Medicine, 6th edition*. Hamilton, Ontario, Canada: BC Decker (2003). Available online at: https://www.ncbi.nlm.nih.gov/books/NBK13447/.

7. Vogelstein B, Papadopoulos N, Velculescu VE, Zhou S, Diaz LA, Kinzler KW. Cancer genome landscapes. *Science*. (2013) 339:1546–58. doi: 10.1126/science.1235122

8. Anderson NM, Simon MC. The tumor microenvironment. *Curr Biol*. (2020) 30: R921–5. Available online at: https://linkinghub.elsevier.com/retrieve/pii/S0960982220309337. (Accessed November 19, 2024).

9. Quail DF, Joyce JA. Microenvironmental regulation of tumor progression and metastasis. *Nat Med*. (2013) 19:1423–37. Available online at: https://www.nature.com/articles/nm.3394. (Accessed February 19, 2025).

10. Krzyszczyk P, Acevedo A, Davidoff EJ, Timmins LM, Marrero-Berrios I, Patel M, et al. The growing role of precision and personalized medicine for cancer treatment. *Technol (Singap World Sci)*. (2018) 6:79–100. doi: 10.1142/S2339547818300020

11. Murciano-Goroff YR, Warner AB, Wolchok JD. The future of cancer immunotherapy: microenvironment-targeting combinations. *Cell Res*. (2020) 30:507–19. Available online at: https://www.nature.com/articles/s41422-020-0337-2. (Accessed March 19, 2025).

12. Mou P, Ge Qh, Sheng R, Zhu Tf, Liu Y, Ding K. Research progress on the immune microenvironment and immunotherapy in gastric cancer. *Front Immunol*. (2023) 14:1291117/full. doi: 10.3389/fimmu.2023.1291117/full

13. Sterner RC, Sterner RM. CAR-T cell therapy: current limitations and potential strategies. *Blood Cancer J*. (2021) 11:69. Available online at: https://www.nature.com/articles/s41408-021-00459-7. (Accessed February 24, 2025).

14. Liu Y, Yang H, Li T, Zhang N. Immunotherapy in liver cancer: overcoming the tolerogenic liver microenvironment. *Front Immunol*. (2024) 15:1460282/full. doi: 10.3389/fimmu.2024.1460282/full

15. Baghban R, Roshangar L, Jahanban-Esfahlan R, Seidi K, Ebrahimi-Kalan A, Jaymand M, et al. Tumor microenvironment complexity and therapeutic implications at a glance. *Cell Commun Signal*. (2020) 18:59. doi: 10.1186/s12964-020-0530-4

16. Maffuid K, Cao Y. Decoding the complexity of immune-cancer cell interactions: empowering the future of cancer immunotherapy. *Cancers (Basel)*. (2023) 15:4188. doi: 10.3390/cancers15164188

17. Whiteside TL. The tumor microenvironment and its role in promoting tumor growth. *Oncogene*. (2008) 27:5904–12. doi: 10.1038/onc.2008.271

18. Binnewies M, Roberts EW, Kersten K, Chan V, Fearon DF, Merad M, et al. Understanding the tumor immune microenvironment (TIME) for effective therapy. *Nat Med*. (2018) 24:541–50. doi: 10.1038/s41591-018-0014-x

19. Berkmen YM, Lande A. Chest roentgenography as a window to the diagnosis of Takayasu's arteritis. *Am J Roentgenol Radium Ther Nucl Med*. (1975) 125:842–6. doi: 10.2214/ajr.125.4.842

20. Gonzalez H, Hagerling C, Werb Z. Roles of the immune system in cancer: from tumor initiation to metastatic progression. *Genes Dev*. (2018) 32:1267–84. doi: 10.1101/gad.314617.118

21. Tie Y, Tang F, Wei Yq, Wei Xw. Immunosuppressive cells in cancer: mechanisms and potential therapeutic targets. *J Hematol Oncol*. (2022) 15:61. doi: 10.1186/s13045-022-01282-8

22. Kay J, Thadhani E, Samson L, Engelward B. Inflammation-induced DNA damage, mutations and cancer. *DNA Repair (Amst)*. (2019) 83:102673. doi: 10.1016/j.dnarep.2019.102673

23. Bilotta MT, Antignani A, Fitzgerald DJ. Managing the TME to improve the efficacy of cancer therapy. *Front Immunol*. (2022) 13:954992/full. doi: 10.3389/fimmu.2022.954992/full

24. Swann JB, Smyth MJ. Immune surveillance of tumors. *J Clin Invest*. (2007) 117:1137–46. doi: 10.1172/JCI31405

25. Li K, Shi H, Zhang B, Ou X, Ma Q, Chen Y, et al. Myeloid-derived suppressor cells as immunosuppressive regulators and therapeutic targets in cancer. *Sig Transduct Target Ther*. (2021) 6:362. Available online at: https://www.nature.com/articles/s41392-021-00670-9. (Accessed February 19, 2025).

26. Mai Z, Lin Y, Lin P, Zhao X, Cui L. Modulating extracellular matrix stiffness: a strategic approach to boost cancer immunotherapy. *Cell Death Dis*. (2024) 15:307. Available online at: https://www.nature.com/articles/s41419-024-06697-4. (Accessed April 28, 2025).

27. Closset L, Gultekin O, Salehi S, Sarhan D, Lehti K, Gonzalez-Molina J. The extracellular matrix – immune microenvironment crosstalk in cancer therapy: Challenges and opportunities. *Matrix Biol*. (2023) 121:217–28. Available online at: https://linkinghub.elsevier.com/retrieve/pii/S0945053X23000811. (Accessed April 28, 2025).

28. Mezu-Ndubuisi OJ, Maheshwari A. The role of integrins in inflammation and angiogenesis. *Pediatr Res*. (2021) 89:1619–26. Available online at: https://www.nature.com/articles/s41390-020-01177-9. (Accessed June 28, 2025).

29. Clark EA, King WG, Brugge JS, Symons M, Hynes RO. Integrin-mediated signals regulated by members of the rho family of GTPases. *J Cell Biol*. (1998) 142:573–86. doi: 10.1083/jcb.142.2.573

30. Zhou Y, Tao L, Qiu J, Xu J, Yang X, Zhang Y, et al. Tumor biomarkers for diagnosis, prognosis and targeted therapy. *Sig Transduct Target Ther*. (2024) 9:132. Available online at: https://www.nature.com/articles/s41392-024-01823-2. (Accessed March 2, 2025).

31. Boudreau N, Bissell MJ. Extracellular matrix signaling: integration of form and function in normal and Malignant cells. *Curr Opin Cell Biol*. (1998) 10:640–6. doi: 10.1016/S0955-0674(98)80040-9

32. Vetsika EK, Koukos A, Kotsakis A. Myeloid-derived suppressor cells: major figures that shape the immunosuppressive and angiogenic network in cancer. *Cells*. (2019) 8:1647. Available online at: https://www.mdpi.com/2073-4409/8/12/1647. (Accessed March 19, 2025).

33. Lv D, Fei Y, Chen H, Wang J, Han W, Cui B, et al. Crosstalk between T lymphocyte and extracellular matrix in tumor microenvironment. *Front Immunol*. (2024) 15:1340702/full. doi: 10.3389/fimmu.2024.1340702/full

34. Xiao Y, Yu D. Tumor microenvironment as a therapeutic target in cancer. *Pharmacol Ther*. (2021) 221:107753. doi: 10.1016/j.pharmthera.2020.107753

35. Justus CR, Dong L, Yang LV. Acidic tumor microenvironment and pH-sensing G protein-coupled receptors. *Front Physiol*. (2013) 4:354/abstract. doi: 10.3389/fphys.2013.00354/abstract

36. Liberti MV, Locasale JW. The Warburg effect: how does it benefit cancer cells? *Trends Biochem Sci*. (2016) 41:211–8. doi: 10.1016/j.tibs.2015.12.001

37. Yang K, Wang X, Song C, He Z, Wang R, Xu Y, et al. The role of lipid metabolic reprogramming in tumor microenvironment. *Theranostics*. (2023) 13:1774–808. doi: 10.7150/thno.82920

38. Liu J, Bai Y, Li Y, Li X, Luo K. Reprogramming the immunosuppressive tumor microenvironment through nanomedicine: an immunometabolism perspective. *EBioMedicine*. (2024) 107:105301. doi: 10.1016/j.ebiom.2024.105301

39. Chen Z, Han F, Du Y, Shi H, Zhou W. Hypoxic microenvironment in cancer: molecular mechanisms and therapeutic interventions. *Sig Transduct Target Ther*. (2023) 8:70. Available online at: https://www.nature.com/articles/s41392-023-01332-8. (Accessed April 22, 2025).

40. Semenza GL. Hypoxia-inducible factors in physiology and medicine. *Cell*. (2012) 148:399–408. doi: 10.1016/j.cell.2012.01.021

41. Averett C, Arora S, Zubair H, Singh S, Bhardwaj A, Singh AP. Molecular targets of honokiol. In: *The Enzymes*. Elsevier, Amsterdam, Netherlands: Elsevier (2014). p. 175–93. Available online at: https://linkinghub.elsevier.com/retrieve/pii/B9780128022153000094. (Accessed April 23, 2025).

42. Wu Q, You L, Nepovimova E, Heger Z, Wu W, Kuca K, et al. Hypoxia-inducible factors: master regulators of hypoxic tumor immune escape. *J Hematol Oncol*. (2022) 15:77. doi: 10.1186/s13045-022-01292-6

43. Siemann DW. The unique characteristics of tumor vasculature and preclinical evidence for its selective disruption by Tumor-Vascular Disrupting Agents. *Cancer Treat Rev*. (2011) 37:63–74. doi: 10.1016/j.ctrv.2010.05.001

44. Chesnokova V, Melmed S. Growth hormone in the tumor microenvironment. *Arch Endocrinol Metab*. (2019) 63:568–75. doi: 10.20945/2359-3997000000186

45. Emami Nejad A, Najafgholian S, Rostami A, Sistani A, Shojaeifar S, Esparvarinha M, et al. The role of hypoxia in the tumor microenvironment and development of cancer stem cell: a novel approach to developing treatment. *Cancer Cell Int*. (2021) 21:62. doi: 10.1186/s12935-020-01719-5

46. Rajabi M, Mousa SA. The role of angiogenesis in cancer treatment. *Biomedicines*. (2017) 5:34. doi: 10.3390/biomedicines5020034

47. Hanahan D, Weinberg RA. Hallmarks of cancer: the next generation. *Cell*. (2011) 144:646–74. Available online at: https://linkinghub.elsevier.com/retrieve/pii/S0092867411001279. (Accessed February 19, 2025).

48. McDonald DM, Baluk P. Significance of blood vessel leakiness in cancer1. *Cancer Res*. (2002) 62:5381–5.

49. Schaaf MB, Garg AD, Agostinis P. Defining the role of the tumor vasculature in antitumor immunity and immunotherapy. *Cell Death Dis*. (2018) 9:115. Available online at: https://www.nature.com/articles/s41419-017-0061-0. (Accessed April 23, 2025).

50. Matuszewska K, Pereira M, Petrik D, Lawler J, Petrik J. Normalizing tumor vasculature to reduce hypoxia, enhance perfusion, and optimize therapy uptake. *Cancers*. (2021) 13:4444. Available online at: https://www.mdpi.com/2072-6694/13/17/4444. (Accessed April 23, 2025).

51. Dameron KM, Volpert OV, Tainsky MA, Bouck N. Control of angiogenesis in fibroblasts by p53 regulation of thrombospondin-1. *Science*. (1994) 265:1582–4. doi: 10.1126/science.7521539

52. Nishida N, Yano H, Nishida T, Kamura T, Kojiro M. Angiogenesis in cancer. *Vasc Health Risk Manage*. (2006) 2:213–9. doi: 10.2147/vhrm.2006.2.3.213

53. Pérez-Tomás R, Pérez-Guillén I. Lactate in the tumor microenvironment: an essential molecule in cancer progression and treatment. *Cancers (Basel)*. (2020) 12:3244. doi: 10.3390/cancers12113244

54. Kim HJ, Ji YR, Lee YM. Crosstalk between angiogenesis and immune regulation in the tumor microenvironment. *Arch Pharm Res*. (2022) 45:401–16. doi: 10.1007/s12272-022-01389-z

55. Webb BA, Chimenti M, Jacobson MP, Barber DL. Dysregulated pH: a perfect storm for cancer progression. *Nat Rev Cancer*. (2011) 11:671–7. Available online at: https://www.nature.com/articles/nrc3110. (Accessed April 4, 2025).

56. Persi E, Duran-Frigola M, Damaghi M, Roush WR, Aloy P, Cleveland JL, et al. Systems analysis of intracellular pH vulnerabilities for cancer therapy. *Nat Commun*. (2018) 9:2997. Available online at: https://www.nature.com/articles/s41467-018-05261-x. (Accessed April 4, 2025).

57. Lee S, Shanti A. Effect of exogenous pH on cell growth of breast cancer cells. *Int J Mol Sci*. (2021) 22:9910. doi: 10.3390/ijms22189910

58. Kellum JA, Song M, Li J. Science review: extracellular acidosis and the immune response: clinical and physiologic implications. *Crit Care*. (2004) 8:331–6. doi: 10.1186/cc2900

59. Wu H, Estrella V, Beatty M, Abrahams D, El-Kenawi A, Russell S, et al. T-cells produce acidic niches in lymph nodes to suppress their own effector functions. *Nat Commun*. (2020) 11:4113. Available online at: https://www.nature.com/articles/s41467-020-17756-7. (Accessed April 22, 2025).

60. Hosonuma M, Yoshimura K. Association between pH regulation of the tumor microenvironment and immunological state. *Front Oncol*. (2023) 13:1175563. doi: 10.3389/fonc.2023.1175563

61. Koppenol WH, Bounds PL, Dang CV. Otto Warburg's contributions to current concepts of cancer metabolism. *Nat Rev Cancer*. (2011) 11:325–37. Available online at: https://www.nature.com/articles/nrc3038. (Accessed April 1, 2025).

62. Tafech A, Stéphanou A. On the importance of acidity in cancer cells and therapy. *Biology*. (2024) 13:225. Available online at: https://www.mdpi.com/2079-7737/13/4/225. (Accessed April 1, 2025).

63. Müller B, Fischer B, Kreutz W. An acidic microenvironment impairs the generation of non-major histocompatibility complex-restricted killer cells. *Immunology*. (2000) 99:375–84. doi: 10.1046/j.1365-2567.2000.00975.x

64. Valiahdi SM, Egger AE, Miklos W, Jungwirth U, Meelich K, Nock P, et al. Influence of extracellular pH on the cytotoxicity, cellular accumulation, and DNA interaction of novel pH-sensitive 2-aminoalcoholatoplatinum(II) complexes. *J Biol Inorg Chem*. (2013) 18:249–60. doi: 10.1007/s00775-012-0970-4

65. Worsley CM, Veale RB, Mayne ES. The acidic tumour microenvironment: Manipulating the immune response to elicit escape. *Hum Immunol*. (2022) 83:399–408. Available online at: https://linkinghub.elsevier.com/retrieve/pii/S0198885922000301. (Accessed April 24, 2025).

66. Erra Díaz F, Dantas E, Geffner J. Unravelling the interplay between extracellular acidosis and immune cells. *Mediators Inflamm*. (2018) 2018:1218297. doi: 10.1155/2018/1218297

67. Estrella V, Chen T, Lloyd M, Wojtkowiak J, Cornnell HH, Ibrahim-Hashim A, et al. Acidity generated by the tumor microenvironment drives local invasion. *Cancer Res*. (2013) 73:1524–35. Available online at: https://aacrjournals.org/cancerres/article/73/5/1524/586608/Acidity-Generated-by-the-Tumor-Microenvironment. (Accessed February 19, 2025).

68. Zhang A, Fan T, Liu Y, Yu G, Li C, Jiang Z. Regulatory T cells in immune checkpoint blockade antitumor therapy. *Mol Cancer*. (2024) 23:251. doi: 10.1186/s12943-024-02156-y

69. Goldmann O, Nwofor OV, Chen Q, Medina E. Mechanisms underlying immunosuppression by regulatory cells. *Front Immunol*. (2024) 15:1328193. doi: 10.3389/fimmu.2024.1328193

70. Saltz J, Gupta R, Hou L, Kurc T, Singh P, Nguyen V, et al. Spatial organization and molecular correlation of tumor-infiltrating lymphocytes using deep learning on pathology images. *Cell Rep*. (2018) 23:181–93.e7. Available online at: https://linkinghub.elsevier.com/retrieve/pii/S2211124718304479. (Accessed March 20, 2025).

71. Iyer SS, Cheng G. Role of interleukin 10 transcriptional regulation in inflammation and autoimmune disease. *Crit Rev Immunol*. (2012) 32:23–63. doi: 10.1615/CritRevImmunol.v32.i1.30

72. Ye C, Yano H, Workman CJ, Vignali DAA. Interleukin-35: structure, function and its impact on immune-related diseases. *J Interferon Cytokine Res*. (2021) 41:391–406. doi: 10.1089/jir.2021.0147

73. Batlle E, Massagué J. Transforming growth factor-β Signaling in immunity and cancer. *Immunity*. (2019) 50:924–40. Available online at: https://linkinghub.elsevier.com/retrieve/pii/S1074761319301414. (Accessed February 19, 2025).

74. Sawant DV, Yano H, Chikina M, Zhang Q, Liao M, Liu C, et al. Adaptive plasticity of IL-10+ and IL-35+ Treg cells cooperatively promotes tumor T cell exhaustion. *Nat Immunol*. (2019) 20:724–35. doi: 10.1038/s41590-019-0346-9

75. Shi J, Fan J, Su Q, Yang Z. Cytokines and abnormal glucose and lipid metabolism. *Front Endocrinol*. (2019) 10:703/full. doi: 10.3389/fendo.2019.00703/full

76. Man K, Kutyavin VI, Chawla A. Tissue immunometabolism: development, physiology, and pathobiology. *Cell Metab*. (2017) 25:11–26. Available online at: https://linkinghub.elsevier.com/retrieve/pii/S1550413116304326. (Accessed April 1, 2025).

77. Zhang S, Carriere J, Lin X, Xie N, Feng P. Interplay between cellular metabolism and cytokine responses during viral infection. *Viruses*. (2018) 10:521. doi: 10.3390/v10100521

78. Hu C, Xuan Y, Zhang X, Liu Y, Yang S, Yang K. Immune cell metabolism and metabolic reprogramming. *Mol Biol Rep*. (2022) 49:9783–95. doi: 10.1007/s11033-022-07474-2

79. Yang L, Li A, Lei Q, Zhang Y. Tumor-intrinsic signaling pathways: key roles in the regulation of the immunosuppressive tumor microenvironment. *J Hematol Oncol*. (2019) 12:125. doi: 10.1186/s13045-019-0804-8

80. Cui JW, Li Y, Yang Y, Yang HK, Dong JM, Xiao ZH, et al. Tumor immunotherapy resistance: Revealing the mechanism of PD-1/PD-L1-mediated tumor immune escape. *Biomed Pharmacother*. (2024) 171:116203. Available online at: https://linkinghub.elsevier.com/retrieve/pii/S0753332224000842. (Accessed April 1, 2025).

81. Zhao H, Wu L, Yan G, Chen Y, Zhou M, Wu Y, et al. Inflammation and tumor progression: signaling pathways and targeted intervention. *Sig Transduct Target Ther*. (2021) 6:263. Available online at: https://www.nature.com/articles/s41392-021-00658-5. (Accessed December 4, 2024).

82. Katopodi T, Petanidis S, Charalampidis C, Chatziprodromidou I, Eskitzis P, Tsavlis D, et al. Tumor-infiltrating dendritic cells: decisive roles in cancer immunosurveillance, immunoediting, and tumor T cell tolerance. *Cells*. (2022) 11:3183. doi: 10.3390/cells11203183

83. Muntjewerff EM, Meesters LD, Van Den Bogaart G. Antigen cross-presentation by macrophages. *Front Immunol*. (2020) 11:1276/full. doi: 10.3389/fimmu.2020.01276/full

84. Del Prete A, Salvi V, Soriani A, Laffranchi M, Sozio F, Bosisio D, et al. Dendritic cell subsets in cancer immunity and tumor antigen sensing. *Cell Mol Immunol*. (2023) 20:432–47. Available online at: https://www.nature.com/articles/s41423-023-00990-6. (Accessed April 22, 2025).

85. Beatty GL, Gladney WL. Immune escape mechanisms as a guide for cancer immunotherapy. *Clin Cancer Res*. (2015) 21:687–92. doi: 10.1158/1078-0432.CCR-14-1860

86. Ghorani E, Swanton C, Quezada SA. Cancer cell-intrinsic mechanisms driving acquired immune tolerance. *Immunity*. (2023) 56:2270–95. Available online at: https://linkinghub.elsevier.com/retrieve/pii/S1074761323004090. (Accessed April 1, 2025).

87. Fulda S, Gorman AM, Hori O, Samali A. Cellular stress responses: cell survival and cell death. *Int J Cell Biol*. (2010) 2010:214074. doi: 10.1155/2010/214074

88. Li X, Zhong J, Deng X, Guo X, Lu Y, Lin J, et al. Targeting myeloid-derived suppressor cells to enhance the antitumor efficacy of immune checkpoint blockade therapy. *Front Immunol*. (2021) 12:754196. doi: 10.3389/fimmu.2021.754196

89. Lee DY, Im E, Yoon D, Lee YS, Kim GS, Kim D, et al. Pivotal role of PD-1/PD-L1 immune checkpoints in immune escape and cancer progression: Their interplay with platelets and FOXP3+Tregs related molecules, clinical implications and combinational potential with phytochemicals. *Semin Cancer Biol.* (2022) 86:1033–57. Available online at: https://linkinghub.elsevier.com/retrieve/pii/S1044579X20302583. (Accessed March 19, 2025).

90. Labani-Motlagh A, Ashja-Mahdavi M, Loskog A. The tumor microenvironment: A milieu hindering and obstructing antitumor immune responses. *Front Immunol.* (2020) 11:940. doi: 10.3389/fimmu.2020.00940

91. Buchbinder EI, Desai A. CTLA-4 and PD-1 pathways: similarities, differences, and implications of their inhibition. *Am J Clin Oncol.* (2016) 39:98–106. doi: 10.1097/COC.0000000000000239

92. Sakaguchi S, Yamaguchi T, Nomura T, Ono M. Regulatory T cells and immune tolerance. *Cell.* (2008) 133:775–87. Available online at: https://linkinghub.elsevier.com/retrieve/pii/S0092867408006247. (Accessed April 10, 2025).

93. Noyes D, Bag A, Oseni S, Semidey-Hurtado J, Cen L, Sarnaik AA, et al. Tumor-associated Tregs obstruct antitumor immunity by promoting T cell dysfunction and restricting clonal diversity in tumor-infiltrating CD8+ T cells. *J Immunother Cancer.* (2022) 10:e004605. doi: 10.1136/jitc-2022-004605

94. Chen Y, Hu H, Tan S, Dong Q, Fan X, Wang Y, et al. The role of neutrophil extracellular traps in cancer progression, metastasis and therapy. *Exp Hematol Oncol.* (2022) 11:99. doi: 10.1186/s40164-022-00345-3

95. Jaboury S, Wang K, O'Sullivan KM, Ooi JD, Ho GY. NETosis as an oncologic therapeutic target: a mini review. *Front Immunol.* (2023) 14:1170603. doi: 10.3389/fimmu.2023.1170603

96. Huang X, Nepovimova E, Adam V, Sivak L, Heger Z, Valko M, et al. Neutrophils in Cancer immunotherapy: friends or foes? *Mol Cancer.* (2024) 23:107. doi: 10.1186/s12943-024-02004-z

97. Zhang F, Xia Y, Su J, Quan F, Zhou H, Li Q, et al. Neutrophil diversity and function in health and disease. *Sig Transduct Target Ther.* (2024) 9:343. Available online at: https://www.nature.com/articles/s41392-024-02049-y. (Accessed June 2, 2025).

98. Kwak JW, Nguyen HQ, Camai A, Huffman GM, Mekvanich S, Kenney NN, et al. CXCR1/2 antagonism inhibits neutrophil function and not recruitment in cancer. *OncoImmunology.* (2024) 13:2384674. doi: 10.1080/2162402X.2024.2384674

99. Vivier E, Tomasello E, Baratin M, Walzer T, Ugolini S. Functions of natural killer cells. *Nat Immunol.* (2008) 9:503–10. doi: 10.1038/ni1582

100. Chester C, Fritsch K, Kohrt HE. Natural killer cell immunomodulation: targeting activating, inhibitory, and co-stimulatory receptor signaling for cancer immunotherapy. *Front Immunol.* (2015) 6:601. doi: 10.3389/fimmu.2015.00601

101. Wang W, Erbe AK, Hank JA, Morris ZS, Sondel PM. NK cell-mediated antibody-dependent cellular cytotoxicity in cancer immunotherapy. *Front Immunol.* (2015) 6:368. doi: 10.3389/fimmu.2015.00368

102. Sivori S, Vacca P, Del Zotto G, Munari E, Mingari MC, Moretta L. Human NK cells: surface receptors, inhibitory checkpoints, and translational applications. *Cell Mol Immunol.* (2019) 16:430–41. doi: 10.1038/s41423-019-0206-4

103. Terrén I, Orrantia A, Mosteiro A, Vitallé J, Zenarruzabeitia O, Borrego F. Metabolic changes of Interleukin-12/15/18-stimulated human NK cells. *Sci Rep.* (2021) 11:6472. Available online at: https://www.nature.com/articles/s41598-021-85960-6. (Accessed June 2, 2025).

104. Peng L, Sferruzza G, Yang L, Zhou L, Chen S. CAR-T and CAR-NK as cellular cancer immunotherapy for solid tumors. *Cell Mol Immunol.* (2024) 21:1089–108. Available online at: https://www.nature.com/articles/s41423-024-01207-0. (Accessed June 2, 2025).

105. Masmoudi D, Villalba M, Alix-Panabières C. Natural killer cells: the immune frontline against circulating tumor cells. *J Exp Clin Cancer Res.* (2025) 44:118. doi: 10.1186/s13046-025-03375-x

106. Takeuchi Y, Nishikawa H. Roles of regulatory T cells in cancer immunity. *Int Immunol.* (2016) 28:401–9. doi: 10.1093/intimm/dxw025

107. Ha D, Tanaka A, Kibayashi T, Tanemura A, Sugiyama D, Wing JB, et al. Differential control of human Treg and effector T cells in tumor immunity by Fc-engineered anti–CTLA-4 antibody. *Proc Natl Acad Sci USA.* (2019) 116:609–18. doi: 10.1073/pnas.1812186116

108. Lv B, Wang Y, Ma D, Cheng W, Liu J, Yong T, et al. Immunotherapy: reshape the tumor immune microenvironment. *Front Immunol.* (2022) 13:844142. doi: 10.3389/fimmu.2022.844142

109. Qiu Y, Ke S, Chen J, Qin Z, Zhang W, Yuan Y, et al. FOXP3+ regulatory T cells and the immune escape in solid tumours. *Front Immunol.* (2022) 13:982986. doi: 10.3389/fimmu.2022.982986

110. Xie L, Fang J, Yu J, Zhang W, He Z, Ye L, et al. The role of CD4+ T cells in tumor and chronic viral immune responses. *MedComm (2020).* (2023) 4:e390. doi: 10.1002/mco2.390

111. Montauti E, Oh DY, Fong L. CD4+ T cells in antitumor immunity. *Trends Cancer.* (2024) 10:969–85. Available online at: https://linkinghub.elsevier.com/retrieve/pii/S2405803324001572. (Accessed June 2, 2025).

112. Condamine T, Gabrilovich DI. Molecular mechanisms regulating myeloid-derived suppressor cell differentiation and function. *Trends Immunol.* (2011) 32:19–25. doi: 10.1016/j.it.2010.10.002

113. Noonan KA, Ghosh N, Rudraraju L, Bui M, Borrello I. Targeting immune suppression with PDE5 inhibition in end-stage multiple myeloma. *Cancer Immunol Res.* (2014) 2:725–31. doi: 10.1158/2326-6066.CIR-13-0213

114. Haile LA, Greten TF, Korangy F. Immune suppression: the hallmark of myeloid derived suppressor cells. *Immunol Invest.* (2012) 41:581–94. doi: 10.3109/08820139.2012.680635

115. Zhao Y, Du J, Shen X. Targeting myeloid-derived suppressor cells in tumor immunotherapy: Current, future and beyond. *Front Immunol.* (2023) 14:1157537. doi: 10.3389/fimmu.2023.1157537

116. He S, Zheng L, Qi C. Myeloid-derived suppressor cells (MDSCs) in the tumor microenvironment and their targeting in cancer therapy. *Mol Cancer.* (2025) 24:5. doi: 10.1186/s12943-024-02208-3

117. Boscardin SB, Dudziak D, Münz C, Rosa DS. Editorial: harnessing the participation of dendritic cells in immunity and tolerance. *Front Immunol.* (2020) 11:595841. doi: 10.3389/fimmu.2020.595841

118. Maldonado RA, von Andrian UH. How tolerogenic dendritic cells induce regulatory T cells. *Adv Immunol.* (2010) 108:111–65. doi: 10.1016/B978-0-12-380995-7.00004-5

119. Knelson EH, Ivanova EV, Tarannum M, Campisi M, Lizotte PH, Booker MA, et al. Activation of tumor-cell STING primes NK-cell therapy. *Cancer Immunol Res.* (2022) 10:947–61. Available online at: https://aacrjournals.org/cancerimmunolres/article/10/8/947/707172/Activation-of-Tumor-Cell-STING-Primes-NK-Cell. (Accessed June 2, 2025).

120. Taylor JL, Kokolus KM, Basse PH, Filderman JN, Cosgrove CE, Watkins SC, et al. Therapeutic anti-tumor efficacy of DC-based vaccines targeting TME-associated antigens is improved when combined with a chemokine-modulating regimen and/or anti-PD-L1. *Vaccines (Basel).* (2024) 12:777. doi: 10.3390/vaccines12070777

121. Boal LH, Glod J, Spencer M, Kasai M, Derdak J, Dombi E, et al. Pediatric PK/PD phase I trial of pexidartinib in relapsed and refractory leukemias and solid tumors including neurofibromatosis type I–related plexiform neurofibromas. *Clin Cancer Res.* (2020) 26:6112–21. Available online at: https://aacrjournals.org/clincancerres/article/26/23/6112/82939/Pediatric-PK-PD-Phase-I-Trial-of-Pexidartinib-in. (Accessed June 2, 2025).

122. Lu Q, Chen X, Wang S, Lu Y, Yang C, Jiang G. Potential new cancer immunotherapy: anti-CD47-SIRPα Antibodies. *Onco Targets Ther.* (2020) 13:9323–31. doi: 10.2147/OTT.S249822

123. Duan Z, Luo Y. Targeting macrophages in cancer immunotherapy. *Sig Transduct Target Ther.* (2021) 6:127. Available online at: https://www.nature.com/articles/s41392-021-00506-6. (Accessed June 2, 2025).

124. Tan Y, Wang M, Zhang Y, Ge S, Zhong F, Xia G, et al. Tumor-associated macrophages: A potential target for cancer therapy. *Front Oncol.* (2021) 11:693517. doi: 10.3389/fonc.2021.693517

125. Huang R, Kang T, Chen S. The role of tumor-associated macrophages in tumor immune evasion. *J Cancer Res Clin Oncol.* (2024) 150:238. doi: 10.1007/s00432-024-05777-4

126. Seager RJ, Hajal C, Spill F, Kamm RD, Zaman MH. Dynamic interplay between tumour, stroma and immune system can drive or prevent tumour progression. *Converg Sci Phys Oncol.* (2017) 3:034002. doi: 10.1088/2057-1739/aa7e86

127. De Visser KE, Joyce JA. The evolving tumor microenvironment: From cancer initiation to metastatic outgrowth. *Cancer Cell.* (2023) 41:374–403. Available online at: https://linkinghub.elsevier.com/retrieve/pii/S1535610823000442. (Accessed February 19, 2025).

128. Tang T, Huang X, Zhang G, Hong Z, Bai X, Liang T. Advantages of targeting the tumor immune microenvironment over blocking immune checkpoint in cancer immunotherapy. *Sig Transduct Target Ther.* (2021) 6:72. Available online at: https://www.nature.com/articles/s41392-020-00449-4. (Accessed February 19, 2025).

129. Sun D, Liu J, Zhou H, Shi M, Sun J, Zhao S, et al. Classification of tumor immune microenvironment according to programmed death-ligand 1 expression and immune infiltration predicts response to immunotherapy plus chemotherapy in advanced patients with NSCLC. *J Thorac Oncol.* (2023) 18:869–81. Available online at: https://linkinghub.elsevier.com/retrieve/pii/S1556086423001946. (Accessed February 19, 2025).

130. Waldman AD, Fritz JM, Lenardo MJ. A guide to cancer immunotherapy: from T cell basic science to clinical practice. *Nat Rev Immunol.* (2020) 20:651–68. Available online at: https://www.nature.com/articles/s41577-020-0306-5. (Accessed March 19, 2025).

131. Dean I, Lee CYC, Tuong ZK, Li Z, Tibbitt CA, Willis C, et al. Rapid functional impairment of natural killer cells following tumor entry limits anti-tumor immunity. *Nat Commun.* (2024) 15:683. Available online at: https://www.nature.com/articles/s41467-024-44789-z. (Accessed February 20, 2025).

132. Villa R, Shiau YP, Mahri S, Racacho KJ, Tang M, Zong Q, et al. Immunomodulatory nanoplatforms with multiple mechanisms of action in cancer treatment. *Nanomedicine.* (2025) 20:1321–38. doi: 10.1080/17435889.2025.2500906

133. Oltolina F, Colangelo D, Miletto I, Clemente N, Miola M, Verné E, et al. Tumor targeting by monoclonal antibody functionalized magnetic nanoparticles. *Nanomaterials (Basel).* (2019) 9:1575. doi: 10.3390/nano9111575

134. Fucikova J, Kepp O, Kasikova L, Petroni G, Yamazaki T, Liu P, et al. Detection of immunogenic cell death and its relevance for cancer therapy. *Cell Death Dis.* (2020)

11:1013. Available online at: https://www.nature.com/articles/s41419-020-03221-2. (Accessed February 19, 2025).

135. Ahmed A, Tait SWG. Targeting immunogenic cell death in cancer. *Mol Oncol*. (2020) 14:2994–3006. doi: 10.1002/1878-0261.12851

136. Krysko O, Løve Aaes T, Bachert C, Vandenabeele P, Krysko DV. Many faces of DAMPs in cancer therapy. *Cell Death Dis*. (2013) 4:e631–1. Available online at: https://www.nature.com/articles/cddis2013156. (Accessed February 19, 2025).

137. Galluzzi L, Buqué A, Kepp O, Zitvogel L, Kroemer G. Immunogenic cell death in cancer and infectious disease. *Nat Rev Immunol*. (2017) 17:97–111. Available online at: https://www.nature.com/articles/nri.2016.107. (Accessed February 19, 2025).

138. Fu J, Zhang W, Jiang T. Immunogenic cell death mediation patterns reveal novel paradigm for characterizing the immune microenvironment and immunotherapeutic responses in bladder cancer. *Front Genet*. (2022) 13:1035484/full. doi: 10.3389/fgene.2022.1035484/full

139. Liu P, Zhao L, Pol J, Levesque S, Petrazzuolo A, Pfirschke C, et al. Crizotinib-induced immunogenic cell death in non-small cell lung cancer. *Nat Commun*. (2019) 10:1486. Available online at: https://www.nature.com/articles/s41467-019-09415-3. (Accessed February 19, 2025).

140. Li Y, Wang J, Ma X, Tan L, Yan Y, Xue C, et al. A review of neoadjuvant chemoradiotherapy for locally advanced rectal cancer. *Int J Biol Sci*. (2016) 12:1022–31. doi: 10.7150/ijbs.15438

141. Kasi A, Abbasi S, Handa S, Al-Rajabi R, Saeed A, Baranda J, et al. Total neoadjuvant therapy vs standard therapy in locally advanced rectal cancer: A systematic review and meta-analysis. *JAMA Netw Open*. (2020) 3:e2030097. doi: 10.1001/jamanetworkopen.2020.30097

142. Huang KCY, Chiang SF, Yang PC, Ke TW, Chen TW, Hu CH, et al. Immunogenic cell death by the novel topoisomerase I inhibitor TLC388 enhances the therapeutic efficacy of radiotherapy. *Cancers (Basel)*. (2021) 13:1218. doi: 10.3390/cancers13061218

143. Sun L, Zhou H, Zhu Z, Yan Q, Wang L, Liang Q, et al. Ex vivo and *in vitro* effect of serum amyloid A in the induction of macrophage M2 markers and efferocytosis of apoptotic neutrophils. *J Immunol*. (2015) 194:4891–900. Available online at: https://academic.oup.com/jimmunol/article/194/10/4891/7960770. (Accessed March 19, 2025).

144. Cutolo M, Campitiello R, Gotelli E, Soldano S. The role of M1/M2 macrophage polarization in rheumatoid arthritis synovitis. *Front Immunol*. (2022) 13:867260/full. doi: 10.3389/fimmu.2022.867260/full

145. Serhan CN, Chiang N, Dalli J, Levy BD. Lipid mediators in the resolution of inflammation. *Cold Spring Harb Perspect Biol*. (2015) 7:a016311. doi: 10.1101/cshperspect.a016311

146. Sugimoto MA, Sousa LP, Pinho V, Perretti M, Teixeira MM. Resolution of inflammation: what controls its onset? *Front Immunol*. (2016) 7:160/abstract. doi: 10.3389/fimmu.2016.00160/abstract

147. Park MD, Silvin A, Ginhoux F, Merad M. Macrophages in health and disease. *Cell*. (2022) 185:4259–79. Available online at: https://linkinghub.elsevier.com/retrieve/pii/S0092867422013228. (Accessed March 19, 2025).

148. Rodríguez-Morales P, Franklin RA. Macrophage phenotypes and functions: resolving inflammation and restoring homeostasis. *Trends Immunol*. (2023) 44:986–98. Available online at: https://linkinghub.elsevier.com/retrieve/pii/S1471490623002119. (Accessed March 19, 2025).

149. Kim J, Bae JS. Tumor-associated macrophages and neutrophils in tumor microenvironment. *Mediators Inflammation*. (2016) 2016:1–11. Available online at: http://www.hindawi.com/journals/mi/2016/6058147/. (Accessed March 19, 2025).

150. Quail DF, Amulic B, Aziz M, Barnes BJ, Eruslanov E, Fridlender ZG, et al. Neutrophil phenotypes and functions in cancer: A consensus statement. *J Exp Med*. (2022) 219:e20220011. Available online at: https://rupress.org/jem/article/219/6/e20220011/213202/Neutrophil-phenotypes-and-functions-in-cancer-A. (Accessed March 19, 2025).

151. Fridlender ZG, Granot Z. Neutrophils in the tumor microenvironment – when a company becomes a crowd. *Cell Mol Immunol*. (2024) 21:313–4. Available online at: https://www.nature.com/articles/s41423-024-01147-9. (Accessed March 31, 2025).

152. Di Ceglie I, Carnevale S, Rigatelli A, Grieco G, Molisso P, Jaillon S. Immune cell networking in solid tumors: focus on macrophages and neutrophils. *Front Immunol*. (2024) 15:1341390/full. doi: 10.3389/fimmu.2024.1341390/full

153. Hsu BE, Shen Y, Siegel PM. Neutrophils: orchestrators of the Malignant phenotype. *Front Immunol*. (2020) 11:1778/full. doi: 10.3389/fimmu.2020.01778/full

154. Francisco LM, Sage PT, Sharpe AH. The PD-1 pathway in tolerance and autoimmunity. *Immunol Rev*. (2010) 236:219–42. doi: 10.1111/j.1600-065X.2010.00923.x

155. Tai X, Van Laethem F, Pobezinsky L, Guinter T, Sharrow SO, Adams A, et al. Basis of CTLA-4 function in regulatory and conventional CD4+ T cells. *Blood*. (2012) 119:5155–63. Available online at: https://ashpublications.org/blood/article/119/22/5155/105494/Basis-of-CTLA4-function-in-regulatory-and. (Accessed March 19, 2025).

156. Pardoll DM. The blockade of immune checkpoints in cancer immunotherapy. *Nat Rev Cancer*. (2012) 12:252–64. Available online at: https://www.nature.com/articles/nrc3239. (Accessed March 31, 2025).

157. Qiao G, Li S, Pan X, Xie P, Peng R, Huang X, et al. Surgical tumor–derived nanoplatform targets tumor-associated macrophage for personalized postsurgical cancer immunotherapy. *Sci Adv*. (2024) 10:eadk7955. doi: 10.1126/sciadv.adk7955

158. Akira S, Uematsu S, Takeuchi O. Pathogen recognition and innate immunity. *Cell*. (2006) 124:783–801. Available online at: https://linkinghub.elsevier.com/retrieve/pii/S0092867406001905. (Accessed March 19, 2025).

159. Banchereau J, Steinman RM. Dendritic cells and the control of immunity. *Nature*. (1998) 392:245–52. Available online at: https://www.nature.com/articles/32588. (Accessed March 19, 2025).

160. Bhardwaj N. Processing and presentation of antigens by dendritic cells: implications for vaccines. *Trends Mol Med*. (2001) 7:388–94. Available online at: https://linkinghub.elsevier.com/retrieve/pii/S1471491401021013. (Accessed March 19, 2025).

161. Thomas IJ, Petrich De Marquesini LG, Ravanan R, Smith RM, Guerder S, Flavell RA, et al. CD86 has sustained costimulatory effects on CD8 T cells. *J Immunol*. (2007) 179:5936–46. Available online at: https://journals.aai.org/jimmunol/article/179/9/5936/38190/CD86-Has-Sustained-Costimulatory-Effects-on-CD8-T. (Accessed March 19, 2025).

162. Fu C, Jiang A. Dendritic cells and CD8 T cell immunity in tumor microenvironment. *Front Immunol*. (2018) 9:3059/full. doi: 10.3389/fimmu.2018.03059/full

163. Koliaraki V, Henriques A, Prados A, Kollias G. Unfolding innate mechanisms in the cancer microenvironment: The emerging role of the mesenchyme. *J Exp Med*. (2020) 217:e20190457. Available online at: https://rupress.org/jem/article/217/4/e20190457/133714/Unfolding-innate-mechanisms-in-the-cancer. (Accessed March 19, 2025).

164. Dutertre CA, Becht E, Irac SE, Khalilnezhad A, Narang V, Khalilnezhad S, et al. Single-cell analysis of human mononuclear phagocytes reveals subset-defining markers and identifies circulating inflammatory dendritic cells. *Immunity*. (2019) 51:573–589.e8. Available online at: https://linkinghub.elsevier.com/retrieve/pii/S1074761319303346. (Accessed March 19, 2025).

165. Galassi C, Chan TA, Vitale I, Galluzzi L. The hallmarks of cancer immune evasion. *Cancer Cell*. (2024) 42:1825–63. Available online at: https://linkinghub.elsevier.com/retrieve/pii/S1535610824003581. (Accessed March 31, 2025).

166. Kim SK, Cho SW. The evasion mechanisms of cancer immunity and drug intervention in the tumor microenvironment. *Front Pharmacol*. (2022) 13:868695/full. doi: 10.3389/fphar.2022.868695/full

167. Pitt JM, Marabelle A, Eggermont A, Soria JC, Kroemer G, Zitvogel L. Targeting the tumor microenvironment: removing obstruction to anticancer immune responses and immunotherapy. *Ann Oncol*. (2016) 27:1482–92. Available online at: https://linkinghub.elsevier.com/retrieve/pii/S0923753419347209. (Accessed February 20, 2025).

168. Ohue Y, Nishikawa H. Regulatory T (Treg) cells in cancer: Can Treg cells be a new therapeutic target? *Cancer Sci*. (2019) 110:2080–9. doi: 10.1111/cas.14069

169. Zhang Z, Liu S, Zhang B, Qiao L, Zhang Y, Zhang Y. T cell dysfunction and exhaustion in cancer. *Front Cell Dev Biol*. (2020) 8:17. doi: 10.3389/fcell.2020.00017

170. Melssen MM, Sheybani ND, Leick KM, Slingluff CL. Barriers to immune cell infiltration in tumors. *J Immunother Cancer*. (2023) 11:e006401. doi: 10.1136/jitc-2022-006401

171. Yamauchi M, Barker TH, Gibbons DL, Kurie JM. The fibrotic tumor stroma. *J Clin Invest*. (2018) 128:16–25. doi: 10.1172/JCI93554

172. Nissen NI, Karsdal M, Willumsen N. Collagens and Cancer associated fibroblasts in the reactive stroma and its relation to Cancer biology. *J Exp Clin Cancer Res*. (2019) 38:115. doi: 10.1186/s13046-019-1110-6

173. Mao X, Xu J, Wang W, Liang C, Hua J, Liu J, et al. Crosstalk between cancer-associated fibroblasts and immune cells in the tumor microenvironment: new findings and future perspectives. *Mol Cancer*. (2021) 20:131. doi: 10.1186/s12943-021-01428-1

174. Yang D, Liu J, Qian H, Zhuang Q. Cancer-associated fibroblasts: from basic science to anticancer therapy. *Exp Mol Med*. (2023) 55:1322–32. Available online at: https://www.nature.com/articles/s12276-023-01013-0. (Accessed March 31, 2025).

175. Chhabra Y, Weeraratna AT. Fibroblasts in cancer: Unity in heterogeneity. *Cell*. (2023) 186:1580–609. Available online at: https://linkinghub.elsevier.com/retrieve/pii/S0092867423002775. (Accessed March 31, 2025).

176. Yaseen MM, Abuharfeil NM, Darmani H, Daoud A. Mechanisms of immune suppression by myeloid-derived suppressor cells: the role of interleukin-10 as a key immunoregulatory cytokine. *Open Biol*. (2020) 10:200111. doi: 10.1098/rsob.200111

177. Cicchese JM, Evans S, Hult C, Joslyn LR, Wessler T, Millar JA, et al. Dynamic balance of pro- and anti-inflammatory signals controls disease and limits pathology. *Immunol Rev*. (2018) 285:147–67. doi: 10.1111/imr.12671

178. Pham K, Parikh K, Heinrich EC. Hypoxia and inflammation: insights from high-altitude physiology. *Front Physiol*. (2021) 12:676782. doi: 10.3389/fphys.2021.676782

179. Scott EN, Gocher AM, Workman CJ, Vignali DAA. Regulatory T cells: barriers of immune infiltration into the tumor microenvironment. *Front Immunol*. (2021) 12:702726/full. doi: 10.3389/fimmu.2021.702726/full

180. Qin D, Zhang Y, Shu P, Lei Y, Li X, Wang Y. Targeting tumor-infiltrating tregs for improved antitumor responses. *Front Immunol*. (2024) 15:1325946/full. doi: 10.3389/fimmu.2024.1325946/full

181. Antonioli L, Pacher P, Vizi ES, Haskó G. CD39 and CD73 in immunity and inflammation. *Trends Mol Med*. (2013) 19:355–67. Available online at: https://linkinghub.elsevier.com/retrieve/pii/S1471491413000543. (Accessed April 02, 2025).

182. Schneider E, Winzer R, Rissiek A, Ricklefs I, Meyer-Schwesinger C, Ricklefs FL, et al. CD73-mediated adenosine production by CD8 T cell-derived extracellular vesicles constitutes an intrinsic mechanism of immune suppression. *Nat Commun*. (2021) 12:5911. Available online at: https://www.nature.com/articles/s41467-021-26134-w. (Accessed March 19, 2025).

183. Cha JH, Chan LC, Li CW, Hsu JL, Hung MC. Mechanisms controlling PD-L1 expression in cancer. *Mol Cell*. (2019) 76:359–70. doi: 10.1016/j.molcel.2019.09.030

184. Han Y, Liu D, Li L. PD-1/PD-L1 pathway: current researches in cancer. *Am J Cancer Res*. (2020) 10:727–42.

185. Hu A, Sun L, Lin H, Liao Y, Yang H, Mao Y. Harnessing innate immune pathways for therapeutic advancement in cancer. *Sig Transduct Target Ther*. (2024) 9:68. Available online at: https://www.nature.com/articles/s41392-024-01765-9. (Accessed April 02, 2025).

186. Lin X, Kang K, Chen P, Zeng Z, Li G, Xiong W, et al. Regulatory mechanisms of PD-1/PD-L1 in cancers. *Mol Cancer [Internet]*. (2024) 23(1). Available from: https://molecular-cancer.biomedcentral.com/articles/10.1186/s12943-024-02023-w.

187. Pashayan N, Antoniou AC, Ivanus U, Esserman LJ, Easton DF, French D, et al. Personalized early detection and prevention of breast cancer: ENVISION consensus statement. *Nat Rev Clin Oncol*. (2020) 17:687–705. Available online at: https://www.nature.com/articles/s41571-020-0388-9. (Accessed March 19, 2025).

188. Fu Z, Mowday AM, Smaill JB, Hermans IF, Patterson AV. Tumour hypoxia-mediated immunosuppression: mechanisms and therapeutic approaches to improve cancer immunotherapy. *Cells*. (2021) 10:1006. doi: 10.3390/cells10051006

189. Santiago-Sánchez GS, Hodge JW, Fabian KP. Tipping the scales: Immunotherapeutic strategies that disrupt immunosuppression and promote immune activation. *Front Immunol*. (2022) 13:993624. doi: 10.3389/fimmu.2022.993624

190. Zahavi D, Weiner L. Monoclonal antibodies in cancer therapy. *Antibodies (Basel)*. (2020) 9:34. doi: 10.3390/antib9030034

191. Liu D, Che X, Wang X, Ma C, Wu G. Tumor vaccines: unleashing the power of the immune system to fight cancer. *Pharm (Basel)*. (2023) 16:1384. doi: 10.3390/ph16101384

192. Ghemrawi R, Abuamer L, Kremesh S, Hussien G, Ahmed R, Mousa W, et al. Revolutionizing cancer treatment: recent advances in immunotherapy. *Biomedicines*. (2024) 12:2158. Available online at: https://www.mdpi.com/2227-9059/12/9/2158. (Accessed April 04, 2025).

193. Disis ML. Mechanism of action of immunotherapy. *Semin Oncol*. (2014) 41:S3–13. Available online at: https://linkinghub.elsevier.com/retrieve/pii/S0093775414001973. (Accessed April 02, 2025).

194. Castelli MS, McGonigle P, Hornby PJ. The pharmacology and therapeutic applications of monoclonal antibodies. *Pharmacol Res Perspect*. (2019) 7:e00535. doi: 10.1002/prp2.535

195. Malik B, Ghatol A. Understanding how monoclonal antibodies work. In: *StatPearls*. StatPearls Publishing, Treasure Island (FL (2025). Available online at: http://www.ncbi.nlm.nih.gov/books/NBK572118/.

196. Su PC, Chen CY, Yu MH, Kuo IY, Yang PS, Hsu CH, et al. Fully human chitinase-3 like-1 monoclonal antibody inhibits tumor growth, fibrosis, angiogenesis, and immune cell remodeling in lung, pancreatic, and colorectal cancers. *Biomed Pharmacother*. (2024) 176:116825. Available online at: https://linkinghub.elsevier.com/retrieve/pii/S0753332224007091. (Accessed March 02, 2025).

197. Goleva E, Lyubchenko T, Kraehenbuehl L, Lacouture ME, Leung DYM, Kern JA. Our current understanding of checkpoint inhibitor therapy in cancer immunotherapy. *Ann Allergy Asthma Immunol*. (2021) 126:630–8. doi: 10.1016/j.anai.2021.03.003

198. Barrueto L, Caminero F, Cash L, Makris C, Lamichhane P, Deshmukh RR. Resistance to checkpoint inhibition in cancer immunotherapy. *Trans Oncol*. (2020) 13:100738. Available online at: https://linkinghub.elsevier.com/retrieve/pii/S1936523319305376. (Accessed February 24, 2025).

199. Lao Y, Shen D, Zhang W, He R, Jiang M. Immune checkpoint inhibitors in cancer therapy-how to overcome drug resistance? *Cancers (Basel)*. (2022) 14:3575. doi: 10.3390/cancers14153575

200. Immune checkpoint inhibitors - NCI. Available online at: https://www.cancer.gov/about-cancer/treatment/types/immunotherapy/checkpoint-inhibitors. (Accessed March 21, 2025).

201. Tawbi HA, SChadendorf D, Lipson EJ, Ascierto PA, Matamala L, Castillo Gutiérrez E, et al. Relatlimab and nivolumab versus nivolumab in untreated advanced melanoma. *N Engl J Med*. (2022) 386:24–34. doi: 10.1056/NEJMoa2109970

202. Long L, Zhang X, Chen F, Pan Q, Phiphatwatchara P, Zeng Y, et al. The promising immune checkpoint LAG-3: from tumor microenvironment to cancer immunotherapy. *Genes Cancer*. (2018) 9:176–89. doi: 10.18632/genesandcancer.180

203. Huo JL, Wang YT, Fu WJ, Lu N, Liu ZS. The promising immune checkpoint LAG-3 in cancer immunotherapy: from basic research to clinical application. *Front Immunol*. (2022) 13:956090/full. doi: 10.3389/fimmu.2022.956090/full

204. Melero I, Yau T, Kang YK, Kim TY, Santoro A, Sangro B, et al. Nivolumab plus ipilimumab combination therapy in patients with advanced hepatocellular carcinoma previously treated with sorafenib: 5-year results from CheckMate 040. *Ann Oncol*. (2024) 35:537–48. Available online at: https://linkinghub.elsevier.com/retrieve/pii/S0923753424000826. (Accessed April 03, 2025).

205. Tian Z, Liu M, Zhang Y, Wang X. Bispecific T cell engagers: an emerging therapy for management of hematologic Malignancies. *J Hematol Oncol*. (2021) 14:75. doi: 10.1186/s13045-021-01084-4

206. Zhu WM, Middleton MR. Combination therapies for the optimisation of Bispecific T-cell Engagers in cancer treatment. *Immunother Adv*. (2023) 3:ltad013. doi: 10.1093/immadv/ltad013

207. Huehls AM, Coupet TA, Sentman CL. Bispecific T-cell engagers for cancer immunotherapy. *Immunol Cell Biol*. (2015) 93:290–6. doi: 10.1038/icb.2014.93

208. Subklewe M. BiTEs better than CAR T cells. *Blood Adv*. (2021) 5:607–12. doi: 10.1182/bloodadvances.2020001792

209. Ross SL, Sherman M, McElroy PL, Lofgren JA, Moody G, Baeuerle PA, et al. Bispecific T cell engager (BiTE®) antibody constructs can mediate bystander tumor cell killing. *PloS One*. (2017) 12:e0183390. doi: 10.1371/journal.pone.0183390

210. Simão DC, Zarrabi KK, Mendes JL, Luz R, Garcia JA, Kelly WK, et al. Bispecific T-cell engagers therapies in solid tumors: focusing on prostate cancer. *Cancers (Basel)*. (2023) 15:1412. doi: 10.3390/cancers15051412

211. Zhou S, Liu M, Ren F, Meng X, Yu J. The landscape of bispecific T cell engager in cancer treatment. *biomark Res*. (2021) 9:38. doi: 10.1186/s40364-021-00294-9

212. Braig F, Brandt A, Goebeler M, Tony HP, Kurze AK, Nollau P, et al. Resistance to anti-CD19/CD3 BiTE in acute lymphoblastic leukemia may be mediated by disrupted CD19 membrane trafficking. *Blood*. (2017) 129:100–4. Available online at: https://ashpublications.org/blood/article/129/1/100/35801/Resistance-to-antiCD19CD3-BiTE-in-acute. (Accessed June 02, 2025).

213. Einsele H, Borghaei H, Orlowski RZ, Subklewe M, Roboz GJ, Zugmaier G, et al. The BiTE (bispecific T-cell engager) platform: Development and future potential of a targeted immuno-oncology therapy across tumor types. *Cancer*. (2020) 126:3192–201. doi: 10.1002/cncr.32909

214. Paredes-Moscosso SR, Nathwani AC. 10 years of BiTE immunotherapy: an overview with a focus on pancreatic cancer. *Front Oncol*. (2024) 14:1429330. doi: 10.3389/fonc.2024.1429330

215. Rafiq S, Hackett CS, Brentjens RJ. Engineering strategies to overcome the current roadblocks in CAR T cell therapy. *Nat Rev Clin Oncol*. (2020) 17:147–67. Available online at: https://www.nature.com/articles/s41571-019-0297-y. (Accessed February 24, 2025).

216. Zhang G, Wang L, Cui H, Wang X, Zhang G, Ma J, et al. Anti-melanoma activity of T cells redirected with a TCR-like chimeric antigen receptor. *Sci Rep*. (2014) 4:3571. Available online at: https://www.nature.com/articles/srep03571. (Accessed February 24, 2025).

217. Brudno JN, Maus MV, Hinrichs CS. CAR T cells and T-cell therapies for cancer: A translational science review. *JAMA*. (2024) 332:1924. Available online at: https://jamanetwork.com/journals/jama/fullarticle/2825799. (Accessed April 04, 2025).

218. Maude SL, Laetsch TW, Buechner J, Rives S, Boyer M, Bittencourt H, et al. Tisagenlecleucel in children and young adults with B-cell lymphoblastic leukemia. *N Engl J Med*. (2018) 378:439–48. doi: 10.1056/NEJMoa1709866

219. Shah BD, Ghobadi A, Oluwole OO, Logan AC, Boissel N, Cassaday RD, et al. KTE-X19 for relapsed or refractory adult B-cell acute lymphoblastic leukaemia: phase 2 results of the single-arm, open-label, multicentre ZUMA-3 study. *Lancet*. (2021) 398:491–502. Available online at: https://linkinghub.elsevier.com/retrieve/pii/S0140673621012228. (Accessed April 04, 2025).

220. Jonnalagadda M, Mardiros A, Urak R, Wang X, Hoffman LJ, Bernanke A, et al. Chimeric antigen receptors with mutated IgG4 Fc spacer avoid fc receptor binding and improve T cell persistence and antitumor efficacy. *Mol Ther*. (2015) 23:757–68. doi: 10.1038/mt.2014.208

221. Watanabe K, Kuramitsu S, Posey AD, June CH. Expanding the therapeutic window for CAR T cell therapy in solid tumors: the knowns and unknowns of CAR T cell biology. *Front Immunol*. (2018) 9:2486. doi: 10.3389/fimmu.2018.02486

222. Liu J, Fu M, Wang M, Wan D, Wei Y, Wei X. Cancer vaccines as promising immuno-therapeutics: platforms and current progress. *J Hematol Oncol*. (2022) 15:28. doi: 10.1186/s13045-022-01247-x

223. Lin MJ, Svensson-Arvelund J, Lubitz GS, Marabelle A, Melero I, Brown BD, et al. Cancer vaccines: the next immunotherapy frontier. *Nat Cancer*. (2022) 3:911–26. Available online at: https://www.nature.com/articles/s43018-022-00418-6. (Accessed April 04, 2025).

224. Grunwitz C, Salomon N, Vascotto F, Selmi A, Bukur T, Diken M, et al. HPV16 RNA-LPX vaccine mediates complete regression of aggressively growing HPV-positive mouse tumors and establishes protective T cell memory. *Oncoimmunology*. (2019) 8:e1629259. doi: 10.1080/2162402X.2019.1629259

225. Sahin U, Oehm P, Derhovanessian E, Jabulowsky RA, Vormehr M, Gold M, et al. An RNA vaccine drives immunity in checkpoint-inhibitor-treated melanoma. *Nature*. (2020) 585:107–12. Available online at: https://www.nature.com/articles/s41586-020-2537-9. (Accessed March 07, 2025).

226. Chow S, Berek JS, Dorigo O. Development of therapeutic vaccines for ovarian cancer. *Vaccines (Basel)*. (2020) 8:657. doi: 10.3390/vaccines8040657

227. Al-Hawary SIS, Saleh EAM, Mamajanov NA, S. Gilmanova N, Alsaab HO, Alghamdi A, et al. Breast cancer vaccines; A comprehensive and updated review. *Pathol - Res Pract*. (2023) 249:154735. Available online at: https://linkinghub.elsevier.com/retrieve/pii/S0344033823004351. (Accessed April 04, 2025).

228. Kaczmarek M, Poznańska J, Fechner F, Michalska N, Paszkowska S, Napierała A, et al. Cancer vaccine therapeutics: limitations and effectiveness-A literature review. *Cells*. (2023) 12:2159. doi: 10.3390/cells12172159

229. Janes ME, Gottlieb AP, Park KS, Zhao Z, Mitragotri S. Cancer vaccines in the clinic. *Bioeng Transl Med*. (2024) 9:e10588. doi: 10.1002/btm2.10588

230. Lee KW, Yam JWP, Mao X. Dendritic cell vaccines: A shift from conventional approach to new generations. *Cells*. (2023) 12:2147. doi: 10.3390/cells12172147

231. Lim SH, Bailey-Wood R. Idiotypic protein-pulsed dendritic cell vaccination in multiple myeloma. *Int J Cancer*. (1999) 83:215–22. doi: 10.1002/(SICI)1097-0215(19991008)83:2<215::AID-IJC12>3.0.CO;2-Q

232. Teng CF, Wang T, Wu TH, Lin JH, Shih FY, Shyu WC, et al. Combination therapy with dendritic cell vaccine and programmed death ligand 1 immune checkpoint inhibitor for hepatocellular carcinoma in an orthotopic mouse model. *Ther Adv Med Oncol*. (2020) 12:1758835920922034. doi: 10.1177/1758835920922034

233. Najafi S, Mortezaee K. Advances in dendritic cell vaccination therapy of cancer. *Biomed Pharmacother*. (2023) 164:114954. Available online at: https://linkinghub.elsevier.com/retrieve/pii/S0753332223007448. (Accessed February 24, 2025).

234. Zanotta S, Galati D, De Filippi R, Pinto A. Enhancing dendritic cell cancer vaccination: the synergy of immune checkpoint inhibitors in combined therapies. *Int J Mol Sci*. (2024) 25:7509. doi: 10.3390/ijms25147509

235. Wang L, Wang N, Zhang W, Cheng X, Yan Z, Shao G, et al. Therapeutic peptides: current applications and future directions. *Sig Transduct Target Ther*. (2022) 7:48. Available online at: https://www.nature.com/articles/s41392-022-00904-4. (Accessed April 04, 2025).

236. Nhàn NTT, Yamada T, Yamada KH. Peptide-based agents for cancer treatment: current applications and future directions. *Int J Mol Sci*. (2023) 24:12931. doi: 10.3390/ijms241612931

237. Smith RJ, Bryant RG. Metal substitutions incarbonic anhydrase: a halide ion probe study. *Biochem Biophys Res Commun*. (1975) 66:1281–6. doi: 10.1016/0006-291X(75)90498-2

238. Jäger E, Chen YT, Drijfhout JW, Karbach J, Ringhoffer M, Jäger D, et al. Simultaneous Humoral and Cellular Immune Response against Cancer–Testis Antigen NY-ESO-1: Definition of Human Histocompatibility Leukocyte Antigen (HLA)-A2–binding Peptide Epitopes. *J Exp Med*. (1998) 187:265–70. Available online at: https://rupress.org/jem/article/187/2/265/7398/Simultaneous-Humoral-and-Cellular-Immune-Response. (Accessed April 04, 2025).

239. Oka Y, Tsuboi A, Taguchi T, Osaki T, Kyo T, Nakajima H, et al. Induction of *WT1* (Wilms' tumor gene)-specific cytotoxic T lymphocytes by WT1 peptide vaccine and the resultant cancer regression. *Proc Natl Acad Sci U S A*. (2004) 101:13885–90. doi: 10.1073/pnas.0405884101

240. Mittendorf EA, Clifton GT, Holmes JP, Clive KS, Patil R, Benavides LC, et al. Clinical trial results of the HER-2/*neu* (E75) vaccine to prevent breast cancer recurrence in high-risk patients: From US Military Cancer Institute Clinical Trials Group Study I-01 and I-02. *Cancer*. (2012) 118:2594–602. doi: 10.1002/cncr.26574

241. Walter S, Weinschenk T, Stenzl A, Zdrojowy R, Pluzanska A, Szczylik C, et al. Multipeptide immune response to cancer vaccine IMA901 after single-dose cyclophosphamide associates with longer patient survival. *Nat Med*. (2012) 18:1254–61. Available online at: https://www.nature.com/articles/nm.2883. (Accessed April 04, 2025).

242. Vansteenkiste J, Zielinski M, Linder A, Dahabreh J, Gonzalez EE, Malinowski W, et al. Adjuvant MAGE-A3 immunotherapy in resected non–small-cell lung cancer: phase II randomized study results. *JCO*. (2013) 31:2396–403. doi: 10.1200/JCO.2012.43.7103

243. Mittendorf EA, Clifton GT, Holmes JP, Schneble E, Van Echo D, Ponniah S, et al. Final report of the phase I/II clinical trial of the E75 (nelipepimut-S) vaccine with booster inoculations to prevent disease recurrence in high-risk breast cancer patients. *Ann Oncol*. (2014) 25:1735–42. Available online at: https://linkinghub.elsevier.com/retrieve/pii/S0923753419351002. (Accessed April 04, 2025).

244. Odunsi K, Matsuzaki J, James SR, Mhawech-Fauceglia P, Tsuji T, Miller A, et al. Epigenetic potentiation of NY-ESO-1 vaccine therapy in human ovarian cancer. *Cancer Immunol Res*. (2014) 2:37–49. Available online at: https://aacrjournals.org/cancerimmunolres/article/2/1/37/466839/Epigenetic-Potentiation-of-NY-ESO-1-Vaccine. (Accessed April 04, 2025).

245. Ghaffari-Nazari H, Tavakkol-Afshari J, Jaafari MR, Tahaghoghi-Hajghorbani S, Masoumi E, Jalali SA. Improving multi-epitope long peptide vaccine potency by using a strategy that enhances CD4+ T help in BALB/c mice. *PLoS One*. (2015) 10:e0142563. doi: 10.1371/journal.pone.0142563

246. Malonis RJ, Lai JR, Vergnolle O. Peptide-based vaccines: current progress and future challenges. *Chem Rev*. (2020) 120:3210–29. doi: 10.1021/acs.chemrev.9b00472

247. Zamani P, Teymouri M, Nikpoor AR, Navashenaq JG, Gholizadeh Z, Darban SA, et al. Nanoliposomal vaccine containing long multi-epitope peptide E75-AE36 pulsed PADRE-induced effective immune response in mice TUBO model of breast cancer. *Eur J Cancer*. (2020) 129:80–96. Available online at: https://linkinghub.elsevier.com/retrieve/pii/S0959804920300241. (Accessed February 24, 2025).

248. Araldi RP, Sant'Ana TA, Módolo DG, De Melo TC, Spadacci-Morena DD, De Cassia Stocco R, et al. The human papillomavirus (HPV)-related cancer biology: An overview. *Biomed Pharmacother*. (2018) 106:1537–56. Available online at: https://linkinghub.elsevier.com/retrieve/pii/S0753332218328178. (Accessed March 02, 2025).

249. Wang R, Huang H, Yu C, Li X, Wang Y, Xie L. Current status and future directions for the development of human papillomavirus vaccines. *Front Immunol*. (2024) 15:1362770. doi: 10.3389/fimmu.2024.1362770

250. Di Donato V, Caruso G, Petrillo M, Kontopantelis E, Palaia I, Perniola G, et al. Adjuvant HPV Vaccination to Prevent Recurrent Cervical Dysplasia after Surgical Treatment: A Meta-Analysis. *Vaccines*. (2021) 9:410. Available online at: https://www.mdpi.com/2076-393X/9/5/410. (Accessed March 02, 2025).

251. Sethi SK, Bradley CE, Bialkowski L, Pang YY, Thompson CD, Schiller JT, et al. Repurposing anti-viral subunit and mRNA vaccines T cell immunity for intratumoral immunotherapy against solid tumors. *NPJ Vaccines*. (2025) 10:84. Available online at: https://www.nature.com/articles/s41541-025-01131-y. (Accessed April 25, 2025).

252. Jahanafrooz Z, Baradaran B, Mosafer J, Hashemzaei M, Rezaei T, Mokhtarzadeh A, et al. Comparison of DNA and mRNA vaccines against cancer. *Drug Discov Today*. (2020) 25:552–60. doi: 10.1016/j.drudis.2019.12.003

253. Paudyal R, Shah AD, Akin O, Do RKG, Konar AS, Hatzoglou V, et al. Artificial intelligence in CT and MR imaging for oncological applications. *Cancers*. (2023) 15:2573. Available online at: https://www.mdpi.com/2072-6694/15/9/2573. (Accessed August 01, 2025).

254. Zheng S, Cui X, Ye Z. Integrating artificial intelligence into radiological cancer imaging: from diagnosis and treatment response to prognosis. *Cancer Biol Med*. (2025) 22:6–13. Available online at: https://www.cancerbiomed.org/content/22/1/6. (Accessed August 01, 2025).

255. Bhinder B, Gilvary C, Madhukar NS, Elemento O. Artificial intelligence in cancer research and precision medicine. *Cancer Discov*. (2021) 11:900–15. doi: 10.1158/2159-8290.CD-21-0090

256. Rangamuwa K, Aloe C, Christie M, Asselin-Labat ML, Batey D, Irving L, et al. Methods for assessment of the tumour microenvironment and immune interactions in non-small cell lung cancer. A narrative review. *Front Oncol*. (2023) 13:1129195. doi: 10.3389/fonc.2023.1129195

257. Crouigneau R, Li YF, Auxillos J, Goncalves-Alves E, Marie R, Sandelin A, et al. Mimicking and analyzing the tumor microenvironment. *Cell Rep Methods*. (2024) 4:100866. Available online at: https://linkinghub.elsevier.com/retrieve/pii/S2667237524002443. (Accessed March 02, 2025).

258. Bajwa J, Munir U, Nori A, Williams B. Artificial intelligence in healthcare: transforming the practice of medicine. *Future Healthc J*. (2021) 8:e188–94. doi: 10.7861/fhj.2021-0095

259. Chen M, Zhou K, Dai SY, Tadepalli S, Balakrishnan PB, Xie J, et al. *In vivo* bioluminescence imaging of granzyme B activity in tumor response to cancer immunotherapy. *Cell Chem Biol*. (2022) 29:1556–67.e6. Available online at: https://linkinghub.elsevier.com/retrieve/pii/S2451945622003142. (Accessed March 20, 2025).

260. De Souza Fernandes Pereira M, Thakkar A, Lee DA. Non-invasive fluorescence imaging for tracking immune cells in preclinical models of immunotherapy. In: *Methods in Cell Biology*. Elsevier (2022). p. 163–70. Available online at: https://linkinghub.elsevier.com/retrieve/pii/S0091679X21000595.

261. Um-e-Kalsoom, Wang S, Qu J, Liu L. Innovative optical imaging strategies for monitoring immunotherapy in the tumor microenvironments. *Cancer Med*. (2024) 13:e70155. doi: 10.1002/cam4.70155

262. Gangadaran P, Onkar A, Rajendran RL, Goenka A, Oh JM, Khan F, et al. Noninvasive *in vivo* imaging of macrophages: understanding tumor microenvironments and delivery of therapeutics. *biomark Res*. (2025) 13:20. doi: 10.1186/s40364-025-00735-9

263. Sheng W, Zhang C, Mohiuddin TM, Al-Rawe M, Zeppernick F, Falcone FH, et al. Multiplex immunofluorescence: A powerful tool in cancer immunotherapy. *IJMS*. (2023) 24:3086. Available online at: https://www.mdpi.com/1422-0067/24/4/3086. (Accessed March 20, 2025).

264. Taube JM, Sunshine JC, Angelo M, Akturk G, Eminizer M, Engle LL, et al. Society for Immunotherapy of Cancer: updates and best practices for multiplex immunohistochemistry (IHC) and immunofluorescence (IF) image analysis and data sharing. *J Immunother Cancer*. (2025) 13:e008875. doi: 10.1136/jitc-2024-008875

265. Keren L, Bosse M, Marquez D, Angoshtari R, Jain S, Varma S, et al. A structured tumor-immune microenvironment in triple negative breast cancer revealed by multiplexed ion beam imaging. *Cell*. (2018) 174:1373–87.e19. Available online at: https://linkinghub.elsevier.com/retrieve/pii/S0092867418311000. (Accessed March 20, 2025).

266. Ptacek J, Locke D, Finck R, Cvijic ME, Li Z, Tarolli JG, et al. Multiplexed ion beam imaging (MIBI) for characterization of the tumor microenvironment across tumor types. *Lab Invest*. (2020) 100:1111–23. Available online at: https://linkinghub.elsevier.com/retrieve/pii/S0023683722003786. (Accessed March 20, 2025).

267. Kapoor M, Kasi A. PET scanning. In: *StatPearls*. StatPearls Publishing, Treasure Island (FL) (2025). Available online at: http://www.ncbi.nlm.nih.gov/books/NBK559089/.

268. Wei W, Jiang D, Ehlerding EB, Luo Q, Cai W. Noninvasive PET imaging of T cells. *Trends Cancer*. (2018) 4:359–73. doi: 10.1016/j.trecan.2018.03.009

269. Vijayakumar S, Yang J, Nittala MR, Velazquez AE, Huddleston BL, Rugnath NA, et al. Changing role of PET/CT in cancer care with a focus on radiotherapy. *Cureus*. (2022) 14(12):e32840. Available online at: https://www.cureus.com/articles/125505-changing-role-of-petct-in-cancer-care-with-a-focus-on-radiotherapy. (Accessed February 19, 2025).

270. Trumbull DA, Lemini R, Bagaria SP, Elli EF, Colibaseanu DT, Wallace MB, et al. Intravital microscopy (IVM) in human solid tumors: novel protocol to examine tumor-associated vessels. *JMIR Res Protoc*. (2020) 9:e15677. Available online at: http://www.researchprotocols.org/2020/10/e15677/. (Accessed February 19, 2025).

271. Fisher DT, Muhitch JB, Kim M, Doyen KC, Bogner PN, Evans SS, et al. Intraoperative intravital microscopy permits the study of human tumour vessels. *Nat Commun*. (2016) 7:10684. Available online at: https://www.nature.com/articles/ncomms10684. (Accessed March 19, 2025).

272. Israel LL, Galstyan A, Holler E, Ljubimova JY. Magnetic iron oxide nanoparticles for imaging, targeting and treatment of primary and metastatic tumors of the brain. *J Controlled Release*. (2020) 320:45–62. Available online at: https://linkinghub.elsevier.com/retrieve/pii/S0168365920300171. (Accessed March 15, 2025).

273. Mallidi S, Luke GP, Emelianov S. Photoacoustic imaging in cancer detection, diagnosis, and treatment guidance. *Trends Biotechnol*. (2011) 29:213–21. Available online at: https://linkinghub.elsevier.com/retrieve/pii/S0167779911000175. (Accessed March 20, 2025).

274. Brown E, Brunker J, Bohndiek SE. Photoacoustic imaging as a tool to probe the tumour microenvironment. *Dis Models Mech*. (2019) 12:dmm039636. Available online at: https://journals.biologists.com/dmm/article/12/7/dmm039636/3378/Photoacoustic-imaging-as-a-tool-to-probe-the. (Accessed March 20, 2025).

275. Bera K, Schalper KA, Rimm DL, Velcheti V, Madabhushi A. Artificial intelligence in digital pathology — new tools for diagnosis and precision oncology. *Nat Rev Clin Oncol*. (2019) 16:703–15. Available online at: https://www.nature.com/articles/s41571-019-0252-y. (Accessed March 20, 2025).

276. Keyl J, Kasper S, Wiesweg M, Götze J, Schönrock M, Sinn M, et al. Multimodal survival prediction in advanced pancreatic cancer using machine learning. *ESMO Open*. (2022) 7:100555. Available online at: https://linkinghub.elsevier.com/retrieve/pii/S2059702922001831. (Accessed March 20, 2025).

277. Alum EU. AI-driven biomarker discovery: enhancing precision in cancer diagnosis and prognosis. *Discov Onc*. (2025) 16:313. doi: 10.1007/s12672-025-02064-7

278. Duchemann B, Remon J, Naigeon M, Cassard L, Jouniaux JM, Boselli L, et al. Current and future biomarkers for outcomes with immunotherapy in non-small cell lung cancer. *Transl Lung Cancer Res*. (2021) 10:2937–54. doi: 10.21037/tlcr-20-839

279. Passaro A, Al Bakir M, Hamilton EG, Diehn M, André F, Roy-Chowdhuri S, et al. Cancer biomarkers: Emerging trends and clinical implications for personalized treatment. *Cell*. (2024) 187:1617–35. doi: 10.1016/j.cell.2024.02.041

280. Daud AI, Wolchok JD, Robert C, Hwu WJ, Weber JS, Ribas A, et al. Programmed death-ligand 1 expression and response to the anti–programmed death 1 antibody pembrolizumab in melanoma. *JCO*. (2016) 34:4102–9. doi: 10.1200/JCO.2016.67.2477

281. Hellmann MD, Ciuleanu TE, Pluzanski A, Lee JS, Otterson GA, Audigier-Valette C, et al. Nivolumab plus ipilimumab in lung cancer with a high tumor mutational burden. *N Engl J Med*. (2018) 378:2093–104. doi: 10.1056/NEJMoa1801946

282. Wang T, Zhang KH. New blood biomarkers for the diagnosis of AFP-negative hepatocellular carcinoma. *Front Oncol*. (2020) 10:1316/full. doi: 10.3389/fonc.2020.01316/full

283. Bayat Mokhtari R, Homayouni TS, Baluch N, Morgatskaya E, Kumar S, Das B, et al. Combination therapy in combating cancer. *Oncotarget*. (2017) 8:38022–43. doi: 10.18632/oncotarget.16723

284. Plant D, Barton A. Adding value to real-world data: the role of biomarkers. *Rheumatol (Oxford)*. (2020) 59:31–8. doi: 10.1093/rheumatology/kez113

285. Ling SP, Ming LC, Dhaliwal JS, Gupta M, Ardianto C, Goh KW, et al. Role of immunotherapy in the treatment of cancer: A systematic review. *Cancers (Basel)*. (2022) 14:5205. doi: 10.3390/cancers14215205

286. Johnson KB, Wei WQ, Weeraratne D, Frisse ME, Misulis K, Rhee K, et al. Precision medicine, AI, and the future of personalized health care. *Clin Transl Sci*. (2021) 14:86–93. doi: 10.1111/cts.12884

287. Farina E, Nabhen JJ, Dacoregio MI, Batalini F, Moraes FY. An overview of artificial intelligence in oncology. *Future Sci OA*. (2022) 8:FSO787. doi: 10.2144/fsoa-2021-0074

288. Sinha S, Vegesna R, Mukherjee S, Kammula AV, Dhruba SR, Wu W, et al. PERCEPTION predicts patient response and resistance to treatment using single-cell transcriptomics of their tumors. *Nat Cancer*. (2024) 5:938–52. Available online at: https://www.nature.com/articles/s43018-024-00756-7. (Accessed March 20, 2025).

289. Liang CW, Yang HC, Islam MM, Nguyen PAA, Feng YT, Hou ZY, et al. Predicting hepatocellular carcinoma with minimal features from electronic health records: development of a deep learning model. *JMIR Cancer*. (2021) 7:e19812. Available online at: https://cancer.jmir.org/2021/4/e19812. (Accessed March 02, 2025).

290. Sato M, Morimoto K, Kajihara S, Tateishi R, Shiina S, Koike K, et al. Machine-learning approach for the development of a novel predictive model for the diagnosis of hepatocellular carcinoma. *Sci Rep*. (2019) 9:7704. Available online at: https://www.nature.com/articles/s41598-019-44022-8. (Accessed March 02, 2025).

291. Mansur A, Vrionis A, Charles JP, Hancel K, Panagides JC, Moloudi F, et al. The role of artificial intelligence in the detection and implementation of biomarkers for hepatocellular carcinoma: outlook and opportunities. *Cancers (Basel)*. (2023) 15:2928. doi: 10.3390/cancers15112928

292. Magaki S, Hojat SA, Wei B, So A, Yong WH. An introduction to the performance of immunohistochemistry. *Methods Mol Biol*. (2019) 1897:289–98. doi: 10.1007/978-1-4939-8935-5_25

293. Oien KA, Dennis JL. Diagnostic work-up of carcinoma of unknown primary: from immunohistochemistry to molecular profiling. *Ann Oncol*. (2012) 23:x271–7. Available online at: https://linkinghub.elsevier.com/retrieve/pii/S0923753419417936. (Accessed March 02, 2025).

294. Wang X, Zhao J, Marostica E, Yuan W, Jin J, Zhang J, et al. A pathology foundation model for cancer diagnosis and prognosis prediction. *Nature*. (2024) 634:970–8. Available online at: https://www.nature.com/articles/s41586-024-07894-z. (Accessed March 02, 2025).

295. Sarkisian ZA, Sagatelian ZA. Treatment of patients with the vertebrogenic lumbosacral radicular syndrome using sinusoidal currents with pulse-duration modulation. *Vopr Kurortol Fizioter Lech Fiz Kult*. (1986), 21–3.

296. Weerarathna IN, Kamble AR, Luharia A. Artificial intelligence applications for biomedical cancer research: A review. *Cureus*. (2023) 15:e48307. doi: 10.7759/cureus.48307

297. Robinson JP, Ostafe R, Iyengar SN, Rajwa B, Fischer R. Flow cytometry: the next revolution. *Cells*. (2023) 12:1875. Available online at: https://www.mdpi.com/2073-4409/12/14/1875. (Accessed April 30, 2025).

298. Fiorin A, López Pablo C, Lejeune M, Hamza Siraj A, Della Mea V. Enhancing AI research for breast cancer: A comprehensive review of tumor-infiltrating lymphocyte datasets. *J Digit Imaging Inform Med*. (2024) 37:2996–3008. doi: 10.1007/s10278-024-01043-8

299. Huhulea EN, Huang L, Eng S, Sumawi B, Huang A, Aifuwa E, et al. Artificial intelligence advancements in oncology: A review of current trends and future directions. *Biomedicines*. (2025) 13:951. Available online at: https://www.mdpi.com/2227-9059/13/4/951. (Accessed April 30, 2025).

300. Bian C, Wang Y, Lu Z, An Y, Wang H, Kong L, et al. ImmunoAIzer: A deep learning-based computational framework to characterize cell distribution and gene mutation in tumor microenvironment. *Cancers*. (2021) 13:1659. Available online at: https://www.mdpi.com/2072-6694/13/7/1659. (Accessed April 30, 2025).

301. Cross JL, Choma MA, Onofrey JA. Bias in medical AI: Implications for clinical decision-making. *PLoS Digit Health*. (2024) 3:e0000651. doi: 10.1371/journal.pdig.0000651

302. Kolla L, Parikh RB. Uses and limitations of artificial intelligence for oncology. *Cancer*. (2024) 130:2101–7. doi: 10.1002/cncr.35307

303. Norori N, Hu Q, Aellen FM, Faraci FD, Tzovara A. Addressing bias in big data and AI for health care: A call for open science. *Patterns (N Y)*. (2021) 2:100347. doi: 10.1016/j.patter.2021.100347

304. Harishbhai Tilala M, Kumar Chenchala P, Choppadandi A, Kaur J, Naguri S, Saoji R, et al. Ethical considerations in the use of artificial intelligence and machine learning in health care: A comprehensive review. *Cureus*. (2024) 16:e62443. doi: 10.7759/cureus.62443

305. Holzinger A. Interactive machine learning for health informatics: when do we need the human-in-the-loop? *Brain Inf*. (2016) 3:119–31. doi: 10.1007/s40708-016-0042-6

306. Washington P. A perspective on crowdsourcing and human-in-the-loop workflows in precision health. *J Med Internet Res*. (2024) 26:e51138. Available online at: https://www.jmir.org/2024/1/e51138. (Accessed July 30, 2025).

307. Nazer LH, Zatarah R, Waldrip S, Ke JXC, Moukheiber M, Khanna AK, et al. Bias in artificial intelligence algorithms and recommendations for mitigation. *PloS Digit Health*. (2023) 2:e0000278. doi: 10.1371/journal.pdig.0000278

308. Hasanzadeh F, Josephson CB, Waters G, Adedinsewo D, Azizi Z, White JA. Bias recognition and mitigation strategies in artificial intelligence healthcare applications. *NPJ Digit Med*. (2025) 8(1). Available online at: https://www.nature.com/articles/s41746-025-01503-7.

309. Li N, Lewin A, Ning S, Waito M, Zeller MP, Tinmouth A, et al. Privacy-preserving federated data access and federated learning: Improved data sharing and AI model development in transfusion medicine. *Transfusion*. (2025) 65:22–8. doi: 10.1111/trf.18077

310. Hoeben A, Joosten EAJ, van den Beuken-van Everdingen MHJ. Personalized medicine: recent progress in cancer therapy. *Cancers (Basel)*. (2021) 13:242. doi: 10.3390/cancers13020242

311. Stefanicka-Wojtas D, Kurpas D. Personalised medicine—Implementation to the healthcare system in Europe (Focus group discussions). *JPM*. (2023) 13:380. Available online at: https://www.mdpi.com/2075-4426/13/3/380. (Accessed June 03, 2025).

312. Uscanga-Palomeque AC, Chávez-Escamilla AK, Alvizo-Báez CA, Saavedra-Alonso S, Terrazas-Armendáriz LD, Tamez-Guerra RS, et al. CAR-T cell therapy: from the shop to cancer therapy. *IJMS*. (2023) 24:15688. Available online at: https://www.mdpi.com/1422-0067/24/21/15688. (Accessed March 20, 2025).

313. Zhao Y, Deng J, Rao S, Guo S, Shen J, Du F, et al. Tumor infiltrating lymphocyte (TIL) therapy for solid tumor treatment: progressions and challenges. *Cancers*. (2022) 14:4160. Available online at: https://www.mdpi.com/2072-6694/14/17/4160. (Accessed March 20, 2025).

314. Davila ML, Brentjens RJ. CD19-Targeted CAR T cells as novel cancer immunotherapy for relapsed or refractory B-cell acute lymphoblastic leukemia. *Clin Adv Hematol Oncol*. (2016) 14:802–8.

315. Zhang X, Zhu L, Zhang H, Chen S, Xiao Y. CAR-T cell therapy in hematological Malignancies: current opportunities and challenges. *Front Immunol*. (2022) 13:927153/full. doi: 10.3389/fimmu.2022.927153/full

316. Sheykhhasan M, Ahmadieh-Yazdi A, Vicidomini R, Poondla N, Tanzadehpanah H, Dirbaziyan A, et al. CAR T therapies in multiple myeloma:

unleashing the future. *Cancer Gene Ther*. (2024) 31:667–86. Available online at: https://www.nature.com/articles/s41417-024-00750-2. (Accessed March 20, 2025).

317. Guzman G, Reed MR, Bielamowicz K, Koss B, Rodriguez A. CAR-T therapies in solid tumors: opportunities and challenges. *Curr Oncol Rep*. (2023) 25:479–89. doi: 10.1007/s11912-023-01380-x

318. Garg P, Pareek S, Kulkarni P, Horne D, Salgia R, Singhal SS. Next-generation immunotherapy: advancing clinical applications in cancer treatment. *J Clin Med*. (2024) 13:6537. doi: 10.3390/jcm13216537

319. Chen T, Wang M, Chen Y, Liu Y. Current challenges and therapeutic advances of CAR-T cell therapy for solid tumors. *Cancer Cell Int*. (2024) 24:133. doi: 10.1186/s12935-024-03315-3

320. Grosser R, Cherkassky L, Chintala N, Adusumilli PS. Combination immunotherapy with CAR T cells and checkpoint blockade for the treatment of solid tumors. *Cancer Cell*. (2019) 36:471–82. Available online at: https://linkinghub.elsevier.com/retrieve/pii/S153561081930426X. (Accessed March 20, 2025).

321. Rodriguez-Garcia A, Lynn RC, Poussin M, Eiva MA, Shaw LC, O'Connor RS, et al. CAR-T cell-mediated depletion of immunosuppressive tumor-associated macrophages promotes endogenous antitumor immunity and augments adoptive immunotherapy. *Nat Commun*. (2021) 12:877. Available online at: https://www.nature.com/articles/s41467-021-20893-2. (Accessed March 20, 2025).

322. Altvater B, Kailayangiri S, Spurny C, Flügge M, Meltzer J, Greune L, et al. CAR T cells as micropharmacies against solid cancers: Combining effector T-cell mediated cell death with vascular targeting in a one-step engineering process. *Cancer Gene Ther*. (2023) 30:1355–68. Available online at: https://www.nature.com/articles/s41417-023-00642-x. (Accessed June 30, 2025).

323. Grzywa TM, Paskal W, Włodarski PK. Intratumor and intertumor heterogeneity in melanoma. *Trans Oncol*. (2017) 10:956–75. Available online at: https://linkinghub.elsevier.com/retrieve/pii/S1936523317302759. (Accessed June 30, 2025).

324. Bartoszewska E, Tota M, Kisielewska M, Skowron I, Sebastianka K, Stefaniak O, et al. Overcoming antigen escape and T-cell exhaustion in CAR-T therapy for leukemia. *Cells*. (2024) 13:1596. doi: 10.3390/cells13181596

325. El-Sayes N, Vito A, Mossman K. Tumor heterogeneity: A great barrier in the age of cancer immunotherapy. *Cancers (Basel)*. (2021) 13:806. doi: 10.3390/cancers13040806

326. Schmidts A, Srivastava AA, Ramapriyan R, Bailey SR, Bouffard AA, Cahill DP, et al. Tandem chimeric antigen receptor (CAR) T cells targeting EGFRvIII and IL-13Rα2 are effective against heterogeneous glioblastoma. *Neuro-Oncology Adv*. (2023) 5:vdac185. doi: 10.1093/noajnl/vdac185/6956903

327. Gómez-Melero S, Hassouneh F, Vallejo-Bermúdez IM, Agüera-Morales E, Solana R, Caballero-Villarraso J. Tandem CAR-T cell therapy: recent advances and current challenges. *Front Immunol*. (2025) 16:1546172. doi: 10.3389/fimmu.2025.1546172

328. Tong C, Zhang Y, Liu Y, Ji X, Zhang W, Guo Y, et al. Optimized tandem CD19/CD20 CAR-engineered T cells in refractory/relapsed B-cell lymphoma. *Blood*. (2020) 136:1632–44. doi: 10.1182/blood.2020005278

329. Sordo-Bahamonde C, Lorenzo-Herrero S, Gonzalez-Rodriguez AP, Martínez-Pérez A, Rodrigo JP, García-Pedrero JM, et al. Chemo-immunotherapy: A new trend in cancer treatment. *Cancers (Basel)*. (2023) 15:2912. doi: 10.3390/cancers15112912

330. Chauhan VP, Martin JD, Liu H, Lacorre DA, Jain SR, Kozin SV, et al. Angiotensin inhibition enhances drug delivery and potentiates chemotherapy by decompressing tumour blood vessels. *Nat Commun*. (2013) 4(1). Available online at: https://www.nature.com/articles/ncomms3516.

331. Pauken KE, Wherry EJ. Overcoming T cell exhaustion in infection and cancer. *Trends Immunol*. (2015) 36:265–76. doi: 10.1016/j.it.2015.02.008

332. Vanneman M, Dranoff G. Combining immunotherapy and targeted therapies in cancer treatment. *Nat Rev Cancer*. (2012) 12:237–51. doi: 10.1038/nrc3237

333. Butterfield LH, Najjar YG. Immunotherapy combination approaches: mechanisms, biomarkers and clinical observations. *Nat Rev Immunol*. (2024) 24:399–416. Available online at: https://www.nature.com/articles/s41577-023-00973-8. (Accessed March 02, 2025).

334. Barbari C, Fontaine T, Parajuli P, Lamichhane N, Jakubski S, Lamichhane P, et al. Immunotherapies and combination strategies for immuno-oncology. *Int J Mol Sci*. (2020) 21:5009. doi: 10.3390/ijms21145009

335. Lu L, Zhan M, Li XY, Zhang H, Dauphars DJ, Jiang J, et al. Clinically approved combination immunotherapy: Current status, limitations, and future perspective. *Curr Res Immunol*. (2022) 3:118–27. doi: 10.1016/j.crimmu.2022.05.003

336. Janjigian YY, Shitara K, Moehler M, Garrido M, Salman P, Shen L, et al. First-line nivolumab plus chemotherapy versus chemotherapy alone for advanced gastric, gastro-oesophageal junction, and oesophageal adenocarcinoma (CheckMate 649): a randomised, open-label, phase 3 trial. *Lancet*. (2021) 398:27–40. Available online at: https://linkinghub.elsevier.com/retrieve/pii/S0140673621007972. (Accessed March 31, 2025).

Frontiers in Immunology

Explores novel approaches and diagnoses to treat immune disorders.

The official journal of the International Union of Immunological Societies (IUIS) and the most cited in its field, leading the way for research across basic, translational and clinical immunology.

Discover the latest Research Topics

See more →

Frontiers

Avenue du Tribunal-Fédéral 34
1005 Lausanne, Switzerland
frontiersin.org

Contact us

+41 (0)21 510 17 00
frontiersin.org/about/contact